Evidence-Based Complementary and Alternative Medicine

The Role and Mechanism of Electroacupuncture for Neurological Diseases 2021

Lead Guest Editor: Feng Zhang
Guest Editors: Yuchuan Ding, Chun-Lei Shan, and Wei-Lin Liu

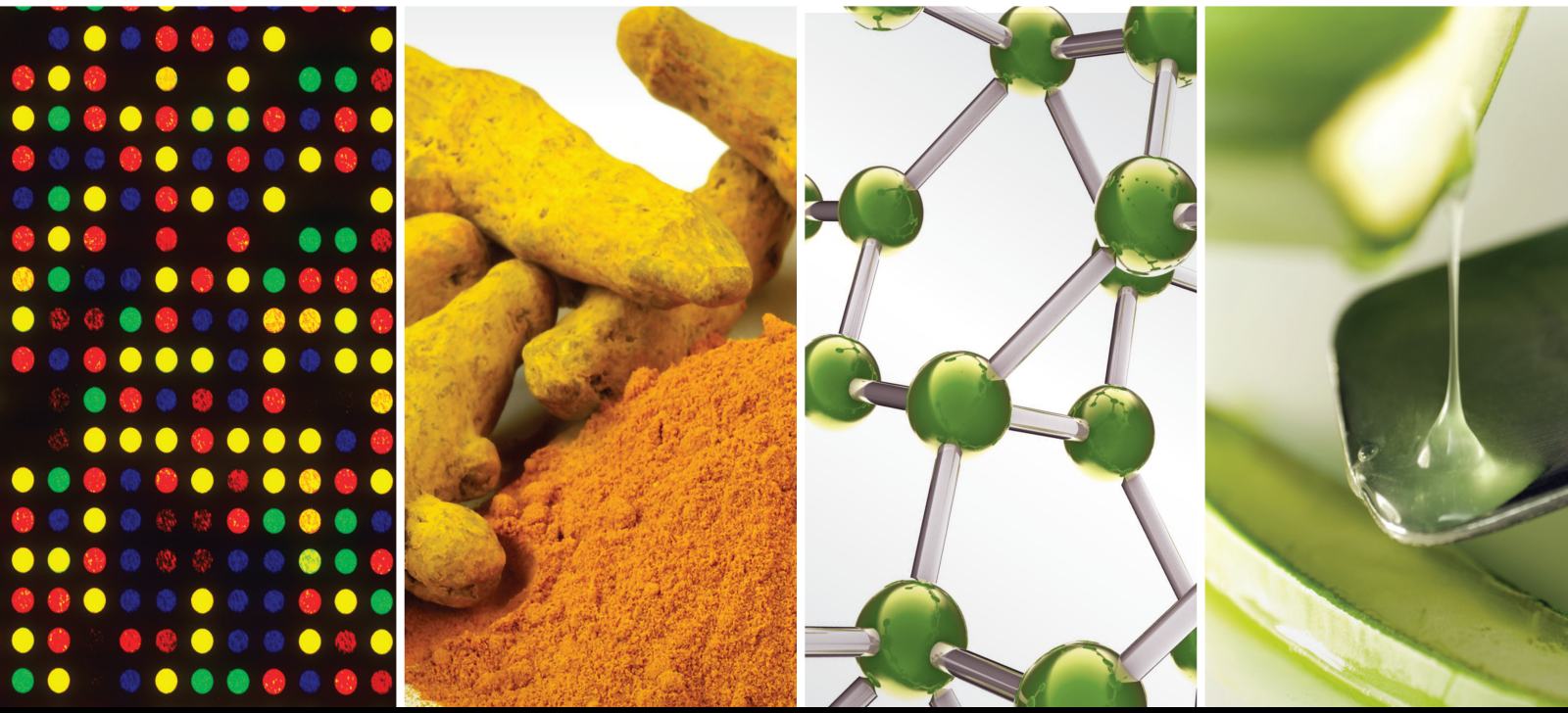

The Role and Mechanism of Electroacupuncture for Neurological Diseases 2021

Evidence-Based Complementary and Alternative Medicine

The Role and Mechanism of Electroacupuncture for Neurological Diseases 2021

Lead Guest Editor: Feng Zhang
Guest Editors: Yuchuan Ding, Chun-Lei Shan, and Wei-Lin Liu

Chief Editor

Associate Editors

Academic Editors

Contents

Contents

Hindawi
Evidence-Based Complementary and Alternative Medicine
Volume 2022, Article ID 3849441, 10 pages
https://doi.org/10.1155/2022/3849441

Research Article

Electroacupuncture Attenuates Learning and Memory Impairment via PI3K/Akt Pathway in an Amyloid $\beta_{25\text{-}35}$-Induced Alzheimer's Disease Mouse Model

Si-Mai Shao,[1] **Kyung Hye Park**,[2] **Ye Yuan**,[2] **Zijuan Zhang**,[1,2] **Yanwen You**,[1] **Zhenqiang Zhang**,[2] **and Li Hao**[1,2]

[1]*Medical College, Henan University of Chinese Medicine, Zhengzhou, China*
[2]*Academy of Chinese Medical Sciences, Henan University of Chinese Medicine, Zhengzhou, China*

Correspondence should be addressed to Zhenqiang Zhang; zhang_zhenqiang@126.com and Li Hao; haoli66@126.com

Received 22 August 2021; Revised 18 November 2021; Accepted 10 February 2022; Published 15 April 2022

Academic Editor: Feng Zhang

The main characteristic of Alzheimer's disease (AD) is the progressive decline of learning and memory ability. Electroacupuncture (EA) may improve AD-related learning and memory ability. However, the underlying molecular mechanism of action remains unclear. The objective of the present study was to assess the effects and the molecular mechanism of EA on learning and memory in an amyloid $\beta_{25\text{-}35}$ ($A\beta_{25\text{-}35}$) induced AD mouse model. The AD model was established by intracerebroventricular (ICV) administration of $A\beta_{25\text{-}35}$ oligomers. AD mice were electroacupunctured with wisdom three-needle combined with Baihui (GV20) five times per week for three consecutive weeks. The Morris water maze (MWM) and Y maze tests were applied to evaluate spatial learning and memory ability. A transmission electron microscope (TEM) was used to measure mitochondria and autophagy of hippocampal neurons, and western blot was applied to observe molecular changes in the mice hippocampus. The results suggested that EA treatment significantly alleviated learning and memory impairment related to AD, reduced mitochondria damage, improved autophagy, increased mitochondrial protein 2 (Mfn2), Beclin 1, and LC3B, and decreased the expressions of fission protein 1 (Fis1) level. Furthermore, EA further upregulated the protein expression of phosphatidylinositol 3-kinase (PI3K) and the ratio of p-Akt/Akt in the hippocampus of AD mice. This study demonstrates that EA treatment attenuates cognitive deficits, modulates mitochondrial fusion and fission, and enhances autophagy via the PI3K/Akt pathway in a mouse AD model.

1. Introduction

Alzheimer's disease (AD), the most common type of dementia, is one of the most prevalent neurodegenerative diseases affecting millions of older adults globally and is characterized by amyloid β ($A\beta$) deposition, phosphorylated tau accumulation, neuroinflammation, oxidative stress, and mitochondrial dysfunction [1–3]. Among them, $A\beta$ deposition and phosphorylated tau accumulation are widely studied and considered the main pathological features of AD. In recent years, mitochondrial dysfunction has gradually gained attention and is considered to be closely related to various injuries in AD [4].

Studies suggest that mitochondrial damage and dysfunction are early pathological changes in AD and may precede the development of $A\beta$ and tau pathology [5, 6]. Impaired mitochondrial function leads to inadequate bioenergy production, increased reactive oxygen species, and oxidative stress, which exacerbate $A\beta$ deposition and tau protein phosphorylation, subsequently causing abnormal synaptic function and cognitive impairment [3]. Mitochondrial dysfunction is caused by abnormal mitochondrial dynamics, energy metabolism, and transport. Mitochondrial dynamics means the equalization between the two opposite processes of fusion and fission, which regulates mitochondria's number, morphology, and function in the cytoplasm

[7]. Fusion helps to homogenize the composition of damaged mitochondria, thereby elongating the mitochondria. Fission leads to mitochondrial fragmentation [8]. Studies have confirmed that the accumulation of oligomeric Aβ in neurons of AD mice can cause increased mitochondrial fission, reduced fusion, mitochondrial and synaptic defects, and ultimately neurodegeneration [9, 10]. Impaired balance of mitochondrial dynamics in an AD mouse model has been associated with increased mitochondrial fragmentation [11]. Once the mitochondria are fragmented, the mitochondria's ability to produce ATP will be compromised and then it will be cleared.

Autophagy is an intracellular degradation process that degrades and recycles damaged organelles and proteins within the cell to maintain normal cellular homeostasis [12]. Therefore, autophagy is involved in clearing intracellular fragmented mitochondria, which is vital for regulating the mitochondrial number and maintaining physiological functions. Enhanced autophagy reduced AD-related tau hyperphosphorylation in neurons and reversed memory impairment in transgenic mice [13]. When autophagy is blocked, dysfunction of mitochondria transport and dynamics occurs in neurons, aggravating pathological changes in AD. Experiments have revealed that, in the early stages of AD, autophagy levels and the expression of Beclin 1 and LC3 are reduced and phosphatidylinositol 3-kinase (PI3K)/Akt pathway is also altered [14]. The PI3K/Akt pathway significantly mediates cellular autophagy and survival functions [15]. Increased autophagy and enhanced PI3K/Akt signaling in the brain can improve memory in AD mice [16]. It has been shown that induction of autophagy via the PI3K/Akt/mTOR pathway can reduce Aβ deposition in neurons [17]. Acupuncture improves autophagy in the brains of double transgenic AD mice, which may be associated with the PI3K/Akt pathway [18].

Acupuncture, an essential part of Chinese medicine, has progressed in clinical treatment and basic research on AD. Acupuncture can ameliorate cognitive deficits in patients with AD [19]. Previous studies have suggested that EA could upregulate enzymes involved in Aβ clearance, reduce the deposition of Aβ, protect hippocampal neurons, and improve AD-related learning and memory ability [20]. Wisdom three-needle is an acupuncture method that includes Shenting and Benshen and has been used clinically in China to treat neurodegenerative diseases such as dementia and stroke [21]. However, its molecular mechanism has not been clarified. Therefore, the aim of this study was to evaluate the molecular mechanism of wisdom three-needle combined with Baihui (GV20) electroacupuncture (EA) to improve the cognitive and mitochondrial dynamics in an amyloid $\beta_{25\text{-}35}$ ($A\beta_{25\text{-}35}$) induced AD mouse model.

2. Materials and Methods

2.1. Animals. Two-month-old male mice of C57Bl/6J (the classic standard laboratory mouse strain) were purchased from the Animal Experiment Center of Henan University of Chinese Medicine (Zhengzhou, China) (license number: SYXK (HA) 2020–0004). The mice were housed up to 3 per cage under laboratory animal ventilation system; the standard conditions are 12 h light/dark cycle, $22 \pm 2^{\circ}$C controlled ambient temperature, and 50%–60% relative humidity, with ad libitum free access to food and water. All procedures involving animals and collection of tissue used in this study were in accordance with the "National Institutes of Health (NIH) Guide for the Care and Use of Laboratory Animals" and were approved by the Animal Welfare Committee of the Henan University of Chinese Medicine (approval number: DWLL201907311).

Forty mice were randomly assigned to four separate groups ($n = 10$/each): (1) the mice in the control group received bilateral hippocampal stereotactic microinjection of saline; (2) the mice in the model group received bilateral hippocampal stereotactic microinjection of $A\beta_{25-35}$; (3) the mice in the EA group received wisdom three-needle combined with Baihui EA treatment after $A\beta_{25-35}$ injection; (4) the mice in the nonacup group received EA at nonacupoints (0.5 cm above the root of the tail and 0.3 cm beside the midline) after $A\beta_{25-35}$ injection.

2.2. Stereotactic Injection. $A\beta_{25\text{-}35}$ (118M4893V; Sigma-Aldrich, MO, USA) was dissolved in 0.9% saline to a concentration of 3 mg/mL and incubated at 37°C for 7 days to induce aggregation [22]. After isoflurane anesthesia, the mice were fixed on the brain stereotactic apparatus, and the bilateral lateral ventricle (0.6 mm behind the anterior fontanel, 1.5 mm beside the midline, and 1.7 mm depth) was chosen as the site of microinjection. $A\beta_{25\text{-}35}$ was injected into the lateral ventricles of mice in the model, EA, and sham-EA groups using a microsyringe at 3.5 μL per side, and the injection was fully completed within 15 min. Mice in the control group were injected with equal sterile saline in the lateral ventricles (Figure 1(a)). No animals died during experimental injection and behavioral testing.

2.3. Electroacupuncture Treatment. Acupuncture points used in this study were according to the World Health Organization Standard Acupuncture Nomenclature. Baihui (GV20) is located at the midpoint of the parietal bone. Shenting (GV24) is 0.5 cm in front of Baihui. Benshen (GB13) is 0.3 cm beside Shenting. EA treatment was administered at 9 : 00 each day for 15 min, five days each week for three consecutive weeks. The disposable sterile needles were connected to the EA device's output terminals (G6805; Suzhou Medical Instrument Factory, Suzhou, China) using a 1~20 Hz discrete wave and electric current of 1 mA. Mice in the EA group were treated with 0.30×13 mm needles (Suzhou Medical and Health Material Co., Ltd., Suzhou, China), with a 2-3 mm depth at the GV20, GV24, and GB13 points. Mice in the nonacup group were acupunctured at 0.5 cm above the root of the tail and 0.3 cm beside the midline (Figure 1(a)). They were also connected to an EA instrument but not energized.

2.4. Morris Water Maze (MWM) Test. To assess spatial cognitive performance in mice, the MWM (RWD Life Science Co., Ltd., Shenzhen, China) test was conducted from day 1 to day 6 after $A\beta_{25\text{-}35}$ and EA administration. The

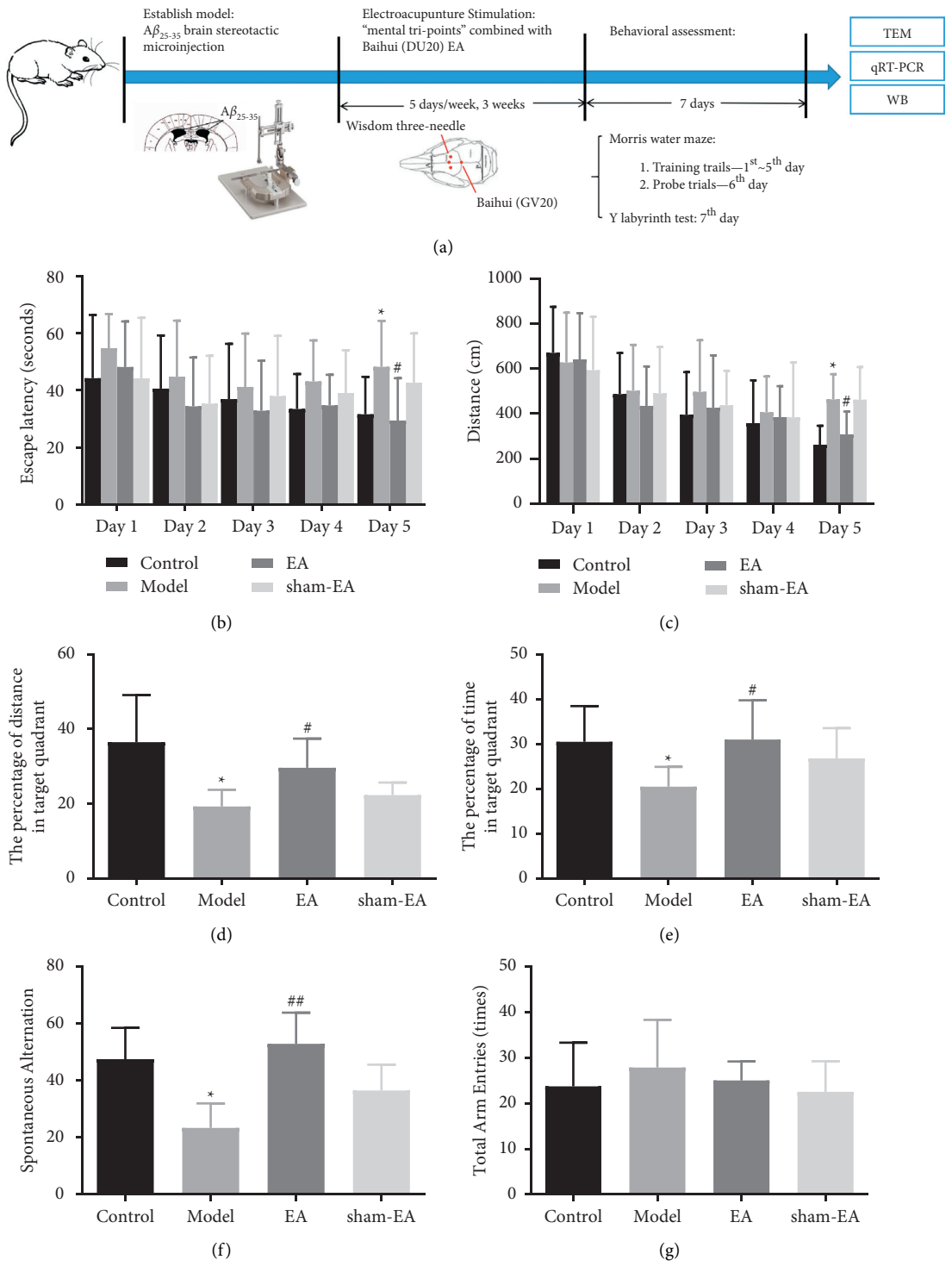

FIGURE 1: Behavioral test analysis of MWM test and Y-maze test has demonstrated that EA treatment could ameliorate learning and memory deficits in the AD mouse model. (a) The schematic diagram of the experimental design for this study. Mice were administered wisdom three-needle combined with Baihui EA therapy after bilateral hippocampal A$\beta_{25\text{-}35}$ injections. Hippocampal tissue was collected after the last EA treatment. (b, c) The escape latency and total distance to reach the hidden platform were used to assess acquisition of the training trials in the MWM test. EA therapy shortened escape latency and total swimming distance in AD model mice on day 5. (d, e) The percentage of distance and time spent in target quadrant is shown which was calculated for probe trials in the MWM task. EA administration decreased the percentage of swimming distance and the percentage of time in the target quadrant in AD model mice on day 6. (f, g) The percentage of alternative behavior and the number of times of total arm entries as a measure of Y-maze test. EA significantly enhanced spontaneous alternation in AD mice. Data are represented as mean ± SD. $^{*}P < 0.05$ vs. the control group; $^{\#}P < 0.05$ and $^{\#\#}P < 0.01$ vs. the model group.

experimental apparatus consisted of a circular tank with a diameter of 130 cm, a height of 50 cm, and an escape platform with a diameter of 10 cm. The tank was conceptually divided into four quadrants and filled with water ($22 \pm 2^{\circ}$C) made opaque by the milk powder. The platform was circular and hidden 1.5 cm below the surface. MWM was equipped with an infrared tracking camera computer and SMART 3.0 software (Panlab SL, Barcelona, Spain). The MWM test included training trial and probe trial.

Training trial: each mouse was tested four times per day for five consecutive days. The platform was hidden in the same quadrant. During training, the mice were randomly placed in the water facing the wall of the tank and permitted to search the hidden platform for 60 seconds. If the mice failed to find the platform within 60 seconds, they were directed to the platform and maintained for 15 seconds. Escape latency (the time for mice to find the hidden platform) and total distance were recorded and analyzed.

Probe trial: the probe trial was conducted on day 6. At the end of the training test, the platform was removed. The percentage of distance and time in the target quadrant (where the platform was located during the training trial) was recorded and analyzed. Ten mice per group participated in the MWM test.

2.5. Y-Maze Test. The Y-maze (RWD Life Technology Co., Ltd., Shenzhen, China) test was performed on the 7th day after $A\beta_{25\text{-}35}$ and EA administration in this study (Figure 1(a)). The Y-maze consisted of three arms of equal length, and the angle between adjacent arms was 120. Mice were positioned in the middle of the Y-maze with the head facing the same arm and allowed to explore for 5 minutes. The SMART 3.0 software was employed to record the total times of arms entered. The number of alternations of the three arms accessed in the sequence divided by the alternation (total number of arms accessed minus 2) multiplied by 100 was the spontaneous alternation. Ten mice per group participated in this test.

2.6. Sample Preparation. Mice were executed after behavioral testing. The whole brains were removed after anesthesia with 20% (w/v) urethane, and the bilateral hippocampi were dissected on ice immediately and stored at −80°C for subsequent mRNA and protein assays, respectively. In addition, the hearts were perfused with precooled 4% paraformaldehyde (Damao Chemical Factory, Tianjin, China) and glutaraldehyde (Aladdin Industrial Co., Ltd., Shanghai, China). The CA1 region of the hippocampus was removed and quickly cut into small 1 mm^3 tissue slices and placed in 4% glutaraldehyde fixative for transmission electron microscopy (TEM) analysis.

2.7. Transmission Electron Microscope. TEM was applied to investigate the mitochondrial ultrastructure and autophagy of hippocampal neurons. After sample preparation, the tissues were cut into 1 mm^3 tissue blocks, postfixed in 2.5% paraformaldehyde solution for more than 2 h at room temperature, then rinsed with 0.1 M phosphoric acid (PBS) (P1010; Solarbio Life Sciences, Beijing, China) for 45 min, and then fixed in 1% osmic acid for 2 h at room temperature. After that, graded dehydration takes place for 20 min for each step in ethanol from water through 30%-50%-70%-85%–95% ethanol and twice for 30 min in 100% ethanol, followed by twice for 20 min in 50% ethanol/50% acetone (1 : 1) and twice for 20 min in 100% pure acetone. For embedding, tissues were incubated in pure acetone and embedding solution (2 : 1) at room temperature for 3 h, in pure acetone and embedding solution (1 : 2) at room temperature overnight, and in pure embedding solution at 37°C for 3 h. Tissues were dried at 37°C overnight, 45°C for 12 h, and 60°C for 24 h. Ultrathin 70 nm sections were obtained using an ultrathin sectioning machine and collected on 100-mesh copper grids. After staining with uranyl acetate and lead citrate (Head Bio Co., Ltd., Beijing, China), mitochondrial substructures and neuronal autophagy were observed on the sections by TEM (JEM-1400; Japan Electronics Co., Ltd, Japan). TEM analysis was performed by the Electron Microscopy Center of the Academy of Chinese Medicine, Henan University of Chinese Medicine. Three mice per group participated in this assay.

2.8. Quantitative Real-Time Polymerase Chain Reaction (qRT-PCR). The mRNA levels of Mfn2, Fis1, Beclin 1, and LC3B were measured by qRT-PCR. Total RNA was extracted from the hippocampus with TRIzol reagent (15596026; Invitrogen, Thermo Fisher Scientific, MA, USA). The concentration of total RNA was measured with an ultraviolet spectrophotometer (ES-A01-NanoDrop 2000/2000c; Thermo Fisher Scientific, MA, USA). cDNA was synthesized using the PrimeScript™ RT reagent kit (RR037; Takara Biotechnology, Dalian, China). The ABI7500 system (Applied Biosystems, Foster City, CA, USA) was used to quantify the mRNA levels of Mfn2, Fis1, Beclin 1, and LC3B using the TB Green Premix Ex Taq kit (RR420; Takara Biotechnology, Dalian, China). The values were standardized to GAPDH. Data were analyzed with the $2^{-\Delta\Delta Ct}$ (cycle threshold, Ct) approach. The PCR primers (Sangon Biotech, Shanghai, China) were as follows Table 1. Five mice from each group attended the measurement.

2.9. Western Blot. Western blot was executed as indicated previously [23]. After sample preparation, frozen hippocampi were homogenized with tissue lysis buffer (R0010; Solarbio Life Science, Beijing, China) until lysis was complete. The supernatant was extracted following centrifugation. Moreover, the protein was quantified by using the BCA assay kit (Cat # PC0020; Solarbio Life Science, Beijing, China). The equal volume SDS-PAGE sample buffer (P1040; Solarbio Life Science, Beijing, China) was mixed into the protein supernatant and boiled at 100°C for 5 min until denaturation. Proteins were separated by polyacrylamide gel electrophoresis and transferred to a nitrocellulose membrane (IPVH00010, size 0.45 μm; Merck Millipore Ltd., MA,

Table 1: The primer sequences used in qRT-PCR.

Genes	Primer
Mfn2	Forward: 5′-TGCACCGCCATATAGAGGAAG-3′
	Reverse: 5′-TCTGCAGTGAACTGGCAATG-3′
Fis1	Forward: 5′-CAAAGAGGAACAGCGGGACT-3′
	Reverse: 5′-ACAGCCCTCGCACATACTTT-3′
Beclin 1	Forward: 5′-ATGGAGGGGTCTAAGGCGTC-3′
	Reverse: 5′-TGGGCTGTGGTAAGTAATGGA-3′
LC3B	Forward: 5′-GATAATCAGACGGCGCTT-3′
	Reverse: 5′-ACTTCGGAGATGGGAGTG-3′
GAPDH	Forward: 5′-TTCCCGTTCAGCTCTGGG-3′
	Reverse: 5′-CCCTGCATCCACTGGTGC-3′

USA). The membranes were blocked with 5% nonfat milk and then incubated with primary antibodies Fis1 (1 : 1000, ab96764; Abcam, Cambridge, UK), Mfn2 (1 : 1000, ab124773; Abcam, Cambridge, UK), LC3B (1 : 1000, ab48394; Abcam, Cambridge, UK), Beclin 1 (1 : 2000, ab207612; Abcam, Cambridge, UK), PI3K (1 : 1000, ab139307; Abcam, Cambridge, UK), Akt (1 : 1000, ab179463; Abcam, Cambridge, UK), p-Akt [S473P] (1 : 1000, ab81283; Abcam, Cambridge, UK), and β-actin (1 : 2000, ab8226; Abcam, Cambridge, UK) at 4°C overnight. Afterward, the membrane was incubated with horseradish peroxidase (HRP) conjugated goat anti-rabbit IgG and goat anti-rabbit IgG (1 : 5000, Boster, Wuhan, China) for 1 h. The proteins were measured by ECL chemiluminescence (VJ312149; Thermo Fisher Scientific, Massachusetts, USA). Quantification of all bands was performed using Image J v1.51 (National Institutes of Health, Bethesda, Maryland). Three mice per group participated in this assay.

2.10. Statistical Analysis. The results obtained from the experiments were expressed as mean ± standard deviation (SD). Statistical significance differences were assessed with one-way analysis of variance (ANOVA) followed by a Bonferroni's post hoc test. Behavioral tests from day 1 to day 5 of the MWM were analyzed by two-way ANOVA. Statistical analyses and figures were based on GraphPad Prism 8.0 software (GraphPad Software, CA, USA). P values less than 0.05 were considered statistically significant.

3. Results

3.1. EA Ameliorated Learning and Memory Deficits in an AD Mouse Model. The MWM test was used to detect the effect of wisdom three-needle combined with Baihui (GV20) EA on AD mice's cognitive abilities. In the training trials, there was no significant difference in escape latency and total swimming distance among four groups from day 1 to day 4. However, the escape latency and total swimming distance of the model group were significantly longer than those of the control group on day 5 ($P < 0.05$), and the escape latency and total swimming distance of the EA group were significantly shorter than those of the model group ($P < 0.05$). In addition, there was no significant difference between AD model group and sham-EA group (Figures 1(b) and 1(c)). In the probe trials, the percentage of swimming distance and the percentage of time in the target quadrant of the model group were less than those of the control group ($P < 0.05$). Moreover, the percentage of swimming distance and the percentage of time in the target quadrant of the EA group were more than those of the model group ($P < 0.05$). Furthermore, there was still no statistical difference between the model and the sham-EA groups (Figures 1(d) and 1(e)).

The Y-maze test was carried out to test mice's spatial working and reference memory. Spontaneous alternation was assessed by exploring the three arms of the maze in mice. The spontaneous alternation of the model group was less than that of the control group ($P < 0.05$), and the spontaneous alternation of the EA group was more than that of the model group ($P < 0.01$) (Figure 1(f)). However, there were no differences in total entrances among the four groups (Figure 1(g)).

In general, behavioral data showed that wisdom three-needle combined with Baihui (GV20) EA could improve AD-related learning and memory deficits.

3.2. EA Regulated Mitochondrial Fusion/Fission Dynamics in an AD Mouse Model. Studies have confirmed that cognitive deficits in AD were accompanied by changes in the mitochondrial dynamics of hippocampal neurons [24]. Therefore, we hypothesized that EA treatment reduced cognitive deficits by regulating mitochondrial dynamics. To test this hypothesis, we evaluated the mitochondrial morphology of hippocampal neurons of the mice in all groups by TEM. The results indicated that $A\beta_{25\text{-}35}$ caused the morphological changes of mitochondria in hippocampal neurons of AD mice. It can be demonstrated by the decrease in the number of mitochondria, swelling and breakage of the cristae, and the rupture of the membrane. EA treatment improved mitochondrial morphology in the hippocampus of AD mice. There was no difference between the model group and the sham-EA group (Figure 2(a)).

To study the potential mechanism of EA treatment on improving mitochondrial morphology, we further measured some genes and proteins related to mitochondrial dynamics. It has been shown that Fis1 promotes mitochondrial fission [25] and the mRNA and protein expression of Fis1 was significantly increased in the hippocampus of AD mice compared to that of the control group ($P < 0.05$). EA treatment decreased the mRNA and protein levels of Fis1 in AD mice. Mfn2 contributes to mitochondrial fusion, and the mRNA and protein levels of Mfn2 in the hippocampus of AD mice decreased compared with those of the control group ($P < 0.05$), whereas EA treatment significantly increased its mRNA and protein levels (Figures 2(b)–2(d)). There was no difference in Fis1 and Mfn2 between the control group and the sham-EA group. These results suggested that EA treatment reduced mitochondrial fission and promoted mitochondrial fusion, which in turn regulates mitochondrial dynamics.

3.3. EA Improved Autophagy in an AD Mouse Model. In the pathogenesis of AD, abnormal autophagy can cause mitochondrial dysfunction, reduced ATP synthesis, and energy metabolism inhibition, leading to neuronal cell loss [26]. To

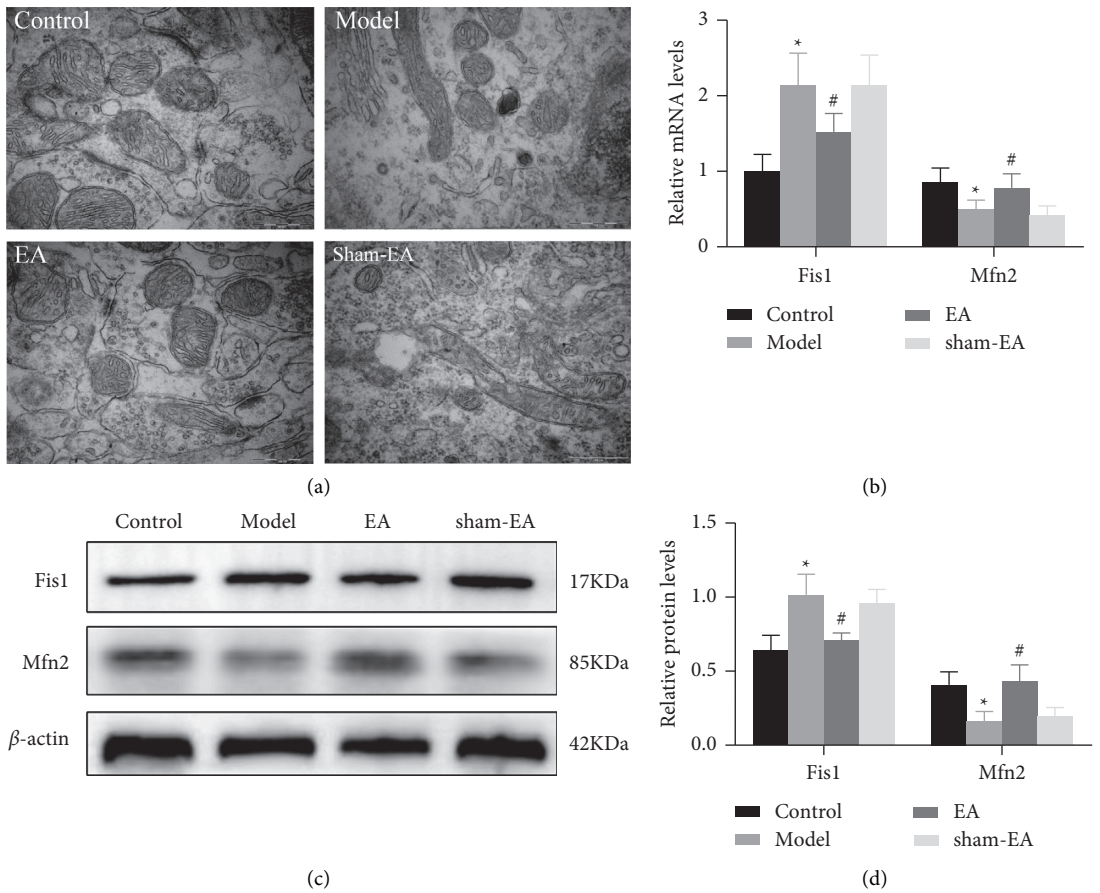

Figure 2: Transmission electron microscope and western bolt results showed that EA treatment modulated mitochondrial fusion/fission dynamics in AD mouse models. (a) TEM detected the mitochondrial structure of hippocampal neurons in each group in the CA1 regions of mice brain. Scale bar in (a) = 500 nm (magnification = 50000x). EA therapy improved mitochondrial morphology of neurons in the hippocampus of AD mice. (b) Mitochondrial dynamics correlation genes Fis1 and Mfn2 in the hippocampus of the mouse were detected by qRT-PCR. EA downregulated Fis1 and upregulated Mfn2 mRNA levels, respectively. (c, d) Protein levels of Fis1 and Mfn2 in the mouse hippocampus were measured by quantitative immunoblot analysis. β-actin was used as a loading control. EA administration decreased Fis1 and increased Mfn2 protein expression, respectively. The data ($n = 3$) are represented as mean ± SD. $^{*}P < 0.05$ vs. the control group; $^{\#}P < 0.05$ vs. the model group.

investigate the reason of mitochondrial dynamics dysfunction, autophagy was examined by transmission electron microscopy. Autophagosome is the primary basis to evaluate the appearance of autophagy, which is characterized by double or multilayer vacuole structure. The TEM results showed decreased intracellular autophagosomes in hippocampal neurons in the AD model group compared with the control group and increased intracellular autophagosomes in hippocampal neurons in the EA group compared with the model group. Nevertheless, there was no difference between the model group and the sham-EA group (Figure 3(a)). Beclin 1 is a critical protein in the formation of autophagosomes. During autophagy, LC3B-I is modified and processed by the ubiquitin system, producing small molecules of LC3B-II that are localized into autophagosomes. Thus, both the presence of LC3B and high levels of LC3B-II are considered molecular markers of autophagy in cells undergoing ferroptosis [27]. We found that AD model mice had a significantly decreased mRNA expression of Beclin 1 and LC3B and protein levels of Beclin 1 and LC3B-II compared with that of control mice ($P < 0.05$) (Figures 3(b)–3(d)). Wisdom three-needle combined with Baihui (GV20) EA treatment significantly increased the mRNA expression of Beclin 1 and LC3B and the protein levels of Beclin 1 and LC3B-II ($P < 0.05$). These results indicated that EA treatment enhanced neuronal autophagy, contributing to the improved learning and memory impairment in AD mice.

3.4. EA Ameliorated Autophagy through PI3K/Akt Pathway. The PI3K/Akt pathway was found to play an essential role in regulating neuronal autophagy [28]. To further elucidate the underlying molecular mechanisms of EA improving autophagy, we detected the expression level of PI3K, Akt, and its activated form p-Akt (Ser473) in the hippocampus of AD model mice. The expression levels of PI3K and p-Akt/Akt were significantly lower in AD mice, and these changes were restored partly by wisdom three-needle combined with Baihui (GV20) EA treatment. However, no changes were observed in the sham-EA group (Figures 4(a)–4(c)). These

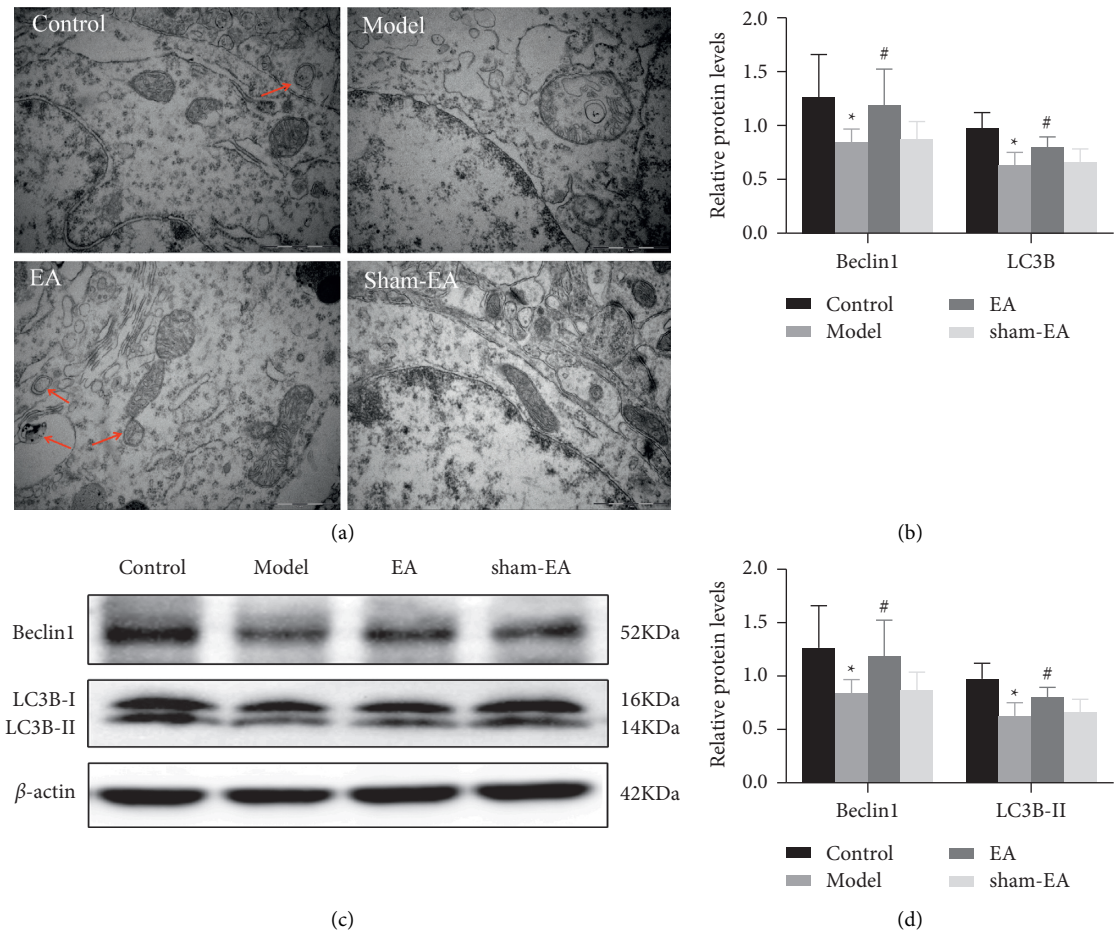

FIGURE 3: Transmission electron microscope and western bolt results showed that EA treatment improved autophagy in AD mouse models. (a) TEM observation of autophagosome in the CA1 regions of mice brains in each group. EA therapy resulted in an increase in the number of autophagosomes in hippocampal neurons of AD mice. Scale bar in (a) = 1 μm (magnification = 20000x). (b) Autophagy-related genes Beclin 1 and LC3B in the hippocampus of the mouse were measured by qRT-PCR. EA treatment enhanced the mRNA levels of Beclin 1 and LC3B. (c, d) Beclin 1 and LC3B-II in hippocampus of the mouse were detected by immunoblotting quantitative analysis. β-actin was used as a loading control. EA administration elevated the protein expression of Beclin 1 and LC3B-II. The data ($n = 3$) are represented as mean ± SD.$^{*}P < 0.05$ vs. the control group; $^{\#}P < 0.05$ vs. the model group.

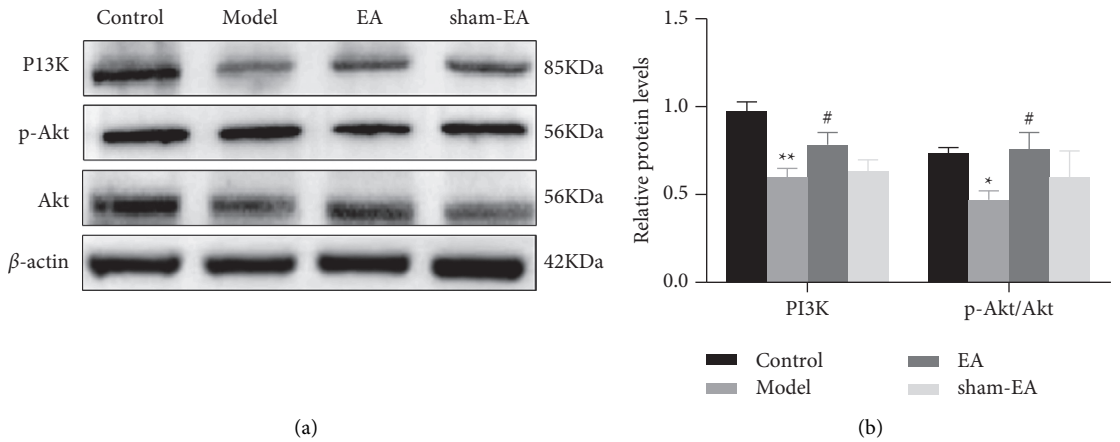

FIGURE 4: Western bolt results showed that EA treatment regulated the PI3K/Akt pathway. (a, b) The protein levels of PI3K, Akt, and p-Akt in the hippocampus of the mouse measured by western blot analysis. β-actin was used as a loading control. The data ($n = 3$) are represented as mean ± SD.$^{*}P < 0.05$ and $^{**}P < 0.01$ vs. the control group; $^{\#}P < 0.05$ vs. the model group.

results suggested that EA treatment has a specific ameliorative effect on autophagy, which may be related to the downregulation of PI3K and p-Akt/Akt.

4. Discussion

In the present study, we identified the neuroprotective role of wisdom three-needle combined with Baihui (GV20) EA treatment, which attenuated mitochondrial damage and enhanced neuronal autophagy in AD model mice and its mechanism of this protection. In addition, we observed a neuroprotective role of the PI3k/Akt pathway in EA treatment of A$\beta_{25\text{-}35}$-induced cognitive impairment.

MWM and Y-maze play an essential role in validating animal models of cognitive impairment such as AD and aging [29]. In this investigation, wisdom three-needle combined with Baihui (GV20) EA treatment reduced the escape latency and upregulated the percentage of swimming distance and residence time in the target quadrant compared with AD mice. Simultaneously, we found that EA could improve spontaneous alternation behavior in AD mice. Therefore, the behavior test results suggested that wisdom three-needle combined with Baihui (GV20) EA treatment enhanced the learning and memory abilities in AD mice.

Consistent with the behavioral test results, we revealed that wisdom three-needle combined with Baihui (GV20) EA treatment attenuated mitochondrial damage. In the hippocampus neurons of A$\beta_{25\text{-}35}$-induced mice, damaged mitochondria with an indistinct morphology were observed. Notably, this type of damaged mitochondria was not observed in mice treated with EA. Mitochondrial dysfunction and accumulated damaged mitochondria are prevalent in AD patients and transgenic AD model animals. It has been demonstrated that Aβ aggregation caused an imbalance of mitochondrial fission and fusion, mitochondrial fragmentation, and morphological and functional changes, leading to mitochondrial damage [30]. Fis1 and Mfn2 are closely associated with mitochondrial fission and fusion, respectively. The mRNA and protein levels of Fis1 and Mfn2 decreased and increased with EA treatment, suggesting that EA can modulate mitochondrial dynamics.

The primary way to eliminate damaged mitochondria and mitochondrial fragmentation is autophagy in AD [31]. Autophagy, the selective removal of damaged mitochondria by autophagosomes followed by catabolism by lysosomes, is essential for maintaining mitochondrial homeostasis, ATP production, and neuronal survival [32]. LC3B-II is considered as a marker molecule in autophagosomes [33]. It was found that the expression of LC3B-II and Beclin 1 in the AD brain was low, which resulted in decreased autophagy and Aβ accumulation in the brain of the transgenic mouse model [34]. In this study, EA administration also increased the mRNA expression of Beclin 1 and LC3B and the protein levels of Beclin 1 and LC3B-II in AD model mice, indicating that EA can enhance neuronal autophagy.

The PI3K/Akt signaling pathway has been found to regulate neuronal autophagy, and its deregulation results in decreased autophagy. Activation of PI3K/Akt prevents neuronal cell death in AD; moreover, activation of PI3K/Akt in neurons has been reported as neuroprotective in AD rats [35]. Given that the PI3K/Akt pathway is involved in neuronal autophagy, survival, and synaptic plasticity, it has attracted much attention as a therapeutic target [36]. Therefore, we speculated that EA treatment improved abnormal mitochondrial dynamics and enhanced autophagy by activating the PI3K/Akt pathway in hippocampal neurons. This speculation underlines the potential beneficial effects of EA, as EA might activate the PI3K/Akt pathway when triggers such as mitochondrial damage and reduced levels of autophagy are encountered. As a critical molecule in the PI3K/Akt pathway, Akt governs the survival and loss of neurons [37]. Enhanced Akt activation facilitates increased autophagy and neuroprotective effects in the AD brain. Akt has two major phosphorylation sites, thr308 and Ser473, and the activation of Akt mainly requires phosphorylation of Ser473 [38]. In the current experiments, p-Akt (Ser473) expression was significantly reduced in the hippocampus of AD mice and EA reversed this reduction; however, Akt expression was not substantially altered, indicating that Akt exerts its function through phosphorylation rather than regulation.

In conclusion, our study sheds light on the potential of EA to attenuate cognitive deficits, modulate mitochondrial dynamics, and enhance autophagy in AD mice via the PI3K/Akt pathway. This result lays the experimental foundation for the application of wisdom three-needle combined with Baihui (GV20) to treat neurodegenerative diseases.

Data Availability

The experimental data supporting this study's findings are available from the corresponding authors upon reasonable request.

Ethical Approval

The study was approved by the Experimental Animal Ethics Committee of Henan University of Traditional Chinese Medicine (ethical approval number: DWLL201907311).

Conflicts of Interest

The authors declare that they have no conflicts of interest.

Acknowledgments

This project was funded by a grant to CH from Zhongyuan Science and Technology Innovation Leading Talent (no. 204200510022), Scientific and Technological Project of Henan Province (nos. 202102310078, 212102310828, and 172102310286), and Key Scientific Research Project of Universities in Henan Province (no. 19A310012).

References

[1] C. A. Lane, J. Hardy, and J. M. Schott, "Alzheimer's disease," *European Journal of Neurology*, vol. 25, no. 1, pp. 59–70, 2017.

[2] M. K. Bai, R. Ammu, and N. S. Ping, "Current concepts of neurodegenerative mechanisms in Alzheimer's disease," *BioMed Research International*, vol. 3, no. 8, pp. 1–12, 2018.

[3] A. Chakravorty, C. T. Jetto, and R. Manjithaya, "Dysfunctional mitochondria and mitophagy as drivers of Alzheimer's disease pathogenesis," *Frontiers in Aging Neuroscience*, vol. 11, p. 311, 2019.

[4] J. Tang, A. Oliveros, and M. H. Jang, "Dysfunctional mitochondrial bioenergetics and synaptic degeneration in alzheimer disease," *International Neurourology Journal*, vol. 2, no. 23, pp. S5–S10, 2019.

[5] C.-X. Gong, I. Grundke-Iqbal, and K. Iqbal, "Targeting tau protein in Alzheimer's disease," *Drugs & Aging*, vol. 27, no. 5, pp. 351–365, 2010.

[6] B. Thomas and A. R. Hicks, "Mitochondrial dysfunction and neurodegenerative proteinopathies: mechanisms and prospects for therapeutic intervention," *Biochemical Society Transactions*, vol. 46, no. 4, pp. 829–842, 2018.

[7] M. Liesa, M. Palacín, and A. Zorzano, "Mitochondrial dynamics in mammalian Health and disease," *Physiological Reviews*, vol. 89, no. 3, pp. 799–845, 2009.

[8] N. N. Wu, Y. Zhang, and J. Ren, "Mitophagy, mitochondrial dynamics, and homeostasis in cardiovascular aging," *Oxidative Medicine And Cellular Longevity*, vol. 2019, Article ID 9825061, 15 pages, 2019.

[9] M. J. Calkins, M. Manczak, P. Mao, U. Shirendeb, and P. H. Reddy, "Impaired mitochondrial biogenesis, defective axonal transport of mitochondria, abnormal mitochondrial dynamics and synaptic degeneration in a mouse model of Alzheimer's disease," *Human Molecular Genetics*, vol. 20, no. 23, pp. 4515–4529, 2011.

[10] M. Maria, M. J. Calkins, and R. P. Hemachandra, "Impaired mitochondrial dynamics and abnormal interaction of amyloid beta with mitochondrial protein Drp1 in neurons from patients with Alzheimer's disease: implications for neuronal damage," *Human Molecular Genetics*, vol. 20, no. 13, pp. 2495–2509, 2011.

[11] P. J. Flannery and E. Trushina, "Mitochondrial dynamics and transport in Alzheimer's disease," *Molecular and Cellular Neuroscience*, vol. 98, pp. 109–120, 2019.

[12] M. Komatsu, S. Waguri, T. Chiba et al., "Loss of autophagy in the central nervous system causes neurodegeneration in mice," *Nature*, vol. 441, no. 7095, pp. 880–884, 2006.

[13] E. F. Fang, Y. Hou, K. Palikaras et al., "Mitophagy inhibits amyloid-β and tau pathology and reverses cognitive deficits in models of Alzheimer's disease," *Nature Neuroscience*, vol. 22, no. 3, pp. 401–412, 2019.

[14] A. Tramutola, J. C. Triplett, D. M. Niedowicz et al., "Alteration of mTOR signaling occurs early in the progression of Alzheimer disease (AD): analysis of brain from subjects with preclinical AD, amnestic mild cognitive impairment and late-stage AD," *Journal of Neurochemistry*, vol. 133, no. 5, pp. 739–749, 2015.

[15] F. Xu, L. Na, Y. Li, and L Chen, "Roles of the PI3K/AKT/mTOR signalling pathways in neurodegenerative diseases and tumours," *Cell & Bioscience*, vol. 10, no. 1, pp. 54–12, 2020.

[16] S. Gabbouj, S. Ryhänen, M. Marttinen et al., "Altered insulin signaling in Alzheimer's disease brain-special emphasis on PI3K-Akt pathway," *Frontiers in Neuroscience*, vol. 13, p. 629, 2019.

[17] A. Wani, M. Gupta, M. Ahmad et al., "Alborixin clears amyloid-β by inducing autophagy through PTEN-mediated inhibition of the AKT pathway," *Autophagy*, vol. 15, no. 10, pp. 1810–1828, 2019.

[18] C. C. Yu, Y. J. Du, and S. Q. Wang, "Experimental evidence of the benefits of acupuncture for Alzheimer's disease: an updated review," *Frontiers in Neuroscience*, vol. 14, p. 1307, 2020.

[19] R. Zhong and L. Xiao, "Progress of researches on mechanisms of acupuncture therapy in regulating brain plasticity," *Zhen Ci Yan Jiu*, vol. 43, no. 10, pp. 674–677, 2018.

[20] Y. N. Wu, J. X. Chen, and J. Tao, "Effects of electroacupuncture at Baihui on learning and memory ability and Tau phosphorylation in APP/PS1 transgenic mice," *Chinese Journal of Rehabilitation Medicine*, vol. 30, no. 5, pp. 432–436, 2015.

[21] J. T. Huang, S. Y. Cui, and C. Z. Tang, "Effect of zhisan needle on the expression of chat and Glut3 in the brain of ad model rats," *Chinese Journal of Basic Medicine in Traditional Chinese Medicine*, vol. 22, no. 07, pp. 915–917+1003, 2016.

[22] H. K. Ji, Q. Wang, and M. C. Ji, "Protective role of caffeic acid in an Aβ25-35-induced Alzheimer's disease model," *Nutrition Research & Practice*, vol. 9, no. 5, p. 480, 2015.

[23] Z. Zhang, L. Hao, M. Shi et al., "Neuroprotective effects of a GLP-2 analogue in the MPTP Parkinson's disease mouse model," *Journal of Parkinson's Disease*, vol. 11, no. 2, pp. 529–543, 2021.

[24] P. Pantiya, C. Thonusin, N. Chattipakorn, and S. C. Chattipakorn, "Mitochondrial abnormalities in neurodegenerative models and possible interventions: focus on Alzheimer's disease, Parkinson's disease, Huntington's disease," *Mitochondrion*, vol. 55, pp. 14–47, 2020.

[25] L. C. Gomes and L. Scorrano, "High levels of Fis1, a pro-fission mitochondrial protein, trigger autophagy," *Biochimica et Biophysica Acta*, vol. 1777, no. 7-8, pp. 860–866, 2008.

[26] C. Martínez-Cué and N. Rueda, "Cellular senescence in neurodegenerative diseases," *Frontiers in Cellular Neuroscience*, vol. 14, no. 16, 2020.

[27] Y. Kabeya, N. Mizushima, and T. Ueno, "LC3, a mammalian homologue of yeast Apg8p, is localized in autophagosome membranes after processing," *The EMBO Journal*, vol. 19, no. 21, pp. 5720–5728, 2000.

[28] A. Nakagawa, K. D. Sullivan, and D. Xue, "Caspase-activated phosphoinositide binding by CNT-1 promotes apoptosis by inhibiting the AKT pathway," *Nature Structural & Molecular Biology*, vol. 21, no. 12, pp. 1082–1090, 2014.

[29] K. S. Min, G. K. Hong, and K. L. Kim, "A novel trimeric peptide, Neuropep-1-stimulating brain-derived neurotrophic factor expression in rat brain improves spatial learning and memory as measured by the Y-maze and Morris water maze," *Journal of Neurochemistry*, vol. 116, no. 2, pp. 205–216, 2011.

[30] X. Wang, B. Su, S. L. Siedlak et al., "Amyloid- overproduction causes abnormal mitochondrial dynamics via differential modulation of mitochondrial fission/fusion proteins," *Proceedings of the National Academy of Sciences*, vol. 105, no. 49, pp. 19318–19323, 2008.

[31] V. K. Medala, B. Gollapelli, S. Dewanjee, G. Ogunmokun, R. Kandimalla, and J. Vallamkondu, "Mitochondrial dysfunction, mitophagy, and role of dynamin-related protein 1 in Alzheimer's disease," *Journal of Neuroscience Research*, vol. 99, no. 4, pp. 1120–1135, 2021.

[32] E. F. Fang, "Mitophagy and NAD+ inhibit Alzheimer disease," *Autophagy*, vol. 15, no. 6, pp. 1112–1114, 2019.

[33] J. Dancourt and T. J. Melia, "Lipidation of the autophagy proteins LC3 and GABARAP is a membrane-curvature dependent process," *Autophagy*, vol. 10, no. 8, pp. 1470-1471, 2014.

[34] F. Pickford, E. Masliah, M. Britschgi et al., "The autophagy-related protein beclin 1 shows reduced expression in early Alzheimer disease and regulates amyloid beta accumulation in mice," *Journal of Clinical Investigation*, vol. 118, no. 6, pp. 2190–2199, 2008.

[35] R. J. Griffin, A. Moloney, M. Kelliher et al., "Activation of Akt/PKB, increased phosphorylation of Akt substrates and loss and altered distribution of Akt and PTEN are features of Alzheimer's disease pathology," *Journal of Neurochemistry*, vol. 93, no. 1, pp. 105–117, 2005.

[36] Y. Wang, A. Zheng, H. Yang et al., ""Olfactory three-needle" acupuncture enhances synaptic function in Aβ1-42-induced Alzheimer's disease via activating PI3K/AKT/GSK-3β signaling pathway," *Journal of Integrative Neuroscience*, vol. 20, no. 1, pp. 55–65, 2021.

[37] C. Kim and S. Park, "IGF-1 protects SH-SY5Y cells against MPP+-induced apoptosis via PI3K/PDK-1/Akt pathway," *Endocrine connections*, vol. 7, no. 3, pp. 443–455, 2018.

[38] Y. Wei, J. Zhou, H. Yu, and X. Jin, "AKT phosphorylation sites of Ser473 and Thr308 regulate AKT degradation," *Bioscience Biotechnology and Biochemistry*, vol. 83, no. 3, pp. 429–435, 2019.

Hindawi
Evidence-Based Complementary and Alternative Medicine
Volume 2022, Article ID 3311250, 10 pages
https://doi.org/10.1155/2022/3311250

Research Article

Inhibition of PDE10A-Rescued TBI-Induced Neuroinflammation and Apoptosis through the cAMP/PKA/NLRP3 Pathway

Jin Huang,[1] Dang Tang,[1] Yiqiang Cao,[1] Yonggang Wang,[1] Jiang Long,[1] Lin Wei,[2] and Hai Song[1]

[1]*Department of Neurosurgery, First Affiliated Hospital of Kunming Medical University, Kunming 650032, China*
[2]*Department of Ultrasound, First Affiliated Hospital of Kunming Medical University, Kunming 650032, China*

Correspondence should be addressed to Hai Song; ydyysonghai@163.com

Received 30 August 2021; Revised 22 January 2022; Accepted 22 March 2022; Published 12 April 2022

Academic Editor: Feng Zhang

Phosphodiesterase 10A (PDE10A) is a dual-substrate phosphodiesterase that is highly expressed in the striatal complex. PDE10A is an important target for the treatment of ganglion dysfunction and neuroinflammation-related diseases, but its possible impact on traumatic brain injury (TBI) is still unclear. This study aims to investigate the protective effects of inhibiting PDE10A on neuroinflammation post-TBI injury and its possible molecular mechanism. The expression of PDE10A in rats and HT22 cells was determined by Western blotting. The neurological dysfunction of these rats was detected by Nissl staining, hematoxylin-eosin (HE) staining, and Morris water maze test. The activity of HT22 cells was measured by MTT. The findings of this study suggest that PDE10A is highly expressed in the brain tissue of TBI rats and HT22 cells induced by mechanical injury. Inhibition of PDE10A reduces the expression of interleukin-1β (IL-1β) and interleukin 6 (IL-6) and tumor necrosis factor alpha (TNF-α) in HT22 cells induced by mechanical injury to inhibit cell apoptosis. Simultaneously, inhibition of PDE10A in TBI rats reduces the time to find a visible platform in the same pool, while cAMP/PKA activator treatment alleviates all of the abovementioned phenomena. Additionally, it is further confirmed that inhibition of PDE10A activates the cAMP/PKA pathway and downregulates the expression of NRLP3. These findings demonstrate that inhibition of PDE10A exerts neuroprotection by inhibiting apoptosis and inflammation following TBI, at least partially by the cAMP/PKA/NLRP3 pathway.

1. Introduction

Traumatic brain injury (TBI) is the main cause of neurological dysfunction, death, and disability [1, 2]. Primary brain injury is direct physical damage to the brain tissue caused by external shocks, which is usually irreversible. Secondary brain injury includes neuroinflammation andapoptosis, which can be reversed in most cases [3, 4]. TBI leading to secondary brain injury occurs after a primary injury, subsequently contributeing to brain tissue damage and neuronal cell death [5, 6]. Brain injury causes nerve cells to activate and release pro-inflammatory factors, leading to neuroinflammation, which is the main sign of TBI. Previous studies have confirmed that brain injury induces an inflammatory response by activating neuroinflammatory mediators [7]. However, the underlying molecular mechanism of neuroinflammation post TBI is still elusive.

PDE10A is a dual-substrate phosphodiesterase that can catalyze cAMP and cGMP simultaneously. PDE10A is highly expressed in the striatal complex, which is the major entry structure to the basal ganglia [8]. Thus, PDE10A is considered to be an important target for the treatment of diseases related to ganglion dysfunction [9]. In recent years, it has been found that inhibition of PDE10A has an anti-inflammatory effect under neuroinflammatory conditions. The PDE10A inhibitor Papaverine is effective in optic neuropathy, LPS-stimulated macrophages/microglia mediated inflammation [10–12]. The PDE10A inhibitor MP-10 inhibits microglia activation in LPS-induced neuroinflammation and MPTP-induced Parkinson's disease mouse models, improving the development of neurodegenerative disease [13]. Our previous study found that PDE10A is highly expressed in TBI rats, but the specific mechanism is still unclear. Therefore, further study is needed to clarify the correlation between PDE10A and TBI.

In this study, we exposed HT22 cells to mechanical injury to mimic the neuronal inflammation caused by TBI in vitro [14, 15] and combined with TBI rat experiments to study the protective effect of inhibiting PDE10A on neuroinflammation post-TBI injury and its possible molecular mechanism.

2. Materials and Methods

2.1. Reagents and Antibodies. MP-10 was brought from Pharma Resources Inc. (Shanghai, China). The MTT assay kit was bought from Sigma-Aldrich (St. Louis, MO, USA). 8-Bromo-cAMP was brought from Selleck (Houston, Texas, USA). Antibodies PDE10A, TNF-α, IL-1β, IL-6, Bax, Bcl-2, caspase-3, NLRP3, and caspase-1 were purchased from Santa Cruz Biotechnology (Santa Cruz, CA, USA).

2.2. Animal Model. We followed the previous method as stated in [16]. Briefly, Sprague-Dawley rats (270–300 g, purchased from the Laboratory Animal Center of Kunming Medical University) were randomly divided into 4 experimental subgroups ($n = 3$ per group). Rats were installed in a stereotactic frame and a single metal pendulum of 1450 g was impacted on the parietooccipital bone to induce TBI. The rat in the sham group were kept under the same environmental except TBI. All protocols were conducted in accordance with guidelines set forth by the National Institutes of Health (NIH) Guide for the Care and Use of Laboratory Animals and were approved by the Ethics Committee of Kunming Medical University. Intracerebroventricular administration was performed as previously described [17]. In brief, after being anesthetized with 2% pentobarbital, rats were fixed on a stereotaxic instrument. The drugs were then injected directly into right lateral ventricles by using a 10 μl Hamilton syringe (Hamilton Company, Reno, NV). We refer to Shen et al.'s coordinates: 1.5 mm below the horizontal plane of the skull and 1.0 mm and 3.2 mm horizontally [18]. MP-10 and 8-Bromo-cAMP were administered by ICV injection at 1 h before TBI modeling. The pcDNA-NLRP3 vector was injected 20 days before modeling.

2.3. HT22 Cell Culture and Treatments. According to the method of Rachmany et al. [14], HT22 is used to construct an in vitro sublethal stretched TBI model (mechanical injury treatment). The stretched cells maintained cell membrane integrity and function [19]. In brief, mouse hippocampal HT22 cells (BeNa Culture Collection, Beijing, China) were cultured in Dulbecco's modified Eagle's medium (DMEM) containing 10% fetal bovine serum (Gibco, Carlsbad, CA), 1% penicillin, and streptomycin (Thermo Fisher Scientific, Inc., USA). HT22 cells were inoculated in flexible membrane plates (Flexcell International Corporation, Burlington, NC). The HT22 cells were subjected to moderate stretch injury with the cell injury controller II (CIC; Custom Design & Fabrication, Richmond, VA, USA) [20]. The cell Injury Controller II applies a short-duration nitrogen pulse (50 ms) to each hole to instantaneously deform the silicone rubber membrane and achieve a predetermined degree of stretching. In the present study, the pulse injury pressure (PI) was approximately 10.8 psi.

2.4. HT22 Cell Viability. Cell viability was determined using the 3-(4, 5-dimethyl-2-thiazolyl)-2, 5-diphenyltetrazolium bromide (MTT) assay. Briefly, HT22 cells induced by mechanical injury were seeded in 24-well plates in DMEM containing 10% FBS, according to the manufacturer's instructions. HT-22 cells were treated with MP-10, 8-Bromo-cAMP, pcDNA-NLRP3. Next, 50 μL of MTT was added to the medium for another 4 h at 37°C, After the medium was removed, DMSO was added to the plates. An automatic microplate reader was used to determine the absorbance at 470 nm. The experiment was repeated three times.

2.5. Western Blotting Assay. We prepared protein extracts from rats' brain tissue and HT22 cells. For rat's brain tissue, Briefly, rats were killed by decapitation; whole brains were removed and frozen at −80°C brain. Tissue lysates were prepared from frozen brain tissues, brain tissues were homogenized in RIPA buffer supplemented with protease and phosphatase inhibitors (Roche). Next, protein concentrations in the supernatant were determined using a BCA assay kit (Beyotime, Shanghai, China). An equal volume of 15 μg of proteins (extracted from the rats brain tissue and HT22 cells) were separated on 5–10% SDS-PAGE gels and transferred to the polyvinylidene difluoride membrane followed by blocking in 5% skim milk, next, the following antibodies were added to detect the primary antibodies: PDE10A (1 : 1000), TNF-α (1 : 1000), IL-1β (1 : 1000), IL-6 (1 : 1000), Bax (1 : 1000), Bcl-2 (1 : 1500), caspase-3 (1 : 1000), NLRP3 (1 : 1000), caspase-1 (1 : 1500), and GAPDH (1 : 2000). Next day, the membranes were incubated with horseradish peroxidase-conjugated secondary antibodies (1 : 3000) for 1 h; the immunoblots were developed using an ECL chemiluminescence system, according to the manufacturer's instructions (Beyotime, China), and analyzed with Image J software (NIH, Bethesda, MD, USA).

2.6. Morris Water Maze Test. Evaluate rat's learning and memory abilities in the Morris water maze. In brief, a large circular pool was filled with water and a circular escape platform was placed in the center of the southwest. All rats underwent the place navigation task. The tracking camera and analysis software record the escape latency of the rat to the platform, and the camera record the position, swimming distance, swimming time, and swimming path of rats.

2.7. H&E and Nissl Staining. To analyze neuronal cell death and lesion post TBI, we follow the Hengchang et al. method [21], In brief, brain tissues of different treatments were fixed in 4% paraformaldehyde, paraffin-embedded, and cut into 4 μm thick sections. The sections with different treatments were subjected to hematoxylin and eosin (H&E) staining and toluidine blue (Nissl) staining, and the tissue slides were treated in xylene solution for 3 minutes and then mounted. A light microscope was used to examine the staining images.

2.8. Statistical Analysis. All data were presented as mean ± SD. The data of MTT and Western blot were analyzed using *t*-test, and more than two groups was analyzed by one-way analysis of variance (ANOVA). The statistical analyses were performed using GraphPad Prism software. A value of $P < 0.05$ or $P < 0.01$ was considered as statistically significant.

3. Results

3.1. PDE10A Is Highly Expressed in TBI Tissues and HT22 Cell Lines. Based on previous studies [16], we detected the expression of PDE10A in TBI rats and HT22 cells. The results of Western blotting showed that the PDE10A expressed exceptionally high in TBI group compared with the sham group (Figure 1(a)). Simultaneously, we detected the expression of PDE10A in HT22 cells after 12 h mechanical injury, we found that PDE10A expression was up-regulated post mechanical injury treatment (MI; in vitro model of TBI) in HT22 cells compared to control group (Figure 1(b)).

3.2. PDE10A Promoted Neurological Dysfunction in TBI Rats. We further analyze the protective effect of inhibiting PDE10A on neurological dysfunction in TBI rats. Morris water maze test results showed that TBI induced a longer latency to find the platform, PDE10A inhibitor (MP-10; 3 mg/kg) shortens the time to find the platform (Figure 2(a)). Next, we use H&E staining and Nissl staining to observe the hippocampal CA1 region sections. The results of H&E staining and Nissl staining showed that the hippocampal neurons in the sham group were intact with normal morphology and obvious nucleoli. In the TBI group, hippocampal neurons are incomplete, with irregular cell contours and loose chromatin, membrane blebbing, shrunken soma, and concentrated nucleus. In addition, hippocampal neuronal density was significantly reduced. The damaged of neuronal by TBI-induced were ameliorated by prior treatment with PDE10A inhibitor (Figures 2(b) and 2(c)).

3.3. PDE10A Promoted Neuroinflammation of HT22 Cells Post Mechanical Injury. Western blotting results showed that PDE10A inhibitor provoked a loss in the expression of PDE10A compared with the control and mechanical trauma group (Figure 3(a)). In parallel, Western blotting results showed that a PDE10A inhibitor led to a significant decrease of inflammation-related proteins TNF-α, IL-1β, and IL-6 (Figure 3(a)). In addition, the results of MTT and Western blotting showed that PDE10A inhibitor improved mechanical trauma-induced apoptosis and upregulated the expression level of anti-apoptotic protein Bax (Figures 3(b) and 3(c)). Therefore, the PDE10A inhibitor alleviates neuroinflammation and apoptosis of HT22 cells post-mechanical Injury.

3.4. PDE10A Inhibits the cAMP/PKA Pathway. We measured the expression of cAMP/PKA pathway. Western blotting results showed that cAMP and p-PKA are significantly downregulated in mechanical trauma-induced cells. PDE10A inhibitor (MP-10; 5 μM; for 1 h) activates the cAMP/PKA pathway and upregulates the expression of CAMP and p-PKA (Figure 4). Thus, the inhibition of PDE10A activates the cAMP/PKA signaling pathway.

3.5. cAMP/PKA Inhibits the NLPR3 Expression. We measured the effect of cAMP/PKA on the expression of NLRP3. Western blotting results showed that cAMP/PKA (8-Bromo-cAMP; 4 μM; for 1 h) activation caused the down-regulation of NLPR3. Simultaneously, the PKA inhibitor (H-89; 10 μM; 1 hour) significantly upregulated the expression of NLPR3 (Figure 5).

3.6. cAMP/PKA Alleviated TBI Damage by Inhibiting NLPR3. We further studied the regulation of cAMP/PKA and NLRP3. Western blotting results showed that cAMP/PKA (8-Bromo-cAMP; 4 μM; for 1 h) activation causes down-regulation of NLPR3 and caspase-1 compared with the control and mechanical trauma group (Figure 6(a)). Simultaneously, the expression of NLRP3 was upregulated after transfection of pcDNA-NLRP3 in cells (Figure 6(b)). In addition, Western blotting results showed that cAMP/PKA activation resulted in the downregulation of inflammation-related proteins TNF-α, IL-1β, and IL-6 (Figure 6(c)). In addition, the results of MTT and Western blotting showed that cAMP/PKA activation alleviated mechanical trauma-induced apoptosis (Figures 6(d) and 6(f)). The pcDNA-NLRP3 group (50 nM transfected into HT22 cells) upregulated the expression of TNF-α, IL-1β, and IL-6 and promoted cell apoptosis compared with the cAMP/PKA activator group (Figures6(c) and 6(f)). The Morris water maze test showed that cAMP/PKA activator (8-Bromo-cAMP; 5 mg/kg) shortened the platform search time compared with the pcDNA-NLRP3 group (5 μL/rat) and the TBI group (Figure 6(d)).

4. Discussion

Our previous study used iTRAQ-based proteomics to analyze the brain proteome of normal and different type of rat mTBI models found that the expression of PDE10A was significantly upregulated in mTBI rats [16]. Changes in PDE10A expression are expected to become a marker of disease progression, drug target identification, and treatment response in TBI. According to reports, PDE10A plays a key role in neurological complications by affecting synaptic transmission, neuronal excitability, and synaptic plasticity [13, 22]. In parallel, PDE10A has neuroinflammation-promoting effects. However, the specific mechanism of PDE10A on TBI-induced inflammation and neuronal apoptosis is still unclear. In this study, we demonstrated that inhibition of PDE10A has a protective effect on TBI-induced inflammation and neuronal apoptosis. The inhibition of PDE10A reduced the expression of TNF-α, IL-1β, and IL-6 in HT22 cells induced by mechanical injury and inhibited cell apoptosis; simultaneously, inhibiting PDE10A in TBI rats shortens the time to find a platform. In addition,

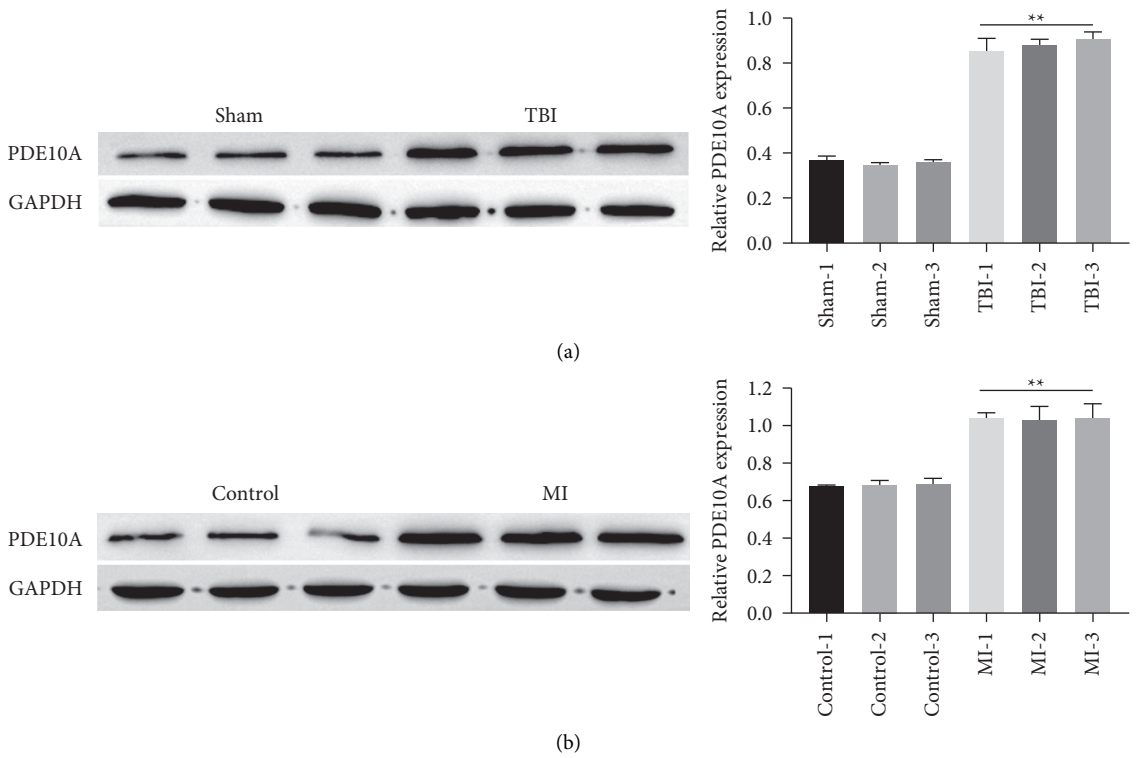

Figure 1: PDE10A is highly expressed in TBI tissues and HT22 cell lines. The expression of PDE10A in tissues and HT22 cells were measured by Western blotting (a, b). **Significant compared to sham/control (**$P < 0.01$).

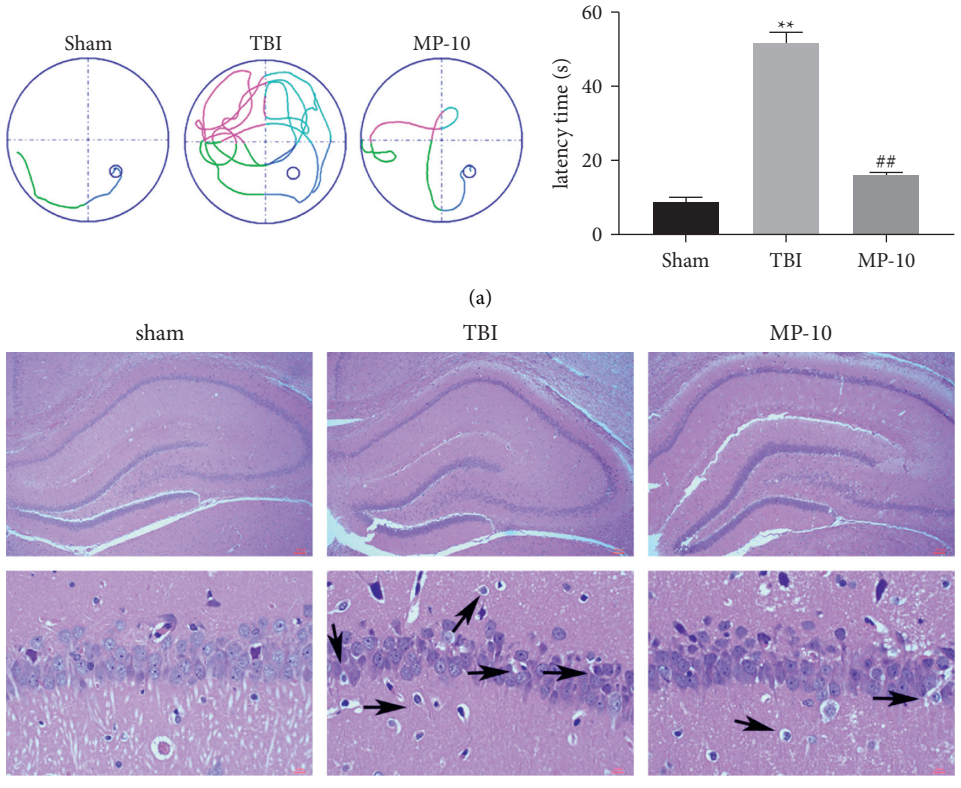

Figure 2: Continued.

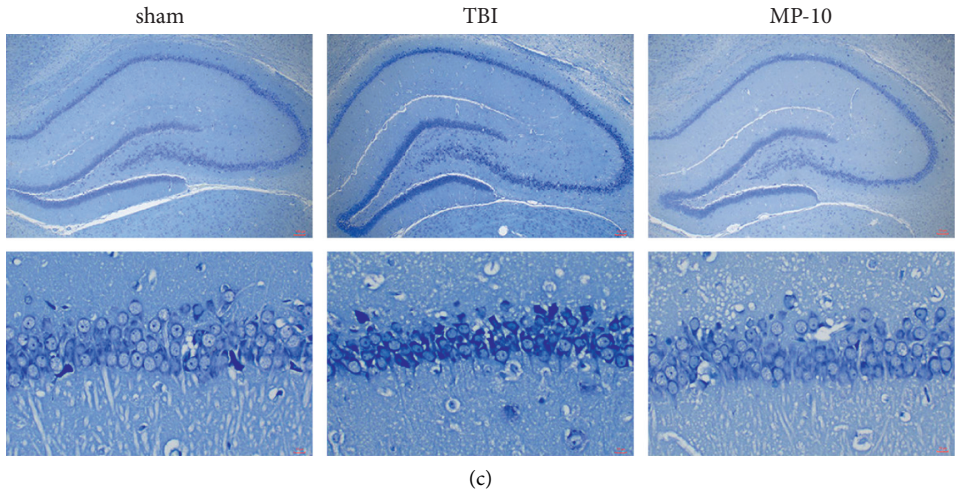

Figure 2: PDE10A promotes neurological dysfunction in TBI rats. Representative images of the escape track of rats in the Morris water maze test (a). The hematoxylin and eosin (H&E)-stained and Nissl-stained hippocampal sections (×100) (b) and (c). **Significant compared to sham/control (** $P < 0.01$).

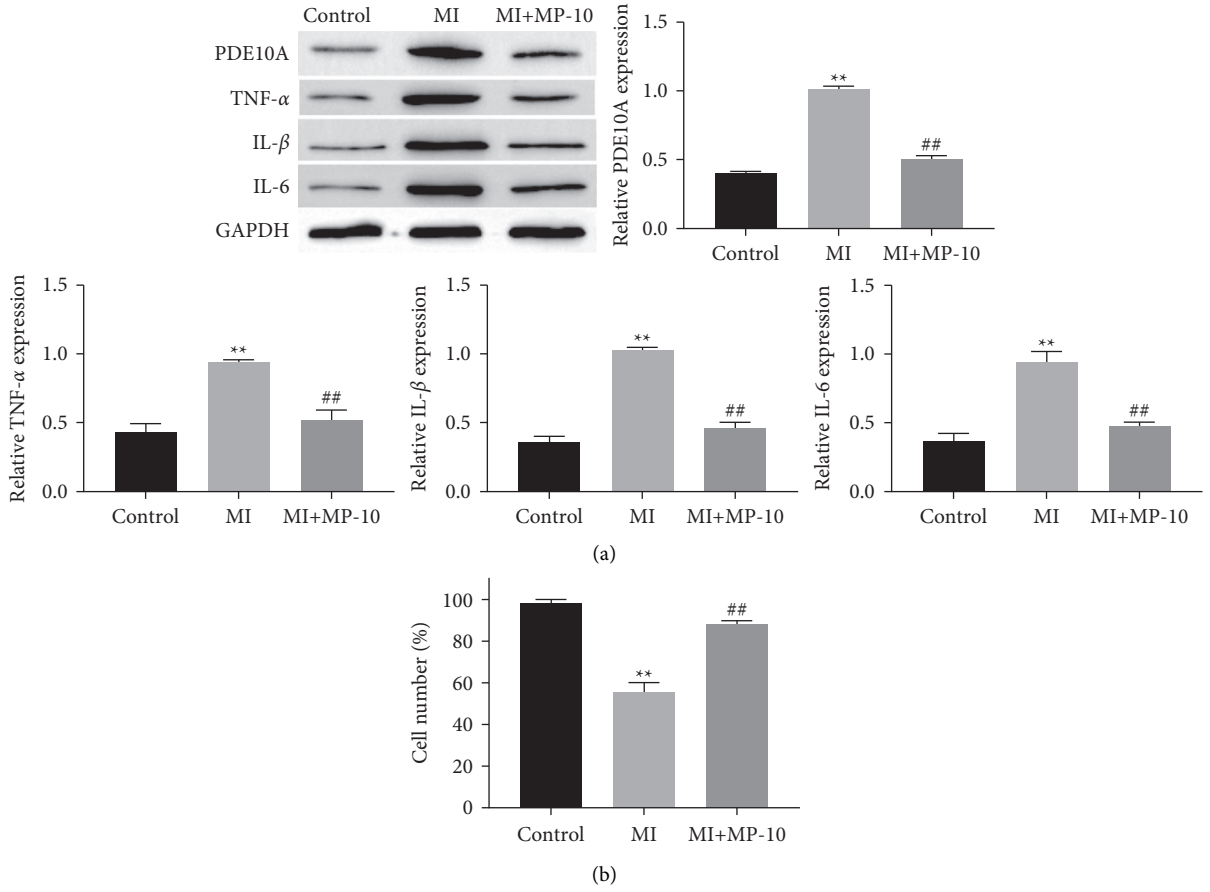

Figure 3: Continued.

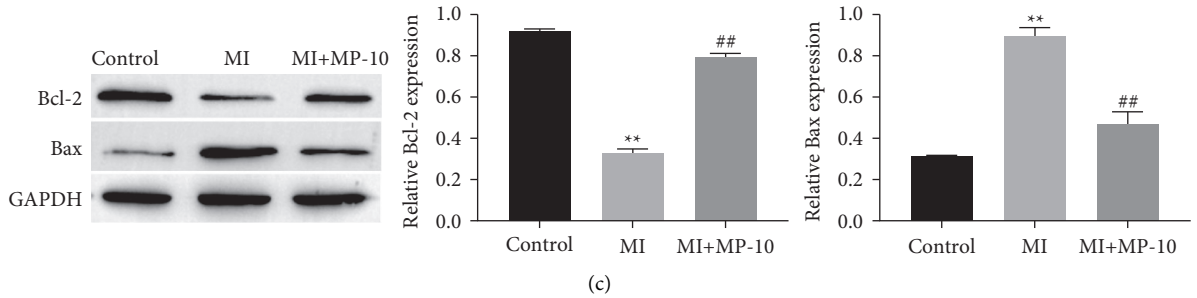

Figure 3: PDE10A promotes neuroinflammation of HT22 cells post mechanical injury. The expression of TNF-α, IL-1β, IL-6, Bax, Bcl-2, and caspase-3 in HT22 cells were measured by Western blotting (a) and (c). HT22 cells viability was measured by the MTT assay (b). **Significant compared to control ($^{**}P < 0.01$). ##Significant compared to PDE10A inhibitor treatment ($^{\#\#}P < 0.01$).

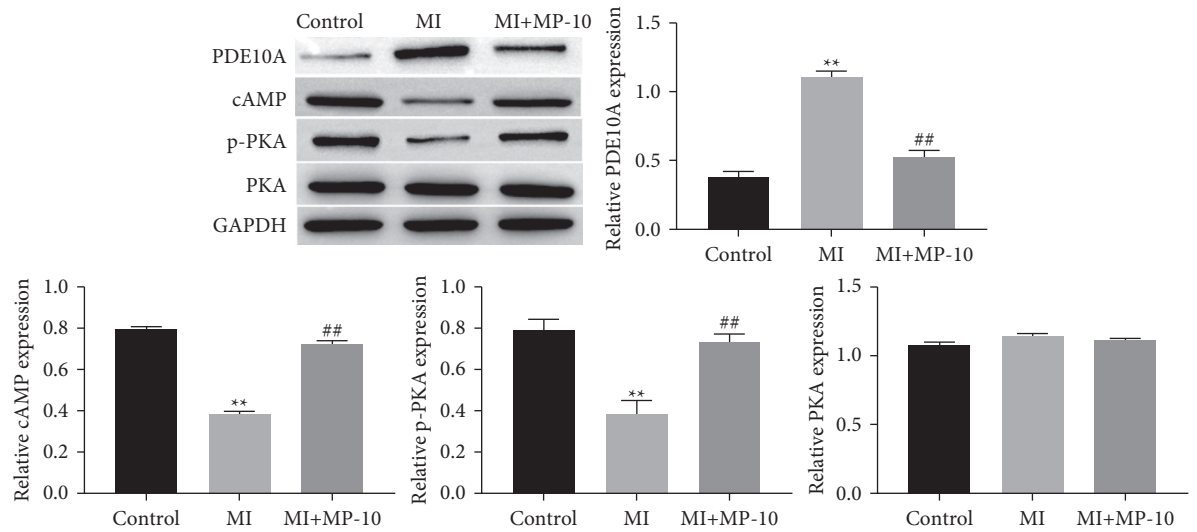

Figure 4: PDE10A inhibiting the cAMP/PKA pathway. The expression of cAMP p-PKA and PKA in HT22 cells were measured by Western blotting. HT22 **significant compared to control ($^{**}P < 0.01$). ##Significant compared to MI ($^{\#\#}P < 0.01$).

PDE10A inhibited the activation of cAMP/PKA, and the inhibition of PDE10A upregulated the expression of cAMP and p-PKA. Moreover, the activation of the cAMP/PKA pathway reduced the expression of TNF-α, IL-1β, and IL-6 induced by mechanical injury through downregulation of NLRP3 and inhibiting cell apoptosis. In our study, the effects of inhibiting the anti-inflammatory and neuroprotective effects of PDE10A indicate the importance of the PDE10A/cAMP/PKA/NLRP3 pathway in mediating these effects.

TBI is accompanied by neuroinflammation [23, 24]. A rapid rise in the levels of cytokines (IL-1β, IL-6, and TNF-α) and chemokines following TBI [25] leads to the rapid development of inflammatory response [26]. In this study, we exposed HT22 cells to mechanical injury to mimic the neuronal inflammation caused by TBI in vitro. It is worth mentioning that previous studies have used LPS and mechanical injury to mimic a cellular model of induce TBI [14]. In contrast, we believe that mechanical injury induction is more in line with the damage environment caused by TBI to neurons. In HT22 cells induced by mechanical injury, IL-1β, IL-6, and TNF-α are significantly high expression, while the survival rate of HT22 cells is reduced. Recently, PDE10A has been increasingly appreciated as important mediators of neurological dysfunction progression. PDE10A can regulate synaptic transmission, neuronal excitability, and synaptic plasticity, playing key roles in neurological dysfunction [27]. In addition, PDE10A abnormal expression in neurological and psychiatric disorders [8, 28]. In order to understand the expression of PDE10A after TBI, we determined the amount of PDE10A protein in vivo and in vitro after TBI injury. We found that PDE10A is highly expressed in TBI rats. Simultaneously, when we inhibited the expression of PDE10A in rats, it effectively shortened the time for rats to find the platform and alleviated brain damage in rats. On the other hand, the inhibition of PDE10A significantly downregulated the expression of TNF-α, IL-1β, and IL-6 in mechanical trauma-induced HT22 cells and inhibited apoptosis. Therefore, the increase of PDE10A expression is correlated with TBI pathogenesis.

cAMP is the second messenger, which plays a major role in cytokine secretion and cell signal transduction [29, 30]. In cells, the expression of cAMP is regulated by adenosine A2A receptor (A2AR) and PDE10A [31, 32]. The inhibition of

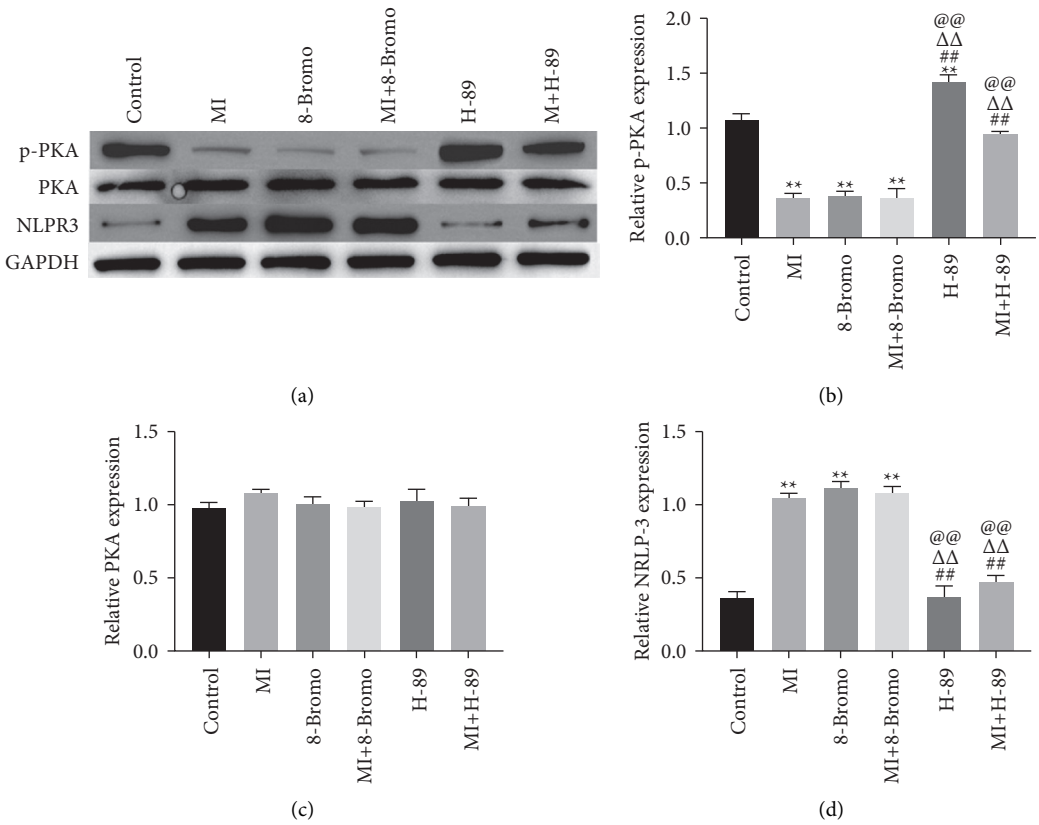

Figure 5: cAMP/PKA inhibits NLPR3 expression. The expression of p-PKA, PKA, and NLRP3 in HT22 cells were measured by Western blotting. HT22 **significant compared to control ($^{**}P < 0.01$). $^{\#\#}$Significant compared to MI ($^{\#\#}P < 0.01$). $^{\Delta\Delta}$ was considered significant compared to cAMP/PKA activator treatment ($^{\Delta\Delta}P < 0.01$). $^{@@}$Significant compared to MI + cAMP/PKA activator treatment ($^{@@}P < 0.01$).

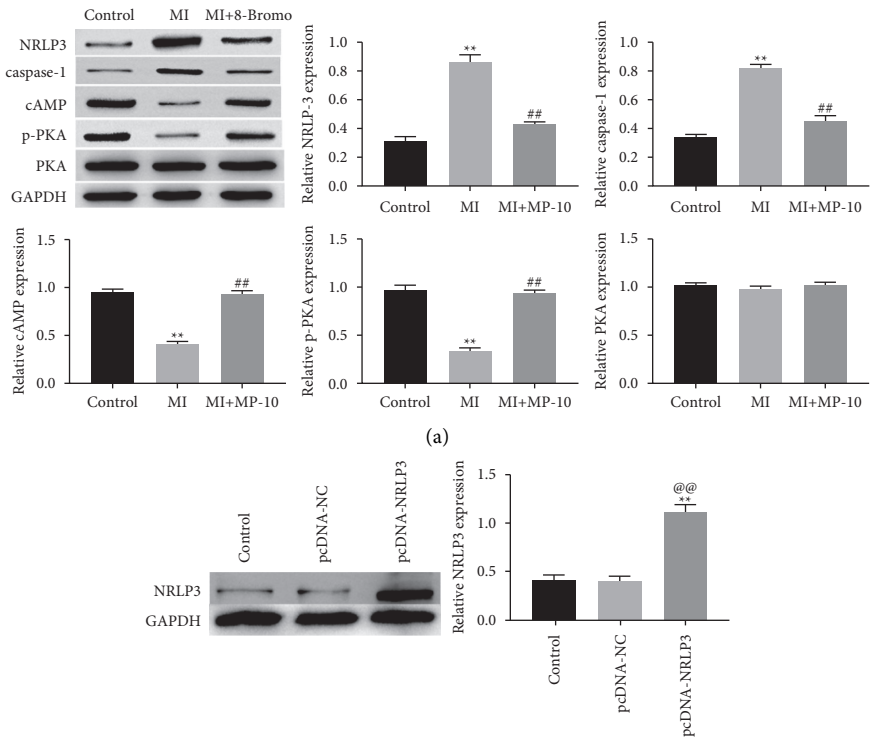

Figure 6: Continued.

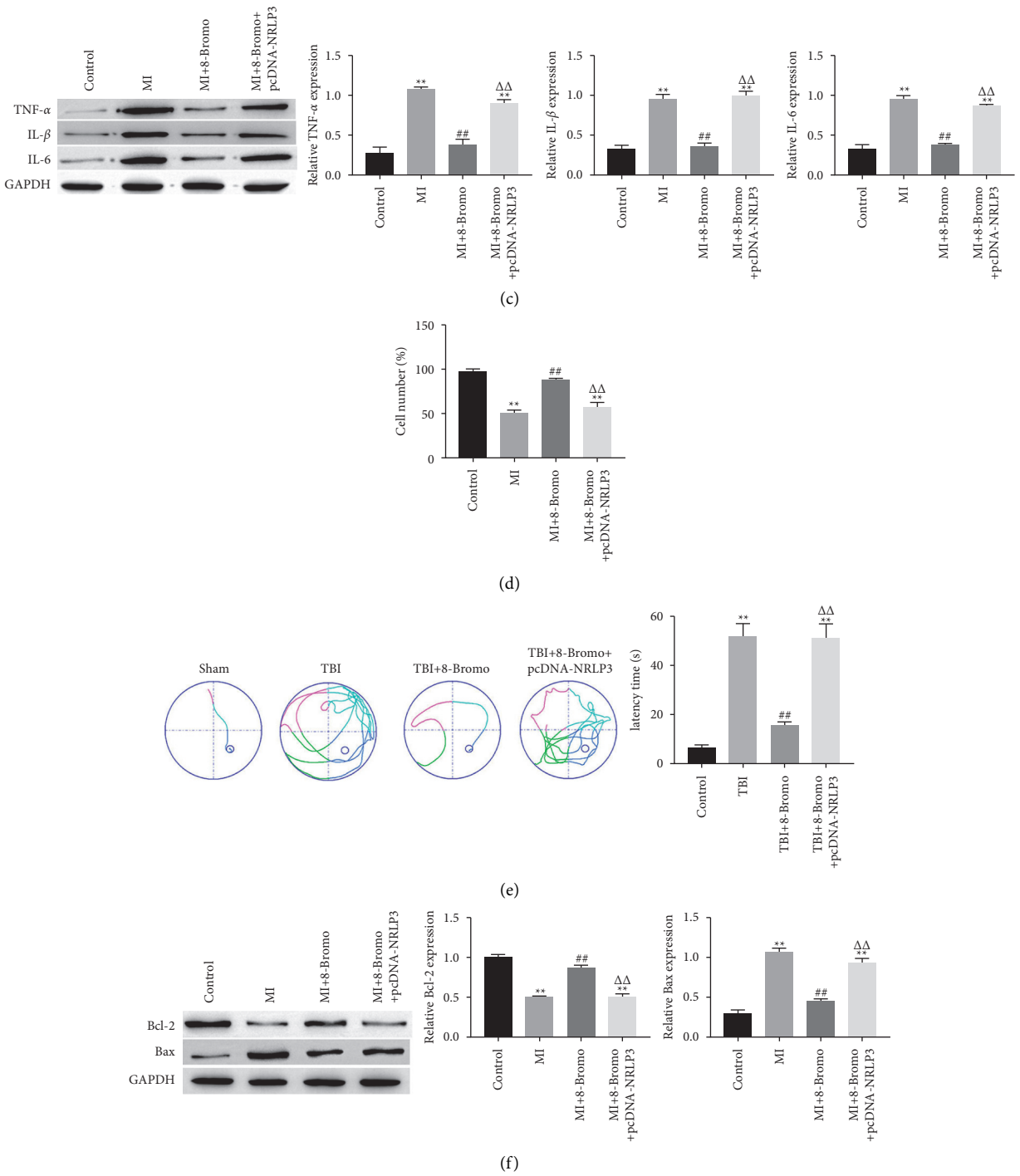

Figure 6: cAMP/PKA alleviated TBI damage by inhibiting NLPR3. The expression of NLPR3, caspase1, TNF-α, IL-1β, IL-6, Bax, Bcl-2, and caspase-3 in HT22 cells was measured by Western blotting (a–c) and (f). HT22 cells viability was measured by the MTT assay (d). Representative images of the escape track of rats in the Morris water maze test (e). **Significant compared to control ($^{**}P < 0.01$). $^{\#\#}$Significant compared to MI/TBI ($^{\#\#}P < 0.01$). $^{\Delta\Delta}$Significant compared to cAMP/PKA activator treatment ($^{\Delta\Delta}P < 0.01$).

PDE10A leads to increased intracellular cAMP levels and activates the PKA signaling pathway [29]. PKA-phosphorylation promotes CREB transcriptional activation and further promotes the combination of CREB and transcriptional co-activator CBP to form a complex that blocks the transcription of inflammatory genes [33]. In this study, cAMP/PKA is low expressed in HT22 cells induced by mechanical injury, and it was found that activation of cAMP/PKA inhibits the inflammatory response of TBI. In addition, PDE10A is overexpressed in TBI rats and HT22 cells induced by mechanical injury, demonstrating a correlation between the PDE10A/cAMP/PKA levels and TBI.

The cAMP/PKA pathway contributes to the resolution of inflammation [34, 35]. This anti-inflammatory effect is closely related to PKA-phosphorylation-mediated upregulation of the anti-inflammatory cytokine and inhibition of proinflammatory cytokines such as IL-1β, IL-6, and TNF-α [10, 36]. In addition, studies have shown a prominent role of the cAMP/PKA signaling pathway in regulating NLRP3-related inflammation [37]. As a core part of the inflammatory response, activation of the NLRP3 inflammasome promoted the release of proinflammatory cytokines [38, 39]. Simultaneously, cAMP has been shown to inhibit the phosphorylation of NLRP3 [40]. In our studies, we found that pcDNA-NLRP3 upregulated the expression of TNF-α, IL-1β, and IL-6 and promoted cell apoptosis in HT22 cells induced by mechanical injury compared with the cAMP/PKA activator group.

In conclusion, our results indicate that PDE10A is highly expressed post-TBI. inhibition of PDE10A exhibits a neuroprotective effect against TBI by relieving neuroinflammation via downregulates the NLRP3 inflammasome through activation of the cAMP/PKA pathway.

Data Availability

The data used to support the findings of this study are available from the corresponding author upon reasonable request.

Conflicts of Interest

The authors declare that they have no conflicts of interest.

Authors' Contributions

HS designed the experiments. JH and DT wrote the original manuscript. JH, DT, YQC, and YGW carried out the experiment and collected the experimental data. JH, XFH, and SL collected and analyzed the experimental data. HS participated in the supervision and revision of the paper. All authors participated in the revision of the manuscript and read and approved the final manuscript. JH and DT contributed equally.

Acknowledgments

This work was supported by the Applied Basic Research of Yunnan Neurological Disease Diagnosis and Treatment Center (ZX2019-03-05).

References

[1] L. Hu, J. Liu, H. Xue et al., "Mirna-92a-3p regulates osteoblast differentiation in patients with concomitant limb fractures and tbi via ibsp/pi3k-akt inhibition," *Molecular Therapy—Nucleic Acids*, vol. 23, pp. 1345–1359, 2021.

[2] J. D. Finan, "Biomechanical simulation of traumatic brain injury in the rat," *Clinical Biomechanics*, vol. 64, pp. 114–121, 2019.

[3] X. Feng, W. Ma, J. Zhu, W. Jiao, and Y. Wang, "Dexmedetomidine alleviates early brain injury following traumatic brain injury by inhibiting autophagy and neuroinflammation through the ros/nrf2 signaling pathway," *Molecular Medicine Reports*, vol. 24, no. 3, p. 24, 2021.

[4] Y. Wang, M. Zhao, L. Shang et al., "Homer1a protects against neuronal injury via pi3k/akt/mtor signaling pathway," *International Journal of Neuroscience*, vol. 130, no. 6, pp. 621–630, 2020.

[5] B. He, W. Chen, J. Zeng, W. Tong, and P. Zheng, "Long noncoding rna nkila transferred by astrocyte-derived extracellular vesicles protects against neuronal injury by upregulating nlrx1 through binding to mir-195 in traumatic brain injury," *Aging*, vol. 13, no. 6, pp. 8127–8145, 2021.

[6] S. I. Alam, M. G. Jo, T. J. Park et al., "Quinpirole-mediated regulation of dopamine d2 receptors inhibits glial cell-induced neuroinflammation in cortex and striatum after brain injury," *Biomedicines*, vol. 9, no. 1, p. 47, 2021.

[7] K. Krukowski, A. Nolan, M. Becker et al., "Novel microglia-mediated mechanisms underlying synaptic loss and cognitive impairment after traumatic brain injury," *Brain, Behavior, and Immunity*, vol. 98, 2021.

[8] A. M. García, I. G. Salado, D. I. Perez et al., "Pharmacological tools based on imidazole scaffold proved the utility of pde10a inhibitors for Parkinson's disease," *Future Medicinal Chemistry*, vol. 9, no. 8, pp. 731–748, 2017.

[9] A. Jankowska, A. Świerczek, E. Wyska et al., "Advances in discovery of pde10a inhibitors for cns-related disorders. part 1: overview of the chemical and biological research," *Current Drug Targets*, vol. 20, no. 1, pp. 122–143, 2018.

[10] Y.-Y. Lee, J.-S. Park, Y.-H. Leem et al., "The phosphodiesterase 10 inhibitor papaverine exerts anti-inflammatory and neuroprotective effects via the pka signaling pathway in neuroinflammation and Parkinson's disease mouse models," *Journal of Neuroinflammation*, vol. 16, no. 1, p. 246, 2019.

[11] K. Tamada, S. Nakajima, N. Ogawa et al., "Papaverine identified as an inhibitor of high mobility group box 1/receptor for advanced glycation end-products interaction suppresses high mobility group box 1-mediated inflammatory responses," *Biochemical and Biophysical Research Communications*, vol. 511, no. 3, pp. 665–670, 2019.

[12] Y. Yamazaki and Y. Kawano, "Inhibitory effects of herbal alkaloids on the tumor necrosis factor-.ALPHA: and nitric oxide production in lipopolysaccharide-stimulated RAW264 macrophages," *Chemical and Pharmaceutical Bulletin*, vol. 59, no. 3, pp. 388–391, 2011.

[13] D.-Y. Kim, J.-S. Park, Y.-H. Leem, J.-E. Park, and H.-S. Kim, "The potent pde10a inhibitor mp-10 (pf-2545920) suppresses microglial activation in lps-induced neuroinflammation and mptp-induced Parkinson's disease mouse models," *Journal of Neuroimmune Pharmacology*, vol. 16, no. 2, pp. 470–482, 2021.

[14] L. Rachmany, D. Tweedie, V. Rubovitch et al., "Exendin-4 attenuates blast traumatic brain injury induced cognitive impairments, losses of synaptophysin and in vitro tbi-induced hippocampal cellular degeneration," *Scientific Reports*, vol. 7, no. 1, p. 3735, 2017.

[15] J. Chen, H. Wang, C. Luo et al., "Chd8 rescued tbi-induced neurological deficits by suppressing apoptosis and autophagy via wnt signaling pathway," *Cellular and Molecular Neurobiology*, vol. 40, no. 7, pp. 1165–1184, 2020.

[16] H. Song, S. Fang, J. Gao et al., "Quantitative proteomic study reveals up-regulation of camp signaling pathway-related proteins in mild traumatic brain injury," *Journal of Proteome Research*, vol. 17, no. 2, pp. 858–869, 2018.

[17] Q. Rui, H. Ni, F. Gao et al., "Lrrk2 contributes to secondary brain injury through a p38/drosha signaling pathway after

traumatic brain injury in rats," *Frontiers in Cellular Neuroscience*, vol. 12, p. 51, 2018.

[18] H. Shen, Z. Chen, Y. Wang et al., "Role of neurexin-1β and neuroligin-1 in cognitive dysfunction after subarachnoid hemorrhage in rats," *Stroke*, vol. 46, no. 9, pp. 2607–2615, 2015.

[19] M. Arundine, M. Aarts, A. Lau, and M. Tymianski, "Vulnerability of central neurons to secondary insults after in vitro mechanical stretch," *Journal of Neuroscience*, vol. 24, no. 37, pp. 8106–8123, 2004.

[20] S.-X. Cheng, Z.-W. Xu, T.-L. Yi et al., "Itraq-based quantitative proteomics reveals the new evidence base for traumatic brain injury treated with targeted temperature management," *Neurotherapeutics*, vol. 15, no. 1, pp. 216–232, 2018.

[21] H. Li, C. Lu, W. Yao, L. Xu, J. Zhou, and B. Zheng, "Dexmedetomidine inhibits inflammatory response and autophagy through the circlrp1b/mir-27a-3p/dram2 pathway in a rat model of traumatic brain injury," *Aging*, vol. 12, no. 21, pp. 21687–21705, 2020.

[22] A. Bhat, V. Tan, B. Heng et al., "Papaverine, a phosphodiesterase 10a inhibitor, ameliorates quinolinic acid-induced synaptotoxicity in human cortical neurons," *Neurotoxicity Research*, vol. 39, no. 4, pp. 1238–1250, 2021.

[23] R. Hummel, M. Lang, S. Walderbach et al., "Single intracerebroventricular progranulin injection adversely affects the blood-brain barrier in experimental traumatic brain injury," *Journal of Neurochemistry*, vol. 158, no. 2, pp. 342–357, 2021.

[24] R. J. Henry, S. J. Doran, J. P. Barrett et al., "Inhibition of mir-155 limits neuroinflammation and improves functional recovery after experimental traumatic brain injury in mice," *Neurotherapeutics*, vol. 16, no. 1, pp. 216–230, 2019.

[25] D. W. Simon, M. J. Mcgeachy, H. Bayır, R. S. B. Clark, D. J. Loane, and P. M. Kochanek, "The far-reaching scope of neuroinflammation after traumatic brain injury," *Nature Reviews Neurology*, vol. 13, no. 3, pp. 171–191, 2017.

[26] F. Corrigan, K. A. Mander, A. V. Leonard, and R. Vink, "Neurogenic inflammation after traumatic brain injury and its potentiation of classical inflammation," *Journal of Neuroinflammation*, vol. 13, no. 1, p. 264, 2016.

[27] Y. Zhang, B. Gao, F. Zheng et al., "The phosphodiesterase 10a inhibitor pf-2545920 enhances hippocampal excitability and seizure activity involving the upregulation of glua1 and nr2a in post-synaptic densities," *Frontiers in Molecular Neuroscience*, vol. 10, p. 100, 2017.

[28] P. Fazio, C. J. Fitzer-Attas, L. Mrzljak et al., "Pet molecular imaging of phosphodiesterase 10a: an early biomarker of Huntington's disease progression," *Movement Disorders*, vol. 35, no. 4, pp. 606–615, 2020.

[29] Z.-Q. Zou, J.-J. Chen, H.-F. Feng et al., "Novel phosphodiesterase 4 inhibitor FCPR03 alleviates lipopolysaccharide-induced neuroinflammation by regulation of the cAMP/PKA/CREB signaling pathway and NF-κB inhibition," *Journal of Pharmacology and Experimental Therapeutics*, vol. 362, no. 1, pp. 67–77, 2017.

[30] P. Jin, S. Deng, M. Tian et al., "Int-777 prevents cognitive impairment by activating takeda g protein-coupled receptor 5 (tgr5) and attenuating neuroinflammation via camp/pka/creb signaling axis in a rat model of sepsis," *Experimental Neurology*, vol. 335, Article ID 113504, 2021.

[31] É. Mota, S. Bompierre, D. Betolngar, L. R. V. Castro, and P. Vincent, "Pivotal role of phosphodiesterase 10a in the integration of dopamine signals in mice striatal d1 and d2 medium-sized spiny neurones," *British Journal of Pharmacology*, vol. 178, 2021.

[32] A. Nishi, M. Kuroiwa, D. B. Miller et al., "Distinct roles of pde4 and pde10a in the regulation of camp/pka signaling in the striatum," *Journal of Neuroscience*, vol. 28, no. 42, pp. 10460–10471, 2008.

[33] W. Xie, F. Li, Y. Han et al., "Neuropeptide y1 receptor antagonist promotes osteoporosis and microdamage repair and enhances osteogenic differentiation of bone marrow stem cells via camp/pka/creb pathway," *Aging*, vol. 12, no. 9, pp. 8120–8136, 2020.

[34] Y. Tao, L. Li, B. Jiang et al., "Cannabinoid receptor-2 stimulation suppresses neuroinflammation by regulating microglial m1/m2 polarization through the camp/pka pathway in an experimental gmh rat model," *Brain, Behavior, and Immunity*, vol. 58, pp. 118–129, 2016.

[35] J. Lu, C. Zhang, J. Lv et al., "Antiallergic drug desloratadine as a selective antagonist of 5HT 2A receptor ameliorates pathology of Alzheimer's disease model mice by improving microglial dysfunction," *Aging Cell*, vol. 20, no. 1, Article ID e13286, 2021.

[36] B. Zhang, J. Zhao, P. Guo et al., "Effects of naodesheng tablets on amyloid beta-induced dysfunction: a traditional Chinese herbal formula with novel therapeutic potential in Alzheimer's disease revealed by systems pharmacology," *Biomedicine & Pharmacotherapy*, vol. 141, Article ID 111916, 2021.

[37] L. Wang, T. Guo, Y. Guo, and Y. Xu, "Asiaticoside produces an antidepressant-like effect in a chronic unpredictable mild stress model of depression in mice, involving reversion of inflammation and the PKA/pCREB/BDNF signaling pathway," *Molecular Medicine Reports*, vol. 22, no. 3, pp. 2364–2372, 2020.

[38] W. Liu, X. Zhang, M. Zhao et al., "Activation in m1 but not m2 macrophages contributes to cardiac remodeling after myocardial infarction in rats: a critical role of the calcium sensing receptor/nrlp3 inflammasome," *Cellular Physiology and Biochemistry*, vol. 35, no. 6, pp. 2483–2500, 2015.

[39] M. Dai, L. Wu, K. Yu et al., "D-carvone inhibit cerebral ischemia/reperfusion induced inflammatory response tlr4/nlrp3 signaling pathway," *Biomedicine & Pharmacotherapy*, vol. 132, Article ID 110870, 2020.

[40] L. Mortimer, F. Moreau, J. A. Macdonald, and K. Chadee, "Nlrp3 inflammasome inhibition is disrupted in a group of auto-inflammatory disease caps mutations," *Nature Immunology*, vol. 17, no. 10, pp. 1176–1186, 2016.

Hindawi
Evidence-Based Complementary and Alternative Medicine
Volume 2022, Article ID 9199856, 7 pages
https://doi.org/10.1155/2022/9199856

Research Article

Triage Nurse-Activated Emergency Evaluation Reduced Door-to-Needle Time in Acute Ischemic Stroke Patients Treated with Intravenous Thrombolysis

Xiao Liang,[1] **Wenhui Gao**,[1] **Jiali Xu**,[2] **Sara Saymuah**,[3] **Xiaojie Wang**,[4] **Jing Wang**,[1] **Wenbo Zhao**,[2] **Xiurong Xing**,[1] **Changyuan Wang**,[1] **Fangyan Liu**,[1] **Lei Feng**,[5] **and Sijie Li**[1,5,6]

[1]*Department of Emergency, Xuanwu Hospital Capital Medical University, Beijing, China*
[2]*Department of Neurology, Xuanwu Hospital Capital Medical University, Beijing, China*
[3]*Wayne State University School of Medicine, Detroit, USA*
[4]*Department of Neurology, Shenzhen Qianhai Shekou Free Trade Zone Hospital, Shenzhen, China*
[5]*Beijing Institute of Brain Disorders, Capital Medical University, Beijing, China*
[6]*Beijing Key Laboratory of Hypoxic Conditioning Translational Medicine, Xuanwu Hospital, Capital Medical University, Beijing, China*

Correspondence should be addressed to Sijie Li; phoenix0537@sina.com

Received 27 August 2021; Accepted 20 January 2022; Published 3 March 2022

Academic Editor: Feng Zhang

Background and Purpose. Shorter door-to-needle time (DNT) is associated with a better outcome in acute ischemic stroke (AIS) patients who accept intravenous thrombolysis. We aimed to explore whether triage nurse-activated emergency evaluation would reduce DNT compared with doctor-activated emergency evaluation in AIS patients treated with intravenous thrombolysis who failed to use emergency medical services (EMSs). *Methods*. This was a retrospective analysis in a general hospital emergency department in Beijing, China. 212 adult AIS patients treated with thrombolysis who failed to use EMSs were included. In addition to DNT, door-to-vein open time (DVT), door-to-blood sample deliver time (DBT), and 7-day NIHSS scores were evaluated. *Results*. 137 (64.6%) patients were in the triage nurse-activated group and 75 (35.4%) patients were in the doctor-activated group. The DNT of the triage nurse-activated group was significantly reduced compared with the doctor-activated group (28 (26, 32.5) min vs. 30 (28, 40) min, $p = 0.001$). DNT less than 45 min was seen in 95.6% of patients in the triage nurse-activated group and 84% of patients in the doctor-activated group ($p = 0.011$, OR 3.972, 95% CI 1.375–11.477). In addition, DVT (7 (4, 10) min vs. 8 (5, 12) min, $P = 0.025$) and DBT (15 (13, 21) min vs. 19 (15, 26) min, $p = 0.001$) of the triage nurse-activated group were also shorter than those of the doctor-activated group ($p < 0.05$). The 7-day NIHSS scores were not statistically different between the two groups. *Conclusions*. Triage nurse-activated urgent emergency evaluation could reduce the door-to-needle time, which provides a feasible opportunity to optimize the emergency department service for AIS patients who failed to use emergency medical services.

1. Introduction

Ischemic stroke is one of the leading causes of mortality and disability in China [1, 2]. Intravenous thrombolysis has become a crucial treatment for acute ischemic stroke during the past two decades [3–7]. Data show that earlier reperfusion therapy performance leads to more salvaged brain tissue [8–10]. 1.9 million neurons are lost every minute after an ischemic stroke, which demonstrated that even a small reduction in treatment time may have great benefit to patients' prognosis [11]. Door-to-needle time (DNT) is defined as the time interval from hospital arrival to the onset of the pharmacological (tissue plasminogen activator) infusion, which has been strongly associated with a lower risk of hemorrhagic transformation, mortality, and better functional outcomes at 3 months [12, 13]. A recent study also

found an association between shorter DNT and long-term lower all-cause mortality and readmission at one year [14]. Thus, it is critical to explore approaches to reduce DNT to ensure patients receive reperfusion therapy as rapidly as possible.

Currently, several approaches have been reported to reduce DNT [15]. The use of emergency medical services (EMSs) system was independently associated with earlier emergency department (ED) arrival, quicker ED evaluation, and more rapid treatment, which also shortens the DNT [16]. However, only about 59% of all stroke patients acquire EMSs [17]. As per protocol, suspected stroke patients arriving via EMSs would be preliminarily assessed by the in-clinic ED neurologist immediately after hospital arrival. The emergency evaluation was initiated by the multicomponent hospital stroke team if patients met eligibility. Nevertheless, patients who were presented directly to the ED without EMSs would have a waiting period between the triage and preliminary assessment performed by neurologists in the clinic. As a result of the waiting period, postponed initiation of the emergency evaluation performed by the hospital stroke team could contribute to a delay in reperfusion treatment, especially for patients with mild symptoms.

Since triage is the first step for patients who arrive at the ED without EMSs, there is an opportunity for professionally trained triage nurses to directly assess patients and activate the stroke team, theoretically reducing the time until neurologist evaluation in the ED clinic. This study aimed to determine whether triage nurse-activated emergency evaluation would reduce the DNT.

2. Materials and Methods

2.1. Study Design and Setting. This was an observational retrospective cross-sectional study and was carried out in the emergency department (ED) of Xuanwu Hospital in Beijing from January 2019 to December 2019. This hospital has set a stroke center at the ED to provide emergency evaluation for suspected stroke patients and stroke units to provide comprehensive management for patients with a final diagnosis of stroke. The emergency evaluation was carried out by the hospital stroke team which mainly composed of neurologists and neurosurgeons and depended on multidisciplinary cooperation among the emergency department, intervention center, radiology department, laboratory department, and vascular ultrasound department. Suspected stroke patients were accompanied by the stroke team throughout assessment, examination, and treatment.

2.2. Participants. Acute ischemic stroke (AIS) patients diagnosed by computed tomography (CT) or magnetic resonance imaging (MRI) who received emergency evaluation services at ED were screened in this study. Eligible patients were aged ≥18 years and accepted intravenous thrombolysis with informed consent. The exclusion criteria are as follows: (1) patients transported by EMSs; (2) patients with laboratory and/or imaging examinations at other hospitals; and (3) patients with incomplete clinical data. A total of 212 AIS patients were finally included in this study and divided into two groups according to the type of personnel who initiated the urgent emergency evaluation service. 137 patients received the urgent emergency evaluation, activated by triage nurses, and 75 patients were activated by doctors (Figure 1).

2.3. Procedure. Procedure of the doctor-activated group: in the doctor-activated group, nurses triaged suspected stroke patients to a higher visit grade and priority if they presented within 4.5 hours of symptom onset or at a time when patients were known to be well by themselves. Doctors in the Neurology Clinic of the emergency department then performed a preliminary examination and assessment and activated the hospital stroke team if patients met eligible criteria. In the meantime, the disease severity of suspected stroke patients would be evaluated by the stroke team as ED nurses insert an indwelling catheter to collect and send blood samples for examination. Subsequently, the radiology department would be contacted to perform a head CT scan for definitive diagnosis. Under the cooperation of the stroke team and emergency department personnel, intravenous thrombolysis therapy was performed in the emergency room for patients who met the indications of intravenous thrombolysis and completed informed consent.

Procedure of the triage nurse-activated group: 6 nurses cooperated with the study and were designated as triage nurses. The criteria for triage nurses were as follows: (1) emergency specialist nurses with more than 5-year work experience; (2) nurses with a bachelor's degree or above; (3) nurses with 3 months of clinical practice in cerebrovascular units; and (4) nurses who were trained in the process of stroke rescue, with solid theoretical knowledge and practical skills in stroke care. They were also trained to master the fast diagnosis of AIS to acquire certification. The 6 triage nurses would directly participate in the evaluation, treatment, and transport of the suspected AIS patients. Triage nurses would first measure vital signs and evaluate suspected stroke patients using the Face-Arm-Speech-Time (FAST) scale, which includes sudden face numbness or weakness, arm(s) numbness or weakness, and slurred or hard-to-understand speech. Triage nurses would then directly initiate the emergency evaluation implemented by the hospital stroke team if the patient suffered any of the above symptoms and the time from symptom onset was within 4.5 hours [18]. The subsequent procedure of treatment was the same as the doctor-activated group (Figure 2).

2.4. Data Collection. Patients' general demographic information, route of transportation to the ED (visit on their own or transfer by ambulance), prehospital call (yes or no), and time of visit were collected by exporting from the triage system. The time metrics were recorded by filling in the self-made "Emergency Evaluation Form for Stroke Patients," including the patient's arrival, venipuncture, blood sample delivery, and the onset of the pharmacological infusion. Disease condition and prognosis information including scores of the 7-day National Institute of Health Stroke Scale

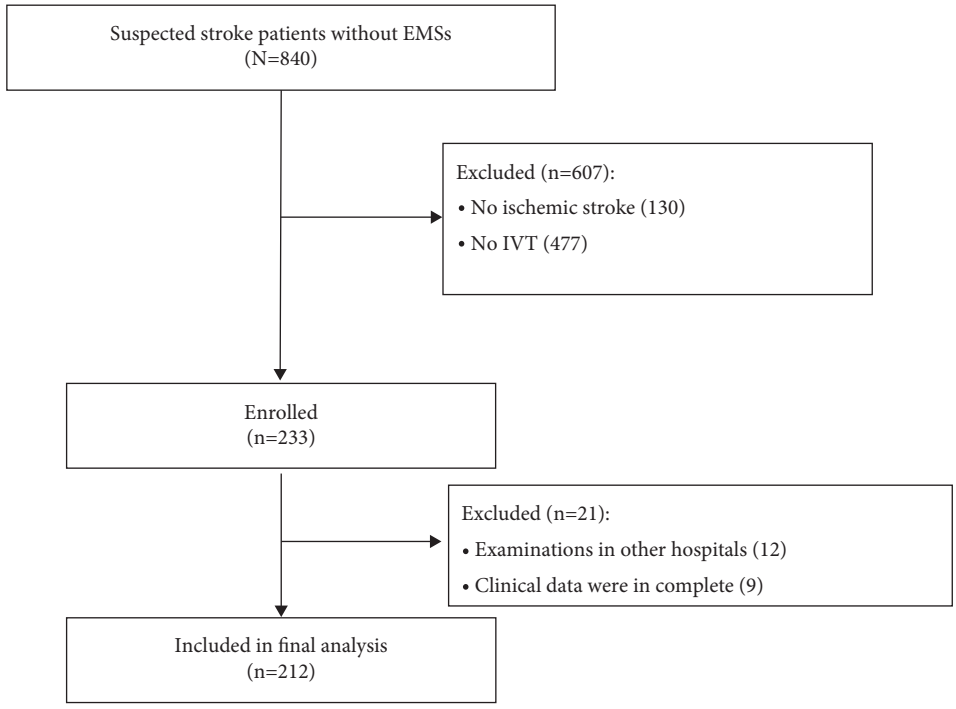

Figure 1: Screening flowchart of participants.

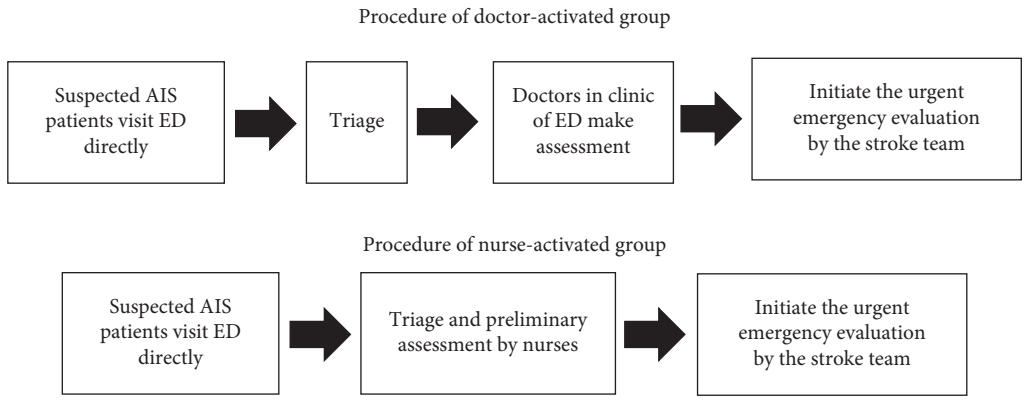

Figure 2: Procedure of the doctor-activated or nurse-activated group.

(NIHSS) was also evaluated by physicians of the hospital stroke team.

The accuracy rate of triaging-possible AIS patients is referred to as the proportion of patients with definitive AIS among all patients who received emergency evaluation services from the hospital stroke team.

In addition, DNT is defined as the time interval between when the patient enters the ED and the onset of pharmacological (tissue plasminogen activator) infusion; door-to-vein open time (DVT) is defined as the time interval from patients entering the ED to indwelling needle puncture completion; and door-to-blood sample delivery time (DBT) is defined as the time interval from patients entering the ED to the reception of the blood sample in the clinical lab.

2.5. Statistical Analysis. The constituent ratios of variables such as sex, the route of transportation to the ED, prehospital call, and visit time were compared using Chi-squared tests. Variables with normal distributions were presented as mean ± SD and were tested for significance using an independent *t*-test. Variables with skewed distributions such as time metrics, scores of NIHSS, and 7-day NIHSS were presented as medians (P_{25} and P_{75}) and compared using the Mann–Whitney *U* test. The accuracy rate of triaging-possible AIS patients among two groups was compared using Chi-squared tests. We considered *P* values less than 0.05 as statistically significant. Multiple analysis was performed using logistic analysis. All statistical analyses were conducted using Software Statistical Product and Service Solutions (SPSS) Version 23.0.

3. Results

A total of 840 suspected stroke patients without EMSs were screened, with 554 and 286 patients activated by triage nurses and doctors, respectively. There were no significant differences between the two groups with the accuracy of finally diagnosing stroke patients (triage nurse-activated group: 83.9% vs. doctor-activated group: 85.7%, $P = 0.291$).

3.1. Baseline Characteristics of Patients. A total of 212 AIS patients accepted intravenous thrombolysis and were included in this study, of whom 137 (64.6%) received triage nurse-activated emergency evaluation. The age of all participants ranged from 20 to 97 years. The mean age of the triage nurse-activated group was 61.20 ± 11.75 years, and 73.0% of participants were male. There was a median NIHSS score of 5.

There was no significant difference between the two groups with regard to the distribution of sex, visit time ($P > 0.05$), average age ($P > 0.05$), and median score of NIHSS ($P = 0.094$), and detailed data are listed in Table 1.

3.2. Door-to-Needle Time in Two Groups. DNT of the triage nurse-activated group was significantly reduced compared with the doctor-activated group (28 (26, 32.5) min vs. 30 (28, 40) min, $P = 0.001$). In addition, DVT (7 (4, 10) min vs. 8 (5, 12) min, $P = 0.025$) and DBT (15 (13, 21) min vs. 19 (15, 26) min, $P = 0.001$) in the triage nurse-activated group were also shorter than those in the doctor-activated group (Table 2).

After adjustment for age, sex, and the severity of stroke, DNT less than 45 min was seen in 95.6% of patients in the triage nurse-activated group and 84% of the other group ($P = 0.011$, OR 3.972, 95% CI 1.375–11.477), which indicated that triage nurse-activated emergency evaluation was strongly associated with DNT less than 45 min (Table 3).

3.3. 7-Day NIHSS Score. There was no significant difference in median 7-day NIHSS scores between the two groups (case group: 2 vs. control group: 1, $P = 0.893$).

4. Discussion

This retrospective study revealed that triage nurse-activated urgent emergency evaluation could significantly reduce DNT as well as DVT and DBT with comparable accuracy of final diagnosis among stroke patients with doctor-activated emergency evaluation. In addition, nurse-activated emergency evaluation of the hospital stroke team was strongly associated with DNT less than 45 minutes.

Since intravenous thrombolysis has proven effective for acute ischemic stroke (AIS) patients [19, 20], the association between shorter DNT and a better functional outcome has been widely explored [3, 4]. In addition to better short-term functional outcomes, a recent study published in JAMA revealed that shorter DNT was also correlated with better long-term outcomes and each 15-minute increase in DNT was distinctively associated with higher all-cause mortality within 90 minutes after ED arrival [14]. Thus, it is pivotal to reduce DNT for better functional outcomes. EMSs have been reported to be an effective prehospital strategy to reduce the time metrics of stroke treatment. However, many patients still failed to use EMSs. Other promising in-hospital opportunities to reduce DNT still need to be explored for patients who do not use EMSs.

As the first contact medical personnel and the whole-process manager of stroke patients, nurses perform a vital role in evaluation, diagnosis, and treatment [21, 22]. Recent studies have demonstrated the effectiveness of nurses in the treatment of stroke patients [22]. A nurse-led stroke team implementation may be an effective method for improving time-sensitive metrics of stroke care and increasing institutional compliance with recommended national guidelines [23]. Furthermore, improving the ability to recognize and care for stroke patients by more specific training in stroke nurses is an important factor, which can reduce the delay of intravenous thrombolysis in the hospital and help expedite AIS-presenting patients' arrival to the hospital after stroke [24]. In our study, nurse-activated emergency evaluation decreased DNT as well as other time metrics of treatment for AIS patients.

The benchmark of DNT was set at 60 minutes by some guidelines [25, 26], yet Man et al. indicated that patients that accepted IVT whose DNT was less than 45 minutes had the lowest mortality and readmission rates [14]. Therefore, in our study, we also revealed a significant association between nurse-activated emergency evaluation and the DNT within 45 minutes, which further clarified the efficacy of nurse-activated emergency evaluation. Recently, hospitals have set a DNT goal within 60 minutes for at least 75% of patients and a DNT within 45 minutes for at least 50% of patients [27, 28]. In our study, the proportion of patients with DNT less than 45 minutes had reached 95.6% in the triage nurse-activated group.

Hence, implementation of triage nurse-activated emergency evaluation achieved elimination of the waiting period between triage and clinical reception with advancement of the evaluation and diagnosis of stroke patients in the meantime. The score of 7-day NIHSS had no significant difference between the two groups in our study, which may be due to the small sample size and short-term follow-up. And, our results showed male gender was negatively associated with DNT less than 45 min, which may also be due to the selection bias brought by the small sample size.

The successful implementation of nurse-activated emergency evaluation depends on experienced triage nurses and suitable tools in stroke recognition. The lack of knowledge and ability of triage nurses were one of the critical factors for the delay in the treatment of stroke patients [29]. It is crucial for a qualified triage nurse to have the clinical acumen and recognition of complicated conditions, strong organization skills, and proficient management and coordination abilities. Strict admittance requirements and standardized training are effective measures to guarantee the ability of triage nurses. In our study, the triage nurses were well-trained for stroke recognition, assessment, and treatment. The recognition of stroke was the first and most pivotal step for suspected AIS patients [30]. Numerous stroke recognition instruments have been developed for EMS and ED personnel to improve the sensitivity and

Table 1: Baseline patient characteristics.

	Triage nurse-activated, $n = 137$	Doctor-activated, $n = 75$	P value
Male (%)	73.0	72.0	0.873
Age (yr)	61.20 ± 11.75	63.99 ± 11.40	0.094
Visit time			
2am to 8am	15	6	0.591
8am to 5pm	62	39	
5pm to 2am	60	30	
NIHSS			
Median (P_{25}, P_{75})	5 (4, 7)	4 (3, 7)	0.094

Table 2: Outcome indicators in two groups.

Outcome indicators	Triage nurse-activated, $n = 137$	Doctor-activated, $n = 75$	P value
DNT	28 (26, 32.5)	30 (28, 40)	0.001
DVT	7 (4, 10)	8 (5, 12)	0.025
DBT	15 (13, 21)	19 (15, 26)	0.001
7-day NIHSS	2 (0, 4)	1 (0, 5)	0.893
Patients with DNT less than 45 min	131	63	0.004

Table 3: The association between nurse-activated emergency evaluation and DNT less than 45 min.

	Adjusted OR	95% CI	P
Nurse-activated emergency evaluation	3.972	1.375–11.477	0.011
Age	0.971	0.925–1.018	0.225
Male	0.268	0.096–0.752	0.012
NHISS	0.993	0.901–1.094	0.887

specificity of identification [31]. The FAST scale has been reported as one of the triage protocols in reducing door-to-CT time and DNT in patients who presented directly to the ED, which has an extremely high sensitivity for stroke recognition when used by paramedics [32, 33]. Besides, the FAST scale is easy to use and boasts a 76.9% sensitivity and a 69.4% specificity of identification for community-dwelling mild stroke patients [34]. In our study, the accuracy of diagnosing stroke patients in the triage nurse-activated group was comparable to that of the doctor-triage group.

We made great efforts focused on the elimination of the delay between triage and neurologist-performed preliminary assessment for suspected stroke patients. Our study also indicated that stroke nurses have an indispensable effect on the ED management of stroke patients. An increasing number of countries and regions have implemented stroke nurses in the ED to provide patients with whole visit services [22, 35]. Stroke nurses are not only practitioners of medical advice but also serve as managers, coordinators, and leaders of thrombolytic procedures. Stroke nurses participating in the treatment of stroke patients in the ED would increase the rescue efficiency and improve the prognosis of patients [36]. Finally, our study also provides a reference for the establishment of nurse-led stroke teams in China.

5. Limitations and Future Directions

The single source, limited size of the sample, and short period of data collection limit the statistical power of this study and the generalizability of the study results. The outcomes of AIS patients were limited by 7-day NIHSS scores without observing the outcomes of 90 days or longer. The results of our study should be tested in a multicenter study with a larger sample size in the future. Future studies may also focus on extending the study period and increasing the evaluation indexes.

The remaining opportunity for improving stroke management involves advancing triage to prehospital treatment by establishing a mobile stroke unit focused on providing whole stroke management, including prehospital, in-hospital, and posthospital treatment. Finally, the integration of screening, treating, and rehabilitation by interdisciplinary care teams is an integral area of study to facilitate quality improvement of ED services.

6. Conclusion

The emergency evaluation services activated by triage nurses would shorten the time of treatment for AIS patients based on comparable accuracy of recognition with neurologists in the ED clinic in this study, which provides a feasible opportunity to optimize the emergency department service for AIS patients who failed to use emergency medical services.

Data Availability

All supporting data are included within the article.

Conflicts of Interest

The authors declare that they have no conflicts of interest.

Acknowledgments

This study was supported by the National Natural Science Foundation of China (Nos. 81801313, 81971114, and 82001257), National Key R&D Program of China (No. 2017YFC1308405), Beijing Hospitals Authority Youth Program (No. QML20180801), General Project of Science and Technology of Beijing Municipal Education Commission(No. KM202110025018), and Beijing Municipal Administration of Hospitals Incubating Program (No. PX2019028).

References

[1] Y. Hua, L. Jia, Y. Xing et al., "Distribution pattern of atherosclerotic stenosis in Chinese patients with stroke: a multicenter registry study," *Aging and Disease*, vol. 10, no. 1, pp. 62–70, 2019.

[2] Y. Ma, Y. Liu, Z. Zhang, and G.-Y. Yang, "Significance of complement system in ischemic stroke: a comprehensive review," *Aging and Disease*, vol. 10, no. 2, pp. 429–462, 2019.

[3] J. Emberson, K. R. Lees, P. Lyden et al., "Effect of treatment delay, age, and stroke severity on the effects of intravenous thrombolysis with alteplase for acute ischaemic stroke: a meta-analysis of individual patient data from randomised trials," *The Lancet*, vol. 384, no. 9958, pp. 1929–1935, 2014.

[4] IST-3 Collaborative Group, "Effect of thrombolysis with alteplase within 6 h of acute ischaemic stroke on long-term outcomes (the third international stroke trial [ist-3]): 18-month follow-up of a randomised controlled trial," *The Lancet Neurology*, vol. 12, pp. 768–776, 2013.

[5] W. J. Powers, A. A. Rabinstein, T. Ackerson et al., "Guidelines for the early management of patients with acute ischemic stroke: 2019 update to the 2018 guidelines for the early management of acute ischemic stroke: a guideline for healthcare professionals from the american heart association/american stroke association," *Stroke*, vol. 50, no. 12, pp. e344–e418, 2019.

[6] Z. Cheng, X. Geng, J. Gao et al., "Intravenous administration of standard dose tirofiban after mechanical arterial recanalization is safe and relatively effective in acute ischemic stroke," *Aging and Disease*, vol. 10, no. 5, pp. 1049–1057, 2019.

[7] C. Borlongan, E. Russo, H. Nguyen, T. Lippert, J. Tuazon, and E. Napoli, "Mitochondrial targeting as a novel therapy for stroke," *Brain Circulation*, vol. 4, no. 3, pp. 84–94, 2018.

[8] O. Glushakova, A. Glushakov, E. Miller, A. Valadka, and R. Hayes, "Biomarkers for acute diagnosis and management of stroke in neurointensive care units," *Brain Circulation*, vol. 2, no. 1, pp. 28–47, 2016.

[9] K. Nagarajan, D. Chatterjee, S. Narayan, and R. Narasimhan, "Regional leptomeningeal collateral score by computed tomographic angiography correlates with 3-month clinical outcome in acute ischemic stroke," *Brain Circulation*, vol. 6, no. 2, pp. 107–115, 2020.

[10] X. Ji, "Forward thinking in stroke treatment: advances in cerebrovascular reperfusion and neurorehabilitation," *Brain Circulation*, vol. 1, no. 1, pp. 1-2, 2015.

[11] J. L. Saver, "Time is brain-quantified," *Stroke*, vol. 37, no. 1, pp. 263–266, 2006.

[12] J. L. Saver, G. C. Fonarow, E. E. Smith et al., "Time to treatment with intravenous tissue plasminogen activator and outcome from acute ischemic stroke," *JAMA*, vol. 309, no. 23, pp. 2480–2488, 2013.

[13] M. G. Lansberg, M. Schrooten, E. Bluhmki, V. N. Thijs, and J. L. Saver, "Treatment time-specific number needed to treat estimates for tissue plasminogen activator therapy in acute stroke based on shifts over the entire range of the modified rankin scale." *Stroke*, vol. 40, no. 6, pp. 2079–2084, 2009.

[14] S. Man, Y. Xian, D. N. Holmes et al., "Association between thrombolytic door-to-needle time and 1-year mortality and readmission in patients with acute ischemic stroke," *JAMA*, vol. 323, no. 21, pp. 2170–2184, 2020.

[15] N. Kamal, E. E. Smith, T. Jeerakathil, and M. D. Hill, "Thrombolysis: improving door-to-needle times for ischemic stroke treatment-a narrative review," *International Journal of Stroke*, vol. 13, no. 3, pp. 268–276, 2018.

[16] O. J. Ekundayo, J. L. Saver, G. C. Fonarow et al., "Patterns of emergency medical services use and its association with timely stroke treatment," *Circulation: Cardiovascular Quality and Outcomes*, vol. 6, no. 3, pp. 262–269, 2013.

[17] H. Mochari-Greenberger, Y. Xian, A. S. Hellkamp et al., "Racial/ethnic and sex differences in emergency medical services transport among hospitalized us stroke patients: analysis of the national get with the guidelines-stroke registry," *Journal of American Heart Association*, vol. 4, no. 8, Article ID e002099, 2015.

[18] Y. Ding, H. Choi, Z. Fan et al., "Recent advances in magnetic resonance imaging for stroke diagnosis," *Brain Circulation*, vol. 1, no. 1, pp. 26–37, 2015.

[19] T. Leng and Z.-G. Xiong, "Treatment for ischemic stroke: from thrombolysis to thrombectomy and remaining challenges," *Brain Circulation*, vol. 5, no. 1, pp. 8–11, 2019.

[20] R. Leigh, P. Heidari, S. Blayney, J. Butler, E. Hitomi, and M. Luby, "Frequency of thrombolytic targets in stroke patients presenting in an extended time window," *Brain Circulation*, vol. 6, no. 3, pp. 163–168, 2020.

[21] Y. Ding, K. Elkin, U. Khan, and M. Hussain, "Developments in hybrid operating room, neurointensive care unit, and ward composition and organization for stroke management," *Brain Circulation*, vol. 5, no. 2, pp. 84–89, 2019.

[22] S. Middleton, S. Dale, N. W. Cheung et al., "Nurse-initiated acute stroke care in emergency departments," *Stroke*, vol. 50, no. 6, pp. 1346–1355, 2019.

[23] C. J. Heiberger, S. Kazi, T. I. Mehta, C. Busch, J. Wolf, and D. Sandhu, "Effects on stroke metrics and outcomes of a nurse-led stroke triage team in acute stroke management," *Cureus*, vol. 1, Article ID e5590, 2019.

[24] Z. Liu, Y. Zhao, D. Liu et al., "Effects of nursing quality improvement on thrombolytic therapy for acute ischemic stroke," *Frontiers in Neurology*, vol. 9, p. 1025, 2018.

[25] M. J. Alberts, G. Hademenos, R. E. Latchaw, A. Jagoda, J. R. Marler, and M. R. Mayberg, "Recommendations for the establishment of primary stroke centers," *JAMA*, vol. 283, no. 23, pp. 3102–3109, 2000.

[26] W. J. Powers, A. A. Rabinstein, T. Ackerson et al., "2018 guidelines for the early management of patients with acute ischemic stroke: a guideline for healthcare professionals from the American heart association/American stroke association," *Stroke*, vol. 49, no. 3, pp. e46–e110, 2018.

[27] Y. Xian, H. Xu, B. Lytle et al., "Use of strategies to improve door-to-needle times with tissue-type plasminogen activator in acute ischemic stroke in clinical practice: findings from target: stroke," *Circulation: Cardiovascular Quality and Outcomes*, vol. 10, no. 1, 2017.

[28] G. C. Fonarow, E. E. Smith, J. L. Saver et al., "Improving door-to-needle times in acute ischemic stroke: the design and rationale for the american heart association/american stroke

association's target: Stroke initiative," *Stroke*, vol. 42, no. 10, pp. 2983–2989, 2011.

[29] A. Mowla, H. Kamal, M. Ahmed et al., "Strokes occurring in the hospital: symptom recognition and eligibility for treatment in the intensive care units versus hospital wards," *Brain Circulation*, vol. 6, no. 3, pp. 196–199, 2020.

[30] H. F. Li, L. Yang, N. N. Li et al., "Review of influencing factors of prehospital and in-hospital delay among stroke patients," *Journal of Nursing Science*, vol. 16, pp. 98–101, 2018.

[31] M. Rudd, D. Buck, G. A. Ford, and C. I. Price, "A systematic review of stroke recognition instruments in hospital and prehospital settings," *Emergency Medicine Journal*, vol. 33, no. 11, pp. 818–822, 2016.

[32] I. Sibon, F. Rouanet, W. Meissner, and J. M. Orgogozo, "Use of the triage stroke panel in a neurologic emergency service," *The American Journal of Emergency Medicine*, vol. 27, no. 5, pp. 558–562, 2009.

[33] R. T. Fothergill, J. Williams, M. J. Edwards, I. T. Russell, and P. Gompertz, "Does use of the recognition of stroke in the emergency room stroke assessment tool enhance stroke recognition by ambulance clinicians?" *Stroke*, vol. 44, no. 11, pp. 3007–3012, 2013.

[34] B. B. Sun, B. Yao, C. Fang, Y. X. Wang, M. X. Li, and L. Ma, "Comparison of application value of three stroke screening scales in rapid referral of suspected stroke patients in community," *Chinese Journal of Stroke*, vol. 15, pp. 126–129, 2020.

[35] S. Mainali, S. Stutzman, S. Sengupta et al., "Feasibility and efficacy of nurse-driven acute stroke care," *Journal of Stroke and Cerebrovascular Diseases*, vol. 26, no. 5, pp. 987–991, 2017.

[36] P. Zhang, T. T. Zhang, L. J. Yu et al., "Impact of stroke nurses on treatment efficiency of acute ischemic stroke," *Chinese Journal of Stroke*, vol. 5, pp. 425–429, 2018.

Hindawi
Evidence-Based Complementary and Alternative Medicine
Volume 2022, Article ID 8550307, 11 pages
https://doi.org/10.1155/2022/8550307

Research Article

miR-96-5p Induces Orbital Fibroblasts Differentiation by Targeting Smad7 and Promotes the Development of Thyroid-Associated Ophthalmopathy

Jianshu Kang, Yunqin Li, Yue Zou, Zhijian Zhao, Linan Jiao, and Hong Zhang

Department of Ophthalmology, The Affiliated Hospital of Yunnan University, Kunming 650021, China

Correspondence should be addressed to Hong Zhang; jaccy6688@163.com

Received 31 August 2021; Revised 1 December 2021; Accepted 27 January 2022; Published 27 February 2022

Academic Editor: Feng Zhang

Background. Recent evidence shows that adipogenic differentiation of orbital fibroblasts (OFs) promotes the development of thyroid-associated ophthalmopathy (TAO), an organ-specific immune disease. Furthermore, miR-96-5p has been linked to adipogenic differentiation of C2C12 myoblasts and is significantly correlated with the severity of TAO. The purpose of this study is to look into the role of miR-96-5p in the adipogenesis of OFs with TAO. *Methods*. The orbital tissues from TAO patients and non-TAO participants were collected, and primary OFs were isolated and cultured for further analysis. miR-96-5p expression was examined using qRT-PCR. The adipogenic differentiation of OFs was then studied. *Results*. Orbital fibroblasts isolated from adipose tissues of TAO patients (t-OFs) demonstrated greater adipogenic differentiation ability than OFs isolated from adipose tissues of non-TAO participants. miR-96-5p was found to be overexpressed in the orbital tissues of TAO patients and t-OFs. Further research revealed that miR-96-5p, by targeting Smad7, could exacerbate PPAR-γ/C/EBPα signaling-induced adipogenic differentiation of t-OFs. However, inhibiting miR-96-5p could block t-OFs adipogenic differentiation-mediated adipogenesis via Smad7/PPAR-γ/C/EBPα. *Conclusions*. miR-96-5p plays a critical regulatory role in the development of TAO by targeting Smad7 and promoting adipogenic differentiation of OFs.

1. Introduction

Thyroid-associated ophthalmopathy (TAO), also known as Graves' ophthalmopathy, is an organ-specific immune disease marked by increased adipose/connective tissue volume and the potential for blindness. It is one of the most common ophthalmic diseases in clinical practice, with TAO having the highest prevalence among orbital diseases [1, 2]. TAO, on the other hand, is a common extrathyroid manifestation and has in recent years been linked to hypothyroidism, subacute thyroiditis, and thyroid cancer [3]. At present, TAO research currently focuses primarily on immunology [4], pathology [5], genetic background [6, 7], and environmental factors [8, 9], but the pathogenesis and pathogenesis of TAO remain unknown [10].

Emerging evidence shows that TAO symptoms are caused by inflammation of orbital connective tissue. The infiltration of inflammatory cells, the accumulation of extracellular matrix proteins, the proliferation of fibroblasts, and the increasing of orbital adipose tissue causes the expansion of orbital connective tissue This results in orbital tissue fibrosis, orbital tissue remodeling, and destruction of adjacent eyeball structure and function, promoting the development of TAO [11, 12]. Orbital fibroblast (OFs) are thought to be important immune targets and effector cells in the development of TAO [13, 14]. Current research evidence indicates that fibrosis and inflammatory factor secretions mediated by OFs play a role in the development of TAO [15]. Furthermore, adipogenic differentiation of OFs is important in the increase of orbital adipose tissue in TAO [16, 17], and adipogenesis mediated by adipogenic differentiation of

activated OFs may result in the orbital protrusion in TAO patients [18]. However, the molecular mechanism of adipogenic differentiation of orbital fibroblasts during TAO needs to be investigated further.

MicroRNAs (miRNAs) are endogenous single-stranded noncoding small mRNAs. Approximately, 90% of miRNAs are expressed differently in different parts of the human eye, and each miRNA can play a unique role in eye tissues [19]. Moreover, an increasing body of evidence suggests that miRNAs are critical in regulating adipogenesis [20]. miR-96-5p has been linked to adipogenic differentiation of C2C12 myoblasts [21]. A previous study found that miR-96-5p was highly expressed in thyroid tissues of patients with autoimmune thyroid disease and was significantly positively correlated with TAO severity [22]. These findings suggested that high expression of miR-96-5p is associated with higher severity of diseases in patients with Graves' orbitopathy (GO), including active eye disease, goiter, high antibody titer, and/or higher recurrence rate. Previous research on miR-96-5p has mostly focused on its role in tumor occurrence and development [23–25]. Additionally, one study found miR-96-5p to be a potential biomarker for multisystem atrophy, Parkinson's disease, and gestational diabetes mellitus [26]. However, the role of miR-96-5p in the adipogenic differentiation of OFs in TAO is still unknown.

Smad7 is a key negative regulator in the TGF-β signal transduction pathway, and its role in osteogenic differentiation has been well documented [27, 28]. Recent evidence has shown a role for Smad7 in adipogenesis [29, 30]. While peroxisome proliferator-activated receptor-γ (PPAR-γ) signal transduction has been identified as the primary inducer of adipogenesis [31, 32], studies have revealed interactions between TGF-β signaling and PPAR-γ signaling [33]. Studies have shown that the Smad signal plays an important role in periorbital fibrosis in TAO [34–36], and Smad7 is predicted to be one of the target genes of miR-96-5p (StarBase, URL: http://starbase.sysu.edu.cn/agoClipRNA.php?source=mRNA). The present study, however, explores whether miR-96-5p plays a role in adipogenic differentiation of OFs during TAO progression via Smad7/PPAR-γ signaling.

The present study demonstrated that Smad7 is a target gene of miR-96-5p, and miR-96-5p is noticeably overexpressed in TAO orbital adipose/connective tissues and OFs. The findings provide evidence that miR-96-5p promotes adipogenic differentiation of OFs by targeting Smad7 and activating PPAR-γ signaling, thereby promoting TAO adipogenesis.

2. Materials and Methods

2.1. Sample Collection and Cell Culture. Orbital adipose tissue was obtained from 15 TAO patients and 10 non-TAO subjects as described in a previous study [16]. All participants provided informed written consent. The Institutional Review Board (IRB) of the Affiliated Hospital of Yunnan University approved this study (approval no. 2019173). The following were the inclusion criteria for TAO patients: (1) patients had orbital decompression for proptosis correction; (2) patients were euthyroid and had inactive TAO status at the time of surgery; (3) patients had not been treated with steroids or radiation therapy for at least 3 months. For non-TAO subjects: (1) age- and sex-matched to TAO subjects; (2) no thyroid or other inflammatory diseases were present; (3) control subjects underwent cosmetic upper and lower blepharoplasty.

Cultures of primary orbital fibroblasts (OFs) were grown following previously described methods [37]. Briefly, the tissue blocks were cut into pieces and placed in a DMEM medium containing 20% FBS, 100 U/mL penicillin, and 20 μg/mL gentamicin from Hyclone Laboratories (Logan, UT). The explants were cultured until fibroblasts formed a monolayer and grew out of the explants. The monolayer cells were then mildly digested with trypsin/EDTA, and subcultured in a DMEM medium containing 10% FBS in a humidified 5% CO_2 incubator at 37°C. Following cell sorting and flow cytometry detection of the surface antigen of the obtained cells, cells of the third to seventh generations in good condition were used for subsequent cell experiments. In comparison to OFs obtained from orbital adipose tissues of non-TAO subjects (n-OFs), the orbital adipose tissues obtained from TAO patients were referred to as t-OFs in the following study.

2.2. Cell Transfection. Orbital fibroblasts were transfected with the miR-96-5p inhibitor, siRNA of Smad7 (siSmad7), and each control following the manufacturer's protocols. The miR-96-5p inhibitor and siSmad7 were obtained from Guangzhou RiboBio Biotechnology Co., Ltd. (Guangzhou; China). Cells were transfected with 50 nM of miR-96-5p inhibitor or siSmad7 using commercial Lipofectamine® 2000 transfection reagent (Invitrogen; Thermo Fisher Scientific, Inc.; USA) following the manufacturer's instructions and recent study [38]. Briefly, the cells were incubated with 50 nM of miR-96-5p inhibitor or siSmad7 for 48 to 72 hours and maintained under normal growth conditions. At 72 hours, qRT-PCR was used to confirm the efficiency of transfection of miR-96-5p inhibitor and siSmad7.

2.3. Dual-Luciferase Reporter Assay. The binding sites between miR-96-5p and Smad7 were predicted with StarBase (URL: http://starbase.sysu.edu.cn/agoClipRNA.php?source=mRNA). Luciferase vectors containing the 3'UTR of human Smad7 with the miR-96-5p binding sites and mutant miR-96-5p binding sites were purchased from Shanghai GenePharma Co., Ltd. The vectors were cotransfected into 293T cells with miR-96-5p mimics by Lipofectamine® 2000 transfection reagent (Invitrogen; Thermo Fisher Scientific, Inc.; USA). The luciferase reporter activity was measured after 48 h using a Dual-Luciferase® eporter Assay System (Promega Corporation). This assay was performed according to the previous description [38].

2.4. Quantitative Real-Time Polymerase Chain Reaction (qRT-PCR). The expression level of RNA was determined by qRT-PCR according to the previous study [38]. In detail, total

RNA was extracted from tissues and cells using Trizol reagent (Invitrogen; Thermo Fisher Scientific, Inc.; USA) according to the manufacturer's instructions to detect the expression levels of miR-96-5p in orbital tissues and OFs. miRNA qRT-PCR was performed using a TaqMan™ MicroRNA Reverse Transcription kit (Applied Biosystems; Thermo Fisher Scientific, Inc.; USA) and a TaqMan Universal PCR Master Mix (Applied Biosystems; Thermo Fisher Scientific, Inc.; USA). The $2^{-\Delta\Delta Cq}$ method [39] was used to present the relative expressions of miRNA as fold changes, and U6 was used to normalize the miRNA level. The primer sequences used were as follows: human U6, forward: 5′-CTCGCTTCGGCAGCACATATACT-3′and reverse: 5′-ACGCTTCACGAATTTGCGTGTC-3′; human miR-96-5p, forward: 5′- CAGTCGTTTTTACACGATCAC-3′ and reverse: 3′- GGTCCAGTTTTTTTTTTTTTTTAAACC-5′.

2.5. Western Blotting. Orbital tissues and fibroblast cells were harvested and lysed in RIPA buffer containing protease inhibitors (Invitrogen; USA), and protein concentrations were determined using the Pierce BCA assay (Invitrogen; USA), following the manufacturer's protocols. The proteins in lysates (40 μg of each sample) were then separated by SDS-PAGE and transferred to PVDF membranes. The membranes were blocked with 5% nonfat milk for 1 h at room temperature and subsequently incubated with primary antibodies overnight at 4°C. Expression levels of the proteins of interest were analyzed using primary antibodies against Smad7, PPAR-γ, C/EBPα, adiponectin, and FABP-4 purchased from Abcam, UK, at a dilution of 1 : 1000. Membranes were rinsed three times with 1X Tris-buffered saline containing 0.5% Tween-20 (TBST) and then incubated for 1 h with anti-rabbit IgG (1 : 2000, Abcam, UK) horseradish peroxidase-conjugated secondary antibody. Membranes were rinsed three times with TBST and examined with an ECL kit (Bio-Rad Laboratories, Inc.). The protein bands were quantified using the ImageJ software (version 1.52a; National Institutes of Health), and GAPDH (1 : 1000, Abcam, UK) was used as a loading control. Each experiment was performed in triplicate.

2.6. Oil Red O Staining. Briefly, cells were fixed in 4% paraformaldehyde (PFA) for 15 min and then washed three times with PBS for 5 min each. After that, cells were incubated for 10–15 min with oil red O working solution (oil red: distilled water = 3 : 2) at room temperature. Following that, 60% isopropanol was used to separate the samples for 30 s before washing with distilled water for 1 min. Finally, the filter paper was used to absorb the surrounding water, and the cells were sealed with glycerin gelatin. As a result, the lipid droplets stained orange-red to bright red.

2.7. Statistical Analyses. All experiments were performed at least three times independently, with at least three cell cultures harvested from different individuals. The results are presented in the form of the mean ± standard deviation. Differences between groups were assessed by Students' *t*-tests and one-way ANOVA or two-way ANOVA followed by Bonfferroni's multiple comparisons test. In all analyses, $P < 0.05$ denoted statistical significance.

3. Results

3.1. miR-96-5p Is Highly Expressed in Orbital Tissue and Orbital Fibroblasts of TAO Patients. The expression of miR-96-5p in orbital tissues and OFs from TAO patients was investigated in qRT-PCR assays. The results showed that miR-96-5p was significantly upregulated in the orbital tissues of TAO patients compared to non-TAO participants (Figure 1(a)). Furthermore, the expression of miR-96-5p in t-OFs was noticeably higher than that in n-OFs (Figure 1(b)), whereas the relative expression level of miR-96-5p in t-OFs was nearly 1.5 times that of n-OFs. These findings suggested that miR-96-5p upregulation may play an important role in the progression of TAO and influence the bioactivity of t-OFs.

3.2. t-OFs Show a Higher Ability of Adipogenesis. PPAR-γ/C/EBPα signaling is important in adipogenic differentiation; as such, the expression of PPAR-γ/C/EBPα signaling related proteins as well as adipogenesis markers such as adiponectin and FABP-4 in n-OFs and t-OFs was determined using western blotting. The expressions of PPAR-γ, C/EBPα, adiponectin, and FABP-4 in t-OFs were significantly increased (Figures 2(a)–2(e)). Furthermore, oil red O staining revealed noticeable lipid accumulation in t-OFs, whereas no lipid accumulated in n-OFs (Figures 2(f), 2(g)). These data indicate that the number of red O-positive cells in t-OFs was nearly 3 times greater than that in n-OFs. Collectively, the findings demonstrate that t-OFs have a greater capacity for adipogenesis than n-OFs, which may be due to the high activation of PPAR-γ/C/EBPα signaling.

3.3. miR-96-5p Inhibition Reduces Adipogenesis of t-OFs. To confirm the role of miR-96-5p in t-OF adipogenesis, a miR-96-5p inhibitor was transfected into t-OFs, and the expression of miR-96-5p and related proteins as well as t-OF lipid accumulation were measured. The miR-96-5p inhibitor significantly impeded the expression of miR-96-5p in t-OFs (Figure 3(a)). Also, the miR-96-5p inhibitor significantly decreased the expressions of PPAR-γ, C/EBPα, adiponectin, and FABP-4 in t-OFs (Figures 3(b)–3(f)). Furthermore, miR-96-5p inhibition reduced t-OF lipid accumulation (Figures 3(g), 3(h)); of note, following miR-96-5p inhibition, the positive rate of oil red O staining in t-OFs cells decreased by more than 1.5 times. These findings suggest that knocking out miR-96-5p can inhibit t-OF adipogenesis.

3.4. miR-96-5p Targets and Inhibits the Expression of Smad7. Previous research revealed that Smad7 is involved in the regulation of adipogenesis [29, 30]; as such, we examined the expression of Smad7 in t-OFs western blotting. The results showed lower Smad7 expression in t-OFs than in n-OFs (Figure 4(a)). Meanwhile, miR-96-5p inhibition promoted

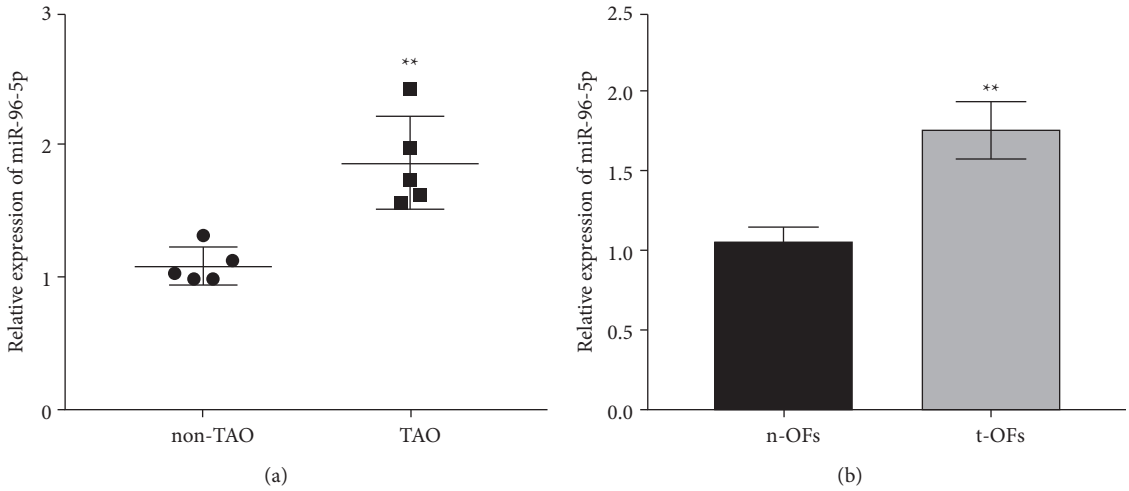

Figure 1: The expression of miR-96-5p in orbital tissues and orbital fibroblasts from non-TAO and TAO participants. (a) The relative expression of miR-96-5p in orbital tissues measured by qRT-PCR. (b) The relative expression levels of miR-96-5p in OFs separated from adipose tissues with or without TAO. $^{**}P < 0.01$ vs non-TAO or n-OFs group by two-tailed Students' *t*-test.

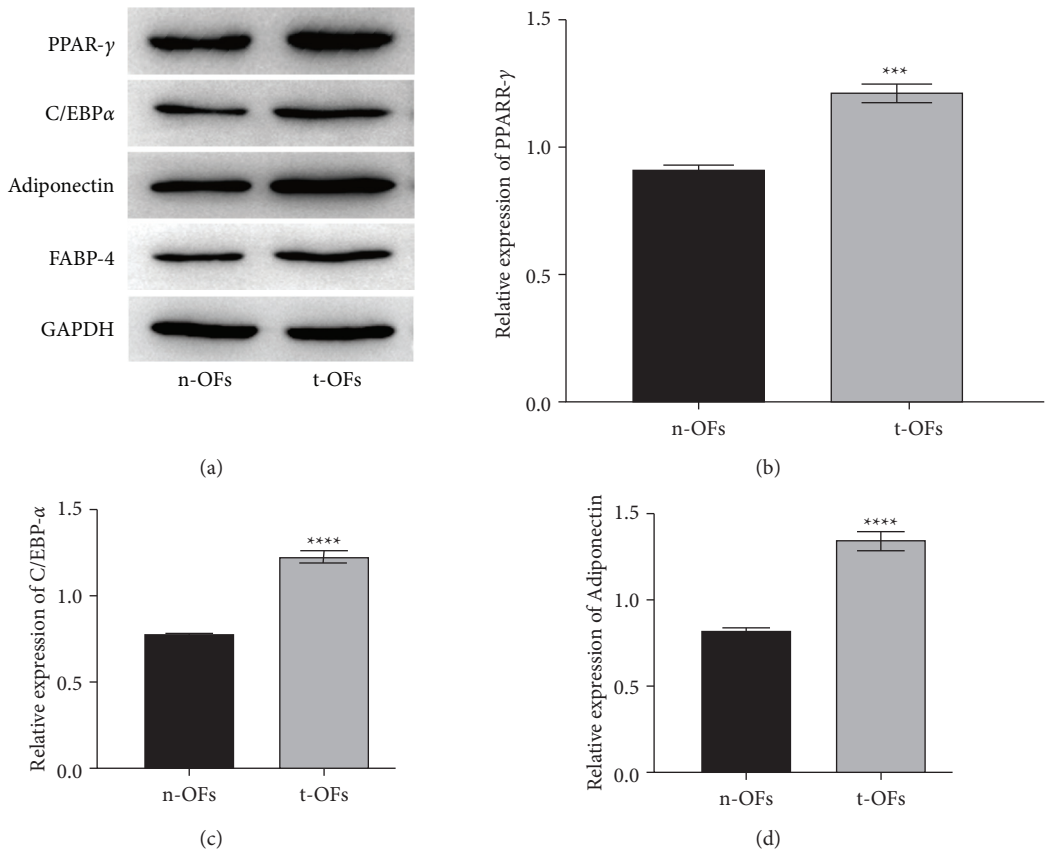

Figure 2: Continued.

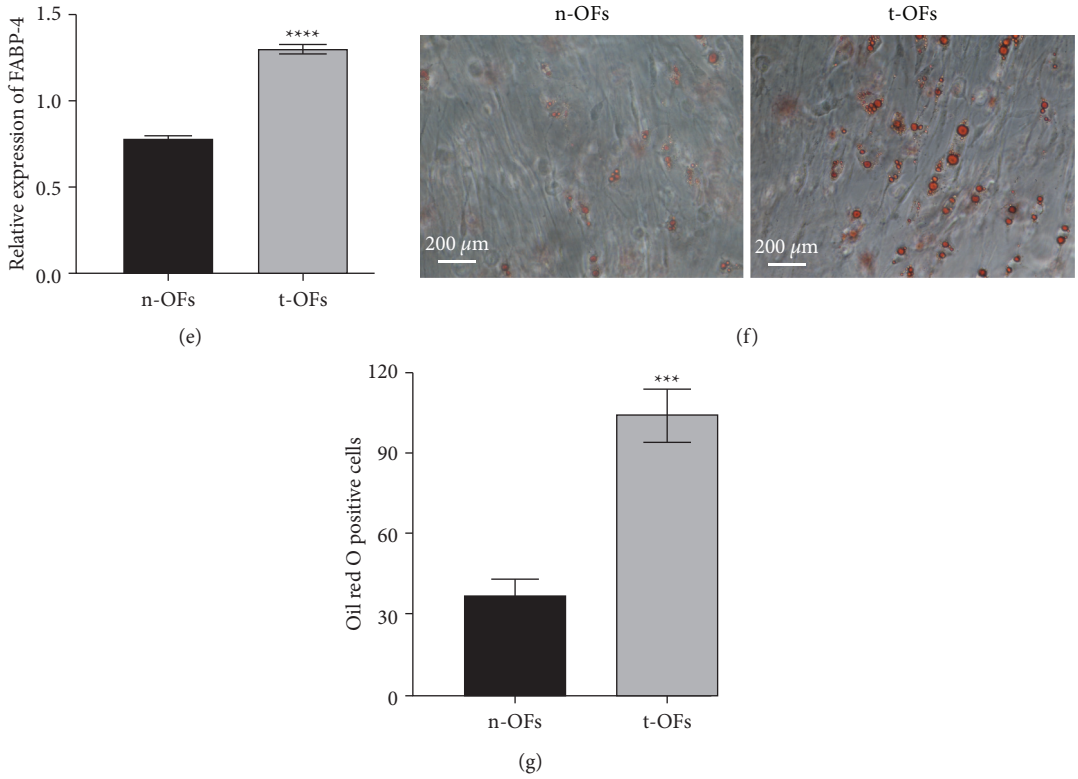

Figure 2: The adipogenesis ability of OFs from non-TAO and TAO participants. (a) The representative bands of western blotting for PPAR-γ, C/EBPα, adiponectin, and FABP-4. (b–e) The relative expression levels of PPAR-γ, C/EBPα, adiponectin, and FABP-4 in n-OFs and t-OFs. (f) The representative images of oil red O staining on n-OFs and t-OFs. (g) Relative oil red O-positive cell rate measured by ImageJ. $^{***}P < 0.001$, $^{****}P < 0.0001$vs n-OFs group by two-tailed Students' t-test.

Smad7 expression in t-OFs (Figure 4(b)). Furthermore, Smad7 was predicted to be one of the target genes of miR-96-5p, and there was a binding site between miR-96-5p and 3'UTR of Smad7 (Figure 4(c)). A dual-luciferase reporter assay confirmed that miR-96-5p could precisely bind to wild-type Smad7 3'UTR (Figure 4(d)). These findings suggested that miR-96-5p may promote t-OF adipogenesis by targeting Smad7.

3.5. miR-96-5p Inhibition Decreases t-OF Adipogenesis by Increasing Smad7 Expression. To investigate whether miR-96-5p promotes t-OFs adipogenic differentiation of t-OFs, miR-96-5p inhibitor and siSmad7 were cotransfected into t-OFs, and protein expressions and lipid accumulation in t-OFs were measured. Smad7 expression was increased by inhibiting miR-96-5p but decreased by siSmad7 (Figures 5(a) and 5(b)). siSmad7 also increased the expressions of PPAR-γ, C/EBPα, adiponectin, aind FABP-4 in t-OFs, which were inhibited by the miR-96-5p inhibitor (Figures 5(c)–5(g)). Of note, the lipid accumulation in t-OFs inhibited by miR-96-5p inhibition was also reversed by siSmad7 (Figures 5(h) and 5(i)), and after miR-96-5p inhibition, the positive rate of oil red O staining in t-OFs cells decreased by about 2 times, but after adding siSmad7 to inhibit the expression of Smad7, the positive rate of oil red O staining in t-OFs cells increased to about 90% of that in the control group. These findings suggested that miR-96-5p promotes t-OF adipogenic differentiation by specifically inhibiting Smad7 expression and that miR-96-5p inhibition can block t-OF adipogenic differentiation by upregulating Smad7 expression and inhibiting PPAR-γ/C/EBPα signaling.

4. Discussion

Thyroid-related ophthalmopathy (TAO) is a common ophthalmic disease, with the highest incidence among orbital diseases that can cause blindness [1, 2]. TAO is distinguished by an increase in adipose/connective tissues. Compelling evidence shows that TAO symptoms are caused by inflammation of the orbital connective tissue [11, 12]. Also, researchers have demonstrated that adipogenesis mediated by adipogenic differentiation of orbital fibroblasts (OFs) plays an important role in TAO progression [16, 17]. Previous research has shown that many genes and signal transduction pathways, such as insulin-like growth factor-1 receptor, FABP4/5, APOE, PPARG and ADIPOQ, PI3K Akt signal transduction, cAMP signal transduction, AGE-RAGE signal, and Wnt signal pathway, are involved in the adipogenesis of TAO patients [40, 41]. This study confirmed that OFs isolated from adipose tissues of TAO patients had greater adipogenic differentiation ability than OFs isolated from adipose tissues of non-TAO participants. PPAR-γ/C/

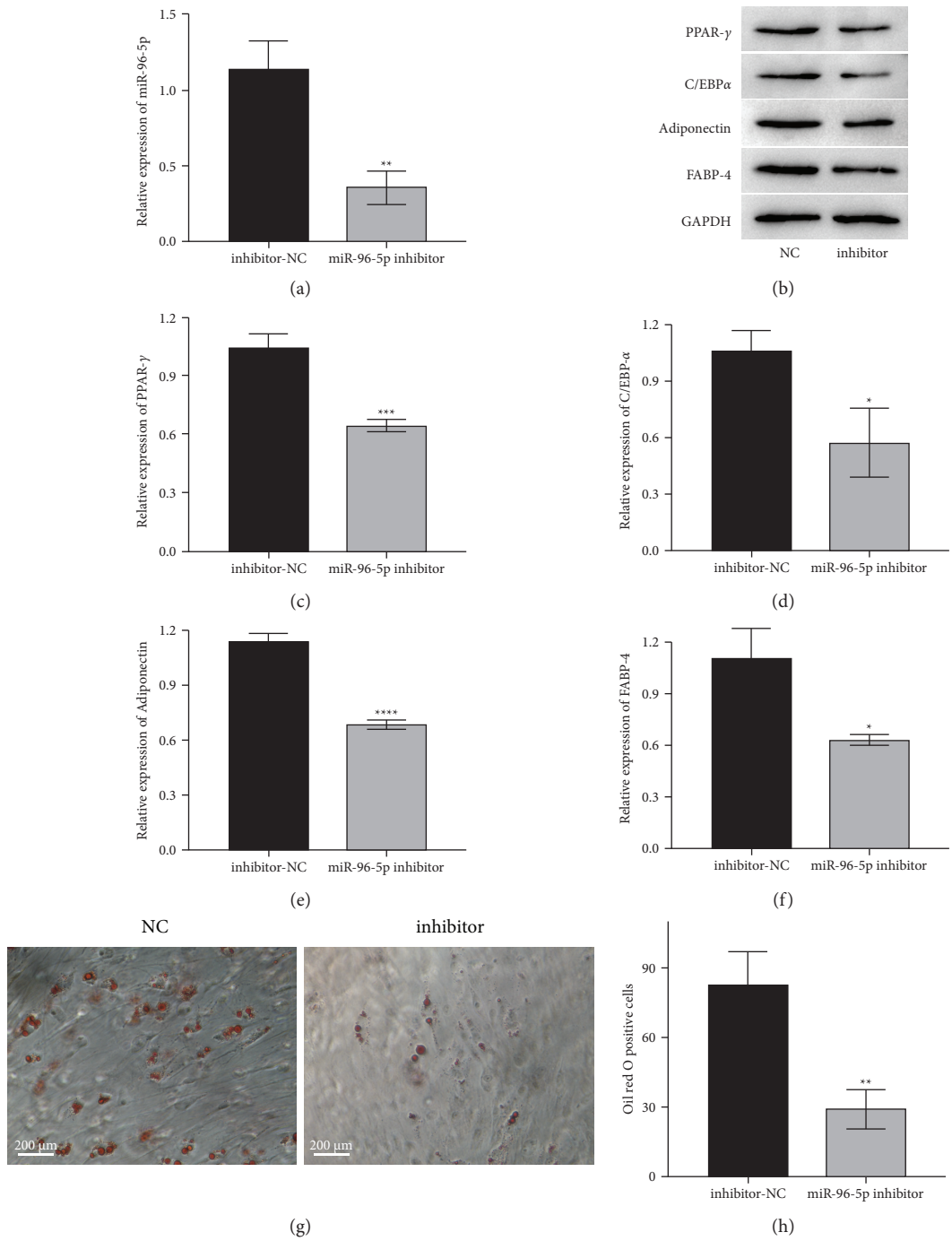

Figure 3: The role of miR-96-5p knockdown in adipogenic differentiation of t-OFs. (a) The relative expression of miR-96-5p in different groups of t-OFs. (b) The representative bands of western blotting for PPAR-γ, C/EBPα, adiponectin, and FABP-4. (c–f), The relative expression levels of PPAR-γ, C/EBPα, adiponectin, and FABP-4 in different groups of t-OFs. (g) The representative images of oil red O staining on t-OFs. (h) Relative oil red O-positive cell rate measured by ImageJ. $^{*}P < 0.05$, $^{**}P < 0.01$, $^{***}P < 0.001$, $^{****}P < 0.0001$, vs inhibitor-NC group by two-tailed Students' t-test.

EBPα signaling is linked to adipogenic differentiation; adiponectin and FABP-4 are adipogenic markers, and their expressions were upregulated in t-OFs.

Recent evidence shows that miRNAs play an important role in the development of TAO. For instance, Jang et al. revealed that miR-27 could inhibit the adipogenic differentiation of OFs in Graves' disease patients [16]. Elsewhere, miR-183 and miR-96 were found to potentially contribute to the progression of Graves' orbitopathy by regulating T cell activation [42], whereas miR-146a could regulate the fibrosis of OFs in Graves' orbitopathy [35, 43]. miR-96-5p was found to be significantly positively correlated with TAO severity [22], and it was also revealed to play a role in adipogenic differentiation of C2C12 myoblasts [21]. In the present

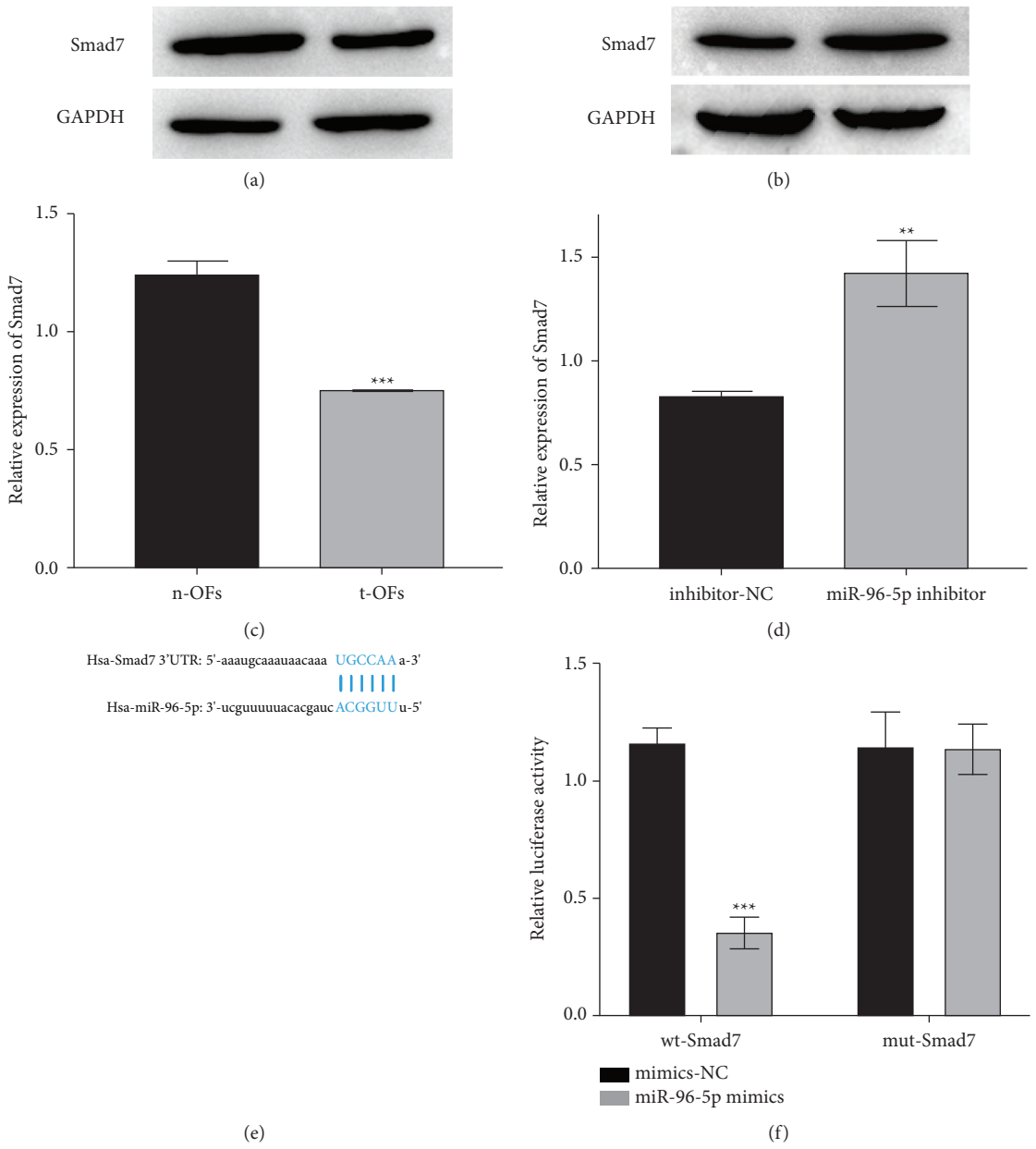

Figure 4: The relationship between miR-96-5p and Smad7. (a) The expression of Smad7 in n-OFs and t-OFs. (b) The expression of Smad7 in t-OFs with or without miR-96-5p inhibitor transfection. (c) The binding site between miR-69-5p and 3'UTR of Smad7. (d) The results of the dual-luciferase report assay. $^{**}P < 0.01$, $^{***}P < 0.001$, vs their control group, (a, b) were detected by two-tailed Students' *t*-test, and (c) was detected by two-way ANOVA.

study, we discovered that miR-96-5p was overexpressed in orbital tissues and OFs of TAO patients. Further research revealed that miR-96-5p could aggravate PPAR-γ/C/EBPα pathway-induced adipogenic differentiation of t-OFs by specifically inhibiting Smad7 expression. Inhibiting miR-96-5p, on the other hand, could inhibit t-OF adipogenic differentiation-mediated adipogenesis via Smad7/PPAR-γ/C/EBPα. Notably, in addition to adipogenic differentiation, OFs-mediated orbital fibrosis and inflammatory factor release are important in the development and progression of TAO [15]. Meanwhile, miRNA expression acted as a key regulator in OFs-mediated orbital fibrosis and inflammatory factor release. Previous research found that miR-146a could inhibit TGF-β-induced OFs fibrosis [35]. Other studies have demonstrated that miR-146a could promote OFs proliferation and proinflammatory IL-6 expression by targeting Notch2 [43, 44] and that miR-21 and miR-155 could also be involved in fibrosis and inflammation caused by OFs in orbital tissues [36, 45, 46]. These findings suggest that miRNAs play an important role in the development of TAO and that miRNAs may be potential biomarkers and therapeutic targets for TAO.

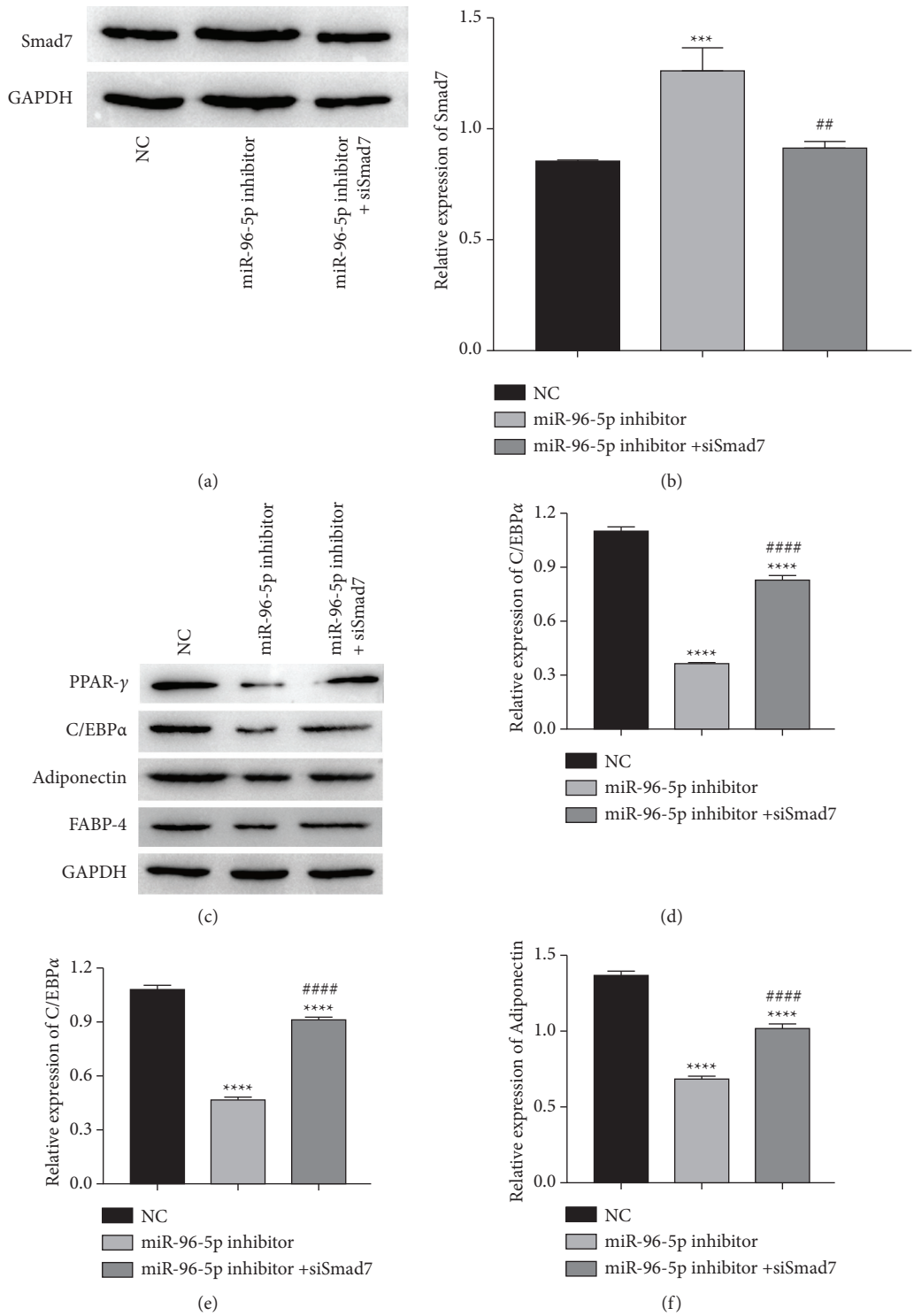

Figure 5: Continued.

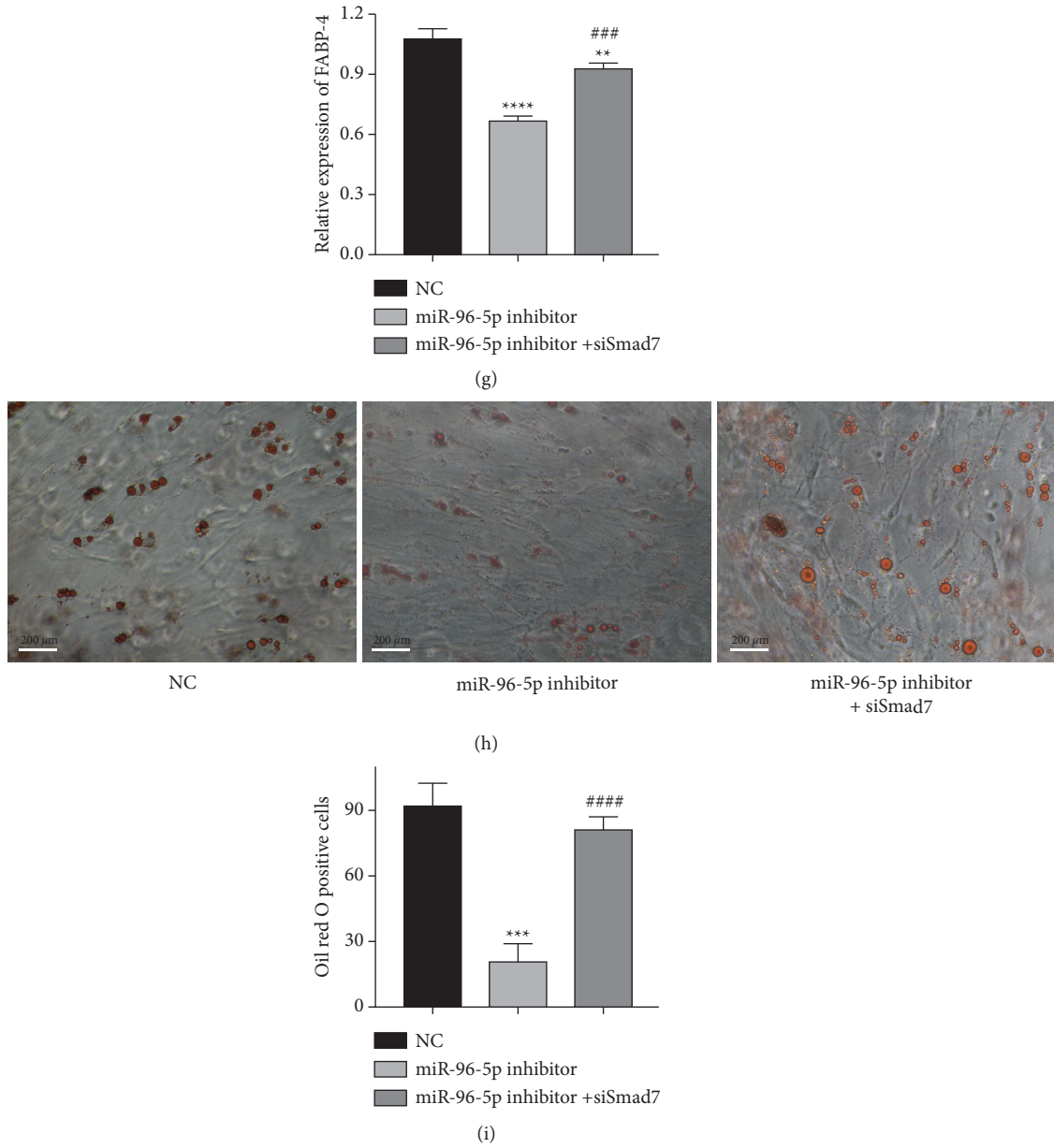

Figure 5: The effect of Smad7 on miR-96-5p knockdown mediated the inhibition of t-OFs adipogenesis. (a, b) The expression of Smad7 in each group of t-OFs. (c–g) The expression of PPAR-γ, C/EBPα, adiponectin, and FABP-4 in each group of t-OFs. (h, i) The representative images of oil red O staining on t-OFs and relative oil red O-positive cell rate. $^{**}P < 0.01$, $^{***}P < 0.001$, $^{****}P < 0.0001$ vs NC group, $^{\#\#}P < 0.01$, $^{\#\#\#}P < 0.001$, $^{\#\#\#\#}P < 0.0001$, vs miR-96-5p inhibitor group by one-way ANOVA.

In conclusion, the present study demonstrates a role for miR-96-5p in adipogenesis of orbital fibroblast in TAO patients. The results revealed that miR-96-5p is highly expressed in orbital tissues of TAO patients and t-OFs and that miR-96-5p can promote t-OF adipogenesis by specifically inhibiting Smad7 expression. Furthermore, miR-96-5p knockdown potentially inhibits t-OF adipogenic differentiation via Smad7/PPAR-γ/C/EBPα signaling. This research suggests that miR-96-5p could be a biomarker and potential therapeutic target for TAO. However, because this is our preliminary work to investigate the role of miR-96-5p in TAO, it has significant limitations. We will improve the experimental design in subsequent studies, including cell experiments, animal model construction, and clinical sample detection and verification.

Data Availability

The datasets used and/or analyzed during the current study are available from the corresponding author upon reasonable request.

Conflicts of Interest

The authors declare that they have no conflicts of interest.

Authors' Contributions

All authors contributed substantially to this manuscript. JS Kang contributed majorly for this manuscript with participating in all the experiments and writing the manuscript. YQ Li contributed equally as JS Kang with participating primarily in all the experiments, data analysis, and manuscript proofreading. Y Zou contributed mainly to the assays of western blotting and qRT-PCR. ZJ Zhao and LN Jiao contributed majorly to cell culture and oil red O staining. H Zhang contributed to the conception and design of this study and guided the writing of the manuscript. All authors read and approved the final manuscript. JS Kang and YQ Li authors contributed equally to this study.

Acknowledgments

This study was supported by grants from the Yunnan Health Science and Technology Plan Project (2016NS183).

References

[1] R. Le Moli, P. Malandrino, M. Russo et al., "Corticosteroid pulse therapy for Graves' ophthalmopathy reduces the relapse rate of Graves' hyperthyroidism," *Frontiers in Endocrinology*, vol. 11, no. 11, p. 367, 2020.

[2] A. Vagge, B. Federico, D. N. Chiara et al., "In vivo confocal microscopy morphometric analysis of meibomian glands in patients with graves ophthalmopathy," *Cornea*, vol. 40, no. 4, 2020.

[3] T. J. Fox and C. Anastasopoulou, "Graves orbitopathy," in *StatPearls.*StatPearls Publishing LLC, McLean, VA, USA, 2020.

[4] A. Antonelli, P. Fallahi, G. Elia et al., "Graves' disease: clinical manifestations, immune pathogenesis (cytokines and chemokines) and therapy," *Best Practice & Research Clinical Endocrinology & Metabolism*, vol. 34, no. 1, Article ID 101388, 2020.

[5] P. N. Taylor, L. Zhang, R. W. J. Lee et al., "New insights into the pathogenesis and nonsurgical management of Graves orbitopathy," *Nature Reviews Endocrinology*, vol. 16, no. 2, pp. 104–116, 2020.

[6] S. Wu, T. Cai, F. Chen, X. He, and Z. Cui, "Genetic associations of FCRL3 polymorphisms with the susceptibility of Graves ophthalmopathy in a Chinese population," *International Journal of Clinical and Experimental Medicine*, vol. 8, no. 9, pp. 16948–16954, 2015.

[7] B. Jurecka-Lubieniecka, R. Ploski, D. Kula et al., "Association between polymorphisms in the TSHR gene and Graves' orbitopathy," *PloS one*, vol. 9, no. 7, Article ID e102653, 2014.

[8] T. Planck, B. Shahida, H. Parikh et al., "Smoking induces overexpression of immediate early genes in active Graves' ophthalmopathy," *Thyroid*, vol. 24, no. 10, pp. 1524–1532, 2014.

[9] S. M. Ferrari, P. Fallahi, A. Antonelli, and S. Benvenga, "Environmental issues in thyroid diseases," *Frontiers in Endocrinology*, vol. 8, p. 50, 2017.

[10] Y. Huang, S. Fang, S. Zhang, and H. Zhou, "Progress in the pathogenesis of thyroid-associated ophthalmopathy and new drug development," *Taiwan journal of ophthalmology*, vol. 10, no. 3, pp. 174–180, 2020.

[11] H. Li, C. Ma, W. Liu, J. He, and K. Li, "Gypenosides protect orbital fibroblasts in Graves ophthalmopathy via anti-inflammation and anti-fibrosis effects," *Investigative Opthalmology & Visual Science*, vol. 61, no. 5, p. 64, 2020.

[12] D. H. Slentz, C. C. Nelson, and T. J. Smith, "Teprotumumab: a novel therapeutic monoclonal antibody for thyroid-associated ophthalmopathy," *Expert Opinion on Investigational Drugs*, vol. 29, no. 7, pp. 645–649, 2020.

[13] D. Łacheta, M. Piotr, G. Alicja et al., "Immunological aspects of graves' ophthalmopathy," *BioMed research international*, vol. 2019, Article ID 7453260, 12 pages, 2019.

[14] Z.-M. Wang, Z. Wang, and Y. Lu, "The role of cell mediated immunopathogenesis in thyroid-associated ophthalmopathy," *International Journal of Ophthalmology*, vol. 12, no. 7, pp. 1209–1214, 2019.

[15] W. A. Dik, S. Virakul, and L. van Steensel, "Current perspectives on the role of orbital fibroblasts in the pathogenesis of Graves' ophthalmopathy," *Experimental Eye Research*, vol. 142, pp. 83–91, 2016.

[16] S. Y. Jang, M. K. Chae, J. H. Lee, E. J. Lee, and J. S. Yoon, "MicroRNA-27 inhibits adipogenic differentiation in orbital fibroblasts from patients with Graves' orbitopathy," *PLoS one*, vol. 14, no. 8, 2019.

[17] J. Y. Kim, S. Park, H.-J. Lee, H. Lew, and G. J. Kim, "Functionally enhanced placenta-derived mesenchymal stem cells inhibit adipogenesis in orbital fibroblasts with Graves' ophthalmopathy," *Stem Cell Research & Therapy*, vol. 11, no. 1, p. 469, 2020.

[18] R. Peyster, F. Ginsberg, J. Silber, and L. Adler, "Exophthalmos caused by excessive fat: CT volumetric analysis and differential diagnosis," *American Journal of Roentgenology*, vol. 146, no. 3, pp. 459–464, 1986.

[19] Y. Takuse, M. Watanabe, N. Inoue et al., "Association of IL-10-regulating MicroRNAs in peripheral blood mononuclear cells with the pathogenesis of autoimmune thyroid disease," *Immunological Investigations*, vol. 46, no. 6, pp. 590–602, 2017.

[20] L. Qin, Y. Chen, Y. Niu et al., "A deep investigation into the adipogenesis mechanism: profile of microRNAs regulating adipogenesis by modulating the canonical Wnt/β-catenin signaling pathway," *BMC Genomics*, vol. 11, no. 1, p. 320, 2010.

[21] Y. Hou, L. Fu, J. Li et al., "Transcriptome analysis of potential miRNA involved in adipogenic differentiation of C2C12 myoblasts," *Lipids*, vol. 53, no. 4, pp. 375–386, 2018.

[22] R. Martínez-Hernández, S.-N. Miguel, S.-S. Ana et al., "A MicroRNA signature for evaluation of risk and severity of autoimmune thyroid diseases," *Journal of Clinical Endocrinology & Metabolism*, vol. 103, no. 3, pp. 1139–1150, 2018.

[23] Z. Liu, Y. Cui, S. Wang et al., "MiR-96-5p is an oncogene in lung adenocarcinoma and facilitates tumor progression through ARHGAP6 downregulation," *Journal of Applied Genetics*, vol. 62, no. 4, 2021.

[24] T. Wang, Y. Xu, X. Liu, Y. Zeng, and L. Liu, "miR-96-5p is the tumor suppressor in osteosarcoma via targeting SYK," *Biochemical and biophysical research communications*, vol. 572, pp. 49–56, 2021.

[25] R. Li, Y. Chen, J. Wu et al., "LncRNA FGF14-AS2 represses growth of prostate carcinoma cells via modulating miR-96-5p/AJAP1 axis," *Journal of Clinical Laboratory Analysis*, vol. 35, no. 11, Article ID e24012, 2021.

[26] A. Vallelunga, T. Iannitti, S. Capece et al., "Serum miR-96-5P and miR-339-5P are potential biomarkers for multiple system Atrophy and Parkinson's disease," *Frontiers in Aging Neuroscience*, vol. 13, Article ID 632891, 2021.

[27] Q. L. Wang, H. F. Li, D. P. Wang et al., "Effect of GGCX on the differentiation function of osteoporosis bone marrow

mesenchymal stem cells through regulating TGFβ/smad signaling pathway," *European Review for Medical and Pharmacological Sciences*, vol. 23, no. 17, pp. 7224–7231, 2019.

[28] N. Li, W. Y.-W. Lee, S.-E. Lin et al., "Partial loss of Smad7 function impairs bone remodeling, osteogenesis and enhances osteoclastogenesis in mice," *Bone*, vol. 67, pp. 46–55, 2014.

[29] B.-H. Kim, S. Han, H. Lee et al., "Metformin enhances the anti-adipogenic effects of atorvastatin via modulation of STAT3 and TGF-β/Smad3 signaling," *Biochemical and biophysical research communications*, vol. 456, no. 1, pp. 173–178, 2015.

[30] D. Ouyang, L. Xu, L. Zhang et al., "MiR-181a-5p regulates 3T3-L1 cell adipogenesis by targetingSmad7andTcf7l2," *Acta biochimica et biophysica Sinica*, vol. 48, no. 11, pp. 1034–1041, 2016.

[31] Y. Li, D. Jin, W. Xie et al., "PPAR-γ and Wnt regulate the differentiation of MSCs into adipocytes and osteoblasts respectively," *Current Stem Cell Research and Therapy*, vol. 13, no. 3, pp. 185–192, 2018.

[32] H. Zhuang, X. Zhang, C. Zhu et al., "Molecular mechanisms of PPAR-γ; governing MSC osteogenic and adipogenic differentiation," *Current Stem Cell Research and Therapy*, vol. 11, no. 3, pp. 255–264, 2016.

[33] A. Vallée, Y. Lecarpentier, R. Guillevin, and J. N. Vallée, "Interactions between TGF-β1, canonical WNT/β-catenin pathway and PPAR γ in radiation-induced fibrosis," *Oncotarget*, vol. 8, no. 52, pp. 90579–90604, 2017.

[34] M. Hao, J. Sun, Y. Zhang et al., "Exploring the role of SRC in extraocular muscle fibrosis of the Graves' ophthalmopathy," *Frontiers in Bioengineering and Biotechnology*, vol. 8, p. 392, 2020.

[35] S. Y. Jang, S. J. Park, M. K. Chae, J. H. Lee, E. J. Lee, and J. S. Yoon, "Role of microRNA-146a in regulation of fibrosis in orbital fibroblasts from patients with Graves' orbitopathy," *British Journal of Ophthalmology*, vol. 102, no. 3, pp. 407–414, 2018.

[36] B. D. Tong, M. Y. Xiao, J. X. Zeng, and W. Xiong, "MiRNA-21 promotes fibrosis in orbital fibroblasts from thyroid-associated ophthalmopathy," *Molecular Vision*, vol. 21, pp. 324–334, 2015.

[37] J. S. Yoon, M. K. Chae, S. Y. Jang, S. Y. Lee, and E. J. Lee, "Antifibrotic effects of quercetin in primary orbital fibroblasts and orbital fat tissue cultures of Graves' orbitopathy," *Investigative Opthalmology & Visual Science*, vol. 53, no. 9, pp. 5921–5929, 2012.

[38] R. Yuan, X. Dai, Y. Li, C. Li, and L. Liu, "Exosomes from miR-29a-modified adipose-derived mesenchymal stem cells reduce excessive scar formation by inhibiting TGF-β2/Smad3 signaling," *Molecular Medicine Reports*, vol. 24, no. 5, 2021.

[39] K. J. Livak and T. D. Schmittgen, "Analysis of relative gene expression data using real-time quantitative PCR and the 2−ΔΔCT method," *Methods*, vol. 25, no. 4, pp. 402–408, 2001.

[40] D. W. Kim, K. Taneja, T. Hoang et al., "Transcriptomic profiling of control and thyroid-associated orbitopathy (TAO) orbital fat and TAO orbital fibroblasts undergoing adipogenesis," *Investigative Opthalmology & Visual Science*, vol. 62, no. 9, p. 24, 2021.

[41] S. Jung, Y. J. Choi, T. K. Park et al., "Wnt signalling inhibits adipogenesis in orbital fibroblasts from patients with Graves' orbitopathy," *British Journal of Ophthalmology*, 2021.

[42] J. Thiel, C. Alter, S. Luppus et al., "MicroRNA-183 and microRNA-96 are associated with autoimmune responses by regulating T cell activation," *Journal of Autoimmunity*, vol. 96, pp. 94–103, 2019.

[43] S. Y. Jang, M. K. Chae, J. H. Lee, E. J. Lee, and J. S. Yoon, "Role of miR-146a in the regulation of inflammation in an in vitro model of Graves' orbitopathy," *Investigative Opthalmology & Visual Science*, vol. 57, no. 10, pp. 4027–4034, 2016.

[44] N. Wang, F.-E. Chen, and Z.-W. Long, "Mechanism of MicroRNA-146a/notch2 signaling regulating IL-6 in Graves ophthalmopathy," *Cellular Physiology and Biochemistry*, vol. 41, no. 4, pp. 1285–1297, 2017.

[45] J.-Y. Lee, M. Yun, J.-S. Paik, S.-B. Lee, and S.-W. Yang, "PDGF-BB enhances the proliferation of cells in human orbital fibroblasts by suppressing PDCD4 expression via upregulation of microRNA-21," *Investigative Opthalmology & Visual Science*, vol. 57, no. 3, pp. 908–913, 2016.

[46] K. Li, Y. Du, B. L. Jiang, and J. F. He, "Increased microRNA-155 and decreased microRNA-146a may promote ocular inflammation and proliferation in Graves' ophthalmopathy," *Medical Science Monitor: International Medical Journal of Experimental and Clinical Research*, vol. 20, pp. 639–643, 2014.

Hindawi
Evidence-Based Complementary and Alternative Medicine
Volume 2022, Article ID 7710374, 8 pages
https://doi.org/10.1155/2022/7710374

Research Article

Prevalence and Risk Factors Comparison of Anterior and Posterior Intracranial Arterial Stenosis

Yan Zhao,[1] **Beibei Liu**,[2] **Chunxiu Wang**,[3] **Shaochen Guan**,[3] **Chunxiao Liu**,[1] **Yanlei Zhang**,[1] **Chengbei Hou**,[3] **Xiaowei Song**,[4] **Zhongying Zhang**,[1] **Xiaoguang Wu**,[3] **Huihui Li**,[1] **Xiang Gu**,[5] **Shimin Hu**,[6] **Jian Wu**,[4,7] **and Xianghua Fang**[3]

[1]*Department of Geriatrics, Xuanwu Hospital of Capital Medical University, Xicheng District, Beijing 100053, China*
[2]*Department of Vascular Ultrasound, Xuanwu Hospital of Capital Medical University, Xicheng District 100053, Beijing, China*
[3]*Evidence Based Medicine Center, Xuanwu Hospital of Capital Medical University, 45 Changchun Street, Xicheng District, Beijing 100053, China*
[4]*Department of Neurology, Beijing Tsinghua Changgung Hospital, School of Clinical Medicine, Tsinghua University, Changping District, Beijing 102218, China*
[5]*Department of Geriatrics, Beijing Friendship Hospital, Capital Medical University, Beijing 100050, China*
[6]*Department of Neurology, Xuanwu Hospital of Capital Medical University, 45 Changchun Street, Xicheng District, Beijing 100053, China*
[7]*School of Clinical Medicine, Tsinghua University, 30 Shuangqing Road, Haidian District, Beijing 100084, China*

Correspondence should be addressed to Jian Wu; wujianxuanwu@126.com and Xianghua Fang; xhfang163@163.com

Received 31 July 2021; Accepted 2 December 2021; Published 10 January 2022

Academic Editor: Feng Zhang

The prevalence and risk factors of intracranial atherosclerotic stenosis (ICAS) located in the anterior circulation (AC) and posterior circulation (PC) has been scarcely noted in the general population. We aimed to determine ICAS prevalence and risk factor profile of AC and PC in a representative population. Data were from the China Hypertension Survey of Beijing. In total, 4800 people aged 35 years or older were enrolled in this subsurvey for ICAS, and 3954 participants were eligible for analysis. ICAS was assessed by transcranial Doppler. The prevalence of ICAS in AC was much greater than that in PC (11.9% vs. 4.2%), and subjects with ICAS in PC were 3.9 years older than those with ICAS in AC. Multivariable logistics regression showed that the odds of hypertension and diabetes increased by 79% (OR: 1.79, 95% CI: 1.40–2.27) and 35% (OR: 1.35, 95% CI: 1.04–1.75) in those with AC vascular lesions and by 3.35 times (OR: 3.35, 95% CI: 2.49–4.50) and 71% (OR: 1.71, 95% CI: 1.19–2.46) in those with PC vascular lesions compared with those without vascular lesions. Most modifiable vascular risk factors for ICAS appeared to exert similar magnitudes of risk for PC to AC lesions.

1. Introduction

The incidence of stroke in China has increased over the last decades [1], and the rise has mainly been attributed to ischemic stroke, with an annual growth rate of 8.7% [2]. Intracranial atherosclerotic stenosis (ICAS) is a predominant cause for ischemic stroke, particularly for the Asian population. The percentage of ICAS ranged from 37% to 46.6% in ischemic stroke patients from China [3–7] and 30% in patients from Korea [3–7], which is higher than that of western countries of ICAS (8%–27%) [8–10]. Previous studies confirmed the disparity in ICAS prevalence by race/region [11–15], but the epidemiological characteristics of ICAS located in anterior circulation (AC) and posterior circulation (PC) has been scarcely noted. In addition, the ICAS of AC and PC shared risk factors; for example, hypertension and diabetes are both the risk factors of ICAS [16, 17]. Different magnitudes of atherosclerotic lesion's risk for AC compared with PC were less reported in general population. These emerging risk factors associated with the

presence of ICAS according to the anatomic location of intracranial artery (i.e., AC and PC as well as per-vessel) are not yet clarified.

Expanding our understanding of ICAS prevalence by the anatomic location of intracranial artery and the association between risk factors and ICAS by location will afford insight in the pathogenesis of ICAS. This would provide potential implications for precise ICAS prevention. We therefore aimed to fill this knowledge gap by conducting a study to determine ICAS prevalence of AC and PC in a representative population. We were also interested in determining if the profiles of risk factor differed by atherosclerotic location.

2. Materials and Methods

2.1. Survey Participants. Data was used from the Beijing subgroup of the China Hypertension Survey (CHS), a nation-wide survey performed during the period of 2012–2015. The study design and major findings of the survey had been published elsewhere [18, 19]. Briefly, a stratified multistage multicentered national cross-sectional survey was conducted to investigate the prevalence of hypertension in subjects over 15 years old from 31 metropolises/provinces in China. For this substudy, all selected urban and rural areas of 31 metropolises/provinces were stratified into eastern, middle and western regions again according to both geographical locations and economic level. Sixty cities and seventy counties were selected by using the simple random sampling (SRS) method. Beijing was one of the selected cities, and three districts and one county were randomly selected for the survey. Next, three communities or villages were further randomly selected. Only residents with certificated documents from the Administration of Households of the local government were enrolled to exclude immigration effects. According to the protocol of CHS, 4000 residents aged more than 35 years were the designed sample size. Taking nonresponse into account, an additional 20% sample was added, and thus, the final sample size was 4800 participants. All participants were invited to complete a standard questionnaire, blood biochemical testing, and cerebral vascular evaluation by carotid ultrasound and transcranial Doppler (TCD) as a secondary analysis for atherosclerosis. A total of 3954 participants completed the questionnaire and underwent the TCD vascular evaluation with a response rate of 82.4%; thus, they were included in this analysis. The participant screening flowchart was presented in Figure S1. The characteristics between participants included and not included in the analyses are listed in Table S1.

The protocol of this study's design was approved by the ethics committee of the Xuanwu Hospital of Capital Medical University ([2014]-016) and Fuwai Hospital (2012-402). Written informed consent was obtained from all participants before enrollment.

2.2. Training and Data Collection. A standardized questionnaire developed by Fuwai Hospital, the coordination center of this nation-wide survey, was administrated by a trained staff to collect information about demographic characteristics, lifestyle, risk factors, and history of coronary heart disease, stroke, diabetes, and hyperlipidemia [19]. The histories of coronary heart disease and stroke were self-reported and verified by cardiologists or neurologists, respectively. Blood pressure and body weight and height were measured with a standard procedure, and details were described elsewhere [18–20]. After the interview, participants were invited to take laboratory measurements. Blood samples were taken and sent to the National Center for Cardiovascular Disease of Fuwai Hospital for analysis according to predefined protocols to ensure the accuracy and controllability of the results [20].To ensure the quality of survey, all of the investigators received standard training before participation, including the TCD operators. All physical examinations and laboratory testing were conducted strictly as the protocol required.

2.3. Assessment of Intracranial Artery Stenosis. TCD was performed by two independent vascular ultrasound practitioners with more than five years of experience using portable machines. All procedures were carried out as the standard protocol required, and each vessel in the intracranial artery was detected, including the bilateral anterior cerebral artery (ACA), middle cerebral artery (MCA), posterior cerebral artery (PCA), terminal of internal carotid artery (ICA), vertebral artery (VA), and basilar artery (BA). The diagnoses of ICAS referred to Wong's criteria based on peak systolic flow velocity (Vp) [21]. The cutoff value of Vp for ICAS diagnosis was 140 cm/s in the MCA, 120 cm/s in the ACA and internal carotid siphon, and 100 cm/s in the PCA and vertebra-basilar artery. Additional criteria of stenosis in the MCA were as follows: Vp ranged from 140 to 160 cm/s, together with disturbance in echo frequency and turbulence, or Vp reduction by ≥30% compared with the contralateral depth-corresponding homologous segment. Intracranial artery occlusion is considered when low velocity and low resistance discontinuous flow signals are detected along the main intracranial artery. The primary TCD criteria at each site of occlusion was defined as one of four types, such as dampened signal, blunted signal, minimal signal, and absent signal [22]. Apart from the velocity criteria, the subjects' age was also considered. In the absence of good temporal windows, intracranial blood flow signals were detected via orbital window [21]. Any cerebral arteries that could not be detected via both temporal and orbital window were considered nonstenosis due to the failed detection of blood follow by both the temporal and orbital windows. The operators and reviewers of the TCD studies were blind to the clinical information.

2.4. Definition of Vascular Risk Factors. Hypertension was defined as systolic blood pressure ≥140 mmHg and/or diastolic blood pressure ≥90 mmHg or having antihypertension therapy. Diabetes was defined as having a previous history of diabetes or on insulin or oral hypoglycemic medication, or having a fast blood glucose over 7 mmol/L. Hyperlipidemia was defined as total cholesterol

≥6.1 mmol/L or triglyceride ≥2.26 mmol/L or high density lipoprotein cholesterol, <0.9 mmol/L in males and <1.0 mmol/L in female, or under lipid-lowering medication. Smoking was defined as those who were either ex-smokers or current smokers. Body mass index (BMI) was classified as underweight (<18.5), normal (18.5–24.9 kg/m^2), overweight (25.0–29.9 kg/m^2), and obese (>30.0 kg/m^2) [18]. Hyperuricaemia was defined as a serum uric acid level ≥416 μmol/L for male and ≥357 μmol/L for female. Hyperhomocysteinemia was defined as serum homocysteine ≥15 umol/L, and urine microalbuminuria (UMA) was defined as urine microalbumin ≥20 mg/L.

2.5. Statistical Analysis. The CHS was designed to provide accurate estimates for the prevalence of cardiovascular disease and risk factors in the general Chinese population as well as for each selected metropolis/province by sampling weights calculated based on different population census data and sampling scheme and including oversampling for old age and nonresponses. In the current study, we estimated prevalence by age and gender based on the 2010 Beijing municipal population census. Therefore, we could provide prevalent estimates referable to the overall Beijing population. The age- and gender-specific weight-adjusted sample was acquired to estimate the prevalence of ICAS. The association of risk factors with the presence of ICAS was analyzed by ANOVA, student's *t*-test, and chi-squared test. To identify the potential risk factors independently associated with the presence of ICAS, multivariate logistic regression models were allied. Odds ratios (OR) and corresponding 95% confidence intervals (95% CI) were also estimated using multivariate logistic regression analysis.

3. Results

The results of Table 1 showed that the overall weighted prevalence of ICAS was 14.6% (95%CI: 13.5–15.8). The prevalence of ICAS was much lower in population free of stroke than that with a history of stroke (13.8% vs. 32.9%). The prevalence of males was similar to females (14.9% vs. 14.4%), but the increased magnitude across age groups was different by gender (Figure 1(a)), and the increased patterns were similar for population with and without history of stroke (Figures 1(b) and 1(c)).

Table 1 also demonstrates that the ICAS prevalence in AC was much higher than that in PC (11.9% vs. 4.2%). The vascular lesions in PC increased faster than in AC with advanced age, and this rapid increase was attributed mainly to VA lesions.

A total of 987 arteries were detected to have atherosclerotic lesions (892 stenosis and 45 occlusions) among 752 individuals with vascular lesions. The individuals with 1, 2, 3, 4, and 5 or more artery lesions were 302, 122, 46, 44, and 14, respectively.

Risk factors related to ICAS were the highest in the subjects with both ICAS and history of stroke (Table S2). The average age for individuals without ICAS was 61.4 ± 12.8 years old, followed by those with ICAS of AC (66.0 ± 11.2), and those with ICAS in PC had the highest age (69.8 ± 8.8). The frequency and multivariable analyses in the population free of stroke were showed in Tables S3 and 2. The odds of hypertension and diabetes increased by 79% (OR: 1.79, 95% CI: 1.40–2.27) and by 30% (OR: 1.35, 95% CI: 1.04–1.75) in those with AC lesions and by 3.35 times (OR: 3.35, 95% CI: 2.49–4.50) and 71% (OR: 1.71, 95% CI: 1.19–2.46) in those with PC lesions compared with that without ICAS. The odds of overweight or obese were reduced in those with either AC or PC lesions. In addition, the population with PC lesions was more likely to have diabetes, hyperlipidemia, and elevated high-sensitivity C-reactive protein (hi-CRP). Most OR values in PC lesions were greater than those in AC lesion, but all of 95% CIs were overlapped, except age.

The frequency and multivariable analyses in subjects with a history of stroke showed that males were more likely to have lesions in AC, and diabetes was significantly associated with lesions of PC (Tables S4 and S5).

Per-vessel risk factor analysis for subjects without and with a history of stroke is listed in Table S6. The associations of most of the previously mentioned risk factors with each intracranial artery lesion were similar to those with AC and PC lesions. However, in the subpopulation with stroke history, the odds of UMA in those with ICAS of VA were significantly higher compared to those with non-ICAS.

4. Discussion

In this representative general population study of Beijing, China, using TCD to detect the vascular lesions of the intracranial artery, we found that ICAS of AC was the predominant location. Our evidence suggested that most risk factors may differ, but there were no different magnitudes of risk for ICAS of AC compared with PC, except for age. On multivariable analyses, hypertension and diabetes were independent risk factors for ICAS of both AC and PC, while hyperlipidemia and elevated hi-CRP were independently associated with PC lesions. To the best of our knowledge, this is the first population-based study to estimate the prevalence of ICAS by the anatomical location of intracranial atherosclerosis. The large sample and randomly selected population of the current study allowed us to analyse the characteristics by age-gender subgroup. The method for detecting vascular lesions and the criteria for defining atherosclerosis were consistent with most of the previous studies in China [11, 21]. Our ICAS prevalence of 13.8% in the population free of stroke is similar to that in the APCA study [11]. The APAC study was performed on 5353 employees aged 40 years or older and retirees of a large coal mine industry in Kailuan, located 150 km southeast of our study site.

Arteries located in AC were more likely to experience atherosclerosis than those in PC. The finding corresponded with the previous clinical observation studies [7, 11, 23, 24]. About 70–80% of the patients who experienced ischemic stroke had AC lesions, and MCA was the most common affected artery. In the current study, we also found that the atherosclerotic lesion was high in MCA. We also analyzed PC lesions and found that VA was much more likely to have

Table 1: Weighted prevalent rates and 95% CIs of ICAS by the anatomic location.

Age	Prevalence and 95% CI of anterior circulation				Prevalence and 95% CI of posterior circulation			
	Total	Subtotal	ACA	MCA	Subtotal	PCA	VA	BA
Population free of stroke								
35~	8.6 (6.9~10.3)	6.9 (5.3~8.4)	5.4 (4.0~6.9)	3.3 (2.2~4.4)	2.4 (1.4~3.4)	0.2 (0.0~0.5)	2.2 (1.3~3.1)	—
45~	10.9 (8.9~12.9)	10.0 (8.1~11.9)	7.2 (5.5~8.9)	5.7 (4.2~7.2)	1.6 (0.8~2.5)	0.2 (0.0~0.6)	0.9 (0.3~1.6)	0.6 (0.1~1.1)
55~	16.8 (14.3~19.3)	15.5 (13.1~17.9)	10.2 (8.1~12.3)	10.7 (8.5~12.8)	4.9 (3.4~6.4)	1.9 (0.9~2.8)	2.9 (1.7~4.1)	0.7 (0.1~1.3)
65~	22.8 (18.7~27.0)	19.1 (15.2~23.1)	12.4 (8.9~15.9)	13.1 (9.6~16.7)	10.1 (6.9~13.3)	2.3 (0.6~3.9)	7.9 (5.0~10.8)	2.9 (1.0~4.7)
75~	23.1 (17.3~29.0)	18.2 (12.7~23.7)	10.5 (5.9~15.1)	13.6 (8.5~18.6)	12.1 (7.2~16.9)	2.5 (0.1~5.0)	9.5 (5.1~13.9)	3.2 (0.4~5.9)
Total	13.8 (12.6~14.9)	11.9 (10.8~13.0)	8.2 (7.2~9.1)	7.5 (6.6~8.4)	4.2 (3.5~4.9)	1.0 (0.6~1.3)	3.0 (2.4~3.6)	0.8 (0.5~1.1)
P for trend	<0.0001	<0.0001	<0.0001	<0.0001	<0.0001	<0.0001	<0.0001	<0.0001
Population with history of stroke								
35~	—	—	—	—	—	—	—	—
45~	—	—	—	—	—	—	—	—
55~	32.7 (19.5~45.8)	31.3 (18.1~44.4)	25.0 (12.2~37.8)	19.5 (7.4~31.6)	21.4 (9.0~33.8)	13.2 (2.4~23.9)	17.5 (5.7~29.3)	5.7 (0.0~13.4)
65~	32.3 (20.9~43.7)	25.4 (14.3~36.5)	17.0 (6.9~27.1)	18.5 (8.2~28.9)	22.8 (11.9~33.7)	10.2 (1.7~18.7)	17.0 (6.9~27.1)	8.3 (0.5~16.2)
75~	38.1 (23.4~52.8)	27.8 (13.1~42.4)	21.2 (7.3~35.2)	21.2 (7.3~35.2)	29.7 (15.0~44.5)	7.1 (0.0~16.7)	25.7 (11.2~40.2)	10.3 (0.0~21.4)
Total	32.9 (25.7~40.2)	27.0 (19.9~34.2)	20.0 (13.3~26.7)	18.8 (12.2~25.4)	23.4 (16.4~30.4)	10.0 (4.6~15.4)	18.8 (12.2~25.4)	7.7 (2.9~12.5)
P for trend	<0.0001	0.198	0.959	0.729	0.189	0.715	0.203	0.137
Overall population								
35~	8.6 (6.9~10.3)	6.9 (5.3~8.4)	5.4 (4.0~6.9)	3.3 (2.2~4.4)	2.4 (1.4~3.4)	0.2 (−0.1~0.5)	2.2 (1.3~3.1)	
45~	10.9 (8.9~12.8)	9.9 (8.0~11.8)	7.2 (5.5~8.9)	5.6 (4.1~7.1)	1.6 (0.8~2.5)	0.2 (−0.1~0.6)	0.9 (0.3~1.6)	0.6 (0.1~1.1)
55~	17.6 (15.2~20.1)	16.2 (13.8~18.6)	10.9 (8.8~13.0)	11.1 (9.0~13.2)	5.7 (4.2~7.3)	2.4 (1.3~3.5)	3.6 (2.3~4.9)	0.9 (0.2~1.6)
65~	24.2 (20.3~28.1)	20.0 (16.2~23.7)	12.8 (9.5~16.0)	13.6 (10.3~16.9)	11.9 (8.7~15.1)	3.3 (1.5~5.1)	8.7 (5.9~11.5)	3.5 (1.6~5.4)
75~	25.7 (20.2~31.2)	19.7 (14.5~25.0)	12.0 (7.6~16.4)	14.1 (9.4~18.8)	15.2 (10.3~20.0)	3.2 (0.7~5.7)	11.6 (7.2~16.0)	4.2 (1.3~7.0)
Total	14.6 (13.5~15.8)	12.5 (11.5~13.6)	8.6 (7.7~9.5)	7.9 (7.0~8.8)	5.0 (4.3~5.8)	1.3 (0.9~1.7)	3.6 (3.0~4.2)	1.1 (0.7~1.4)
P for trend	<0.0001	<0.0001	<0.0001	<0.0001	<0.0001	<0.0001	<0.0001	<0.0001

atherosclerotic lesions. Several population-based studies of China [11], Japan [25], Korea [13], and Spain [15] demonstrated that MCA was much more likely to have atherosclerotic lesions. Similar findings were also noted in hospitalized ischemic stroke patients in China [3] and European countries such as Italy [26] and Germany [9]. However, the prevalence of each intracranial artery was not reported in these studies. In an autopsy study in France, Mazighi et al. reported that MCA and BA appeared to be the most common location for stenosis >30%. Similarly, Kimura et al. reported that MCA and BA had the highest percentage of severe atherosclerosis from 7260 autopsies in Japan, but the lesions in ACA was the lowest. On the contrary, Suri et al. reported that intracranial artery lesions in PCA were highest in the Atherosclerosis Risk in Community Study of US [27]. Whether the diversity in the location or artery of atherosclerotic lesions among these previous studies was due to the differences in study design, method for detecting vascular lesion, definition of ICAS, or selection of the study population was not clear, and thus, the results should be explained with caution.

We found that the association of demographic characteristics to vascular lesions by location was interesting. The mean age of the subjects with AC lesions was 3.9 years younger than those with PC lesions. The findings are in accordance with hospital-based studies in China [23, 28, 29]. Compared with patients with PC stroke, the patients with AC stroke were 0.9–5.6 years younger. On the contrary, studies from Western countries such as Switzerland, Germany, Austria, and Czech showed that patients with

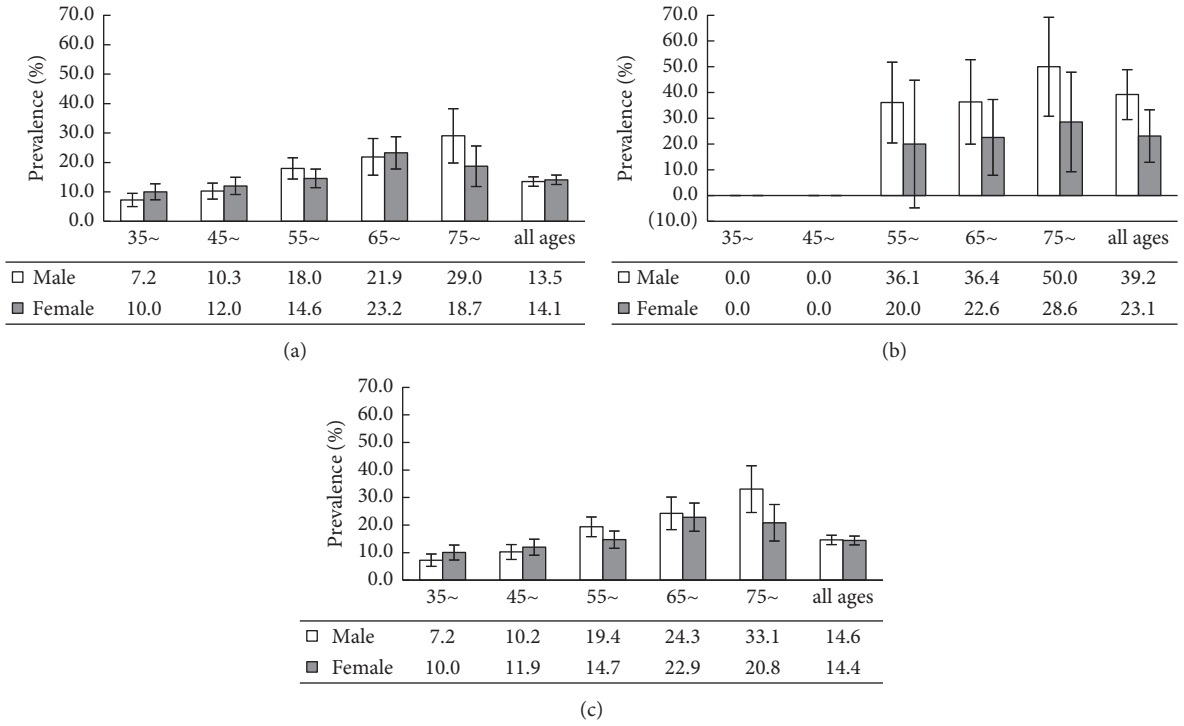

Figure 1: Prevalences and 95% CIs of ICAS by age and gender. (a) Population free of stroke; (b) population with history of stroke; (c) total population.

Table 2: ORs and 95% CIs of ICAS for 3600 individuals free of stroke*.

Risk factors	Anterior circulation		Posterior circulation	
	Crude OR and 95% CI	Fully adjusted OR and 95% CI	Crude OR and 95% CI	Fully adjusted OR and 95% CI
Age (<65 vs. ≥65 years old)	1.79 (1.48~2.17)	1.18 (0.93~1.47)	3.37 (2.46~4.61)	2.16 (1.48~3.15)
Gender (male vs. female)	0.89 (0.73~1.07)	0.88 (0.66~1.17)	1.07 (0.80~1.43)	1.04 (0.68~1.61)
Hypertension (no vs. yes)	1.99 (1.65~2.41)	1.79 (1.40~2.27)	3.35 (2.49~4.50)	2.54 (1.76~3.69)
Diabetes (no vs. yes)	1.76 (1.42~2.17)	1.35 (1.04~1.75)	2.42 (1.80~3.25)	1.71 (1.19~2.46)
Hyperlipidemia (no vs. yes)	1.12 (0.93~1.36)	1.05 (0.83~1.32)	1.52 (1.13~2.04)	1.49 (1.04~2.16)
History of CAD (no vs. yes)	2.00 (1.32~3.01)	1.23 (0.71~2.12)	3.72 (2.30~6.00)	1.86 (0.97~3.56)
Smoking status				
Never	Reference	Reference	Reference	Reference
Current smoker	1.06 (0.84~1.34)	1.00 (0.71~1.39)	0.97 (0.68~1.39)	1.25 (0.75~2.08)
Ex-smoker	1.38 (1.02~1.88)	1.22 (0.81~1.83)	1.19 (0.74~1.91)	1.02 (0.54~1.92)
Normal weight	Reference	Reference	Reference	Reference
Underweight	0.83 (0.35~1.97)	1.19 (0.45~3.13)	0.61 (0.15~2.57)	0.96 (0.22~4.20)
Overweight	1.01 (0.83~1.23)	0.93 (0.73~1.18)	0.82 (0.61~1.11)	0.61 (0.42~0.88)
Obese	0.87 (0.63~1.20)	0.61 (0.40~0.92)	0.69 (0.42~1.15)	0.33 (0.17~0.65)
Hyperuricaemia (no vs. yes)	1.31 (1.02~1.68)	1.17 (0.87~1.58)	1.65 (1.17~2.33)	1.07 (0.69~1.67)
Hyperhomocysteinemia (no vs. yes)	0.99 (0.80~1.22)	0.94 (0.74~1.18)	1.04 (0.76~1.44)	0.94 (0.66~1.34)
hi-CRP(mg/dl)				
1st tertile (≤0.70)	Reference	Reference	Reference	Reference
2nd tertile (0.71–1.80)	0.77 (0.61~0.98)	1.02 (0.77~1.35)	0.84 (0.58~1.20)	1.07 (0.68~1.67)
3rd tertile (>1.80)	0.98 (0.78~1.22)	1.27 (0.97~1.67)	1.37 (1.00~1.89)	1.69 (1.12~2.56)
UMA (no vs. yes)	1.21 (0.99~1.47)	1.27 (0.97~1.67)	1.59 (1.19~2.12)	1.23 (0.87~1.75)

*Population with neither ICAS nor stroke was the reference group, and the frequencies of risk factors are listed in Supplementary Table S3.

posterior circulation infarction were 3–5 years younger than those with anterior circulation infarction [30–33]. The earlier occurrence of ICAS in AC in the current study can well explain why the age at the first stroke onset in China was about 10 years younger than that in the Western population [34]. However, we did not find that ICAS had sex differences

in our population despite the fact that stroke incidence is generally higher in males than females [1]. The average age of females with ICAS was younger than males, which suggested that vascular lesions occur earlier in females. But age-specific prevalence suggested that the vascular lesion might develop faster in males than females, which consequently led to the higher ICAS prevalence in males than females after the age of 55 years. This gender–age change pattern was similar to the Asymptomatic Polyvascular Abnormalities Community (APCA) Study [11]. We could not explain the earlier onset and the slower progression of vascular lesions in females compared with males. It is known that the risk of stroke and majority of risk factors in women are closer to those in men after menopause [35]. Female sex hormones may be implicated in vascular outcomes [35].One possible explanation might be that unhealthy lifestyles (i.e., smoking and physical inactivity) are more prevalent in men than women across the life span.

The modifiable risk factors associated with ICAS in current study were much similar to a previous Chinese population-based study [11]. Hypertension, diabetes, and elevated hi-CRP were independent risk factors for ICAS [36], while overweight and obesity appeared to have a protective effect against vascular damage [11]. We failed to find any unique potential risk factor that can explain the high prevalence of ICAS in our population. It is known that the prevalence of smoking [37] and hyperhomocysteinemia [38] are generally higher in Chinese population than the Western population. However, we did not find the significant differences of these two risk factors between individuals with and without ICAS. Perhaps, some unmeasured characteristics associated with the development of ICAS may explain the high incidence of ICAS in the Asian population and need to be elucidated in the future.

Our analysis showed that the modifiable risk factors in lesions between AC and PC were similar, except for age, which is not in line with the previous studies [2, 11–15]. To date, there has been no study attempting to discern the comparative role of these risk factors by the anatomic location of intracranial artery lesions in general population. Several hospital-based studies showed the disparity of risk factor profile in ischemic stroke patients located in AC and PC existed. Compared with patients with AC ischemic stroke, patients with PC ischemic stroke had 50% higher prevalence of diabetes and 16% higher prevalence of hypertension, and TG was high, while HDL-C was lower in Chinese ischemic stroke patients [28]. Subramanian et al. found that diabetes was independently associated with an increase in the odds of PC to AC ischemic stroke in 849 Canadian patients with acute ischemic stroke [39]. The authors presumed a neurovascular origin of anterior and posterior circulation differed and the arteries of PC might be more susceptible to metabolic disorders. We did not find the difference in these modifiable risk factors in the population with history of stroke. The values of ORs were greater than these of AC, but all of 95% CIs were overlapped. Our findings implied that an intensive administration of those modifiable vascular risk factors in the population free of stroke and that with a history of stroke could reduce of the risk of ICAS; hence, risk of the first-ever and recurrence of stroke would decrease. Controlling diabetes at population level might decrease the risk of ICAS in PC, which may reduce the risk of PC strokes and generally have worse outcomes compared with AC strokes [28].

Limitations of the current study have to be mentioned. First, the ICAS assessment was by TCD and was not further validated by vessel imaging (CTA or MRA). The application of the golden standard measurements, that is, DSA, CTA, or MRA, is not feasible in large population studies. TCD was applied to detect intracranial artery lesions in most population-based surveys in China [11, 21, 40], and the sensitivity was validated by a previous study [41, 42]. With an identical criterion to define vascular lesions, our results were comparable with those of previous studies [11, 21, 40]. Second, subjects had an acoustic window failure, and they were defined as non-ICAS, which would lead to misclassification of ICAS and underestimation of ICAS burdens. We failed to detect blood flow using the temporal or orbital windows in only 34 subjects. Therefore, the impact on the prevalence of CAS was not big enough to change the overall prevalence. Third, the cross-sectional design of this study limits the ability to draw definitive associations of risk factors with the development of ICAS. We will follow this population for several years, so the causal relationship between the development of ICAS and risk factors can be explored.

In conclusion, our results showed that the prevalence of ICAS in AC was predominate to that in PC. The vascular lesion in PC developed faster than that in AC with aging. Advanced age in patients with ICAS appeared to exert different magnitudes of risk for PC to AC lesions. The ICAS of AC and PC shared the most modifiable risk factors.

Data Availability

The data that support the findings of this study are available from the corresponding author upon reasonable request.

Conflicts of Interest

The authors declare that they have no conflicts of interest.

Authors' Contributions

X. H. F. and J. W. were responsible for the conceptualization. X. H. F. was responsible for the methodology. C. B. H. and X. G. W. were responsible for software. Y. Z., B. B. L., and C. X. W. were responsible for the validation. Y. Z. and X. W. S. were responsible for the formal analysis. Y. Z., S. C. G., C. X. L., H. H. L., X. G., and Y. L. Z. were responsible for the investigation. X. H. F. was responsible for the resources. X. G. W. and S. S. H. were responsible for the data curation. Y. L. Z. prepared the original draft. X. H. F. and J. W. reviewed and edited the manuscript. Y. Z. was responsible for the visualization. X. H. F. was responsible for the supervision. X. H. F. and J. W. were responsible for the project administration. X. H. F. was responsible for the funding acquisition.

Acknowledgments

This study was supported by the National Key Program in the Twelfth Five-year Plan (grant no. 2011BAI 11 B01) from the Chinese Ministry of Science and Technology; Commission of Science and Technology of Beijing (grant no. D121100004912002), Beijing Municipal Science & Technology Commission (Z171100001017019), and Beijing Municipal Administration of Hospitals' Ascent Plan (DFL20152201).

Supplementary Materials

Supplementary Figure 1: the screening flowchart of participants. Supplementary Table 1: characteristics (i.e., age, sex, smoking and alcohol consumption, and chronic diseases). Supplementary Tables 2–4: frequency of risk factors (i.e., old age, male, hypertension and history of coronary heart disease, smoking, obesity, and laboratory testing results) in the population with or without history of stroke by anatomic location of ICAS. Supplementary Tables 5–6: ORs and 95% CIs of ICAS in the intracranial anterior and posterior circulation and branches for individuals with or without history of stroke. (*Supplementary Materials*)

References

[1] W. Wang, B. Jiang, H. Sun et al., "Prevalence, incidence, and mortality of stroke in China: results from a nationwide population-based survey of 480 687 adults," *Circulation*, vol. 135, no. 8, pp. 759–771, 2017.

[2] D. Zhao, J. Liu, W. Wang et al., "Epidemiological transition of stroke in China: twenty-one-year observational study from the Sino-MONICA-Beijing project," *Stroke*, vol. 39, no. 6, pp. 1668–1674, 2008.

[3] Y. Wang, X. Zhao, L. Liu et al., "Prevalence and outcomes of symptomatic intracranial large artery stenoses and occlusions in China: the Chinese Intracranial Atherosclerosis (CICAS) Study," *Stroke*, vol. 45, no. 3, pp. 663–669, 2014.

[4] K. S. Wong and H. Li, "Long-term mortality and recurrent stroke risk among Chinese stroke patients with predominant intracranial atherosclerosis," *Stroke*, vol. 34, no. 10, pp. 2361–2366, 2003.

[5] Y. D. Kim, H. Y. Choi, H. J. Cho et al., "Increasing frequency and burden of cerebral artery atherosclerosis in Korean stroke patients," *Yonsei Medical Journal*, vol. 51, no. 3, pp. 318–325, 2010.

[6] J. T. Kim, S. H. Yoo, J.-H. Kwon, S. U. Kwon, and J. S. Kim, "Subtyping of ischemic stroke based on vascular imaging: analysis of 1,167 acute, consecutive patients," *Journal of clinical neurology (Seoul, Korea)*, vol. 2, no. 4, pp. 225–230, 2006.

[7] K. S. Wong, H. Li, Y. L. Chan et al., "Use of transcranial Doppler ultrasound to predict outcome in patients with intracranial large-artery occlusive disease," *Stroke*, vol. 31, no. 11, pp. 2641–2647, 2000.

[8] R. L. Sacco, D. E. Kargman, Q. Gu, and M. C. Zamanillo, "Race-ethnicity and determinants of intracranial atherosclerotic cerebral infarction. The Northern Manhattan Stroke Study," *Stroke*, vol. 26, no. 1, pp. 14–20, 1995.

[9] C. Weimar, M. Goertler, L. Harms, and H.-C. Diener, "Distribution and outcome of symptomatic stenoses and occlusions in patients with acute cerebral ischemia," *Archives of Neurology*, vol. 63, no. 9, pp. 1287–1291, 2006.

[10] G. Tsivgoulis, K. Vadikolias, I. Heliopoulos et al., "Prevalence of symptomatic intracranial atherosclerosis in Caucasians: a prospective, multicenter, transcranial Doppler study," *Journal of Neuroimaging: Official Journal of the American Society of Neuroimaging*, vol. 24, no. 1, pp. 11–17, 2014.

[11] S. Zhang, Y. Zhou, Y. Zhang et al., "Prevalence and risk factors of asymptomatic intracranial arterial stenosis in a community-based population of Chinese adults," *European Journal of Neurology*, vol. 20, no. 11, pp. 1479–1485, 2013.

[12] Q. Sun, Q. Wang, X. Wang et al., "Prevalence and cardiovascular risk factors of asymptomatic intracranial arterial stenosis: the Kongcun town study in Shandong, China," *European Journal of Neurology*, vol. 27, no. 4, pp. 729–735, 2020.

[13] K.-Y. Park, C.-S. Chung, K. H. Lee, G.-M. Kim, Y.-B. Kim, and K. Oh, "Prevalence and risk factors of intracranial atherosclerosis in an asymptomatic Korean population," *Journal of Clinical Neurology (Seoul, Korea)*, vol. 2, no. 1, pp. 29–33, 2006.

[14] Y. Qiao, F. K. Suri, Y. Zhang et al., "Racial differences in prevalence and risk for intracranial atherosclerosis in a US community-based population," *JAMA Cardiology*, vol. 2, no. 12, pp. 1341–1348, 2017.

[15] E. López-Cancio, L. Dorado, M. Millán et al., "The barcelona-asymptomatic intracranial atherosclerosis (AsIA) study: prevalence and risk factors," *Atherosclerosis*, vol. 221, no. 1, pp. 221–225, 2012.

[16] P. Chaturvedi, A. Singh, V. Tiwari, and A. Thacker, "Brain-derived neurotrophic factor levels in acute stroke and its clinical implications," *Brain circulation*, vol. 6, no. 3, pp. 185–190, 2020.

[17] R. G. Eaton, V. S. Shah, D. Dornbos et al., "Demographic age-related variation in Circle of Willis completeness assessed by digital subtraction angiography," *Brain circulation*, vol. 6, no. 1, pp. 31–37, 2020.

[18] Z. Wang, X. Wang, G. Hao et al., "A national study of the prevalence and risk factors associated with peripheral arterial disease from China: the China hypertension survey, 2012–2015," *International Journal of Cardiology*, vol. 275, pp. 165–170, 2019.

[19] Z. Wang, L. Zhang, Z. Chen et al., "Survey on prevalence of hypertension in China: background, aim, method and design," *International Journal of Cardiology*, vol. 174, no. 3, pp. 721–723, 2014.

[20] X. Song, J. Li, Y. Hua et al., "Chronic kidney disease is associated with intracranial artery stenosis distribution in the middle-aged and elderly population," *Journal of Atherosclerosis and Thrombosis*, vol. 27, no. 3, pp. 245–254, 2020.

[21] K. S. Wong, Y. N. Huang, H. B. Yang et al., "A door-to-door survey of intracranial atherosclerosis in Liangbei county, China," *Neurology*, vol. 68, no. 23, pp. 2031–2034, 2007.

[22] A. M. Demchuk, I. Christou, T. H. Wein et al., "Accuracy and criteria for localizing arterial occlusion with transcranial Doppler," *Journal of Neuroimaging: Official Journal of the American Society of Neuroimaging*, vol. 10, no. 7, pp. 1–12, 2000.

[23] Y. Hua, L. Jia, Y. Xing et al., "Distribution pattern of atherosclerotic stenosis in Chinese patients with stroke: a multicenter registry study," *Aging and disease*, vol. 10, no. 1, pp. 62–70, 2019.

[24] T. Uehara, M. Tabuchi, and E. Mori, "Risk factors for occlusive lesions of intracranial arteries in stroke-free Japanese,"

European Journal of Neurology, vol. 12, no. 3, pp. 218–222, 2005.

[25] W. Duan, Y. Pu, H. Liu et al., "Association between leukoaraiosis and symptomatic intracranial large artery stenoses and occlusions: the Chinese intracranial atherosclerosis (CICAS) study," *Aging and disease*, vol. 9, no. 6, pp. 1074–1083, 2018.

[26] C. Baracchini, G. P. Anzola, S. Cenciarelli et al., "Italian symptomatic intracranial atherosclerosis study (ISIDE): a multicenter transcranial ultrasound evaluation," *Neurological Sciences*, vol. 37, no. 10, pp. 1645–1651, 2016.

[27] M. F. K. Suri, Y. Qiao, X. Ma et al., "Prevalence of intracranial atherosclerotic stenosis using high-resolution magnetic resonance angiography in the general population: the atherosclerosis risk in communities study," *Stroke*, vol. 47, no. 5, pp. 1187–1193, 2016.

[28] Y. Luo, Z. Li, J. Zhang, J. Li, and Z. Lu, "Dyslipidaemia was correlated to the posterior circulation infarction in non-diabetic populations," *Lipids in Health and Disease*, vol. 17, no. 1, p. 150, 2018.

[29] Q. Zeng, W. Tao, C. Lei, W. Dong, and M. Liu, "Etiology and risk factors of posterior circulation infarction compared with anterior circulation infarction," *Journal of Stroke and Cerebrovascular Diseases*, vol. 24, no. 7, pp. 1614–1620, 2015.

[30] P. Sommer, A. Posekany, W. Serles et al., "Is functional outcome different in posterior and anterior circulation stroke?" *Stroke*, vol. 49, no. 11, pp. 2728–2732, 2018.

[31] E. Zürcher, B. Richoz, M. Faouzi, and P. Michel, "Differences in ischemic anterior and posterior circulation strokes: a clinico-radiological and outcome analysis," *Journal of Stroke and Cerebrovascular Diseases: The Official Journal of National Stroke Association*, vol. 28, no. 3, pp. 710–718, 2019.

[32] T. Dorňák, M. Král, M. Hazlinger et al., "Posterior vs. anterior circulation infarction: demography, outcomes, and frequency of hemorrhage after thrombolysis," *International Journal of Stroke: Official Journal of the International Stroke Society*, vol. 10, no. 8, pp. 1224–1228, 2015.

[33] B. von Sarnowski, U. Schminke, U. Grittner et al., "Posterior versus anterior circulation stroke in young adults: a comparative study of stroke aetiologies and risk factors in stroke among young fabry patients (sifap1)," *Cerebrovascular Diseases*, vol. 43, no. 3-4, pp. 152–160, 2017.

[34] V. L. Feigin, C. M. Lawes, D. A. Bennett, S. L. Barker-Collo, and V. Parag, "Worldwide stroke incidence and early case fatality reported in 56 population-based studies: a systematic review," *The Lancet Neurology*, vol. 8, no. 4, pp. 355–369, 2009.

[35] L. Lisabeth and C. Bushnell, "Stroke risk in women: the role of menopause and hormone therapy," *The Lancet Neurology*, vol. 11, no. 1, pp. 82–91, 2012.

[36] A. O. Almobarak, S. Badi, W. M. Elmadhoun, H. Tahir, and M. H. Ahmed, "The prevalence and risk factors of stroke among Sudanese individuals with diabetes: cross-sectional survey," *Brain Circulation*, vol. 6, no. 1, pp. 26–30, 2020.

[37] S. Liu, M. Zhang, L. Yang et al., "Prevalence and patterns of tobacco smoking among Chinese adult men and women: findings of the 2010 national smoking survey," *Journal of Epidemiology & Community Health*, vol. 71, no. 2, pp. 154–161, 2017.

[38] Y. Huo, J. Li, X. Qin et al., "Efficacy of folic acid therapy in primary prevention of stroke among adults with hypertension in China: the CSPPT randomized clinical trial," *JAMA*, vol. 313, no. 13, pp. 1325–1335, 2015.

[39] G. Subramanian, J. Silva, F. L. Silver et al., "Risk factors for posterior compared to anterior ischemic stroke: an observational study of the registry of the Canadian stroke network," *Neuroepidemiology*, vol. 33, no. 1, pp. 12–16, 2009.

[40] K. S. Wong, P. W. Ng, A. Tang, R. Liu, V. Yeung, and B. Tomlinson, "Prevalence of asymptomatic intracranial atherosclerosis in high-risk patients," *Neurology*, vol. 68, no. 23, pp. 2035–2038, 2007.

[41] J. Röther, A. Schwartz, K. U. Wentz, W. Rautenberg, and M. Hennerici, "Middle cerebral artery stenoses: assessment by magnetic resonance angiography and transcranial Doppler ultrasound," *Cerebrovascular Diseases*, vol. 4, no. 4, pp. 273–279, 1994.

[42] A. Mowla, B. Shakibajahromi, R. Kabir, Z. Garami, and J. Volpi, "Transcranial Doppler and magnetic resonance angiography assessment of intracranial stenosis: an analysis of screening modalities," *Brain Circulation*, vol. 6, no. 3, pp. 181–184, 2020.

Hindawi
Evidence-Based Complementary and Alternative Medicine
Volume 2022, Article ID 3747285, 20 pages
https://doi.org/10.1155/2022/3747285

Research Article

Systematic Understanding of Mechanism of Danggui Shaoyao San against Ischemic Stroke Using a Network Pharmacology Approach

Sijie Li,[1,2] Yong Yang,[3] Wei Zhang,[1,2,3] Haiyan Li,[1,2] Wantong Yu,[1,2] Chen Gao,[1,2] Jiali Xu,[1,2] Wenbo Zhao,[1,2] and Changhong Ren[1,2]

[1]*Beijing Key Laboratory of Hypoxia Translational Medicine, Xuanwu Hospital, Capital Medical University, Beijing 100053, China*
[2]*Center of Stroke, Beijing Institute for Brain Disorder, Capital Medical University, Beijing 100053, China*
[3]*School of Chinese Medicine, Beijing University of Chines Medicine, Beijing 100029, China*

Correspondence should be addressed to Changhong Ren; rench@xwhosp.org

Received 8 September 2021; Accepted 7 December 2021; Published 5 January 2022

Academic Editor: Feng Zhang

Purpose. Danggui Shaoyao San (DSS) was developed to treat the ischemic stroke (IS) in patients and animal models. The purpose of this study was to explore its active compounds and demonstrate its mechanism against IS through network pharmacology, molecular docking, and animal experiment. *Methods*. All the components of DSS were retrieved from the pharmacology database of TCM system. The genes corresponding to the targets were retrieved using OMIM, CTD database, and TTD database. The herb-compound-target network was constructed by Cytoscape software. The target protein-protein interaction network was built using the STRING database. The core targets of DSS were analyzed by Gene Ontology (GO) and Kyoto Encyclopedia of Genes and Genomes (KEGG). Then, we achieved molecular docking between the hub proteins and the key active compounds. Finally, animal experiments were performed to verify the core targets. Triphenyltetrazolium chloride (TTC) staining was used to calculate the infarct size in mice. The protein expression was determined using the Western blot. *Results*. Compound-target network mainly contained 51 compounds and 315 corresponding targets. Key targets contained MAPK1, SRC, PIK3R1, HRAS, AKT1, RHOA, RAC1, HSP90AA1, and RXRA FN1. There were 417 GO items in GO enrichment analysis ($p < 0.05$) and 119 signaling pathways ($p < 0.05$) in KEGG, mainly including negative regulation of apoptosis, steroid hormone-mediated signaling pathway, neutrophil activation, cellular response to oxidative stress, and VEGF signaling pathway. MAPK1, SRC, and PIK3R1 docked with small molecule compounds. According to the Western blot, the expression of p-MAPK 1, p-AKT, and p-SRC was regulated by DSS. *Conclusions*. This study showed that DSS can treat IS through multiple targets and routes and provided new insights to explore the mechanisms of DSS against IS.

1. Introduction

Stroke has the characteristics of high incidence, high recurrence rate, high fatality rate, high disability rate, and high economic burden, which seriously threatens human health and quality of life. Ischemic stroke (IS) accounts for 70% to 80% of all strokes, which results from sudden interruption of the blood supply to areas of the brain [1]. Neurological deficits such as disturbances to consciousness, cognitive and behavioral changes, paralysis, dysphagia, and aphasia are the major sequels of stroke. In China, stroke is the leading cause of death and contributes to a heavy disease burden [2]. The most effective treatment is currently recognized as intravenous thrombolysis and/or endovascular treatment, which prevent irreversible brain tissue damage by restoring blood flow reperfusion in time [3]. Although in situ clot retrieval can improve the recanalization rate of patients with ischemic stroke (mTICI of 2b/3) to 80–90%, it still exceeds 73% of patients who are left with functional disability or death (90 days of mRS $\geq$ 2) [4]. Therefore, it is

necessary to explore neuroprotective drug to promote neurological function after IS and improve the prognosis of stroke [5].

Traditional Chinese medicine (TCM) has played an important part in maintaining health for thousands of years. In recent years, traditional Chinese drugs have been reported to possess protective effects on the nervous system, which has attracted the attention of researchers worldwide [6]. Danggui Shaoyao San (DSS) is a famous herbal formula composed of the following 6 raw herbs: Paeoniae Radix Alba (PRA), Atractylodes macrocephala Koidz. (AMK), Chuanxiong Rhizoma (CR), Angelicae Sinensis Radix (ASR), Poria cocos (Schw.) Wolf (PCW), and Alisma orientale (Sam.) Juz. (AOJ), which has been widely used in the treatment of various gynecological diseases [7, 8]. Recently, it was found that DSS is a potential therapeutic agent for the treatment of cognitive impairment and depression [9]. It is reported that DSS not only prevents cognitive impairment from Alzheimer's disease (AD) but also improves microcirculation in patients with asymptomatic cerebral infarction [10]. A number of studies indicate the potentials of DSS for improving neurological functions in poststroke treatment [11, 12]. DSS treatment also promotes focal angiogenesis and neurogenesis, attenuates neurological deficit scores, and improves memory functions in experimental rat models of cerebral ischemic-reperfusion injury [13, 14]. However, the underlying neuroprotection mechanisms of DSS against IS remain largely unknown.

Compared with the single-target therapeutic effect of chemical drugs, TCM compound ingredients have the overall therapeutic effect, which is usually modulated through various pathways and targets [15]. System biology, such as network pharmacology, contributes to reveal the biological networks in which drugs work. The integration strategy of network biology and multidirectional pharmacology is conducive to expand the available drug target space and is expected to enhance therapeutic efficacy, elevate clinical trial success rate, and decrease drug discovery costs [16]. In recent years, it has been well applied for drug discovery, especially in the field of research and development of Chinese medicine formulae [17].

According to the description above, DSS is an ideal TCM in the application of treatment to IS. However, the underlying pharmacological mechanisms of DSS on IS treatment remain unclear. In this study, we used the emerging traditional Chinese medicine network pharmacology method to predict the targets of DSS and systematically predict the mechanism of action of DSS in IS. An outline of the method is shown in Figure 1. Our results offered the systematic mechanism of DSS in the treatment of IS and clearly clarified the synergy mechanism of DSS multicomponent and multitarget.

2. Materials and Methods

2.1. DSS Ingredient Collection and Target Gene Prediction. The traditional Chinese medicine systems pharmacology database and analysis platform (TCMSP, https://tcmsp-e.com/) was used for the active ingredient screening [18]. The names of herbs were used as the keywords to retrieve all components. We filtered active compounds by setting the pharmacokinetic index that the oral bioavailability (OB) was greater than 30% and the drug-like (DL) index was >0.18. Target genes were predicted using TCMSP, the PubChem website (pubchem.ncbi.nlm.nih.gov), and the PharmMapper database (http://www.lilabecust.cn/pharmmapper) after identifying the active ingredients [19].

2.2. Acquisition of Potential Therapeutic Targets for DSS Anti-IS. Online Mendelian Inheritance in Man (OMIM, http://omim.org) database, Comparative Toxicogenomics Database (CTD, http://ctdbase.org/) [20], and Therapeutic Target Database (TTD, http://db.idrblab.net/ttd/) were selected to obtain IS-related target gene [21]. All the databases used "ischemic stroke" as the keyword. The potential therapeutic targets of DSS in the treatment of IS were derived from the overlapping targets of DSS-related targets and IS-related targets. Subsequently, we used Cytoscape software (version 3.7.2) to construct a network diagram of "Drug active ingredient-target gene interaction network." The topology analysis of the composition-target network was carried out using the function of "Network Analyzer" in the software.

2.3. Protein-Protein Interaction (PPI) Analysis. The obtained intersection targets were inputted to the STRING database (http://string-db.org/cgi/inpup.pl) with the species set to "*Homo sapiens*" to construct a protein-protein interaction (PPI) network [22]. The minimum required interaction score was set to "highest confidence (0.900)," and the hide disconnected nodes were set. Then, we obtained the PPI network. Next, the interaction files were downloaded and imported into Cytoscape software (version 3.7.2) to visualize the PPI network and analyze the topological value [23]. Then, the targets with the degree and betweenness centrality (BC), which were greater than the average value, were recognized as the key targets of DSS for the treatment of IS.

2.4. Enrichment Analysis of Gene Ontology (GO) and Kyoto Encyclopedia of Genes and Genomes (KEGG). The predicted targets were imported into the Database for Annotation, Visualization, and Integrated Discovery (DAVID database, https://david.ncifcrf.gov) for GO and KEGG enrichment analyses [24]. GO enrichment analysis includes biological process (BP), cellular component (CC), and molecular function (MF). The enrichment results of GO and KEGG were obtained by setting the FDR value, and the bubble map was made according to the enrichment results [25].

2.5. Molecular Docking. The top three key compounds analyzed by "Network Analyzer" were obtained in the TCMSP database in mol2 format, and the top three key target proteins in the PPI network were obtained in the PDB database (http://www.rcsb.org). The software AutoDock Vina was used to carry out molecular docking between the key active ingredients and the key targets [26]. The binding energy was used as the evaluation index to evaluate the

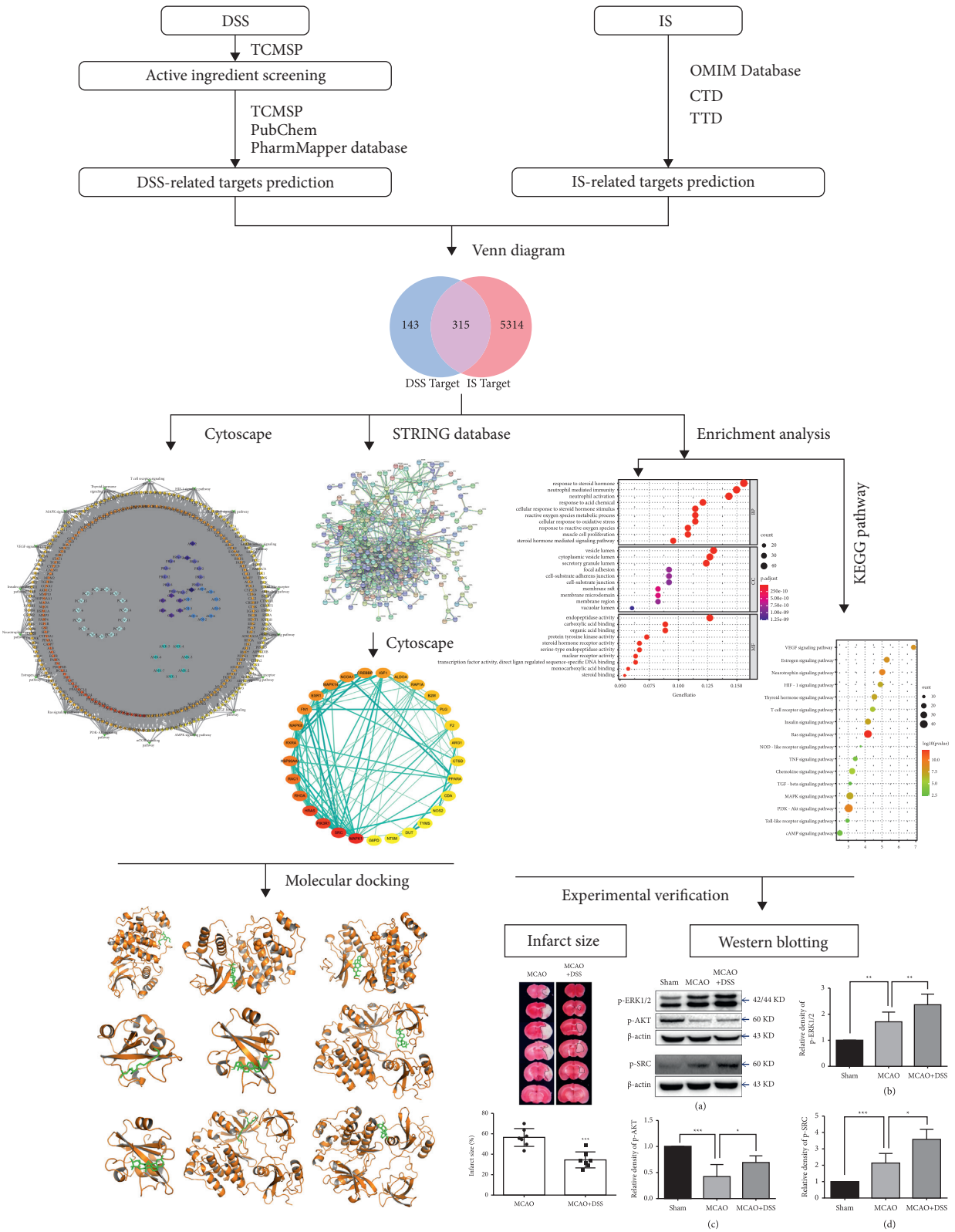

Figure 1: Flowchart of this study.

docking results, and the results were displayed by the software PyMOL [27].

2.6. Animal Model and Drug Administration. All animal experiments were approved by the Institutional Animal Care and Use Committee of Capital Medical University (XW-20210228-1) and in accordance with the principles outlined in the National Institutes of Health Guide for the Care and Use of Laboratory Animals. Male C57/BL6 mice (21–23 g) were used. Transient focal ischemia was induced by right middle cerebral artery occlusion (MCAO) using the intraluminal vascular occlusion method as previously described [28]. In brief, the right common carotid artery and the right external carotid artery (ECA) were exposed. The ECA was then dissected distally, ligated, and coagulated. The right MCA was occluded using a heparinized intraluminal filament. After 60 min, the suture was withdrawn. During surgery, rectal temperature was maintained at $37 \pm 0.5^{\circ}$C with a thermostat-controlled heating pad. Sham-operated mice underwent an identical surgery except that the MCA was not occluded. Sixty minutes after occlusion, the filament was removed and a laser speckle contrast imaging (PSI System, Perimed Inc.) was used to observe the local cerebral blood flow. The mice were randomly assigned to the sham, MCAO, and MCAO + DSS groups. The MCAO + DSS group was administered DSS (20 g/kg) via the intragastric route at the time of reperfusion.

2.7. Preparation of DSS. The materials of DSS were purchased from Tong Ren Tang Pharmaceutical Company (Beijing, China) and were then authenticated by Dr. Weipeng Yang in the China Academy of Chinese Medical Sciences. The DSS dilution was prepared as described previously [14]. In brief, the 6 raw herbs were mixed in their dry weight ratios of 3 : 16 : 3:8 : 4:4 (ASR : PRA : CR : AOJ: PCW : AMK). The mixture was soaked in distilled water (1 : 8 w/v) for 30 minutes at room temperature, boiled for 1.5 h, and the extract was filtered thereafter. The boiling and extraction procedures were repeated three times. The extracted filtrate was concentrated using a rotary evaporator, and the final concentration of the extract is 1 g/ml (equivalent to the dry weight of the raw materials). The DSS extract was then stored at 4°C.

2.8. Two-Dimensional Laser Speckle Imaging. Regional cerebral blood flow (CBF) was monitored by the two-dimensional laser speckle imaging before ischemia and after the onset of ischemia (10 min after MCAO). We calculated the blood flow ratio of the two cerebral hemispheres (right/left), and at a ratio less than 20%, the MCAO model was considered successful (Figures 2(a)–2(b)).

2.9. Infarct Size Measurement. Infarct size was measured according to previous methods [28]. Twenty-four hours after surgery, the mice ($n = 7$ per group) were anesthetized with 1% pentobarbital sodium, and then, the brains were removed and sectioned coronally at 1-mm intervals to generate 6 slices. The slices were then incubated with 2% solution of 2, 3, 4-triphenyltetrazolium chloride (TTC). The infarct area and the corresponding contralateral area were measured by a blinded observer using the Image-Pro Plus software 5.0 (Rockville, MD, USA). Infarct size was calculated as a percentage of the size of contralateral hemisphere.

2.10. Western Blot. Tissue samples were collected from the ischemic hemisphere at 24 hours and 7 days, respectively, after reperfusion for the Western blot analysis. The samples at 24 hours after reperfusion were used for the detection of phosphorylated MAPK1 (p-ERK1/2) and phosphorylated RAC-alpha serine/threonine-protein kinase (p-AKT). The samples at 7 days after reperfusion were used for the detection of phosphorylated proto-oncogene tyrosine-protein kinase Src (p-SRC). Protein (40 μg) was electrophoresed on 10% SDS polyacrylamide gels (Beijing Biotides Biotechnology Co., Ltd, Beijing, China) and then transferred to a polyvinylidene fluoride membrane (Millipore Corporation, USA). The membrane was probed with primary antibody: anti-p-ERK1/2 antibody (Cell Signaling; 1 : 1000 dilution), anti-p-AKT antibody (Cell Signaling; 1 : 1000 dilution), and anti-p-SRC antibody (Cell Signaling; 1 : 1000 dilution). The specific reaction was visualized through the use of a chemiluminescent substrate (GE Healthcare, UK) [29]. β-Actin was used to verify equal loading. The optical density of protein was measured using ImageJ software (NIH, Bethesda, MD, USA) according to the manufacturer's instructions ($n = 7$ per group).

2.11. Statistical Analysis. For two groups, the differences were analyzed for statistical significance by Student's t-test. For three or more groups, the differences were analyzed for statistical significance by the one-way ANOVA followed by Tukey's post hoc test. All the data were expressed as mean ± SD. The statistical analysis was performed with SPSS for Windows, version 21.0 (SPSS Inc.). The p-value <0.05 was considered significant.

3. Results

3.1. DSS Ingredient Collection and Target Gene Prediction. According to the two screening conditions of OB value and DL index, 54 active ingredients of DSS were obtained from TCMSP, including 13 ingredients in PRA, 7 ingredients in CR, 7 ingredients in AMK, 2 ingredients in ASR, 15 ingredients in PCW, and 10 ingredients in AOJ. ASR and PRA share one ingredient. PRA, AOJ, and CR share one ingredient (Table 1). Then, the target genes of 54 active ingredients were collected for target gene prediction in TCMSP and PubChem. A total of 14978 predicted targets were obtained. After removing the other species gene targets and duplicate values, 458 relevant human gene targets were obtained, including ASR (232), PRA (432), AOJ (377), CR(433), PCW (409), and AMK (359).

3.2. Drug Active Ingredient-Target Gene Interaction Network. The overlapping targets of DSS-related targets and IS-related targets were considered as potential therapeutic targets for

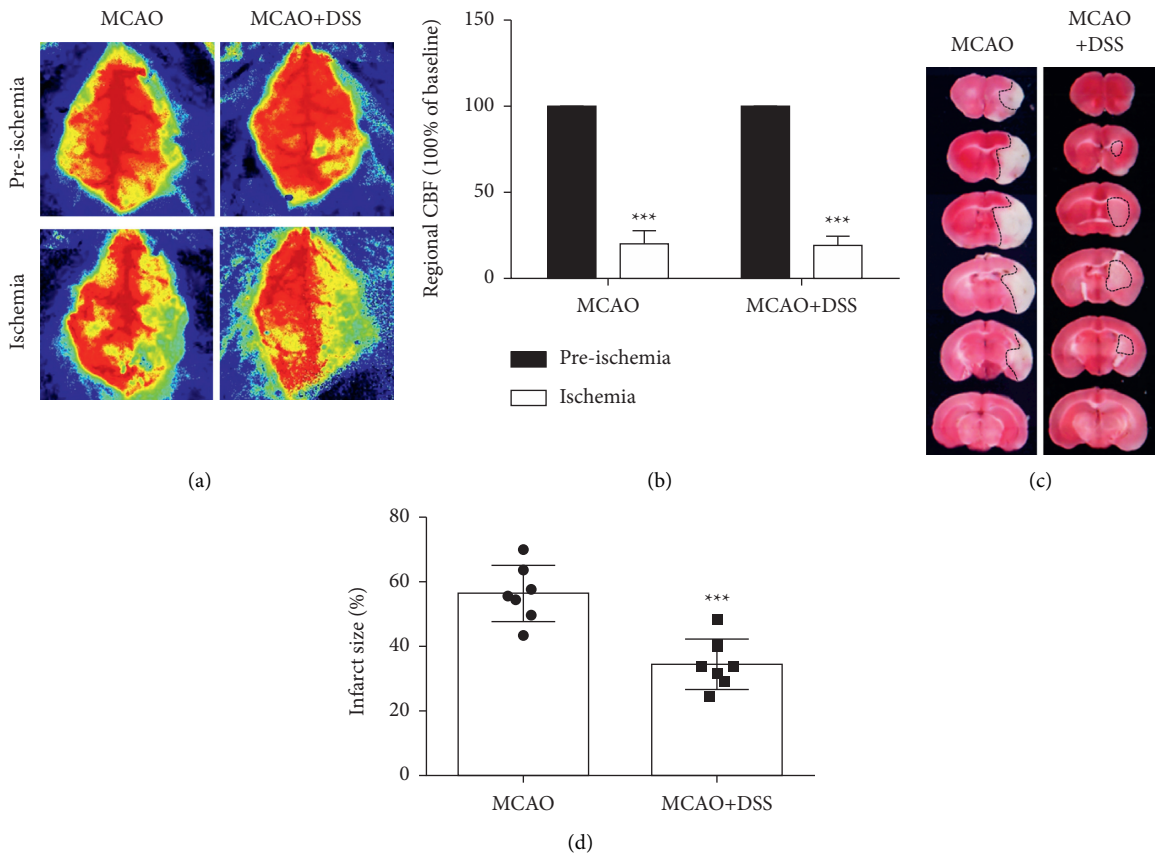

Figure 2: DSS treatment reduced infarct volume. (a) Regional cerebral blood flow (CBF) was monitored by the two-dimensional laser speckle imaging. (b) The blood flow ratio of two cerebral hemispheres (right/left), and a ratio less than 20% considered that the MCAO model is successful ($P < 0.05$). (c) Representative brain slices with infarcts stained by triphenyltetrazolium chloride from each group at 24 h after MCAO. (d) Quantification of infarct size at 24 h after MCAO. $N = 7$ per group. $^{***}P < 0.001$, vs. MCAO group, by Student's t-test.

DSS anti-IS. As shown in Figure 1, a total of 315 intersection targets were obtained by screening drug ingredient targets and IS targets (Figure 3(a)). Six kinds of drugs have 182 common targets (Table 2) (Figure 3(b)). Drug active component-target gene interaction network contained 366 nodes (including 51 herb compound nodes and 315 target gene nodes) and 11146 edges. The degree value of a node represents the number of lines connected to the node in the network. The larger node means more importance. Among 315 target gene nodes, the higher the degree of disease correlation, the redder the color (Figure 4). In addition, in the network pharmacological map of a single herb, the higher the degree value of the target gene to the herb, the closer it is to the herb component (Figure 5). The topology analysis showed that the average degree value of each node in the network was 208.4706, and the average medium was 0.016732. There were 17 compound nodes with both degree and intermediate values above the mean (Table 3), suggesting that these compounds may be key compounds in the treatment of stroke.

3.3. Construction of the PPI Network and Core Target Screening. 315 selected target genes were introduced into the STRING database to construct PPI network (Figure 6(a)). The PPI network contains 268 nodes and 1184 edges, indicating that 268 targets can interact with each other in the network, resulting in a total of 1184 interactions. After the analysis of topology parameters, the average node degree is 8.670412, and the average medium is 0.20796. There are 30 nodes with degree and intermediate values above the average, which were considered to be core targets of DSS in the treatment of IS (Figure 6(b), Table 4). According to the degree values, the top 10 core targets were identified as MAPK1, SRC, PIK3R1, HRAS, AKT1, RHOA, RAC1, HSP90AA1, RXRA, and FN1.

3.4. GO and KEGG Enrichment Analyses. 315 targets screened by the DAVID database were used for GO functional enrichment analysis and KEGG signaling pathway enrichment analysis (FDR < 0.01). As a result, we obtained 417 GO terms, including 288 biological processes (BPs), 86 molecular functions (MFs), and 43 cellular components (CCs). BP mainly includes negative regulation of apoptosis, steroid hormone-mediated signaling pathway, neutrophil activation, and cellular response to oxidative stress. MF mainly includes the activity of steroid hormone receptor and protein tyrosine kinase. CC mainly includes cytoplasm and extracellular bodies. The top 10 screened BP, MF, and CC

Table 1: Pharmaceutical ingredients.

Chinese name	Latin name	Molecule ID	Active ingredients	Ingredient code
Danggui	*Angelicae Sinensis Radix*	MOL000358	Beta-sitosterol	ASR-1
		MOL000449	Stigmasterol	ASR-2
Baishao	*Paeoniae Radix Alba*	MOL001921	Lactiflorin	PRA-1
		MOL001924	Paeoniflorin	PRA-2
		MOL000211	Mairin	PRA-3
		MOL000358	Beta-sitosterol	ASR-1
		MOL000359	Sitosterol	PRA-4
		MOL001930	Benzoyl paeoniflorin	PRA-5
		MOL001919	Palbinone	PRA-6
		MOL001925	Paeoniflorin	PRA-7
		MOL001910	11alpha,12alpha-epoxy-3beta-23-Dihydroxy-30-nor--olean-20-en-28,12beta-olide	PRA-8
		MOL001918	Paeoniflorin genome	PRA-9
		MOL001928	Albiflorin	PRA-10
		MOL000492	Cianidanol	PRA-11
		MOL000422	Kaempferol	PRA-12
Zexie	*Alisma Orientale* (Sam.) Juz.	MOL000856	Alisol C monoacetate	AOJ-1
		MOL000853	Alisol B	AOJ-2
		MOL000832	Alisol B 23-acetate	AOJ-3
		MOL000830	Alisol B	AOJ-4
		MOL000854	Alisol C	AOJ-5
		MOL000862	Alisol B 23-acetate	AOJ-6
		MOL000831	Alisol B monoacetate	AOJ-7
		MOL000849	16β-Methoxyalisol B monoacetate	AOJ-8
		MOL000359	Sitosterol	PRA-4
		MOL002464	1-Monolinolein	AOJ-9
Chuanxiong	*Chuanxiong Rhizoma*	MOL000359	Sitosterol	PRA-4
		MOL002157	Wallichilide	CR-1
		MOL000433	Folsaeure	CR-2
		MOL002135	Myricanone	CR-3
		MOL002140	Perlolyrine	CR-4
		MOL002151	Senkyunone	CR-5
		MOL001494	Mandenol	CR-6
Fuling	*Poria cocos* (Schw.) Wolf.	MOL000300	Dehydroeburicoic acid	PCW-1
		MOL000285	Polyporenic acid C	PCW-2
		MOL000280	Dehydrotumulosic acid	PCW-3
		MOL000273	16alpha-Hydroxydehydrotrametenolic acid	PCW-4
		MOL000283	Ergosterol peroxide	PCW-5
		MOL000276	7, 9 (11)-dehydropachymic acid	PCW-6
		MOL000289	Pachymic acid	PCW-7
		MOL000287	Eburicoic acid	PCW-8
		MOL000275	Trametenolic acid	PCW-9
		MOL000279	Cerevisterol	PCW-10
		MOL000290	Poricoic acid A	PCW-11
		MOL000296	Hederagenin	PCW-12
		MOL000292	Poricoic acid C	PCW-13
		MOL000291	Poricoic acid B	PCW-14
		MOL000282	Stellasterol	PCW-15
Baizhu	*Atractylodes macrocephala Koidz.*	MOL000033	(24S)-24-Propylcholesta-5-ene-3beta-ol	AMK-1
		MOL000028	A-Amyrin	AMK-2
		MOL000021	14-Acetyl-12-senecioyl-2E, 8E, 10E-atractylentriol	AMK-3
		MOL000022	14-Acetyl-12-senecioyl-2E, 8Z, 10E-atractylentriol	AMK-4
		MOL000020	12-Senecioyl-2E, 8E, 10E-atractylentriol	AMK-5
		MOL000049	3β-Acetoxyatractylone	AMK-6
		MOL000072	8β-Ethoxy atractylenolide III	AMK-7

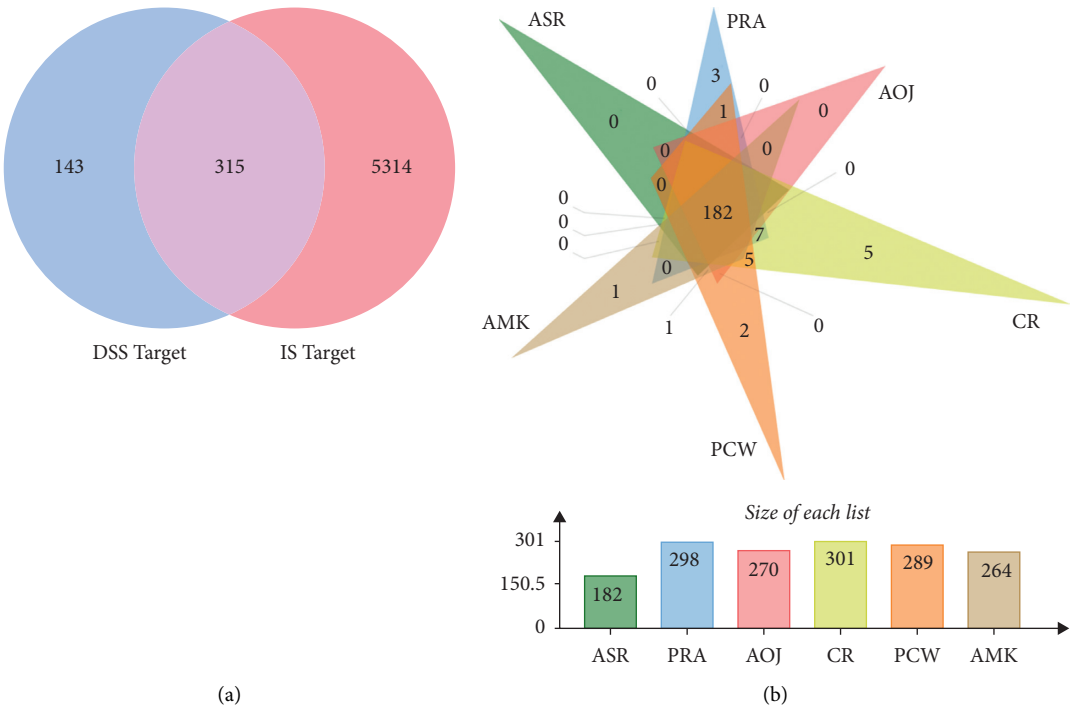

Figure 3: Identification of the drug-target interaction. (a) Venn diagram. (b) Drug-disease target analysis of traditional Chinese medicine. 182 represents the common targets of six Chinese medicines, and other figures indicate the unique targets of each Chinese medicine. PRA, *Paeoniae Radix Alba*. AMK, *Atractylodes macrocephala Koidz.*, CR, *Chuanxiong Rhizoma*. ASR, *Angelicae Sinensis Radix*. PCW, *Poria cocos* (Schw.) Wolf. AOJ, *Alisma orientale* (Sam.) Juz.

Table 2: Drug active ingredient-target gene (common targets of six drugs).

Gene	Gene ID
CASP3	836
SOD2	6648
NOS3	4846
HMOX1	3162
MAPK1	5594
F2	2147
MMP2	4313
GSK3B	2932
MAPK8	5599
IL-2	3558
PPARG	5468
NR3C1	2908
MAPK14	1432
REN	5972
F3	2152
IGF-1	3479
BCL2L1	598
PARP1	142
EGFR	1956
CASP7	840
ALB	213
CYP19A1	1588
PPARA	5465
GSR	2936
FABP4	2167
IGF-1R	3480
MMP3	4314
MAOA	4128

Table 2: Continued.

Gene	Gene ID
NQO1	1728
MMP13	4322
HSP90AA1	3320
CCNA2	890
AKR1C3	8644
MDM2	4193
TGFBR1	7046
CALM1	801
PGR	5241
TGFB2	7042
CYP2C9	1559
ESR1	2099
NR3C2	4306
KDR	3791
GSTP1	2950
F7	2155
AR	367
NR1I2	8856
AURKA	6790
MAP2K1	5604
B2M	567
CASP1	834
HSPA8	3312
MAOB	4129
FGFR1	2260
HSP90AB1	3326
HMGCR	3156
JAK2	3717
MME	4311
CTSB	1508
LCN2	3934
HSD11B1	3290
SRC	6714
XIAP	331
SULT1E1	6783
VDR	7421
GSTA1	2938
GCK	2645
INSR	3643
CDK2	1017
NCOA2	10499
S100A9	6280
FABP5	2171
BMP2	650
TEK	7010
MET	4233
CDK6	1021
CYP2C8	1558
CTSK	1513
PSAP	5660
THRB	7068
PDPK1	5170
ADAM17	6868
KIT	3815
EPHX2	2053
FKBP1A	2280
MMP12	4321
CTSS	1520
MAPK10	5602
FABP3	2170

Table 2: Continued.

Gene	Gene ID
RARA	5914
MAPKAPK2	9261
PIK3R1	5295
PDE4D	5144
LSS	4047
AKT2	208
PIM1	5292
AKR1B1	231
PLA2G2A	5320
NR1I3	9970
OAT	4942
DUSP6	1848
PGF	5228
CHEK1	1111
ESRRA	2101
PPIA	5478
TNNC1	7134
AKR1C1	1645
GSTM1	2944
HCK	3055
SULT2A1	6822
PDK2	5164
F10	2159
RORA	6095
NR1H3	10062
AKR1C2	1646
EIF4E	1977
BRAF	673
CA2	760
AMD1	262
MMP8	4317
JAK3	3718
NCOA1	8648
NR1H4	9971
THRA	7067
PDE4B	5142
PTPN11	5781
GART	2618
RBP4	5950
PDE5A	8654
BACE1	23621
WAS	7454
GRB2	2885
PTPN1	5770
PROCR	10544
SDS	10993
PPP5C	5536
PRKCQ	5588
BCHE	590
ACADM	34
DHFR	1719
FGFR2	2263
TTR	7276
PYGL	5836
GC	2638
ANXA5	308
CES1	1066
LCK	3932
DPP4	1803
FKBP1B	2281

Table 2: Continued.

Gene	Gene ID
FABP7	2173
FECH	2235
STS	412
ELANE	1991
BAG1	573
ERBB4	2066
GM2A	2760
TPX2	22974
PLK1	5347
TYMS	7298
DCK	1633
BHMT	635
CTNNA1	1495
CRABP2	1382
ESRRG	2104
RXRA	6256
MTAP	4507
SHBG	6462
NCOA5	57727
PPARD	5467
ABL1	25
TTPA	7274
FKBP3	2287
GRB14	2888
PCTP	58488
CTSF	8722
ADK	132
HSD17B1	3292
KIF11	3832
RFK	55312
FNTB	2342
YARS1	8565
HNMT	3176
BCAT2	587

were selected as bubble charts through R language-related procedures (Figure 7).

The enrichment and screening of KEGG pathways resulted in 119 signaling pathways (FDR < 0.01) and 16 pathways related to stroke (Figure 8). The main pathway included VEGF signaling pathway, estrogen signaling pathway, neurotrophin signaling pathway, HIF-1 signaling pathway, and thyroid hormone signaling pathway.

3.5. Molecular Docking. The top 3 key target proteins (MAPK1, PIK3R1, and SRC) in PPI network were selected to dock with the top 3 key active compounds ("11alpha, 12alpha-epoxy-3beta-23-dihydroxy-30-norolean-20-en-28,12beta-olide," "eburicoic acid," "12-senecioyl-2E, 8E, 10E-atractylentriol"). The PyMOL software was used to visualize the docking results of key active ingredients and core targets, as shown in Figure 9 and Table 5.

3.6. DSS Treatment Reduced Infarct Size. To confirm the neuroprotection of DSS in focal ischemic stroke, the MCAO mice were treated with DSS, and 24 hours later, the infarct size was detected by TTC stain. Compared with the MCAO group (56.47 ± 3.30), the infarct size was reduced by 39% in the MCAO + DSS group (34.49 ± 2.94) ($P = 0.0003$) (Figure 2).

3.7. DSS Modulated the Expression of p-AKT, p-ERK1/2, and p-SRC. To evaluate the performance of the core target screening approach used in this study, we selected the three major target proteins for analysis by the Western blot. The level of p-ERK1/2 was significantly increased in the MCAO mice (MCAO vs. sham, $p < 0.01$) and further significantly increased after LRIC treatment (MCAO + DSS vs. MCAO, $p < 0.01$) (Figure 10). Moreover, compared with the sham group, the expression of p-AKT in the MCAO group was decreased ($P < 0.001$), but that in the DSS group was significantly upregulated compared with the MCAO group ($p < 0.05$) (Figure 2). We also measured the expression levels of p-SRC at day 7 after MCAO surgery, finding that, when compared with the sham group, the levels of p-SRC in the MCAO mice were significantly increased ($P < 0.001$). DSS treatment for 7 days increased the levels of p-SRC compared with those found in the MCAO group ($P < 0.05$) (Figure 10).

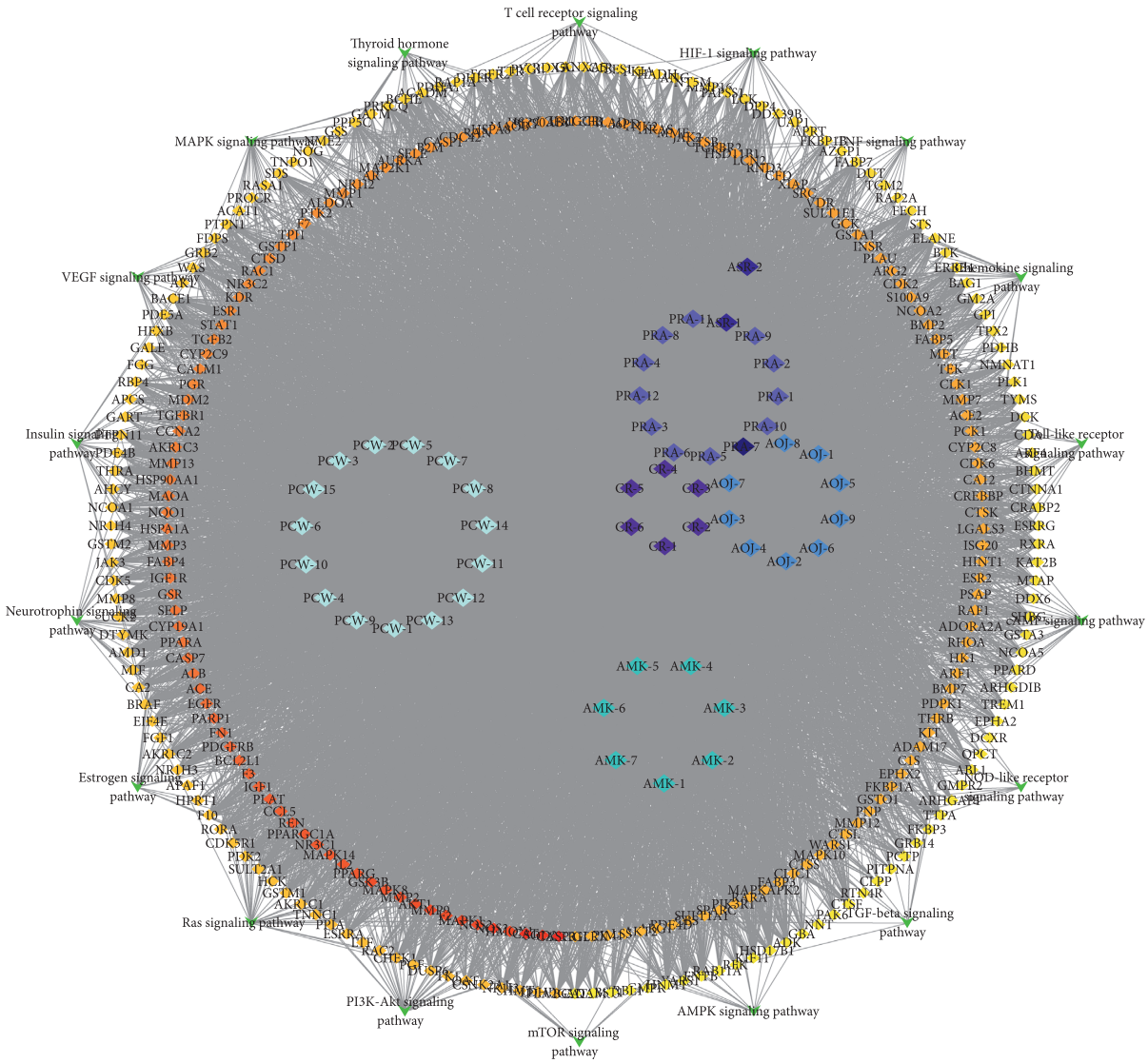

Figure 4: DSS prescription compositions of active ingredient-target pathway network. Rhombus represents the active ingredients of herbs contained in DSS. The degree value of a node represents the number of lines connected to the node in the network. The higher the degree value, the more important the node. The round nodes represent disease targets. The higher the degree of disease correlation, the redder the color is.

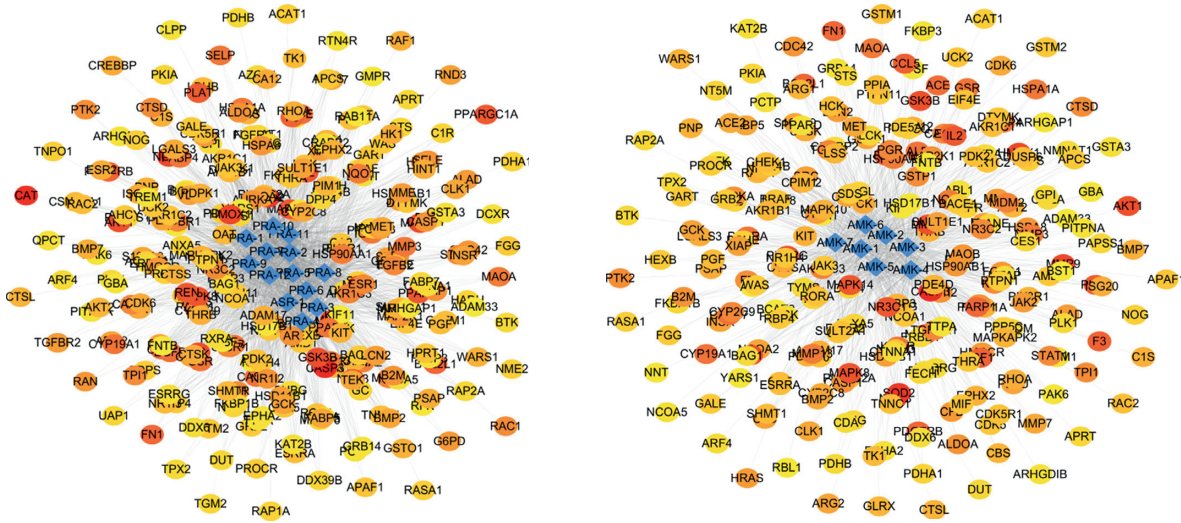

(a) (b)

Figure 5: Continued.

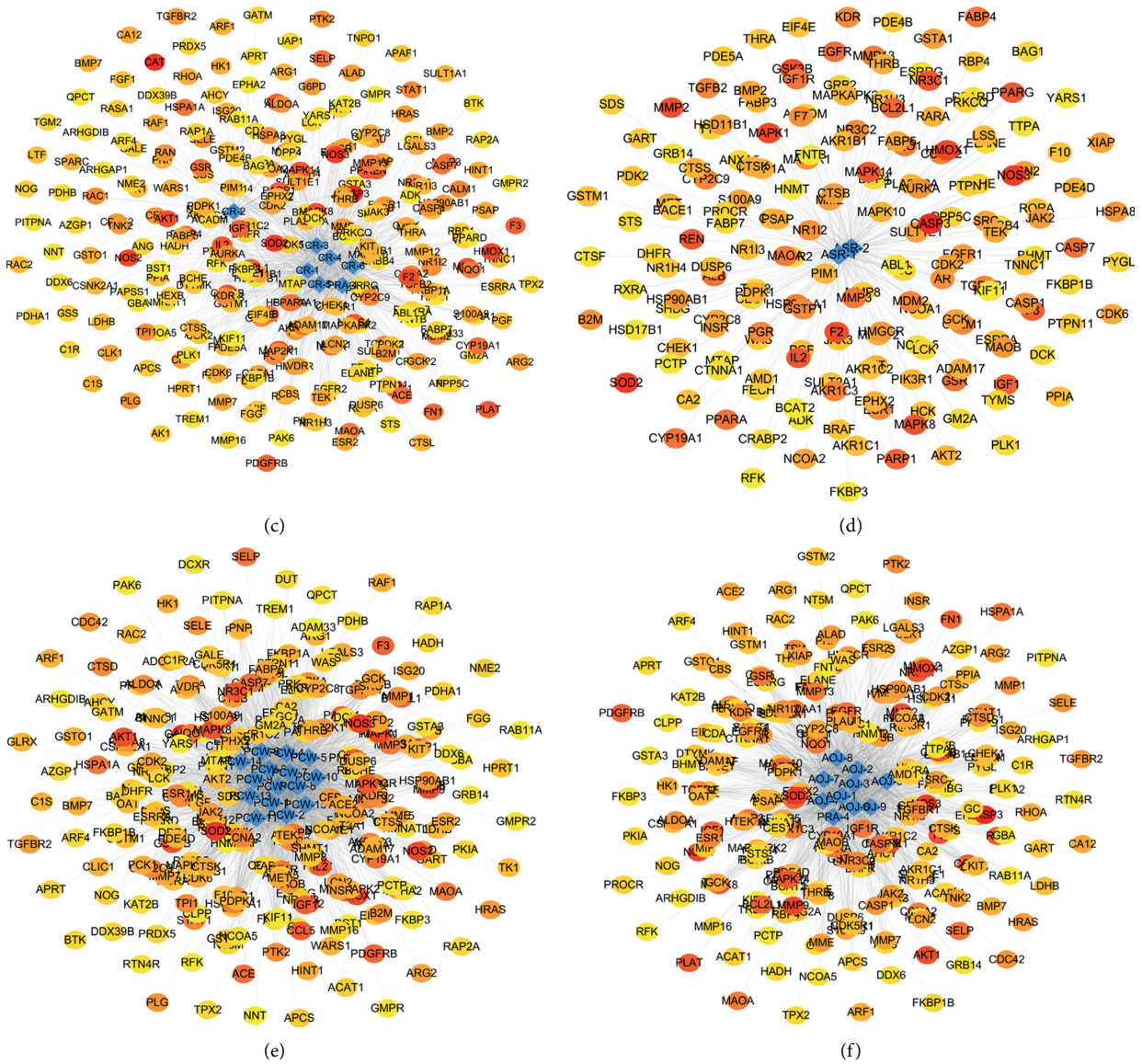

FIGURE 5: The network pharmacological diagram of a single herb. (a) PRA, *Paeoniae Radix Alba*. (b) AMK, *Atractylodes macrocephala Koidz*. (c) CR, *Chuanxiong Rhizoma*. (d) ASR, *Angelicae Sinensis Radix*. (e) PCW, *Poria cocos* (Schw.) Wolf. (f) AOJ, *Alisma orientale* (Sam.) Juz. Rhombus represents the active ingredients of herbs contained in DSS. The round nodes represent disease targets. The higher the degree of disease correlation, the redder the color is. The higher the degree value of the target gene to the herb, the closer it is to the herb component.

TABLE 3: Key compounds. (The average degree value is 208.4706, and the average medium is 0.016732.)

Compound	Compound ID	Degree	Betweenness centrality
11alpha,12alpha-epoxy-3beta-23-Dihydroxy-30-nor-olean-20-en-28,12beta-olide	PRA-8	228	0.024789
Eburicoic acid	PCW-8	226	0.017975
12-Senecioyl-2E, 8E, 10E-atractylentriol	AMK-5	225	0.021314
Dehydroeburicoic acid	PCW-1	225	0.01739
14-Acetyl-12-senecioyl-2E, 8Z, 10E-atractylentriol	PRA-11	223	0.028611
Cianidanol	AMK-4	223	0.01698
Alisol C	AOJ-5	221	0.017782
16alpha-Hydroxydehydrotrametenolic acid	PCW-4	221	0.017585
Poricoic acid C	PCW-13	220	0.021088
Palbinone	PRA-6	219	0.024345
Cerevisterol	PCW-10	217	0.017087
Poricoic acid A	PCW-11	216	0.02044
Kaempferol	PRA-12	215	0.032249
Paeoniflorin	PRA-2	215	0.017069
Lactiflorin	PRA-1	214	0.016884
Poricoic acid B	PCW-14	213	0.021272
Myricanone	CR-3	209	0.041457

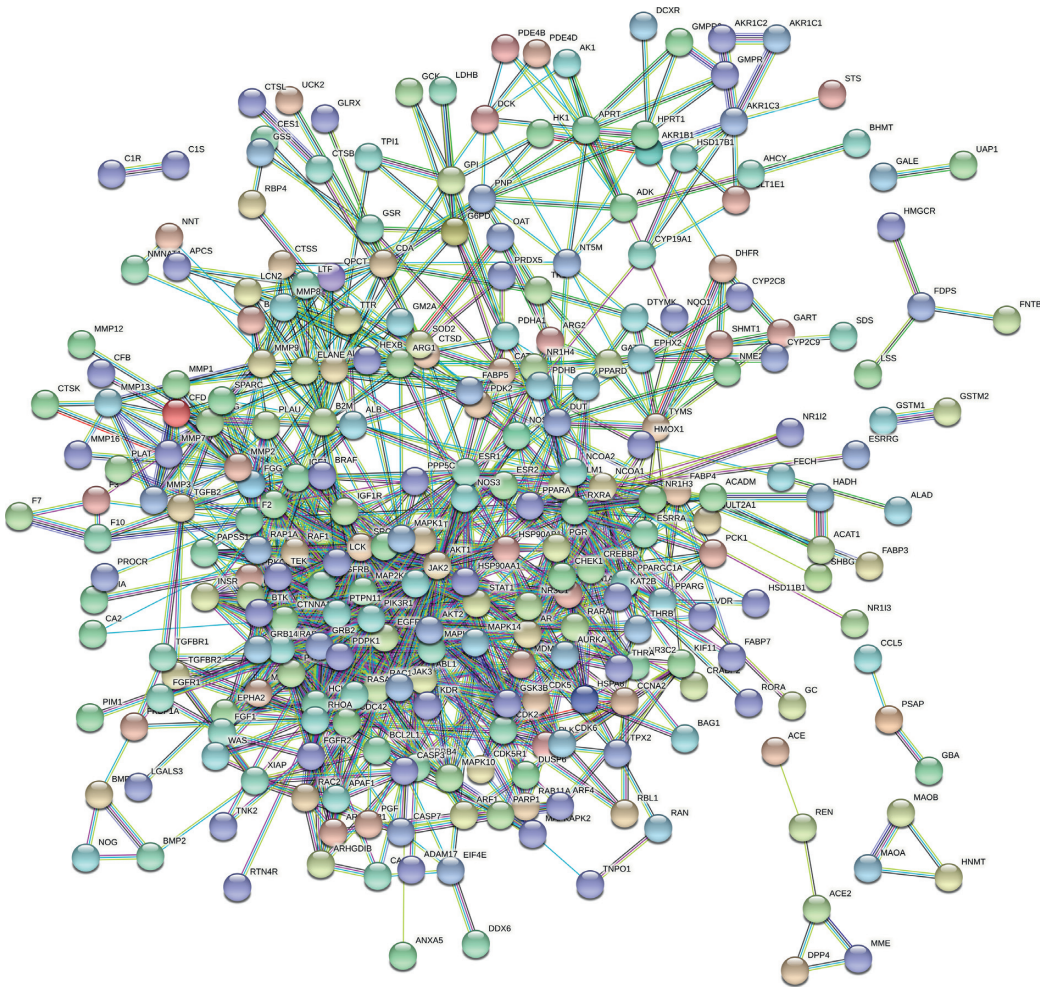

(a)

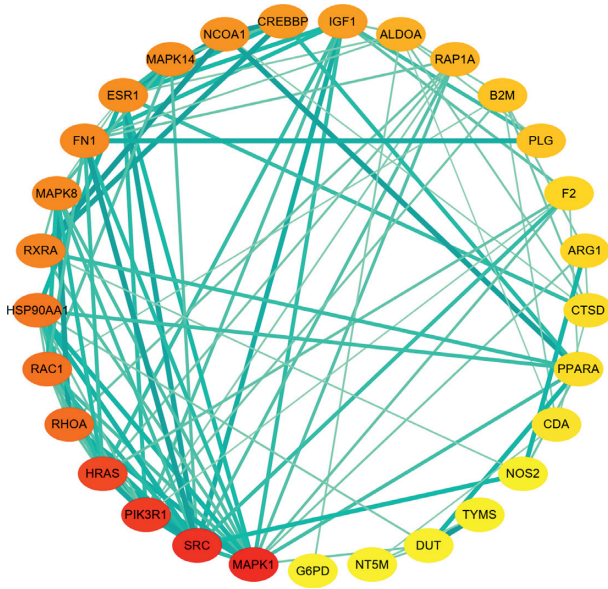

(b)

FIGURE 6: PPI network and top 30 hub genes for DSS anti-IS. (a) PPI network constructed with the STRING database. (b) Top 30 hub genes for DSS anti-IS were obtained using the degree and betweenness centrality algorithm. The node size and color indicate the degree value. The heavier the color, the greater the degree value and the wider the line and the heavier its color, indicating the closer the connection between the two proteins.

Table 4: Drug targets of IS. (The average degree value is 8.670412, and the average medium is 0.20796.)

Gene	Protein name	Degree	Betweenness centrality
MAPK1	Mitogen-activated protein kinase 1	53	0.126385
SRC	Proto-oncogene tyrosine-protein kinase Src	50	0.052449
PIK3R1		47	0.047873
HRAS	GTPase HRas	44	0.033552
AKT1	Phosphatidylinositol 3-kinase regulatory subunit alpha	40	0.109791
RHOA	Transforming protein RhoA	35	0.047081
RAC1	Ras-related C3 botulinum toxin substrate 1	34	0.0268
HSP90AA1	Heat shock protein HSP 90-alpha	33	0.059285
RXRA	Retinoic acid receptor alpha , RAR-alpha	30	0.067159
FN1	Fibronectin 1	29	0.023024
MAPK8	Mitogen-activated protein kinase 8	29	0.022235
ESR1	Estrogen receptor	28	0.091184
MAPK14	Mitogen-activated protein kinase 14	28	0.058202
NCOA1	Nuclear receptor coactivator 1	27	0.039326
CREBBP	CREB binding protein	26	0.03777
IGF-1	Insulin-like growth factor I	25	0.024056
ALDOA	Fructose-bisphosphate aldolase A	22	0.065989
RAP1A	Ras-related protein Rap-1A	21	0.026304
B2M	Beta-2-microglobulin	19	0.034377
PLG	Plasminogen	19	0.023626
F2	Prothrombin	16	0.028418
ARG1	Arginase-1	16	0.021575
CTSD	Cathepsin D	15	0.037545
PPARA	Peroxisome proliferator-activated receptor alpha	15	0.028961
CDA	Cytidine deaminase	14	0.059555
TYMS	Thymidylate synthase	11	0.037145
NOS3	Nitric oxide synthase 3	11	0.036816
DUT	Deoxyuridine triphosphatase	9	0.057749
NT5M	5′(3′)-Deoxyribonucleotidase, mitochondrial	9	0.048718
G6PD	Glucose-6-phosphate dehydrogenase	9	0.027099

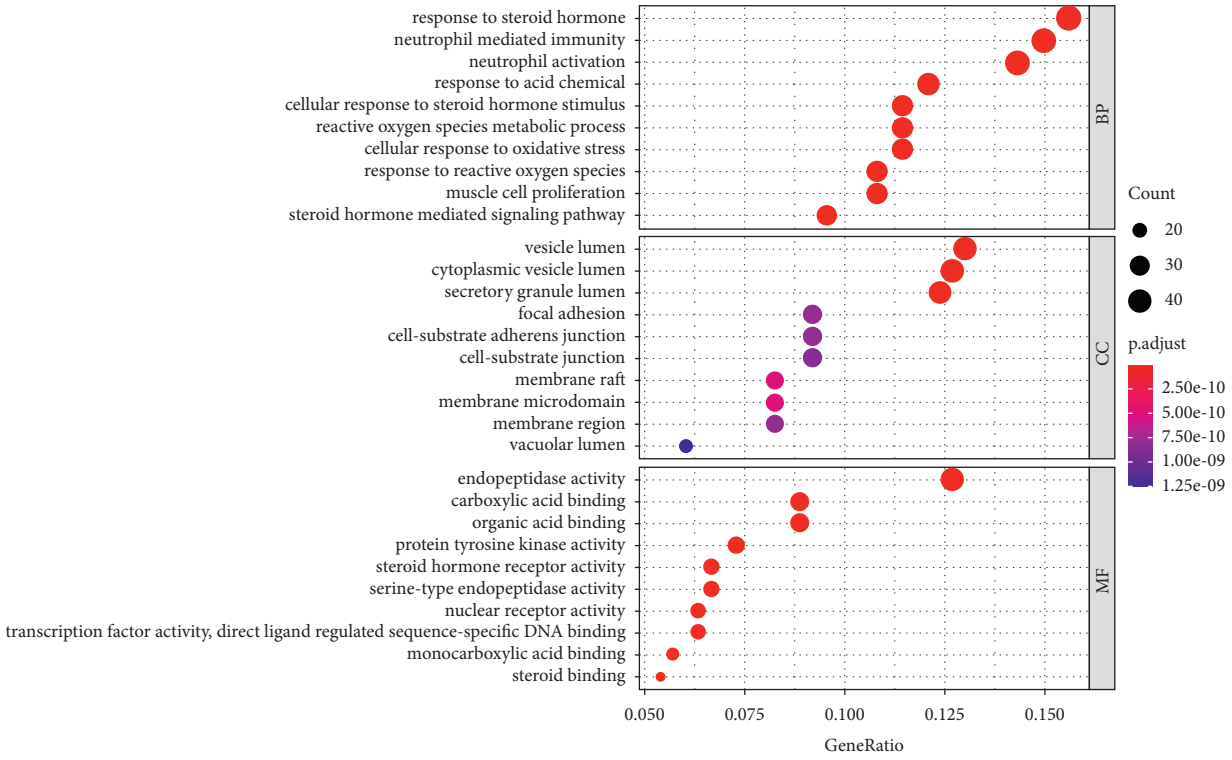

Figure 7: Functional classification of drug-disease targets by bioinformatic analysis. The biological process (BP), cellular component (CC), and molecular function (MF). Gene ratio refers to the ratio of enriched genes to all target genes, and counts refer to the number of the enriched genes.

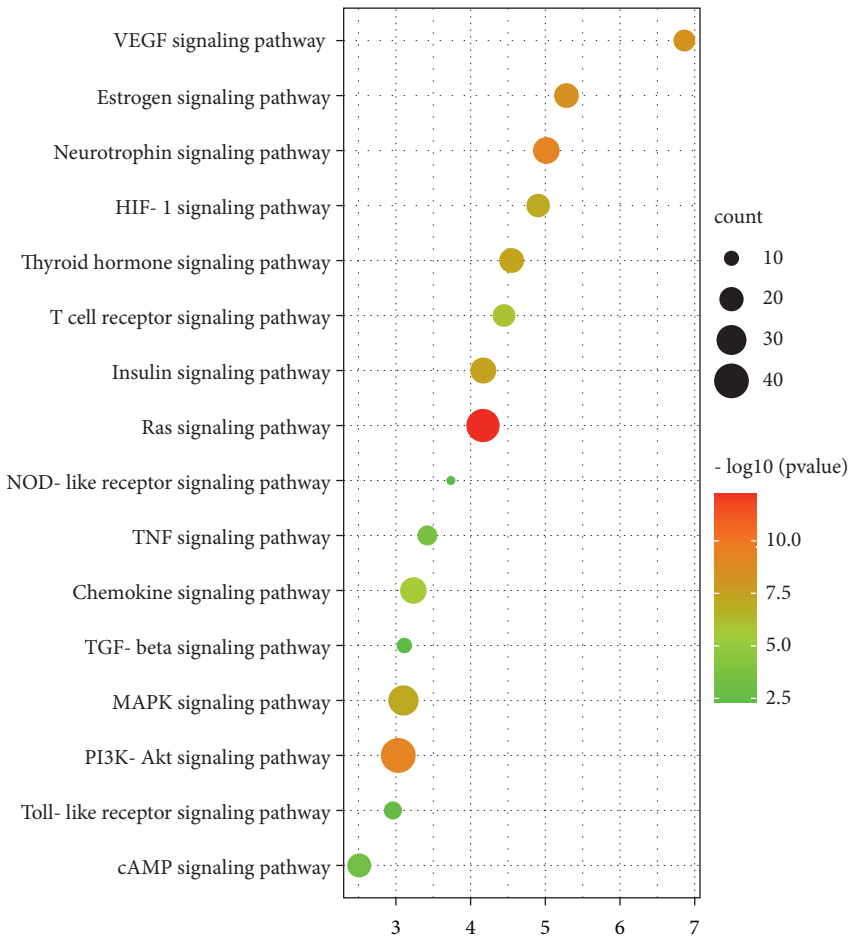

Figure 8: KEGG signaling pathway enrichment of screened genes. The bar chart showed the 16 pathways related to stroke. "Rich factor" represents the ratio of the number of target genes belonging to a pathway and the number of the annotated genes located in the pathway. A higher rich factor represents a higher level of enrichment. The size of the dot indicates the number of target genes in the pathway, and the color of the dot reflects the different *P* values.

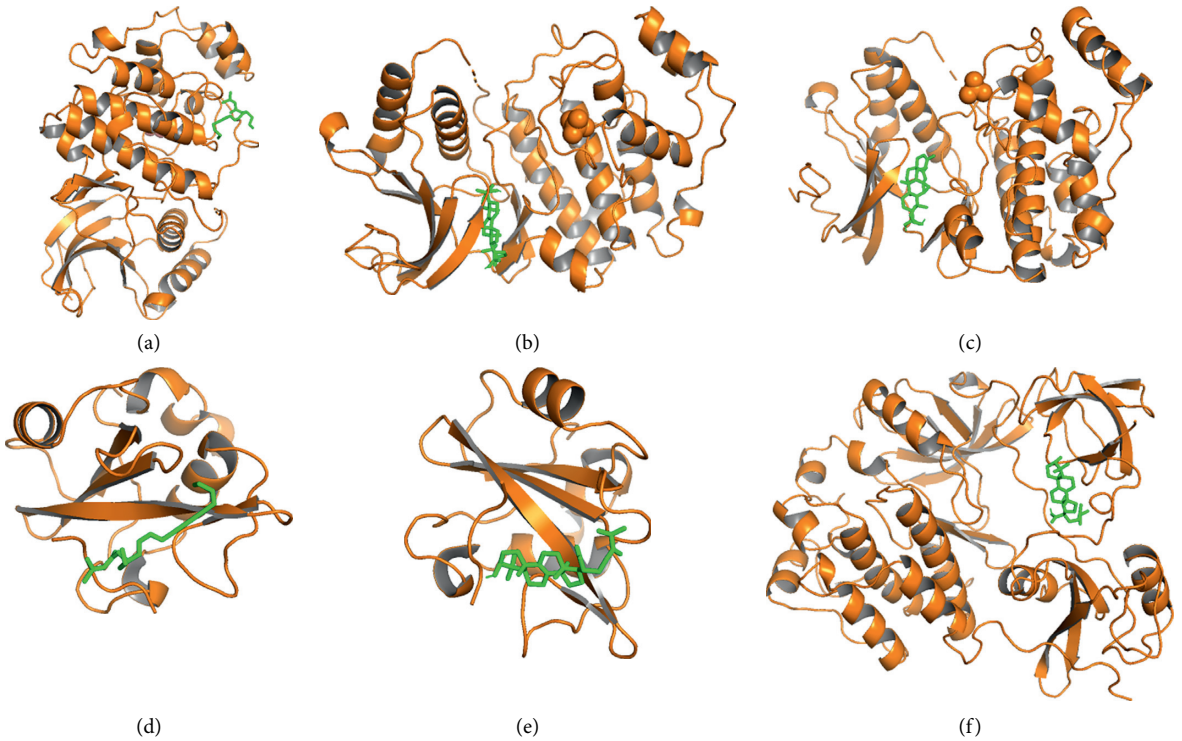

Figure 9: Continued.

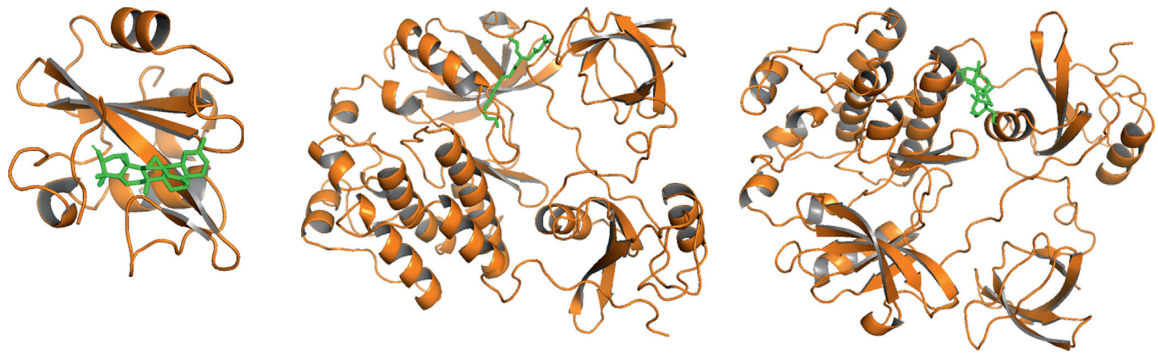

(g) (h) (i)

Figure 9: Docking results of the key ingredient and three hub target proteins. (a) 12-senecioyl-2E, 8E, 10E-atractylentriol and MAPK1; (b) eburicoic acid and MAPK1; (c) 11alpha,12alpha-epoxy-3beta-23-dihydroxy-30-nor-olean-20-en-28,12beta-olide and MAPK1; (d) 12-senecioyl-2E, 8E, 10E-atractylentriol and PI3K; (e) eburicoic acid and PI3K; (f) 11alpha,12alpha-epoxy-3beta-23-dihydroxy-30-nor-olean-20-en-28,12beta-olide and PI3K; (g) 12-senecioyl-2E, 8E, 10E-atractylentriol and SRC; (h) eburicoic acid and SRC; (i) 11alpha,12alpha-epoxy-3beta-23-dihydroxy-30-nor-olean-20-en-28,12beta-olide and SRC.

Table 5: Binding energy between the key ingredients and target proteins.

NO.	Receptor protein	Molecule ID	Ligand component	Binding energy (kcal·mol-1)
1	MAPK1	MOL000020	12-Senecioyl-2E, 8E, 10E-atractylentriol	−5.99
2	MAPK1	MOL000287	Eburicoic acid	−8.64
3	MAPK1	MOL001910	11alpha,12alpha-epoxy-3beta-23-Dihydroxy-30-nor-olean-20-en-28, 12beta-olide	−9.32
4	PIK3R1	MOL000020	12-Senecioyl-2E, 8E, 10E-atractylentriol	−6.66
5	PIK3R1	MOL000287	Eburicoic acid	−9.24
6	PIK3R1	MOL001910	11alpha,12alpha-epoxy-3beta-23-Dihydroxy-30-nor-olean-20-en-28, 12beta-olide	−10.18
7	SRC	MOL000020	12-Senecioyl-2E, 8E, 10E-atractylentriol	−7.57
8	SRC	MOL000287	Eburicoic acid	−9.42
9	SRC	MOL001910	11alpha,12alpha-epoxy-3beta-23-Dihydroxy-30-nor-olean-20-en-28, 12beta-olide	−9

4. Discussion

In this study, the anti-IS mechanism underlying the effect of DSS was explored using network pharmacology through data mining and subsequent computational modeling. It was noteworthy that our findings partially elucidate the complex anti-IS mechanism in the DSS, and they provide insight into the integrated understanding of the therapeutic efficacy and pharmaceutical activity of DSS. First, a total of 534 active ingredients were extracted from DSS. The possible targets of DSS were mined using the TCMSP database. PPI data were used to construct the core PPI network. Then, 30 candidate anti-IS targets of DSS were identified as the pivotal hub genes in the core PPI network according to the specific topological importance. In addition, GO and KEGG pathway analyses were carried out to demonstrate the candidate target biological significance after the pivotal hub genes were incorporated into ClueGO. Finally, we evaluate the neuroprotection role of DSS in IS stroke mice and detected the effect of DSS on the major drug targets in IS treatment using the Western blot.

4.1. DSS May Contribute to the Treatment of IS by Diminishing Apoptosis, Reducing Inflammation, and Oxidative Stress at Acute Stage. Cerebral ischemia-reperfusion injury induces a complex pathophysiological cascade that includes a wide range of aberrant cellular processes [30]. In the ischemic phase, reduced blood supply rapidly leads to failure of ionic gradients, excitotoxicity, and neuronal death. During the reperfusion phase, the return of oxygen contributes to oxidative stress, and the restoration of blood introduces factors that promote inflammation and edema, thereby further increasing the vulnerability of the affected tissue to death [30].

The increasing number of reports shows that apoptosis may contribute to a significant proportion of neuron death following IS [31]. Mechanistic studies have established that decreasing pro-apoptotic proteins or enhancing pro-survival proteins protects the brain after cerebral ischemia. We found that MAPK1 is the key target of DSS in the treatment of IS, and AKT1, GSK3, CASP3, and BCL2 are also among the targets. MAPK includes the extracellular signal-regulated kinase 1/2 (ERK1/2) subfamily. The phosphatidylinositol 3-

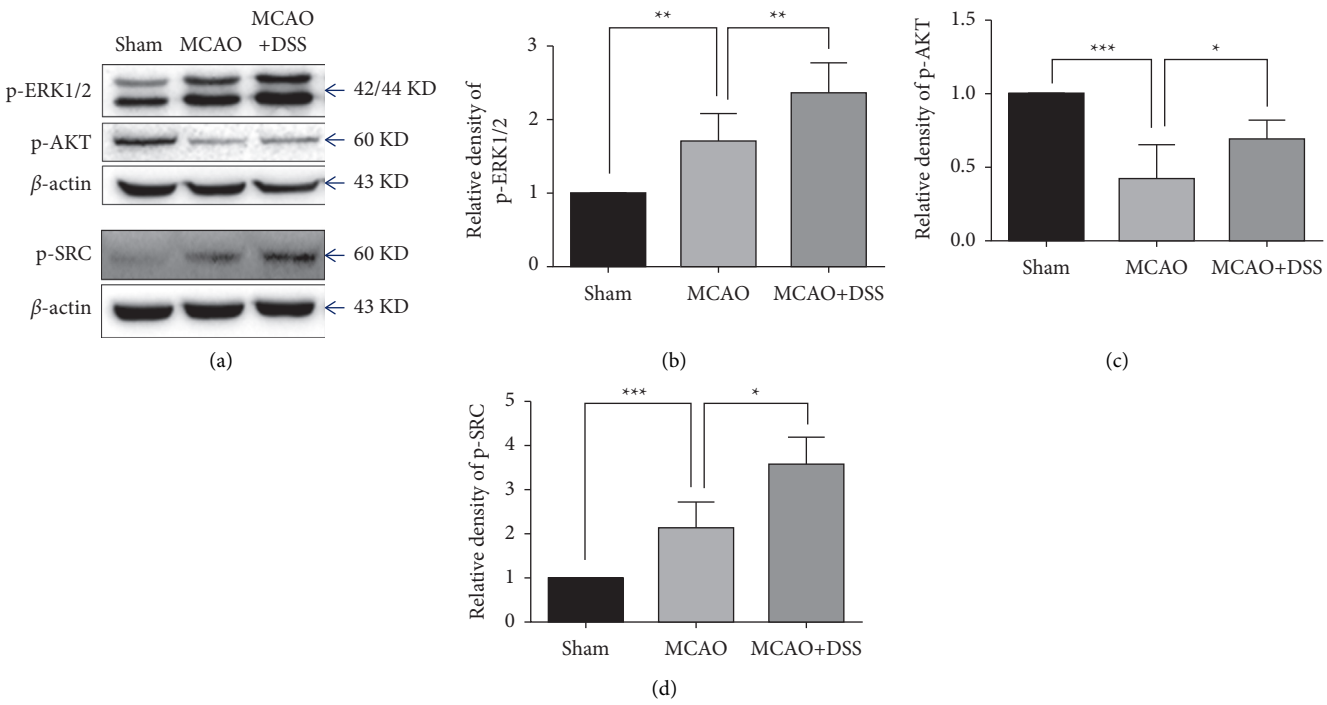

Figure 10: Expression of protein detected through the Western blot. (a) Representative Western blots of p-ERK1/2 and p-AKT at day 1 after MCAO surgery and the levels of p-SRC at day 7 after MCAO surgery. (b-d) Quantification of p-ERK1/2, p-AKT, and p-SRC, respectively. Values are mean ± SD. $^{*}P < 0.05$, $^{**}P < 0.01$, $^{***}P < 0.001$. $N = 7$ per group.

kinase/Akt (PI3K/Akt) is an important signaling pathway involved in the regulation of cell apoptosis after stroke [32]. Many studies have shown that the activation of AKT and ERK1/2 can effectively inhibit apoptosis by regulating the expression of the anti-apoptosis gene Bcl-2 [33, 34]. Activated Akt promotes cell survival and suppresses apoptosis partly via inhibiting glycogen synthase kinase-3β (GSK3β), an apoptosis-related molecule [31]. Caspase-3 is considered to play an executing role at the final step of apoptosis-producing DNA fragmentation [31]. The report showed that DSS reduced the expression of caspase-3 and upregulated the expression of Bcl-2 at the MCAO rat model [11]. In this study, the Western blot results revealed that DSS significantly regulated the expression of p-ERK1/2, p-AKT, and Bcl-2. MAPK1 (ERK1/2) and PI3K, the two key targets, created 3D graphs of docking and analysis. Docking their crystal structures with the compounds, we showed that the two genes could be attached to the active pocket of the protein.

Inflammation after cerebral ischemia is a complicated pathological process starting from the activation of microglia, circulating leukocyte infiltrate (such as neutrophils, lymphocytes, and macrophages), and releasing of pro-inflammatory mediators mediated by ischemic cells and immune cells [30, 35]. Our GO analysis showed that DSS regulated neutrophil activation and neutrophil mediated immunity. Experimental models have shown that the inhibition of neutrophilic inflammatory mechanisms reduces neurodegeneration and improves functional outcome after cerebral ischemia [36]. Based on the KEGG pathway analysis, DSS influences TNF signaling pathway. TNF signaling pathway mediates a wide range of cellular processes including inflammation, proliferation, cell migration, apoptosis, and necrosis [37]. Studies confirm that the inhibition of TNF signaling pathway might be associated with reducing neuroinflammation in IS [38].

An imbalance between free radical production and antioxidant activity leads to oxidative stress, which is a major pathologic mechanism of secondary brain damage after cerebral ischemia [30]. Our GO analysis showed that the mechanism of DSS in the treatment of IS was related to cellular response to oxidative stress and reactive oxygen species metabolic process. Superoxide dismutase 2 (SOD2) and peroxisome proliferator-activated receptor alpha (PPARA) are the core targets of DSS in IS treatment. SOD2 is an enzymatic antioxidant that catalyzes the conversion of H2O2 and helps maintain the redox balance by diffusing the superoxide. Therapeutically increasing the levels of SOD2 could be an important treatment strategy in oxidative stress-induced pathology [39]. PPARA is a member of the PPAR nuclear receptor subfamily. Several studies have demonstrated that PPARA-mediated reduction in oxidative stress correlates with improved outcomes in rodent stroke models [40]. Recently, the study showed that DSS could attenuate oxidative stress against cerebral ischemic-reperfusion injury via SIRT1-dependent manner [11].

4.2. DSS May Contribute to the Treatment of IS by Increased Angiogenesis and Neurogenesis at Chronic Stage. Spontaneous neurogenesis and angiogenesis in the post-acute phase are highly coordinated responses and may

contribute to the improvement in neurologic function after stroke. Accumulating experimental studies showed that promoting post-ischemic angiogenesis and neurogenesis can improve neurological function [41]. Ischemic stroke promotes neurogenesis by several growth factors including FGF-2, IGF-1, BDNF, VEGF, and chemokines including SDF-1 and MCP-1. Stroke-induced angiogenesis is similarly regulated by many factors most notably eNOS and CSE, VEGF/VEGFR2, and Ang-1/Tie2 [41]. KEGG enrichment analysis showed that VEGF signaling pathway and FGF signaling pathway were part of the ten major signaling pathways, suggesting that the mechanisms of DSS in the treatment of IS were related to the angiogenesis. SRC is the top three targets of DSS in the IS treatment. SRC is the downstream of VEGF to regulate angiogenesis. Our Western blot analysis confirmed that DSS significantly modulated the activity of SRC. We found that IGF-1, FGFR2, NOX3 (eNOS), MMP13, and EIF4E are the key targets of DSS in the treatment of IS. VEGF confers neuroprotection and promotes neurogenesis and cerebral angiogenesis after ischemic stroke [42]. VEGF signaling promotes endothelial nitric oxide synthase (eNOS) phosphorylation and is related to the angiogenesis [43]. Our previous study showed that DSS treatment promoted focal angiogenesis at 14 days after MCAO. Our previous study showed that DSS promotes angiogenesis and neurogenesis in rat following MCAO via upregulation of VEGF protein expression and increased eNOS activity [14]. The above studies have shown that DSS can not only inhibit apoptosis, inflammatory response, and oxidative stress in the acute phase of stroke but also improve neurological function by increasing neurogenesis and angiogenesis in the chronic recovery period. It suggests that DSS can be used in any period of stroke.

4.3. DSS May Contribute to the Treatment of IS by Modulate Estrogen Level. DSS is a famous herbal formulary from the Synopsis of the Golden Chamber, which was used to treat gynecological disease, especially female abdominal pain. At present, DSS is widely used in neurological diseases [7, 14]. Therefore, it is speculated that DSS might be able to regulate estrogen levels. Both GO and KEGG results showed that DSS responds to steroid hormone and regulates the estrogen signaling pathway. A number of evidence shows that the biological effects of estrogen extend beyond the gonads to other body systems, including the brain and behavior [44]. The results of preclinical studies have shown that estrogen has neuroprotective effects in various experimental models of IS [44]. Many different biological effects of estrogen are modulated by estrogen receptor (ESR), e.g., ESR1 and ESR2. Our result showed that ESR1 is a major target of DSS for IS treatment. The reports showed that estrogen reduces the ischemic oxidative damage via an ESR1-mediated inhibition of NADPH oxidase activation [45]. Dubal et al. showed that ESR1-/-mice have more severe brain damage after MCAO [46]. The above results might in part explain why DSS can treat both gynecological diseases and stroke.

Despite abundant new findings in this study, some limitations still exist. First, the corresponding experimental validation covered only a small number of mechanisms. Second, the compounds, targets, and pathways contained in these databases may not be exhaustive. In conclusion, the study, combined with network pharmacology, molecular docking, and animal experiments, offers the systematic mechanism of DSS in the treatment of IS and clearly clarifies the synergy mechanism of DSS multicomponent and multitarget. DSS may contribute to the treatment of IS by diminishing apoptosis, reducing inflammation and oxidative stress, increasing angiogenesis and neurogenesis, and modulating estrogen level. Our results indicate that DSS can not only reduce brain injury in the acute phase of stroke but also promote neurological recovery in the chronic phase of stroke.

Data Availability

The data that support the findings of this study are available from the corresponding author upon reasonable request.

Conflicts of Interest

The authors declare that there are no conflicts of interest regarding the publication of this article.

Authors' Contributions

C. R. and Y. Y. conceived and designed the study. S.L. developed the methodology. S.L., J.X, and W.Z. performed the data acquisition. C. R. performed data analysis and interpretation. S. L., C.G., H. L., W.Y., and W.Z did animal experiments and molecular biology experiments. C. R. drafted, reviewed, and revised the manuscript. All authors read and approved the final manuscript.

Acknowledgments

This work was supported by the National Natural Science Foundation of China (Grant Nos. 81971114, 81573867, 81801313, and 81801142) and the National Key R&D Program of China (2017YFC1308402).

References

[1] V. L. Feigin, G. Nguyen, K. Cercy et al., "Global, regional, and country-specific lifetime risks of stroke, 1990 and 2016," *New England Journal of Medicine*, vol. 379, no. 25, pp. 2429–2437, 2018.

[2] GBD 2019 Diseases and Injuries Collaborators, "Global burden of 369 diseases and injuries in 204 countries and territories, 1990–2019: a systematic analysis for the Global Burden of Disease Study 2019," *Lancet (London, England)*, vol. 396, pp. 1204–1222, 2020.

[3] W. J. Powers, A. A. Rabinstein, T. Ackerson et al., "Guidelines for the early management of patients with acute ischemic stroke: 2019 update to the 2018 guidelines for the early management of acute ischemic stroke: a guideline for Healthcare professionals from the American heart association/American stroke association," *Stroke*, vol. 50, no. 12, pp. e344–e418, 2019.

[4] M. Goyal, B. K. Menon, W. H. van Zwam et al., "Endovascular thrombectomy after large-vessel ischaemic stroke: a meta-analysis of individual patient data from five randomized trials," *The Lancet*, vol. 387, no. 10029, pp. 1723–1731, 2016.

[5] X. Ji, W. Zhao, C. Wu et al., "Multiphase adjuvant neuroprotection: a novel paradigm for improving acute ischemic stroke outcomes," *Brain circulation*, vol. 6, no. 1, pp. 11–18, 2020.

[6] Z. Xu, "Modernization: one step at a time," *Nature*, vol. 480, no. 7378, pp. S90–S92, 2011.

[7] T. Itoh, S. Michijiri, S. Murai et al., "Regulatory effect of Danggui-Shaoyao-San on central cholinergic nervous system dysfunction in mice," *The American Journal of Chinese Medicine*, vol. 24, no. 03n04, pp. 205–217, 1996.

[8] L. Chen, J. Qi, Y.-X. Chang, D. Zhu, and B. Yu, "Identification and determination of the major constituents in Traditional Chinese Medicinal formula Danggui-Shaoyao-San by HPLC-DAD-ESI-MS/MS," *Journal of Pharmaceutical and Biomedical Analysis*, vol. 50, no. 2, pp. 127–137, 2009.

[9] X. Fu, Q. Wang, Z. Wang, H. Kuang, and P. Jiang, "Danggui-Shaoyao-San: new hope for Alzheimer's disease," *Aging and Disease*, vol. 7, no. 4, pp. 502–513, 2016.

[10] Y. Kitabayashi, K. Shibata, T. Nakamae, J. Narumoto, and K. Fukui, "Effect of traditional Japanese herbal medicine Toki-Shakuyaku-San for mild cognitive impairment: SPECT study," *Psychiatry and Clinical Neurosciences*, vol. 61, no. 4, pp. 447-448, 2007.

[11] Y. Luo, H. Chen, B. Tsoi, Q. Wang, and J. Shen, "Danggui-Shaoyao-San (DSS) ameliorates cerebral ischemia-reperfusion injury via activating SIRT1 signaling and inhibiting NADPH oxidases," *Frontiers in Pharmacology*, vol. 12, Article ID 653795, 2021.

[12] Y. Ren, Y. Zhao, and S. Lu, "Clinical observation on effect of Danggui Shaoyao powder Combined with rehabilitation technique in treatment of 60 cases cerebral infarction," *Liaoning University Traditional Chinese Medical*, vol. 087, no. 8, 2013.

[13] I. Hatip-Al-Khatib, F. B. Hatip, Y. Yoshimitsu et al., "Effect of Toki-Shakuyaku-san on acetylcholine level and blood flow in dorsal hippocampus of intact and twice-repeated ischemic rats," *Phytotherapy Research*, vol. 21, no. 3, pp. 291–294, 2007.

[14] C. Ren, B. Wang, N. Li, K. Jin, and X. Ji, "Herbal formula Danggui-Shaoyao-San promotes neurogenesis and angiogenesis in rat following middle cerebral artery occlusion," *Aging and Disease*, vol. 6, no. 4, pp. 245–253, 2015.

[15] J. Qiu, "A culture in the balance," *Nature*, vol. 448, no. 7150, pp. 126–128, 2007.

[16] F. Cheng, I. A. Kovács, and A. L. Barabási, "Network-based prediction of drug combinations," *Nature Communications*, vol. 10, p. 1197, 2019.

[17] J. Zhao, P. Jiang, and W. Zhang, "Molecular networks for the study of TCM pharmacology," *Briefings in Bioinformatics*, vol. 11, no. 4, pp. 417–430, 2010.

[18] J. Ru, P. Li, J. Wang et al., "TCMSP: a database of systems pharmacology for drug discovery from herbal medicines," *Journal of Cheminformatics*, vol. 6, p. 13, 2014.

[19] X. Wang, Y. Shen, S. Wang et al., "PharmMapper 2017 update: a web server for potential drug target identification with a comprehensive target pharmacophore database," *Nucleic Acids Research*, vol. 45, no. W1, pp. W356–w360, 2017.

[20] A. P. Davis, T. C. Wiegers, J. Wiegers et al., "CTD Anatomy: analyzing chemical-induced phenotypes and exposures from an anatomical perspective, with implications for environmental health studies," *Current Research in Toxicology*, vol. 2, pp. 128–139, 2021.

[21] Y. Wang, S. Zhang, F. Li et al., "Therapeutic target database 2020: enriched resource for facilitating research and early development of targeted therapeutics," *Nucleic Acids Research*, vol. 48, pp. D1031–d1041, 2020.

[22] D. Szklarczyk, J. H. Morris, H. Cook et al., "The STRING database in 2017: quality-controlled protein-protein association networks, made broadly accessible," *Nucleic Acids Research*, vol. 45, no. D1, pp. D362–d368, 2017.

[23] C. H. Chin, S. H. Chen, H. H. Wu, C. W. Ho, M. T. Ko, and C. Y. Lin, "CytoHubba: identifying hub objects and sub-networks from complex interactome," *BMC Systems Biology*, vol. 8, no. Suppl 4, 2014.

[24] X. Jiao, B. T. Sherman, D. W. Huang et al., "DAVID-WS: a stateful web service to facilitate gene/protein list analysis," *Bioinformatics*, vol. 28, no. 13, pp. 1805-1806, 2012.

[25] M. Kanehisa, M. Araki, S. Goto et al., "KEGG for linking genomes to life and the environment," *Nucleic Acids Research*, vol. 36, no. Database, pp. D480–D484, 2008.

[26] O. Trott and A. J. Olson, "AutoDock Vina: improving the speed and accuracy of docking with a new scoring function, efficient optimization, and multithreading," *Journal of Computational Chemistry*, vol. 31, pp. 455–461, 2010.

[27] J. Chang, L. Liu, Y. Wang, Y. Sui, H. Li, and L. Feng, "Investigating the multitarget mechanism of traditional Chinese medicine prescription for cancer-related pain by using network pharmacology and molecular docking approach," *Evidence-Based Complementary and Alternative Medicine*, vol. 2020, Article ID 7617261, 11 pages, 2020.

[28] X. Ji, C. Ren, S. Li et al., "Enhanced oxidative stress response and neuroprotection of combined limb remote ischemic conditioning and atorvastatin after transient ischemic stroke in rats," *Brain Circulation*, vol. 3, no. 4, pp. 204–212, 2017.

[29] C. Ren, Y. Liu, C. Stone et al., "Limb remote ischemic conditioning ameliorates cognitive impairment in rats with chronic cerebral hypoperfusion by regulating glucose transport," *Aging and Disease*, vol. 12, no. 5, pp. 1197–1210, 2021.

[30] G. Li, K. C. Morris-Blanco, M. S. Lopez et al., "Impact of microRNAs on ischemic stroke: from pre- to post-disease," *Progress in Neurobiology*, vol. 163-164, pp. 59–78, 2018.

[31] D. Radak, N. Katsiki, I. Resanovic et al., "Apoptosis and acute brain ischemia in ischemic stroke," *Current Vascular Pharmacology*, vol. 15, no. 2, pp. 115–122, 2017.

[32] U. Kilic, A. B. Caglayan, M. C. Beker et al., "Particular phosphorylation of PI3K/Akt on Thr308 via PDK-1 and PTEN mediates melatonin's neuroprotective activity after focal cerebral ischemia in mice," *Redox Biology*, vol. 12, pp. 657–665, 2017.

[33] N. Sawe, G. Steinberg, and H. Zhao, "Dual roles of the MAPK/ERK1/2 cell signaling pathway after stroke," *Journal of Neuroscience Research*, vol. 86, no. 8, pp. 1659–1669, 2008.

[34] E. Kilic, Ü. Kilic, J. Soliz, C. L. Bassetti, M. Gassmann, and D. M. Hermann, "Brain-derived erythropoietin protects from focal cerebral ischemia by dual activation of ERK-1/-2 and Akt pathways," *The FASEB Journal*, vol. 19, no. 14, pp. 2026–2028, 2005.

[35] L. Belayev, N. Bazan, A. Obenaus et al., "Blocking pro-inflammatory platelet-activating factor receptors and activating cell survival pathways: a novel therapeutic strategy in experimental ischemic stroke," *Brain Circulation*, vol. 6, no. 4, pp. 260–268, 2020.

[36] L. Zhang, Z. G. Zhang, R. L. Zhang, M. Lu, M. Krams, and M. Chopp, "Effects of a selective CD11b/CD18 antagonist and

recombinant human tissue plasminogen activator treatment alone and in combination in a rat embolic model of stroke," *Stroke*, vol. 34, no. 7, pp. 1790–1795, 2003.

[37] J. Bradley, "TNF-mediated inflammatory disease," *The Journal of Pathology*, vol. 214, no. 2, pp. 149–160, 2008.

[38] M. Liguz-Lecznar, R. Zakrzewska, and M. Kossut, "Inhibition of TNF-α R1 signaling can rescue functional cortical plasticity impaired in early post-stroke period," *Neurobiology of Aging*, vol. 36, no. 10, pp. 2877–2884, 2015.

[39] S. Orellana-Urzúa, I. Rojas, L. Libran, and R. Rodrigo, "Pathophysiology of ischemic stroke: role of oxidative stress," *Current Pharmaceutical Design*, vol. 26, pp. 4246–4260, 2020.

[40] A. C. Boese, J.-P. Lee, and M. H. Hamblin, "Neurovascular protection by peroxisome proliferator-activated receptor α in ischemic stroke," *Experimental Neurology*, vol. 331, Article ID 113323, 2020.

[41] L. Ruan, B. Wang, Q. ZhuGe, and K. Jin, "Coupling of neurogenesis and angiogenesis after ischemic stroke," *Brain Research*, vol. 1623, pp. 166–173, 2015.

[42] D. A. Greenberg and K. Jin, "From angiogenesis to neuropathology," *Nature*, vol. 438, no. 7070, pp. 954–959, 2005.

[43] S. C. Bir, Y. Xiong, C. G. Kevil, and J. Luo, "Emerging role of PKA/eNOS pathway in therapeutic angiogenesis for ischaemic tissue diseases," *Cardiovascular Research*, vol. 95, no. 1, pp. 7–18, 2012.

[44] E. C. Koellhoffer and L. D. McCullough, "The effects of estrogen in ischemic stroke," *Translational Stroke Research*, vol. 4, no. 4, pp. 390–401, 2013.

[45] Q.-G. Zhang, L. Raz, R. Wang et al., "Estrogen attenuates ischemic oxidative damage via an estrogen receptor-mediated inhibition of NADPH oxidase activation," *Journal of Neuroscience*, vol. 29, no. 44, pp. 13823–13836, 2009.

[46] D. B. Dubal, H. Zhu, J. Yu et al., "Estrogen receptor alpha, not beta, is a critical link in estradiol-mediated protection against brain injury," *Proceedings of the National Academy of Sciences*, vol. 98, no. 4, pp. 1952–1957, 2001.

Hindawi
Evidence-Based Complementary and Alternative Medicine
Volume 2021, Article ID 6510383, 14 pages
https://doi.org/10.1155/2021/6510383

Research Article

Transcranial Ultrasound Stimulation of the Anterior Cingulate Cortex Reduces Neuropathic Pain in Mice

Xiangjun Feng,[1,2,3] Lili Niu,[3,4,5] Meng Long,[3,4,5] Kaixuan Luo,[1,3] Xiaowei Huang,[3] Moxian Chen,[1] Zhengrong Lin,[3] Wei Zhou,[3] Shasha Yi,[1,3] and Lijuan Ao[1]

[1]*The School of Rehabilitation, Kunming Medical University, 1168 West Chunrong Road, Chenggong, Kunming 650500, China*
[2]*General Surgery Department of Geriatrics, The First Affiliated Hospital of Kunming Medical University, 295 Xichang Road, Kunming 650032, China*
[3]*Institute of Biomedical and Health Engineering, Shenzhen Institutes of Advanced Technology, Chinese Academy of Sciences, 1068 Xueyuan Avenue, Shenzhen 518055, China*
[4]*CAS Key Laboratory of Health Informatics, Shenzhen Institutes of Advanced Technology, 1068 Xueyuan Avenue, Shenzhen 518055, China*
[5]*Guangdong-Hong Kong-Macao Greater Bay Area Center for Brain Science and Brain-Inspired Intelligence, 1068 Xueyuan Avenue, Guangzhou 518055, China*

Correspondence should be addressed to Lijuan Ao; aolijuan69@gmail.com

Received 10 August 2021; Accepted 22 November 2021; Published 31 December 2021

Academic Editor: Feng Zhang

Focused ultrasound (FUS) is a potential tool for treating chronic pain by modulating the central nervous system. Herein, we aimed to determine whether transcranial FUS stimulation of the anterior cingulate cortex (ACC) effectively improved chronic pain in the chronic compress injury mice model at different stages of neuropathic pain. The mechanical threshold of pain was recorded in the nociceptive tests. We found FUS stimulation elevated the mechanical threshold of pain in both short-term ($p < 0.01$) and long-term ($p < 0.05$) experiments. Furthermore, we determined protein expression differences in ACC between the control group, the intervention group, and the Sham group to analyze the underlying mechanism of FUS stimulation in improving neuropathic pain. Additionally, the results showed FUS stimulation led to alterations in differential proteins in long-term experiments, including cellular processes, cellular signaling, and information storage and processing. Our findings indicate FUS may effectively alleviate mechanical neuropathic pain via the ACC's stimulation, especially in the chronic state.

1. Introduction

Chronic pain is a severe condition that considerably interferes with daily functioning [1], and the estimated prevalence of chronic pain ranges from 8.7% to 64.4% [2, 3]. Neuropathic pain (NP) is a prominent type of chronic pain. Chronic pain causes not only stress on the body, including strained muscles, diminished motion range, inadequate power, and appetite changes, but also emotional effects, such as depression, anger, anxiety, and fear of reinjury, which may limit the ability to return to routine work or leisure activities [4]. The treatment is mainly medication or physical therapy, but the effect is not significant due to the complicated etiology [5, 6]. Therefore, it is necessary to develop effective strategies to improve these issues.

The use of the S-size ultrasound probe in pulsed mode stimulation over a skin incision has been reported to improve the mechanical and thermal retraction threshold of the NP model [7]. A previous study reported that axonal regeneration in autograft nerves was improved following low-intensity pulsed ultrasound with 250 mW/cm^2 compared with that following high-intensity ultrasound [8]. Therefore, focused ultrasound (FUS) may be a nonpharmacological nonablative neuromodulatory technique that improves peripheral nerve injury or NP. Additionally, Hameroff et al. stimulated individuals with chronic pain using transcranial ultrasound and

reported an unexpected analgesic effect [9]. Moreover, Spooner et al. reported that deep brain stimulation over the bilateral cingulate by 130 Hz high-frequency electricity resulted in pain relief in a patient with severe drug-resistant pain syndrome following a complete spinal cord injury [10]. Subsequently, there has been increasing interest in modulating the central nervous system (CNS) for chronic pain treatment.

Thalamus is an important regulatory target for the treatment of pain, and ACC is a possible target for pain management through previous researches. Pain relief using cingulotomy has evoked clinical interest in deep brain stimulation in the dorsal ACC for treating chronic refractory pain, especially when coupled with a substantial affective component, such as distress, resulting in the more complicated treatment [11]. ACC activation improves chronic pain states through several neuronal modulation changes in the CNS [12–14]. Moon et al. reported that optical inhibition of the ACC improved pain-associated behavior and reduced the unusual activity of thalamic sensory neurons in a rat model of trigeminal NP [15]. In addition, various neuromodulation techniques have demonstrated therapeutic value against NP by inhibiting neuronal activity in the ACC, a crucial target in the brain [13, 15–17].

At present, deep brain stimulation, transcranial magnetic stimulation, and transcranial electrical stimulation are the most commonly used regulation programs of the CNS, which may have the disadvantages of high surgical risk and poor accuracy. Recent studies have also shown that FUS is a safe, noninvasive, and accurate technique that modulates neuronal circuits in the CNS [18, 19] of both animal models and humans [20–22]. Moreover, transcranial FUS may treat chronic pain through neuronal regulation of the CNS, including the ACC. However, the treatment effect of FUS-induced ACC activation on chronic pain remains unclear. Consequently, we investigated the therapeutic effects of FUS stimulation of the ACC using the short- and long-term NP chronic compress injury (CCI) mouse model.

2. Materials and Methods

2.1. Animal Preparation. We conducted all animal experiments based on the guidelines approved by the Animal Use Committee and the Ethics Committee of Kunming Medical University (Approval number: KMMU2019075). For short-term experiments, we randomly allocated 18 C57BL/6J mice (age: 8 weeks, weight: 20–23 g, male) to the FUS1 (parameter 1), FUS2 (parameter 2), and control (sham stimulation) groups ($n = 6$ mice/group). For the long-term experiments, we randomly allocated 36 C57BL/6J mice (age: 14 months, weight: 24–36 g, female) to the Control (Sham operation), FUS (parameter 2), and Sham (sham stimulation) groups ($n = 12$ mice/group). All animals were raised in a controlled environment ($22 \pm 2^{\circ}$C) under a regular light-dark cycle (lights on, 7 a.m.; lights off, 7 p.m.) with ad libitum access to food and water.

2.2. Chronic Pain Model. Following a 1-week acclimation of the mice to the maintenance environment, we began the experiment. We used the CCI surgical procedure to establish the NP model [23]. We conducted nociceptive tests, including the mechanical allodynia test, thermal allodynia test, and sciatic nerve functional index, to obtain baseline values before the CCI surgical procedure on the right sciatic nerve. The mice were anesthetized with isoflurane (2% for induction and 1.5% for maintenance, Sigma-Aldrich, St. Louis, Missouri, USA) and placed in the prone position. Next, the right thigh was shaved, and the skin was disinfected with 2% iodine-alcohol. After a skin incision was made in the middle third of the right hind limb to expose the biceps femoris muscle, approximately 5 mm of the sciatic nerve was uncovered, and three ligatures (gut ligatures 6.0, Jinhuang, Shanghai, China) were tied at 1-mm intervals. The tying allowed noticeable nerve constriction without arresting epineurial blood flow. The skin was sutured using Mononylon 4.0 (Johnson & Johnson Medical N.V., Belgium, 2018–2019). Mice in the sham-operated group were operated according to the abovementioned surgical procedure, but after the nerve was exposed, an intestinal ligature was placed on the sciatic nerve trunk three times without ligation; the nerve was repositioned, and the skin was sutured We returned the animals to their cages after surgery and recovery from anesthesia.

2.3. Nociceptive Tests. We conducted nociceptive tests before (baseline) and following surgery in all experimental groups. In the short-term experiment, we started ultrasound stimulation when there was a substantial decrease in the mechanical pain threshold of the entire group (≈0.008 g; ≈6 days following surgery). A substantial reduction in the mechanical pain threshold during the postoperative examination indicated successful establishment of the pain model in the long-term experiment. We started ultrasound stimulation on the 91st days after the surgery and repeated the nociceptive tests every 6–7 days following ultrasound stimulation commencement.

2.3.1. Mechanical Allodynia Test. All the animals were allowed 2–3 days to acclimate to the test environment before the tests or surgery. We placed the mice in a ten-grid Plexiglas box (homemade) with a metal net lid and bottom for about 30 min. Next, we perpendicularly stimulated the bilateral hind paws on the plantar surface in an ascending order of stimulus intensity using Von Frey hairs (Aesthesio, DanMic Global, Campbell, CA) with increasing stiffness (0.008, 0.02, 0.04, 0.07, 0.16, 0.4, 0.6, 1, 1.4, 2, and 4 g). A positive situation was defined when the mice ran away or raised the hind leg following a 5–6 s perpendicular stimulation. We recorded the gradually growing stiffness when a positive result occurred three times in five stimulations separated by more than 3 min. We repeated the process mentioned above 3–5 times at intervals of >15 min and obtained the mean value as the mechanical withdrawal threshold to indicate the mechanical pain tolerance of mice.

2.3.2. Thermal Allodynia Test. We used a laser transmitter (ADR-1805, Xilongguangdian, Shanghai, China) to determine the thermal allodynia value with a near-infrared laser

(wavelength, 787.7 nm; output power, 564 mW) that was calibrated using an infrared thermal imager (R300, NEC Avio, Tokyo, Japan). The calibration warmed the paw sole skin to 50°C at a distance of 0.5 cm within 28 s. The mice were allowed to habituate to the Plexiglas box for at least 30 min. The light was transmitted to the paw sole skin using the laser transmitter at a distance of approximately 0.5 cm. The time from the start of lighting to paw withdrawal was recorded with a 60-s limit to avoid local burn injury. This described procedure was performed twice at a 15-min interval, and the mean value was used as the thermal withdrawal threshold to indicate the thermal pain tolerance of mice.

2.3.3. Sciatic Nerve Functional Index (SFI). We prepared a plastic corridor (5 cm × 10 cm × 15 cm) with paper tape (6 cm × 20 cm, homemade) at the bottom and an ink pad at the beginning of the corridor for the mice to walk through. The mice were briefly placed on the ink pad and walked straight through the corridor while leaving footprints on the paper tape prior to and following the CCI surgery. When there were three clear footprints, we measured the following three parameters: print length (PL), distance from the heel to the third toe; toe spread (TS), distance from the first toe to the fifth toe; and intermediate TS (ITS), distance from the second toe to the fourth toe. We calculated the SFI using the following formula [24]:

$$\mathrm{SFI} = 38.3\left(\frac{\mathrm{EPL}-\mathrm{NPL}}{\mathrm{NPL}}\right) + 109.5\left(\frac{\mathrm{ETS}-\mathrm{NTS}}{\mathrm{NTS}}\right) + 13.3\left(\frac{\mathrm{EITS}-\mathrm{NITS}}{\mathrm{NITS}}\right) - 8.8, \quad (1)$$

where E represents the experimental side and N represents the normal side. A value of 0 indicates the normal function, and −100 indicates total impairment.

2.4. FUS Stimulation Process. We used an arbitrary waveform generator (3102C, Tektronix, Texas, USA) with a power amplifier (LZY-22+, Mini-circuits, Shenzhen, China) to provide an output to apply to a 3.7 MHz focused transducer with a focal diameter and length of 0.7 and 11.1 mm, respectively. We performed FUS stimulation of the ACC (Cg) region of mice to induce pain relief in the mice (the ultrasound pulse parameters were as follows: pulse repetition frequency, 1.5 kHz and duty cycle, 10%. The spatial-peak pulse-averaged acoustic intensity (Isppa) was 15980 mW/cm^2 and 34982 mW/cm^2 for FUS1 and FUS2, respectively. Moreover, the spatial-peak temporal-average intensity (Ispta) was 1598 mW/cm^2 and 3498 mW/cm^2 for FUS1 and FUS2, respectively (Figure 1(a)). These values were obtained using degassed water through an ultrasound test tank system (Precision Acoustics Ltd., Dorchester, United Kingdom) equipped with a calibrated hydrophone (2010, Precision Acoustics Ltd., Dorchester, United Kingdom). We measured the acoustic intensity attenuation through the skull up to 80%, and the focal spot can be located just below the skull. The measured acoustic field distribution shows the measured acoustic pressure of the probe, with or without a fresh mouse skull. The focus distance for projecting across the cingulate cortex area through the collimator filled with degassed water was 11.1 mm (Figure 1(b)).

All the mice were depilated using a depilatory paste (Veet, Reckitt Benckiser, Hubei, China), and we used acoustic coupling gel for FUS treatment (15 min/day for 21 days). The mice underwent ultrasonic stimulation under anesthesia with isoflurane (2% for induction, 0.6% for maintenance, Sigma-Aldrich, St. Louis, Missouri, USA). The mice were depilated and anesthetized; then, the head of the mice was fixed on the mouse-adapted stereotaxic device. The collimator prepared by calculating the focal length of the ultrasound transducer was placed directly above the brain area of ACC (bregma point) and was coupled with a coupling agent to ensure no air was left (Figure 1(a)). Ultrasound stimulation was performed through the collimator, just touching the scalp of the mice using the above parameters, and the sham procedure was performed at the same time, which involved the same procedure of all working processes for equal time, with all equipment turned on, without ultrasonic excitation signal.

First, we performed FUS on the short-term pain model to determine the effect of FUS on the ACC brain area in the early stage of pain. On the 6th day after surgery, we confirmed the successful establishment of the CCI model using the nociceptive tests. On the 7th day, we started FUS stimulation at 15 min/day for 21 days (Figure 2(a)). After completing the short-term experiment, we confirmed that FUS has a better neuromodulation effect when using the FUS2 parameters. Therefore, we conducted long-term experiments to confirm the effectiveness of the ACC regulation with FUS in the chronic pain period using FUS2 parameters. Following successful establishment of the CCI model, the mice were allowed to move freely for 90 days without intervention, and the baseline values of nociceptive tests were determined prior to ultrasound stimulation. On the 91st day, we started the FUS2 stimulation using a similar protocol to that used for the short-term experiment (Figure 3(a)).

2.5. Slice Preparation and Multielectrode Array (MEA) Recordings. To verify the direct effect of ultrasound on neurons in the ACC brain area using FUS2 parameters, we separately recorded three brain slices of three C57BL/6J mice for MEA recordings. The animals were sacrificed using a rodent guillotine (RWD, Shenzhen, China) under deep anesthesia with 5% isoflurane. Next, we collected the brains and placed them in an ice-cold oxygenated high-sucrose cutting solution (0–2°C) that contained the following ingredients (in mM): 60 NaCl, 3 KCl, 7 $MgCl_2$, 1.25 NaH_2PO_4, 25 $NaHCO_3$, 10 D-glucose, 115 sucrose, and 0.5 $CaCl_2$. Subsequently, we prepared 500 μm coronal slices of the ACC area using a vibratome (VT-1200 Series, Leica Biosystems, Wetzlar, Germany). The slices were then equilibrated and incubated in artificial cerebrospinal fluid (ACSF) that contained the following ingredients (in mM): 126 NaCl, 2.5

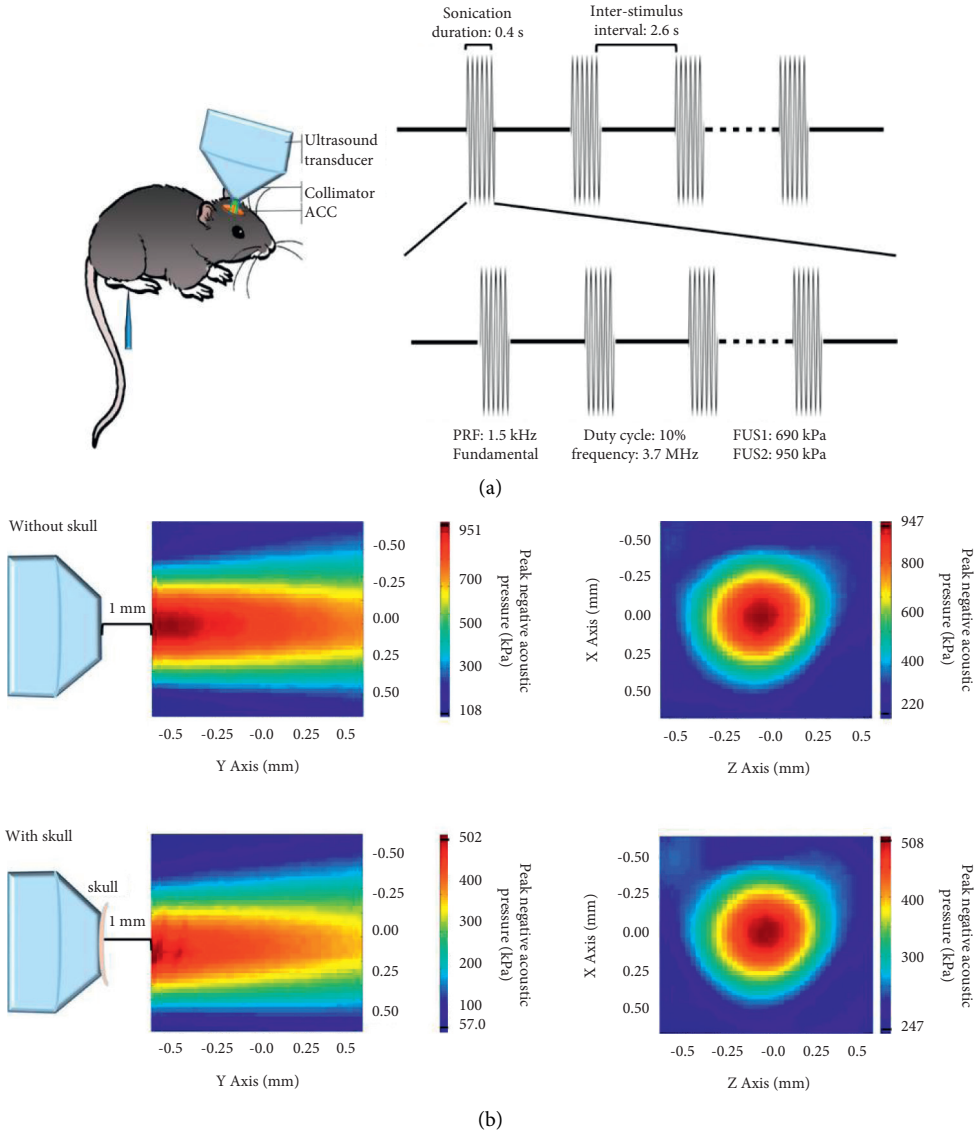

Figure 1: Experimental schematics. Experimental schematic diagram (a). Acoustic field distributions with or without a fresh mouse skull (b).

KCl, 1 $MgCl_2$, 1.25 NaH_2PO_4, 26 $NaHCO_3$, 10 D-glucose, 2 sodium pyruvate, 0.5 L-ascorbic acid, and 2 $CaCl_2$. The ACSF was continuously saturated with 95% O_2-5% CO_2 and maintained at a temperature of 35°C (all the above regents: Sigma-Aldrich, St. Louis, Missouri, USA).

To investigate the FUS-induced modulatory effects, we recorded spikes from the slices using the MEA systems (MCS MEA 2100-IFB, MCS, Reutlingen, Germany), which reliably quantifies neuronal activity [25, 26]. The brain slices were placed in the recording chamber and continuously perfused with ACSF saturated with 95% O_2-5% CO_2 (Figure 4(a)). We applied a solution with higher potassium levels (2.5 mM to 5 mM of KCl in the ACSF) to evoke more discharge from the brain slices. We placed an ultrasound transducer with a coupling cone (homemade) over the ACC slices and adjusted its location to ensure the acoustic field was focused on the stimulation site of the slices. We recorded the baseline value at 100 s before the ultrasound intervention. Following the record of 60-s intervention (parameter 2), we subsequently recorded the measurement value of another 100 s without intervention and identified effective neuronal discharge as those with amplitude 2.5 times greater than the baseline amplitude. There were a total of 29 channels of electrical signals recorded through MEA, indicating that the excitability of 29 neuron cells was recorded. The effective discharge times were counted manually for statistical analysis.

2.6. Detection of Proteins. To preliminarily determine the local protein expression changes of ACC after the neuroregulation of FUS and to understand the possible central control mechanism of pain, we conducted protein detection on the ACC brain area of the long-term experimental group

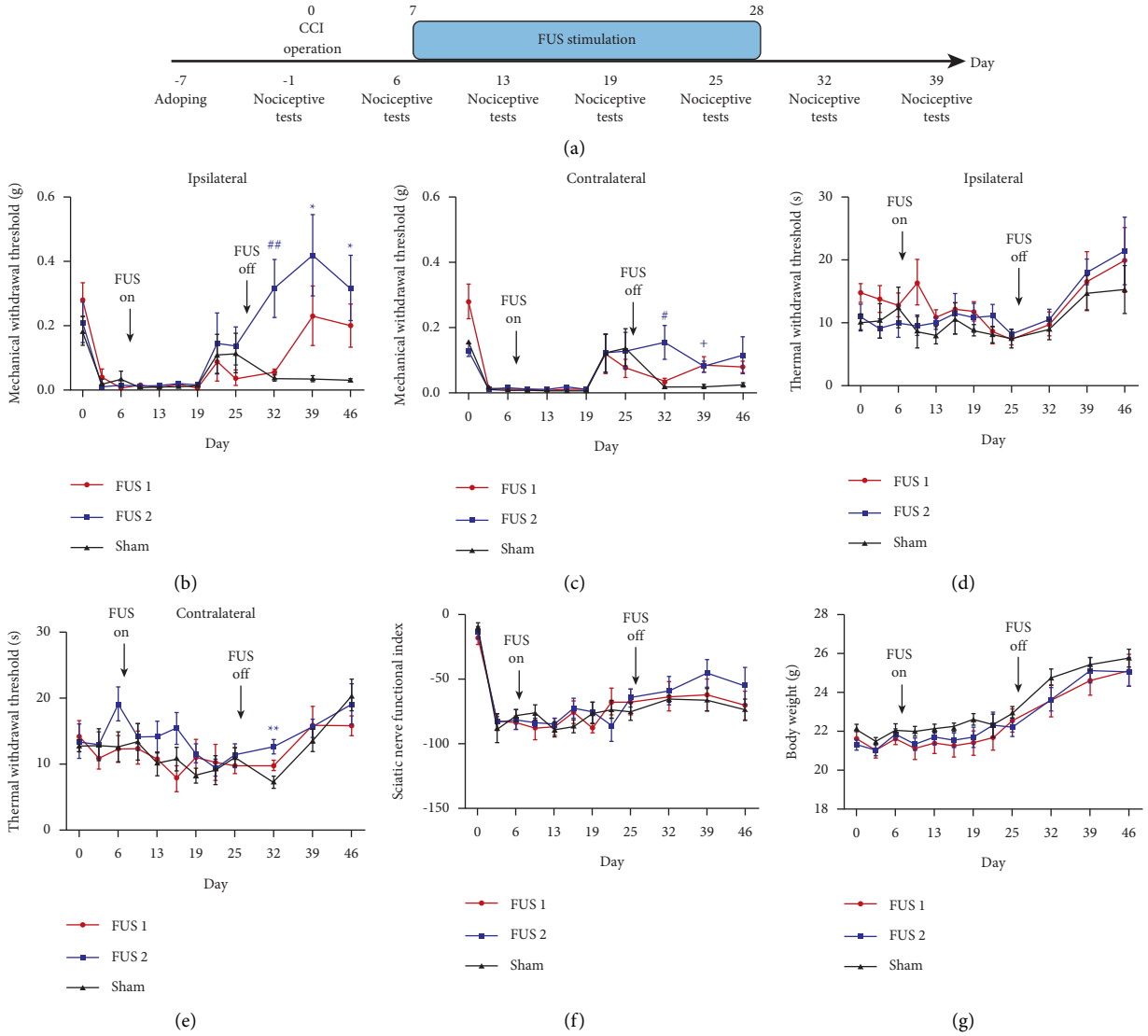

Figure 2: Transcranial FUS stimulation slowly improved the mechanical withdraw threshold in the short-term experiment. Timeline of the short-term experiment ($n = 6$) (a). Ultrasound stimulation increased the mechanical withdrawal thresholds of the surgical side ($^{\#\#}p = 0.003$) (b). The increase in the mechanical and thermal withdrawal thresholds of the contralateral side (c, e). The variation of sciatic nerve index and body weight (f, g). $^{\#}$ represents a statistically significant difference between the FUS2 group and the other two groups. * indicates a statistically significant difference between the FUS2 group and the Sham group. + indicates a statistically significant difference between the FUS1 group and the Sham group.

using an Isobaric tag for relative and absolute quantitation (iTRAQ), which is among the most commonly used methods in quantitative proteomics research. It works on the principle of the reaction of digested polypeptides from different samples with differentially labeled iTRAQ reagents [27]. On the 21st day of the long-term experiment, 12 mice ($n = 6$/group) were cardiacally perfused with a saline solution. Subsequently, the whole brains were quickly removed, and the entire ACC tissue was obtained according to the map [28]. Following multiple sample protein extractions, we performed protein digestion and quantification based on the filter-aided sample preparation method [29]. Further, we vacuum-dried (Savant DNA120, Thermo Scientific, Massachusetts, USA) three samples with the greatest protein concentration in each group for iTRAQ-based identification. We used information-dependent acquisition (IDA) mass spectrum techniques to obtain tandem mass spectrometry (MS) data on a ThermoFisher Q Exactive mass spectrometer (Thermo Scientific, Massachusetts, USA) fitted with a Nano Flex ion source (Thermo Scientific, Massachusetts, USA). We performed the FULL-MS scans with an ion spray voltage of 1.9 kV and an interface heater temperature of 275°C. We obtained survey scans of IDA within 250 ms and a maximum of 20 production scans within 50 ms. With a dynamic exclusion of 25 s, fragmentation was performed with higher-energy collision energy dissociation for 2+ to 4+ charged spectra. We analyzed the MS/MS data for protein identification and quantification using IPeak.

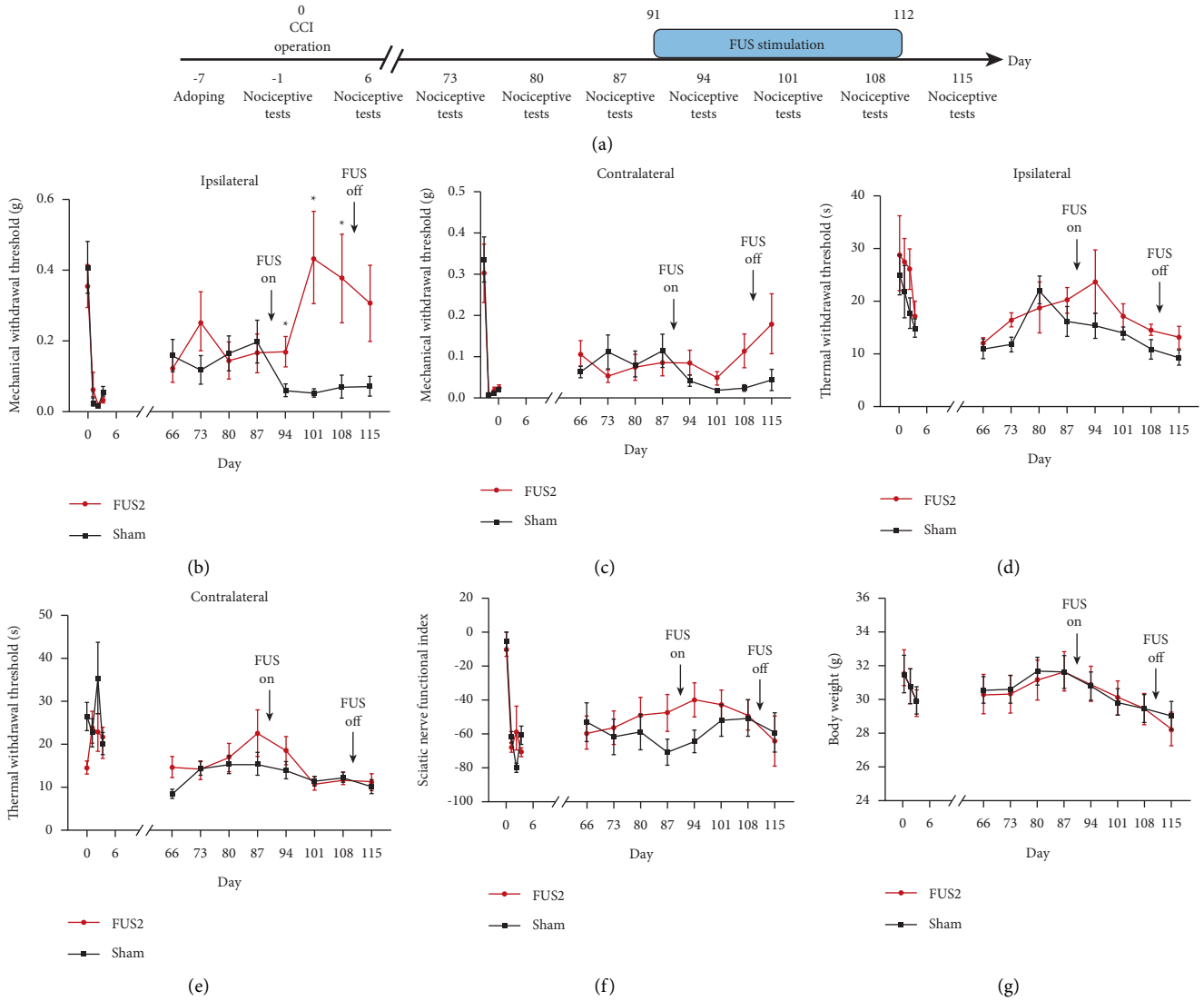

Figure 3: FUS stimulation promptly improved the mechanical withdraw threshold in the long-term experiment. Timeline of the long-term experiment ($n = 12$) (a). Ultrasound stimulation increased the mechanical withdraw threshold of the surgical side ($p < 0.05$) (b). There were no significant changes in the mechanical withdraw threshold of the contralateral side. The bilateral thermal withdraw threshold, body weight, and sciatic nerve index between the FUS2 group and the Sham group (c–f). * indicates statistical significance between the FUS2 group and the Sham group.

2.7. Western Blotting. Total protein was extracted from tissues. Antibodies Hnrnph1, Snrpb, Dhx16, and GAPDH were purchased from Abcam (USA). Antibody Hnrnpd was purchased from CST (USA). Membranes were blocked with 5% milk and incubated with the primary antibodies in 5% bovine serum albumin (BSA) at 4°C overnight. Next day, after washing membrane three times, then it was incubated with 1 : 1000 secondary antibody. Then the signals were detected using an enhanced chemiluminescence-detecting kit (Thermo Fisher, MA, USA), and the density of the bands was analyzed by using ImageJ.

2.8. Safety and Temperature Calculations. Finally, we conducted a safety test. We performed standard hematoxylin-eosin (HE, Sigma-Aldrich, St. Louis, Missouri, USA) staining of the brain and the CCI surgical area after the experiment in all test groups to determine that FUS would not cause further tissue damage and used mathematical modeling to determine the local temperature increase. Specifically, 12 FUS2-stimulated and Sham mice ($n = 6$/group) were used for histological assessment. On the 21st day, 12 mice were cardiacally perfused with phosphate-buffered saline followed by 4% paraformaldehyde. The whole brains were then isolated and fixed in 4% paraformaldehyde (Sigma-Aldrich, St. Louis, Missouri, USA). The brain tissues were dehydrated, defatted, paraffinized, and serially sectioned at 4-μm thicknesses using a pathologic microtome (Leica, RM2016, Wetzlar, Germany). We randomly selected the brain sections for observation under light microscopy. Upon the spread of ultrasonic energy into tissues, wave energy attenuation resulted from absorption or scattering

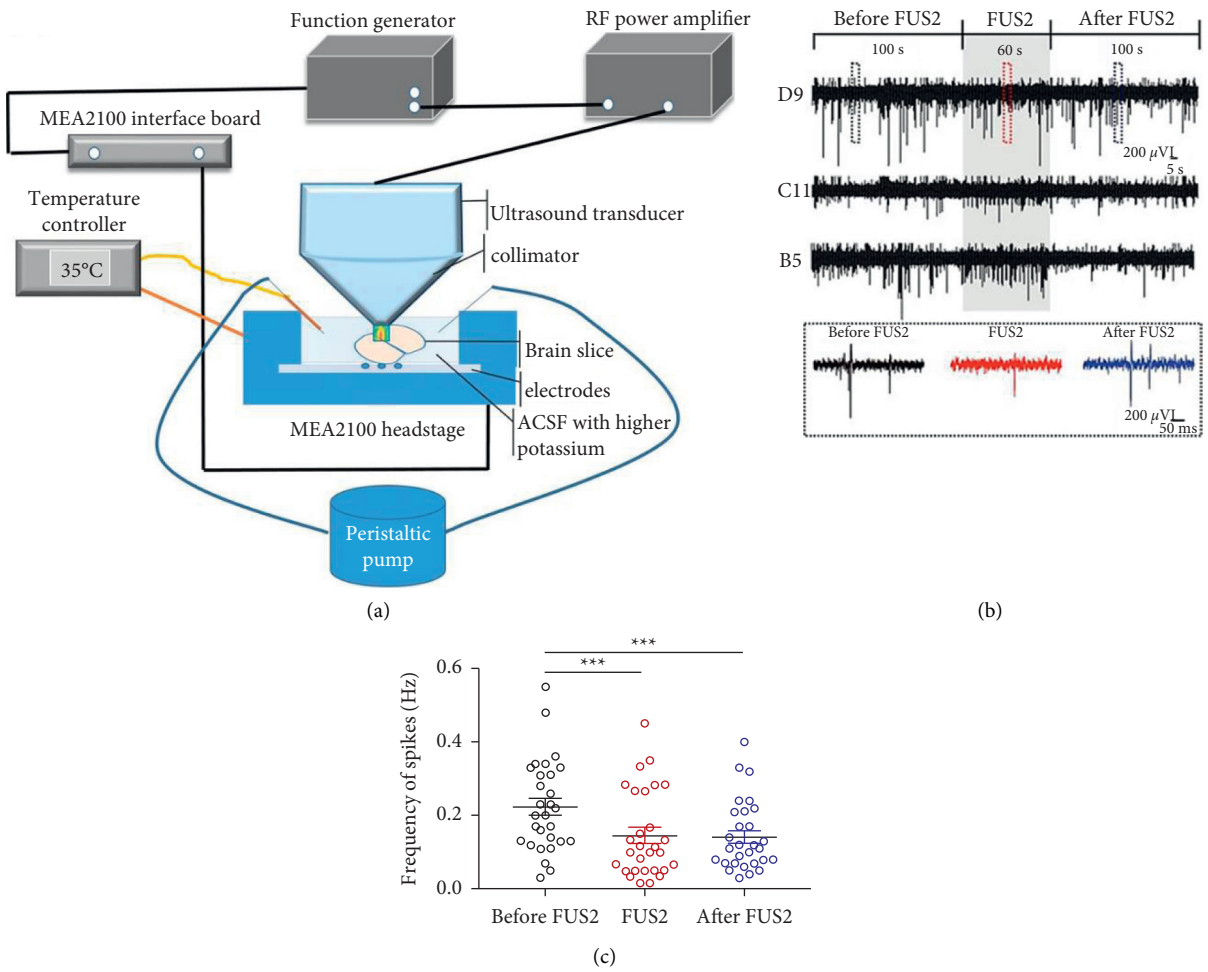

Figure 4: Ultrasound-induced inhibition of neuronal discharges from the ACC slices. Experimental schematics (a). Representative traces randomly selected of the neuronal discharges from the ACC slices obtained using MEA recording (b). Ultrasound stimulation substantially decreased the spike frequency of neuronal discharges (c) (*** $p < 0.001$ (prior to during: $p \leq 0.001$, prior to following: $p = 0.002$)).

with heat conversion or directional change, respectively. The balance between the absorbed energy and heat released results in an ultrasound-induced temperature increase that can be calculated using mathematical modeling techniques under different exposure conditions. Therefore, we calculated the ultrasound-induced local temperature increase to avoid local thermal damage using the following equation:

$$Q = 2\alpha I_{\mathrm{TA}}, \tag{2}$$

where α is the absorption coefficient in the brain tissue, I_{TA} is the temporal-average intensity, and Q is the heat generated per volume [30].

The FUS-induced maximum temperature increase ($\Delta T_{\max}$) in the brain tissue could be described as follows without the heat loss:

$$\Delta T_{\max} = \frac{Q\Delta_t}{c_v} = \frac{Q\Delta_t}{c_\rho}, \tag{3}$$

where Δ_t is the FUS exposure time and C_v is the heat capacity per unit volume for brain tissue defined as the product of C (heat capacity in brain tissue: 3.6 J/g/°C) and ρ (density of brain tissue: 1028 kg/m^3) [31].

2.9. Statistical Analysis. We expressed all experimental data as mean ± standard error (SME) and conducted analyses using independent sample t-tests and one-way ANOVA tests with Tukey's or Bonferroni's post hoc test for parametric analysis. All statistical analyses were performed in IBM® SPSS® Statistics 23 (IBM Corp, Armonk, NY, USA), and the statistical significance was set at $p < 0.05$.

3. Results

3.1. Transcranial FUS Stimulation Slowly Improved the Mechanical Withdraw Threshold in the Short-Term Experiment. The results showed an increase in the mechanical withdraw threshold of the operation side following the end of the FUS2 stimulation period (FUS1 group, 0.06 ± 0.01 g; FUS2 group, 0.32 ± 0.09 g; Sham group, 0.04 ± 0.01 g; $p < 0.01$ ($p = 0.003$)), indicating that the pain tolerance of mice on the surgical side had improved. FUS1 showed a similar but delayed and nonsignificant response. On the contralateral side, FUS2 exerted a similar effect; however, the outcome was not sustained (FUS1 group, 0.04 ± 0.01 g; FUS2 group, 0.15 ± 0.05 g; Sham group, 0.02 ± 0.002 g; $p < 0.05$ ($p = 0.038$) (Figure 2(b)).

Conversely, FUS1 stimulation induced a significant increase after 1 week (FUS1 group, 0.09 ± 0.02 g; FUS2 group, 0.08 ± 0.02 g; Sham group, 0.02 ± 0.005 g; $p < 0.05$ ($p = 0.038$) (Figure 2(c)). There was substantial synchrony in the bilateral mechanical retraction domain following ultrasound stimulation and a significant improvement in the contralateral thermal withdrawal threshold following FUS2 stimulation (FUS1 group, 9.83 ± 0.74 s; FUS2 group, 12.67 ± 1.12 s; Sham group, 7.33 ± 0.92 s; $p < 0.01$ ($p = 0.003$) (Figures 2(d) and 2(e)). Conversely, there were no significant changes in the sciatic nerve index and body weight (Figures2(f) and 2(g)).

3.2. FUS Stimulation Promptly Improved the Mechanical Withdraw Threshold in the Long-Term Experiment. The results showed that the mechanical withdrawal threshold of the surgical side increased in the FUS group compared with that in the Sham group. This increase was sustained until the end of the FUS stimulation period (FUS group, 0.17 ± 0.04 g; Sham group, 0.06 ± 0.02 g; $p < 0.05$ ($p = 0.03$)) (Figure 3(b)). There were no significant changes in the contralateral mechanical withdrawal threshold ($p = 0.19$) (Figure 3(b)), bilateral thermal withdrawal threshold (surgical side $p = 0.21$, other side $p = 0.25$) (Figures 3(d) and 3(e)), body weight ($p = 0.93$) (Figure 3(g)), and sciatic nerve index ($p = 0.49$) (Figure 3(f)) between the FUS and the Sham groups.

3.3. Ultrasound-Induced Inhibition of Neuronal Discharges from the ACC Slices. Representative traces of spikes recorded during three phases in different channels randomly selected showed the ultrasound-induced changes using MEA recording (Figure 4(b)). The assessment of the 29 cells indicated that the spike frequencies in the ACC slices were effectively inhibited during ultrasound, which was sustained following ultrasound stimulation (prior to FUS2, 0.224 ± 0.0023 Hz; during FUS2, 0.145 ± 0.0218 Hz; following FUS2, 0.142 ± 0.0176 Hz, $^{***}p < 0.001$and prior to during: $p \leq 0.001$, prior to following: $p = 0.002$), Student's paired t-test (Figure 4(c)).

3.4. FUS-Induced Differences in Protein Expression Indicated Alterations in Pathways in the ACC. Protein profiling with a threshold of fold change of >1.2 and a T-test revealed differential up- and downregulations of 97 and 49 proteins, respectively; therefore, we observed a total of 146 protein expression changes. The subcellular structures of the proteins were mainly located in the cytoplasm, nucleus, and extracellular fluid (Figure 5(b)). Using EggNOG (EggNOG evolutionary genealogy of genes: Nonsupervised Orthologous Groups version 4.5.1, Computational Biology group-EMBL, Heidelberg), we found that the top 20 items (differential proteins) were involved in cellular processes, cellular signaling, and information storage and processing (Figure 5(a)). This suggests that ACC treatment with FUS alters cellular signal transduction and information processing involved in chronic pain. Further, enriched pathway analysis [32] (Cytoscape 3.7.2, Cytoscape Consortium) revealed that the differential proteins were mainly related to the endocrine, immune, and nervous systems (Figures 5(c) and 5(d)).

3.5. FUS2-Induced Changes in the Expression of Hnrnph1, Hnrnpd, Snrpb, and Dhx16. Based on the plugin cytoHubba in Cytoscape, 4 key genes Hnrnph1, Hnrnpd, Snrpb, and Dhx16 were screened (Table S1). Western blotting results showed that HNRNPH1 and HNRNPD were significantly higher in the brain tissue of CCI mice compared with the normal group and the LUS stimulation group. Snrpb and Dhx16 expression shows no significant differences between CCI sham stimulation group and LUS stimulation group (Figure 6).

3.6. Safety and Temperature Evaluation. The results of HE staining of ACC brain tissue and local parts of CCI operation in the Control group, Sham group, and FUS2 group showed that the sciatic nerve had no neurofibrillation, swelling, or thickening. Further, there were no axon irregularities, the disappearance of changes, or myelin loosening, disintegration, or precise segmental loss. There was no substantial change in the number of nerve cells in the brain, especially the ACC. Moreover, there was no inflammatory cell infiltration between the stroma and blood vessels, nerve cell swelling, ulceration, pyknosis, coagulative necrosis, vesicular degeneration, or vacuolar degeneration (Figure 7).

4. Discussion

Transcranial FUS is a popular technique used for noninvasive neuromodulation in both animal models and humans [20]. Our findings indicated that ultrasound stimulation of the ACC increased the mechanical withdraw threshold in the CCI mice model in both the short- and long-term experiments. In the short experiment, the mechanical threshold of the intervention group started increasing at 2 weeks following the ultrasound, and we observed a substantial difference in the mechanical threshold between the intervention group and the Sham group at 3 weeks. In the long-term experiment, there was an early and sustained increase in the threshold following ultrasound stimulation. Similar to related studies in recent years, protein analysis results of the ACC region showed that it mainly involves the immune system and endocrine system considering the occurrence of pain, especially the occurrence of chronic pain, which may involve changes in the functions of the CNS [33–37]. In addition, HNRNPH1 and HNRNPD may become important regulatory targets for FUS to stimulate reduce neuropathic pain.

Ultrasound stimulation is a noninvasive technique that allows accurate targeting of different neurological diseases. Additionally, it is a safe and cheap therapeutic method [38–41]. The ultrasound is even safer in cases where pacemakers or other important implantable devices are not antimagnetic or antielectric. Compared with TMS and tDCS, focused ultrasound is easier to implement in the deep brain

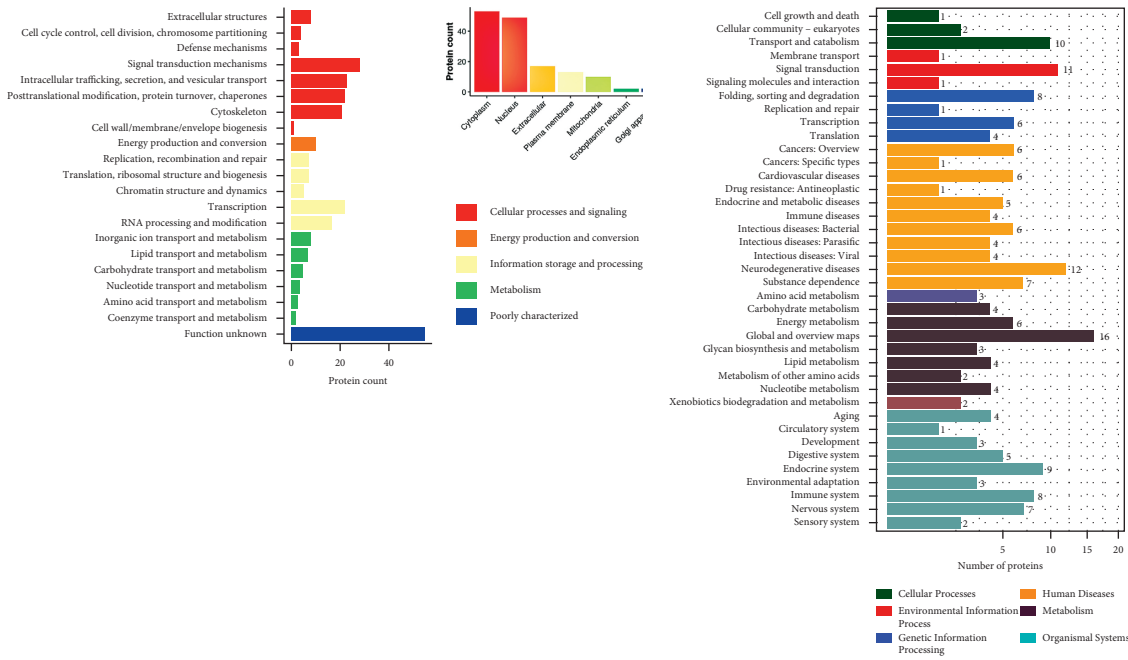

(a) (b)

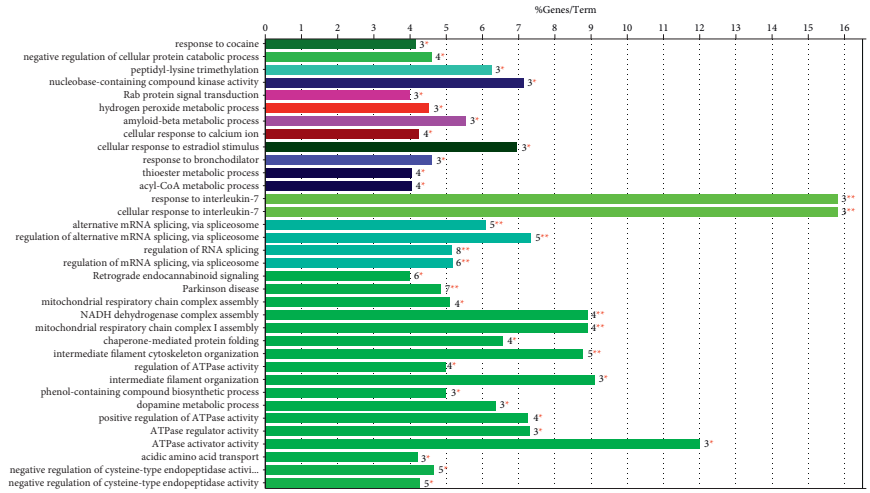

(c)

Figure 5: Continued.

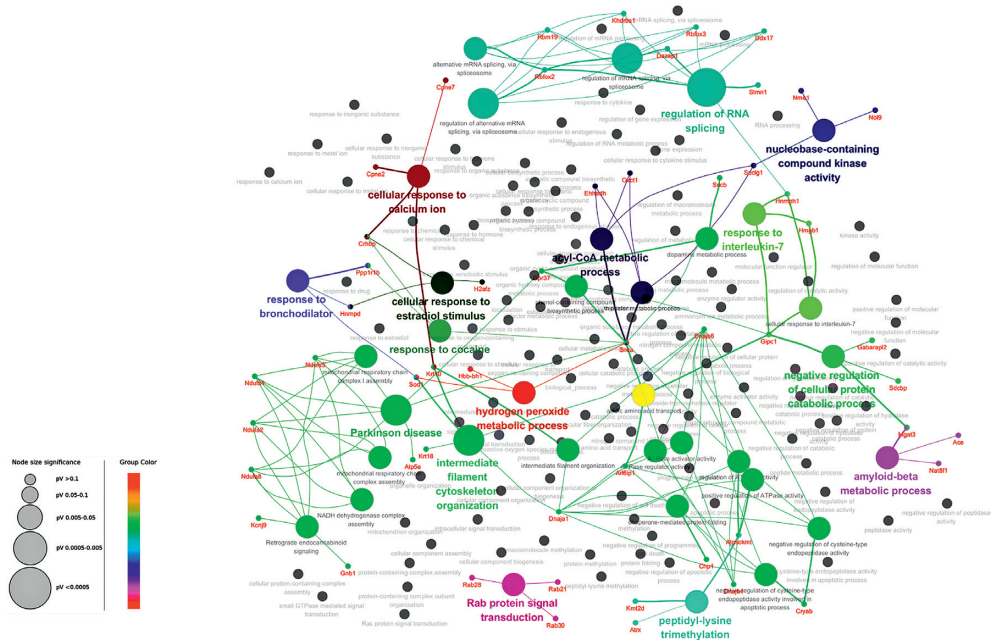

(d)

Figure 5: FUS-induced differences in protein expression indicated alterations in pathways in the ACC. EggNOG entry statistics (a). Subcellular location analysis (b). Visualized functional enrichment (c). Pathway analysis (d).

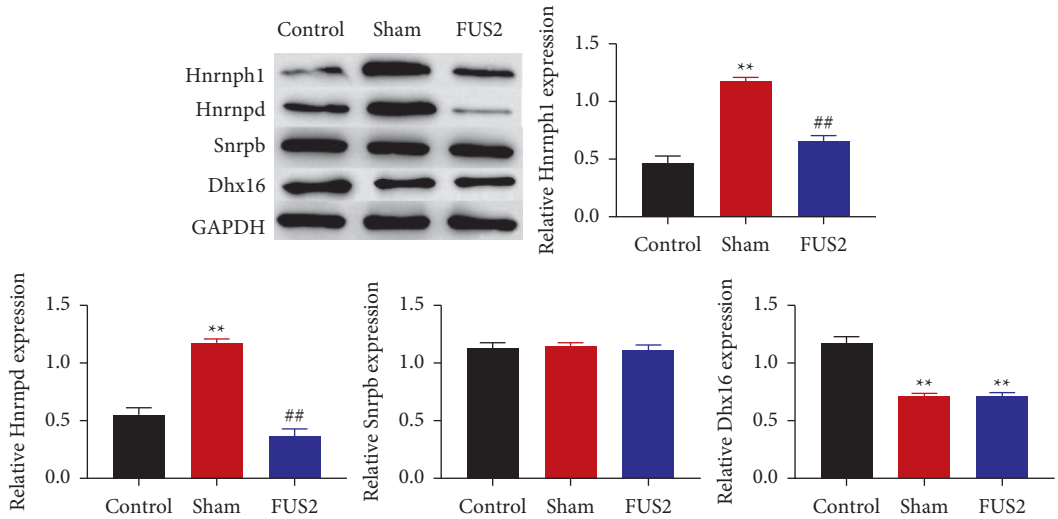

Figure 6: FUS2-induced changes in the expression of Hnrnph1, Hnrnpd, Snrpb, and Dhx16. The expression of Hnrnph1, Hnrnpd, Snrpb, and Dhx16 in tissue was measured by western blotting. * indicates statistical significance between the Sham group and the Control group, the FUS2 group and the Control group. # indicates statistical significance between the FUS2 group and the Sham group.

area, making it safer and more accurate and improving the effects of uneven skull bones in humans or large animals through combination with magnetic resonance imaging (MRI) [42]. Similar to magnetic stimulation, FUS can be used in regions of the peripheral and central nervous systems [43]. Moreover, they both require more effective treatment following repeated stimulation for pain management. The difference between the protocols is that the cortical M1 is a more effective target for central inhibition using repetitive transcranial magnetic stimulation [16, 44]. At present, FUS is also widely used in larger animals. Low-intensity FUS modulated the excitability of regional brain tissues reversibly and safely in awake sheep [45]. In addition, FUS stimulation of female macaque monkeys under the guidance of MRI can double suppressive and excitative modulation of specific functional circuits [46]. FUS is different from other pharmacological or interventional therapies for acute and chronic pain. In our study, FUS stimulation of the ACC was effective in both the short- and long-term experiments, which suggests that FUS is a useful and noninvasive technique for pain management. Yang et al. reported increased neuronal excitability in ACC during nerve injury pain [47],

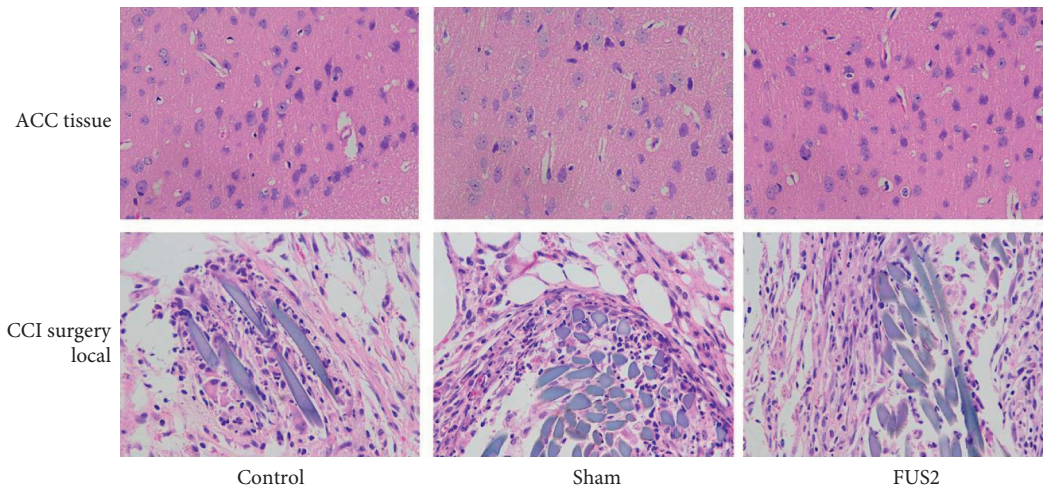

Figure 7: Safety and temperature evaluation. HE staining of the ACC brain tissue and the CCI surgery local site (×400).

especially in the bilateral ACC [48]. Similar to previous reports on other neuroregulatory methods (e.g., optogenetics) [13, 49–51], our MEA recordings revealed that FUS-induced reduction in the nerve excitability of the ACC in the brain slices was involved in pain attenuation, which also suggested that ACC could be an ideal target in CNS regulation of NP. Clennell et al. confirmed that there was a sustained effect until 8 hours after ultrasound stimulation [52], and we had found there was inhibition within 100s after ultrasound stimulation through MEA. In our experiment, the mechanical analgesic effect of ultrasound stimulation lasting for 3 weeks may be due to the continuous inhibition of nerve by repeated stimulation.

Peripheral nociceptor sensitization and durable synaptic plasticity in the CNS contribute to chronic pain in rodent models [53]. Although chronic and acute pain share common neural pathways [54, 55], establishing mechanisms for alleviating acute or chronic pain remains challenging. In a rodent NP model, central sensitization may be indicated by the characteristic potentiation of synaptic responses in the ACC and the development of allodynia at 1–2 weeks following nerve injury [56, 57]. This may explain the earlier presentation of FUS effects in the long-term experiment. Contrastingly, in the short-term experiment, the FUS-induced effects required a longer time (two weeks following the surgery) to appear.

The difference in the time of onset of FUS effects between the short- and long-term experiments indicated that the ACC or the early stage of the pain was not the optimal target for pain improvement in the short-term experiments. Conversely, central sensitization may have been the main target for pain regulation in long-term tests. Our findings indicate that FUS stimulation of the ACC has a therapeutic effect on chronic pain following peripheral nerve injury through changes in the nervous and immune systems of the CNS. Similarly, a previous study that focused on similar peripheral damage reported that the emergence of central sensitization played a vital role in the resulting chronic pain [58]. The regulation of different brain regions would have different results from the literature [59–67], and ultrasound regulation of ACC improved mechanical retraction threshold in the CCI model in our study, suggesting that ultrasound stimulation of different target brain regions can be considered to obtain better curative effect according to the different pain symptoms.

The occurrence and development of NP are caused by many factors and the disorder of genes regulation. Recent studies have found that FUS stimulation can improve the progress of NP by regulating the disordered genes [68]. In this study, we found four key genes Hnrnph1, Hnrnpd, Snrpb, and Dhx16 by analyzing the protein profile of long-term experimental mice. Further research found that Hnrnph1 and Hnrnpd are highly expressed in the brain tissue of NP mice, but downregulated in normal mouse brain tissue and FUS stimulation. HNRNPH1 and HNRNPD (heterogeneous nuclear ribonucleoprotein D) is a multifunctional RNA binding protein (RBP) with roles in regulation of alternative splicing, mRNA transcription, RNA stability, RNA localization, and regulation of target transcript translation. HNRNPH1 is abnormally overexpressed in a variety of tumors. Previous studies have confirmed that the high expression of HNRNPH1 can promote tumor development by inhibiting tumor suppressor genes [69]. However, the role of HNRNPH1 in NP has not been investigated. HNRNPD participates in the regulation of cell oxidative stress and inflammation. And it is also related to the cross-regulation of inflammation [70]. In addition, HNRNPD participates in the apoptosis of diabetic cells [71]. But the role of HNRNPD in NP has not been reported. According to the results of this experiment, we speculate that HNRNPH1 and HNRNPD may play a key role in NP, and, at the same time, FUS stimulation can directly or indirectly downregulate the levels of HNRNPH1 and HNRNPD to improve the development of NP. However, to determine the regulatory mechanism of HNRNPH1 and HNRNPD in NP, further research and investigation are needed.

Ultrasound waves have mechanical, cavitation, and thermal effects on biological tissue. The thermal effects of high-intensity FUS (HIFU >200 W/cm^2) are reported to cause coagulative necrosis of brain tissue through the intact

skull [72, 73]. Findings on HE staining and local temperature increase ($\Delta T < 0.1^{\circ}C$) showed that the treatment was safe and did not cause tissue damage to the target tissue and the surrounding. Moreover, the maximum negative peak pressure was much lower than the inertial cavitation threshold (40 MPa), which prevented tissue damage [74].

In conclusion, previous studies have indicated the safety of transcranial ultrasound stimulation, which is consistent with the results of other studies [21, 75, 76]. Our findings indicate that FUS effectively alleviates mechanical NP via ACC inhibition, especially in the chronic state. The underlying mechanisms may be associated with several central sensitization stages, suggesting that different protocols may be more appropriate for different NP stages. Protein analysis in the long-term experiment demonstrated that FUS-induced neuromodulation of the ACC altered the immune function and several pathways involved in central sensitization. These results suggested great potential for clinical translation. Particularly, it is of significance to select different intervention programs at different clinical stages. However, ultrasound is prone to be off-target due to the heterogeneity of the skull, and MRI is needed to correct the ultrasound stimulation in humans or large animals. Based on ethical principles, we could not use a larger sample of mice to verify every parameter, and there may be more reasonable parameters inducing different effects. Future studies should investigate targeted brain regions, appropriate time points, and response pathways to identify the mechanisms underlying FUS treatment of NP.

Data Availability

The data used to support the findings of this study are available from the corresponding author upon reasonable request.

Disclosure

The funding sources had no role in the study design; in the collection, analysis, and interpretation of data; in the writing of the report; or in the decision to submit the article for publication.

Conflicts of Interest

The authors declare that there are no conflicts of interest regarding the publication of this study.

Acknowledgments

The authors would like to thank Dr. Mian Chen (Biomedical Engineering Department of Shenzhen University) for providing his laser transmitter and technical help. This work was supported by the National Natural Science Foundation of China (grant nos. 81960421, 81660381, 81527901, 11774371, 11574341, 11674347, and 12004410), Guangdong-Hong Kong-Macao Greater Bay Area Center for Brain Science and Brain-Inspired Intelligence Fund (no. 2019024), Guangdong grant "Key Technologies for Treatment of Brain Disorders" (no. 2018B030332001), CAS Key Laboratory of Health Informatics Fund (2011DP173015), and Doctoral Innovation Foundation of Kunming Medical University (no. 2019D007).

Supplementary Materials

Table S1: cytoHubba function results. (*Supplementary Materials*)

References

[1] S.-F. Cho, K.-M. Rau, Y.-Y. Shao et al., "Patients with head and neck cancer may need more intensive pain management to maintain daily functioning: a multi-center study," *Supportive Care in Cancer*, vol. 27, no. 5, pp. 1663–1672, 2019.

[2] J. Gierthmühlen and R. Baron, "Neuropathic pain," *Seminars in Neurology*, vol. 36, pp. 462–468, 2016.

[3] Ó. A. Steingrímsdóttir, T. Landmark, G. J. Macfarlane, and C. S. Nielsen, "Defining chronic pain in epidemiological studies: a systematic review and meta-analysis," *Pain*, vol. 158, no. 11, pp. 2092–2107, 2017.

[4] L. E. Simons, I. Elman, and D. Borsook, "Psychological processing in chronic pain: a neural systems approach," *Neuroscience & Biobehavioral Reviews*, vol. 39, pp. 61–78, 2014.

[5] D. Moulin, A. Boulanger, A. CLArK et al., "Pharmacological management of chronic neuropathic pain: revised consensus statement from the Canadian Pain Society," *Pain Research and Management*, vol. 19, no. 6, pp. 328–335, 2014.

[6] X. Moisset, D. Bouhassira, J. Avez Couturier et al., "Pharmacological and non-pharmacological treatments for neuropathic pain: systematic review and French recommendations," *Revue Neurologique*, vol. 176, no. 5, pp. 325–352, 2020.

[7] C.-H. Hung, P.-C. Huang, J.-I. Tzeng, J.-J. Wang, and Y.-W. Chen, "Therapeutic ultrasound and treadmill training suppress peripheral nerve injury-induced pain in rats," *Physical Therapy*, vol. 96, no. 10, pp. 1545–1553, 2016.

[8] W. Jiang, Y. Wang, J. Tang et al., "Low-intensity pulsed ultrasound treatment improved the rate of autograft peripheral nerve regeneration in rat," *Scientific Reports*, vol. 6, no. 1, Article ID 22773, 2016.

[9] S. Hameroff, M. Trakas, C. Duffield et al., "Transcranial ultrasound (TUS) effects on mental states: a pilot study," *Brain Stimulation*, vol. 6, no. 3, pp. 409–415, 2013.

[10] J. Spooner, H. Yu, C. Kao, K. Sillay, and P. Konrad, "Neuromodulation of the cingulum for neuropathic pain after spinal cord injury. Case report," *Journal of Neurosurgery*, vol. 107, no. 1, pp. 169–172, 2007.

[11] S. M. Farrell, A. Green, and T. Aziz, "The current state of deep brain stimulation for chronic pain and its context in other forms of neuromodulation," *Brain Sciences*, vol. 8, 2018.

[12] T. Chen, K. Koga, G. Descalzi et al., "Postsynaptic potentiation of corticospinal projecting neurons in the anterior cingulate cortex after nerve injury," *Molecular Pain*, vol. 10, p. 33, 2014.

[13] L. Gu, M. L. Uhelski, S. Anand et al., "Pain inhibition by optogenetic activation of specific anterior cingulate cortical neurons," *PLoS One*, vol. 10, Article ID e0117746, 2015.

[14] W. Masocha, "Astrocyte activation in the anterior cingulate cortex and altered glutamatergic gene expression during paclitaxel-induced neuropathic pain in mice," *PeerJ*, vol. 3, Article ID e1350, 2015.

[15] H. C. Moon, W. I. Heo, Y. J. Kim et al., "Optical inactivation of the anterior cingulate cortex modulate descending pain

pathway in a rat model of trigeminal neuropathic pain created via chronic constriction injury of the infraorbital nerve," *Journal of Pain Research*, vol. 10, pp. 2355–2364, 2017.

[16] H. Kumru, S. Albu, J. Vidal, and J. M. Tormos, "Effectiveness of repetitive trancranial or peripheral magnetic stimulation in neuropathic pain," *Disability & Rehabilitation*, vol. 39, no. 9, pp. 856–866, 2017.

[17] V. Levi, R. Cordella, A. D'Ammando et al., "Dorsal anterior cingulate cortex (ACC) deep brain stimulation (DBS): a promising surgical option for the treatment of refractory thalamic pain syndrome (TPS)," *Acta Neurochirurgica*, vol. 161, no. 8, pp. 1579–1588, 2019.

[18] O. Naor, S. Krupa, and S. Shoham, "Ultrasonic neuromodulation," *Journal of Neural Engineering*, vol. 13, Article ID 031003, 2016.

[19] R. F. Dallapiazza, K. F. Timbie, S. HolmberG et al., "Noninvasive neuromodulation and thalamic mapping with low-intensity focused ultrasound," *Journal of Neurosurgery*, vol. 128, no. 3, pp. 875–884, 2018.

[20] L. Di Biase, E. Falato, and V. Di Lazzaro, "Transcranial focused ultrasound (tFUS) and transcranial unfocused ultrasound (tUS) neuromodulation: from theoretical principles to stimulation practices," *Frontiers in Neurology*, vol. 10, p. 549, 2019.

[21] X. Huang, H. Zheng, Z. Lin et al., "Transcranial low-intensity pulsed ultrasound modulates structural and functional synaptic plasticity in rat Hippocampus," *IEEE Transactions on Ultrasonics, Ferroelectrics, and Frequency Control*, vol. 66, no. 5, pp. 930–938, 2019.

[22] H. Zhou, L. Niu, L. Meng et al., "Noninvasive ultrasound deep brain stimulation for the treatment of Parkinson's disease model mouse," *Research: Ideas for Today's Investors*, vol. 2019, Article ID 1748489, 13 pages, 2019.

[23] G. J. Bennett and Y.-K. Xie, "A peripheral mononeuropathy in rat that produces disorders of pain sensation like those seen in man," *Pain*, vol. 33, no. 1, pp. 87–107, 1988.

[24] V. V. Monte-Raso, C. H. Barbieri, N. Mazzer, A. C. Yamasita, and G. Barbieri, "Is the sciatic functional index always reliable and reproducible?" *Journal of Neuroscience Methods*, vol. 170, no. 2, pp. 255–261, 2008.

[25] A. Becchetti, F. Gullo, G. Bruno, E. Dossi, M. Lecchi, and E. Wanke, "Exact distinction of excitatory and inhibitory neurons in neural networks: a study with GFP-GAD67 neurons optically and electrophysiologically recognized on multielectrode arrays," *Frontiers in Neural Circuits*, vol. 6, p. 63, 2012.

[26] Q. Jiang, G. Li, H. Zhao et al., "Temporal neuromodulation of retinal ganglion cells by low-frequency focused ultrasound stimulation," *IEEE Transactions on Neural Systems and Rehabilitation Engineering*, vol. 26, no. 5, pp. 969–976, 2018.

[27] S. Wiese, K. A. Reidegeld, H. E. Meyer, and B. Warscheid, "Protein labeling by iTRAQ: a new tool for quantitative mass spectrometry in proteome research," *Proteomics*, vol. 7, no. 3, pp. 340–350, 2007.

[28] G. Paxinos and K. B. J. Franklin, "The mouse brain in stereotaxic coordinates," Elsevier, Amsterdam, Netherlands, 2nd edition, 2001.

[29] J. R. Wisniewski, A. Zougman, N. Nagaraj, and M. Mann, "Universal sample preparation method for proteome analysis," *Nature Methods*, vol. 6, pp. 359–362, 2009.

[30] D. Zhang, H. Li, J. Sun et al., "Antidepressant-like effect of low-intensity transcranial ultrasound stimulation," *IEEE Transactions on Biomedical Engineering*, vol. 66, no. 2, pp. 411–420, 2019.

[31] W. D. O'brien JR., "Ultrasound-biophysics mechanisms," *Progress in Biophysics and Molecular Biology*, vol. 93, pp. 212–255, 2007.

[32] P. Shannon, A. Markiel, O. Ozier et al., "Cytoscape: a software environment for integrated models of biomolecular interaction networks," *Genome Research*, vol. 13, no. 11, pp. 2498–2504, 2003.

[33] F. Marchand, M. Perretti, and S. B. Mcmahon, "Role of the immune system in chronic pain," *Nature Reviews Neuroscience*, vol. 6, no. 7, pp. 521–532, 2005.

[34] R. Geenen and J. W. J. Bijlsma, "Deviations in the endocrine system and brain of patients with fibromyalgia: cause or consequence of pain and associated features?" *Annals of the New York Academy of Sciences*, vol. 1193, no. 1, pp. 98–110, 2010.

[35] K. Ren and R. Dubner, "Interactions between the immune and nervous systems in pain," *Nature Medicine*, vol. 16, no. 11, pp. 1267–1276, 2010.

[36] F. Tennant, "The physiologic effects of pain on the endocrine system," *Pain and Therapy*, vol. 2, no. 2, pp. 75–86, 2013.

[37] S. K. Totsch and R. E. Sorge, "Immune system involvement in specific pain conditions," *Molecular Pain*, vol. 13, Article ID 1744806917724559, 2017.

[38] M. E. Downs, S. A. Lee, G. Yang, S Kim, Q. Wang, and E. E. Konofagou, "Non-invasive peripheral nerve stimulation via focused ultrasound in vivo," *Physics in Medicine and Biology*, vol. 63, p. 035011, 2018.

[39] K. Eguchi, T. Shindo, K. Ito et al., "Whole-brain low-intensity pulsed ultrasound therapy markedly improves cognitive dysfunctions in mouse models of dementia - crucial roles of endothelial nitric oxide synthase," *Brain Stimulation*, vol. 11, no. 5, pp. 959–973, 2018.

[40] V. Cotero, Y. Fan, T. Tsaava et al., "Noninvasive sub-organ ultrasound stimulation for targeted neuromodulation," *Nature Communications*, vol. 10, no. 1, p. 952, 2019.

[41] H. Zhou, L. Niu, X. Xia et al., "Wearable ultrasound improves motor function in an MPTP mouse model of Parkinson's disease," *IEEE Transactions on Biomedical Engineering*, vol. 66, 2019.

[42] A. Bystritsky, A. S. Korb, P. K. Douglas et al., "A review of low-intensity focused ultrasound pulsation," *Brain Stimulation*, vol. 4, no. 3, pp. 125–136, 2011.

[43] E. Hattapoglu, I. Batmaz, B. Dilek, M. Karakoç, S. Em, and R. Çevik, "Efficiency of pulsed electromagnetic fields on pain, disability, anxiety, depression, and quality of life in patients with cervical disc herniation: a randomized controlled study," *Turkish Journal of Medical Sciences*, vol. 49, pp. 1095–1101, 2019.

[44] A. Leung, M. Donohue, R. Xu et al., "rTMS for suppressing neuropathic pain: a meta-analysis," *The Journal of Pain*, vol. 10, no. 12, pp. 1205–1216, 2009.

[45] H. C. Kim, W. Lee, J. Kunes et al., "Transcranial focused ultrasound modulates cortical and thalamic motor activity in awake sheep," *Scientific Reports*, vol. 11, Article ID 19274, 2021.

[46] P.-F. Yang, M. A. Phipps, S. Jonathan et al., "Bidirectional and state-dependent modulation of brain activity by transcranial focused ultrasound in non-human primates," *Brain Stimulation*, vol. 14, no. 2, pp. 261–272, 2021.

[47] Z. Yang, Q. Tan, D. Cheng et al., "The changes of intrinsic excitability of pyramidal neurons in anterior cingulate cortex in neuropathic pain," *Frontiers in Cellular Neuroscience*, vol. 12, p. 436, 2018.

[48] R. Zhao, H. Zhou, L. Huang et al., "Neuropathic pain causes pyramidal neuronal hyperactivity in the anterior cingulate cortex," *Frontiers in Cellular Neuroscience*, vol. 12, p. 107, 2018.

[49] M. F. Dossantos, N. Ferreira, R. L. Toback, A. C. Carvalho, and A. F. DaSilva, "Potential mechanisms supporting the value of motor cortex stimulation to treat chronic pain syndromes," *Frontiers in Neuroscience*, vol. 10, p. 18, 2016.

[50] D. L. Juarez-Salinas, J. M. Braz, A. Etlin, S. Gee, V. Sohal, and A. I. Basbaum, "GABAergic cell transplants in the anterior cingulate cortex reduce neuropathic pain aversiveness," *Brain*, vol. 142, no. 9, pp. 2655–2669, 2019.

[51] D. J. Lee, C. S. Lozano, R. F. Dallapiazza, and A. M. Lozano, "Current and future directions of deep brain stimulation for neurological and psychiatric disorders," *Journal of Neurosurgery*, vol. 131, no. 2, pp. 333–342, 2019.

[52] B. Clennell, T. G. J. Steward, M. Elley et al., "Transient ultrasound stimulation has lasting effects on neuronal excitability," *Brain Stimulation*, vol. 14, no. 2, pp. 217–225, 2021.

[53] M. Zhuo, "Cortical excitation and chronic pain," *Trends in Neurosciences*, vol. 31, no. 4, pp. 199–207, 2008.

[54] A. V. Apkarian, M. C. Bushnell, R.-D. Treede, and J.-K. Zubieta, "Human brain mechanisms of pain perception and regulation in health and disease," *European Journal of Pain*, vol. 9, no. 4, p. 463, 2005.

[55] M. C. Bushnell, M. Čeko, and L. A. Low, "Cognitive and emotional control of pain and its disruption in chronic pain," *Nature Reviews Neuroscience*, vol. 14, no. 7, pp. 502–511, 2013.

[56] X.-Y. Li, H.-G. Ko, T. Chen et al., "Alleviating neuropathic pain hypersensitivity by inhibiting PKMzeta in the anterior cingulate cortex," *Science*, vol. 330, no. 6009, pp. 1400–1404, 2010.

[57] K. Koga, G. Descalzi, T. Chen et al., "Coexistence of two forms of LTP in ACC provides a synaptic mechanism for the interactions between anxiety and chronic pain," *Neuron*, vol. 85, no. 2, pp. 377–389, 2015.

[58] C. Den Boer, L. Dries, B. Terluin et al., "Central sensitization in chronic pain and medically unexplained symptom research: a systematic review of definitions, operationalizations and measurement instruments," *Journal of Psychosomatic Research*, vol. 117, pp. 32–40, 2019.

[59] H. Sun and V. Neugebauer, "mGluR1, but not mGluR5, activates feed-forward inhibition in the medial prefrontal cortex to impair decision making," *Journal of Neurophysiology*, vol. 106, no. 2, pp. 960–973, 2011.

[60] L. Luongo, V. De Novellis, L. Gatta et al., "Role of metabotropic glutamate receptor 1 in the basolateral amygdala-driven prefrontal cortical deactivation in inflammatory pain in the rat," *Neuropharmacology*, vol. 66, pp. 317–329, 2013.

[61] C. Giordano, L. Cristino, L. Luongo et al., "TRPV1-dependent and -independent alterations in the limbic cortex of neuropathic mice: impact on glial caspases and pain perception," *Cerebral Cortex*, vol. 22, no. 11, pp. 2495–2518, 2012.

[62] W. E. Wang, R. L. M. Ho, B. Gatto et al., "Cortical dynamics of movement-evoked pain in chronic low back pain," *The Journal of Physiology*, vol. 599, no. 1, pp. 289–305, 2021.

[63] M. Zhuo, "Neural mechanisms underlying anxiety-chronic pain interactions," *Trends in Neurosciences*, vol. 39, no. 3, pp. 136–145, 2016.

[64] K. Carlsson, J. Andersson, P. Petrovic, K. M. Petersson, A. Öhman, and M. Ingvar, "Predictability modulates the affective and sensory-discriminative neural processing of pain," *NeuroImage*, vol. 32, no. 4, pp. 1804–1814, 2006.

[65] C. A. Brown, B. Seymour, Y. Boyle, W. El-Deredy, and A. K. P. Jones, "Modulation of pain ratings by expectation and uncertainty: behavioral characteristics and anticipatory neural correlates," *Pain*, vol. 135, no. 3, pp. 240–250, 2008.

[66] G.-Q. Wang, C. Cen, C. Li et al., "Deactivation of excitatory neurons in the prelimbic cortex via Cdk5 promotes pain sensation and anxiety," *Nature Communications*, vol. 6, no. 1, p. 7660, 2015.

[67] B. W. Badran, K. A. Caulfield, S. Stomberg-Firestein et al., "Sonication of the anterior thalamus with MRI-Guided transcranial focused ultrasound (tFUS) alters pain thresholds in healthy adults: a double-blind, sham-controlled study," *Brain Stimulation*, vol. 13, no. 6, pp. 1805–1812, 2020.

[68] Y. H. Liao, B. Wang, M. X. Chen, Y. Liu, and Li-J. Ao, "LIFU alleviates neuropathic pain by improving the KCC(2) expression and inhibiting the CaMKIV-KCC(2) pathway in the L4-L5 section of the spinal cord," *Neural Plasticity and Neuropathic Pain*, vol. 2021, Article ID 6659668, 2021.

[69] M. Liu, L. Yang, X. Liu et al., "HNRNPH1 is a novel regulator of cellular proliferation and disease progression in chronic myeloid leukemia," *Frontiers in Oncology*, vol. 11, Article ID 682859, 2021.

[70] T. Ishii, H. Hayakawa, T. Sekiguchi, N. Adachi, and M. Sekiguchi, "Role of Auf1 in elimination of oxidatively damaged messenger RNA in human cells," *Free Radical Biology and Medicine*, vol. 79, pp. 109–116, 2015.

[71] E. C. Vanzela and A. K. Cardozo, "Is ARE/poly(U)-binding factor 1 (AUF1) a new player in cytokine-mediated beta cell apoptosis?" *Diabetologia*, vol. 55, no. 6, pp. 1572–1576, 2012.

[72] W. J. Elias, D. Huss, T. Voss et al., "A pilot study of focused ultrasound thalamotomy for essential tremor," *New England Journal of Medicine*, vol. 369, no. 7, pp. 640–648, 2013.

[73] V. Krishna, F. Sammartino, P. Agrawal et al., "Prospective tractography-based targeting for improved safety of focused ultrasound thalamotomy," *Neurosurgery*, vol. 84, pp. 160–168, 2019.

[74] D. Dalecki, "Mechanical bioeffects of ultrasound," *Annual Review of Biomedical Engineering*, vol. 6, no. 1, pp. 229–248, 2004.

[75] T. Deffieux, Y. Younan, N. Wattiez, M. Tanter, P. Pouget, and J.-F. Aubry, "Low-intensity focused ultrasound modulates monkey visuomotor behavior," *Current Biology*, vol. 23, no. 23, pp. 2430–2433, 2013.

[76] Z. Zhang, W. Qiu, H. Gong et al., "Low-intensity ultrasound suppresses low-Mg(2+)-induced epileptiform discharges in juvenile mouse hippocampal slices," *Journal of Neural Engineering*, vol. 16, Article ID 036006, 2019.

Hindawi
Evidence-Based Complementary and Alternative Medicine
Volume 2021, Article ID 5671998, 7 pages
https://doi.org/10.1155/2021/5671998

Research Article

Effect of Specific Acupuncture Therapy Combined with Rehabilitation Training on Incomplete Spinal Cord Injury: A Randomized Clinical Trial

Feng Xiong,[1,2,3] **Jingkang Lu**,[1,2] **Hongxia Pan**,[1,2] **Fengyi Wang**,[1,2] **Yaqin Huang**,[1,2] **Yiwei Liu**,[1,2] **Lingxin Li**,[1,2] **Rengang Zhang**,[1,2] **Yulong Wang**,[3] **Chengqi He**,[1,2] **and Wei Quan**[1,2]

[1]*Department of Rehabilitation Medicine Center and Institute of Rehabilitation Medicine, West China Hospital, Sichuan University, Chengdu, Sichuan, China*
[2]*Key Laboratory of Rehabilitation Medicine in Sichuan Province, Chengdu, Sichuan, China*
[3]*Department of Rehabilitation, Shenzhen Second People's Hospital, The First Affiliated Hospital of Shenzhen University, Shenzhen, China*

Correspondence should be addressed to Yulong Wang; ylwang668@163.com and Wei Quan; weiquan@scu.edu.cn

Received 12 August 2021; Accepted 2 December 2021; Published 26 December 2021

Academic Editor: Feng Zhang

Acupuncture therapies were used to treat spinal cord injury (SCI) and its complications. To assess the effect of a specific acupuncture therapy combined with rehabilitation training for inpatients with incomplete SCI, we conducted an assessor-blinded, randomized controlled clinical trial in the Department of Rehabilitation Medicine Center in West China Hospital, Sichuan University. Seventy-two participants diagnosed with incomplete SCI were randomly assigned into 3 groups of 24 patients each, with data collection completed in December, 2019. Participants were randomly assigned (1 : 1 : 1) to 3 groups to receive treatment for 4 weeks, 5 times/week of acupuncture for Continuous Acupuncture Treatment (CAT) group, 3 times/week for Intermittent Acupuncture Treatment (IAT) group, and no acupuncture for Control group; all 3 groups received routine rehabilitation training. The primary outcome was the change of American Spinal Injury Association (ASIA) motor score from baseline to week 4. Secondary outcomes included sensory score, Modified Barthel Index (MBI). At week 4, CAT group had a higher motor score and MBI score increase than the control group (mean difference 10.52, 17.36; $p < 0.001$, $p < 0.01$, respectively). CAT group had more increase in motor score and MBI than IAT group (mean difference 5.55, 14.77; $p < 0.05$, $p < 0.05$, respectively). But the difference among groups in the increase of sensory score was not statistically significant. Acupuncture resulted in a higher motor score and MBI after 4 weeks. And the dosage of 5/week led to more improvement in motor score and MBI than that of 3/week. The results suggested that a dosage of 5/week of acupuncture is safe and more effective for SCI than 3/week. But further research is needed to determine the best intervention dosage, long-term efficacy, and underlying mechanism. This trial is registered with ChiCTR1900021530.

1. Introduction

Spinal cord injury (SCI) is a neurological condition that is common in the clinic but is often severe; most of the patients ended up with quadriplegia or paraplegia. At present, rehabilitation treatments for SCI have been proven to be effective [1], but the effects are often slow and limited [2], so it is necessary to seek better rehabilitation treatments.

Acupuncture has a wide range of applications, and acupuncture treatments for SCI have been studied across the world, but there have been only a few randomized controlled trials reporting treatment effects on neural function (motor and sensory) in English [3–6]. Most of the existing literature regarding the clinical effect of acupuncture on SCI only reported other outcomes such as pain scale or molecular indicators [3–9]. At present, the acupoints used in most of

the studies investigating acupuncture treatment for SCI were mainly on the abdomen, the back, and the lower extremities [3–6]. Acupuncture relies on mobilizing the energy within the human body itself, but because of the stagnation of Qi and blood below the damaged segment after SCI, it is difficult to obtain a satisfactory result using treatments consisting mostly of acupoints below the injured segment.

Besides the location and number of acupoints, the dosage of acupuncture for SCI also varied between centers. Some of the common dosages are three times, five times, or seven times per week. Up until now, there has not been a trial investigating the dosage of acupuncture treatments for SCI.

To help solve the problem of dosage, this study aimed to investigate the intervention frequency of acupuncture therapy on incomplete SCI.

2. Methods

This assessor-blinded, randomized controlled clinical study was conducted in West China Hospital in Sichuan, China. The medical ethical committee of West China Hospital, Sichuan University, approved the study protocol (no. 2018-253). The trial was registered at the Chinese Clinical Trial Registry (ChiCTR1900021530). This study was supported by the National Natural Science Foundation of China (grant no. 81572231). Written informed consent was obtained from all participants. The study process was shown in Figure 1.

2.1. Participants. Patients with SCI were recruited from inpatients at the Department of Rehabilitation Medicine, West China Hospital, Sichuan University, between August, 2018, and December, 2019. Interested patients were initially screened according to the inclusion and exclusion criteria at the neural rehabilitation ward. Participants were not compensated for study participation. Participants' self-reported ethnicity information was routinely collected without ethnic discrimination.

2.2. Inclusion Criteria. The inclusion criteria were as follows: age 18 to 75 years, a clear history of trauma by surgery or accidents of the spinal cord, diagnosis with SCI by magnetic resonance imaging and clinical symptoms, classification as grade C or D according to the American Spinal Injury Association (ASIA) 2011 classification of SCI, passing the shock phase of SCI, already went through surgery (if needed), stable vital signs, clear consciousness, the liability to cooperate with the treatments and tests and answer the questionnaire, and agreement to participate and sign informed consent.

2.3. Exclusion Criteria. The exclusion criteria included: shock phase of SCI, complete SCI, inability to complete the sessions due to various reasons, severe deep vein thrombosis, open fractures, infection, severe osteoporosis, and other complications that may prevent the patients from participating in the rehabilitation sessions; heart failure, cardiovascular and cerebrovascular accidents within 1 year, malignant tumors, and other serious diseases that may lead to interruption of the experiment or the observation of outcome indicators; and skin infections around the acupuncture points, history of severe fainting during acupuncture, and other conditions that may prevent the patients from receiving acupuncture.

2.4. Randomization and Blinding. Seventy-two participants were randomly assigned to 3 groups according to the random sequences generated using Excel software. The random sequences were each sealed in envelopes and were not to be opened until each patient's enrollment. The 3 groups were CAT group, IAT group, and the control group, with ratio 1 : 1 : 1, 24 participants in each group. The outcome assessors, therapists (rehabilitation therapists other than an acupuncturist), and statisticians were blinded to treatment allocation. Acupuncturists were not blinded due to the nature of the intervention. Acupuncturists, other therapists, outcome assessors, and statisticians are four separate groups of people.

2.5. Intervention. Hwato brand disposable acupuncture needles (size 0.25×40 mm, or 0.25×75 mm, manufactured by Wuxi Jiajian Medical Devices Co., Ltd) were used.

2.5.1. Routine Rehabilitation. All three groups of patients were treated with routine rehabilitation training, and the necessary symptomatic treatment (for example, catheterization) was performed for complications. Both CAT group and IAT group received acupuncture treatments: 5/week (Monday to Friday) for CAT group and 3/week (Monday, Wednesday, and Friday) for IAT group. The treatments lasted for 4 weeks.

All included patients received routine rehabilitation training. It mainly included passive training, upright bed treatment, active training, sitting balance, wheelchair shift, the activity of daily life training, and counseling of patients and their families.

For patients with neurogenic bladder, intermittent catheterization was also required. The urine was drained from the bladder according to the bladder sensation or a timetable using a catheter. A drinking-catheterization plan was made for each patient before the experiment.

2.5.2. Acupuncture Treatments. Besides the rehabilitation treatment mentioned above, the acupuncture groups (CAT group and IAT group) shall receive acupuncture treatment.

Acupuncture treatment began on the first Monday after enrollment. The selected area should be disinfected with 75% alcohol, and the doctor's hand should be disinfected by washing with soap or quick-drying disinfectant. To prevent fainting, patients should be prevented from exercising vigorously within 1 hour before treatment, avoid acupuncture when hungry, and properly communicate with and comfort the patient to avoid mental stress. The patient was placed in a supine position during treatment exposing to the skin at the corresponding location. The room temperature was adjusted, and an infrared heater was used to maintain the surface body temperature of the patient if necessary.

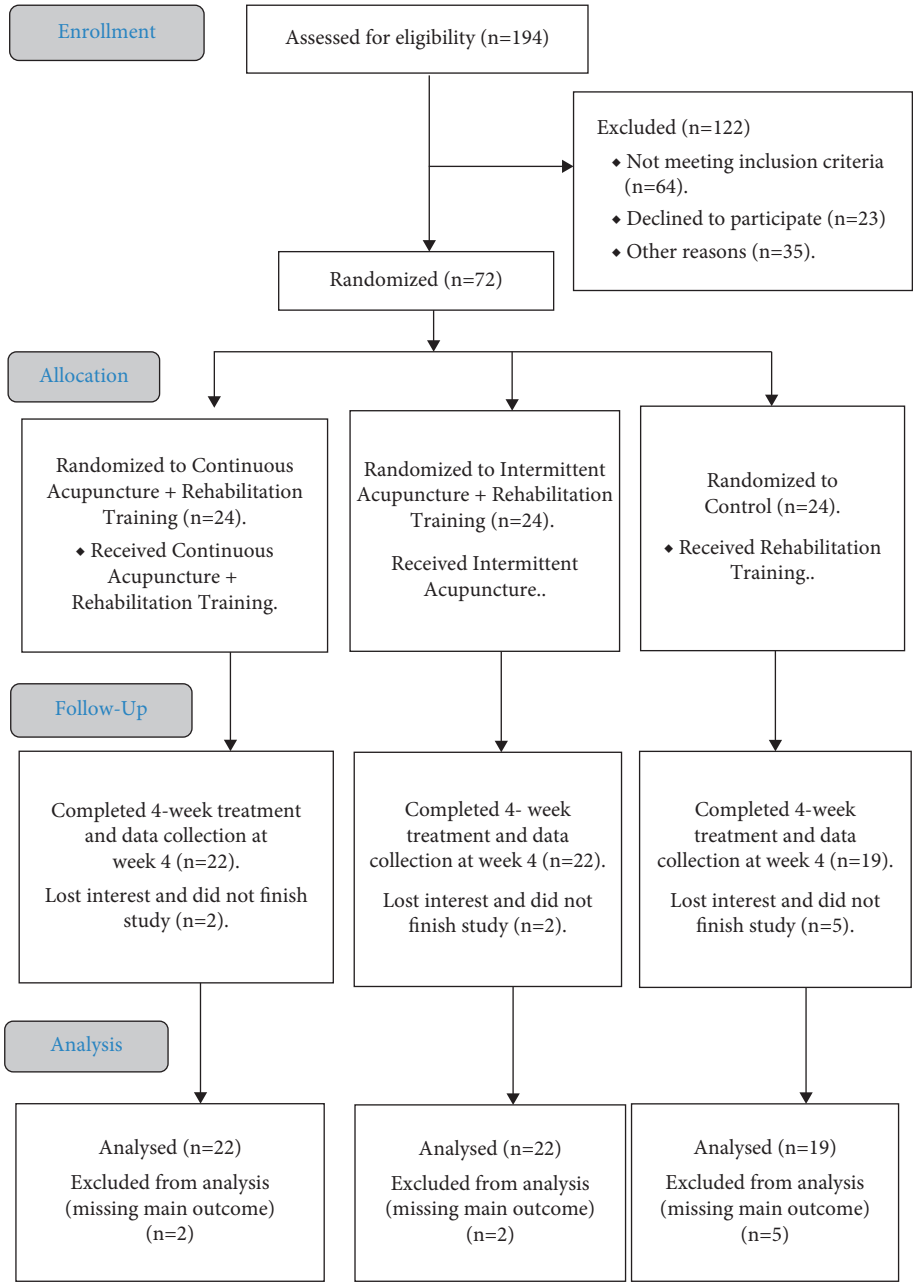

Figure 1: Consolidated Standards Of Reporting Trials (CONSORT) 2010.

Baihui (GV20) 0.5 to 0.8 cun (about 15 degrees angle with the skin, needle tip pointing to the lower back), bilateral *Hegu* (LI4) 0.5 to 0.8 cun (the palm in a relaxed position), bilateral *Wangu* (SI4) 0.3 to 0.5 cun, bilateral *Houxi* (SI3) 0.5 to 1.0 cun, bilateral *Yemen* (TE2) 0.3 ~ 0.5 cun, bilateral *Zhigou* (SJ6) 0.5 to 1cun, bilateral *Shaofu* (HT8) 0.3 ~ 0.5 cun, bilateral *Quchi* (LI11) 1.0 to 2.5 cun, bilateral *Jianyu* (LI15) (the tip of the needle points to the direction of *Jiquan* [HT1], 2 to 3 cun deep), and *Shousanli* (LI10) 1 to 2 cun [10] were applied (for all the above acupoints, the needle is inserted perpendicularly into the skin, if not specifically instructed otherwise).

Ren meridian acupoints: [11] the position opposite to the injury point, for example, the lumbosacral region, corresponds to the upper chest, and the upper part of the thoracic spinal cord corresponds to the lower abdomen. The specific correspondence of the acupoints to the injured segments is shown in Table 1. And the cervical segments correspond to the *Houxi* (SI3) and the *Shenmai* (BL62).

After needle insertion, small manipulations of twirling were performed on the needles to reach de qi sensation, which is believed to be essential for acupuncture efficacy [12]. Each session lasted 30 minutes and then the needles were carefully removed and counted.

The depth of acupuncture is measured by the unit "cun," which is the width of the thumb joint of the patient in most cases.

Table 1: The acupoints on the Ren meridian corresponding to segments of the spinal cord.

Spinal cord segment	Acupoints	Spinal cord segment	Acupoints
T1	*Qugu* (RN2), *Zhongji* (RN3)	T10	*Xiawan* (RN10), *Jianli* (RN11), *Zhongwan* (RN12)
T2	*Qugu* (RN2), *Zhongji* (RN3), *Guanyuan* (RN4)	T11	*Jianli* (RN11), *Zhongwan* (RN12)
T3	*Zhongji* (RN3), *Guanyuan* (RN4)	T12	*Zhongwan* (RN12), *Shangwan* (RN13)
T4	*Zhongji* (RN3), *Guanyuan* (RN4), *Shimen* (RN5)	L1	*Shangwan* (RN13), *Juque* (RN14)
T5	*Guanyuan* (RN4), *Shimen* (RN5), *Yinjiao* (RN7)	L2	*Shangwan* (RN13), *Juque* (RN14), *Zhenwei* (RN15)
T6	*Shimen* (RN5), *Yinjiao* (RN7), *Shenque* (RN8)	L3	*Juque* (RN14), *Zhenwei* (RN15)
T7	*Yinjiao* (RN7), *Shenque* (RN8), *Shuifen* (RN9)	L4	*Zhenwei* (RN15), *Zhongting* (RN16), *Danzhong* (RN17)
T8	*Shenque* (RN8), *Shuifen* (RN9), *Xiawan* (RN10)	L5	*Zhongting* (RN16), *Danzhong* (RN17), *Yutang* (RN18)
T9	*Xiawan* (RN10), *Jianli* (RN11)	S1	*Danzhong* (RN17), *Yutang* (RN18), *Zigong* (RN19)

The specific location of all the acupoints mentioned above was determined according to WHO standard acupuncture point locations in the Western Pacific region (Manila: World Health Organization; 2008). And all acupuncture procedures were performed by professional acupuncturists with years of experience.

Participants in the rehabilitation group received only routine rehabilitation.

Throughout the trial, aside from the acupuncture intervention, the participants were treated the same as nonparticipants, and proper treatments (medicine or therapies) were given for SCI-related complications.

2.6. Outcome Measures. The main outcome was a change of motor score from baseline to week 4 (28 days).

The secondary outcome included sensory score, light touch (LT) and pinprick (PP), and Modified Barthel Index (MBI).

Adverse events were documented throughout the trial.

Based on their potential association with the acupuncture needling procedure, adverse events were categorized by acupuncturists and related specialists as treatment-related or non–treatment-related within 24 hours of occurrence.

3. Statistical Analysis

Data were presented as mean ± standard deviation (SD). The statistical analysis was conducted using SPSS software version 20. The comparisons of continuous variables between treatment groups were assessed using the *t*-test. The primary outcome was analyzed according to the intention-to-treat principle. The change from baseline in the motor score at week 4 was analyzed by fitting a mixed-effect model using baseline value as a covariate, treatment as a fixed effect, and interaction between treatments as random effects accounting for acupuncturist differences. Kappa analysis was used to analyze the distribution of the injured segment.

4. Results

Among the 72 randomized participants (mean [SD] age, 43.36 [14.43] years), 63 completed the study and 9 withdrew from the study due to reasons unrelated to the study (2 in CAT group, 2 in the IAT group, and 5 in the control group).

No statistical differences were found in the age and injured segment (Table 2).

The mean motor score at baseline was 59.91 for the CAT group, 57.86 for the IAT group, and 60.42 for the control group (no statistical difference between the 3 groups, $p > 0.05$) (Table 2). At week 4, the CAT group (15.05) had a greater increase in motor score than the IAT group, and the IAT group had a greater increase (9.50) than the control group: mean differences were 10.52 (95% CI, 6.14 to 14.90; $p < 0.001$) between CAT group (15.05) and the control group (4.53), 4.97 (95% CI, 0.43 to 9.52; $p < 0.05$) between the IAT group (9.50) and the control group (4.53), and 5.55 (95% CI, 0.32 to 10.77; $p < 0.05$) between the CAT group (15.05) and the IAT group (9.50) (Table 3).

The mean LT score at baseline was 81.19 for the CAT group, 71.70 for the IAT group, and 68.00 for the control group (no statistical difference between each group, $p > 0.05$) (Table 2). At week 4, the difference in the increase of LT score between each two of the three groups was not statistically significant: mean differences were 0.23 (95% CI, −11.05 to 10.60; $p > 0.05$) between CAT group (7.95) and the control group (8.18), 1.02 (95% CI, −10.63 to 12.68; $p > 0.05$) between IAT group (9.20) and the control group (8.18), and 1.25 (95% CI, −9.47 to 6.97; $p > 0.05$) between CAT group (7.95) and IAT group (9.20) (Table 3).

The mean PP score at baseline was 74.76 for the CAT group, 69.60 for the IAT group, and 62.82 for the control group (no statistical difference between each group, $p > 0.05$) (Table 2). At week 4, the difference in the increase of PP score between each two of the three groups was not statistically significant: the mean difference was 3.84 (95% CI, −16.05 to 8.37; $p > 0.05$) between the CAT group (8.33) and control group (11.41), 3.61 (95% CI, −16.56 to 9.34; $p > 0.05$) between the IAT group (7.80) and

Table 2: Data of the Control, IAT, and CAT groups at baseline.

Group	Control	IAT group	CAT group	P
Size	$N = 24$	$N = 24$	$N = 24$	
Age*	44.00 (14.10)	44.17 (12.71)	41.92 (16.70)	0.257
Injured segment				
Cervical	9	8	8	
Thoracic	9	9	8	0.976, (Likelihood ratio = 0.444)
Lumbar	6	7	8	
Initial motor score+	60.42 (26.70)	57.86 (18.77)	59.91 (18.66)	0.255
Initial MBI score+	28.29 (27.08)	32.22 (26.44)	18.87 (19.99)	0.360
Initial LT score+	68.00 (29.14)	71.70 (25.98)	81.19 (21.10)	0.282
Initial PP score+	62.82 (30.48)	69.60 (29.35)	74.00 (24.59)	0.272

*Data were presented as mean (SD). SD = standard mean difference; MBI = Modified Barthel Index; LT = light touch; PP = Pinprick; IAT = intermittent acupuncture treatment; CAT = continuous acupuncture treatment group.

Table 3: Outcome data of the control, IAT, and CAT groups at 4 weeks.

Group	Control group	IAT group	CAT group	P		
N	19	22	22	CAT vs. control	IAT vs. control	CAT vs. IAT
MS	64.95 (26.42)	67.36 (22.06)	74.95 (17.87)			
Change+	4.53 (4.62)	9.50 (8.79)	15.05 (8.39)	<0.001	0.160	0.038
MBI	44.46 (30.00)	49.63 (30.05)	52.39 (22.65)			
Change+	16.17 (17.75)	18.75 (18.10)	33.52 (20.93)	0.004	0.620	0.013
LT score	76.18 (24.95)	80.90 (24.21)	89.14 (20.26)			
Change+	8.18 (19.26)	9.20 (14.64)	7.95 (10.92)	0.966	0.859	0.760
PP score	74.24 (28.44)	77.40 (23.91)	82.33 (22.43)			
Change+	11.41 (21.13)	7.80 (16.73)	8.33 (13.83)	0.609	0.573	0.912

Data were presented as mean (SD). +The change from baseline to 4 weeks. SD = standard mean; MS = Mortar Score; MBI = Modified Barthel Index; LT = Light touch; PP = Pinprick; IAT = intermittent acupuncture treatment; CAT = continuous acupuncture treatment group.

the control group (11.41), and −0.23 (95% CI, −9.97 to 9.51; $p > 0.05$) between CAT group (8.33) and IAT group (7.80) (Table 3).

The mean MBI at baseline was 18.87 for the CAT group, 32.22 for the IAT group, and 28.29 for the control group (no statistical difference between each group, $p > 0.05$) (Table 2). At week 4, the CAT group had a greater increase in MBI (33.52) than the control group (16.17), and the CAT group (33.52) had more increase than the IAT group (18.75). But the difference between the IAT group (18.75) and the control group (16.17) in the increase of MBI was not statistically significant: mean differences were 17.36 (95% CI, 5.92 to 28.79; $p < 0.01$) between the CAT group (33.52) and the control group (16.17), 2.58 (95% CI, −7.83 to 13.00; $p > 0.05$) between the IAT group (18.75) and the control group (16.17), and 14.77 (95% CI, 3.24 to 26.30; $p < 0.05$) between the CAT group (33.52) and the IAT group (18.75) (Table 3).

No treatment-related severe adverse events (such as acupuncture fainting that persisted after the acupuncture procedure, severe pain or infection around acupoints, bleeding of more than 1 mL of the acupoints after acupuncture, and damage of major nerve or vessels around the acupoints) were reported during the trial. And no severe advancements of SCI-related complications (such as neurogenic bladder, neurogenic bowel, and pressure sores) were found during the trial.

5. Discussion

The purpose of this randomized controlled trial is to determine the ideal dosage of acupuncture therapy combined with rehabilitation training for SCI in improving neural function and daily living ability.

Acupuncture improved ASIA Motor Score and Modified Barthel Index in patients with SCI and seemed to have no effect in improving the sensory score in this study.

The acupuncture therapy did not result in a better outcome in the sensory score. It could be that this specific acupuncture therapy does not have enough effect in improving sensory function or the sample size is still limited, or the frequent needling may have built up the patients' tolerance for mild stimulus.

Significant differences in the motor score and MBI were observed between the CAT group and IAT group, meaning that increased dosage of acupuncture treatment led to more improvement in motor function and daily living ability; the dosage of 5/week can be considered as safe and more effective.

The IAT group did not show improvement in motor, sensory, and MBI score, meaning that intermittent therapy (3/week) may not have enough effect on patients with SCI to show a statistical difference, or the IAT lacked stimulus to start certain molecular pathways which existed in CAT

group, or the sample size was not big enough to show statistical difference.

Acupuncture has not been used as a routine treatment for SCI, except in several Asian countries [4]. Most of the previous studies emphasized acupuncture treatment for complications of SCI such as neurogenic bladder, while less attention was paid to the motor and sensory function or daily living ability. Previous randomized clinical trials investigating acupuncture for SCI reported a dosage of once per day [13–17], 6/week [13, 18], or 5/week [11, 19], but no trials have done the comparison between different dosages [20].

Skilled acupuncturists design useful acupuncture treatment plans by following ancient wisdom but lacking modern scientific interpretation. Take dosage, for example, the underlying mechanisms of it, what dosage works best and why, may just be the key to deciphering the secrets in Chinese Traditional Medicine.

The Bian Que needle method which was used to select acupoints in this study is from the Classical Acupuncture method, one of the four famous methods of Taiwan acupuncture, and was inherited from the acupuncture masters Zuoyu Zhou and Peirong Sun. [21] Classical Acupuncture is specialized in midnight-noon ebb-flow, Linggui Bafa, Wumen Shibian method, Bian Que needle, et cetera [21]. And its effectiveness on a few other diseases has been studied and proved [22, 23].

Admittedly, it would be better that the sample size of this study was bigger. Due to the limited number of participants, this study has not been able to analyze certain outcome measures and if acupuncture affects them. And the study did not contain a long time follow-up to study long-term effects. And since all the participants were Chinese thus not easily fooled by sham acupuncture and the acupoints used in this study were not easy to conceal, we did not design a sham acupuncture group. And due to the popularity of acupuncture among Chinese residents, there might have been a placebo effect on the two acupuncture groups which may have affected the results.

The strengths of this study are as follows. The dosage of acupuncture treatment for SCI had not been studied in any previous trials investigating SCI; it is the first time that the topic has been properly studied. And the sample size is relatively large compared with previous randomized controlled trials studying acupuncture for SCI, [3, 4] and the results showed that acupuncture is an effective and safe treatment and that the treatment frequency of 5/per week is better than 3/week. This result may be useful for clinical practice and further research.

Although we did conclude the more effective dosage of acupuncture for SCI, it may not be the best dosage there is; the mechanisms beneath it and whether it applies to other illnesses are still unknown.

6. Conclusion

In conclusion, based on the findings of this clinical trial, the recommended dosage of acupuncture for SCI is 5/week. We hope there will be more related studies in the future, to allow a deeper understanding of acupuncture.

Data Availability

The data used to support the findings of this study are available from the corresponding author upon request. .

Disclosure

The funders had no role in study design, data collection, analysis, decision to publish, or preparation of the manuscript.

Conflicts of Interest

The authors declare that they have no conflicts of interest.

Authors' Contributions

Feng Xiong, Jingkang Lu, and Hongxia Pan contributed equally to this work.

Acknowledgments

This work was supported by the Project of the Science and Technology Department in Sichuan Province (grant no. 2019YJ0119).

Supplementary Materials

Supplement File: STRICTA (Standards for Reporting Interventions in Clinical Trials of Acupuncture) Checklist for this study. . (*Supplementary Materials*)

References

[1] C. S. Ahuja, J. R. Wilson, S. Nori et al., "Traumatic spinal cord injury," *Nature Reviews Disease Primers*, vol. 3, no. 1, p. 17018, 2017.

[2] M.-P. Côté, M. Murray, and M. A. Lemay, "Rehabilitation strategies after spinal cord injury: inquiry into the mechanisms of success and failure," *Journal of Neurotrauma*, vol. 34, no. 10, pp. 1841–1857, 2017.

[3] R. Ma, X. Liu, J. Clark, G. M. Williams, and S. A. Doi, "The impact of acupuncture on neurological recovery in spinal cord injury: a systematic review and meta-analysis," *Journal of Neurotrauma*, vol. 32, no. 24, pp. 1943–1957, 2015.

[4] Q. Fan, O. Cavus, L. Xiong, and Y. Xia, "Spinal cord injury: how could acupuncture help?" *Journal of acupuncture and meridian studies*, vol. 11, no. 4, pp. 124–132, 2018.

[5] I. Heo, B.-C. Shin, Y.-D. Kim, E.-H. Hwang, C. W. Han, and K.-H. Heo, "Acupuncture for spinal cord injury and its complications: a systematic review and meta-analysis of randomized controlled trials," *Evidence-based Complementary and Alternative Medicine*, vol. 2013, Article ID 364216, 18 pages, 2013.

[6] B.-C. Shin, M. S. Lee, J. C. Kong, I. Jang, and J. J. Park, "Acupuncture for spinal cord injury survivors in Chinese literature: a systematic review," *Complementary Therapies in Medicine*, vol. 17, no. 5-6, pp. 316–327, 2009.

[7] I. Estores, K. Chen, B. Jackson, L. Lao, and P. H. Gorman, "Auricular acupuncture for spinal cord injury related neuropathic pain: a pilot controlled clinical trial," *The journal of spinal cord medicine*, vol. 40, no. 4, pp. 432–438, 2017.

[8] R. Zhang, L. Lao, K. Ren, and B. M. Berman, "Mechanisms of acupuncture-electroacupuncture on persistent pain," *Anesthesiology*, vol. 120, no. 2, pp. 482–503, 2014.

[9] J. Liu, "Reviews on acupuncture for cellular signal transduction in spinal cord injury," *Zhongguo zhen jiu = Chinese acupuncture & moxibustion*, vol. 37, pp. 680–684, 2017.

[10] X. G. Wang, X. Guan, and Q. C. Guo, "Effect of acupuncture on trunk control ability and balance function in patients with spinal cord injury above lumber," *Chinese Journal of Rehabilitation Theory and Practice*, pp. 1180–1182, 2013.

[11] C. A. L. Deng, "Observation on the efficacy of jiaji electroacupuncture in treating incomplete spinal cord injury," *Shanxi Journal of Traditional Chinese Medicine*, pp. 30-31, 2012.

[12] K. Zhou, J. Fang, X. Wang et al., "Characterization of de qi with electroacupuncture at acupoints with different properties," *Journal of Alternative & Complementary Medicine*, vol. 17, no. 11, pp. 1007–1013, 2011.

[13] H. a. W. Xiao, "Influence of acupuncture combined with rehabilitation training on ADL of spinal cord injury patients," *Journal of New Chinese Medicine*, pp. 46-47, 2003.

[14] X. M. Cui, X. M. Pan, X. M. Zhang, H. Z. Deng, and S. Y. Yao, "The rehabilitation function of electroacupuncture treatment in patients with traumatic spinal cord injury," *Journal of Guangdong Medical College*, pp. 170-171, 2004.

[15] L. X. Chen, J. F. Duan, X. R. Zhan, Q. Xie, and Q. H. Long, "Electrical and auricular acupuncture for patients with acute spinal cord injury," *Chinese Journal of Rehabilitation Theory and Practice*, vol. 11, pp. 934-935, 2005.

[16] X. D. Gu, Y. H. Yao, M. Gu, J. M. Fu, Y. Ren, and H. K. Yin, "Clinical study on functional independence measure for patients with spinal cord injury of trauma treated by electroacupuncture," *Acupuncture Research*, pp. 175–178, 2005.

[17] J. L. Wang, T. Y. Bai, and X. Wang, "Observation on the efficacy of electroacupuncture plus rehabilitation training in treating spinal cord injury," *Shanghai Journal of Acupuncture and Moxibustion*, pp. 369–371, 2010.

[18] Z. G. Chen, J. J. Zhang, Z. M. Wong, H. L. Li, and A. L. Zhang, "The clinical study of Governor vessel electroacupuncture treatment on the lower extremity spasticity in patients with spinal cord injury," *Journal of Clinical Acupuncture and Moxibustion*, pp. 6-7, 1995.

[19] A. M. K. Wong, C.-P. Leong, T.-Y. Su, S.-W. Yu, W.-C. Tsai, and C. P. C. Chen, "Clinical trial of acupuncture for patients with spinal cord injuries," *American Journal of Physical Medicine & Rehabilitation*, vol. 82, no. 1, pp. 21–27, 2003.

[20] F. Xiong, C. Fu, Q. Zhang et al., "The effect of different acupuncture therapies on neurological recovery in spinal cord injury: a systematic review and network meta-analysis of randomized controlled trials," *Evidence-Based Complementary and Alternative Medicine*, vol. 2019, Article ID 2371084, 12 pages, 2019.

[21] K. Chiahsin, *Research of Taiwan Classical Acupuncture*, Nanjing University of Chinese Medicine, Nanjing, China, 2018.

[22] H. Y. Wu Yhao, "Clinical application of wumen shibian-acupuncture method," *Chinese Acupuncture and Moxibustion*, pp. 801–804, 2014.

[23] H. Y. Wu Yuhao, "The matching method of Bian Que acupuncture and its application," *China Journal of Traditional Chinese Medicine and Pharmacy*, pp. 894–896, 2016.

Hindawi
Evidence-Based Complementary and Alternative Medicine
Volume 2021, Article ID 4358163, 9 pages
https://doi.org/10.1155/2021/4358163

Research Article

Protective Effect of NGR1 against Glutamate-Induced Cytotoxicity in HT22 Hippocampal Neuronal Cells by Upregulating the SIRT1/Wnt/β-Catenin Pathway

Dong Wang,[1] Bibo Gao,[2] Tao Yang,[3] Huiying Sun,[1] Xiaoping Ran,[1] and Wen Lin[1]

[1]*Department of Neurological Diseases, Ziyang People's Hospital of Sichuan Province, Ziyang, Sichuan 641300, China*
[2]*Department of Neurosurgery, First Affiliated Hospital of Kunming Medical University, Kunming, Yunnan 650030, China*
[3]*Department of Neurosurgery, The General Hospital of Western Theater Command, Chengdu, Sichuan 610000, China*

Correspondence should be addressed to Wen Lin; zysrmyylw@163.com

Received 1 August 2021; Revised 13 November 2021; Accepted 25 November 2021; Published 15 December 2021

Academic Editor: Feng Zhang

Notoginsenoside R1 (NGR1) is an active compound isolated from *Panax notoginseng*. Despite the NGR1 having been used as a traditional medicine, little is known about the neuroprotective effects. In this study, we investigate the protective effects of NGR1 against glutamate-induced cytotoxicity in HT22 cells and its possible molecular mechanism. We assessed the toxicity of NGR1 and the protective activity by MTT assay. The levels of oxidative stress indices superoxide dismutase (SOD), glutathione (GSH), and mitochondrial membrane potential (MMP) were measured by the kits. The levels of reactive oxygen species (ROS) and Ca^{2+} concentration were measured by flow cytometry. Furthermore, we determined the expression of mitochondrial dysfunction related protein PINK1, Parkin, silent mating type information regulation 2 homolog-1 (sirtuin 1; SIRT1), and Wnt/β-catenin by Western blotting. Here, we discovered that glutamate treatment led to cell viability loss, apoptosis facilitation, Ca^{2+} upregulation, MMP fluorescence intensity downregulation, and ROS generation of HT22 cells. In parallel, expression of Parkin was declined by glutamate. While, NGR1 treatment alleviated all the above phenomena. We further clarified that NGR1 alleviated glutamate-induced oxidative stress, apoptosis, and mitochondrial dysfunction by upregulating SIRT1 to activate Wnt/β-catenin pathways. These findings demonstrate that NGR1 alleviated glutamate-induced cell damage, and NGR1 may play a protective role in neurological complications.

1. Introduction

Oxidative stress caused by the accumulation of reactive oxygen species (ROS) is related to the development of many neurological complications [1, 2]. Normally, ROS are generated in the mitochondrial respiratory chain. Excessive ROS induces oxidative stress and apoptosis in neuronal cells [3]. Currently, extracting compounds with antioxidant activity and neuroprotective effects from plants is a potential alternative therapy for neurological complications [4], Therefore, the identification of compounds of plants that inhibit oxidative stress in neuronal cells is crucial to protect the nervous system complications.

Notoginsenoside R1 (NGR1) is an active compound isolated from *Panax notoginseng* [5, 6]. It has antioxidant, anti-inflammatory, antiapoptotic, and antitumor effects [7]. Previous studies have confirmed that NGR1 effectively prevents neurological diseases. In addition, increasing studies have shown that NGR1 can prevent the oxidation, inflammation, and other damages of primary neurons, PC12, and other nerve cells. Like, in PC12 neurotoxicity induced by acrylamide, NGR1 protects PC12 cells by upregulating Trx1 [8]. In diabetic peripheral neuropathy, NGR1 acts as a protective agent by promoting the survival of RSC96 cells [9]. However, there are few studies on the protective effect of NGR1 in HT22 cells.

Glutamate is the main excitatory neurotransmitter in the brain and is considered to be one of the initiating factors of neuronal damage [10–12]. In our study, we exposed HT22 cells to glutamate and investigated the possible mechanism

of NGR1's protective effect. According to this study, we found that NGR1 alleviated glutamate-induced oxidative stress and apoptosis by upregulating SIRT1 to activate the Wnt/β-catenin pathway.

2. Materials and Methods

2.1. Reagents and Antibodies. L-glutamic acid, notoginsenoside R1 (NGR1), 98% (HPLC), 2′, 7′dichlorodihydrofluorescein diacetate (H2DCFDA), MTT, and nicotinamide were brought from Sigma-Aldrich (St. Louis, MO, USA). Wnt/β-catenin agonist SKL2001 (S8302) was brought from Selleck Chemicals (Houston, TX, USA). Superoxide dismutase (SOD), lactate dehydrogenase (LDH), and glutathione (GSH) assay kits were brought from Nanjing Jiancheng Bioengineering Institute (Nanjing, China). Primary antibodies against Parkin, PINK1, SIRT1, Wnt1, β-catenin, cyclin D1, GAPDH, and secondary antibodies were all brought from Cell Signaling Technology (New England Biolabs, Ipswich, MA, USA).

2.2. Cell Culture and Treatments. Mouse hippocampal HT22 cells were bought from the Procell Cell Bank (Wuhan, China). HT22 cells were cultured in the DMEM with 10% fetal bovine serum (Gibco, Grand Island, NY), supplemented with penicillin-streptomycin (HyClone, Logan, UT, USA) at 37°C with 5% CO_2 in a humidified incubator. When cell confluency reached 80%, cells were passaged. All experiments were performed on third passage cells and next, treated with 5 mM glutamate and different concentrations of NGR1.

2.3. Cell Viability. Cell viability was detected by the MTT assay. We followed the methods of Wang et al. [13]. Briefly, HT22 cells were seeded into 24-well plates at a density of 1×10^4 cells/cm^2, according to the manufacturer's instructions. Cells were treated with 5 mM glutamate and different concentrations of NGR1 for 24 h. After treatment, MTT solution (50 μL) was added to the cell culture medium at 37°C for 4 h and added DMSO to plates. Absorbance was measured at 570 nm using a microplate reader. The experiment was repeated three times.

2.4. Western Blotting Assay [13]. In the HT22 cells after treatment, add RIPA buffer (Invitrogen; USA) to collect total protein, and the concentration of protein was determined by a bicinchoninic acid protein assay kit (Invitrogen; USA). An equivalent of total protein was resolved on SDS-PAGE and transferred to the polyvinylidene fluoride membrane. Next, the membranes were blocked with 5% nonfat milk and probed with the following primary antibodies overnight at 4°C : SIRT1 (1 : 1000), PINK1(1 : 1000), Parkin (1 : 1000), Wnt1 (1 : 1000), β-catenin (1 : 1000), and GAPDH (1 : 2000). Then, they were incubated with diluted secondary antibodies (1 : 3000). followed by immunodetection using an enhanced chemiluminescence kit (Beyotime, China) and analyzed with Image *J* software (NIH, Bethesda, MD, USA).

2.5. LDH Release Assay. LDH activity was detected by LDH assay kit. Briefly, cells were collected after glutamate and NGR1 treatment, and separate the supernatant; next, cells' supernatant was incubated with 2,4-dinitrophenylhydrazine; the release of LDH was examined by measurement of the absorbance at 450 nm. The experiment was repeated three times.

2.6. ROS Assay. HT22 cells in 6-well plates (1×10^4 cells/well) were treated by NGR1, glutamate, or both. 10 μM H2DCFDA was added into cells and reacted for 20 min at 37°C in the dark. HT22 cells were washed with the serum-free medium for three times. The ROS generation was examined by the flow cytometer (Bender Med Systems, CA, USA).

2.7. Flow Cytometry. HT22 cells were treated by NGR1, glutamate, or both. Collect cells and incubate with 5 μL FITC-Annexin V and 1 μL PI (Beyotime Biotechnology, China) working solution for 15 min (in dark). Finally, the fluorescence intensity was measured by flow cytometry (Bender Med Systems, CA, USA).

2.8. Determination of Mitochondrial Membrane Potential (MMP). We followed the methods of Parinee et al. [14]. MMP was evaluated using the commercial kit (Cell Signaling, USA). In brief, HT22 cells were treated by NGR1, glutamate, or both, incubation with TMRE fluorescent dye, and the plate was placed in an incubator for 20 min. Then, after the cells were washed in PBS, the samples were measured with a microplate reader at 488 nm excitation and 574 nm emission.

2.9. Statistical Analysis. In our study, all experimental data are presented as mean ± standard error of mean. The difference between two groups was compared by using the *t*-test. Statistical analysis was performed using GraphPad Prism 7.0 software. A value of $P < 0.05$ was considered as statistically significant ($^{**}P < 0.01$; $^{\#\#}P < 0.01$; $^{\triangle\triangle}P < 0.01$; $^{\$\$}P < 0.01$).

3. Results

3.1. The Effects of NGR1 on Glutamate-Induced Cytotoxicity in HT22 Cells. The MTT assay was used to evaluate the effect of NGR1 on the viability of HT22 cells. The cell viability assays showed that the viability of HT22 cells was unchanged by NGR1 treatment (Figure 1(a)); after the cells were treated with 5 mM glutamate, cell viability was significantly reduced, and NGR1 treatment alleviated the cell death caused by glutamate (Figure 1(a) and Figure 1(c)). Based on the results of the MTT assay, we choose 50 μM NGR1 as optimum dosage for the following experiments (Glu + NGR1 30 μM: 88.72 ± 3.76%; Glu + NGR1 50 μM: 96.48 ± 2.17%; Glu + NGR1 100 μM: 91.66 ± 2.85%). Simultaneously, treatment with 50 μM NGR1 significantly inhibited Glu-induced LDH leakage (Figure 1(b)). These changes indicated that NGR1 might alleviated the cell death induced by glutamate.

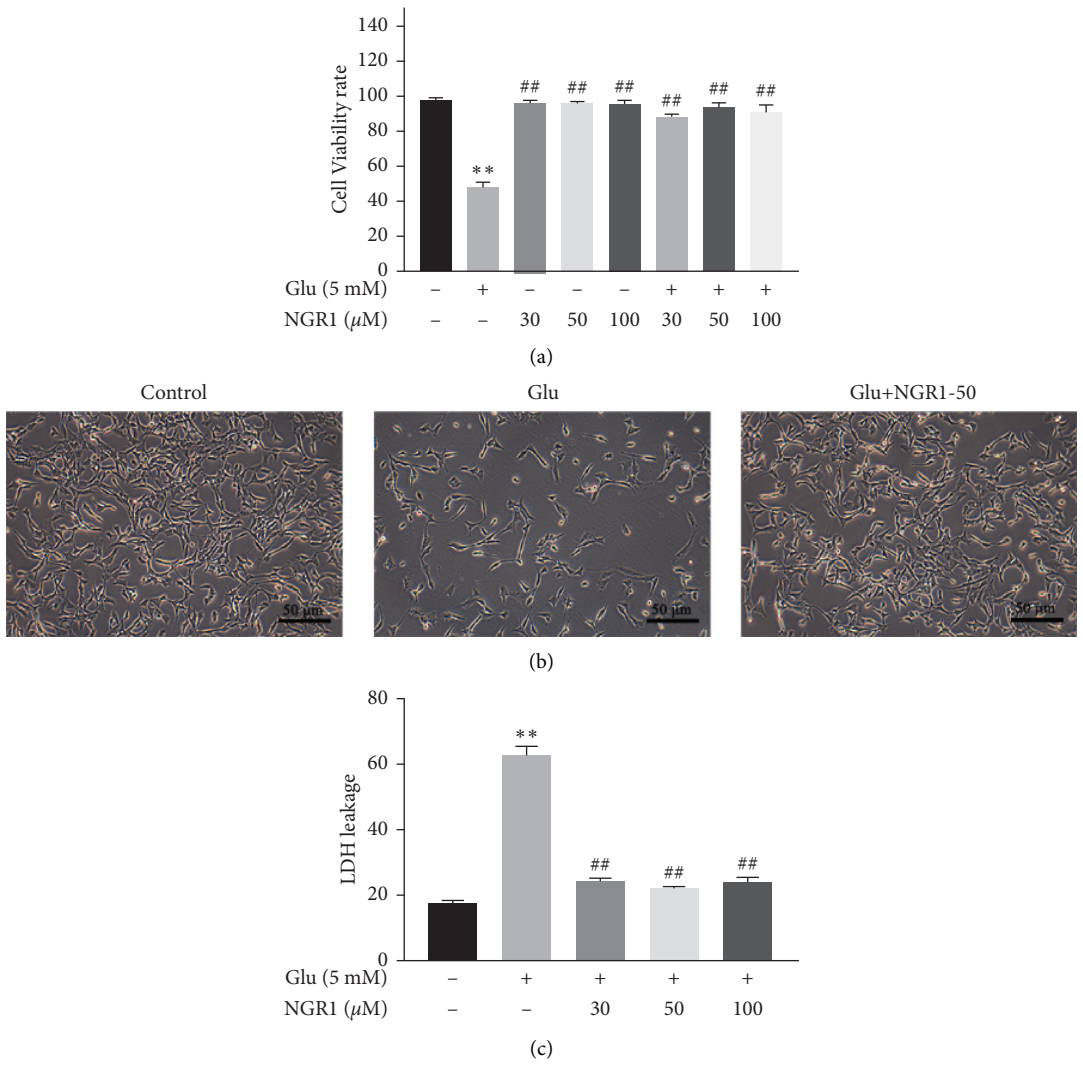

FIGURE 1: NGR1 alleviated cytotoxicity in the glutamate-induced HT22 cells. HT22 cells viability measured by the MTT assay (48 h) (a). HT22 cells viability observed by microscopic examination (100 ×) (b). The LDH release measured by the LDH assay kit (c). ** was considered significant compared to control ($^{**}P < 0.01$); ## was considered significant compared to glutamate treatment ($^{\#\#}P < 0.01$).

3.2. NGR1 Alleviated Glutamate-Induced Apoptosis and Oxidative Stress. We assessed three oxidative stress-associated indicators and levels of Bcl-2, Bax, and apoptosis rate. Our preliminary results showed that treatment with 50 μM NGR1 significantly increased the SOD and GSH content. The levels of ROS were decreased with the treatment of NGR1 (Figure 2(a)). Simultaneously, 50 μM NGR1 significantly reduced glutamate-induced apoptosis (Figure 2(b)). We next evaluated the protein expression of Bax and Bcl-2 and found that treatment with NGR1 significantly upregulated Bcl-2 expression and downregulated Bax expression (Figure 2(c)). Thus, NGR1 alleviated apoptosis and oxidative stress in glutamate-induced HT22 cells.

3.3. NGR1 Alleviates the Increase of Ca^{2+} and Mitochondrial Dysfunction in HT22 Cells Induced by Glutamate. Glutamate induces the further development of oxidative stress in HT22 cells, leads to cell mitochondrial dysfunction, increased Ca^{2+} concentration, and ultimately leads to cellular apoptosis. Next, we wanted to evaluate the effect of NGR1 on mitochondrial dysfunction and Ca^{2+} concentration in glutamate-induced HT22 cells. Our results showed that glutamate significantly decreased the expression levels of Parkin and increased the concentration of Ca^{2+}; treatment with 50 μM NGR1 significantly enhanced the expression levels of Parkin and decreased the concentration of Ca^{2+}, and PINK1 is upregulated in both glutamate and NGR1 treatments (Figure 3(a) and Figure 3(b)).

3.4. NGR1 Alleviates HT22 Cells Apoptosis, Oxidative Stress, Increase of $Ca2^{+}$, and Mitochondrial Dysfunction through Upregulating SIRT1. SIRT1 is a protein that is downregulated in neurological complications; to find out whether NGR1 could alleviated cytotoxicity in the glutamate-induced HT22 cells by acting on SIRT1, we use SIRT1 inhibitor nicotinamide (20 μM; for 30 min) to treat cells. The result

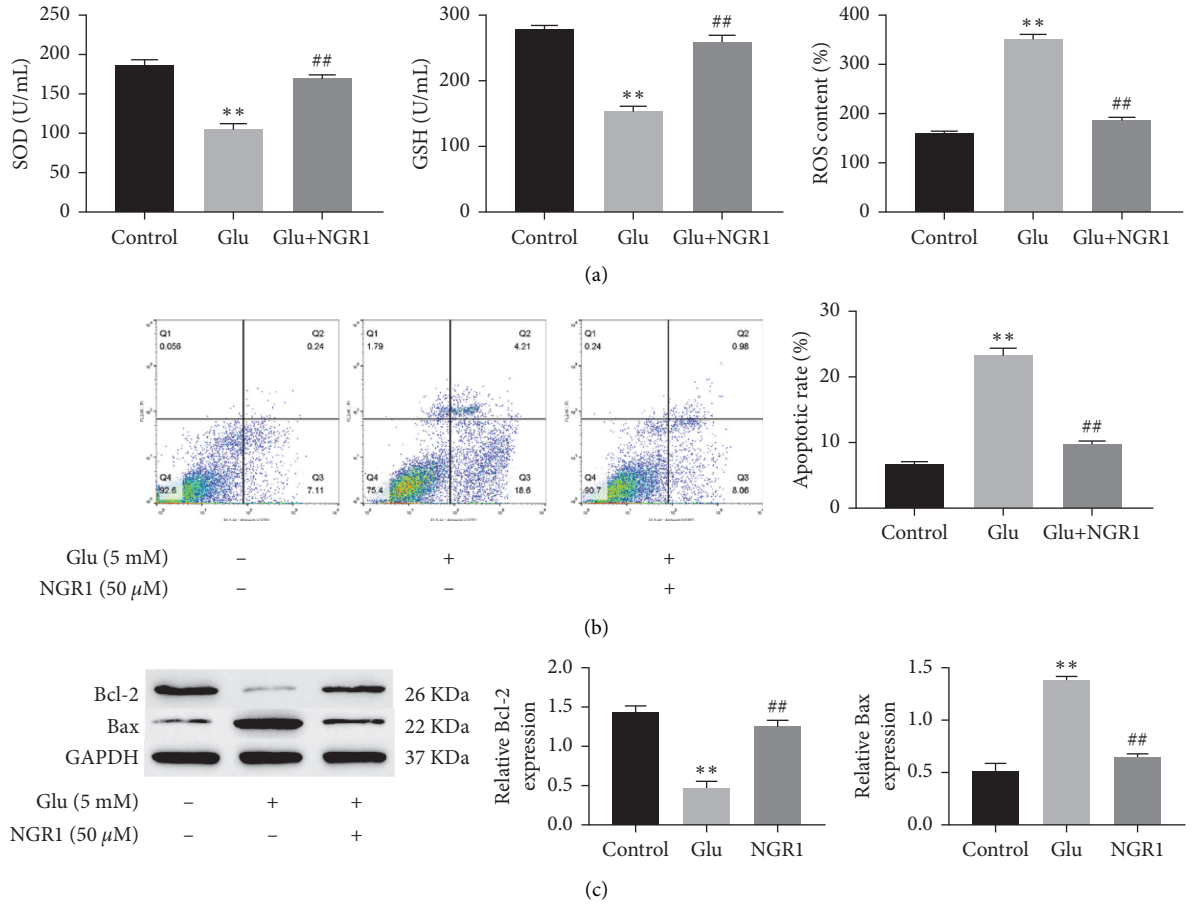

Figure 2: NGR1 alleviated apoptosis and oxidative stress in the glutamate-induced HT22 cells. The levels of SOD and GSH were measured by assay kits. The level of ROS measured by flow cytometry (a). The apoptotic ratio detected by flow cytometry (b). The expressions of Bcl-2 and Bax in cells measured by Western blotting (c). ** was considered significant compared to control ($^{**}P < 0.01$); ## was considered significant compared to glutamate treatment ($^{\#\#}P < 0.01$).

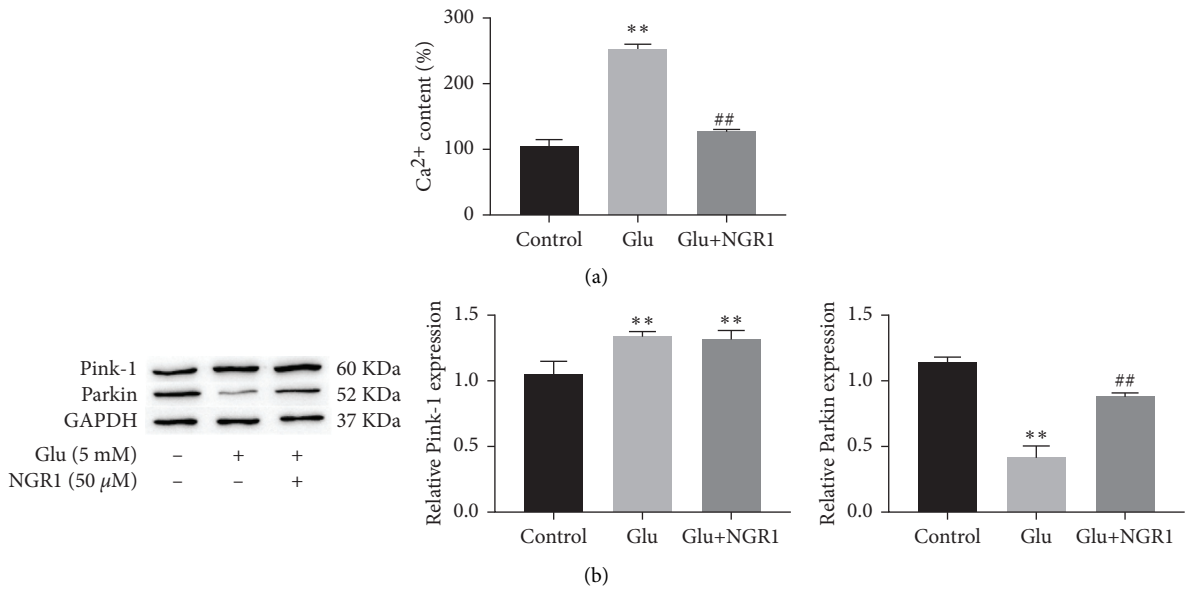

Figure 3: NGR1 alleviates the increase of Ca^{2+} and mitochondrial dysfunction in HT22 cells induced by glutamate. The level of Ca^{2+} measured by flow cytometry (a). The expression of PINK1 and Parkin in HT22 cells measured by Western blotting (b). ** was considered significant compared to control ($^{**}P < 0.01$); ## was considered significant compared to glutamate treatment ($^{\#\#}P < 0.05$).

showed that viability of HT22 cells was unchanged by nicotinamide (20 μM) treatment alone. However, treatment with nicotinamide (20 μM) significantly reduced the cell viability of HT22 cells treated with NGR1 (Figure 4(a)). In addition, Western blotting results showed that SITR1 expression decreased in glutamate-induced HT22 cells, treatment with 50 μM NGR1 significantly enhanced the expression levels of SITR1, and the effect of nicotinamide can be used to reverse this result (Figure 4(b)). Likewise, nicotinamide treatment increased ROS levels and decreased GSH content and SOD activities in cells (Figure 4(c)). Next, we evaluated the apoptosis rate and the protein expression of Bax and Bcl-2; we found that nicotinamide induced cell apoptosis; simultaneously, nicotinamide treatment significantly downregulated Bcl-2 expression and upregulated Bax expression (Figure 4(d) and Figure 4(e)). In addition, nicotinamide treatment decreased the expression levels of Parkin and increased the concentration of Ca^{2+} in HT22 cells, and PINK1 is upregulated in nicotinamide treatment (Figure 4(f) and Figure 4(g)). Thus, NGR1 alleviates HT22 cells apoptosis, oxidative stress, increase of Ca^{2+}, and mitochondrial dysfunction through upregulating SIRT1.

3.5. Effect of NGR1 on MMP. We examined the change of MMP in HT22 cells by TMRE staining. The results showed that glutamate significantly reduces the fluorescence intensity of HT22 cells, compared to the control group. Treatment with 50 μM NGR1 significantly enhanced the TMRE fluorescence intensity. In contrast, the effects of NGR1 were reversed by nicotinamide treatment (Figures 5(a) and 5(b)).

3.6. NGR1 Activates the Wnt/β-Catenin Pathway by Upregulating SIRT1. We measured the expression level of Wnt/β-catenin. The results showed that Wnt1, β-catenin, and cyclin D1 were significantly downregulated in glutamate-induced cells. After treatment with NGR1, Wnt1, β-catenin, and cyclin D1 expressions were significantly increased. However, the expression of Wnt1, c-myc, and cyclin D1 decreased after the nicotinamide treatment. Wnt/β-catenin agonist (SKL2001; 10 μM; for 30 min) inhibited the effect of nicotinamide (Figures 6(a) and 6(b)).

4. Discussion

Oxidative stress caused by the accumulation of reactive oxygen species (ROS) in nerve cells is associated with neurological complications, including Alzheimer's disease, Parkinson's disease, Huntington's disease, and neuropathic pain [15–17]. The antioxidants are the first defense to detoxify ROS [14]. Identification of effective antioxidant active chemical components from plants or natural products, eliminating active oxygen and maintaining homeostasis, is one of the hotspots of the current research [18, 19]. NGR1 has been reported to treated neurological complications [8, 9]; in addition, NGR1 has anti-inflammatory and antioxidative stress effects [20]. However, the neuroprotective potential of NGR1 against glutamate-induced mediated neurological complications in HT22 cells is unclear. In our present study, we demonstrated the antiapoptosis and antioxidative stress effects of NGR1 on glutamate-induced HT22 cells. We provide evidence that NGR1 alleviates glutamate-induced apoptosis, oxidative stress, and mitochondrial dysfunction, simultaneously restoring Ca^{2+} back to near normal. In addition, SITR1 and Wnt/β-catenin is highly expressed under NGR1 treatment. Although previous studies have found the protective effects of SITR1 and Wnt/β-catenin in nerves [13], there is no report on the effects of NGR1, SITR1, and Wnt/β-catenin. In our study, we demonstrated for the first time that NGR1 prevented glutamate-induced HT22 cells injury by alleviating oxidative stress, the levels of Ca^{2+}, and mitochondrial dysfunction through the SIRT1/Wnt/β-catenin signaling pathway. Neurons are the functional unit of the nervous system [21–23]. The oxidative stress induced by glutamate will trigger the changes in the structure and function of the neurons and cause the death of neurons [14, 24]. Earlier studies showed that plant extracts and compounds with strong antioxidant activity protected glutamate-induced neuronal death [4, 25]. In the current study, we used mouse-derived hippocampal HT22 cells to study the neuroprotective effect of NGR1 against glutamate-induced cell apoptosis and to explore the neuroprotective mechanism of action. In our study, we found that NGR1 alone is not neurocytotoxic even at high concentrations. However, glutamate alone inhibited HT22 activity, promoted apoptosis, increased levels of LDH, and activated oxidative stress; this is consistent with the results in previous studies [26]. In addition, NGR1 pretreatment significantly protected HT22 cells against glutamate-induced neurocytotoxic by decreasing levels of LDH, inhibiting apoptosis, and oxidative stress. Therefore, these results confirm that NGR1 is an effective antioxidant that exhibits neuroprotective effects by inhibiting the activation of oxidative stress in cells.

Glutamate induces the further development of oxidative stress in HT22 cells, leads to cell mitochondrial dysfunction, increased Ca^{2+} concentration, reduced mitochondrial membrane potential, and ultimately leads to cellular apoptosis [27]. Mitochondrial dysfunction has an integral role in the development of oxidative stress and leads to increased oxidative stress, while the ultrastructure of mitochondria is destroyed, which further exacerbates mitochondrial dysfunction [28]. Plant extracts with antioxidant activity can inhibit glutamate-induced mitochondrial dysfunction and increase in Ca^{2+} concentration in HT22 cells [25]. In this study, we found that NGR1 has an effect on mitochondrial dysfunction and Ca^{2+} concentration. When mitochondria are damaged, activated PINK1 aggregates on the outer mitochondrial membrane and induces mitochondrial autophagy through direct/indirect activated Parkin [29], thereby protecting mitochondrial DNA from reactive oxygen species and stimulating the self-repair process of mitochondria [19]. In this study, we found that NGR1 treatment activates the PINK1/Parkin pathway and upregulates Parkin expression. Simultaneously, NGR1 treatment reduces Ca^{2+} concentration and increases the level of mitochondrial membrane potential in HT22 cells.

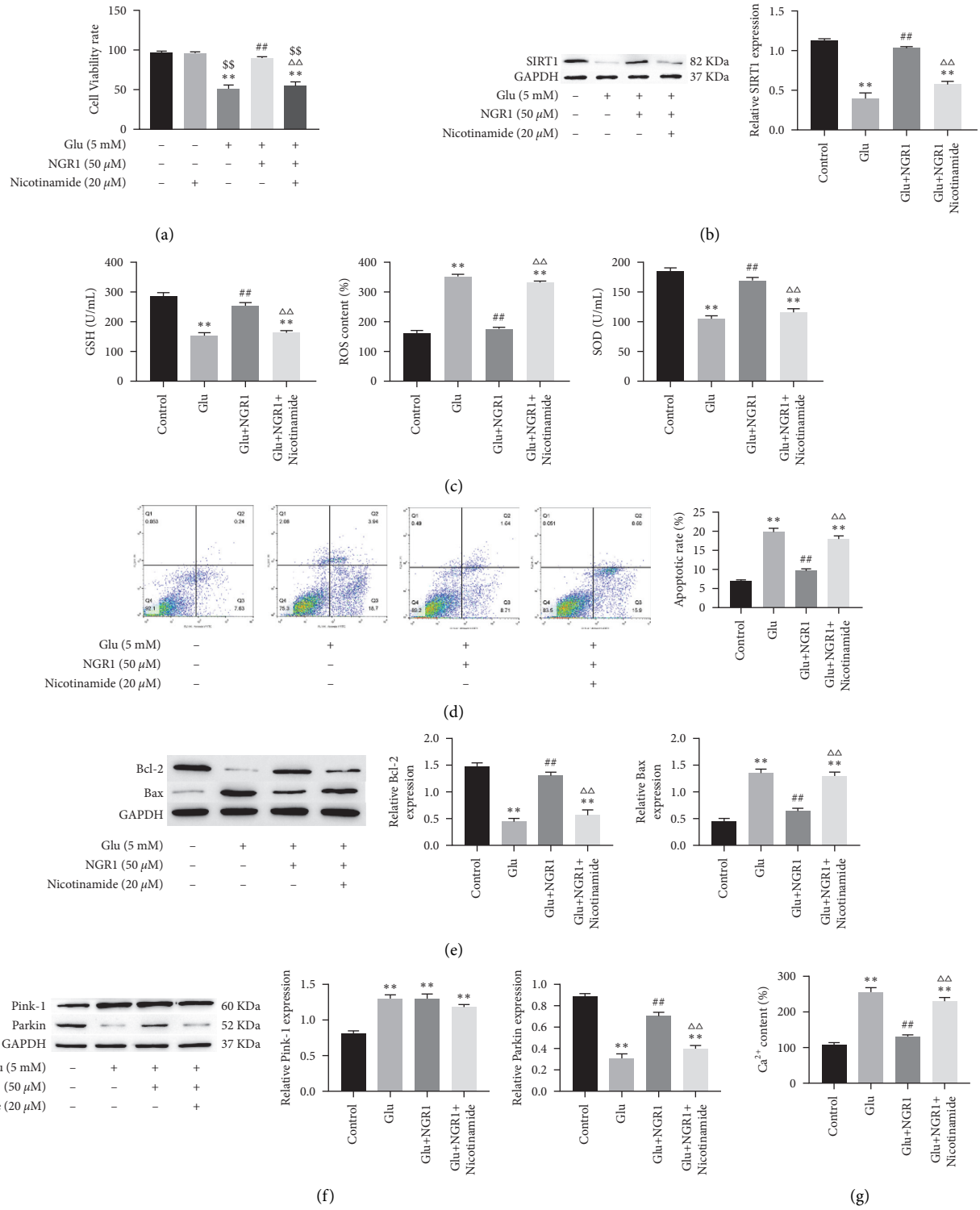

FIGURE 4: NGR1 alleviates HT22 cells apoptosis, oxidative stress, increase of Ca^{2+}, and mitochondrial dysfunction through upregulating SIRT1. HT22 cells viability was measured by the MTT assay (48 h) (a). The expression of SIRT, PINK1, Parkin, Bcl-2, and Bax in cells measured by Western blotting (b), (f), and (e). The levels of SOD and GSH were measured by assay kits. The level of ROS measured by flow cytometry (c). The apoptotic ratio and the level of Ca^{2+} detected by flow cytometry (d) and (g). ** was considered significant compared to control ($^{**}P < 0.01$); ## was considered significant compared to Glu treatment ($^{\#\#} < 0.01$); △△ was considered significant compared to Glu and NGR1 treatment ($^{\Delta\Delta}P < 0.01$); $$ was considered significant compared to nicotinamide treatment ($^{\$\$}P < 0.01$).

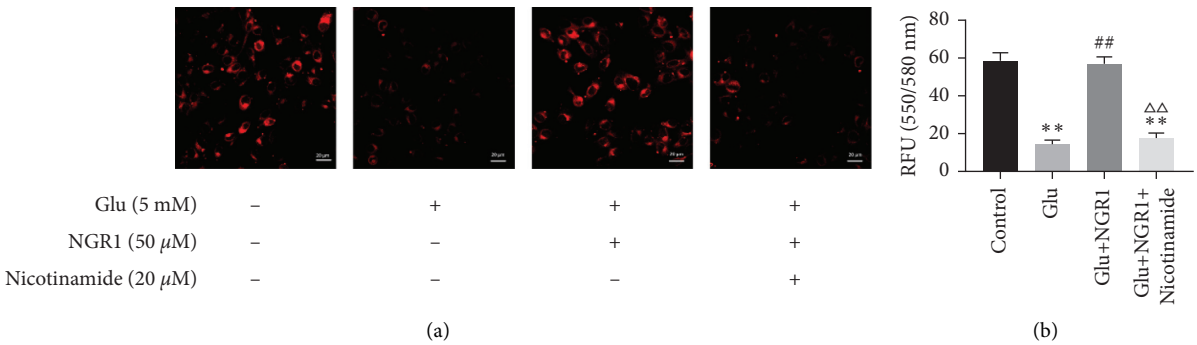

Figure 5: Effect of NGR1 on MMP by upregulating SIRT1. The micrograph of TMRE stained fluorescence was taken with a fluorescence microscope. ** was considered significant compared to control ($^{**}P < 0.01$); ## was considered significant compared to Glu treatment ($^{\#\#} < 0.01$); △△ was considered significant compared to Glu and NGR1 treatment ($^{\Delta\Delta}P < 0.01$).

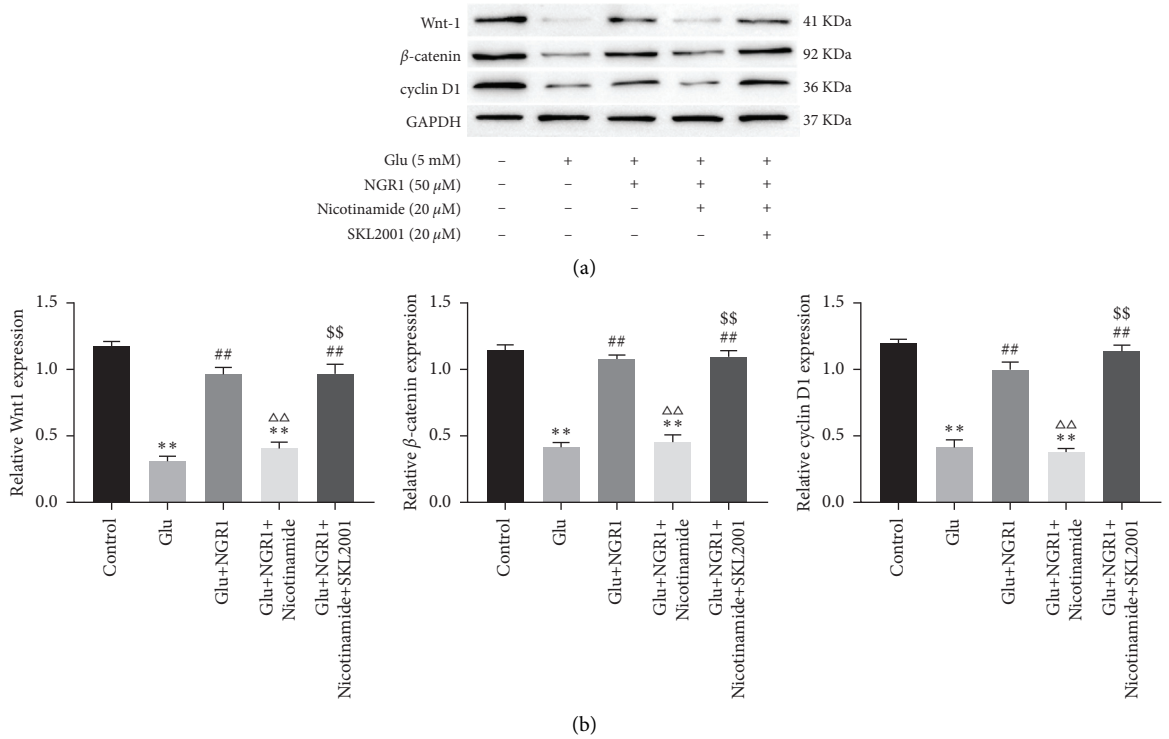

Figure 6: NGR1 activates the Wnt/β-catenin pathway by upregulating SIRT1. The expression of Wnt-1, β-catenin, and cyclin D1 in HT22 cells measured by Western blotting (a). ** was considered significant compared to control ($^{**}P < 0.01$); ## was considered significant compared to Glu treatment ($^{\#\#} < 0.01$); △△ was considered significant compared to Glu and NGR1 treatment ($^{\Delta\Delta}P < 0.01$). $$ was considered significant compared to Glu, NGR1, and nicotinamide treatment ($^{\$\$}P < 0.01$).

As the main regulator of neurological diseases, SIRT1 plays a protective role in neurological diseases by regulating inflammation, oxidative stress, and cell apoptosis [19]. Previous studies demonstrated that activation of SIRT1 alleviates neuronal apoptosis and oxidative injury [30]. In parallel, SIRT1 has been identified as the upstream of the PINK1/Parkin pathway. SIRT1 upregulation mediates mitochondrial autophagy by activating the PINK1-Parkin pathway [31]. In addition, Zhu et al. found that NGR1 can upregulate SIRT1 levels [32]. In the present study, we found that NGR1 significantly increased the expression of SIRT1 in HT22 cells, and the SIRT1 inhibitor nicotinamide weakened the effect of NGR1. Simultaneously, nicotinamide downregulated the expression level of Parkin and weakened the fluorescence intensity of MMP. The Wnt/β-catenin signaling system is an important pathway in the development of the CNS [33]. Previous studies have shown that SIRT1, as an activator of the Wnt/β-catenin signaling pathway, can increase the transcriptional activity of Wnt1 and β-catenin by affecting the stability of c-myc, promote the nuclear transfer of β-catenin, and activates the Wnt/β-catenin signaling pathway [32, 34]. Moreover, we also observed that the Wnt/

β-catenin signaling pathway participates in the development process of neurological diseases [35, 36]. In this study, we found that glutamate treatment downregulated the expression of SIRT1, Wnt1, β-catenin, and cyclin D1. NGR1 treatment upregulated the expression of SIRT1, Wnt1, β-catenin, and cyclin D1. Furthermore, the effects of SIRT1 inhibitor nicotinamide and Wnt/β-catenin inhibitor SKL2001 both affect the regulation of SIRT1/Wnt/β-catenin by NGR1.

In summary, this study demonstrated that NGR1 plays a neuroprotective role in glutamate-induced cytotoxicity. To the best of our knowledge, this is the first report to show NGR1-protecting HT22 cells against glutamate-induced cytotoxicity by upregulating SIRT1 to activate the Wnt/β-catenin pathway. However, one limitation should not be ignored in this study; it is necessary to further verify the mechanism of NGR1 regulation in animal models of neurological diseases.

Data Availability

The data used to support the findings of this study are available from the corresponding author upon request.

Conflicts of Interest

The authors declare that they no conflicts of interest.

Authors' Contributions

WL designed the experiments. DW and WL wrote the article. DW, BBG, TY, HYS, and XPR performed experiments. HYS and XPR analyzed this data. All the authors read and approved the final manuscript.

References

[1] N. Yan, Z. Xu, C. Qu, and J. Zhang, "Dimethyl fumarate improves cognitive deficits in chronic cerebral hypoperfusion rats by alleviating inflammation, oxidative stress, and ferroptosis via NRF2/ARE/NF-κB signal pathway," *International Immunopharmacology*, vol. 98, Article ID 107844, 2021.

[2] A. Perrelli and S. F. Retta, "Polymorphisms in genes related to oxidative stress and inflammation: emerging links with the pathogenesis and severity of cerebral cavernous malformation disease," *Free Radical Biology and Medicine*, vol. 172, pp. 403–417, 2021.

[3] S. Sharma, D. Advani, A. Das et al., "Pharmacological intervention in oxidative stress as a therapeutic target in neurological disorders," *Journal of Pharmacy and Pharmacology*, vol. rgab064, 2021.

[4] C. Duangjan, P. Rangsinth, S. Zhang, G. Xiaojie, and W. Michael, "Vitis vinifera leaf extract protects against glutamate-induced oxidative toxicity in ht22 hippocampal neuronal cells and increases stress resistance properties in caenorhabditis elegans," *Front Nutr*, vol. 8, Article ID 634100, 2021.

[5] L. Wang, H. Fu, W. Wang et al., "Notoginsenoside r1 functionalized gelatin hydrogels to promote reparative dentinogenesis," *Acta Biomaterialia*, vol. 122, pp. 160–171, 2021.

[6] P. Zhou, W. Xie, X. Meng et al., "Notoginsenoside R1 ameliorates diabetic retinopathy through PINK1-dependent activation of mitophagy," *Cells*, vol. 8, no. 3, Article ID 213, 2019.

[7] H. L. Qin, X. J. Wang, B. X. Yang, B. Du, and X. L. Yun, "Notoginsenoside R1 attenuates breast cancer progression by targeting CCND2 and YBX3," *Chinese Medical Journal*, vol. 134, no. 5, pp. 546–554, 2021.

[8] W. Wang, L. Huang, Y. Hu, E. Thomas, and X. Li, "Neuroprotective effects of notoginsenoside R1 by upregulating Trx-1 on acrylamide-induced neurotoxicity in PC12," *Human & Experimental Toxicology*, vol. 39, no. 6, pp. 797–807, 2020.

[9] W. Wang, Y. Hao, and F. Li, "Notoginsenoside R1 alleviates high glucose-evoked damage in RSC96 cells through down-regulation of miR-503," *Artificial Cells, Nanomedicine, and Biotechnology*, vol. 47, no. 1, pp. 3947–3954, 2019.

[10] S. H. Tai, W. T. Lee, A. C. Lee et al., "Therapeutic window for YC-1 following glutamate-induced neuronal damage and transient focal cerebral ischemia," *Molecular Medicine Reports*, vol. 17, pp. 6490–6496, 2018.

[11] J. Yang, M. D. C. Vitery, J. Chen, J. Osei-Owusu, J. Chu, and Z. Qiu, "Glutamate-releasing swell1 channel in astrocytes modulates synaptic transmission and promotes brain damage in stroke," *Neuron*, vol. 102, no. 4, pp. 813–827, Article ID e816, 2019.

[12] J. H. Kang, M. H. Kim, H. J. Lee, J.-W. Huh, H.-S. Lee, and D.-S. Lee, "Peroxiredoxin 4 attenuates glutamate-induced neuronal cell death through inhibition of endoplasmic reticulum stress," *Free Radical Research*, vol. 54, no. 4, pp. 207–220, 2020.

[13] J. Huang, L. Zhou, J. Chen et al., "Hyperoside attenuate inflammation in HT22 cells via upregulating SIRT1 to activities wnt/β-catenin and sonic hedgehog pathways," *Neural Plasticity*, vol. 2021, pp. 1–10, 2021.

[14] P. Kittimongkolsuk, N. Pattarachotanant, S. Chuchawankul, M. Wink, and T. Tencomnao, "Neuroprotective effects of extracts from tiger milk mushroom lignosus rhinocerus against glutamate-induced toxicity in ht22 hippocampal neuronal cells and neurodegenerative diseases in caenorhabditis elegans," *Biology*, vol. 10, no. 1, p. 30, 2021.

[15] Q. Pan, Y. Ban, and L. Xu, "Silibinin-albumin nanoparticles: characterization and biological evaluation against oxidative stress-stimulated neurotoxicity associated with alzheimer's disease," *Journal of Biomedical Nanotechnology*, vol. 17, no. 6, pp. 1123–1130, 2021.

[16] Y. Zhang, L. Wang, G. Li, and J. Gao, "Berberine-albumin nanoparticles: preparation, thermodynamic study and evaluation their protective effects against oxidative stress in primary neuronal cells as a model of alzheimer's disease," *Journal of Biomedical Nanotechnology*, vol. 17, no. 6, pp. 1088–1097, 2021.

[17] J.-S. Chan, P.-J. Hsiao, W.-F. Chiang, and P. Roy-Chaudhury, "The role of oxidative stress markers in predicting acute thrombotic occlusion of haemodialysis vascular access and progressive stenotic dysfunction demanding angioplasty," *Antioxidants*, vol. 10, no. 4, Article ID 569, 2021.

[18] J. Y. Baek, K. Jung, Y.-M. Kim, H.-Y. Kim, K. S. Kang, and Y.-W. Chin, "Protective effect of γ-mangostin isolated from the peel of Garcinia mangostana against glutamate-induced cytotoxicity in HT22 hippocampal neuronal cells," *Biomolecules*, vol. 11, no. 2, Article ID 170, 2021.

[19] S. Kang, J. Li, Z. Yao, and J. Liu, "Cannabidiol induces autophagy to protects neural cells from mitochondrial dysfunction by upregulating SIRT1 to inhibits NF-κB and NOTCH pathways," *Frontiers in Cellular Neuroscience*, vol. 15, Article ID 654340, 2021.

[20] J. Zhao, L. Cui, J. Sun et al., "Notoginsenoside r1 alleviates oxidized low-density lipoprotein-induced apoptosis, inflammatory response, and oxidative stress in huvecs through modulation of xist/mir-221-3p/traf6 axis," *Cellular Signalling*, vol. 76, Article ID 109781, 2020.

[21] Y. Fang, B. Shi, X. Liu et al., "Xiaoyao pills attenuate inflammation and nerve injury induced by lipopolysaccharide in hippocampal neurons in vitro," *Neural Plasticity*, vol. 2020, pp. 1–12, 2020.

[22] N. Vergnolle and C. Cirillo, "Neurons and glia in the enteric nervous system and epithelial barrier function," *Physiology*, vol. 33, no. 4, pp. 269–280, 2018.

[23] D. K. Wilton, L. Dissing-Olesen, and B. Stevens, "Neuron-Glia signaling in synapse elimination," *Annual Review of Neuroscience*, vol. 42, no. 1, pp. 107–127, 2019.

[24] D. Lee, H. G. Choi, J. H. Hwang, S. H. Shim, and K. S. Kang, "Neuroprotective effect of tricyclic pyridine alkaloids from fusarium lateritium ssf2, against glutamate-induced oxidative stress and apoptosis in the ht22 hippocampal neuronal cell line," *Antioxidants*, vol. 9, no. 11, Article ID 1115, 2020.

[25] D. H. Park, J. Y. Park, K. S. Kang, and G. S. Hwang, "Neuroprotective effect of gallocatechin gallate on glutamate-induced oxidative stress in hippocampal ht22 cells," *Molecules*, vol. 26, no. 5, Article ID 1387, 2021.

[26] J. Kwon, H. Hwang, B. Selvaraj et al., "Phenolic constituents isolated from senna tora sprouts and their neuroprotective effects against glutamate-induced oxidative stress in ht22 and r28 cells," *Bioorganic Chemistry*, vol. 114, Article ID 105112, 2021.

[27] H.-J. Park, M. Kwak, and S.-H. Baek, "Neuroprotective effects of dendropanax morbifera leaves on glutamate-induced oxidative cell death in ht22 mouse hippocampal neuronal cells," *Journal of Ethnopharmacology*, vol. 251, Article ID 112518, 2020.

[28] S. Jiang, P. Nandy, W. Wang et al., "Mfn2 ablation causes an oxidative stress response and eventual neuronal death in the hippocampus and cortex," *Molecular Neurodegeneration*, vol. 13, no. 1, p. 5, 2018.

[29] F. Mouton-Liger, M. Jacoupy, J.-C. Corvol, and O. Corti, "Pink1/parkin-dependent mitochondrial surveillance: from pleiotropy to Parkinson's disease," *Frontiers in Molecular Neuroscience*, vol. 10, Article ID 120, 2017.

[30] Q. Zhu, T. Tang, H. Liu et al., "Pterostilbene attenuates cocultured bv-2 microglial inflammation-mediated sh-sy5y neuronal oxidative injury via sirt-1 signalling," *Oxidative Medicine and Cellular Longevity*, vol. 2020, pp. 1–11, 2020.

[31] T. Liu, Q. Yang, X. Zhang et al., "Quercetin alleviates kidney fibrosis by reducing renal tubular epithelial cell senescence through the sirt1/pink1/mitophagy axis," *Life Sciences*, vol. 257, Article ID 118116, 2020.

[32] T. Zhu, W.-j. Xie, L. Wang et al., "Notoginsenoside R1 activates the NAMPT-NAD+-SIRT1 cascade to promote post-ischemic angiogenesis by modulating Notch signaling," *Biomedicine & Pharmacotherapy*, vol. 140, Article ID 111693, 2021.

[33] N. Feng, Q. Han, J. Li et al., "Generation of highly purified neural stem cells from human adipose-derived mesenchymal stem cells by sox1 activation," *Stem Cells and Development*, vol. 23, no. 5, pp. 515–529, 2014.

[34] Q. Wu, Y. Wang, M. Qian et al., "Sirt1 suppresses Wnt/βCatenin signaling in liver cancer cells by targeting βCatenin in a PKAα-dependent manner," *Cellular Signalling*, vol. 37, pp. 62–73, 2017.

[35] B. Zhao, P. Wang, J. Yu, and Y. Zhang, "MicroRNA-376b-5p targets SOX7 to alleviate ischemic brain injury in a mouse model through activating Wnt/β-catenin signaling pathway," *Life Sciences*, vol. 270, Article ID 119072, 2021.

[36] B. Gong, L. Jiao, X. Du et al., "Ghrelin promotes midbrain neural stem cells differentiation to dopaminergic neurons through Wnt/β-catenin pathway," *Journal of Cellular Physiology*, vol. 235, no. 11, pp. 8558–8570, 2020.

Hindawi
Evidence-Based Complementary and Alternative Medicine
Volume 2021, Article ID 7219293, 10 pages
https://doi.org/10.1155/2021/7219293

Review Article

A Meta-Analysis: Whether Repetitive Transcranial Magnetic Stimulation Improves Dysfunction Caused by Stroke with Lower Limb Spasticity

Yu Liu[1], **Hong Li**[1], **Jun Zhang**[2], **Qing-qing Zhao**[1,3], **Hao-nan Mei**[1,3] and **Jiang Ma**[1]

[1]*Department of Rehabilitation Medicine, Shijiazhuang People's Hospital, Shijiazhuang 050030, Hebei, China*
[2]*Rehabilitation District of Taihe Hospital, Shiyan 442000, Hubei, China*
[3]*School of Nursing and Rehabilitation, North China University of Science and Technology, Tangshan 063210, Hebei, China*

Correspondence should be addressed to Jiang Ma; majiangtutor@sina.com

Received 10 June 2021; Accepted 21 October 2021; Published 28 November 2021

Academic Editor: Feng Zhang

Objective. To evaluate the efficacy of repetitive transcranial magnetic stimulation (rTMS) in improving lower limb spasticity after stroke. *Methods*. The PubMed, Web of Science, Cochrane Library, EMBASE, China National Knowledge Infrastructure (CNKI), China Biology Medicine (CBM) disc, China Science and Technology Journal Database (VIP), and Wanfang databases were searched online from their inception to May 2021 for randomized controlled trials (RCTs) involving repetitive transcranial magnetic stimulation for lower extremity spasticity after stroke. Valid data were extracted from the included literature, and the quality evaluation was conducted with the Cochrane Handbook for Systematic Reviews of Interventions along with the Physiotherapy Evidence Database scale (PE-Dro scale). The data that met the quality requirements were systematically analysed using Review Manager 5.4 software. *Results*. A total of 554 patients from seven articles (nine studies) were quantitatively analysed. Outcomes included the Modified Ashworth Scale (MAS), Fugl–Meyer Assessment of Lower Extremity (FMA-LE), Modified Barthel Index (MBI), and Timed Up and Go (TUG), measured as the effect of rTMS compared with controls conditions after treatment. The systematic review showed that rTMS reduced MAS and increased MBI scores, respectively (SMD = −0.24, 95% CI [−0.45, −0.03], $P = 0.02$; MD = 6.14, 95% CI [−3.93,8.35], $P < 0.00001$), compared with control conditions. Low-frequency rTMS (LF-rTMS) significantly improved FMA-LE scores (SMD = 0.32, 95% CI [0.13, 0.51], $P = 0.001$). However, there was no significant difference in FMA-LE scores when using high-frequency rTMS (HF-rTMS) ($P > 0.1$) and in TUG times ($P > 0.1$) between the treatment and control groups. *Conclusions*. rTMS was effective in improving spasticity and activities of daily living. LF-rTMS has positive clinical effects on enhancing motor function in patients who experience lower extremity spasticity after stroke. To better validate the above conclusions, more multicentre, high-quality, and double-blind randomized controlled trials are needed.

1. Introduction

Stroke is a common disease worldwide and causes serious disabilities for patients. More than two-thirds of stroke survivors develop poststroke sequelae that involve impairment of motor function, balance, gait, and activities of daily living [1, 2]. Poststroke spasticity (PSS) is a common motor dysfunction after stroke that clinically manifests as increased muscle tone, positive pathological signs, and tendon hyperreflexia [3], with a prevalence from 4% to 42.6% [2]. Current management of poststroke spasticity has shown that although drug therapy (such as botulinum toxin injection, oral baclofen, dantrolene, sodium, and tizanidine) is effective for improving spasticity and widely used in clinical practice, it had side effects and produced unsatisfied clinical effects such as muscle weakness [4]. Nondrug therapy, such as neuromuscular electrical stimulation and physical therapy, temporarily relieved poststroke spasticity and motor dysfunction. However, some of these interventions demand active participants to become involved, and the duration of

the efficacy was relatively short [5, 6]. rTMS has been gradually applied in the clinical treatment of poststroke dysfunction due to its noninvasiveness and safety on the basis of conventional treatment of stroke sequelae. But most of the research focused on motor dysfunction, cognitive disorder, aphasia, and so on. There are few studies on the application of rTMS in poststroke spasticity, and the mechanism is unclear. What is more, rTMS has a significant impact on public acceptance due to the relatively high clinical costs and being excluded in the health insurance in some cities [7–9]. A recent meta-analysis explored the use of rTMS in stroke patients. Two meta-analyses published by McIntyre et al. [10] and Peng et al. [11] analysed the effect of rTMS in the rehabilitation of spasticity after stroke. However, they did not include RCTs for the treatment of lower limb spasticity after stroke, and some new RCTs have been published since then. Moreover, the efficacy of repetitive transcranial magnetic stimulation in improving lower limb spasticity after stroke remains unknown. As a result, the purpose of this study was to perform a systematic review of RCTs that explored the efficacy of rTMS in treating patients with lower limb spasticity after stroke.

2. Methods

2.1. Literature Search Strategy. We performed a search in the PubMed, Web of Science, Cochrane Library, EMBASE, CNKI, CBM, VIP, and Wanfang databases published up to May 2021. The search terms were "stroke" OR "hemiplegia" OR "cerebrovascular accident" OR "ischemic stroke" OR "hemorrhagic stroke" OR "CVA" OR "apoplexy" AND "repetitive transcranial magnetic stimulation" OR "rTMS" OR "transcranial magnetic stimulation" OR "TMS" AND "spasticity" AND "lower limb" OR "lower extremity".

2.2. Inclusion and Exclusion Criteria. The relevant articles were selected based on the following eligibility criteria: (1) the involved patients were clinically diagnosed with lower limb spasticity after stroke by relevant examinations; (2) the experimental group used rTMS and traditional physical therapy, while the control group underwent traditional physical therapy plus sham rTMS (or only with traditional physical therapy); (3) the outcome measures included the MAS, FMA-LE, MBI, and TUG; and (4) the included articles were RCTs.

Articles meeting with the following criteria were excluded: (1) total sample size of fewer than 10 participants in each study; (2) study with incomplete data; (3) meta-analysis, case report, literature review, guidelines, dissertation, and others; and (4) non-RCTs.

2.3. Literature Screening and Data Extraction. Two researchers independently searched and screened the literature based on the above search strategy and removed the studies that did not meet the predefined criteria by reading the abstracts and full texts. Any inconsistencies between the two authors were resolved by discussion or in consultation with the third author. The following data were extracted: study characteristics (authors, year of publication, study design, sample sizes, age, and course of disease) and intervention details (intervention measures, treatment time, stimulated sites, treatment parameters, and outcome measures).

2.4. Literature Quality Evaluation. The quality of the included articles was evaluated by two authors using the Cochrane Handbook for Systematic Reviews of Interventions [12] and PE-Dro [13]. In cases of disagreement, a third person made the final decision. Three levels (level A, level B, and level C) were used to rank the quality of each study when using the former method [12]. Regarding the PE-Dro, 0–3 points indicated low quality, 4–7 points indicated medium quality, and 8–11 indicated high-quality [14].

2.5. Data Synthesis and Statistical Methods. The outcomes in both the treatment and control groups after the intervention period were extracted. The results were shown by the histogram in one study [15], and we estimated the results based on the X and Y axes and the corresponding parameters. A six-point scale (0, 1, 1^+, 2, 3, and 4) was denoted as the MAS scale [16]. To quantify the score for analysis, we calculated 1^+ as 1.5. If the results were not presented as the means and standard deviations, we calculated the original data using SPSS 25.0 [17] or the method of Wan et al. [18]. The data from the first phase for both groups were extracted in randomized controlled crossover studies [15, 19, 20]. If the variable between two groups in an article was only rTMS, we divided the one article into two studies [17, 21]. Quantitative analysis was performed using Review Manager version 5.4 by two authors. Concerning the continuous variables (excluding H_{max}/M_{max}), the mean difference (MD) or the standardized mean difference (SMD) with 95% CI were calculated for the outcome. The heterogeneity among the included studies was assessed by the χ^2 test and Higgins I^2 values. If there was clear heterogeneity ($I^2 > 50\%$ or $P < 0.1$), a random effects model was used. Otherwise, a fixed effects model was applied.

3. Results

3.1. Characteristics of the Studies. A total of 113 entries were retrieved from Chinese and English databases, including 33 in Chinese and 80 in English (Figure 1); 50 duplicates were removed through EndNote X9; and 63 articles were screened. Then, 21 were excluded because the article type was not a clinical trial. A total of 42 full-text studies were obtained for eligibility. Then, 35 studies were rejected: 25 due to the population, 4 owing to the intervention, 3 because of the study design, and 3 because of the assessed outcome. Finally, seven articles with a total of 554 patients [15, 17, 19–23] were included. Two articles had two separate data sets [17, 21], and the others had one data set each. Table 1 shows the characteristics of the included articles. All the included studies were randomized controlled trials with quality level B, and three of them were crossover trials [15, 19, 20]. The risk of bias of the included RCT is shown in Figure 2. The total score on the PE-Dro was 51, with an

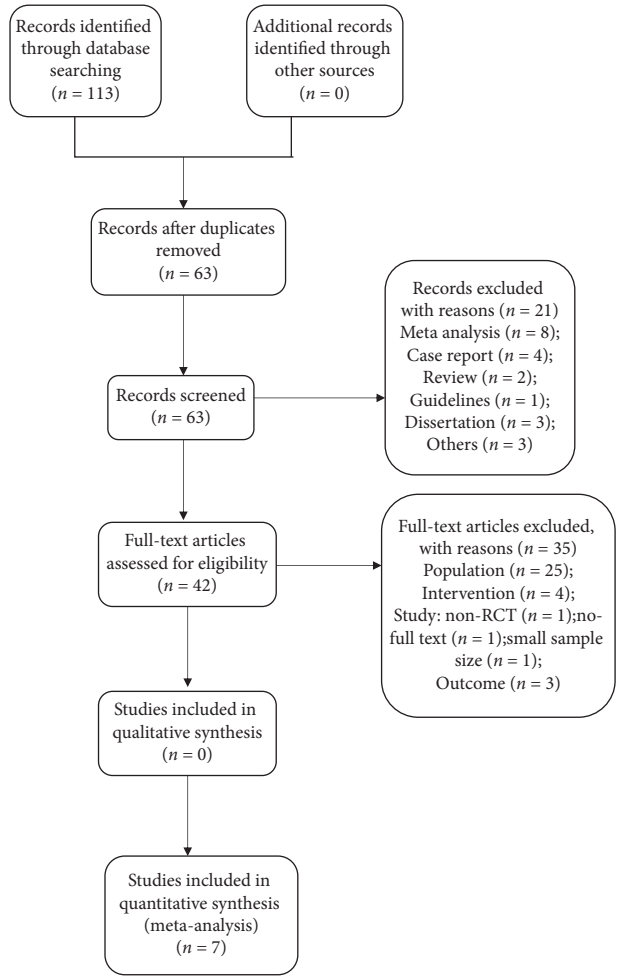

Figure 1: Flow diagram of study selection.

Table 1: Characteristics of included articles.

Author/ year	Sample size	Mean age (y)	Course of disease (m)	Intervention	Treatment duration	Stimulated site	Treatment parameters	RCT type	Outcome
			Treatment/control						
Chieffo et al., 2020 [19]	6/6	58.67 ± 10.33/ 61.17 ± 8.70	41.50 ± 26.77/ 41.00 ± 26.54	$r + c$/ sham + c	15 min/day, 11 sessions	Bilateral leg motor cortex	20 Hz, 80%–90% RMT, H-coil	Crossover trial	FMA-LE, MAS, 10-MT, 6MWT
Rastgoo et al., 2016 [15]	7/7	54.60 ± 11.75/ 49.70 ± 11.00	30.2 ± 18.3/ 27.4 ± 20.1	r/sham	20 min/day, 5 days	Leg motor cortex of the unaffected hemisphere	1 Hz, 90% RMT, eight coil	Crossover trial	MMAS, FMA-LE, H_{max}/ $M_{max,}$ TUG
Yijie, 2018 [20]	70/70	55.20 ± 11.50/ 51.30 ± 12.10	31.60 ± 11.5/ 51.3 ± 12.1	$r + R$/ sham + R	20 min/day, 5 days	Contralateral cerebral cortex	1 Hz, 90% RMT, eight coil	Crossover trial	MAS, FMA-LE, H_{max}/ M_{max}, TUG
Jing et al., 2018 [21]	24/24	56.55 ± 13.11/ 57.33 ± 12.00	3.58 ± 2.44/ 4.01 ± 2.89 days	$r + R/R$	15 min/day, 1 month	Primary motor cortex of the unaffected hemisphere	1 Hz, 90% RMT	Factorial trial	MAS, FMA-LE, MBI, BBS

Table 1: Continued.

Author/year	Sample size	Mean age (y)	Course of disease (m) Treatment/control	Intervention	Treatment duration	Stimulated site	Treatment parameters	RCT type	Outcome
Jing et al., 2018 [21]	24/24	56.21 ± 11.68/ 55.93 ± 13.88	4.33 ± 2.57/ 4.41 ± 2.69 days	*r* + *B* + *R*/ *B* + *R*	15 min/day, 1 month	Primary motor cortex of the unaffected hemisphere	1 Hz, 90% RMT	Factorial trial	MAS, FMA-LE, MBI, BBS
Yang et al., 2015 [22]	60/60	58.7 ± 3.5/ 59.2 ± 3.3	4.6 ± 1.2/ 4.3 ± 1.4	*r* + *R*/*r*	15 min/day, 5 days/ week, 8 weeks	M1 of the affected hemisphere	2 Hz, 90% RMT butterfly shaped coils	Parallel trial	FMA, FAC, CSI, 10-MT
Hong et al., 2016 [17]	20/20	62.18 ± 13.66/ 61.23 ± 14.24	3.98 ± 2.05/ 4.61 ± 2.50 days	*r* + *R*/*R*	20 min/day, 6 days/ week, 4 weeks	Primary motor cortex of the unaffected hemisphere	1 Hz, 90% RMT circular coil	Factorial trial	MAS, FMA-LE, MBI
Hong et al., 2016 [17]	20/20	61.99 ± 15.02/ 60.89 ± 15.16	4.02 ± 3.17/ 4.35 ± 3.28 days	*r* + *B* + *R*/ *r* + *B*	20 min/day, 6 days/ week, 4 weeks	Primary motor cortex of the unaffected hemisphere	1 Hz, 90% RMT circular coil	Parallel trial	MAS, FMA-LE, MBI
Huayao et al., 2019 [23]	47/45	43.33 ± 9.18/ 44.33 ± 9.94	———	*r* + *F*/ sham + *F*	20 min/day, 5 days/ week, 4 weeks	M1 of the affected brain hemisphere	1 Hz	Parallel trial	MAS, FMA-LE, MEP

r: rehabilitation; sham: sham rTMS; c: cycling; *B*: BTX-A; *R*: rehabilitation; *F*: FES (functional electrical stimulation).

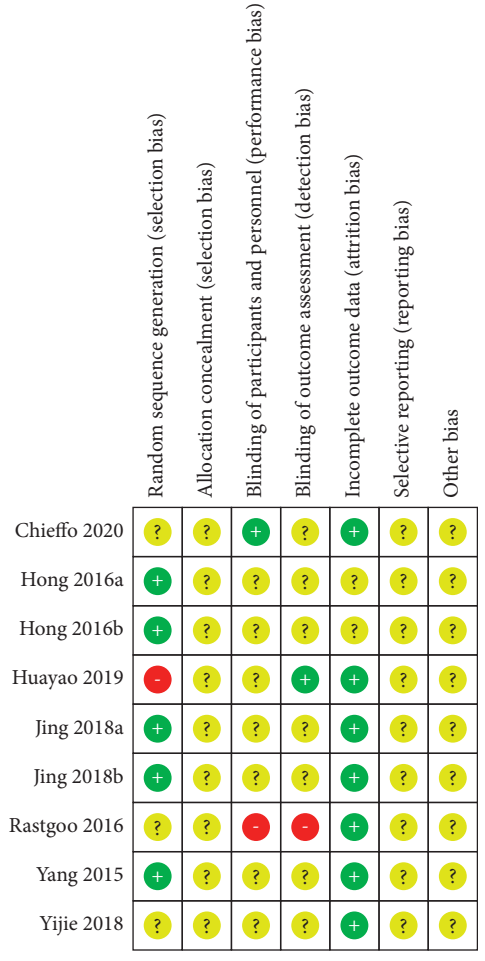

(a)

Figure 2: Continued.

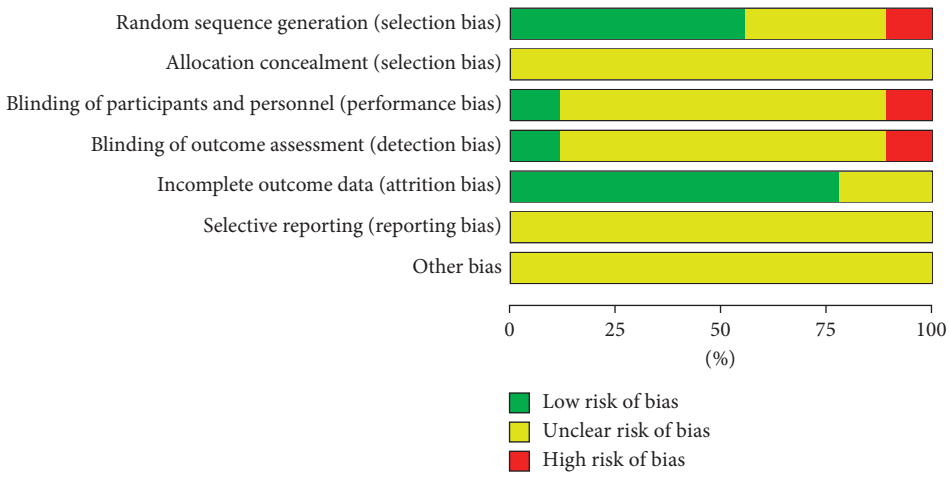

(b)

Figure 2: (a) Risk of bias graph. (b) Risk of bias summary.

average of 7.29. Two articles were of high quality [17, 19], and five were of medium quality (Table 2).

3.2. Effects of rTMS on Spasticity of the Lower Limbs in Stroke Patients

3.2.1. MAS. Five articles (seven studies) [17, 19, 21, 23] with 420 patients were included. The forest plot (Figure 3(a)) shows that statistical heterogeneity was not observed ($I^2 = 44\%$, $P = 0.10$). We used the fixed effects model because heterogeneity was not observed after two studies were [19, 21] excluded through sensitivity analysis ($I^2 = 0\%$, $P = 0.78$). The meta-analysis showed that rTMS had a significant beneficial effect on MAS scores in patients with lower limb spasticity after stroke (SMD = −0.24, 95% CI [−0.45, 0.03], $P = 0.02$) (Figure 3(b)).

3.3. Effects of rTMS on Spasticity of the Lower Limbs in Stroke Patients

3.3.1. FMA. A total of seven articles (nine studies) with 554 patients [15, 17, 19–23] presented effects on the FMA. Subgroup analysis based on low- and high-frequency indicated seven studies with LF-rTMS and two with HF-rTMS. The difference between groups among those using low-frequency rTMS showed a statistically significant effect on FMA scores (SMD = 0.32, 95% CI [0.13, 0.51], $P = 0.001$) with no statistical heterogeneity ($I^2 = 1\%$, $P = 0.42$). There was no statistical significance between the two groups in the studies using high-frequency rTMS ($P = 0.72$) (Figure 4).

3.4. Effects of rTMS on Spasticity of the Lower Limbs in Stroke Patients

3.4.1. MBI. Two articles (four studies) [17, 21] with 176 patients assessed this outcome. The random effects model was used with $I^2 = 40\%$ and $P = 0.17$ (Figure 5(a)). Jing was the source of the heterogeneity after sensitivity analysis (Figure 5(b)). We found that there was a significant difference between the two groups (MD = 6.14, 95% CI [3.93, 8.35], $P < 0.00001$).

3.5. Effects of rTMS on Spasticity of the Lower Limbs in Stroke Patients

3.5.1. TUG Scores. Two studies [15, 20] showed that rTMS did not have a significant effect on MBI scores in the patients with lower limb spasticity (Figure 6).

3.6. Others. The electrophysiological index H_{max}/M_{max} was described in two studies [15, 20] and showed that the index decreased in the treatment group without a significant difference compared with the control group.

The included articles reported adverse effects except for Hong [17]. Three studies [15, 20, 21] showed that patients had good tolerance to LF-rTMS in their studies. Chieffo et al. [19] reported transitory dizziness and muscle twitches in the shoulders of three patients, and they subsequently completed the remaining treatment after the intensity was decreased to 80% RMT. In another study, the patients had muscle pain and fatigue symptoms that were relieved after two to three days [21]. Huayao et al. [23] reported adverse effects without a significant difference between the two groups. In the treatment group, transitory headache was found in two patients, which diminished after suspension of the treatment [22].

4. Discussion

Velocity-dependent increases in muscle tone, hyperexcitable stretch reflexes, and hyperreflexia tendon jerks are often described as features of spasticity that appear in patients with stroke [24]. The reason for muscle spasticity in stroke patients is the hyperreflexia of the stretch reflex from the spine. The excitability and inhibitory imbalance of spinal

Table 2: PE-Dro scale of the included study.

Study	Item 1	Item 2	Item 3	Item 4	Item 5	Item 6	Item 7	Item 8	Item 9	Item 10	Item 11	Total
Chieffo et al., 2020 [19]	1	1	0	1	1	1	1	1	0	1	1	9
Rastgoo et al., 2016 [15]	1	1	0	1	1	0	0	0	1	1	1	7
Yijie, 2018 [20]	1	0	0	1	1	0	0	1	1	0	1	6
Jing et al., 2018 [21]	1	1	0	1	1	0	0	1	1	1	1	7
Yang et al., 2015 [22]	1	1	0	1	0	0	0	1	1	1	1	7
Hong et al., 2016 [17]	1	1	0	1	0	0	1	1	1	1	1	8
Huayao et al., 2019 [23]	1	0	0	1	0	0	1	1	1	1	1	7

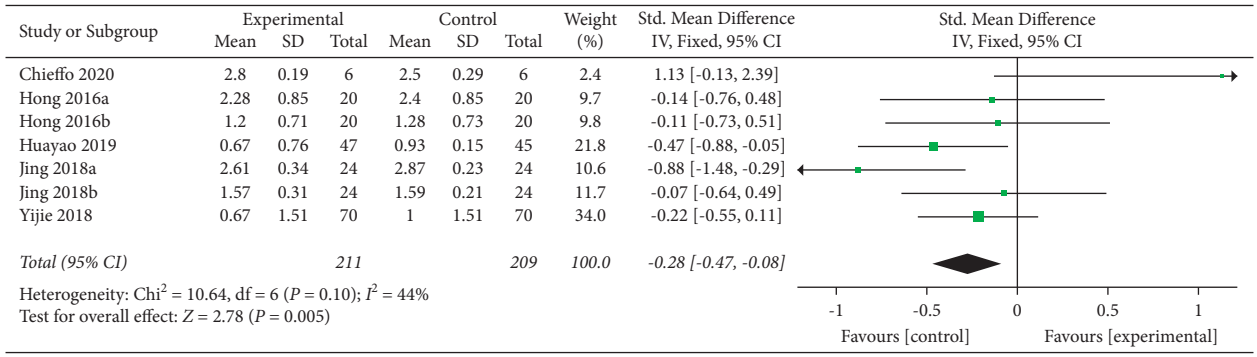

(a)

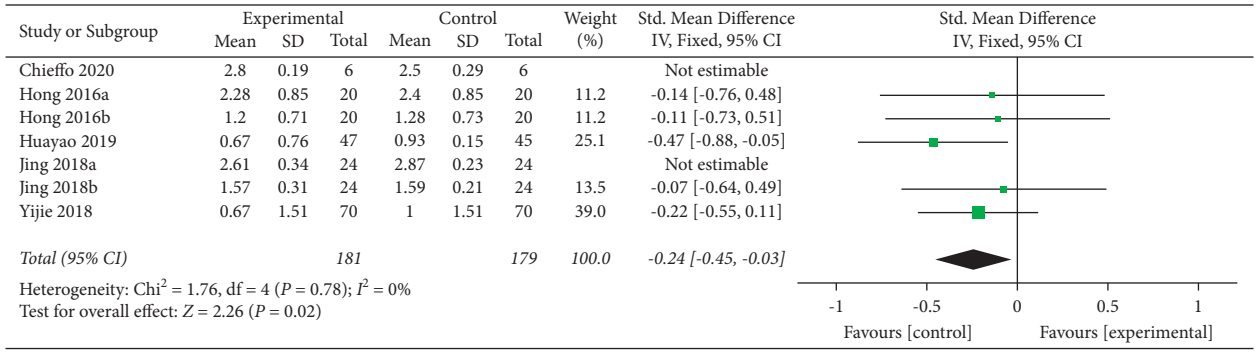

(b)

Figure 3: (a) Forest plot for MAS scores. (b) Forest plot for MAS scores when excluding two studies with high sensitivity.

descending fibres was considered the main cause of hyperreflexia of the stretch reflex. The disorder presents with high excitability of the reticular spine [25]. In addition, there has also been evidence that the vestibular spinal cord was less inhibitory [26], which reduces the inhibition of the spinal cord. Stroke patients with lower limb spasticity generally manifest hip adduction, knee extension, and ankle plantar flexion impacting the recovery of motor function and gait [27].

At present, the conventional treatment for lower limb spasticity after stroke includes drugs, motor therapy, and neuromuscular electrical stimulation [6]. However, the effect of conventional rehabilitation is limited. Thus some ways of complementary and alternative medicine are needed. Previous studies have shown that rTMS can be used to treat patients with lower limb spasticity after stroke with different results and unclear mechanisms. Naghdi et al. [28] reported that improvements in ankle plantar flexor and knee extensor spasticity were significant, but H_{max}/M_{max} showed no statistical improvement after five consecutive LF-rTMS sessions. Terreaux et al. [29] showed that 1 Hz rTMS reduced the excitability of the ankle plantar flexor reflex without modifying clinical signs of spasticity, but there was no change during 10-Hz rTMS. Because these studies were a nonrandomized controlled trial [28] or had a small sample size [29], our research group performed a systematic analysis including the most recent randomized controlled trials with more participants to further increase the quality of the included studies.

The results indicated that rTMS was effective in improving lower limb spasticity and activities of daily living; LF-rTMS had a positive influence on enhancing motor function in patients who experienced lower extremity spasticity after stroke, whereas HF-rTMS did not have a

Study or Subgroup	Experimental Mean	SD	Total	Control Mean	SD	Total	Weight (%)	Std. Mean Difference IV, Fixed, 95% CI
3.3.1 LF-rTMS								
Hong 2016a	7.98	1.87	20	8.18	2.14	20	7.9	-0.10 [-0.72, 0.52]
Hong 2016b	12.83	1.09	20	11.27	3.12	20	7.4	0.65 [0.02, 1.29]
Huayao 2019	14.33	8.41	47	12.17	8.04	45	17.9	0.26 [-0.15, 0.67]
Jing 2018a	11.61	2.34	24	10.57	2.03	24	9.2	0.47 [-0.11, 1.04]
Jing 2018b	17.31	2.18	24	17.29	1.51	24	9.5	0.01 [-0.56, 0.58]
Rastgoo 2016	16.93	7.9	7	18.07	8.08	7	2.7	-0.13 [-1.18, 0.92]
Yijie 2018	27.6	5.6	70	24.9	5.2	70	26.7	0.50 [0.16, 0.83]
Subtotal (95% CI)			*212*			*210*	*81.3*	*0.32 [0.13, 0.51]*
Heterogeneity: $Chi^2 = 6.06$, df = 6 ($P = 0.42$); $I^2 = 1\%$								
Test for overall effect: $Z = 3.26$ ($P = 0.001$)								
3.3.2 HF-rTMS								
Chieffo 2020	22	0.9	6	23.1	1.2	6	2.0	-0.96 [-2.18, 0.27]
Yang 2015	25.7	3.89	60	18.5	4.04	60	16.6	1.80 [1.38, 2.23]
Subtotal (95% CI)			*66*			*66*	*18.7*	*1.51 [1.10, 1.91]*
Heterogeneity: $Chi^2 = 17.43$, df = 1 ($P < 0.0001$); $I^2 = 94\%$								
Test for overall effect: $Z = 7.32$ ($P < 0.00001$)								
Total (95% CI)			*278*			*276*	*100.0*	*0.54 [0.37, 0.72]*
Heterogeneity: $Chi^2 = 50.52$, df = 8 ($P < 0.00001$); $I^2 = 84\%$								
Test for overall effect: $Z = 6.10$ ($P < 0.00001$)								
Test for subgroup differences: $Chi^2 = 27.04$, df = 1 ($P < 0.00001$); $I^2 = 96.3\%$								

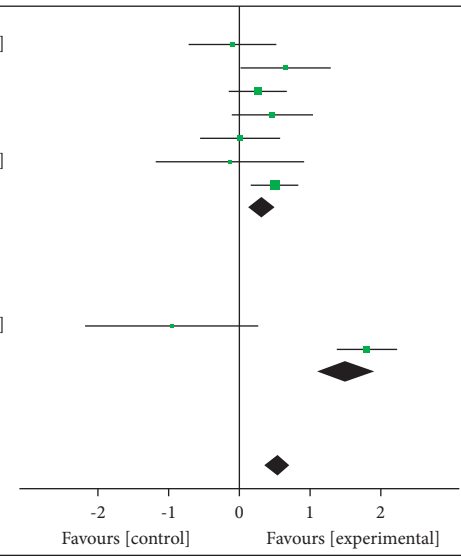

Figure 4: Forest plot of FMA.

Study or Subgroup	Experimental Mean	SD	Total	Control Mean	SD	Total	Weight (%)	Mean Difference IV, Fixed, 95% CI
Hong 2016a	68.15	14.55	20	66.39	13.17	20	6.6	1.76 [-6.84, 10.36]
Hong 2016b	81.99	18.39	20	80.23	19.98	20	3.5	1.76 [-10.14, 13.66]
Jing 2018a	62.14	6.11	24	53.92	3.88	24	58.3	8.22 [5.32, 11.12]
Jing 2018b	78.26	6.57	24	74.56	7.32	24	31.6	3.70 [-0.24, 7.64]
Total (95% CI)			*88*			*88*	*100.0*	*6.14 [3.93, 8.35]*
Heterogeneity: $Chi^2 = 4.98$, df = 3 ($P = 0.17$); $I^2 = 40\%$								
Test for overall effect: $Z = 5.44$ ($P < 0.00001$)								

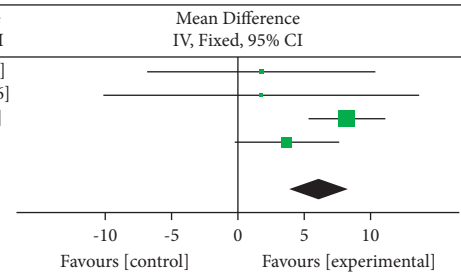

(a)

Study or Subgroup	Experimental Mean	SD	Total	Control Mean	SD	Total	Weight (%)	Mean Difference IV, Fixed, 95% CI
Hong 2016a	68.15	14.55	20	66.39	13.17	20	15.9	1.76 [-6.84, 10.36]
Hong 2016b	81.99	18.39	20	80.23	19.98	20	8.3	1.76 [-10.14, 13.66]
Jing 2018a	62.14	6.11	24	53.92	3.88	24		Not estimable
Jing 2018b	78.26	6.57	24	74.56	7.32	24	75.8	3.70 [-0.24, 7.64]
Total (95% CI)			*64*			*64*	*100.0*	*3.23 [-0.20, 6.66]*
Heterogeneity: $Chi^2 = 0.23$, df = 2 ($P = 0.89$); $I^2 = 0\%$								
Test for overall effect: $Z = 1.85$ ($P = 0.06$)								

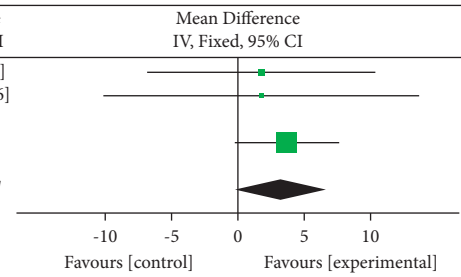

(b)

Figure 5: (a) Forest plot for MBI scores. (b) Forest plot for MBI scores after removing one study.

Study or Subgroup	Experimental Mean	SD	Total	Control Mean	SD	Total	Weight (%)	Std. Mean Difference IV, Fixed, 95% CI
Rastgoo 2016	15.5	27.1	7	15.73	28.29	7	9.1	-0.01 [-1.06, 1.04]
Yijie 2018	23.7	20.6	70	24	21.5	70	90.9	-0.01 [-0.35, 0.32]
Total (95% CI)			*77*			*77*	*100.0*	*-0.01 [-0.33, 0.30]*
Heterogeneity: $Chi^2 = 0.00$, df = 1 ($P = 0.99$); $I^2 = 0\%$								
Test for overall effect: $Z = 0.08$ ($P = 0.93$)								

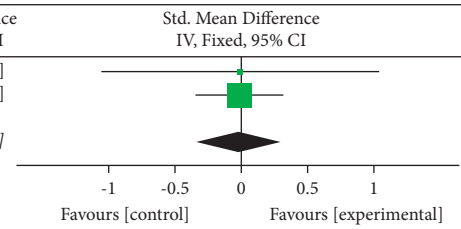

Figure 6: Forest plot for TUG times.

significant effect on motor function. Furthermore, rTMS did not have an additional significant effect on TUG times or H_{max}/M_{max}. McIntyre et al. [10] performed a systematic review regarding the use of rTMS in patients with spasticity after stroke and discovered that rTMS improved spasticity in the elbow, wrist, and finger flexors in uncontrolled pre-post studies, whereas there was no significant influence on spasticity in the wrist in two RCTs. Another meta-analysis by Xu et al. [11] was published in 2020 and reported no benefits on the use of rTMS for upper limb spasticity after stroke, which was different from our research.

Sensitivity analyses of the included studies found that the cause of high bias of risk in Jing and Yan [21] may have been the short duration of treatment and the poor baseline condition of the patients. Rastgoo [15] and Yijie [20] reported that the reason why gait function was improved in both the treatment and control groups after the treatment was that patients were similar regarding TUG measures (TUG refers to the time it takes for the subject to stand up after hearing the instruction, walk straight for three meters, and return to the sitting position with the quickest speed [30]). Few of them had barriers to walking. Electrophysiological changes (H_{max}/M_{max}) were [31] not accompanied by clinical improvement in spasticity in Rastgoo et al. [15], which was similar to the result of Dos Santos et al. [32]. $H_{max}/M_{max,}$ which has been related to an increase in muscle tone in spasticity to a certain extent, is the ratio of the maximum amplitude of *H* reflexion and *M* wave recorded by surface electromyography. H_{max}/M_{max} does not completely reflect the excitability of neurons with measurement of error, and H_{SLP}/M_{SLP} was proposed as a better outcome [33]. H_{SLP}/M_{SLP} (the ratio of the slope of *H* and *M*-waves) was more sensitive to represent the excitability of motor neuron of the anterior horn of the spinal cord [34]. In addition, the reasons for unsynchronized changes were that the treatment times of rTMS were short with only five sessions and the relationship between H_{max}/M_{max} and MAS is not exact, which may not change with the change of MAS [35]. There were no serious adverse effects reported during the process of treatment. Five studies [15, 17, 20–22] followed up patients after therapy, and Jing [21] reported that FMA, MAS, and MBI scores were significantly different between the treatment and control groups after the 12-month follow-up. rTMS is based on the principle of electromagnetic induction and produces changes at the stimulated site and transsynaptically in distant cortical regions. Sustained physiological effects were a feature of rTMS, namely, long-term potential and long-term depression [36], while neuromuscular electrical stimulation had a short duration of the therapeutic effect without the above features [37], as previously mentioned.

The mechanism by which rTMS improves spasticity is not clear. There are two commonly used models of rTMS: (1) a high-frequency (>1 Hz) facilitatory mode, which is applied to the affected brain region to increase cortical excitability and thus reduce spasticity and improve upper limb motor function, and (2) a low-frequency (≤1 Hz) inhibitory mode, which decreases excitability in the unaffected hemisphere and therefore reduces inhibition from the contralateral hemisphere to the ipsilateral hemisphere [31, 38, 39]. We concluded from the subgroup analysis that the LF-rTMS group showed a significant influence on lower limb motor function, while there were no benefits of HF-rTMS. The better therapy between high- or low-frequency stimulation has been controversial. Based on the guidelines written by Lefaucheur et al. [40], LF-rTMS over the contralesional hemisphere promoted poststroke recovery of motor function in chronic stroke patients. Owing to the limited studies we included, the curative effect of HF-rTMS remains to be discussed. Guo et al. [41] reported that the reorganization of the motor network was found with both HF-rTMS and LF-rTMS, and both improved motor recovery; HF-rTMS had more positive effects on the functional connectivity reorganization of the ipsilesional motor network. In addition to stimulation frequency, the stimulation parameters of rTMS also include stimulation duration and intensity. Further studies about parameters selection that make rTMS optimally effective need to be conducted.

The stimulated site included in this study was the leg motor cortex, which is associated with a deep position that is located on the inner side of the anterior central gyrus under a thick skull [42]. To ensure that rTMS has a good effect on the rehabilitation of patients with lower limb spasticity after stroke, the requirement for stimulation depth was quite high. In addition to the intensity of the rTMS used in the adopted studies (i.e., 80%–90% RMT), the rTMS coil itself also played a pivotal role in the effects of lower limb spasticity after stroke. The types of coils were different across studies included in our analysis: Rastgoo et al. [15] and Yijie [20] used a figure-8-shaped coil with higher focal stimulation and less white matter penetration. Chieffo et al. [19] found that the reason that the use of an H coil with deeper stimulation did not improve spasticity and walking function was that rTMS combined with cycling did not influence the functional networks involved in the coordination of gait and skilled walking. This was also considered the reason for the heterogeneity observed in this meta-analysis. Although the circular coil had deep penetration, the short duration of treatment with unconcentrated stimulation was the reason for the lack of improvements in lower limb MAS scores [17].

The limitations of this study are as follows: first, the risk of bias was slightly high. The three crossover trials included in this paper only contributed data from the first stage to this analysis; thus, the testing power was reduced. In addition, the affected region of the brain is a factor that influences spasticity after stroke, and subgroup analyses of the main muscle groups in the context of lower extremity spasticity were not conducted. The MAS, FMA, and MBI are semiquantitative indicators, and the evaluators may have introduced subjectivity when assessing them. More large-scale and high-quality randomized controlled trials with targeted and precise quantitative indicators as outcomes are expected in the future.

In summary, rTMS was effective in improving spasticity and activities of daily living in patients with lower limb spasticity after stroke. LF-rTMS had a positive effect on enhancing motor function.

Data Availability

All the data supporting this systematic review and meta-analysis are included in this study.

Disclosure

Yu Liu and Hong Li are equal contributors and co-first authors.

Conflicts of Interest

The authors declare no conflicts of interest.

Acknowledgments

This study was funded by the S&T Program of Hebei (2037727D).

Authors' Contributions

Yu Liu and Hong Li designed the work, analysed the data, and drafted the manuscript. Jun Zhang and Qing-qing Zhao screened the literature. Nan-Hao Mei assisted in screening the literature. Jiang Ma revised the work and agreed to be accountable for all aspects of the work.

References

[1] S. L. Paul, V. K. Srikanth, and A. G. Thrift, "The large and growing burden of stroke," *Current Drug Targets*, vol. 8, no. 7, pp. 786–793, 2007.

[2] J. Wissel, A. Manack, and M. Brainin, "Toward an epidemiology of poststroke spasticity," *Neurology*, vol. 80, no. 3, Supplement 2, p. S13, 2013.

[3] S. Pundik, J. McCabe, M. Skelly, C. Tatsuoka, and J. J. Daly, "Association of spasticity and motor dysfunction in chronic stroke," *Annals of Physical and Rehabilitation Medicine*, vol. 62, no. 6, pp. 397–402, 2019.

[4] N. Foley, S. Pereira, K. Salter et al., "Treatment with botulinum toxin improves upper-extremity function post stroke: a systematic review and meta-analysis," *Archives of Physical Medicine and Rehabilitation*, vol. 94, no. 5, pp. 977–989, 2013.

[5] A. Chail, R. K. Saini, P. S. Bhat, K. Srivastava, and V. Chauhan, "Transcranial magnetic stimulation: a review of its evolution and current applications," *Industrial Psychiatry Journal*, vol. 27, no. 2, pp. 172–180, 2018.

[6] C. J. Winstein, J. Stein, R. Arena et al., "Guidelines for adult stroke rehabilitation and recovery: a guideline for healthcare professionals from the American heart association/American stroke association," *Stroke*, vol. 47, no. 6, pp. e98–e169, 2016.

[7] F. Moslemi Haghighi, A. Kordi Yoosefinejad, M. Razeghi, A. Shariat, Z. Bagheri, and K. Rezaei, "The effect of high-frequency repetitive transcranial magnetic stimulation on functional indices of affected upper limb in patients with subacute stroke," *Journal of Biomedical Physics and Engineering*, vol. 11, no. 2, pp. 175–184, 2021.

[8] A. Dionísio, I. C. Duarte, M. Patrício, and M. Castelo-Branco, "The use of repetitive transcranial magnetic stimulation for stroke rehabilitation: a systematic review," *Journal of Stroke and Cerebrovascular Diseases*, vol. 27, no. 1, pp. 1–31, 2018.

[9] F. Fisicaro, G. Lanza, A. A. Grasso et al., "Repetitive transcranial magnetic stimulation in stroke rehabilitation: review of the current evidence and pitfalls," *Therapeutic Advances in Neurological Disorders*, vol. 12, pp. 1756286419878317–1756286419878322, 2019.

[10] A. McIntyre, M. Mirkowski, S. Thompson, A. M. Burhan, T. Miller, and R. Teasell, "A systematic review and meta-analysis on the use of repetitive transcranial magnetic stimulation for spasticity poststroke," *PM&R*, vol. 10, no. 3, pp. 293–302, 2018.

[11] P. Xu, Y. Huang, J. Wang et al., "Repetitive transcranial magnetic stimulation as an alternative therapy for stroke with spasticity: a systematic review and meta-analysis," *Journal of Neurology*, vol. 268, pp. 817–832, Article ID 10058-4, 2020.

[12] J. P. T. Higgins, D. G. Altman, P. C. Gotzsche et al., "The Cochrane Collaboration's tool for assessing risk of bias in randomised trials," *BMJ*, vol. 343, p. d5928, 2011.

[13] S. K. Bhogal, R. W. Teasell, N. C. Foley, and M. R. Speechley, "The PEDro scale provides a more comprehensive measure of methodological quality than the Jadad scale in stroke rehabilitation literature," *Journal of Clinical Epidemiology*, vol. 58, no. 7, pp. 668–673, 2005.

[14] L. Harvey, R. Herbert, and J. Crosbie, "Does stretching induce lasting increases in joint ROM? a systematic review," *Physiotherapy Research International*, vol. 7, no. 1, pp. 1–13, 2010.

[15] M. Rastgoo, S. Naghdi, N. Nakhostin Ansari et al., "Effects of repetitive transcranial magnetic stimulation on lower extremity spasticity and motor function in stroke patients," *Disability & Rehabilitation*, vol. 38, no. 19, pp. 1918–1926, 2016.

[16] A. B. Meseguer-Henarejos, J. Sánchez-Meca, J. A. López-Pina, and R. Carles-Hernández, "Inter-and intra-rater reliability of the Modified Ashworth Scale: a systematic review and meta-analysis," *European Journal of Physical and Rehabilitation Medicine*, vol. 54, no. 4, pp. 576–590, 2017.

[17] W. Hong, Y. Hua, M. Xiang et al., "The effect of botulinum toxin type A combined with repetitive transcranial magnetic stimulation on spasticity of lower limbs in stroke patients," *Chinese Journal of Rehabilitation Medicine*, vol. 31, no. 9, pp. 936–940, 2016.

[18] X. Wan, W. Wang, J. Liu, and T. Tong, "Estimating the sample mean and standard deviation from the sample size, median, range and/or interquartile range," *BMC Medical Research Methodology*, vol. 14, no. 1, p. 135, 2014.

[19] R. Chieffo, F. Giatsidis, R. Santangelo et al., "Repetitive transcranial magnetic stimulation with H-coil coupled with cycling for improving lower limb motor function after stroke: an exploratory study," *Neuromodulation: Journal of the International Neuromodulation Society*, vol. 24, pp. 1–7, 2020.

[20] C. Yijie, "Effects of repetitive transcranial magnetic stimulation on spasm and motor function of lower limbs in patints with stroke," *Chongqing Medical Journal*, vol. 47, no. 25, pp. 3292–3298, 2018.

[21] T. Jing and W. Yan, "Long term efficacy and safety of repetitive transcranial magnetic stimulation combined with repeated injection of botulinum toxin type a in the treatment of spasticity of lower limb muscles spasm after stroke," *Journal of Brain and Nervous Diseases*, vol. 26, no. 5, pp. 272–276, 2018.

[22] Y. Yang, H. Lijie, C. Xiguo, C. Liushuan, and Q. Baoyan, "Effect of repetitive transcranial magnetic stimulation on limb function recovery in stroke patients with lower limb spasm," *Chinese Journal of Physical Medicine and Rehabilitation*, vol. 37, no. 8, pp. 602-603, 2015.

[23] H. Hua-yao, D. Hou-Wei, C. Chao, Z. Yi-xian, and C. Qing-fa, "Rehabilitative effect of low-frequency rTMS combined FES

on lower limb spasm and motor function in patients with subacute ischemic stroke," *Chinese Journal of Cardiovascular Rehabilitation Medicine*, vol. 28, no. 2, pp. 134–138, 2019.

[24] S. Li and G. E. Francisco, "New insights into the pathophysiology of post-stroke spasticity," *Frontiers in Human Neuroscience*, vol. 9, p. 192, 2015.

[25] C. B. Ivanhoe and T. A. Reistetter, "Spasticity: the misunderstood part of the upper motor neuron syndrome," *American Journal of Physical Medicine and Rehabilitation*, vol. 83, no. 10 Suppl, pp. S3–S9, 2004.

[26] D. M. Miller, C. S. Klein, N. L. Suresh, and W. Z. Rymer, "Asymmetries in vestibular evoked myogenic potentials in chronic stroke survivors with spastic hypertonia: evidence for a vestibulospinal role," *Clinical Neurophysiology*, vol. 125, no. 10, pp. 2070–2078, 2014.

[27] A. Thibaut, C. Chatelle, E. Ziegler, M.-A. Bruno, S. Laureys, and O. Gosseries, "Spasticity after stroke: physiology, assessment and treatment," *Brain Injury*, vol. 27, no. 10, pp. 1093–1105, 2013.

[28] S. Naghdi, N. N. Ansari, M. Rastgoo, B. Forogh, S. Jalaie, and G. Olyaei, "A pilot study on the effects of low frequency repetitive transcranial magnetic stimulation on lower extremity spasticity and motor neuron excitability in patients after stroke," *Journal of Bodywork and Movement Therapies*, vol. 19, no. 4, pp. 616–623, 2015.

[29] L. Terreaux, R. Gross, F. Leboeuf et al., "Benefits of repetitive transcranial magnetic stimulation (rTMS) for spastic subjects: clinical, functional, and biomechanical parameters for lower limb and walking in five hemiparetic patients," *Science World Journal*, vol. 2014, Article ID 389350, 2014.

[30] D. Podsiadlo and S. Richardson, "The timed "up & go:" a test of basic functional mobility for frail elderly persons," *Journal of the American Geriatrics Society*, vol. 39, no. 2, pp. 142–148, 1991.

[31] M. Kobayashi and A. Pascual-Leone, "Transcranial magnetic stimulation in neurology," *The Lancet Neurology*, vol. 2, no. 3, pp. 145–156, 2003.

[32] R. B. C. Dos Santos, S. C. B. Galvão, L. M. P. Frederico et al., "Cortical and spinal excitability changes after repetitive transcranial magnetic stimulation combined to physiotherapy in stroke spastic patients," *Neurological Sciences*, vol. 40, no. 6, pp. 1199–1207, 2019.

[33] N. N. Ansari and S. Naghdi, "The effect of Bobath approach on the excitability of the spinal alpha motor neurones in stroke patients with muscle spasticity," *Electromyography & Clinical Neurophysiology*, vol. 47, no. 1, pp. 29–36, 2007.

[34] C. P. Phadke, C. T. Robertson, E. G. Condliffe, and C. Patten, "Upper-extremity H-reflex measurement post-stroke: reliability and inter-limb differences," *Clinical Neurophysiology*, vol. 123, no. 8, pp. 1606–1615, 2012.

[35] N. N. Ansari and S. Naghdi, "The effect of Bobath approach on the excitability of the spinal alpha motor neurones in stroke patients with muscle spasticity," *Electromyography & Clinical Neurophysiology*, vol. 47, no. 1, pp. 29–36, 2007.

[36] J. M. Hoogendam, G. M. J. Ramakers, and V. Di Lazzaro, "Physiology of repetitive transcranial magnetic stimulation of the human brain," *Brain Stimulation*, vol. 3, no. 2, pp. 95–118, 2010.

[37] Z. Lin and T. Yan, "Long-term effectiveness of neuromuscular electrical stimulation for promoting motor recovery of the upper extremity after stroke," *Journal of Rehabilitation Medicine*, vol. 43, no. 6, pp. 506–510, 2011.

[38] M. Corti, C. Patten, and W. Triggs, "Repetitive transcranial magnetic stimulation of motor cortex after stroke," *American Journal of Physical Medicine & Rehabilitation*, vol. 91, no. 3, pp. 254–270, 2012.

[39] E. H. Hoyer and P. A. Celnik, "Understanding and enhancing motor recovery after stroke using transcranial magnetic stimulation," *Restorative Neurology and Neuroscience*, vol. 29, no. 6, pp. 395–409, 2011.

[40] J.-P. Lefaucheur, A. Aleman, C. Baeken et al., "Evidence-based guidelines on the therapeutic use of repetitive transcranial magnetic stimulation (rTMS): an update (2014-2018)," *Clinical Neurophysiology*, vol. 131, no. 2, pp. 474–528, 2020.

[41] Z. Guo, Y. Jin, X. Bai et al., "Distinction of high- and low-frequency repetitive transcranial magnetic stimulation on the functional reorganization of the motor network in stroke patients," *Neural Plasticity*, vol. 2021, Article ID 8873221, 2021.

[42] Y. Roth, A. Zangen, and M. Hallett, "A coil design for transcranial magnetic stimulation of deep brain regions," *Journal of Clinical Neurophysiology*, vol. 19, no. 4, pp. 361–370, 2002.

Hindawi
Evidence-Based Complementary and Alternative Medicine
Volume 2021, Article ID 8534466, 16 pages
https://doi.org/10.1155/2021/8534466

Research Article

Effects of Noninvasive Low-Intensity Focus Ultrasound Neuromodulation on Spinal Cord Neurocircuits In Vivo

Ye-Hui Liao,[1,2] **Mo-Xian Chen**,[1] **Shao-Chun Chen**,[1] **Kai-Xuan Luo**,[1] **Bin Wang**,[1] **Yao Liu**,[1] **and Li-Juan Ao**[1]

[1]*School of Rehabilitation, Kunming Medical University, Kunming 650500, Yunnan Province, China*
[2]*Department of Orthopaedics, Affiliated Hospital of Southwest Medical University, Luzhou 646000, Sichuan Province, China*

Correspondence should be addressed to Yao Liu; 175381219@qq.com and Li-Juan Ao; aolijuan@kmmu.edu.cn

Received 7 September 2021; Revised 8 October 2021; Accepted 26 October 2021; Published 27 November 2021

Academic Editor: Feng Zhang

Although neurocircuits can be activated by focused ultrasound stimulation, it is unclear whether this is also true for spinal cord neurocircuits. In this study, we used low-intensity focused ultrasound (LIFU) to stimulate lumbar 4–lumbar 5 (L4–L5) segments of the spinal cord of normal Sprague Dawley rats with a clapper. The activation of the spinal cord neurocircuits enhanced soleus muscle contraction as measured by electromyography (EMG). Neuronal activation and injury were assessed by EMG, western blotting (WB), immunofluorescence, hematoxylin and eosin (H&E) staining, Nissl staining, enzyme-linked immunosorbent assay (ELISA), immunohistochemistry (IHC), somatosensory evoked potentials (SEPs), motor evoked potentials (MEPs), and the Basso–Beattie–Bresnahan locomotor rating scale. When the LIFU intensity was more than 0.5 MPa, LIFU stimulation induced soleus muscle contraction and increased the EMG amplitudes ($P < 0.05$) and the number of c-fos- and GAD65-positive cells ($P < 0.05$). When the LIFU intensity was 3.0 MPa, the LIFU stimulation led to spinal cord damage and decreased SEP amplitudes for electrophysiological assessment ($P < 0.05$); this resulted in coagulation necrosis, structural destruction, neuronal loss in the dorsal horn by H&E and Nissl staining, and increased expression of GFAP, IL-1β, TNF-α, and caspase-3 by IHC, ELISA, and WB ($P < 0.05$). These results show that LIFU can activate spinal cord neurocircuits and that LIFU stimulation with an irradiation intensity ≤1.5 MPa is a safe neurostimulation method for the spinal cord.

1. Introduction

Neurostimulation technology, including focused ultrasound stimulation, transcranial magnetic stimulation (TMS), deep brain stimulation (DBS), and optogenetic stimulation, has become an important neuromodulation method for various neurological conditions. TMS is a noninvasive or minimally invasive neurostimulation technique, which has been widely used for neuromodulation. TMS has advantages for superficial brain regions, while its effects on deeper brain regions are limited given its poor spatial resolution [1]. DBS, including electrical stimulation or epidural electrical stimulation, is a commonly used neurostimulation method. Epidural stimulation of the spinal cord plays a positive role in the functional recovery of the injured spinal cord [2, 3]. However, because of the highly diffuse electric field and lower spatial resolution, it is difficult to locate a specific area of interest using electrical stimulation [4]. Moreover, surgery is also required, and the electrode is inserted in or on the cerebral cortex or epidural space for electrical stimulation [2]. Optogenetic stimulation also requires invasive procedures and genetic manipulation, which are not feasible in humans [5, 6]. Recently, focused ultrasound has attracted much attention and interest due to its high spatial resolution, noninvasive neurostimulation, and effective stimulation of the deep tissues with submillimeter static resolution [7, 8]. Consequently, it has become an alternative modality for neuromodulation [9].

Ultrasound is a mechanical pressure wave with a frequency of >20 kHz, which can be transmitted through bone and soft tissues. An acoustic intensity <500 mw/cm^2 (low-intensity ultrasound) has shown significant biological effects

without producing thermal effects or tissue damage [10, 11]. Moreover, many studies have confirmed that low-intensity ultrasound stimulation can inhibit or stimulate neurons both in vitro and in vivo. Recent research has shown that low-intensity, low-frequency ultrasound stimulation of hippocampal slices excites the neurons and network activity by activating voltage-gated sodium and calcium channels [12, 13]. Further studies have confirmed that low-intensity focused ultrasound (LIFU) activates neurocircuits in both model organisms and humans. Indeed, pulsed focused ultrasonic stimulation has been shown to effectively induce nerve responses and action potentials in the giant fibers of invertebrate animals [14, 15]. Moreover, precise stimulation of the deep brain nuclei and modulation of brain neuronal activity [16–19] have been shown to induce muscle contraction of the limbs of rats and rabbits, as verified by electromyography (EMG) [20, 21]. Primate studies have also found that focused ultrasound stimulation of the brains of two awake macaque rhesus monkeys significantly modulates high-level cognitive behavior [22]. Gavrilov [23] confirmed that ultrasound could induce tactile, thermal, and pain sensations by activation of somatosensory neurons in humans. As a result, low-intensity ultrasound, especially LIFU, has gained widespread attention as a potential clinical neuromodulation technology.

The spinal cord contains complex neurocircuits, the stimulation of which is an important method to treat chronic spine-related conditions, such as failed back surgery syndrome, complex regional pain syndrome, painful diabetic neuropathy, and spinal cord injury [3, 24–28]. Recently, there has been growing interest in ultrasound neuromodulation; however, little is known about whether spinal cord stimulation with LIFU can activate or inhibit spinal cord neurocircuits and whether such stimulation causes injury to the spinal cord. Activation of the spinal cord neurocircuits can induce muscle contractions and produce action potentials, which can be measured by EMG [20]. In this study, LIFU was used to stimulate the L4–L5 segments of the spinal cord in Sprague Dawley (SD) rats, and EMG was used to measure the stimulation success of the spinal cord neurocircuits. Hematoxylin and eosin (H&E) staining, Nissl staining, and biomarker tests were used to evaluate the safety of LIFU stimulation.

2. Materials and Methods

2.1. Animals. Adult male SD rats weighing 220–300 g were acquired from the Kunming Laboratory Animal Center for experimental use. All of the animal protocols were approved by the Animal Ethics Committee of Kunming Medical University (KMMU2020352). All rats were housed at a temperature of 25 ± 2°C with a 12/12-h light/dark cycle, and all rats had free access to food and water.

2.2. Experimental Protocol. After 1 week of adaptation, the SD rats were used for the experiment. The study comprised two protocols. The first study (Study I, $n = 6$) was designed to test the activation of the spinal cord neurocircuits by LIFU stimulation. In this study, the rats were anesthetized with isoflurane (1.5%), and EMG was used to measure the recruitment of the soleus (Sol) muscle when the rats received different acoustic pressure stimulations (radiation intensity (RI) = 0 MPa ($I_{spta} = 0$ mw/cm^2), 0.5 MPa ($I_{spta} = 60$ mw/cm^2), 1.0 MPa ($I_{spta} = 180$ mW/cm^2), 1.5 MPa ($I_{spta} = 320$ mw/cm^2), 2.0 MPa ($I_{spta} = 400$ mw/cm^2), 2.5 MPa ($I_{spta} = 500$ mw/cm^2), or 3.0 MPa ($I_{spta} = 600$ mw/cm^2)) with 20% duty cycle (DC). There was a 5 min interval between different ultrasonic parameter tests. The study protocol is shown in Figure 1(a).

In the second study (Study II, $n = 42$), the safety of LIFU stimulation was detected by electrophysiology, neuromotor function, H&E staining, Nissl staining, enzyme-linked immunosorbent assay (ELISA), and biomarker tests. The rats were divided into four groups as follows: the negative LIFU stimulation group (LIFU$^-$ group, RI = 0 MPa, $n = 6$), the LIFU stimulation 1 group (LIFU^{+1} group, RI = 0.5 MPa, $n = 12$), the LIFU stimulation 2 group (LIFU^{+2} group, RI = 1.5 MPa, $n = 12$), and the LIFU stimulation 3 group (LIFU^{+3} group, RI = 3.0 MPa, $n = 12$). After anesthesia with isoflurane (1.5%), the rats were stimulated with LIFU for 20 min. After LIFU treatment, the safety test was performed according to the protocol shown in Figure 1(b).

2.3. LIFU Stimulation. The LIFU stimulation procedure was performed as follows [29]: after anesthesia, the rats were fixed on a table, and the hair on their backs was removed using a depilating cream to expose the L4–L5 segments of the spinal cord. An ultrasound probe was fixed to the back of the L4–L5 spinal cord segment with a clapper. An ultrasound gel was used to fill the space between the skin and the ultrasound probe. A waveform signal was generated by a two-channel function/arbitrary waveform generator (DG4202, RIGOL, China) and was amplified with a 50 W power amplifier (Dahan Radio Studio, China). The amplified signal activated the ultrasonic probe. Channel I was set to deliver the wave signal with cycles of 1000 Hz/s, a burst duration of 1 s, and a 20% total duty cycle. Channel II was set to deliver the ultrasound probe with a frequency of 4 MHz and 800 cycles for every pulse period (Figures 2(a)–2(b)). The acoustic pressure of the ultrasound was measured using a hydrophone (Onda HNP-1000, ONDA Corporation, Sunnyvale, CA, USA) in a water tank (Figures 2(c)–2(e)).

2.4. Neuromotor Function Assessment. The Basso–Beattie–Bresnahan locomotor rating scale (BBB scale) was used for the hind limb neuromotor function assessment pre- and post-LIFU. The assessment was performed as previously described [30]. The BBB rating scale assesses the coordination of limb movement, paw placement, and tail balance. The scale ranges from 0 to 21 points, where 0 is defined as no visible movement of the legs, and 21 is defined as normal neuromotor function, i.e., the rat can walk continually on the paws, with consistent plantar stepping, coordinated gait, trunk stability, a cocked tail, and parallel throughout the stance.

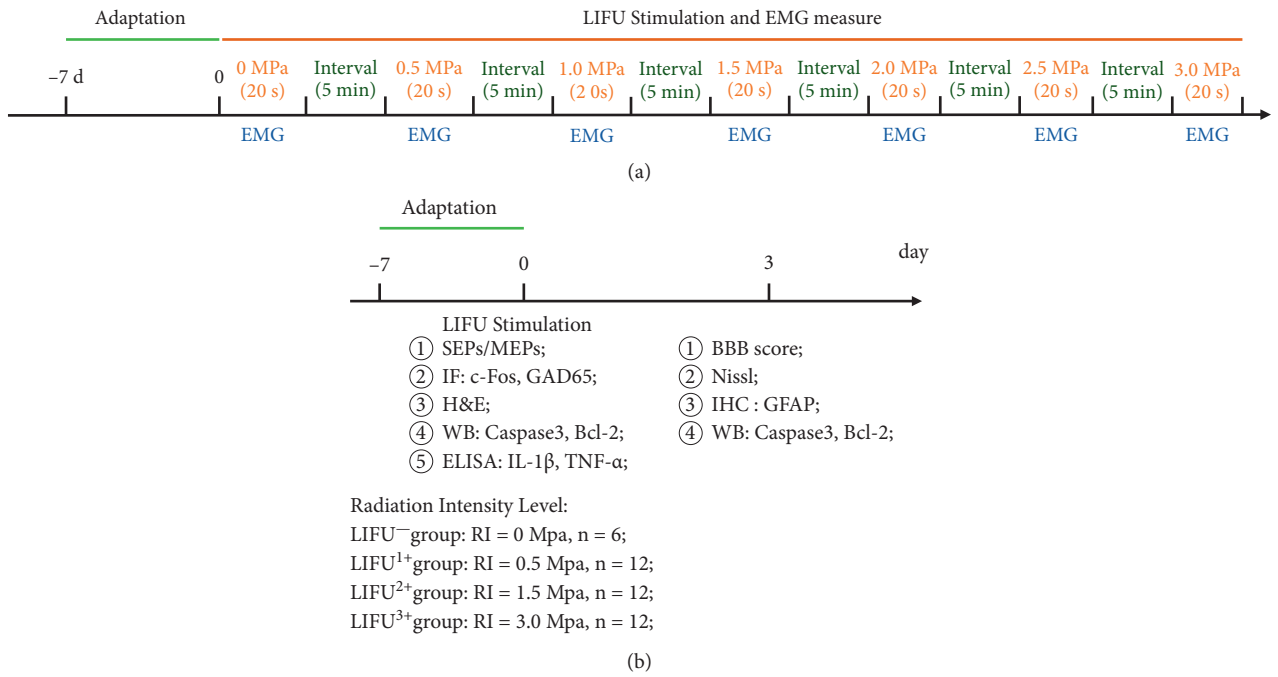

Figure 1: Timeline of study I (a) and II (b) experimental protocols. The rats were killed, and the safety was examined on days 0 and 3 post-low-intensity focused ultrasound (LIFU) stimulation.

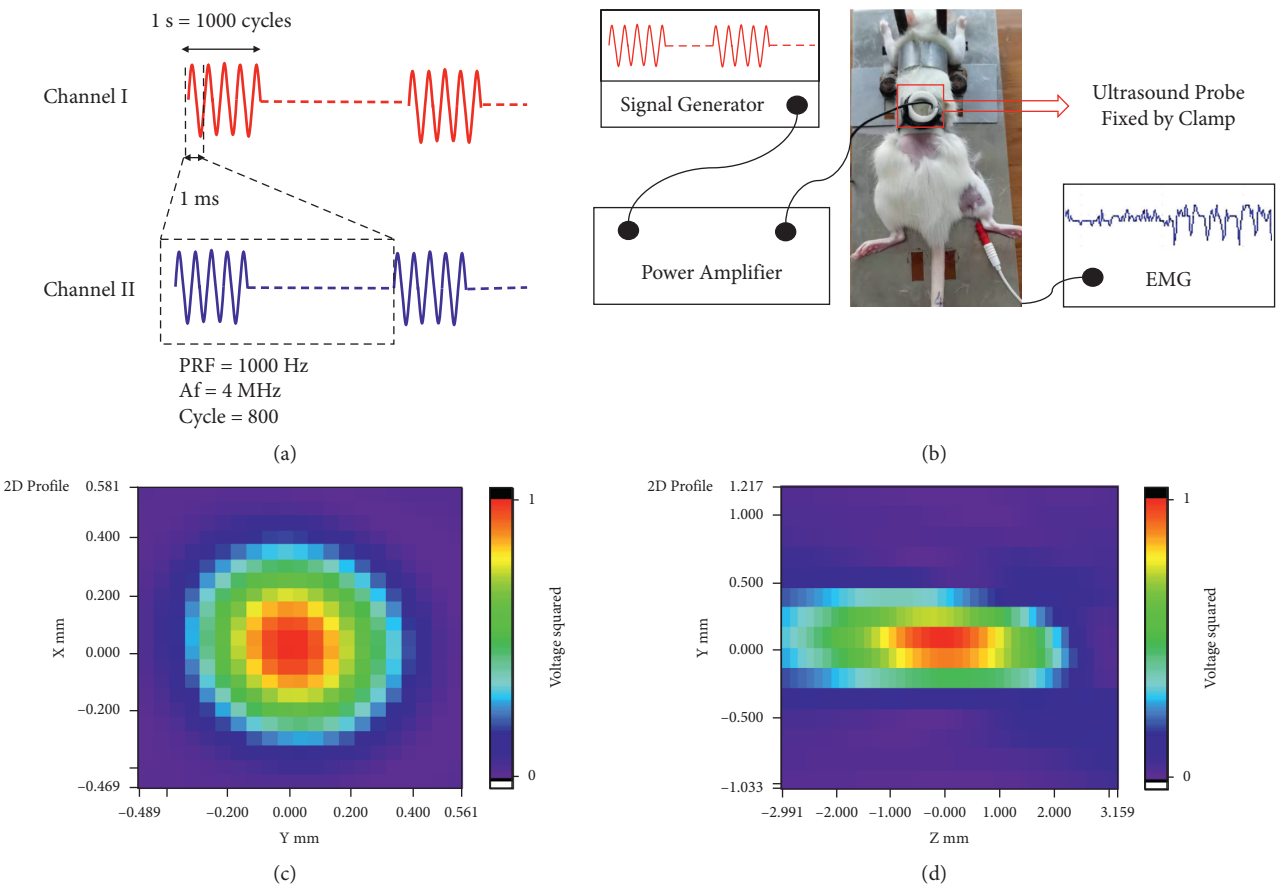

Figure 2: Continued.

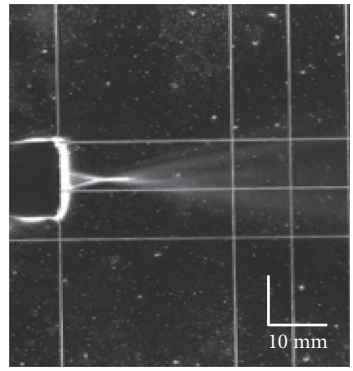

(e)

Figure 2: (a) Schematic of the LIFU pulsing strategy. (b) Schematic of LIFU stimulation of the spinal cord and electromyography (EMG) examination. The signal was generated by the generator, amplified by the amplifier, and then converted into an acoustic signal by the ultrasound probe. The ultrasound probe was fixed by the clamp on the back of the rats at the segment L4–L5 spinal cord level. The recruitment of the soleus muscle was recorded at the time of LIFU spinal cord stimulation. (c–e) Parameters of focal ultrasound, including the acoustic-intensity distribution map from transverse and sagittal planes.

2.5. Electrophysiology Test. The recruitment of Sol muscle was used to assess the activation of spinal neurocircuits and was measured by EMG using an electromyographic evoked potentiometer (Neuropack® S1 MEB-9400, Nihon Kohden, Japan). EMG was conducted as described previously [31, 32]. Briefly, the EMG signal was measured by a concentric circular electrode that was percutaneously inserted into the Sol, and the reference electrode was percutaneously inserted into the tail. The EMG signal was recorded at the same time as the LIFU stimulation of the spinal cord and was filtered at 200 Hz–5 kHz (Figure 2(b)). The amplitude (intensity of recruitment of Sol) was measured between consecutive peaks, i.e., from the positive peak to the neighboring negative peak (μV).

Somatosensory evoked potentials (SEPs) and motor evoked potentials (MEPs) were used to assess the conduction function after the white and gray matter injury of the spinal cord [33]. For the SEP test [34, 35], the recording electrode was placed on the left sensorimotor cortex, the reference electrode was inserted under the skin of the nose, the stimulation electrodes were inserted under the skin of the right ankle, and the ground needle electrode was percutaneously placed in the tail. The stimulation involved sine impulses with a trigger frequency of 2 Hz and an intensity of 3 mA. Signal data (including the latency and amplitude) were recorded from the electrode placed on the sensorimotor cortex and were filtered with a bandpass (10–2000 Hz); we recorded 100 evoked potentials on average for two times with 5 min interval. The latency was defined as the time (ms) between the onset of the stimulus artifact and the first peak (positive or negative). The amplitude (μV) was measured from the positive peak to the negative peak.

For the MEP test, the stimulation electrode was placed on the left motor cortex, the recording electrode was percutaneously inserted into the right fifth palmar interosseous muscle, and the reference and ground needle electrodes were placed as outlined for the SEP test. The stimulation involved sine impulses with an intensity of 4 mA. An analog amplifier (Model 1700 Differential AC Amplifier, AM Systems, USA) was used for amplification (100×), filtering (10 Hz–10 kHz, bandpass), and recording of MEP signals. The latency was defined as the time (ms) between the onset of the stimulus artifact and the first peak (positive or negative).

The EMG, SEPs, and MEPs data were visualized and recorded on a computer for further analysis using a software interface (Signal, Cambridge Electronics Design Ltd., United Kingdom).

2.6. Tissue Preparation. After neuromotor function and electrophysiology assessment, the rats were killed by an overdose of 1% sodium pentobarbital (40 mg/kg). Then, the tissues were collected for western blot, ELISA, and H&E staining, Nissl staining, immunofluorescence staining, and IHC staining. For western blot and ELISA, L4–L5 spinal cord segments were immediately collected and stored at −80°C until use. For the H&E staining, Nissl staining, immunofluorescence staining, and IHC staining, the rats were perfused with 200 mL of 0.1 M phosphate-buffered saline (PBS) and then with 200 mL PBS with 4% paraformaldehyde (pH 7.4). The L4–L5 spinal cord segments were collected, fixed in 4% paraformaldehyde overnight, dehydrated, and embedded in paraffin. Finally, transverse section slices (5 μm thick) of the spinal cord were prepared for H&E staining, Nissl staining, immunofluorescence staining, and IHC staining.

2.7. Western Blotting. The spinal cord tissue (0.1 g) was dissected, ultrasonically homogenized, and lysed with PIPA buffer (RIPA : PMSF = 1 mL : 10 μL) on ice for 30 min. After centrifugation at 12000 r/min for 20 min at 4°C, the supernatant was collected. The concentration of the total protein was quantified using a bicinchoninic acid assay (Enhanced BCA Protein Assay Kit, Beyotime, China), and all samples were equalized to 30 μg/10 μL. The samples (30 μg total protein) were resolved by 10% sodium dodecyl sulfate-

polyacrylamide gel electrophoresis (SDS-PAGE) and transferred to polyvinylidene difluoride membranes (PVDFs, Millipore, MA, USA). The membranes were blocked with 5% fat-free milk at room temperature for 2 h and incubated with primary antibodies at 4°C with gentle shaking overnight. The primary antibodies included polyclonal antibodies against caspase-3 (1 : 2000, Proteintech, USA), polyclonal antibodies against Bcl-2 (1 : 2000, Proteintech, USA), and β-actin (1 : 2000, Santa, USA). Following incubation, the membranes were incubated with the secondary antibody, peroxidase-conjugated AffiniPure goat anti-mouse/rabbit IgG (H + L) (1 : 2000, ZSGB-BIO, China) for 2 h at room temperature. Finally, the protein bands were visualized and quantified using enhanced chemiluminescence (Tanon, Shanghai, China) and the image processing system ImageJ (Rawak Software, Stuttgart, Germany). The protein concentrations were normalized to β-actin.

2.8. ELISA for IL-1β and TNF-α. The expression levels of the inflammatory factors IL-1β and TNF-α in the spinal cord were examined after ultrasound stimulation. Spinal cord tissue (0.1 g) was cut into pieces with ophthalmic scissors after adding precooled 0.1 M PBS (1 mL). Then, the cut tissues were placed in a glass homogenizer and homogenized on ice for 8 min. After centrifugation at 4°C and 5000 r/min for 5 min, the supernatant was obtained, and the total protein concentration was quantified by the bicinchoninic acid assay (Enhanced BCA Protein Assay Kit, Beyotime, China). The ELISA was performed in accordance with the instructions for IL-1β (Bioswamp, RA20020, China: http://www.bio-swamp.com/upload/file/201711/1510793514933161.pdf) and TNF-α (Bioswamp, RA20035, China: http://www.bio-swamp.com/upload/file/201910/1571017094579621.pdf).

2.9. H&E Staining and Nissl Staining. H&E staining and Nissl staining were used to assess the safety of LIFU for use in the spinal cord. The H&E staining was performed as follows: the slices were dewaxed, dehydrated, stained with H&E solution, cleared with xylene, and mounted with resin. Toluidine blue was used to stain for Nissl using the following procedure: the slices were dewaxed, rinsed with tap water, treated with toluidine blue, dehydrated, and sealed with neutral gum. Images of H&E staining and Nissl staining were captured using an optical microscope (Olympus Corporation, Tokyo, Japan). The Nissl substance was identified as navy or dark blue with a light blue or light background.

2.10. Immunofluorescence Staining and IHC Staining. For immunofluorescence staining and IHC staining, paraffin sections (5 μm thick) were prepared. First, the sections were subjected to dewaxing, antigen repair, and H_2O_2 elimination of endogenous peroxidase. For immunofluorescence staining, the slices were incubated with 5% goat serum and 0.03% Triton X-100 in 0.1 M PBS for 2 h. Then, the slices were incubated with primary antibodies, including monoclonal antibodies against c-fos (1 : 200, Proteintech, USA) and GAD65 (1 : 200, CST, USA), at 4°C overnight. Following incubation, the slices were incubated with secondary antibodies, including anti-rabbit IgG (H + L), F(ab′)2 fragment (Alexa Fluor® 594 Conjugate) and anti-mouse IgG (H + L), F(ab′)2 fragment (Alexa Fluor® 488 Conjugate) at room temperature in the dark for 2 h. After 3 × 10 min washing with PBS, the sections were incubated with 4′, 6-diamidino-2-phenylindole (DAPI; Sigma, USA). The images were captured via a fluorescence microscope (Olympus Corporation, Tokyo, Japan), and ImageJ software (NIH, Bethesda, MD, USA) was used to quantify the number of positive cells.

For IHC, the slides were incubated with the primary antibody GFAP (1 : 1000, Cell Signaling, USA) at 4°C overnight. Then, the slides were incubated with secondary antibody labeled with poly-HRP anti-rabbit IgG (1 : 1; Beijing Zhongshan Golden Bridge Biotechnology) for 50 min. After staining with DAB for 20 s and counterstaining with hematoxylin for 8 min at room temperature, the images were captured via a light microscope (Olympus Corporation, Tokyo, Japan), and ImageJ software (Rawak Software) was used to quantify the density of positive regions.

2.11. Statistical Analyses. The data are presented as the mean ± standard error of mean (SEM). SPSS 23.0 (IBM Corp., Armonk, NY, USA) was used for all statistical analyses, and GraphPad Prism software version 8.0 (GraphPad Software Inc., San Diego, CA, USA) was used to prepare the graphs. The amplitude of EMG, the gray intensity of western blot, the number of positive cells in immunofluorescence, and the density data for IHC were calculated. After verifying that all data satisfied the normality of distribution, differences among different intensities of stimulation were determined using analysis of variance (ANOVA). When an ANOVA showed a significant difference, Fisher's protected least significant difference (LSD) tests were used for pairwise comparisons. Differences between pre- and post-LIFU stimulation were analyzed using paired t-tests. Two-tailed P values <0.05 were considered statistically significant.

3. Results

3.1. LIFU Stimulation Enhances the Recruitment of Sol Muscle. As shown in Figure 3, LIFU simulation of the spinal cord enhanced the recruitment of Sol muscle. When the LIFU intensity was >0.5 MPa, the recruitment of Sol muscle was measured on EMG. With the increase in the stimulation intensity, the recruitment intensity (Amp, μV) of the Sol muscle also increased (Supplementary Figure 1). When the stimulation intensity was >1.0 MPa, LIFU ON induced significant muscle recruitment and the EMG amplitude was significantly higher than that at LIFU OFF stimulation ($P < 0.05$). There was no significant difference in the amplitude among LIFU OFF time point ($P > 0.05$) (Supplementary Figure 1).

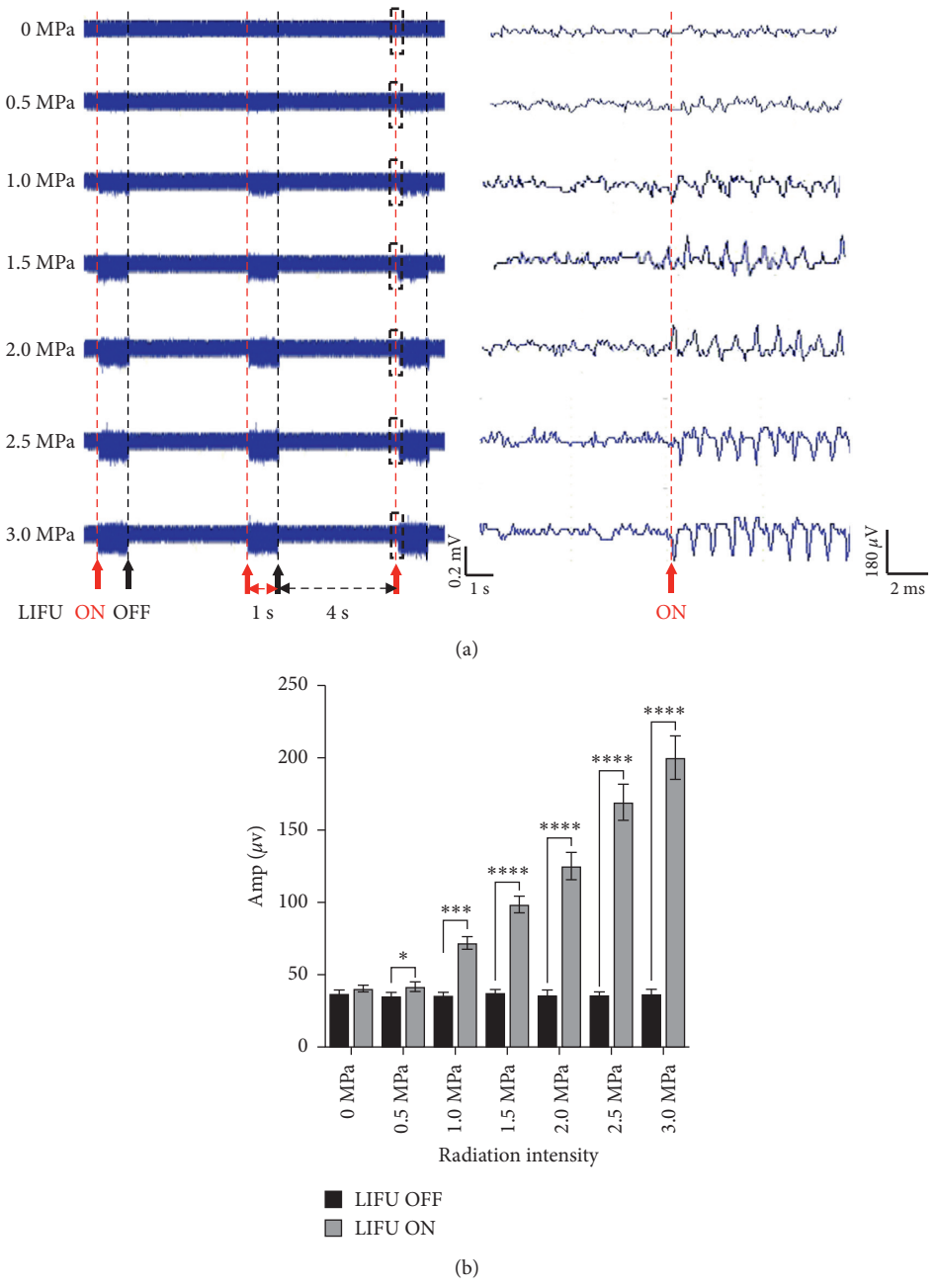

Figure 3: Electromyography (EMG) shows the recruitment of the soleus (Sol) muscle by different intensities of LIFU stimulation. (a) The red arrow shows the moment at which the LIFU was initiated, and the black arrow shows the moment at which the LIFU was stopped. The duration (LIFU on) from the red arrow to the black arrow was 1 s and that from the black to the red arrow (LIFU turned off) was 4 s. The black dotted rectangle shows the recruitment of Sol muscle and activation of EMG. (b) Amplitude of EMG after different irradiation intensity stimulations. $^{*}P < 0.05$, $^{***}P < 0.01$, and $^{****}P < 0.0001$. Each symbol represents the mean ± SEM; paired *t-test*; $n = 6$ rats per assay.

3.2. LIFU Stimulation Enhances the Number of c-fos- and GAD65-Positive Cells. c-fos and GAD65 were used as markers of neuronal and synaptic activity, respectively. Neuronal activation can increase the number of c-fos-positive cells and GAD65-positive cells [36, 37]. We found that the numbers of c-fos-positive cells increased after 0.5 MPa, 1.5 MPa, and 3.0 MPa stimulation and that those of GAD65-positive cells increased after 0.5 MPa and 1.5 MPa stimulation compared to stimulation with 0 MPa (negative stimulation) ($P < 0.05$). However, the highest number of c-fos- and GAD65-positive cells was found in the 1.5 MPa stimulation group (Figure 4).

3.3. Neuromotor Function and Electrophysiological Assessment. The safety of LIFU stimulation was examined at different irradiation intensities (0 MPa, 0.5 MPa, 1.5 MPa, and 3.0 MPa). After ultrasonic stimulation with different

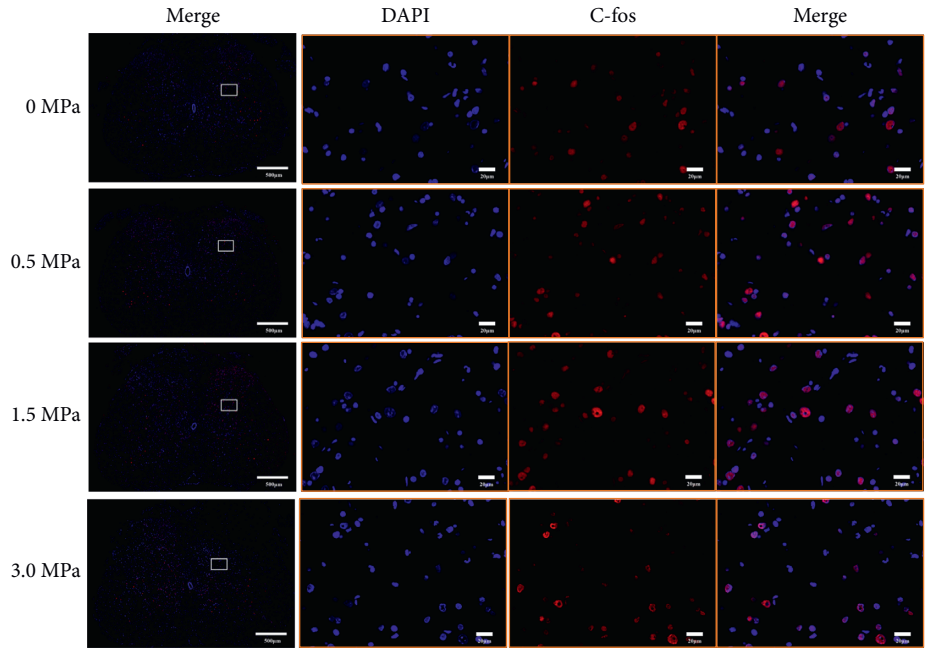

(a)

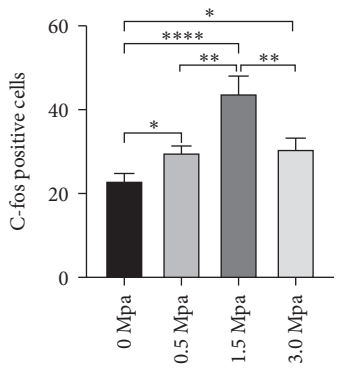

(b)

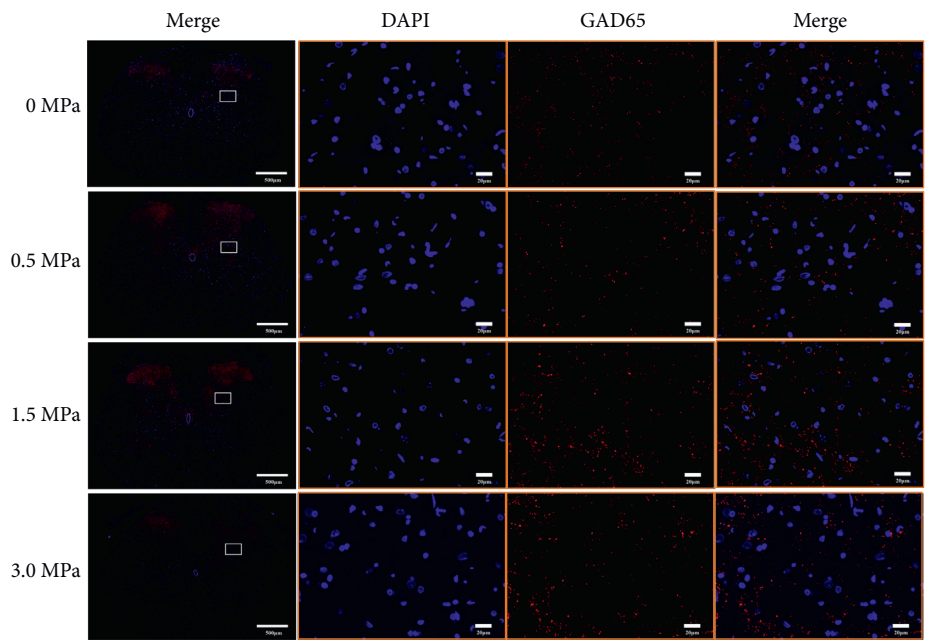

(c)

Figure 4: Continued.

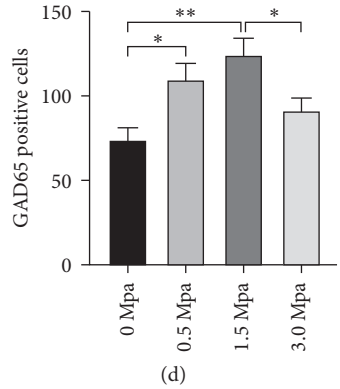

Figure 4: The effect of LIFU stimulation on neuron and synaptic activation in the lumbar spinal cord (×40 and ×400). Scale bar = 500 μm and 20 μm. (a, c) Representative immunofluorescence pictures showing the c-fos-positive (a) and GAD65-positive (c) cells after different intensities of LIFU stimulation of the lumbar spinal cord. (b, d) C-fos- and GAD65-positive cells after different intensities of stimulation. $^{*}P < 0.05$, $^{***}P < 0.01$, and $^{****}P < 0.0001$. Each symbol represents the mean ± SEM; one-way ANOVA, followed by LSD test for pairwise comparisons; $n = 3$ rats per assay.

intensities, the rats showed no changes in BBB score and latency of SEPs and MEPs (Supplementary Figure 2), except that the 3.0 MPa group had decreased SEP amplitudes (Figure 5).

3.4. Inflammatory Factors and Histological Examination. Spinal cord injuries can lead to high expression of inflammatory factors, such as IL-1β and TNF-α. According to the ELISA results, stimulation with 0.5 MPa and 1.5 MPa LIFU did not significantly increase the expression of IL-1β and TNF-α compared to the negative stimulation (0 MPa). In contrast, 3.0 MPa stimulation significantly increased the expression of IL-1β and TNF-α compared to 0 MPa and 0.5 MPa irradiation intensities ($P < 0.05$) (Figure 6).

Among the LIFU^{0+}, LIFU^{1+}, and LIFU^{2+} groups, we found no erythrocyte exudation (or bleeding), immune cell infiltration, or coagulative necrosis in H and E staining, no decrease in the numbers of Nissl bodies in Nissl staining, and no significant difference in the fluorescence intensity of GFAP (Figures 7–9). However, in the LIFU^{3+} group, H&E staining revealed coagulation necrosis of the dorsal horn, especially at the right lateral portion (Figure 7). In the LIFU^{3+} group, Nissl staining also showed significant necrosis on the right side of the dorsal horn, with structural destruction and loss of neurons, and the Nissl bodies showed condensation and darker staining (Figure 8). In the LIFU^{3+} group, the intensity of GFAP also increased compared to that of the LIFU^{0+}, LIFU^{1+}, and LIFU^{2+} groups ($P < 0.05$) (Figure 9).

3.5. Western Blot. We also examined the expression levels of caspase-3 and Bcl-2 as proapoptotic and antiapoptotic markers, respectively. According to the results of western blotting, the expression levels of caspase-3 and Bcl-2 remained unchanged on day 0 after different irradiation intensity stimulations ($P > 0.05$). On day 3 after LIFU stimulation, the 3.0 MPa stimulation significantly increased the expression of caspase-3 and Bcl-2 compared to 0 MPa and 0.5 MPa stimulations ($P < 0.05$), while there was no significant difference among 0 MPa, 0.5 MPa, and 1.5 MPa stimulations ($P > 0.05$) (Figure 10).

4. Discussion

After Wall and Melzack [38] first proposed the concept that "control of pain may be achieved by selectively activating the large, rapidly conducting fibers," spinal cord stimulation has evolved significantly over the past decades [39]. Clinically, spinal cord stimulation or neuromodulation has attracted much attention in the management of chronic spinal conditions, especially for chronic spinal-related pain, such as failed back surgery syndrome/postlaminectomy syndrome, complex regional pain syndrome, and peripheral neuropathic pain [28]. In the past, spinal cord stimulation was induced by electrodes placed in the epidural space with pulse currents of different stimulation modalities, including high-frequency technology, bust stimulation, or other paradigms [40–43]. The electric field formed by electrical stimulation between the electrodes can transfer a specific amount of charge, thus altering the neuronal membrane potential, which is the basis of nerve recruitment [44]. The current study is the first to explore spinal cord neuromodulation with percutaneous LIFU stimulation.

The previous study found that LIFU stimulation of the brain or peripheral nerves can elicit electrophysiological changes [20]. For example, LIFU stimulation of the L5 dorsal root ganglion (DRG) or applied to a peripheral nerve in situ can also alter nerve function, including an increase in mechanical and thermal thresholds and suppression of compound action potentials and sensory action potentials in a neuropathic pain model [45, 46]. Moreover, transcranial LIFU stimulation of the motor cortex activates neurons and evokes motor behavior, and the muscle contraction of limbs has been verified by EMG [20, 21]. In this study, we successfully activated the neurocircuits of the spinal cord by

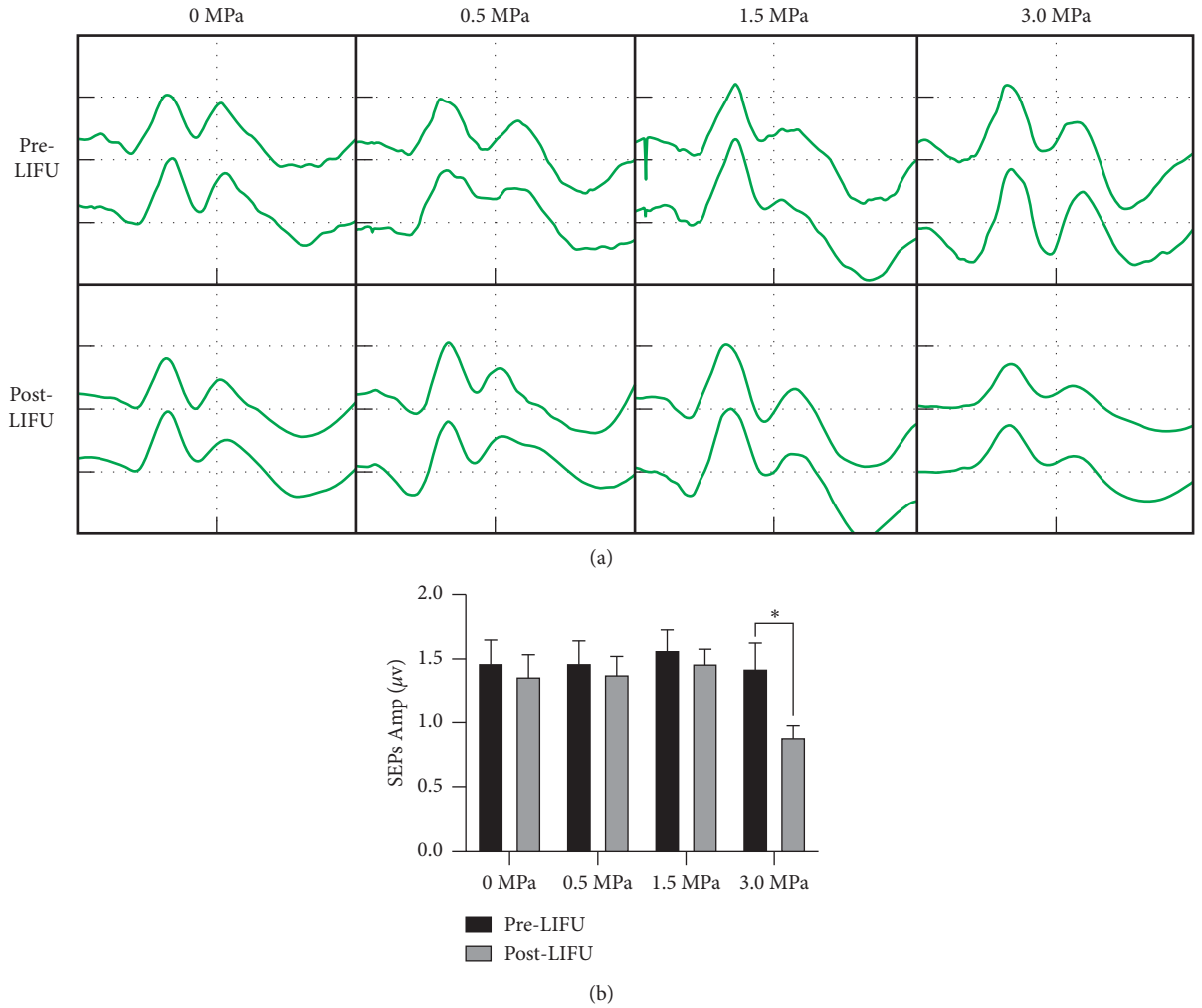

Figure 5: (a) Somatosensory evoked potentials (SEPs) were used to detect somatosensory conduction from the spinal cord. (b) SEP amplitude analyses for different intensities of stimulation. Each symbol represents the mean ± SEM; paired *t-test*; $n = 6$ rats per assay.

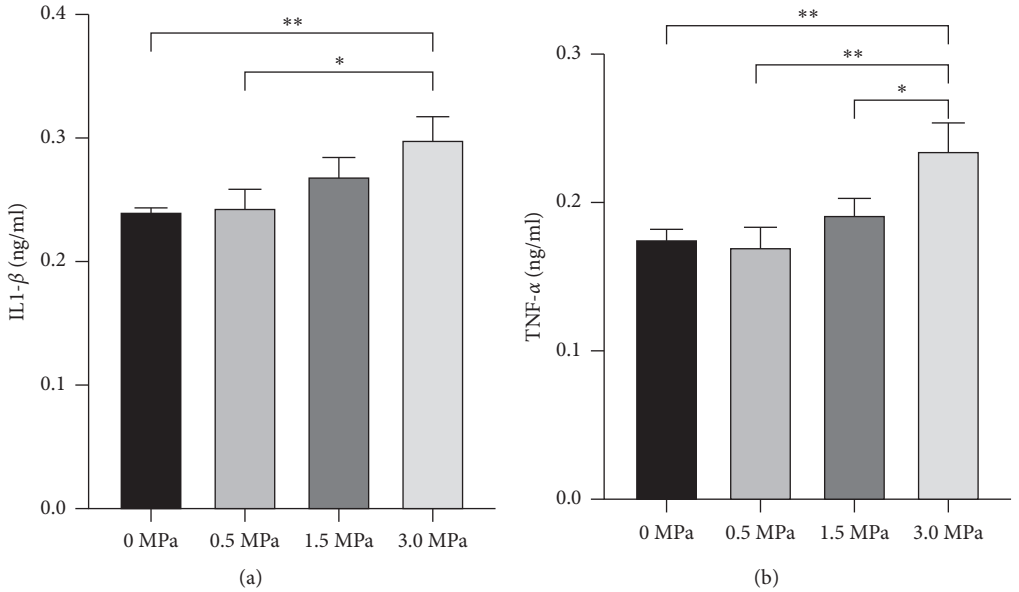

Figure 6: Enzyme-linked immunosorbent assay (ELISA) for detection of the inflammatory factors IL-1β (a) and TNF-α (b). $^{*}P < 0.05$ and $^{**}P < 0.01$. Each symbol represents the mean ± SEM; one-way ANOVA, followed by LSD test for pairwise comparisons; $n = 3$ rats per assay.

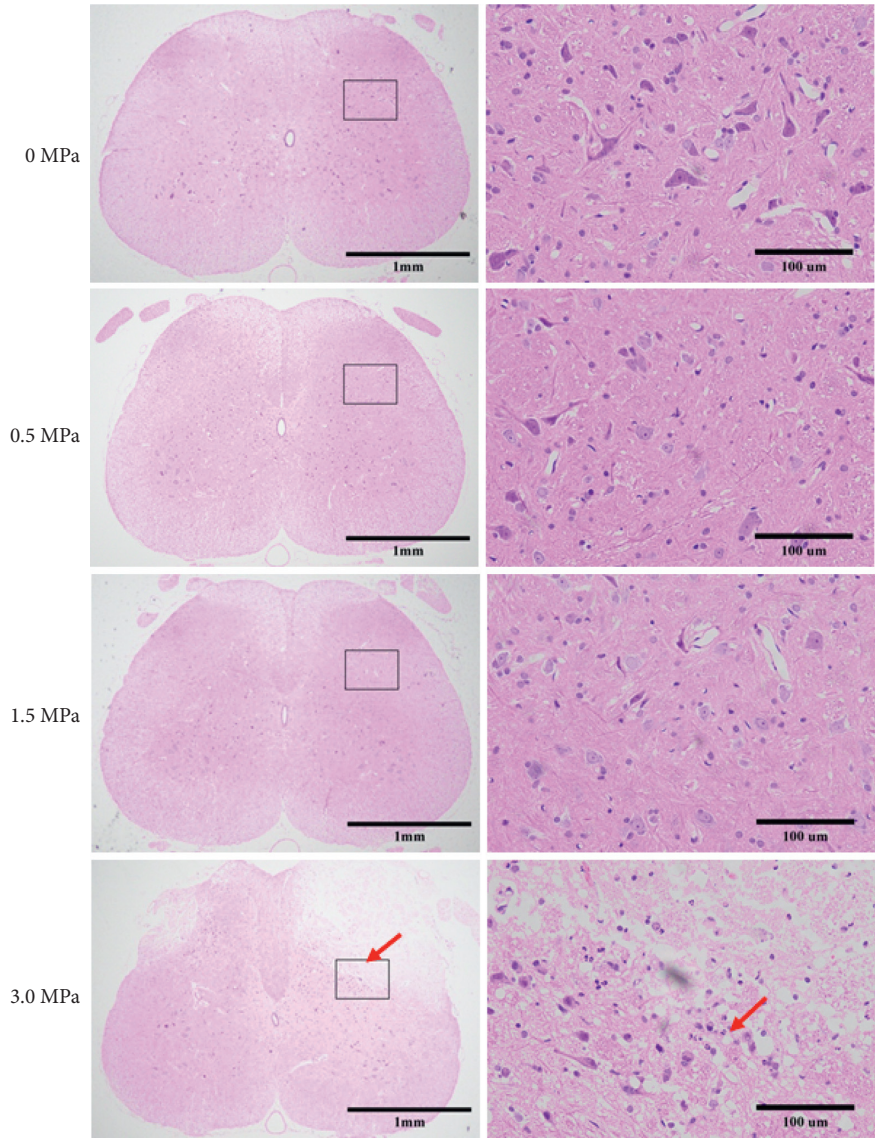

Figure 7: Hematoxylin and eosin (H&E) staining for histological examination of spinal cord injury (×40 and ×400). Scale bars = 1 mm and 100 μm. Comparison of H&E staining among the spinal cord sections after different irradiation intensities of LIFU stimulation. There was no significant difference in histological results among 0 MPa, 0.5 MPa, and 1.5 MPa stimulation groups. In the 3.0 MPa stimulation group, coagulative necrosis was clear at the dorsal horn of the spinal cord (red arrow).

percutaneous stimulation with LIFU when the intensity was >0.5 MPa. Spinal cord activation also induced the recruitment of Sol muscle as measured by EMG.

A previous study has shown that low-intensity ultrasound stimulation can also induce changes in biomarkers. For example, low-intensity ultrasound stimulation of peripheral nerves promoted injured nerve regeneration by stimulating the release of brain-derived neurotrophic factor (BDNF) [47]. Furthermore, transcranial focused ultrasound can decrease the expression of c-fos and increase the expression of GAD65 in the brains of SD rats with epilepsy, indicating that focused ultrasound deactivates excitatory cells and activates GABAergic terminals [37]. Another study has demonstrated that spinal cord activation increases the expression of c-fos and produces analgesia [36]. The increased numbers of c-fos- and GAD65-positive cells indicated the activation of neurons and synapses [36, 37]. In this study, we found that transdermal LIFU increased the numbers of c-fos- and GAD65-positive cells. From the results of EMG and biomarker studies (c-fos and GAD65), we hypothesize that the spinal cord was activated by LIFU.

Our results showed some differences from those of Chen, which showed that transcranial focused ultrasound reduced the number of c-fos-positive cells [37]; the difference may reflect the different animal models adopted. Tissue injury, such as paw inflammation [48], sciatic nerve transection [49], and chronic constriction injury of the sciatic nerve [50], can also increase c-fos expression. A previous study found that the expression of c-fos increased in rats with seizures [51]. However, in this study, normal rats were used, and spinal cord activation by LIFU increased the number of c-fos-positive cells.

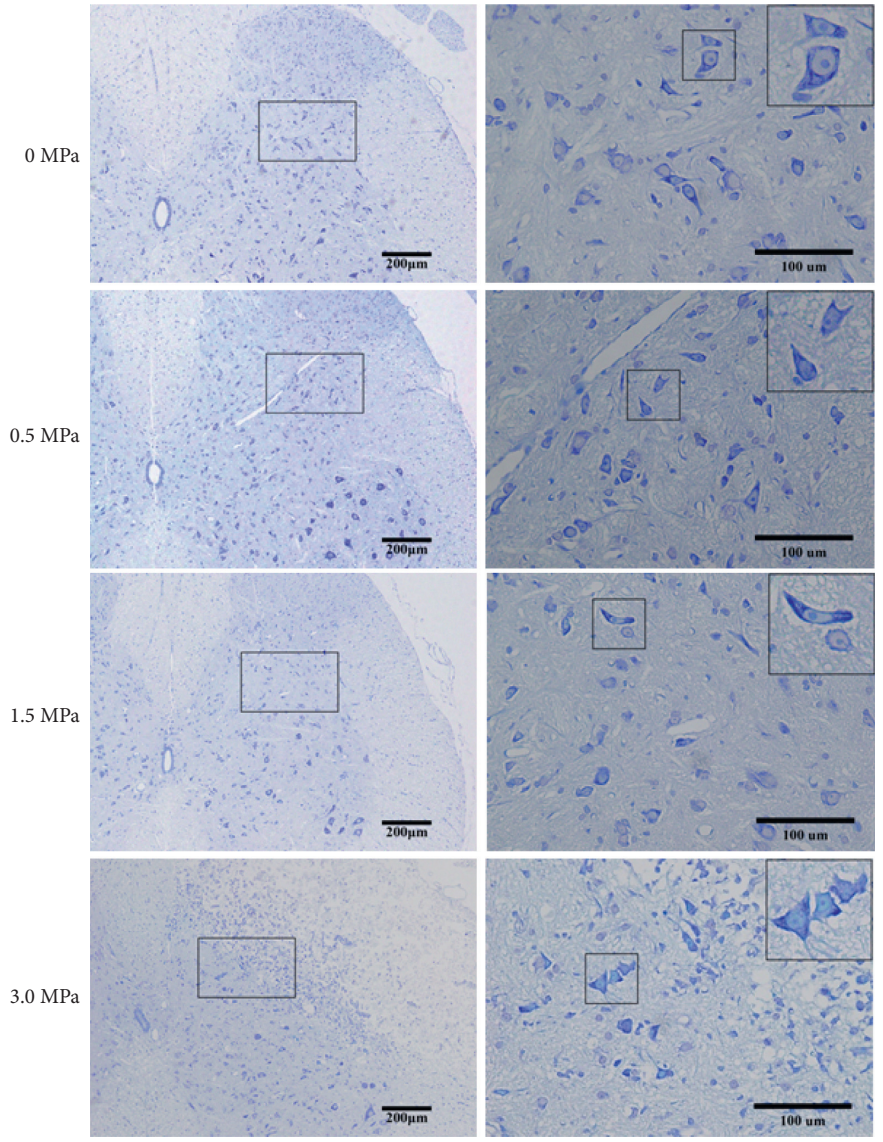

Figure 8: Nissl staining for histological examination of spinal cord injury (×100 and ×400). Scale bars = 200 μm and 100 μm. Comparison of Nissl staining among the spinal cord sections after different irradiation intensities of LIFU stimulation. After 0 MPa, 0.5 MPa, and 1.5 MPa stimulation, the neuron arrangement was regular, the structure was clear, the morphology was normal, and the Nissl body was clear (shown in the black square). After 3.0 MPa irradiation intensity stimulation, the neuron arrangement was irregular, the structure was unclear, the morphology was abnormal, and the Nissl body was unclear (shown in the black square).

Previous studies have shown the many advantages of focused ultrasound stimulation, including high spatial resolution, noninvasive neurostimulation, and effective stimulation of the deep tissues with submillimeter static resolution [7, 8]. Moreover, it has been demonstrated that focused ultrasound can activate cells, brain histology slices, and neurocircuits of nonprimates, primates, and even humans [13, 16, 19, 20, 22]. However, the spinal cord is surrounded by irregular vertebral bones, which could lead to reflection, refraction, diffusion, and absorption of ultrasound beams, all of which may affect the neuromodulatory effects of ultrasound. In this study, we first demonstrated that LIFU enhances Sol muscle contractions and increases the number of c-fos- and GAD65-positive cells, suggesting activation of the spinal cord neurocircuits. The activation of the spinal cord neurocircuits by ultrasound may be due to the use of focused ultrasound, which can converge ultrasound beams onto the target to produce tissue effects [52]. Clearly, the activation of the spinal cord neurocircuits by low-intensity focused ultrasound would also provide an innovative and noninvasive neuromodulation method for spinal cord stimulation.

Safety is an important consideration in neuromodulation. Previous studies have demonstrated that ultrasound can induce different biological effects depending on the exposure parameters; for example, low-intensity ultrasound produces reversible cellular effects, whereas high-intensity ultrasound leads to irreversible cell death. According to the Food and Drug Administration (FDA), the I_{spta} of the diagnostic ultrasound must be ≤720 mw/cm^2 [53],

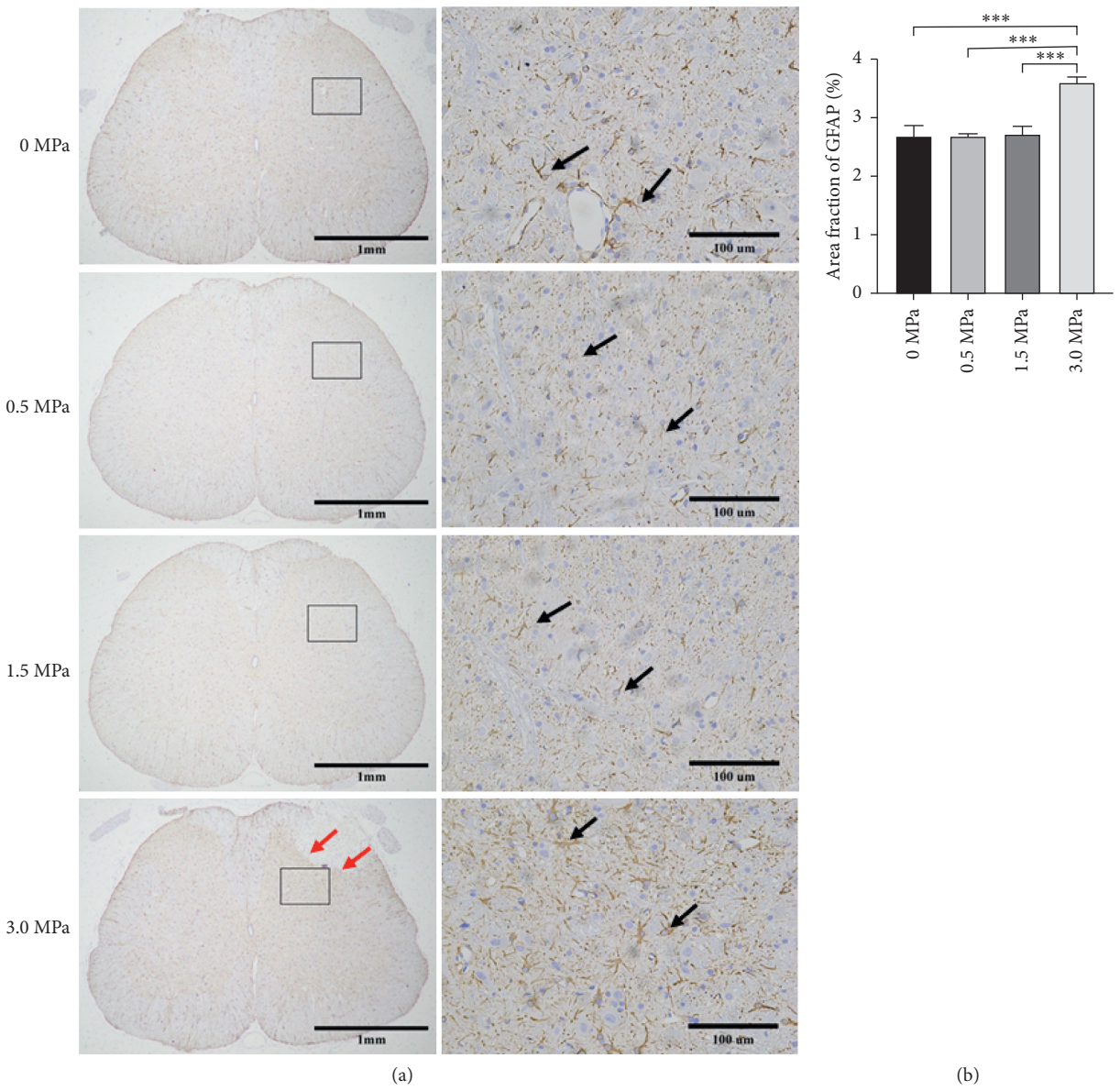

Figure 9: Results of immunohistochemistry (IHC) staining of astrocyte activation in the spinal cord sections after different irradiation intensities of LIFU stimulation (×40 and ×400). Scale bars = 1 mm and 100 μm. (a) Black arrows show the GFAP-positive astrocytes, and the red arrow shows coagulative necrosis of the spinal cord. A diagram indicating a 300 μm × 300 μm square area was defined for further analysis of the positive cells. (b) Intensity analysis of the GFAP-positive area using ImageJ showed that 3.0 MPa stimulation increased the intensity of GFAP. $^{****}P < 0.0001$. Each symbol represents the mean ± SEM; one-way ANOVA, followed by LSD test for pairwise comparisons; $n = 3$ rats per assay.

which has been recognized as the requirement for ultrasonic neuromodulation treatment protocols. The safety of the FDA-recommended limit of ultrasound intensity has been demonstrated by previous studies. Some studies have shown that ultrasound intensity above the FDA limits but below the International Electrotechnical Commission (IEC) set intensity ($I_{spta} = 3\ W/cm^2$) for diagnostic medical ultrasound equipment is still safe [54]. Focused ultrasound with an intensity of 3.2 MPa has also been used to stimulate the peripheral nervous system of the mice, activation of which was detected by EMG, while histological examination showed no evidence of nerve damage [55]. In this study, the neuromotor function, electrophysiology, H&E staining, Nissl staining, and protein expression analyses suggested no injury to the spinal cord after 0.5 MPa or 1.5 MPa stimulation. Moreover, ultrasound has little thermal effect and does not cause tissue injury [10, 11]. However, in this study, 3 MPa stimulation decreased the SEP amplitude and increased the expression levels of IL-1β, TNF-α, caspase-3 and Bcl-2, and GFAP, but it did not affect the neuromotor function or latency of SEPs and MEPs. The decreased amplitude of SEPs indicates damage to the spinal cord sensory pathways. The electrophysiological results were consistent with the H&E staining results, which showed

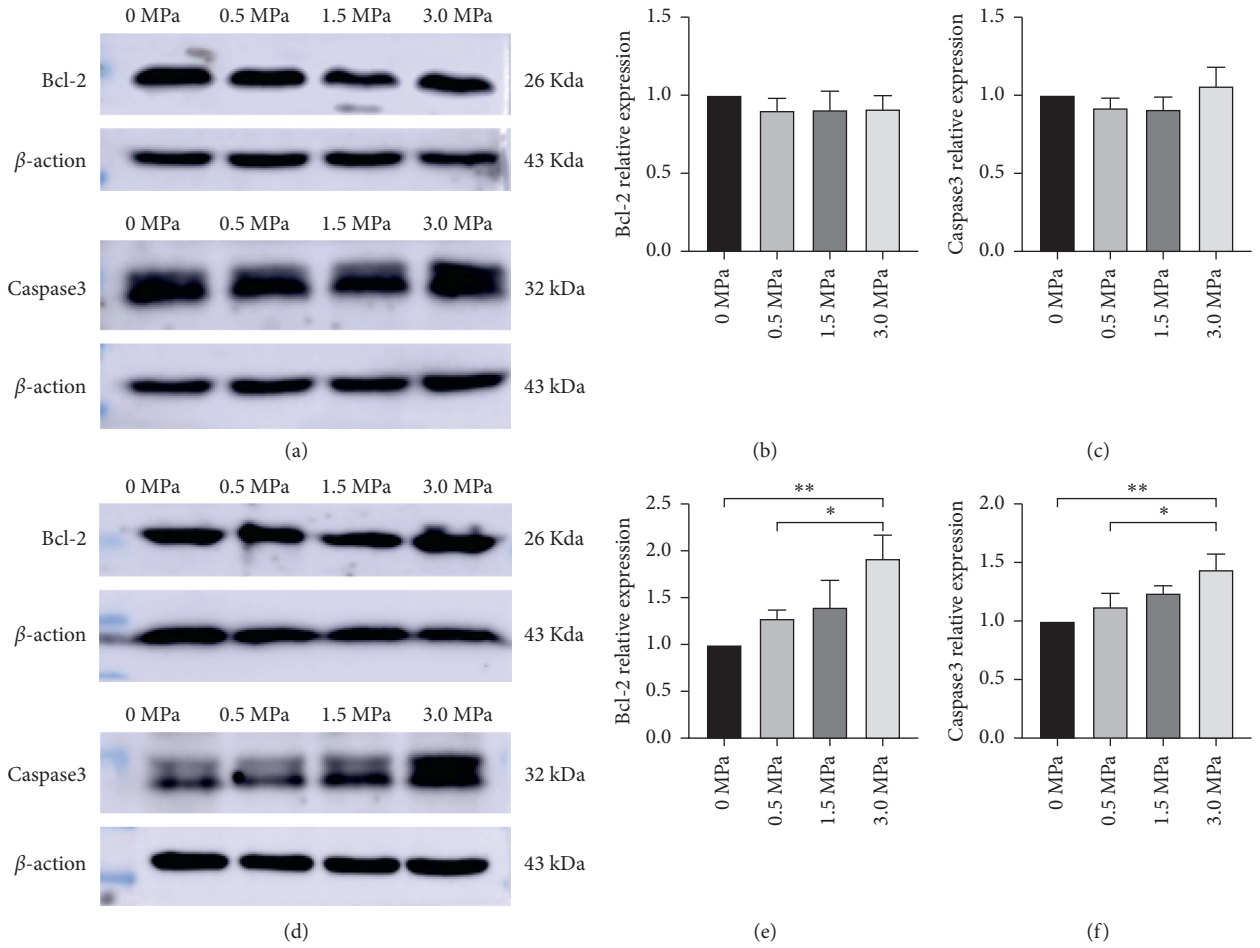

FIGURE 10: LIFU stimulation induces the expression of caspase-3 and Bcl-2 as markers of apoptosis induction and apoptosis inhibition. (a–c) Western blot results showed that LIFU stimulation did not significantly alter the expression levels of caspase-3 and Bcl-2 on day 0 ($P > 0.05$), while (d–f) 3.0 MPa irradiation intensity stimulation increased the expression levels of caspase-3 and Bcl-2 compared to 0 MPa and 0.5 MPa irradiation intensities on day 3 after LIFU stimulation ($P < 0.05$). There were no significant differences among the 0 MPa, 0.5 MPa, and 1.5 MPa irradiation intensity stimulation groups ($P > 0.05$). Values were normalized to β-actin. Each symbol represents the mean ± SEM; $^{*}P < 0.05$, $^{**}P < 0.01$; one-way ANOVA, followed by LSD test for pairwise comparisons; $n = 3$ rats per assay.

coagulative necrosis of the dorsal horn. Furthermore, the WB results showed increased expression of caspase-3, confirming the apoptosis of neurons after spinal cord injury. The increased expression of Bcl-2 suggests that the spinal cord produced an antioxidant response following injury. The differences observed between this study and previous studies may be due to various factors. First, focused ultrasound forms a focal spot in the deep tissue, which has a higher acoustic pressure and stimulation intensity and can produce stronger biological effects. Second, the spinal cord may exhibit a lower tolerance to ultrasonic stimulation than the peripheral nervous system. Finally, we suggest that the irradiation intensity should be strictly controlled when using low-intensity focused ultrasound to stimulate the central nervous system to avoid irreversible neural damage.

5. Limitations

This study has several limitations that warrant discussion. First, although we found that percutaneous low-intensity focused ultrasound activates spinal cord neurocircuits, the detailed mechanism is still unknown. Second, the prestudy confirmed that the temperature change was less than 0.025°C after LIFU stimulation. However, focused ultrasound can lead to spinal cord injury at an irradiation intensity of 3 MPa, and further experiments are needed to clarify the mechanisms underlying spinal cord injuries. Third, we confirmed that LIFU stimulation activates spinal cord neurocircuits, but we did not extend this research to determine how long the effects of LIFU stimulation are maintained.

6. Conclusions

Noninvasive LIFU can effectively activate spinal cord neurocircuits and represents a safe neuromodulation method for spinal cord stimulation when the radiation intensity is <1.5 MPa.

Abbreviations

LIFU: Low-intensity focused ultrasound
EMG: Electromyography
RI: Radiation intensity
BBB scale: Basso–Beattie–Bresnahan locomotor rating scale
Sol: Soleus
SEPs: Somatosensory evoked potentials
MEPs: Motor evoked potentials
Amp: Amplitude
H&E: Hematoxylin and eosin.

Data Availability

The data used to support the findings of this study are included within the article.

Conflicts of Interest

The authors declare that they have no conflicts of interest.

Acknowledgments

This study was supported by the National Natural Science Foundation of China (nos. 81960421 and 82060421), the Science and Technology Innovative Team Grant of Kunming Medical University (no. CXTD201905), and Basic Research Program of Yunnan Science and Technology Department (no. 202101AT070255). The authors also thank LetPub (https://www.letpub.com) for the linguistic assistance during the preparation of this manuscript.

Supplementary Materials

Supplementary Figure 1: the amplitude of EMG after different irradiation intensity stimulations. $^{*}P < 0.05$ and $^{****}P < 0.0001$. Each symbol represents the mean ± SEM; one-way ANOVA, followed by LSD test for pairwise comparisons; $n = 6$ rats per assay. Supplementary Figure 2: (a) the Basso, Beattie, and Bresnahan locomotor rating scale (BBB scale) was used to assess the neuromotor function of the hind limbs and the latency of (b) somatosensory evoked potentials (SEPs) and (d) motor evoked potentials (MEPs) evaluation for the spinal cord. The results show no difference in neuromotor function, latency of SEPs, and latency of MEPs after the different irradiation intensity stimulation ($P > 0.05$). (c) MEPs were used to detect motor conduction for the spinal cord, and the triangle represents the excitation point time. Each symbol represents the mean ± SEM; paired t-test; $n = 6$ rat per assay. (*Supplementary Materials*)

References

[1] P. B. Fitzgerald and Z. J. Daskalakis, "A practical guide to the use of repetitive transcranial magnetic stimulation in the treatment of depression," *Brain Stimulation*, vol. 5, no. 3, pp. 287–296, 2012.

[2] C. Ridler, "Spinal stimulation and physical therapy helps paraplegic patients to walk again," *Nature Reviews Neurology*, vol. 14, no. 11, p. 631, 2018.

[3] S. Li, M. Alam, R. U Ahmed et al., "Ultrasound-driven piezoelectric current activates spinal cord neurocircuits and restores locomotion in rats with spinal cord injury," *Bioelectronic Medicine*, vol. 6, no. 13, p. 13, 2020.

[4] P. Faria, M. Hallett, and P. C. Miranda, "A finite element analysis of the effect of electrode area and inter-electrode distance on the spatial distribution of the current density in tDCS," *Journal of Neural Engineering*, vol. 8, no. 6, Article ID 066017, 2011.

[5] F. Zhang, A. M. Aravanis, A. Adamantidis, L. De Lecea, and K. Deisseroth, "Circuit-breakers: optical technologies for probing neural signals and systems," *Nature Reviews Neuroscience*, vol. 8, no. 8, pp. 577–581, 2007.

[6] E. S. Boyden, "A history of optogenetics: the development of tools for controlling brain circuits with light," *F1000 Biology Reports*, vol. 3, p. 11, 2011.

[7] J. Mueller, W. Legon, A. Opitz, T. F. Sato, and W. J. Tyler, "Transcranial focused ultrasound modulates intrinsic and evoked EEG dynamics," *Brain Stimulation*, vol. 7, no. 6, pp. 900–908, 2014.

[8] S.-S. Yoo, A. Bystritsky, J.-H. Lee et al., "Focused ultrasound modulates region-specific brain activity," *Neuroimage*, vol. 56, no. 3, pp. 1267–1275, 2011.

[9] P. Bowary and B. D. Greenberg, "Noninvasive focused ultrasound for neuromodulation," *Psychiatric Clinics of North America*, vol. 41, no. 3, pp. 505–514, 2018.

[10] G. Ter Haar, "Therapeutic applications of ultrasound," *Progress in Biophysics and Molecular Biology*, vol. 93, no. 1-3, pp. 111–129, 2007.

[11] W. D. O'Brien, "Ultrasound-biophysics mechanisms," *Progress in Biophysics and Molecular Biology*, vol. 93, no. 1–3, pp. 212–255, 2007.

[12] W. J. Tyler, Y. Tufail, M. Finsterwald, M. L. Tauchmann, E. J. Olson, and C. Majestic, "Remote excitation of neuronal circuits using low-intensity, low-frequency ultrasound," *PLoS One*, vol. 3, no. 10, Article ID e3511, 2008.

[13] Z. Lin, X. Huang, W. Zhou et al., "Ultrasound stimulation modulates voltage-gated potassium currents associated with action potential shape in hippocampal CA1 pyramidal neurons," *Frontiers in Pharmacology*, vol. 10, p. 544, 2019.

[14] J. Vion-Bailly, W. A. N'Djin, I. M. Suarez Castellanos, J.-L. Mestas, A. Carpentier, and J.-Y. Chapelon, "A causal study of the phenomenon of ultrasound neurostimulation applied to an in vivo invertebrate nervous model," *Scientific Reports*, vol. 9, no. 1, p. 13738, 2019.

[15] W. Zhou, J. Wang, K. Wang et al., "Ultrasound neuromodulation chip: activation of sensory neurons in *Caenorhabditis elegans* by surface acoustic waves," *Lab on a Chip*, vol. 17, no. 10, pp. 1725–1731, 2017.

[16] W. Legon, T. F. Sato, A. Opitz et al., "Transcranial focused ultrasound modulates the activity of primary somatosensory cortex in humans," *Nature Neuroscience*, vol. 17, no. 2, pp. 322–329, 2014.

[17] G. Leinenga, C. Langton, R. Nisbet, and J. Götz, "Ultrasound treatment of neurological diseases-current and emerging

applications," *Nature Reviews Neurology*, vol. 12, no. 3, pp. 161–174, 2016.

[18] R. F. Dallapiazza, K. F. Timbie, Holmberg et al., "Noninvasive neuromodulation and thalamic mapping with low-intensity focused ultrasound," *Journal of Neurosurgery*, vol. 128, no. 3, pp. 875–884, 2018.

[19] W. Lee, S. D. Lee, Park et al., "Image-guided focused ultrasound-mediated regional brain stimulation in sheep," *Ultrasound in Medicine & Biology*, vol. 42, no. 2, pp. 459–470, 2016.

[20] R. L. King, J. R. Brown, W. T. Newsome, and K. B. Pauly, "Effective parameters for ultrasound-induced in vivo neurostimulation," *Ultrasound in Medicine & Biology*, vol. 39, no. 2, pp. 312–331, 2013.

[21] Y. Tufail, A. Matyushov, Baldwin et al., "Transcranial pulsed ultrasound stimulates intact brain circuits," *Neuron*, vol. 66, no. 5, pp. 681–694, 2010.

[22] T. Deffieux, Y. Younan, N. Wattiez, M. Tanter, P. Pouget, and J.-F. Aubry, "Low-intensity focused ultrasound modulates monkey visuomotor behavior," *Current Biology*, vol. 23, no. 23, pp. 2430–2433, 2013.

[23] L. R. Gavrilov, E. M. Tsirulnikov, and I. A. I. Davies, "Application of focused ultrasound for the stimulation of neural structures," *Ultrasound in Medicine & Biology*, vol. 22, no. 2, pp. 179–192, 1996.

[24] K. Meier, "Spinal cord stimulation: background and clinical application," *Scandinavian Journal of Pain*, vol. 5, no. 3, pp. 175–181, 2014.

[25] K. Chakravarthy, H. Richter, P. J. Christo, K. Williams, and Y. Guan, "Spinal cord stimulation for treating chronic pain: reviewing preclinical and clinical data on paresthesia-free high-frequency therapy," *Neuromodulation: Technology at the Neural Interface*, vol. 21, no. 1, pp. 10–18, 2018.

[26] A. D. Sdrulla, Y. Guan, and S. N. Raja, "Spinal cord stimulation: clinical efficacy and potential mechanisms," *Pain Practice*, vol. 18, no. 8, pp. 1048–1067, 2018.

[27] C. Willyard, "How a revolutionary technique got people with spinal-cord injuries back on their feet," *Nature*, vol. 572, no. 7767, pp. 20–25, 2019.

[28] G. L. Schmidt, "The use of spinal cord stimulation/neuromodulation in the management of chronic pain," *Journal of the American Academy of Orthopaedic Surgeons*, vol. 27, no. 9, pp. e401–e407, 2019.

[29] Y. H. Liao, B. Wang, M. X. Chen, Y. Liu, and L. J. Ao, "LIFU alleviates neuropathic pain by improving the KCC2 expression and inhibiting the CaMKIV-KCC2 pathway in the L4-L5 section of the spinal cord," *Neural Plast*, vol. 2021, Article ID 6659668, 10 pages, 2021.

[30] D. M. Basso, M. S. Beattie, and J. C. Bresnahan, "A sensitive and reliable locomotor rating scale for open field testing in rats," *Journal of Neurotrauma*, vol. 12, no. 1, pp. 1–21, 1995.

[31] J. A. Corleto, M. Bravo-Hernández, Kamizato et al., "Thoracic 9 spinal transection-induced model of muscle spasticity in the rat: a systematic electrophysiological and histopathological characterization," *PLoS One*, vol. 10, no. 12, Article ID e0144642, 2015.

[32] H. Beverungen, S. C. Klaszky, M. Klaszky, and M.-P. Côté, "Rehabilitation decreases spasticity by restoring chloride homeostasis through the brain-derived neurotrophic factor-KCC2 pathway after spinal cord injury," *Journal of Neurotrauma*, vol. 37, no. 6, pp. 846–859, 2020.

[33] T.-Y. Chen, S.-H. Tai, E.-J. Lee et al., "Cinnamophilin offers prolonged neuroprotection against gray and white matter damage and improves functional and electrophysiological outcomes after transient focal cerebral ischemia∗," *Critical Care Medicine*, vol. 39, no. 5, pp. 1130–1137, 2011.

[34] M. G. Schlag, R. Hopf, and H. Redl, "Serial recording of sensory, corticomotor, and brainstem-derived motor evoked potentials in the rat," *Somatosensory & Motor Research*, vol. 18, no. 2, pp. 106–116, 2001.

[35] Y. Liu, G. Lu, Su et al., "Characterization of axon damage, neurological deficits, and histopathology in two experimental models of intracerebral hemorrhage," *Frontiers in Neuroscience*, vol. 12, p. 928, 2018.

[36] R. Melzack and P. D. Wall, "Pain mechanisms: a new theory," *Science*, vol. 150, no. 3699, p. 971, 1965.

[37] T. R. Deer, E. Krames, N. Mekhail et al., "The appropriate use of neurostimulation: new and evolving neurostimulation therapies and applicable treatment for chronic pain and selected disease states," *Neuromodulation: Technology at the Neural Interface*, vol. 17, no. 6, pp. 599–615, 2014.

[38] L. Kapural, C. Yu, M. W. Doust et al., "Comparison of 10-kHz high-frequency and traditional low-frequency spinal cord stimulation for the treatment of chronic back and leg pain," *Neurosurgery*, vol. 79, no. 5, pp. 667–677, 2016.

[39] S. Hou, K. Kemp, and M. Grabois, "A systematic evaluation of burst spinal cord stimulation for chronic back and limb pain," *Neuromodulation: Technology at the Neural Interface*, vol. 19, no. 4, pp. 398–405, 2016.

[40] E. Veizi, S. M. Hayek, J. North et al., "Spinal cord stimulation (SCS) with anatomically guided (3D) neural targeting shows superior chronic axial low back pain relief compared to traditional SCS-LUMINA study," *Pain Medicine (Malden, Mass)*, vol. 18, no. 8, pp. 1534–1548, 2017.

[41] J. P. Miller, S. Eldabe, E. Buchser, L. M. Johanek, Y. Guan, and B. Linderoth, "Parameters of spinal cord stimulation and their role in electrical charge delivery: a review," *Neuromodulation: Technology at the Neural Interface*, vol. 19, no. 4, pp. 373–384, 2016.

[42] R. Vallejo, k. Bradley, and L. Kapural, "Spinal cord stimulation in chronic pain: mode of action," *Spine (Phila Pa 1976)*, vol. 42, no. 14, pp. s53–s60, 2017.

[43] Y.-F. Lee, C.-C. Lin, J.-S. Cheng, and G.-S. Chen, "High-intensity focused ultrasound attenuates neural responses of sciatic nerves isolated from normal or neuropathic rats," *Ultrasound in Medicine & Biology*, vol. 41, no. 1, pp. 132–142, 2015.

[44] Y. Youn, A. Hellman, Walling et al., "High-intensity ultrasound treatment for vincristine-induced neuropathic pain," *Neurosurgery*, vol. 83, no. 5, pp. 1068–1075, 2018.

[45] X.-J. Ni, X.-D. Wang, Y.-H. Zhao et al., "The effect of low-intensity ultrasound on brain-derived neurotropic factor expression in a rat sciatic nerve crushed injury model," *Ultrasound in Medicine & Biology*, vol. 43, no. 2, pp. 461–468, 2017.

[46] S.-G. Chen, C.-H. Tsai, C.-J. Lin et al., "Transcranial focused ultrasound pulsation suppresses pentylenetetrazol induced epilepsy in vivo," *Brain Stimulation*, vol. 13, no. 1, pp. 35–46, 2020.

[47] Y. Maeda, M. Ikeuchi, P. Wacnik, and K. A. Sluka, "Increased c-fos immunoreactivity in the spinal cord and brain following spinal cord stimulation is frequency-dependent," *Brain Research*, vol. 1259, pp. 40–50, 2009.

[48] M. Pinto, D. Lima, and I. Tavares, "Neuronal activation at the spinal cord and medullary pain control centers after joint stimulation: a c-fos study in acute and chronic articular inflammation," *Neuroscience*, vol. 147, no. 4, pp. 1076–1089, 2007.

[49] S.-I. Chi, J. D. Levine, and A. I. Basbaum, "Peripheral and central contributions to the persistent expression of spinal cord fos-like immunoreactivity produced by sciatic nerve transection in the rat," *Brain Research*, vol. 617, no. 2, pp. 225–237, 1993.

[50] K. C. Kajander, A. M. Madsen, M. J. Iadarola, G. Draisci, and S. Wakisaka, "Fos-like immunoreactivity increases in the lumbar spinal cord following a chronic constriction injury to the sciatic nerve of rat," *Neuroscience Letters*, vol. 206, no. 1, pp. 9–12, 1996.

[51] H. Yang, W. Shan, F. Zhu et al., "C-Fos mapping and EEG characteristics of multiple mice brain regions in pentylenetetrazol-induced seizure mice model," *Neurological Research*, vol. 41, no. 8, pp. 749–761, 2019.

[52] G. R. Giammalva, C. Gagliardo, S. Marrone et al., "Focused ultrasound in neuroscience. State of the art and future perspectives," *Brain Science*, vol. 11, no. 1, 2021.

[53] Administration USFaD, *Marketing Clearance of Diagnostic Ultrasound Systems and Transducers. Draft Guidance for Industry and Food and Drug Administration Staff*, Administration USFaD, Silver Spring, USA, 2017.

[54] F. A. Duck, "Medical and non-medical protection standards for ultrasound and infrasound," *Progress in Biophysics and Molecular Biology*, vol. 93, no. 1–3, pp. 176–191, 2007.

[55] M. E. Downs, S. A. Lee, G. Yang, S. Kim, Q. Wang, and E. E. Konofagou, "Non-invasive peripheral nerve stimulation via focused ultrasound in vivo," *Physics in Medicine and Biology*, vol. 63, no. 3, Article ID 035011, 2018.

Hindawi
Evidence-Based Complementary and Alternative Medicine
Volume 2021, Article ID 1418616, 15 pages
https://doi.org/10.1155/2021/1418616

Research Article

Scalp Acupuncture and Treadmill Training Inhibits Neuronal Apoptosis through Activating cIAP1 in Cerebral Ischemia Rats

Qiang Tang[1], **Tao Ye**[2], **Runyu Liang**[3], **Yan Wang**[1], **Hongyu Li**[1], **Jiyao Zhang**[3], **Xingxing Yuan**[4] **and Luwen Zhu**[1]

[1]*The Second Hospital, Heilongjiang University of Chinese Medicine, Harbin, Heilongjiang, China*
[2]*First Affiliated Hospital of Guizhou University of Traditional Chinese Medicine, Guiyang, Guizhou, China*
[3]*Heilongjiang University of Chinese Medicine, Harbin, Heilongjiang, China*
[4]*Heilongjiang Academy of Chinese Medicine, Harbin, Heilongjiang, China*

Correspondence should be addressed to Luwen Zhu; zhuluwen1983@126.com

Received 21 August 2021; Revised 2 October 2021; Accepted 26 October 2021; Published 12 November 2021

Academic Editor: Feng Zhang

Stroke is the leading cause of long-term disability in developed countries. Multitudinous evidence suggests that treadmill training treatment is beneficial for balance and stroke rehabilitation; however, the need for stroke therapy remains unmet. In the present study, a cerebral ischemia rat model was established by permanent middle cerebral artery occlusion (pMCAO) to explore the therapeutic effect and mechanism of scalp acupuncture combined with treadmill training on ischemic stroke. Terminal deoxynucleotidyl transferase-mediated dUTP nick-end labeling and neuronal nuclear protein (NeuN) double staining and cellular inhibitor of apoptosis protein-1 (cIAP1) and NeuN immunofluorescence double staining were used to detect the short-term and long-term neuroprotective effects of scalp acupuncture combined with treadmill training on pMCAO rats. In addition, the antiapoptotic effect of the combined treatment was evaluated in pMCAO rats transfected with cIAP1 shRNA. Western blotting was used to detect the relative protein expression in the caspase-8/-9/-3 activation pathway downstream of cIAP1 to further clarify its regulatory mechanism. Our results showed that scalp acupuncture combined with treadmill training successfully achieved short-term and long-term functional improvement within 14 days after stroke, significantly inhibited neuronal apoptosis, and upregulated the expression of cIAP1 protein in the ischemic penumbra area of the ischemic brain. However, no significant functional improvement and antiapoptotic effect were found in pMCAO rats transfected with cIAP1 shRNA. Western blotting results showed that the combined therapy markedly inhibited the activation of the caspase-8/-9/-3 pathway. These findings indicate that scalp acupuncture combined with treadmill training therapy may serve as a more effective alternative modality in the treatment of ischemic stroke, playing an antiapoptotic role by upregulating the expression of cIAP1 and inhibiting the activation of the caspase-8/-9/-3 pathway.

1. Introduction

Stroke is the leading cause of long-term disability in developed countries and is one of the top causes of mortality worldwide. China accounts for almost one-third of the total stroke deaths in the world; furthermore, over recent years, stroke has been the leading cause of dementia [1]. Ischemic stroke, defined as an acute focal injury of the central nervous system (CNS) which occurs when a blood vessel in the neck or brain is blocked, is one of the most common types of stroke, accounting for approximately 80% of all stroke incidents [2]. Ischemia and hypoxia of brain tissue further result in corresponding neurological deficit symptoms and signs due to brain infarction, necrosis, and the loss of a large number of neurons [3]. Changes in standing ability, sensorimotor function, and postural swing are the main poststroke complications and are closely related to the increased risk of falls and balance disorders [4, 5]. Therefore, balance is often the main focus of interventions in stroke rehabilitation.

Acupuncture is recommended by the World Health Organization as an alternative and complementary strategy. It is defined as the insertion of fine needles or sometimes a finger on the defined points and has been used for patients

with stroke and poststroke rehabilitation for thousands of years [6, 7]. Recent research indicates that manual acupuncture or electroacupuncture activates afferent fibers at particular acupoints and then sends signals to the CNS, playing a role in improving balance, reducing spasms, increasing muscle strength, and general well-being poststroke via molecules identified as possible mediators of specific acupuncture effects, such as neurotransmitters (catecholamine, acetylcholine, 5-hydroxytryptamine, glutamate, and gamma-aminobutyric acid), neuropeptides, cytokines, and growth factors [7–9]. Scalp acupuncture is one of the several specialized acupuncture techniques in which a filiform needle is used to penetrate specific stimulation areas on the scalp, mainly for the treatment of brain diseases [10]. Systematic evidence has suggested that Baihui (GV20)-based scalp acupuncture is beneficial in the treatment of ischemic stroke as it improves infarct volume and neurological function scores and exerts a potential neuroprotective role in experimental ischemic stroke [11, 12]. However, the mechanisms underlying the beneficial effects of acupuncture in stroke rehabilitation remain unclear.

Poststroke rehabilitation training, such as treadmill training, has been shown to be effective in addressing the inefficiencies and gait patterns of poststroke individuals, principally through improving endurance and gait speed [13]. Despite the large number of studies conducted, the potential effects of treadmill training on balance function and postural control in poststroke individuals need to be further improved. In the present study, we hypothesized that scalp acupuncture combined with treadmill training therapy could effectively reduce nerve injury and promote the recovery of limb disorders. The neuronal expression level of cellular inhibitor of apoptosis protein-1 (cIAP1), which is considered the key target of neuroprotection induced by ischemic preconditioning, was examined *in vivo* to further investigate the regulatory effects of scalp acupuncture combined with treadmill training therapy in inhibiting neuronal apoptosis and neuroprotection.

2. Materials and Methods

2.1. Animals. The experiment was approved by the Animal Care and Use Committee of Heilongjiang University of Chinese Medicine (ABX20190508A) and executed following the National Institutes of Health Guidelines. Ten- to twelve-week-old male Sprague-Dawley rats (250 ± 14 g) were acquired from Liaoning Changsheng Biotechnology Co., Ltd. (SCXK 2015–0001) (Liaoning, China) and housed in a clean room with *ad libitum* access to food and water at a room temperature of 23–25°C and 55–65% humidity.

2.2. Development of cIAP1 shRNA. Three shRNAs, each targeting different regions of the rat *cIAP1* gene, and a negative control (NC) shRNA were designed and synthesized by Gene Pharma Co. (Shanghai, China). The target sequences were as follows: shRNA-1 : TTCTAGAG CAGTGGAAGAC, shRNA-2 : CTACAGGACGGTCAGTGAT, and shRNA-3 : CAG CTGCGGAGATTACAAG. shRNA-NC was a negative sequence with no significant homology to any rat gene.

2.3. Cell Culture and Transient Transfection. SH-SY5Y cells were obtained from the cell bank of the Chinese Academy of Science and were seeded into 25 cm^2 flasks with DMEM medium (Sigma-Aldrich, MO, USA) containing 10% FBS and incubated in a 37°C, 5% CO_2 thermostatic incubator. Cells were grown to confluency and passaged with 0.25% trypsin at 2–3-day intervals.

The cell concentration was adjusted to 1×10^6 cells/ml and seeded in six-well plates. When the density of the cell slide reached 90%, they were transfected into five groups as follows: (1) control group, (2) negative group (shRNA-NC), (3) shRNA-1 group, (4) shRNA-2 group, and (5) shRNA-3 group. Transfection was performed according to the manufacturer's protocol. Transfection efficiency was observed by real-time PCR and Western blot at 48 h, and *cIAP1* shRNAs were screened to select the one with the highest interference efficiency for animal experiments.

2.4. Animal Study. The ischemic stroke model was established by permanent middle cerebral artery occlusion (pMCAO) as previously described [14]. Briefly, rats were anesthetized by an intraperitoneal injection of pentobarbital (45 mg/kg body weight). Next, a silicone-coated nylon monofilament was inserted through a small incision in the right common carotid artery and was then advanced to 18 mm distal to the carotid bifurcation through the internal carotid artery to occlude the origin of the middle cerebral artery. In sham-operated animals, the same procedure was performed with the exception of inserting the intraluminal filament.

One hundred and forty male Sprague-Dawley rats were randomly divided into the following five groups: (1) sham operation group (**S-con**), $n = 28$, sham operation without intervention; (2) model group (**M-con**), $n = 28$, pMCAO without intervention; (3) scalp acupuncture group (**SA**), $n = 28$, pMCAO with scalp acupuncture at the Baihui point (GV20) and 2 mm on the left and right sides. Cluster needling was carried out with a 0.25×25 mm acupuncture needle; the depth of needling was 15 mm, and the needle was kept for 2 h after 30 min of scalp electroacupuncture, once daily. The scalp electroacupuncture frequency was 2–15 Hz, and the stimulation intensity was 1 mA, induced by a G6805-2A instrument [15]. The fourth group was the treadmill training group (**TT**), $n = 28$, pMCAO with TT. An electric running platform was used for training: slope: 0°; speed: 8 m/min during day 1 to day 3, 12 m/min during day 4 to day 7, 15 m/min after day 7, 30 min per time, once daily. The fifth group was scalp acupuncture combined with treadmill training group (**SA-T**), $n = 28$, pMCAO with SA and TT, once daily.

In addition, 140 male Sprague-Dawley rats were randomly divided into the following five groups: (1) **S-con**, $n = 28$, sham operation with no intervention; (2) **M-con**, $n = 28$, pMCAO with no intervention; (3) **SA-T**, $n = 28$, pMCAO with SA and TT, once daily; (4) *cIAP1* negative

control group (**SA-T + Lv-cIAP1 NC**), $n = 28$, in addition to SA and TT treatment, a lentiviral vector (1×10^9 TU/ml, 2 μl) negative control (Lv-*cIAP1* NC) was injected into the lateral ventricle 30 min before pMCAO with a stereotaxic instrument after the mice were anesthetized; and (5) the *cIAP1* interference group (**SA-T + Lv-cIAP1**), $n = 28$, in addition to SA and TT treatment, a lentiviral vector (1×10^9 TU/ml, 2 μl) interfering with *cIAP1* (Lv-cIAP1 NC) was injected into the lateral ventricle 30 min before pMCAO with a stereotaxic instrument after the rats were anesthetized. The injection was completed with a 10 μL microsyringe at the rate of 0.2 μL/min. A detailed schematic description of the study design and injection site of Lv-*cIAP1* is shown in Figure 1.

2.5. Behavioral Outcome Evaluation. The behavioral outcomes of rats were evaluated using the modified Bederson test [16], Beam Walk test [17], and Rota-rod test [18] before and 3, 7, and 14 days after modeling.

2.6. Histopathology. Brain tissue was embedded in paraffin, and then, consecutive cross-sections of the brain were cut. Hematoxylin-eosin (HE) staining and Nissl staining were performed to observe the neuronal damage in the ischemic penumbra on the 3rd, 7th, and 14th day after modeling.

2.7. Double Immunofluorescence. For terminal deoxynucleotidyl transferase-mediated dUTP nick-end labeling (TUNEL) and neuronal nuclear protein (NeuN) double staining, paraffin sections of the brain tissue on the 3rd, 7th, and 14th day after modeling were dewaxed and rehydrated by xylene and graded alcohol and then incubated at 37°C in ethylenediaminetetraacetic acid (EDTA) (pH 9.0) for 15 minutes. A TUNEL reaction mixture (Beyotime, China) was added and then blocked with 3% goat serum albumin for 30 min. The sections were then incubated with primary antibody against NeuN (0.72 μg/ml, 24307, CST) at 4°C overnight and Cy3-labeled goat anti-rabbit IgG antibody (0.8 μg/ml, ab6939, Abcam) for 50 min sequentially.

For cIAP1 and NeuN double staining, paraffin sections of the brain tissue on the 3rd, 7th, and 14th day after modeling were dewaxed and rehydrated by xylene and graded alcohol and then incubated in 37°C EDTA (pH 9.0) for 15 minutes. The sections were then incubated with primary antibody against NeuN (0.72 μg/ml, 24307, CST) and cIAP1 (5 μg/ml, ab25939, Abcam) at 4°C overnight. Then, Cy3-labeled goat anti-rabbit IgG antibody (0.8 μg/ml, ab6939, Abcam) was added and incubated for 50 minutes sequentially. Finally, the sections were incubated with DAPI for 10 min prior to visualizing them with a fluorescence microscope (BX51, Olympus, Japan) at 400 magnification.

2.8. TUNEL Assay. The TUNEL assay was performed using the colorimetric TUNEL apoptosis assay kit (Beyotime, China) according to the manufacturer's instructions. Paraffin sections of the brain tissue on the 3rd, 7th, and 14th day after modeling were dewaxed and rehydrated by xylene and graded alcohol and then incubated at room temperature 3% H_2O_2 for 10 minutes. The sections were rinsed and visualized using 3,3′-diaminobenzidine (DAB), followed by the TUNEL reaction mixture. Cell nuclei were counterstained with hematoxylin. Visualization was carried out with an optical microscope (CX41, Olympus, Japan) at 400 magnification. Quantitative analysis was carried out by calculating the number of positive staining cells in the ischemic penumbra.

2.9. Immunohistochemistry Staining for cIAP1. The brain sections were then incubated with a 3% goat serum albumin dissolved in PBS at room temperature for 2 h to remove peroxidase. Next, the sections were incubated with primary antibody against cIAP1 (10 μg/mL, ab25939, Abcam) at 4°C overnight, followed by incubation with a secondary antibody conjugated with HRP (2 μg/mL, ab6721, Abcam) at 37°C for 45 min. Specific labeling was visualized with a DAB kit and appeared tan-colored, while cell nuclei were counterstained with hematoxylin. The visualization was carried out with an optical microscope (CX41, Olympus, Japan) at 400 magnification. Quantitative analysis was carried out by calculating the number of positive staining cells in the ischemic penumbra.

2.10. Western Blot Analysis. Proteins obtained from the SH-SY5Y cells or ischemic penumbra tissue of rats were run by 10% sodium dodecyl sulfate-polyacrylamide gel electrophoresis and then transferred onto a polyvinylidene difluoride membrane. Penumbral tissues were separated according to a previous study [19]. The brain was sectioned into three slices beginning 3 mm from the anterior tip of the frontal lobe. Regions from the right and left hemispheres of Section 2 that corresponded to the ischemic core and penumbra were dissected. We initially identified the midline between the two hemispheres and then made a longitudinal cut (from top to bottom) approximately 2 mm from the midline through each hemisphere. We then made a transverse diagonal cut at approximately the "2 o'clock" position to separate the core (i.e., striatum and overlying cortex) from the penumbra (adjacent cortex). Blots were blocked with 5% skimmed milk for 2 h and then incubated with primary antibodies against cIAP1 (2 μg/mL, ab25939, Abcam), cleaved caspase-9 (0.09 μg/mL, 20750, CST), cleaved caspase-8 (0.133 μg/mL, 9496, CST), cleaved caspase-3 (0.0519 μg/mL, 9661, CST), NeuN (0.036 μg/mL, 24307, CST), and β-actin (0.061 μg/mL, 4970, CST) at 4°C overnight. The following day, blots were incubated with HRP-labeled goat anti-rabbit IgG antibody (1 μg/mL, ab6721, Abcam) for 2 h with shaking. Proteins were detected with enhanced chemiluminescence, and images were taken and examined with a Gel-Pro-Analyzer 4.0 (Media Cybernetics, USA).

2.11. Real-Time Polymerase Chain Reaction. Total RNA was isolated from SH-SY5Y cells using TRIzol reagent (Thermo Fisher, CA, USA) according to the manufacturer's instructions. RNA samples were reverse transcribed into cDNA with the PrimeScript™ RT reagent kit (Takara,

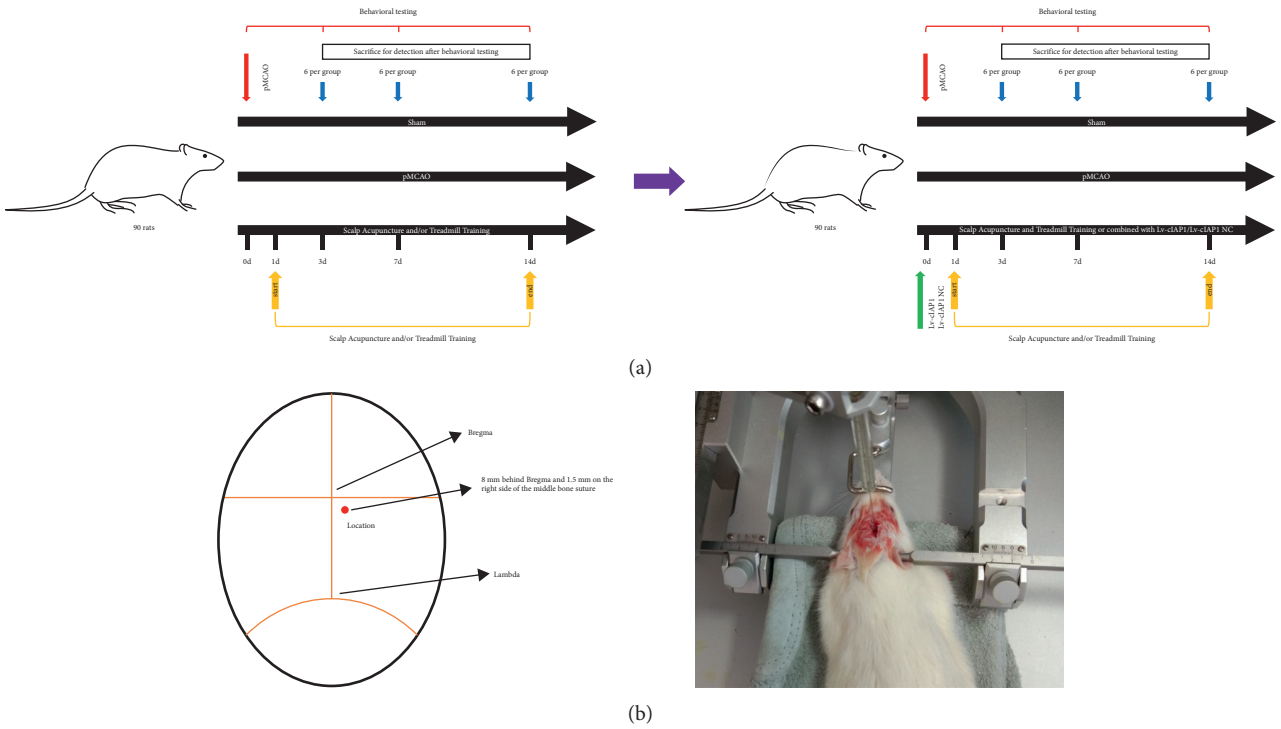

FIGURE 1: Schematic description of the study design and experimental operation. (a) Study design and experimental timeline. (b) Schematic diagram and operation diagram of the injection site of Lv-cIAP1.

Kyoto, Japan). The mRNA expression of target genes was examined by a standard SYBR-Green method in the ABI PRISM 7500 sequence detection system (Applied Biosystems, CA, USA). The reaction conditions were as follows: predenaturation at 93°C for 3 min, 40 cycles of denaturation at 93°C for 30 sec, annealing at 55°C for 45 sec, and extension at 72°C for 45 sec. All results were normalized to the expression levels of *β-actin* and quantified by the comparative ($2^{-\triangle\triangle Ct}$) method. The primer sequences were synthesized by Sangon Biotech (Shanghai, China) as follows: *cIAP1* forward 5′- GCAGGCTTCTACTACACAGGG-3′, reverse 5′-TTGGATACACTAAACCTCTGCG -3′; *β-actin* forward 5′-GGAGATTACTGCCCTGGCTCCTAGC-3′, reverse 5′-GGCCGGACTCATCGTACTCCTGCTT-3′.

2.12. Statistical Analysis. Experimental results are shown as mean ± standard error of the mean. Data were analyzed using SPSS 15.0 software. For analyses with only one factor involved, a one-way analysis of variance (ANOVA) and multiple comparisons followed by Bonferroni tests were applied, while a two-way ANOVA and multiple comparisons followed by Tukey's test were used when two factors were involved. All statistical tests were two-sided and P values <0.05 were considered statistically significant.

3. Results

3.1. Effect of SA-T on the Behavioral Outcomes of the pMCAO Model. The behavioral results showed that SA-T successfully achieved short-term and long-term functional improvements within 14 days after stroke. The difference was statistically significant when compared with the model group ($P < 0.05$). Nevertheless, it should be noted that the difference in these improvements was significant in the SA-T group when compared with the other treatment groups on each day during the evaluation ($P < 0.05$). These results suggest that SA-T has a therapeutic effect on neurological deficits and is superior to SA and TT treatments (Figures 2(a)–2(c)).

3.2. Effect of SA-T on Neuronal Damage in the pMCAO Model. The Nissl body is sensitive to ischemic injury and appeared to decrease or disappear once ischemia occurred. Regarding the neuropathological changes in the cortex penumbra of the ischemic brain, the Nissl staining results showed a significant reduction in neurons of the model group when compared with the sham operation group on the 3rd, 7th, and 14th days after modeling. After treatment with SA, TT, or SA-T, increased Nissl bodies were observed indicating that these treatments were effective for ischemic stroke. It is noteworthy that SA-T was more neuroprotective than SA and TT (Figure 2(d)).

3.3. Effect of SA-T on Neuronal Apoptosis in the pMCAO Model. NeuN is a specific protein expressed in the nucleus and cytoplasm of most neurons in the nervous system. We further examined the effect of SA-T on neuronal apoptosis in the ischemic penumbra area by double immunofluorescence staining (Figure 3). Limited numbers of TUNEL and NeuN positive neurons were observed in the sham operation

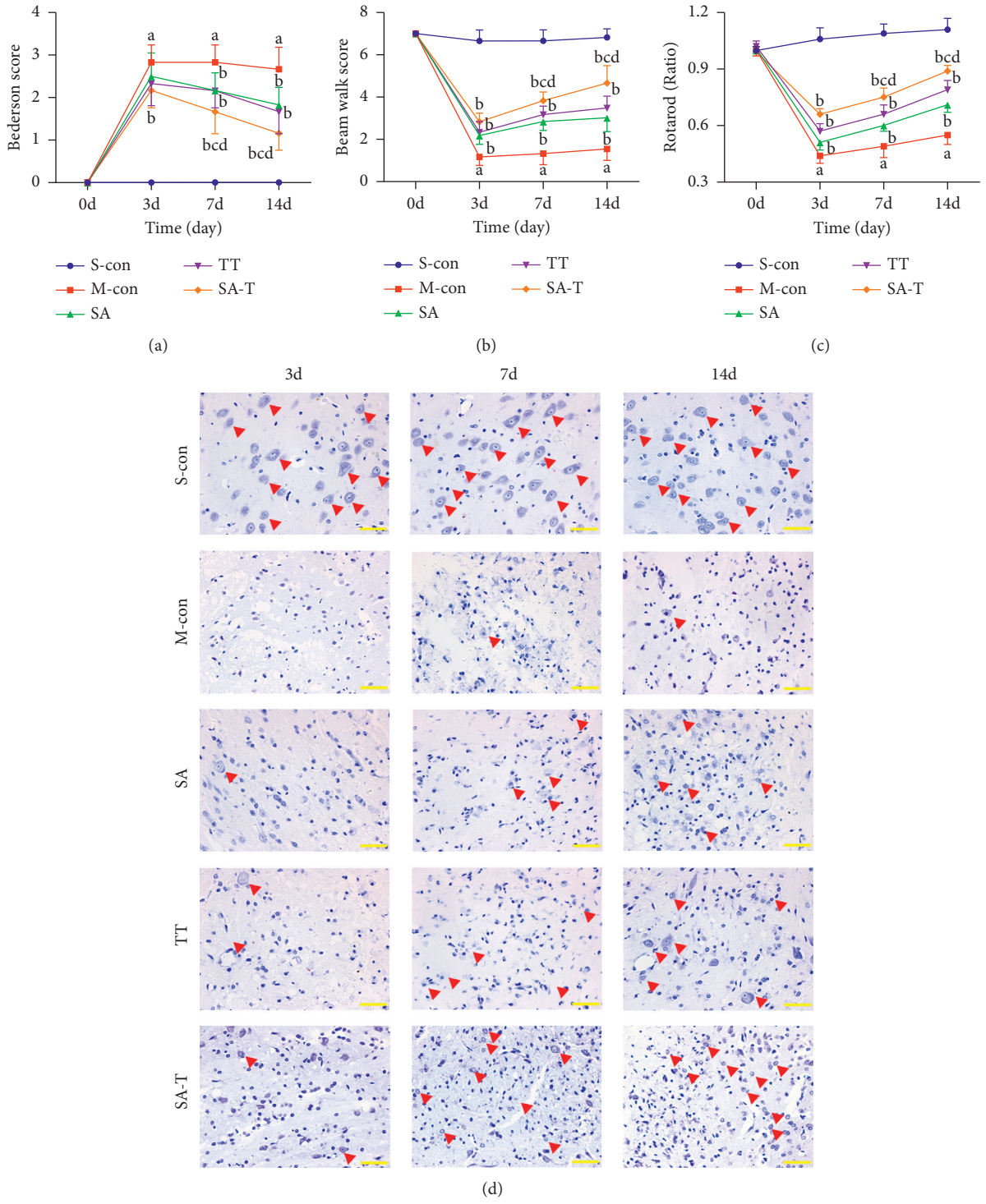

Figure 2: Effect of SA-T on behavioral outcomes and neuronal damage of the pMCAO model. (a), (b), (c) Behavioral outcomes were evaluated using a modified Bederson test, Beam Walk test, and Rota-rod test before and 3, 7, and 14 days upon pMCAO. (d) The brain tissues were stained with cresyl violet and observed using a microscope on the 3rd, 7th, and 14th days upon pMCAO (× 400). The red arrows mark intact neurons. Data are presented as mean ± SEM; $n = 6$ per group at each time point. $^{a}P < 0.05$ vs. S-con group, $^{b}P < 0.05$ vs. M-con group, $^{c}P < 0.05$ vs. SA group, $^{d}P < 0.05$ vs. TT group.

group, while markedly more TUNEL and NeuN positive neurons were found in the model group on the 3rd, 7th, and 14th days ($P < 0.05$). SA, TT, and SA-T treatments significantly decreased the number of TUNEL and NeuN positive neurons in pMCAO rats ($P < 0.05$), and SA-T showed the highest antiapoptotic effect.

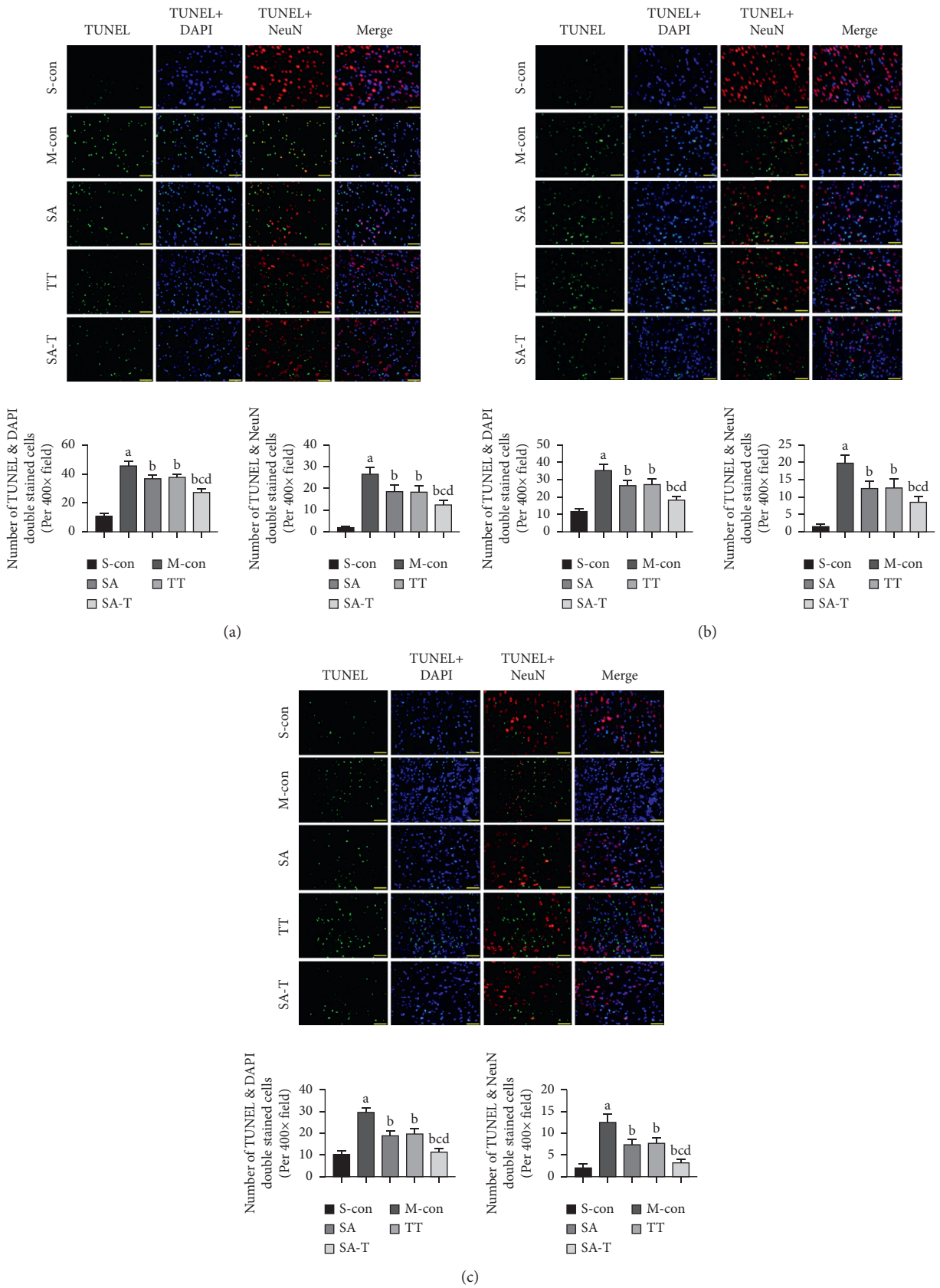

Figure 3: Effect of SA-T on neuronal apoptosis of the pMCAO model. (a) Quantification of TUNEL positive cells and NeuN and TUNEL double-positive cells on the 3rd day. (b) Quantification of TUNEL positive cells and NeuN and TUNEL double-positive cells on the 7th day. (c) Quantification of TUNEL positive cells and NeuN and TUNEL double-positive cells on the 14th day. Double immunofluorescence staining for TUNEL (green), NeuN (red), and nuclei-stained with DAPI (blue). Fluorescence images were captured using a fluorescence microscope (× 400). Data are presented as mean ± SEM; $n = 6$ per group at each time point. $^{a}P < 0.05$ vs. S-con group, $^{b}P < 0.05$ vs. M-con group, $^{c}P < 0.05$ vs. SA group, $^{d}P < 0.05$ vs. TT group.

3.4. Effect of SA-T on cIAP1 Expression in Neurons of the pMCAO Model. Apoptosis is a critical factor for the loss of hypoxic-ischemic neurons in the nervous system, and cIAP1 is an important regulator of apoptosis [20, 21]. The double immunofluorescence staining results showed that multitudinous cIAP1 and NeuN positive neurons existed in the cortex penumbra of the ischemic brain in the sham-operated group (Figure 4). Compared with the sham-operated group, the fluorescence intensity of cIAP1 and NeuN proteins and the number of cIAP1 and NeuN positive neurons were markedly reduced on the 3rd, 7th, and 14th days in the model group ($P < 0.05$). SA, TT, and SA-T significantly increased the fluorescence intensity of cIAP1, NeuN, and the number of cIAP1 and NeuN positive neurons in pMCAO rats ($P < 0.05$), with SA-T showing the highest effect.

3.5. Effects of Three Pairs of shRNA Expression Vectors on cIAP1 Expression. The results of Western blotting and RT-PCR showed that there was no decline in cIAP1 protein or mRNA expression in the negative group (NC) as compared with the control group. However, the expression of cIAP1 protein was decreased by 39%, 75%, and 25% in the shRNA-1, shRNA-2, and shRNA-3 groups, respectively (Figure 5(a)). Moreover, *cIAP1* mRNA expression was decreased in the shRNA-1, shRNA-2, and shRNA-3 groups by ~30%, 75%, and 18%, respectively (Figure 5(b)). These results suggest that shRNA-2 provided the most reliable expression. Therefore, shRNA-2 was selected for the subsequent experiments.

3.6. Effect of SA-T on Behavioral Outcomes in the cIAP1 shRNA Interference pMCAO Model. As shown in Figures 6(a)–6(c), the SA-T + Lv *cIAP1* NC group showed the same trend as SA-T in behavioral outcomes, and there was no difference between the two groups ($P > 0.05$). However, the therapeutic effect of SA-T on cerebral ischemia was completely reversed by Lv *cIAP1*. There was no significant difference between SA-T + Lv *cIAP1* and model groups ($P > 0.05$), and behavioral outcomes in the SA-T + Lv *cIAP1* group were significantly worse than in the SA-T group ($P < 0.05$).

3.7. Effect of SA-T on Neuronal Damage in the cIAP1 shRNA Interference pMCAO Model. HE and Nissl staining were conducted to evaluate the histological damage in the brain. The results of HE staining showed that most cells were arranged disorderly, and neuronal necrosis was observed in the model group. SA-T and SA-T + Lv *cIAP1* NC treatment markedly ameliorated these pathological abnormalities, but no significant difference was observed between the two groups ($P > 0.05$). Compared with the SA-T group, more neuronal necrosis existed in the SA-T + Lv *cIAP1* group, and the difference was statistically significant ($P < 0.05$) (Figure 6(d)). Nissl staining showed a similar trend with HE staining; fewer Nissl bodies were observed in the SA-T + Lv *cIAP1* group when compared with the SA-T group ($P < 0.05$) (Figure 6(e)).

3.8. Effect of SA-T on Neuronal Apoptosis and NeuN Expression in the cIAP1 shRNA Interference pMCAO Model. Neuronal apoptosis in the *cIAP1* shRNA interference pMCAO model was further determined by a TUNEL assay. Treatment with SA-T alone or combined therapy with Lv *cIAP1* NC partly diminished neuronal apoptosis induced by cerebral ischemia (Figure 7(a)). The same results were also confirmed by Western blotting, which showed that the expression level of NeuN protein in the SA-T and SA-T + Lv *cIAP1* NC group significantly increased when compared with the model group ($P < 0.05$) (Figure 7(b)). However, in the SA-T + Lv *cIAP1* group, SA-T showed no significant antiapoptotic effect, and the number of TUNEL positive cells was markedly higher than that in the SA-T group ($P < 0.05$). In addition, Western blotting results showed that the NeuN protein expression level in the SA-T + Lv *cIAP1* group was significantly lower than that in the SA-T group ($P < 0.05$). Even on the 3rd and 7th days, the expression of NeuN protein in the SA-T + Lv *cIAP1* group was significantly lower than that in the model group ($P < 0.05$).

3.9. Effect of SA-T on cIAP1 Expression in the cIAP1 shRNA Interference pMCAO Model. To further investigate the influence of SA-T on the expression patterns of cIAP1 in the cIAP1 shRNA interference pMCAO model, immunohistochemistry and Western blotting were used to compare cIAP1 protein levels in the five groups on the 3rd, 7th, and 14th days (Figures 7(c) and 7(d)). The results showed that the expression level of cIAP1 in the SA-T and SA-T + Lv *cIAP1* NC groups was upregulated when compared with the model group ($P < 0.05$), while no difference was found between the two groups ($P > 0.05$). The expression level of cIAP1 protein in the SA-T + Lv *cIAP1* group was significantly lower than that in the SA-T group ($P < 0.05$), but there was no difference between the SA-T + Lv *cIAP1* and model groups ($P > 0.05$). This further indicates that SA-T mainly plays a neuroprotective role by targeting cIAP1.

3.10. Effect of SA-T on the Caspase-8/-9/-3 Activation Pathway in the cIAP1 shRNA Interference pMCAO Model. Caspases are synthesized as proenzymes, which are activated by the cleavage of the prodomain at a specific aspartic acid cleaving site. As shown in Figure 8, the Western blotting results showed that SA-T significantly attenuated pMCAO-induced caspase-8, caspase-9, and caspase-3 activation ($P < 0.05$), but no additional effect was observed in the combined therapy with Lv *cIAP1* NC. Moreover, we found that SA-T had no significant reversal effect on the activation of caspase-8, caspase-9, and caspase-3 in the Lv *cIAP1*-transfected pMCAO model when compared with the model group ($P > 0.05$), while there were statistically significant increases as compared with the SA-T group ($P < 0.05$).

4. Discussion

Multitudinous clinical practice guidelines recommend early exercise after stroke to promote recovery from physical disability [22]. Yang et al. demonstrated that two weeks of

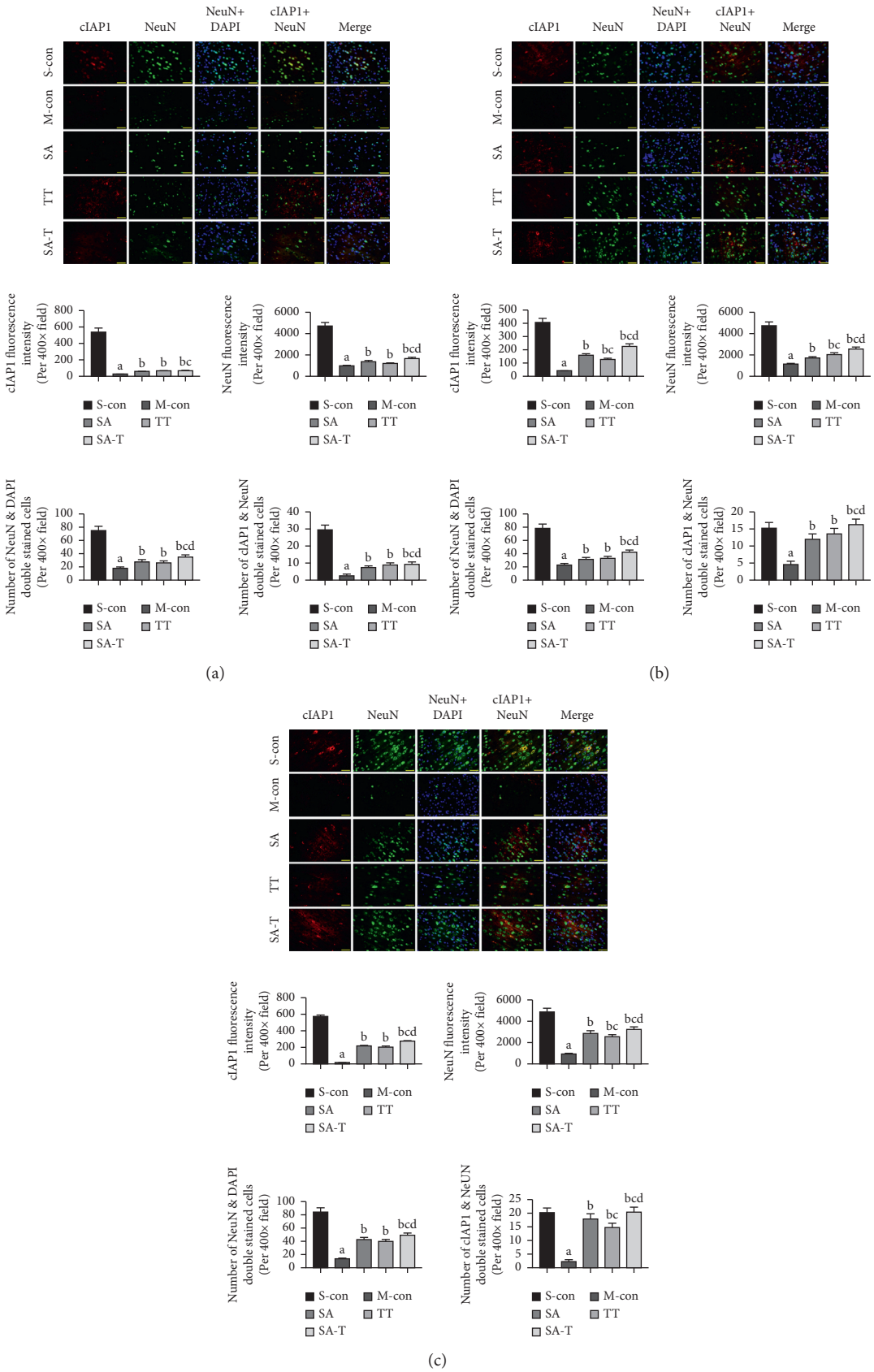

Figure 4: Effect of SA-T on cIAP1 expression in neurons of the pMCAO model on the 3rd day. (a) Quantification of fluorescence intensity of cIAP1 and NeuN and quantification of NeuN positive cells and cIAP1 and NeuN double-positive cells on the 3rd day. (b) Quantification of fluorescence intensity of cIAP1 and NeuN and quantification of NeuN positive cells and cIAP1 and NeuN double-positive cells on the 7th day. (c) Quantification of fluorescence intensity of cIAP1 and NeuN and quantification of NeuN positive cells and cIAP1 and NeuN double-positive cells on the 14th day. Double immunofluorescence staining for cIAP1 (red), NeuN (green), and nuclei-stained with DAPI (blue). Fluorescence images were captured using a fluorescence microscope (× 400). Data are presented as mean ± SEM; $n = 6$ per group at each time point. $^{a}P < 0.05$ vs. S-con group, $^{b}P < 0.05$ vs. M-con group, $^{c}P < 0.05$ vs. SA group, $^{d}P < 0.05$ vs. TT group.

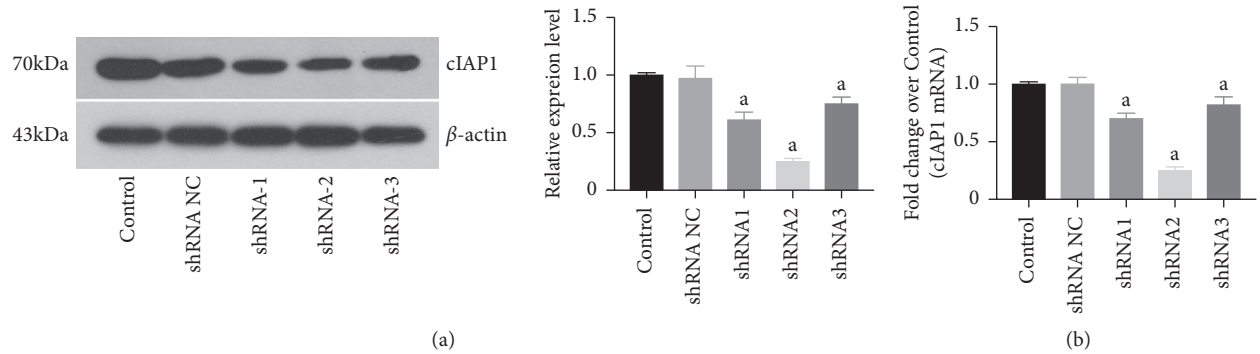

Figure 5: Effect of three pairs of shRNA expression vectors on cIAP1 protein expression. (a) Quantification of cIAP1 protein expression in SH-SY5Y cells. (b) Quantification of cIAP1 mRNA expression in SH-SY5Y cells. Data are presented as mean ± SEM; $n = 3$ per group. $^{a}P < 0.05$ vs. control group, $^{b}P < 0.05$ vs. shRNA-NC group.

early exercise promotes the recovery of motor and spatial memory in rats 24 h after MCAO [23]. Previous studies have shown that exercise could promote angiogenesis, increase microvessel density, improve cerebral blood supply, and, thus, reduce the cerebral infarction volume [24–26]. These possible mechanisms have been used to explain the positive effects of early exercise. In the present study, our results demonstrated that the combination therapy of SA and TT successfully improves the short-term and long-term motor function in pMCAO rats, which is better than using SA or TT alone.

According to the damage pattern of brain neurons, the ischemic area can be divided into the ischemic core area and the ischemic penumbra area. Neurons in the ischemic core area are necrotic immediately after acute ischemia and are rarely rescued. Conversely, neurons in the ischemic penumbra are less damaged and can recover, thus making them the target of various interventions [27]. Moreover, neurons in the ischemic area can be further injured by activating the apoptosis pathway after acute ischemic stroke [28]. Therefore, inhibiting neuronal apoptosis in the ischemic penumbra is a key strategy to potentially improve neurological function recovery after ischemic stroke and improve patient prognosis. Our results also demonstrated that the combination therapy of SA and TT significantly reduces the apoptosis of neurons in the ischemic penumbra, which is better than using SA or TT alone.

Apoptosis, also known as programmed cell death, is a highly regulated mechanism, which mainly activates a series of "caspases" through extrinsic and intrinsic mitochondria pathways to cause nuclear shrinkage, DNA fragmentation, and other apoptosis changes. The caspase-8/-9/-3 activation pathway plays a central role in the execution of apoptosis [29]. The extrinsic pathway, mainly involving the activation of caspase-8 and caspase-10, is initiated by the interaction of cell surface receptors and specific ligands with cell surface receptors such as death receptors, CD95/Fas, and tumor necrosis factor (TNF) [30, 31]. Caspase-9 is involved in the intrinsic mitochondria pathway, which is initiated by various stimuli such as hypoxia and cytotoxic agents, cellular distress, and DNA damage inside the cell [32, 33]. Following the activation of caspase-8 or caspase-9, activated caspase-3 is the final executor of both apoptosis pathways. The activation of caspase-3 results in poly (ADP-ribose) polymerase (PARP) degradation [34]. Previous studies have shown that caspase-8 is a potential target for future therapies, and targeted inhibition of the caspase-8/-3 pathway significantly attenuates the devastating functional losses that result from retinal or cerebral stroke [35]. In the present study, a large number of apoptotic cells were observed in the ischemic penumbra after cerebral ischemia in pMCAO rats when compared with the sham operation group at each time point, and the apoptotic number reached a peak in the acute stage (3 d after ischemia) and gradually decreased in the subacute stage (7 d and 14 d after ischemia). Our results also suggest that SA-T significantly inhibits the activation of the caspase-8/-9/-3 pathway when compared with the model group, so as to play an antiapoptotic role. Therefore, the decrease of neuronal apoptosis mediated by the inactivation of the caspase-8/-9/-3 pathway is an important way for ST-T in the motor function improvement in ischemic stroke (Figure 9).

The inhibitor of apoptosis (IAP) family is involved in various cellular processes, such as cell proliferation, apoptosis, cytokinesis, heavy metal homeostasis, signal transduction, and immunity [36–39]. The IAP family mainly includes cIAP1, cIAP2, X-linked IAP (XIAP), and survivin and is characterized by the presence of at least one baculovirus inhibitor of apoptosis repeat domain that promotes protein-protein interactions. cIAP1 is an important regulator of the apoptosis cascade, which inhibits subsequent exogenous and endogenous apoptosis by blocking caspase activity [40]. Multiple studies have shown that the deficiency of apoptosis caused by the overexpression of cIAP1 is closely related to the occurrence of various tumors and is also related to the poor prognosis of tumors and tumor resistance [41, 42]. Previous studies have confirmed that cIAP1 prevents caspase-3's feed-forward activation of procaspase-9 and can also directly bind to caspase-3 and caspase-7, thus inhibiting their activity [43]. In addition, the degradation of caspase-3 and caspase-7 proteasomes can be mediated by the active ubiquitin dependent on E3 ubiquitin ligase, which is related to the binding of cIAP1 with the IBM structure of activated caspase-3 and caspase-7 through its BIR2 domain [44].

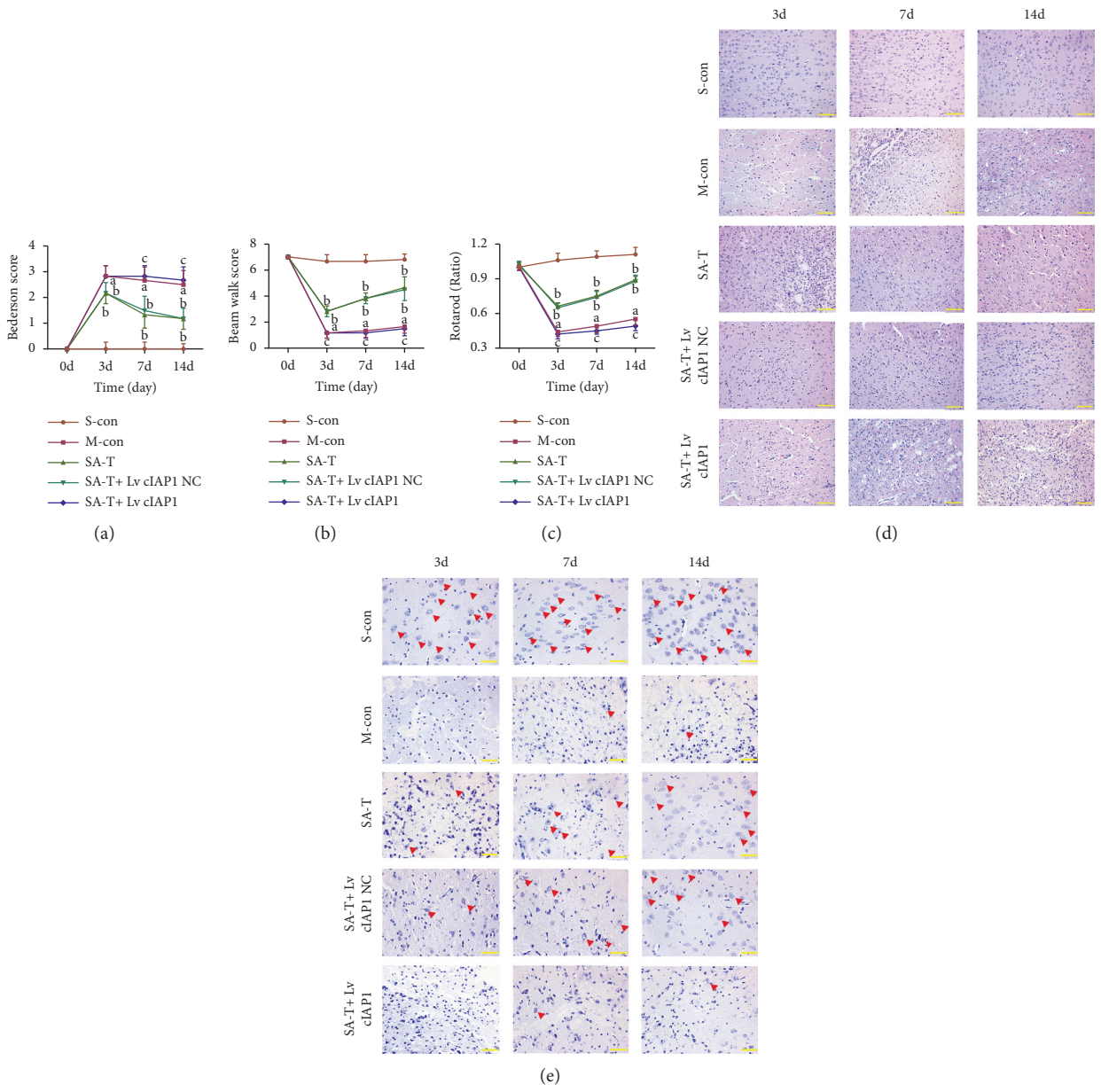

Figure 6: Effect of SA-T on behavioral outcomes in the cIAP1 shRNA interference pMCAO model. (a), (b), (c) Behavioral outcomes were evaluated using the modified Bederson test, Beam Walk test, and Rota-rod test before MCAO on the 3rd, 7th, and 14th day in the cIAP1 shRNA interference pMCAO model. (d) The brain tissues were stained with H&E and observed using a microscope on the 3rd, 7th, and 14th day in the cIAP1 shRNA interference pMCAO model (×200). (e) The brain tissues were stained with cresyl violet and observed using a microscope on the 3rd, 7th, and 14th day in the cIAP1 shRNA interference pMCAO model (× 400). Data are presented as mean ± SEM; $n = 6$ per group at each time point. $^{a}P < 0.05$ vs. S-con group, $^{b}P < 0.05$ vs. M-con group, $^{c}P < 0.05$ vs. SA-T group.

It was also confirmed that the expression of cIAP1 in primary cultured cortical neurons treated with glutamic acid was significantly decreased, and upregulation of cIAP1 could significantly inhibit apoptosis induced by glutamic acid and thus play a neuroprotective role [45]. In contrast, Motomatsu et al. found that hypothermic treatment reduced the levels of TNF-α and other inflammatory mediators and proinflammatory cytokines in the rabbit model of transient spinal cord ischemia and inhibited the expression of cIAP1/2 to promote the survival of neurons [46]. Nevertheless, there are a few studies on cIAP1 in ischemic stroke. A study on neurovascular damage after hypoxic-ischemic neonatal brain tissue shows that cIAP1 is a critical endogenous antiapoptotic brake induced by ischemic preconditioning and has a protective effect on neonatal cerebral neurovascular damage [20]. In this study, the expression level of cIAP1 was significantly downregulated in the pMCAO model and negatively correlated with the level of apoptosis when compared with the sham operation group at each time point. SA, TT, and SA-T treatment significantly upregulated

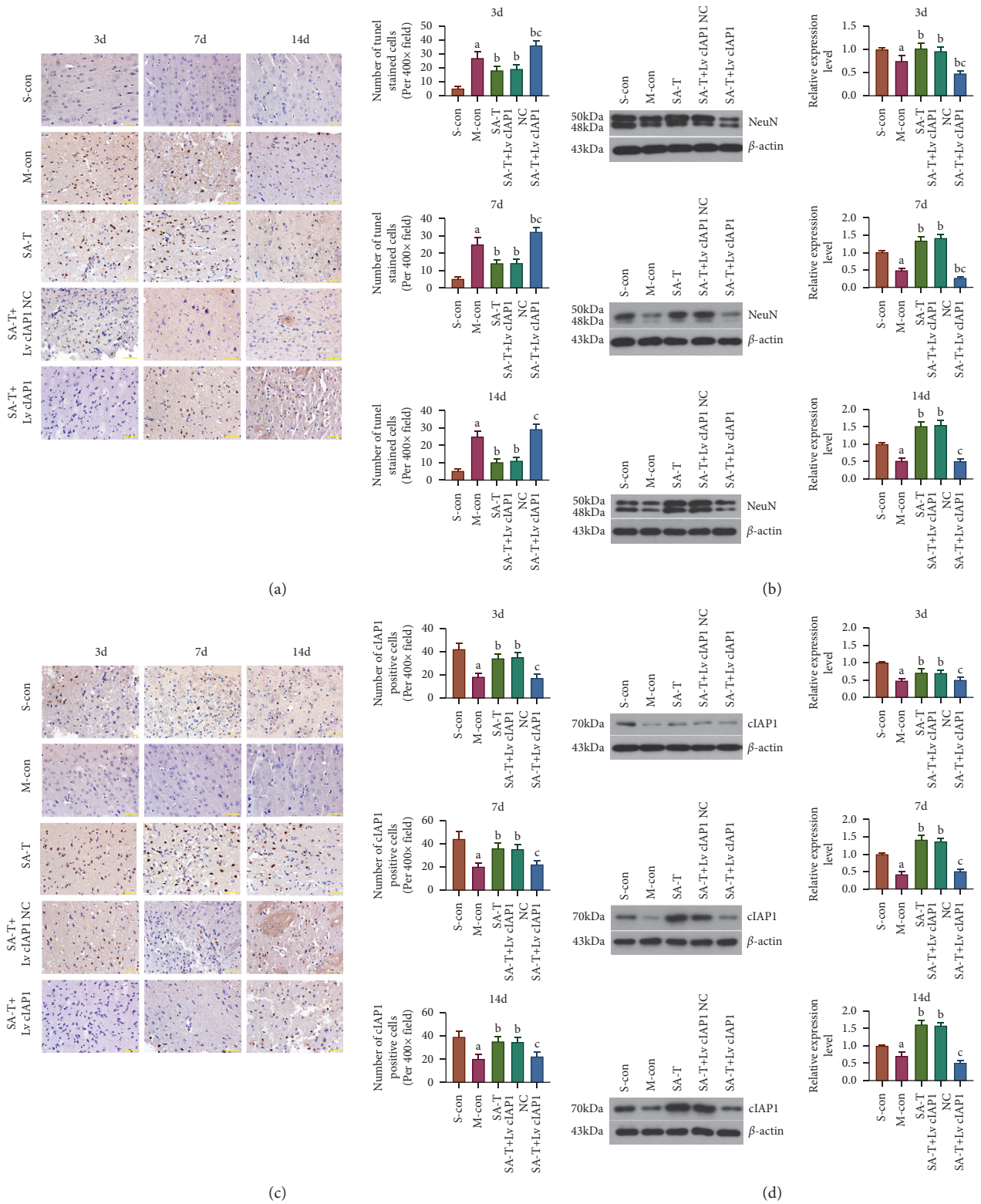

Figure 7: Effect of SA-T on neuronal apoptosis and the expression of NeuN and cIAP1 on the cIAP1 shRNA interference pMCAO model. (a) Quantification of TUNEL positive cells on the 3rd, 7th, and 14th days. Neuronal apoptosis using TUNEL assay. Images were captured using an optical microscope (× 400). (b) Detection of the expression level of NeuN protein in the brain by Western blot on the 3rd, 7th, and 14th days. (c) Quantification of cIAP1 positive cells on the 3rd, 7th, and 14th days. (d) Detection of the expression level of cIAP1 protein in the brain by Western blot on the 3rd, 7th, and 14th days. Data are presented as mean ± SEM; $n = 6$ per group at each time point. [a]$P < 0.05$ vs. S-con group, [b]$P < 0.05$ vs. M-con group, [c]$P < 0.05$ vs. SA-T group.

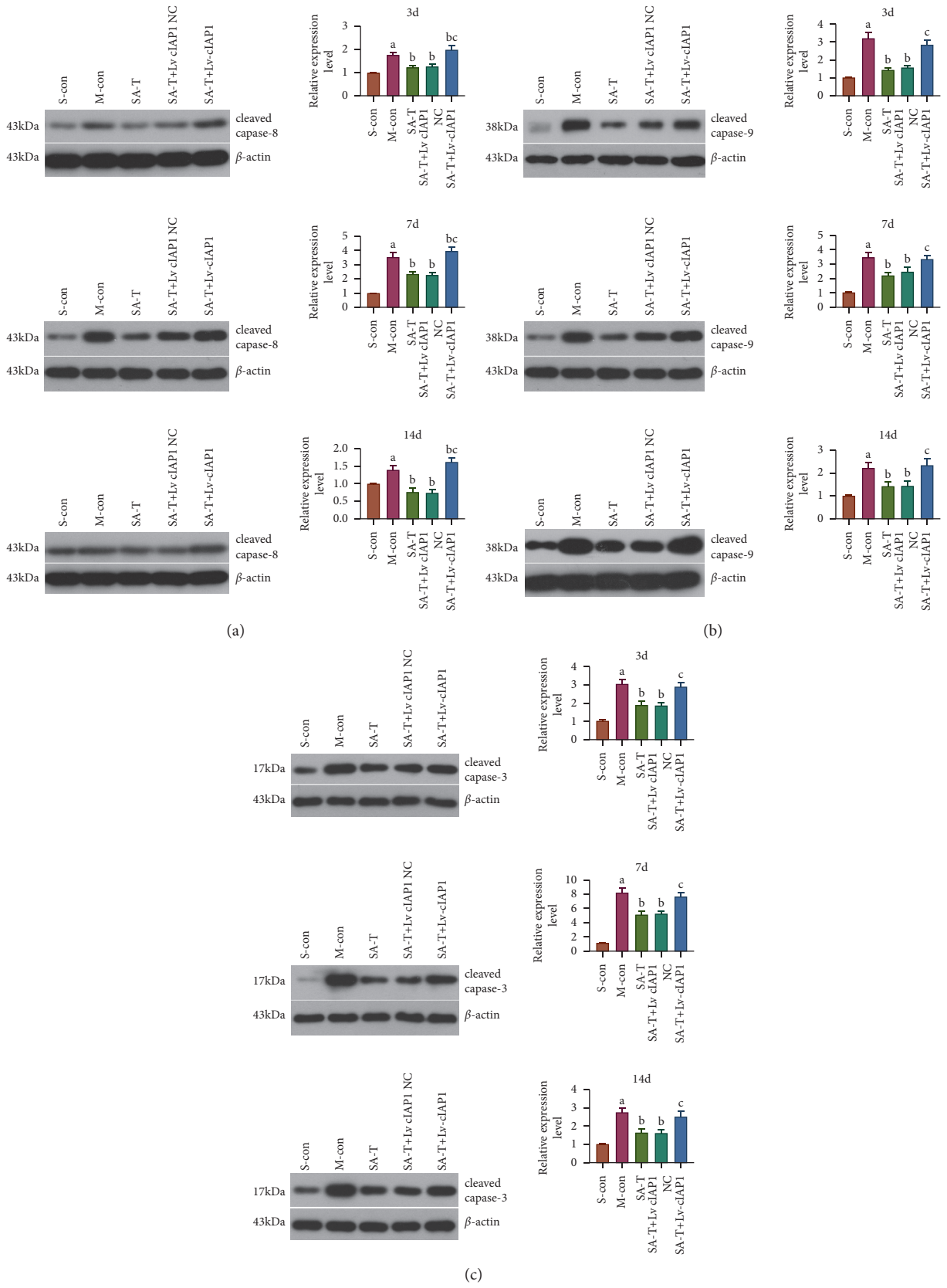

Figure 8: Effect of SA-T on the caspase-8/-9/-3 activation pathway in the cIAP1 shRNA interference pMCAO model. (a) Detection of the expression level of cleaved caspase-8 protein in the brain by Western blot on the 3rd, 7th, and 14th days. (b) Detection of the expression level of cleaved caspase-9 protein in the brain by Western blot on the 3rd, 7th, and 14th days. (c) Detection of the expression level of cleaved caspase-3 protein in the brain by Western blot on the 3rd, 7th, and 14th days. Data are presented as mean ± SEM; $n = 6$ per group at each time point. [a]$P < 0.05$ vs. S-con group, [b]$P < 0.05$ vs. M-con group, [c]$P < 0.05$ vs. SA-T group.

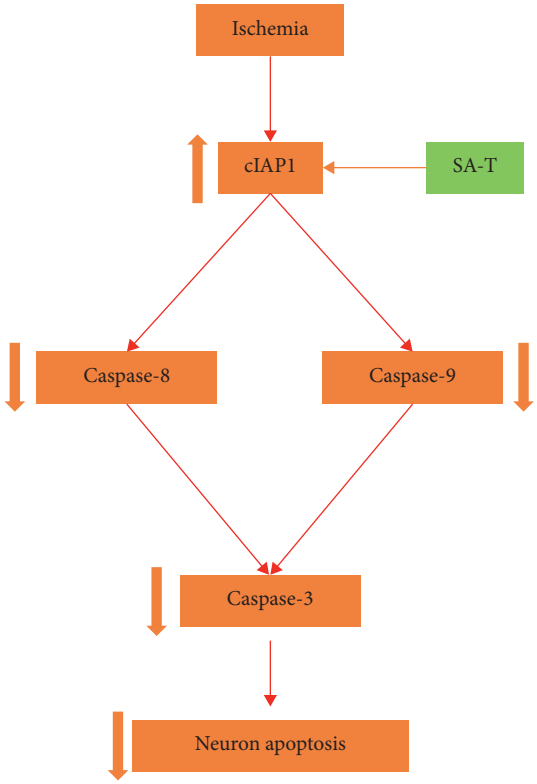

Figure 9: Mechanism diagram. SA-T plays a neuroprotective role through the caspase-independent pathway by upregulating the expression of cIAP1.

the expression level of cIAP1 and inhibited neuronal apoptosis in the ischemic penumbra tissue on the 3rd, 7th, and 14th days after cerebral ischemia.

Herein, our results suggest that the expression level of cIAP1 in the ischemic penumbra tissue is closely related to the apoptosis of neurons. However, the protective effect of SA-T on neurons was not observed in the combined injection of shRNA cIAP1 rats, which further confirmed that the protective effect of SA-T on ischemic neuron injury was mainly dependent on the regulation of cIAP1. Furthermore, the inhibitory effect of SA-T on the caspase-8/-9/-3 activation pathway was completely reversed by intracerebroventricular injection of shRNA cIAP1. These results further confirmed that SA-T regulates the caspase-8/-9/-3 pathway mainly by targeting cIAP1. However, this research has certain time and technical limitations. First of all, this study only explored the neuroprotective mechanism of scalp acupuncture combined with treadmill training therapy from the aspect of nerve apoptosis. Secondly, this study did not conduct in-depth research on the signal transduction pathway of cIAP1 regulating cell apoptosis. Therefore, it has certain limitations. We will further explore from the perspectives of astrocytes and vascular endothelial cells in later studies.

In conclusion, we first report the neuroprotective effect of cIAP1 in ischemic stroke. Mechanistically, cIAP1 inhibits the apoptosis of neurons in the ischemic penumbra by inhibiting the activation of the caspase-8/-9/-3 pathway. Moreover, we found that the combined therapy involving scalp acupuncture and treadmill training improves the motor function by upregulating the expression level of cIAP1, and its short-term and long-term effects are better than scalp acupuncture and treadmill training alone. These results suggest that the combination of scalp acupuncture and treadmill training is a potential rehabilitation strategy for ischemic stroke.

Data Availability

The data extracted from this Institute's Analytical are stored in the FAIRDOMHub database [47] (https://fairdomhub.org/projects/240).

Conflicts of Interest

There are no conflicts of interest to declare.

Acknowledgments

This study received funding from the Natural Science Foundation of China (No. 81473762), the Natural Science Foundation of Heilongjiang Province (ZD2019H007), the Guizhou Province Basic Research Project (Qian Ke He Ji Chu-ZK [2021] General 505), and the Youth Science and Technology Talent Growth Project of the Guizhou Provincial Department of Education (Qian Jiao He KY Zi [2021] 210).

References

[1] M. S. Phipps and C. A. Cronin, "Management of acute ischemic stroke," *BMJ*, vol. 368, Article ID l6983, 2020.

[2] W. J. Powers, A. A. Rabinstein, T. Ackerson et al., "Guidelines for the early management of patients with acute ischemic stroke: 2019 update to the 2018 guidelines for the early management of acute ischemic stroke: a guideline for healthcare professionals from the American heart association/American stroke association," *Stroke*, vol. 50, no. 12, pp. e344–e418, 2019.

[3] Collaborators GBDLRoS, V. L. Feigin, G. Nguyen et al., "Global, regional, and country-specific lifetime risks of stroke, 1990 and 2016," *New England Journal of Medicine*, vol. 379, no. 25, pp. 2429–2437, 2018.

[4] M. Guerra Padilla, F. Molina Rueda, and I. M. Alguacil Diego, "Effect of ankle-foot orthosis on postural control after stroke: a systematic review," *Neurologia*, vol. 29, no. 7, pp. 423–432, 2014.

[5] V. Weerdesteyn, M. d. Niet, H. J. R. van Duijnhoven, and A. C. H. Geurts, "Falls in individuals with stroke," *Journal of Rehabilitation Research and Development*, vol. 45, no. 8, pp. 1195–1213, 2008.

[6] P. Wu, E. Mills, D. Moher, and D. Seely, "Acupuncture in poststroke rehabilitation," *Stroke*, vol. 41, no. 4, pp. e171–9, 2010.

[7] B.-H. Yu, Y. Xing, F. Zhang, and M. Moss, "The therapeutic effect of electroacupuncture therapy for ischemic stroke," *Evidence-based Complementary and Alternative Medicine*, vol. 2020, Article ID 6415083, 9 pages, 2020.

[8] L. Chavez, S.-S. Huang, I. MacDonald, J.-G. Lin, Y.-C. Lee, and Y.-H. Chen, "Mechanisms of acupuncture therapy in ischemic stroke rehabilitation: a literature review of basic

studies," *International Journal of Molecular Sciences*, vol. 18, no. 11, p. 2270, 2017.

[9] Y. Xing, M. Zhang, W.-B. Li, F. Dong, and F. Zhang, "Mechanisms involved in the neuroprotection of electroacupuncture therapy for ischemic stroke," *Frontiers in Neuroscience*, vol. 12, p. 929, 2018.

[10] Z. Liu, L. Guan, Y. Wang, C.-L. Xie, X.-M. Lin, and G.-Q. Zheng, "History and mechanism for treatment of intracerebral hemorrhage with scalp acupuncture," *Evidence-based Complementary and Alternative Medicine*, vol. 2012, Article ID 895032, 9 pages, 2012.

[11] W.-W. Wang, C.-L. Xie, L. Lu, and G.-Q. Zheng, "A systematic review and meta-analysis of Baihui (GV20)-based scalp acupuncture in experimental ischemic stroke," *Scientific Reports*, vol. 4, no. 1, p. 3981, 2014.

[12] Y. Wang, J. Shen, X.-M. Wang et al., "Scalp acupuncture for acute ischemic stroke: a meta-analysis of randomized controlled trials," *Evidence-based Complementary and Alternative Medicine*, vol. 2012, Article ID 480950, 9 pages, 2012.

[13] J. C. Polese, L. Ada, C. M. Dean, L. R. Nascimento, and L. F. Teixeira-Salmela, "Treadmill training is effective for ambulatory adults with stroke: a systematic review," *Journal of Physiotherapy*, vol. 59, no. 2, pp. 73–80, 2013.

[14] G. P. Morris, A. L. Wright, R. P. Tan, A. Gladbach, L. M. Ittner, and B. Vissel, "A comparative study of variables influencing ischemic injury in the longa and koizumi methods of intraluminal filament middle cerebral artery occlusion in mice," *PLoS One*, vol. 11, no. 2, Article ID e0148503, 2016.

[15] X.-D. Feng, H.-L. Wang, F.-L. Liu et al., "Electroacupuncture improves learning and memory functions in a rat cerebral ischemia/reperfusion injury model through PI3K/Akt signaling pathway activation," *Neural Regeneration Research*, vol. 16, no. 6, pp. 1011–1016, 2021.

[16] J. B. Bederson, L. H. Pitts, M. Tsuji, M. C. Nishimura, R. L. Davis, and H. Bartkowski, "Rat middle cerebral artery occlusion: evaluation of the model and development of a neurologic examination," *Stroke*, vol. 17, no. 3, pp. 472–476, 1986.

[17] D. M. Feeney, A. Gonzalez, and W. A. Law, "Amphetamine, haloperidol, and experience interact to affect rate of recovery after motor cortex injury," *Science*, vol. 217, no. 4562, pp. 855–857, 1982.

[18] W. Yang, X. Chen, J. Pan et al., "Malibatol A protects against brain injury through reversing mitochondrial dysfunction in experimental stroke," *Neurochemistry International*, vol. 80, pp. 33–40, 2015.

[19] S. Ashwal, B. Tone, H. R. Tian, D. J. Cole, and W. J. Pearce, "Core and penumbral nitric oxide synthase activity during cerebral ischemia and reperfusion," *Stroke*, vol. 29, no. 5, pp. 1037–1047, 1998.

[20] W.-Y. Lin, Y.-C. Chang, C.-J. Ho, and C.-C. Huang, "Ischemic preconditioning reduces neurovascular damage after hypoxia-ischemia via the cellular inhibitor of apoptosis 1 in neonatal brain," *Stroke*, vol. 44, no. 1, pp. 162–169, 2013.

[21] Y. R. Kim, H. N. Kim, J. Y. Jang et al., "Effects of electroacupuncture on apoptotic pathways in a rat model of focal cerebral ischemia," *International Journal of Molecular Medicine*, vol. 32, no. 6, pp. 1303–1310, 2013.

[22] S. A. Billinger, R. Arena, J. Bernhardt et al., "Physical activity and exercise recommendations for stroke survivors," *Stroke*, vol. 45, no. 8, pp. 2532–2553, 2014.

[23] L. Yang, J. Zhang, Y. Deng, and P. Zhang, "The effects of early exercise on motor, sense, and memory recovery in rats with stroke," *American Journal of Physical Medicine & Rehabilitation*, vol. 96, no. 3, pp. e36–e43, 2017.

[24] F. Matsuda, H. Sakakima, and Y. Yoshida, "The effects of early exercise on brain damage and recovery after focal cerebral infarction in rats," *Acta Physiologica*, vol. 201, no. 2, pp. 275–287, 2011.

[25] C. Morland, K. A. Andersson, Ø. P. Haugen et al., "Exercise induces cerebral VEGF and angiogenesis via the lactate receptor HCAR1," *Nature Communications*, vol. 8, no. 1, Article ID 15557, 2017.

[26] P. Zhang, H. Yu, N. Zhou et al., "Early exercise improves cerebral blood flow through increased angiogenesis in experimental stroke rat model," *Journal of NeuroEngineering and Rehabilitation*, vol. 10, no. 1, p. 43, 2013.

[27] A. J. Yoo, L. A. Verduzco, P. W. Schaefer, J. A. Hirsch, J. D. Rabinov, and R. G. González, "MRI-based selection for intra-arterial stroke therapy," *Stroke*, vol. 40, no. 6, pp. 2046–2054, 2009.

[28] S. Vidale, A. Consoli, M. Arnaboldi, and D. Consoli, "Postischemic inflammation in acute stroke," *Journal of Clinical Neurology*, vol. 13, no. 1, pp. 1–9, 2017.

[29] S.-C. Wang, J.-M. Chow, M.-H. Chien et al., "Cantharidic acid induces apoptosis of human leukemic HL-60 cells via c-Jun N-terminal kinase-regulated caspase-8/-9/-3 activation pathway," *Environmental Toxicology*, vol. 33, no. 4, pp. 514–522, 2018.

[30] V. Viswanath, Y. Wu, R. Boonplueang et al., "Caspase-9 activation results in downstream caspase-8 activation and bid cleavage in 1-methyl-4-phenyl-1,2,3,6-tetrahydropyridine-induced Parkinson's disease," *Journal of Neuroscience*, vol. 21, no. 24, pp. 9519–9528, 2001.

[31] S. Zhuang, M. C. Lynch, and I. E. Kochevar, "Caspase-8 mediates caspase-3 activation and cytochrome c release during singlet oxygen-induced apoptosis of HL-60 cells," *Experimental Cell Research*, vol. 250, no. 1, pp. 203–212, 1999.

[32] J. M. Brown and L. D. Attardi, "The role of apoptosis in cancer development and treatment response," *Nature Reviews Cancer*, vol. 5, no. 3, pp. 231–237, 2005.

[33] S. Elmore, "Apoptosis: a review of programmed cell death," *Toxicologic Pathology*, vol. 35, no. 4, pp. 495–516, 2007.

[34] J. Li and J. Yuan, "Caspases in apoptosis and beyond," *Oncogene*, vol. 27, no. 48, pp. 6194–6206, 2008.

[35] A. P. Shabanzadeh, P. M. D'Onofrio, P. P. Monnier, and P. D. Koeberle, "Targeting caspase-6 and caspase-8 to promote neuronal survival following ischemic stroke," *Cell Death & Disease*, vol. 6, no. 11, e1967 pages, 2015.

[36] A. C. Mita, M. M. Mita, S. T. Nawrocki, and F. J. Giles, "Survivin: key regulator of mitosis and apoptosis and novel target for cancer therapeutics," *Clinical Cancer Research*, vol. 14, no. 16, pp. 5000–5005, 2008.

[37] F. Abadía-Molina, V. Morón-Calvente, S. D. Baird, F. Shamim, F. Martín, and A. MacKenzie, "Neuronal apoptosis inhibitory protein (NAIP) localizes to the cytokinetic machinery during cell division," *Scientific Reports*, vol. 7, no. 1, Article ID 39981, 2017.

[38] S. M. Srinivasula and J. D. Ashwell, "IAPs: what's in a name?" *Molecular Cell*, vol. 30, no. 2, pp. 123–135, 2008.

[39] D. Conte, M. Holcik, C. A. Lefebvre et al., "Inhibitor of apoptosis protein cIAP2 is essential for lipopolysaccharide-induced macrophage survival," *Molecular and Cellular Biology*, vol. 26, no. 2, pp. 699–708, 2006.

[40] A. D. Schimmer, "Inhibitor of apoptosis proteins: translating basic knowledge into clinical practice," *Cancer Research*, vol. 64, no. 20, pp. 7183–7190, 2004.

[41] S. Qi, S. Mogi, H. Tsuda et al., "Expression of cIAP-1 correlates with nodal metastasis in squamous cell carcinoma of the

tongue," *International Journal of Oral and Maxillofacial Surgery*, vol. 37, no. 11, pp. 1047–1053, 2008.

[42] T. Tanimoto, H. Tsuda, N. Imazeki et al., "Nuclear expression of cIAP-1, an apoptosis inhibiting protein, predicts lymph node metastasis and poor patient prognosis in head and neck squamous cell carcinomas," *Cancer Letters*, vol. 224, no. 1, pp. 141–151, 2005.

[43] B. P. Eckelman and G. S. Salvesen, "The human anti-apoptotic proteins cIAP1 and cIAP2 bind but do not inhibit caspases," *Journal of Biological Chemistry*, vol. 281, no. 6, pp. 3254–3260, 2006.

[44] Y. E. Choi, M. Butterworth, S. Malladi, C. S. Duckett, G. M. Cohen, and S. B. Bratton, "The E3 ubiquitin ligase cIAP1 binds and ubiquitinates caspase-3 and -7 via unique mechanisms at distinct steps in their processing," *Journal of Biological Chemistry*, vol. 284, no. 19, pp. 12772–12782, 2009.

[45] J. Y. Jang, H. N. Kim, Y. R. Kim et al., "Hexane extract from Polygonum multiflorum attenuates glutamate-induced apoptosis in primary cultured cortical neurons," *Journal of Ethnopharmacology*, vol. 145, no. 1, pp. 261–268, 2013.

[46] Y. Motomatsu, M. Sakurai, H. Onitsuka, K. Abe, and A. Shiose, "Hypothermia inhibits the expression of receptor interacting protein kinases 1 and 3 after transient spinal cord ischaemia in rabbits," *European Journal of Vascular and Endovascular Surgery*, vol. 59, no. 5, pp. 824–833, 2020.

[47] K. Wolstencroft, O. Krebs, J. L. Snoep et al., "FAIRDOMHub: a repository and collaboration environment for sharing systems biology research," *Nucleic Acids Research*, vol. 45, pp. D404–D407, 2017.

Hindawi
Evidence-Based Complementary and Alternative Medicine
Volume 2021, Article ID 3056963, 8 pages
https://doi.org/10.1155/2021/3056963

Research Article

Electroacupuncture Preconditioning Reduces Oxidative Stress in the Acute Phase of Cerebral Ischemia-Reperfusion in Rats by Regulating Iron Metabolism Pathways

Runyu Liang,[1] **Qiang Tang**,[2] **Wenjing Song**,[1] **Mei Zhang**,[1] **Lili Teng**,[1] **Yuying Kang**,[2] **and Luwen Zhu**[3]

[1]*Heilongjiang University of Chinese Medicine, Harbin, Heilongjiang, China*
[2]*Second Affiliated Hospital of Heilongjiang University of Chinese Medicine, Harbin, Heilongjiang, China*
[3]*Fourth Affiliated Hospital of Heilongjiang University of Chinese Medicine, Harbin, Heilongjiang, China*

Correspondence should be addressed to Luwen Zhu; zhuluwen1983@126.com

Received 4 September 2021; Revised 8 October 2021; Accepted 25 October 2021; Published 8 November 2021

Academic Editor: Feng Zhang

Background. Oxidative stress is an important mechanism of cerebral ischemia-reperfusion injury. Ferroptosis caused by iron overload after cerebral ischemia-reperfusion is considered a common cause of oxidative stress. Many recent studies have shown that electroacupuncture (EA) can regulate the expression of inflammatory factors, and the use of electroacupuncture preconditioning can produce a protective effect, which can reduce injury after cerebral ischemia and reperfusion. We aimed to assess whether EA could be used to reduce oxidative stress. *Methods*. The oxidative stress level of rats during the acute phase of cerebral ischemia and reperfusion was assessed with and without preconditioning with EA. Molecular biology methods were used to detect iron metabolism and oxidative stress-related proteins. *Results*. Rats that had EA preconditioning had lower infarct volumes than rats in the control group. Furthermore, western blot analysis showed that the expression of iron metabolism-related protein FPN-1 was higher in the intervention group than in the model group after reperfusion. In this regard, further investigation also demonstrated higher expression of glutathione and glutathione peroxidase-4, and lower reactive oxygen species values in the brain tissue of the EA group were compared with those of the control group rats. *Conclusions*. Electroacupuncture preconditioning can reduce oxidative stress after cerebral ischemia-reperfusion by regulating iron overload.

1. Introduction

Cerebral ischemia is a disease that endangers human health and quality of life and is the leading cause of death and disability worldwide [1]. After cerebral ischemia occurs, thrombolytic therapy is usually the first-choice treatment, and emboli can be surgically removed. However, when the blood supply is suddenly restored to ischemic and hypoxic brain tissue, it triggers oxidative stress, neuroinflammation, and a series of other complex cell cascade reactions [2]. This collection of conditions is known as ischemia-reperfusion injury and is considered a critical cause of disability after stroke treatment [3]. At present, reperfusion injuries are believed to be caused by immune cells and oxygen atoms in perfused blood [4, 5]. Moreover, reperfusion injury can affect the expression of hepcidin. As a regulator of iron balance, hepcidin can reduce the expression of ferroportin-1(FPN-1) so that iron ions can be retained in cells [6]. The iron ions in the cells cannot be transported in time, leaving the cells in a state of iron overload [7, 8]. In this state, the cell membrane is oxidized and broken by oxidative stress triggered by excessive free iron, resulting in ferroptosis [9, 10]. Nerve cells are greatly affected by damage caused by ferroptosis and other oxidative stress due to high oxygen consumption and difficulty in processing reactive oxygen species (ROS) [11]. Glutathione peroxidase-4 (GPX4) can deplete glutathione (GSH) to resist oxidative stress and is an important mechanism to resist oxidative stress in cells

[12, 13]. Consequently, restoring the activity of GPX4 in cells and increasing GSH content will become a therapeutic strategy in combating oxidative stress damage.

Given the incidence and repercussions of oxidative stress after ischemia-reperfusion, it is vital to develop a treatment strategy that reduces oxidative stress. Administration of electroacupuncture (EA) stimulation before cerebral ischemia has been presented as an effective treatment strategy by several recent studies [14, 15]. EA not only induces ischemic tolerance but also inhibits the oxidative stress caused by reperfusion [16–19].

EA has been used as an effective and safe treatment for various diseases, especially brain diseases and their rehabilitation [20]. The effectiveness of electroacupuncture involves the acupuncture points, interval, intensity, and duration of intervention for stroke treatment [21]. Compared with other acupoints, we chose Baihui (GV20) and Zusanli (ST36). The literature has shown that electrical stimulation of Baihui can increase astrocytes and promote angiogenesis [22]. Electrical stimulation of Zusanli may cause increased cerebral blood flow in normal rats or those with ischemic stroke and can enhance the functional connection between the ipsilateral motor cortex and motor function-related brain areas (including the motor cortex, striatum, and sensory cortex) in focal ischemic rats [23, 24]. Furthermore, EA preconditioning can reduce the injury after cerebral ischemia-reperfusion and induce cerebral ischemic tolerance, and other effects have been confirmed [25, 26]. Therefore, we hypothesize that EA preconditioning can reduce the inflammatory response during cerebral ischemia-reperfusion and reduce the iron overload caused by oxidative stress.

Herein, we determined the effect of EA preconditioning on the acute phase of cerebral ischemia-reperfusion by assessing the levels of iron transport-related proteins and oxidative stress-related proteins during ischemia-reperfusion in a rat model.

2. Materials and Methods

2.1. Animals and Grouping. Male Sprague Dawley rats aged 8–10 weeks (240 ± 20 g) were obtained from Liaoning Changsheng Biotechnology Co., Ltd. (SCXK 2015-0001). Rats were housed in a ventilated room with free access to food and water and maintained at a temperature of 24 ± 2°C, with a humidity of 60 ± 5%, and a day/night cycle was created by alternating between bright and dark lighting every 12 h. The rats were divided into 4 groups of 12 rats, allocated by a random number generator, and reared independently. The rats were divided into four groups: the sham group (sham) ($n = 12$), cerebral ischemia-reperfusion group (I/R), electroacupuncture preconditioning group (EA), and electroacupuncture preconditioning and sham group (EA + S). Each group was subdivided for sacrifice at either 1 day ($n = 6$) or 3 days ($n = 6$) after reperfusion. The experimental protocol is shown in Figure 1(a). The experiment was approved by the Animal Care and Use Committee at the Heilongjiang University of Chinese Medicine, and all animals were euthanized in accordance with the National Institutes of Health Guidelines.

2.2. Electroacupuncture Preconditioning Protocol. EA preconditioning was performed 14 days before Middle Cerebral Artery Occlusion (MCAO) modeling. First, the rat was fixed on a special fixator, and the Baihui point (GV20) was punctured to a depth of 4 mm and Zusanli point (ST36) to a depth of 8 mm and an angle of 15°, with a 0.13×0.25 mm acupuncture needle (Hwato, Suzhou Medical Appliance Factory, China). The EA treatment instrument (G6805-2A, Shanghai Huayi Group, China) was used to simultaneously stimulate the acupoints. The positive pole of the instrument was connected to Baihui (GV20), and the negative pole was connected to Zusanli (ST36) using the density wave, frequency 2/15 Hz, stimulation intensity 1 mA, 30 min per day, 6 days a week, and total two weeks. The sham and I/R groups did not undergo EA preconditioning, but rats were handled daily, similar to those experiencing EA.

2.3. I/R Model. The I/R model was established 24 h after the two-week EA preconditioning, as described previously [27, 28]. Briefly, the rats were placed on an animal anesthesia machine (RWD510, RWD Life Science Inc., China) and anesthetized with 5% isoflurane inhalation. Next, a small opening was made in the common carotid artery on the left, and a wire thread embolus (A4-263450, Beijing Cinotech Co., Ltd., China) with a tip coated with silicone was inserted approximately 18–20 mm and reached the middle cerebral artery; this technique effectively occluded cerebral blood flow. After 2 h of ischemia, the thread embolus was pulled out approximately 10 mm to achieve reperfusion. A laser Doppler flow meter (PeriFlux 5100 Laser Doppler, PERIMED Inc., Sweden) was used to record the situation before ischemia, after ischemia, and after reperfusion to determine the success of ischemia and reperfusion (Figure 1(b)). In the sham groups, except for inserting the thread embolus in the left common carotid artery, the rest of the operations were the same as those in the I/R group. Rats that failed or died were excluded and replaced by rats that met the criteria.

2.4. 2, 3, 5-Triphenyltetrazolium Chloride (TTC) Staining. TTC staining is used to verify the success of the stroke model and determine infarct volume. One day after reperfusion, each rat was deeply anesthetized, sacrificed, and dissected on ice. Brain tissue was removed and placed in a freezer at −20°C for 30 min. The frozen brain tissue was separated from the cerebellum and dissected into 2 mm sections from the optic chiasm. Next, brain tissue was placed in a 2% TTC solution (G3005, Solarbio Inc., China) in a 37°C incubator for 10–15 minutes, and samples were observed and removed when adequate tissue color change was achieved. The successfully stained brain tissue section showed infarcts in white and normal brain tissue in red and was fixed in 4% paraformaldehyde once the desired coloration was achieved. A high-definition camera was used for imaging and calculation of the infarct area, measured by Image-Pro Plus 6.0 software (Media Cybernetics Inc., America). The infarct area was determined as the infarct volume÷ total brain tissue volume × 100% and expressed as a percentage.

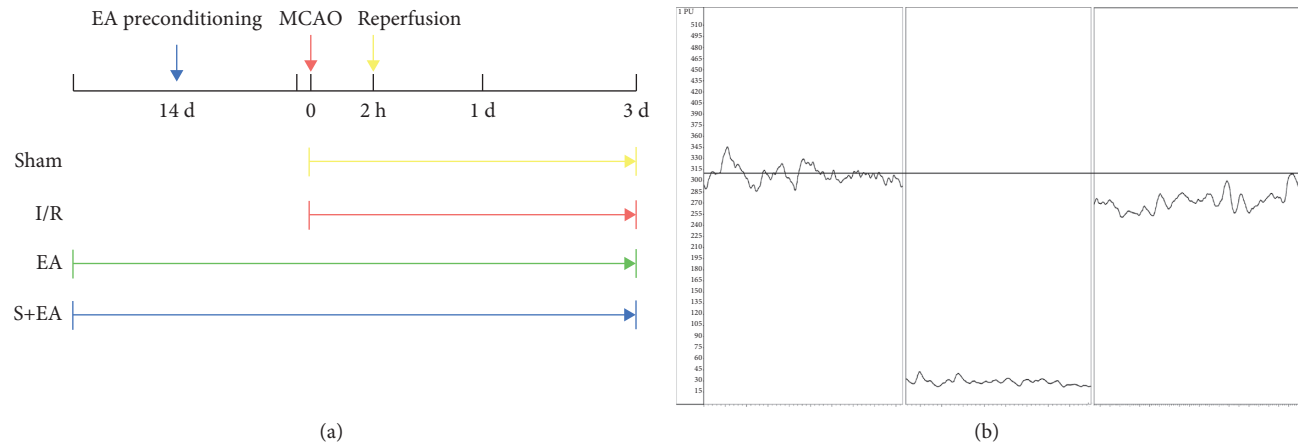

Figure 1: Schematic description of study design (a) and blood flow meter measurement icon (b). MCAO: middle cerebral artery occlusion; S: sham group; I/R: cerebral ischemia-reperfusion group; EA: electroacupuncture preconditioning group; and EA + S: electroacupuncture preconditioning and sham group.

2.5. Hematoxylin-Eosin (HE) Staining. The rat brain, which was perfused with 9% physiological saline and 4% paraformaldehyde placed in the tissue fixative, was used for pathological observation using the hematoxylin and eosin staining method. First, the dehydrated brain tissue was sliced and embedded in paraffin. After gradient xylene and alcohol treatment, the brain tissue was immersed in hematoxylin and eosin staining solutions. The successfully stained tissue sections were fixed for observation and microscopy. The main observation locations are the cerebral cortex and ischemic penumbra.

2.6. Western Blot Analysis. The rat infarcted side cortex or ischemic penumbra brain tissue was treated with RIPA Lysis Buffer (P0013B-RIPA, Beyotime, China) for grinding to extract total protein. After measuring the protein, samples were prepared and run by 10% sodium dodecyl sulfate-polyacrylamide gel electrophoresis and then transferred onto a polyvinylidene difluoride membrane. The imprinted polyvinylidene fluoride (PVDF) membranes were blocked in a sealed bag at room temperature for 2 h with skimmed milk powder dissolved in Tris-buffered saline with Tween solution (50 mmol/L Tris-HCl, pH 8.0, 150 mmol/L NaCl, and 0.1% Tween-20). The membranes were then blocked with FPN-1 primary antibodies (1 μg/mL, 26601-1-AP, Proteintech, China) for 1.5 h at room temperature (25°C ± 1°C), according to the manufacturer's instructions. Finally, the membranes were incubated with HRP-labeled goat anti-rabbit immunoglobin G antibody for 2 h in a shaker. β-Actin polyclonal antibody (0.5 μg/mL, 20536-1-AP, Proteintech, China) was used as an internal reference. Proteins were detected with enhanced ECL chemiluminescence substrate, and images were taken to measure quantitative expression using Gel-Pro-Analyzer 4.0 (Media Cybernetics, USA) and Image J (National Institutes of Health, America).

2.7. Enzyme Linked Immunosorbent Assay (ELISA). ELISA was used to detect the protein content. According to the manufacturer's instructions (MEIMIANbio, China), PBS was used as a protein diluent. The sample (10 μl) was added to a microcuvette coated with hepcidin, GSH, GPX4, and ROS antibodies (MEIMIANbio, China), followed by 50 μl of sample diluent and 100 μl of enzyme-labeled reagent. The microcuvettes were then incubated for 1 h at 37°C. After the initial incubation, the cuvettes were washed five times using the washing solution provided in the kit. The A and B reaction solutions were added, and the cuvettes were incubated for a further 15 min in the dark. Finally, 50 μl of stop solution was added to stop the reaction. The protein content was measured using a microplate reader with a 450 nm filter (Multiskan FC, Thermo Fisher, USA).

2.8. Statistical Analysis. All experimental data were analyzed using SPSS 26.0 (IBM Inc., America) and displayed in the form of mean ± standard deviation. The quantitative data for comparing the two groups were tested using Student's t-test, while multiple groups of data considering single-factor changes were statistically analyzed using analysis of variance, and multiple post hoc comparisons were used to pass the LSD test. Differences were considered statistically significant when P was <0.05.

3. Results

3.1. TTC Staining. TTC staining showed that the infarct volume of rats pretreated with electroacupuncture for two weeks was smaller than that of the I/R group after 1 day of cerebral ischemia and reperfusion. The calculated infarct volume was significantly smaller in the EA group (28.14% ± 1.46%) than in the I/R group (33.48% ± 1.44%) ($P < 0.01$) (Figure 2).

3.2. HE Staining. HE staining more effectively demonstrated the changes in brain tissue after cerebral ischemia and reperfusion. The cells in the sham and EA + S groups were arranged neatly, with clear and complete levels. The brain tissue of the I/R group was loose and edematous, showing

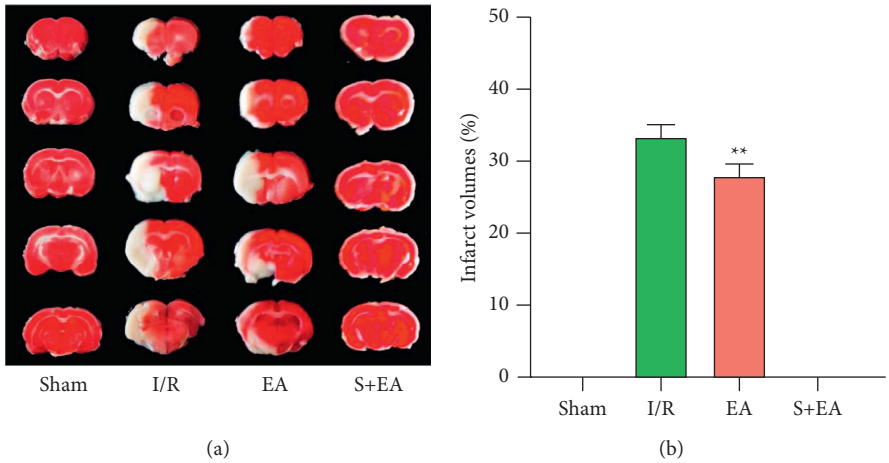

Figure 2: EA preconditioning exerted a neuroprotective role in cerebral ischemia/reperfusion rats. (a) Sequential cerebral slices of tissue from single rats in the group which was sacrificed 1 day were stained with 2% TTC solution. (b) Cerebral infarction volume measurement through Image-Pro Plus ($^{**}P < 0.01$ vs. I/R group). S: sham group; I/R: cerebral ischemia-reperfusion group; EA: electroacupuncture preconditioning group; and EA + S: electroacupuncture preconditioning and sham group.

vacuolar changes, and the nucleus was pyknotic. The degree of brain edema and vacuole changes in the EA group was lower than that in the I/R group, although the degree of damage was different. It should be noted that brain tissue damage increases with time after reperfusion, but EA preconditioning appeared to reduce this damage (Figure 3).

3.3. Western Blot Analysis. The FPN-1 level in the EA group was significantly higher in the brain tissue of the infarct area than in the I/R group ($P < 0.01$), but it was still significantly lower than in the sham and EA + S groups. This phenomenon was still present after 3 days of reperfusion ($P < 0.01$) (Figures 4(a) and 4(b)). Additionally, the hepcidin content in the brain tissue was lower than that in the I/R group at both time points ($P < 0.01$) (Figures 4(c) and 4(d)).

3.4. ELISA. Compared with the I/R group, the EA group had a lower oxidative stress level, as measured by ROS, at 1 and 3 days after reperfusion ($P < 0.01$) (Figure 5(a)). Furthermore, concentrations of GSH and GPX4, which can protect cells by inhibiting oxidative stress and ferroptosis caused by iron overload, were significantly higher in the EA group than in the I/R group, at both time points ($P < 0.05$) (Figures 5(b) and 5(c)).

4. Discussion

Although studies pertaining to the development and progress of stroke have provided a clearer understanding of ischemic diseases, we do not have a perfect treatment plan yet. Even when strokes are detected and treated as early as possible, thrombolysis is still a mode of treatment with certain risks [29]. With prolonged ischemia and hypoxia, the infarction gradually expands. Reversing the injury as soon as possible is preferable, but if a patient has already experienced prolonged ischemia, this can cause reperfusion injury with serious consequences [30].

As a conventional measure, therapy to restore perfusion has more benefits than risks and can improve survival rates. It should be noted that, unlike permanent ischemia, reperfusion injury changes the physiological state after ischemia, in a process more related to inflammation [31]. Not only can ischemic changes cause the expression of various inflammatory factors but also the immune cells in the perfused blood cannot be ignored [32] and can trigger severe inflammation, which is an important mechanism leading to iron overload and ferroptosis in cells [33].

Acupuncture has emerged as a supplementary (available here) and alternative treatment for stroke. The mechanisms of action have been investigated in several studies, which have shown a reduction in reperfusion inflammatory reactions and ferroptosis [34, 35]. EA has the advantages of continuous acupuncture, relatively fixed parameters, and reduced manpower and has been suggested as a strategy to combat damage caused by cerebral ischemia [21]. Baihui (GV20) is often selected as a treatment for cerebral ischemia because it has many functions in traditional Chinese medicine, such as dredge collateral, regulation of qi flow, restoration of consciousness, and benefitting resuscitation [36]. Many studies have demonstrated the neuroprotective effect of treating the Baihui (GV20) point with electroacupuncture [37, 38]. Additionally, Zusanli (ST36) also has an effect that makes the body strong in traditional Chinese medicine; therefore, it is widely used in clinical treatment [36]. Previous studies on the effect of Zusanli in stroke diseases have shown that it enhances limb movement [39]. In summary, we chose the Baihui (GV20) point and Zusanli (ST36) point as the EA preconditioning protocol because they are often used in clinical treatment and have good curative effects. We selected the electrical component of the treatment (stimulus and frequency) based on previous research [40, 41].

TTC staining showed a smaller infarct volume in the EA group than in the I/R group. This finding supported the pathological staining results, demonstrating less damage in the EA group than in the I/R group. We investigated the

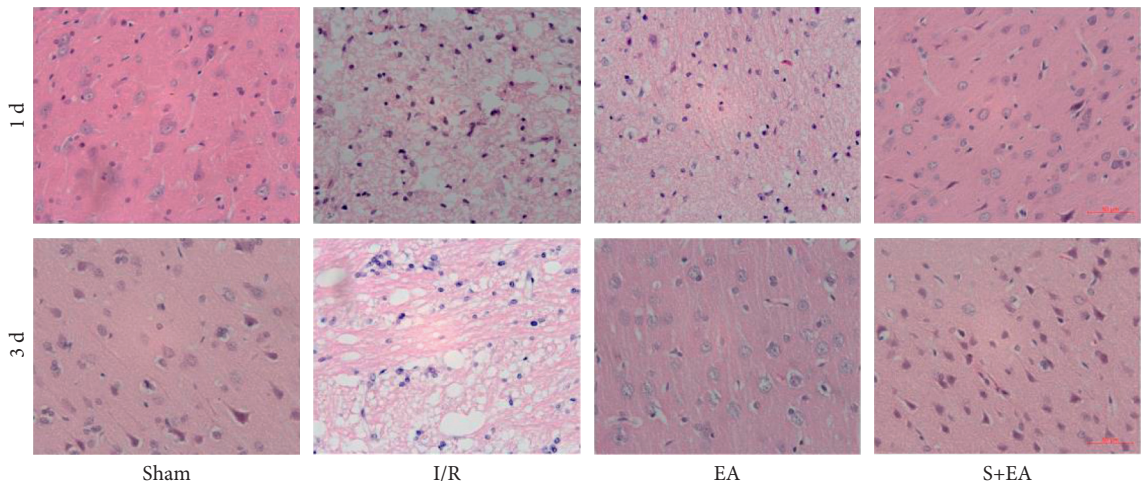

Figure 3: EA preconditioning can reduce acute pathological damage after cerebral ischemia and reperfusion. 1 d: 1 day after reperfusion; 3 d: 3 days after reperfusion; S: sham group; I/R: cerebral ischemia-reperfusion group; EA: electroacupuncture preconditioning group; and EA + S: electroacupuncture preconditioning and sham group.

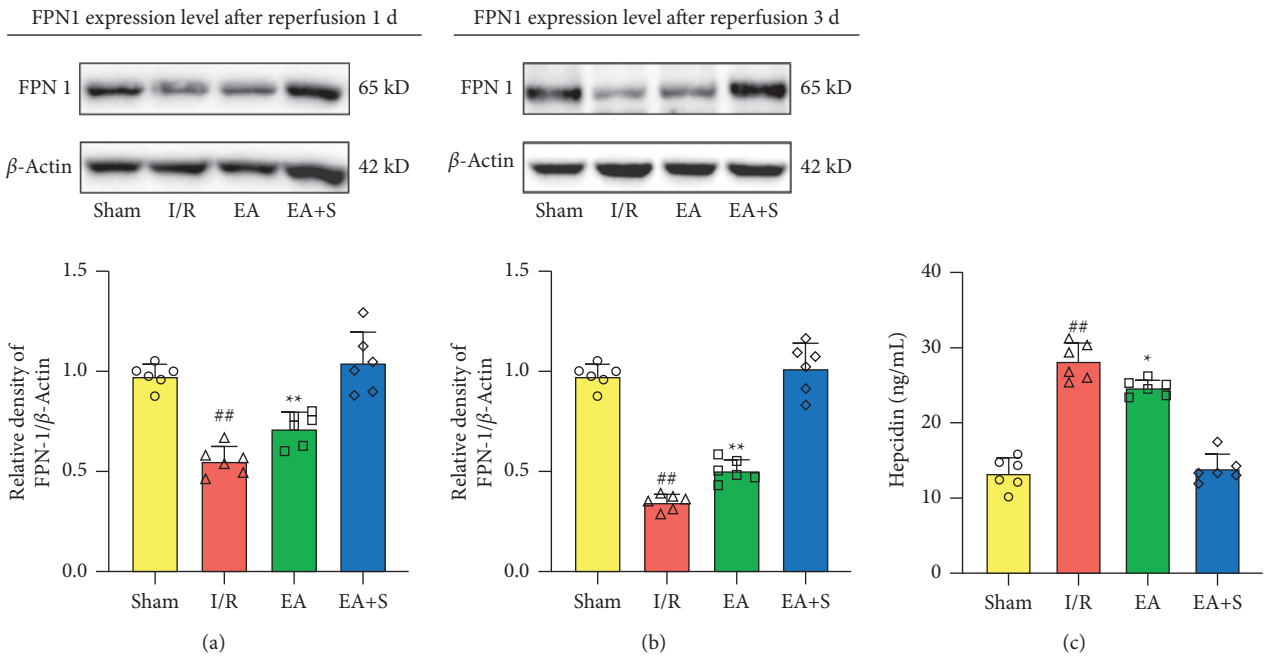

Figure 4: Continued.

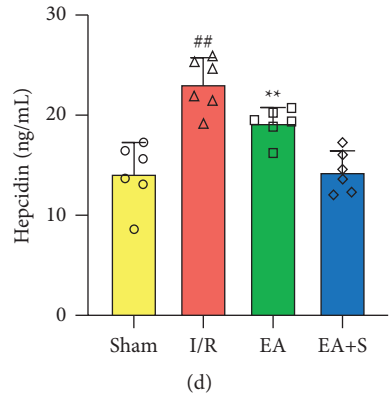

Figure 4: Effect of EA preconditioning on iron transport-related protein in the acute phase of cerebral ischemia and reperfusion. (a) The effect of EA preconditioning on the expression of FPN-1 in rats sacrificed 1 day after reperfusion. (b) The effect of EA preconditioning on the expression of FPN-1 in rats sacrificed 3 days after reperfusion. (c) The effect of EA preconditioning on the content of hepcidin in brain tissues of rats sacrificed 1 day after reperfusion. (d) The effect of EA preconditioning on the content of hepcidin in brain tissues of rats sacrificed 3 days after reperfusion ($^{*}P < 0.05$ vs. I/R group; $^{**}P < 0.01$ vs. I/R group; and $^{\#\#}P < 0.01$ vs. sham group and EA + S group). S: sham group; I/R: cerebral ischemia-reperfusion group; EA: electroacupuncture preconditioning group; and EA + S: electroacupuncture preconditioning and sham group.

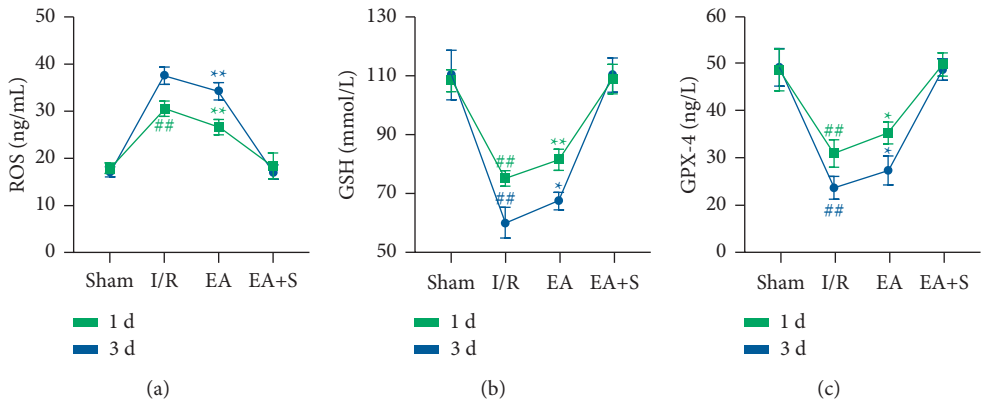

Figure 5: Effect of EA preconditioning on the content of oxidative stress-related proteins. (a) EA preconditioning can reduce the content of ROS in brain tissues in the acute phase after reperfusion. (b) EA preconditioning can reduce the content of GSH in brain tissues in the acute phase after reperfusion. (c) EA preconditioning can reduce the content of GPX4 in brain tissues in the acute phase after reperfusion ($^{*}P < 0.05$ vs. I/R group; $^{**}P < 0.01$ vs. I/R group; and $^{\#\#}P < 0.01$ vs. sham group and EA + S group). S: sham group; I/R: cerebral ischemia-reperfusion group; EA: electroacupuncture preconditioning group; and EA + S: electroacupuncture preconditioning and sham group.

mechanism of this reduction by analyzing the levels of hepcidin and FPN-1 within the cortex tissue. Hepcidin can be activated by the HAMP gene, which is upregulated by the IL-6/JAK/STAT3 signaling pathway [42]. FPN-1, an iron-transporting protein that can transport iron ions from cells to plasma, is downregulated by hepcidin [43]. The results showed that EA preconditioning could reduce the increase of hepcidin caused by cerebral ischemia-reperfusion within 3 days and restore the expression level of FPN-1. The reduction in ROS levels also supports this conclusion as it indicates the absence of excess intracellular iron in the tissue from the EA group rats.

In addition, we assessed the levels of GSH and GPX4 in the brain tissue. GSH and GPX4 can antagonize the Fenton reaction, produced by a large amount of intracellular iron, and protect the cell membrane from oxidative damage [44]. This indicates that EA preconditioning protects against the consumption of GSH and GPX4. Higher levels of GSH and GPX4 also indicate reduced oxidative stress levels in the brain tissue and low occurrence of ferroptosis.

Consequently, we believe that EA can reduce the consumption of GSH and keep GPX4 active to resist lipid peroxidation. Simultaneously, EA can reduce the generation of ROS and protect cells. Taken together, we believe that EA can exert neuroprotective effects after cerebral ischemia and reperfusion. The effect can be sustained, at least in the acute to subacute phase.

Although the experimental results reveal the advantages of EA preconditioning to reduce the injury after cerebral ischemia and reperfusion and exert neuroprotective effects, this experiment also has certain limitations. We demonstrated that EA preconditioning could reduce injury after

ischemia-reperfusion; however, the research is based on animal experiments. Even though we used the left hemisphere of the brain as the object of ischemia, as suggested by a previous review [28], the experiment using only adult male rats does not cover all types of disease. Therefore, future directions will include exploring the limitations of this research and aim to conduct more in-depth research into the mechanisms of action.

As most previous studies focused on the mechanism of electroacupuncture preconditioning, the duration of its effect remains unclear; therefore, in the future, more attention should be paid to calculating the protection time of electroacupuncture preconditioning, and the mechanism should be analyzed to optimize electroacupuncture points, parameters, and intervention cycles, etc., to provide a better reference for clinical services.

5. Conclusions

We found that electroacupuncture preconditioning can protect nerve cells from oxidative stress damage after cerebral ischemia and reperfusion by regulating iron transport-related proteins, which is consistent with previous research and our hypothesis. However, the mechanism of ferroptosis and how to prevent it remains a problem requiring an urgent solution.

Data Availability

The experimental data of this study are stored in the FAIRDOMHub database [45]: https://fairdomhub.org/projects/251/.

Disclosure

This manuscript was submitted as a project in the FAIRDOMHub database on 4 Sep 2021.

Conflicts of Interest

The authors declare no conflicts of interest regarding the publication of this paper.

Acknowledgments

The authors are grateful to Qiang Tang, PhD, and Luwen Zhu, PhD, for their helpful assistance. This work was supported by the National Natural Science Foundation of China (82174477), Young Talents Promotion Project of the China Association of Traditional Chinese Medicine (CACM-2019-QNRC2-B04), and Outstanding Cultivation Fund of Heilongjiang University of Traditional Chinese Medicine (No. 2019JC03).

Supplementary Materials

The ARRIVE Compliance Questionnaire, etc. supporting this study are stored in the FAIRDOMHub database as supplementary files. (*Supplementary Materials*)

References

[1] B. C. V. Campbell and P. Khatri, "Stroke," *The Lancet*, vol. 396, no. 10244, pp. 129–142, 2020.

[2] G. Stoll and B. Nieswandt, "Thrombo-inflammation in acute ischaemic stroke—implications for treatment," *Nature Reviews Neurology*, vol. 15, no. 8, pp. 473–481, 2019.

[3] Y. Lu, C. Li, Q. Chen et al., "Microthrombus-targeting micelles for neurovascular remodeling and enhanced microcirculatory perfusion in acute ischemic stroke," *Advanced Materials*, vol. 31, no. 21, Article ID e1808361, 2019.

[4] Á. Chamorro, U. Dirnagl, X. Urra, and A. M. Planas, "Neuroprotection in acute stroke: targeting excitotoxicity, oxidative and nitrosative stress, and inflammation," *The Lancet Neurology*, vol. 15, no. 8, pp. 869–881, 2016.

[5] Y. Fu, Q. Liu, J. Anrather, and F. D. Shi, "Immune interventions in stroke," *Nature Reviews Neurology*, vol. 11, no. 9, pp. 524–535, 2015.

[6] R. Daher, T. Lefebvre, H. Puy, and Z. Karim, "Extrahepatic hepcidin production: the intriguing outcomes of recent years," *World Journal of Clinical Cases*, vol. 7, no. 15, pp. 1926–1936, 2019.

[7] D.-L. Zhang, M. C. Ghosh, H. Ollivierre, Y. Li, and T. A. Rouault, "Ferroportin deficiency in erythroid cells causes serum iron deficiency and promotes hemolysis due to oxidative stress," *Blood*, vol. 132, no. 19, pp. 2078–2087, 2018.

[8] H. Ding, C. Z. Yan, H. Shi et al., "Hepcidin is involved in iron regulation in the ischemic brain," *PLoS One*, vol. 6, no. 9, Article ID e25324, 2011.

[9] B. Proneth and M. Conrad, "Ferroptosis and necroinflammation, a yet poorly explored link," *Cell Death & Differentiation*, vol. 26, no. 1, pp. 14–24, 2019.

[10] M. Valko, K. Jomova, C. J. Rhodes, K. Kuča, and K. Musílek, "Redox- and non-redox-metal-induced formation of free radicals and their role in human disease," *Archives of Toxicology*, vol. 90, no. 1, pp. 1–37, 2016.

[11] D. M. Ward and S. M. Cloonan, "Mitochondrial iron in human health and disease," *Annual Review of Physiology*, vol. 81, no. 1, pp. 453–482, 2019.

[12] M. Maiorino, M. Conrad, and F. Ursini, "GPx4, lipid peroxidation, and cell death: discoveries, rediscoveries, and open issues," *Antioxidants & Redox Signaling*, vol. 29, no. 1, pp. 61–74, 2018.

[13] F. Ursini and M. Maiorino, "Lipid peroxidation and ferroptosis: the role of GSH and GPx4," *Free Radical Biology and Medicine*, vol. 152, pp. 175–185, 2020.

[14] M. Long, Z. Wang, D. Zheng et al., "Electroacupuncture pretreatment elicits neuroprotection against cerebral ischemia-reperfusion injury in rats associated with transient receptor potential vanilloid 1-mediated anti-oxidant stress and anti-inflammation," *Inflammation*, vol. 42, no. 5, pp. 1777–1787, 2019.

[15] M. M. Wang, M. Zhang, Y. S. Feng et al., "Electroacupuncture Inhibits neuronal autophagy and apoptosis via the PI3K/AKT pathway following ischemic stroke," *Frontiers in Cellular Neuroscience*, vol. 14, p. 134, 2020.

[16] Y. S. Jung, S. W. Lee, J. H. Park, H. B. Seo, B. T. Choi, and H. K. Shin, "Electroacupuncture preconditioning reduces ROS generation with NOX4 down-regulation and ameliorates blood-brain barrier disruption after ischemic stroke," *Journal of Biomedical Science*, vol. 23, no. 1, p. 32, 2016.

[17] Z. Ma, Z. Zhang, F. Bai, T. Jiang, C. Yan, and Q. Wang, "Electroacupuncture pretreatment alleviates cerebral ischemic injury through $\alpha 7$ nicotinic acetylcholine receptor-

mediated phenotypic conversion of microglia," *Frontiers in Cellular Neuroscience*, vol. 13, p. 537, 2019.

[18] T. Guo, Z. Guo, X. Yang et al., "The alterations of IL-1beta, IL-6, and TGF-beta levels in hippocampal CA3 region of chronic restraint stress rats after electroacupuncture (EA) pretreatment," *Evid Based Complement Alternative Medicine*, vol. 2014, Article ID 369158,, 7 pages, 2014.

[19] X. T. Su, L. Wang, S. M. Ma et al., "Mechanisms of acupuncture in the regulation of oxidative stress in treating ischemic stroke," *Oxidative Medicine and Cellular Longevity*, vol. 2020, Article ID 7875396, 15 pages, 2020.

[20] A. Yang, H. M. Wu, J. L. Tang, L. Xu, M. Yang, and G. J. Liu, "Acupuncture for stroke rehabilitation," *Cochrane Database System Review*, vol. 8, Article ID CD004131, 2016.

[21] B. H. Yu, Y. Xing, and F. Zhang, "The therapeutic effect of electroacupuncture therapy for ischemic stroke," *Evidence-Based Complementary and Alternative Medicine : eCAM*, vol. 2020, Article ID 6415083, 9 pages, 2020.

[22] P. Young-Wook, H. Gi Yoon, K. Min Jae, L. Seo-Yeon, C. Byung Tae, and S. Hwa Kyoung, "Subacute electroacupuncture at baihui (GV 20) and dazhui (GV 14) promotes post-stroke functional recovery via neurogenesis and astrogliosis in a photothrombotic stroke mouse model," *Journal Traditional Chinese Medical*, vol. 39, no. 6, pp. 833–841, 2019.

[23] C. L. Hsieh, Q. Y. Chang, I. H. Lin et al., "The study of electroacupuncture on cerebral blood flow in rats with and without cerebral ischemia," *The American Journal of Chinese Medicine*, vol. 34, no. 2, pp. 351–361, 2006.

[24] Z. Li, M. Yang, Y. Lin et al., "Electroacupuncture promotes motor function and functional connectivity in rats with ischemic stroke: an animal resting-state functional magnetic resonance imaging study," *Acupuncture in Medicine*, vol. 39, no. 2, pp. 146–155, 2021.

[25] Y. Shi, Q. Dai, B. Ji et al., "Electroacupuncture pretreatment prevents cognitive impairment induced by cerebral ischemia-reperfusion via adenosine A1 receptors in rats," *Frontiers in Aging Neuroscience*, vol. 13, Article ID 680706, 2021.

[26] Z. G. Mei, Y. G. Huang, Z. T. Feng et al., "Electroacupuncture ameliorates cerebral ischemia/reperfusion injury by suppressing autophagy via the SIRT1-FOXO1 signaling pathway," *Aging*, vol. 12, no. 13, pp. 13187–13205, 2020.

[27] G. P. Morris, A. L. Wright, R. P. Tan, A. Gladbach, L. M. Ittner, and B. Vissel, "A comparative study of variables influencing ischemic injury in the longa and koizumi methods of intraluminal filament middle cerebral artery occlusion in mice," *PLoS One*, vol. 11, no. 2, Article ID e0148503, 2016.

[28] R. Ma, Q. Xie, Y. Li et al., "Animal models of cerebral ischemia: a review," *Biomedicine & Pharmacotherapy*, vol. 131, Article ID 110686, 2020.

[29] K. Shi, M. Zou, D. M. Jia et al., "tPA mobilizes immune cells that exacerbate hemorrhagic transformation in stroke," *Circulation Research*, vol. 128, no. 1, pp. 62–75, 2021.

[30] K. A. Hossmann, "The two pathophysiologies of focal brain ischemia: implications for translational stroke research," *Journal of Cerebral Blood Flow & Metabolism*, vol. 32, no. 7, pp. 1310–1316, 2012.

[31] G. Ford, Z. Xu, A. Gates, J. Jiang, and B. D. Ford, "Expression analysis systematic explorer (EASE) analysis reveals differential gene expression in permanent and transient focal stroke rat models," *Brain Research*, vol. 1071, no. 1, pp. 226–236, 2006.

[32] S. Sakai and T. Shichita, "Inflammation and neural repair after ischemic brain injury," *Neurochemistry International*, vol. 130, Article ID 104316, 2019.

[33] H. K. Eltzschig and T. Eckle, "Ischemia and reperfusion-from mechanism to translation," *Nature Medicine*, vol. 17, no. 11, pp. 1391–1401, 2011.

[34] B. Q. Cao, F. Tan, J. Zhan, and P. H. Lai, "Mechanism underlying treatment of ischemic stroke using acupuncture: transmission and regulation," *Neural Regeneration Research*, vol. 16, no. 5, pp. 944–954, 2021.

[35] G. Li, X. Li, J. Dong, and Y. Han, "Electroacupuncture ameliorates cerebral ischemic injury by inhibiting ferroptosis," *Frontiers in Neurology*, vol. 12, Article ID 619043, 2021.

[36] L. M. Chavez, S. S. Huang, I. MacDonald, J. G. Lin, Y. C. Lee, and Y. H. Chen, "Mechanisms of acupuncture therapy in ischemic stroke rehabilitation: a literature review of basic studies," *International Journal of Molecular Sciences*, vol. 18, no. 11, 2017.

[37] L. Zhu, T. Ye, Q. Tang et al., "Electroacupuncture pretreatment exerts an anti-apoptotic effect in cerebral ischaemia and reperfusion injury in rats," *Acupuncture & Electro-Therapeutics Research*, vol. 46, no. 4, pp. 357–370, 2021.

[38] R. Liu, N. G. Xu, W. Yi, and C. Ji, "Electroacupuncture attenuates inflammation after ischemic stroke by inhibiting NF-κB-mediated activation of microglia," *Evidence-Based Complementary and Alternative Medicine : eCAM*, vol. 2020, Article ID 8163052, 12 pages, 2020.

[39] Z. G. Sun, Y. L. Pi, J. Zhang, M. Wang, J. Zou, and W. Wu, "Effect of acupuncture at ST36 on motor cortical excitation and inhibition," *Brain and Behavior*, vol. 9, no. 9, Article ID e01370, 2019.

[40] Q. Y. Chang, Y. W. Lin, and C. L. Hsieh, "Acupuncture and neuroregeneration in ischemic stroke," *Neural Regeneration Research*, vol. 13, no. 4, pp. 573–583, 2018.

[41] S. Yao, Y. Liu, S. Cui et al., "Effect of different frequencies of electroacupuncture on post-stroke dysphagia in mice," *Journal of Molecular Neuroscience*, vol. 70, no. 11, pp. 1871–1879, 2020.

[42] Y. Kanamori, M. Murakami, M. Sugiyama, O. Hashimoto, T. Matsui, and M. Funaba, "Hepcidin and IL-1β," *Vitamins and Hormones*, vol. 110, pp. 143–156, 2019.

[43] C. B. Billesbølle, C. M. Azumaya, R. C. Kretsch et al., "Structure of hepcidin-bound ferroportin reveals iron homeostatic mechanisms," *Nature*, vol. 586, no. 7831, pp. 807–811, 2020.

[44] N. Kajarabille and G. O. Latunde-Dada, "Programmed cell-death by ferroptosis: antioxidants as mitigators," *International Journal of Molecular Sciences*, vol. 20, no. 19, 2019.

[45] K. Wolstencroft, O. Krebs, J. L. Snoep et al., "FAIRDOMHub: a repository and collaboration environment for sharing systems biology research," *Nucleic Acids Research*, vol. 45, no. D1, pp. D404–D407, 2017, https://fair-dom.org/publication/fairdomhub-a-repository-and-collaboration-%20environment-for-sharing-systems-biology-research/.

Hindawi
Evidence-Based Complementary and Alternative Medicine
Volume 2021, Article ID 1116126, 10 pages
https://doi.org/10.1155/2021/1116126

Research Article

Motor Imagery-Based Brain-Computer Interface Combined with Multimodal Feedback to Promote Upper Limb Motor Function after Stroke: A Preliminary Study

Yi-Qian Hu,[1] **Tian-Hao Gao**,[1] **Jie Li**,[2] **Jia-Chao Tao**,[2] **Yu-Long Bai**,[1] **and Rong-Rong Lu**[1]

[1]*Department of Rehabilitation, Huashan Hospital, Fudan University, No. 12 Middle Wulumuqi Road, Shanghai 200040, China*
[2]*Department of Computer Science and Technology, Tongji University, No. 4800 Cao'an Highway, Shanghai 200092, China*

Correspondence should be addressed to Yu-Long Bai; dr_baiyl@fudan.edu.cn and Rong-Rong Lu; 0356213@fudan.edu.cn

Received 6 September 2021; Accepted 11 October 2021; Published 3 November 2021

Academic Editor: Feng Zhang

Background. Recently, the brain-computer interface (BCI) has seen rapid development, which may promote the recovery of motor function in chronic stroke patients. *Methods*. Twelve stroke patients with severe upper limb and hand motor impairment were enrolled and randomly assigned into two groups: motor imagery (MI)-based BCI training with multimodal feedback (BCI group, $n = 7$) and classical motor imagery training (control group, $n = 5$). Motor function and electrophysiology were evaluated before and after the intervention. The Fugl-Meyer assessment-upper extremity (FMA-UE) is the primary outcome measure. Secondary outcome measures include an increase in wrist active extension or surface electromyography (the amplitude and cocontraction of extensor carpi radialis during movement), the action research arm test (ARAT), the motor status scale (MSS), and Barthel index (BI). Time-frequency analysis and power spectral analysis were used to reflect the electroencephalogram (EEG) change before and after the intervention. *Results*. Compared with the baseline, the FMA-UE score increased significantly in the BCI group ($p = 0.006$). MSS scores improved significantly in both groups, while ARAT did not improve significantly. In addition, before the intervention, all patients could not actively extend their wrists or just had muscle contractions. After the intervention, four patients regained the ability to extend their paretic wrists (two in each group). The amplitude and area under the curve of extensor carpi radialis improved to some extent, but there was no statistical significance between the groups. *Conclusion*. MI-based BCI combined with sensory and visual feedback might improve severe upper limb and hand impairment in chronic stroke patients, showing the potential for application in rehabilitation medicine.

1. Introduction

Stroke remains the leading cause of long-term disability, among which upper limb paralysis is particularly common and prevents patients from returning to self-care [1]. Rehabilitation has been shown to recover some motor functions from stroke. Several clinical controlled trials have confirmed that it is not hard to regain partial control of the shoulder and elbow from positive and intensive rehabilitation training [2–4]. However, it is difficult to improve the recovery of the control of severely paretic wrist and fingers, which prevents patients from returning to family and society [5]. Hence, there exists a pressing need to seek new interventions to improve the motor function of the paralysed upper limb. Sensory disorders, including deep and superficial sensory, are also common in stroke patients [6–8]. Studies have shown that the recovery of sensory impairments promotes the recovery of motor impairments; hence, increasing sensory input and output during exercise training may play an important role [9–11].

The brain-computer interface (BCI) is new technology that has been developing rapidly, and it directly acts on the central nervous system. By collecting and analysing the biological electrical signals from the human brain, BCI

technology could establish a direct communication and control pathway between the human brain and computers or other electronic devices [12]. This unconventional pathway has the potential to help stroke patients regain movement [13–15]. There are many ways to generate brain signals, among which motor imagery (MI) is more common [16,17]. The phenomenon of event-related desynchronisation (ERD)/event-related synchronisation (ERS) occurs when patients perform motor imagination [18]. In fact, many rehabilitation interventions are not appropriate for severely paralysed stroke patients, which means that these patients are excluded from therapy [19]. MI requires patients to have good cognitive function and can be carried out after standardised training and guidance, even for patients with severe hemiplegia [20–22]. Previous clinical studies have shown that MI or a combination of it and physical therapy can promote recovery of the upper extremities, which is important for daily activities and skills [23–25]. EEG is widely used because of its noninvasive, portability, and good temporal resolution. Researchers have demonstrated that MI-based BCI has the potential to be used in stroke rehabilitation [26–28].

BCI training is often combined with virtual reality (VR), which provides a three-dimensional visual interaction during training [29]. Adding VR to BCI might arouse patients' interest, which is conducive to improving patient compliance [30]. Adverse reactions such as dizziness and eyestrain might occur during treatment.

In previous research, BCI was mostly used as an intermediate medium to output signals that can control external devices, such as exoskeleton robots and functional electrical stimulation (FES) [31,32]. Studies have confirmed its clinical efficacy, and the improvement has a certain degree of continuity [33]. In our previous study [34], continuous passive motion (CPM) was used as an external device to improve wrist extension in chronic stroke patients. The results showed that after six weeks of interventions, 81% of the patients who completed the study had regained wrist extension. Meanwhile, the spatial and spectrum pattern of the EEG signal also improved after the training. However, this was before and after study and did not set up a control group. Also, external devices might have some insufficiencies, such as economic costs and patient adaptability. Patients might mainly focus on internal motor imagery during MI-based BCI training if external devices do not exist. In the current study, we further investigated the effect of sensory, visual, and EEG feedback on the recovery of upper limb motor function in chronic stroke patients.

2. Methods

2.1. Participants and Study Design. Twelve stroke patients were enrolled in this preliminary study. The inclusion criteria for participation were as follows:

(1) Diagnosis as cerebrovascular diseases confirmed by CT or MRI;

(2) No active extension of the paretic wrist and manual muscle test (MMT) for wrist extension at grade 0–1;

(3) Disease duration more than two months;

(4) Without cognition impairment (Mini Mental State Examination (MMSE) score >21); and

(5) No hearing or visual impairment.

The exclusion criteria included the following:

(1) The kinaesthetic and visual imagery questionnaire (KVIQ) [35] showing the MI task could not be performed, with a score less than 25;

(2) Patients with contraindications for MRI; and

(3) Participation in other clinical trials.

The current study is a single-centre, single-blinded prospectively randomised controlled study. The intervention was given by a qualified physiatrist, and another physiatrist who did not know the group of participants assessed all the participants at baseline and immediately after all the interventions. The participants were randomly divided into two groups: the MI-based BCI group and the classic MI group. All of them received individualised rehabilitation therapy based on their impairment. The scheme was carried out in accordance with the Helsinki Declaration and approved by the local ethics committee of Huashan Hospital. All the participants signed a written informed consent form before treatment. The clinical trial was registered (ChiCTR2000034725).

2.2. EEG Signal Acquisition and Processing. Only participants in the BCI group would get their EEG signals collected and processed. An 11-channel high-resolution EEG system (g.USBamp, g.tec, Schiedlberg, Austria) was used, and electrodes were attached to the scalp according to the 10–20 international system standard as follows: "FC3," "FC4," "C5," "C3," "C1," "CZ," "C2,""C4," "C6," "CP3," and "CP4". The ground electrodes were placed on the medial frontal cortex. The reference electrodes were, respectively, fixed at the left and right mastoids, and the average value from bilateral electrodes was used as the reference. EEG signals were collected at a sampling rate of 256 Hz.

Then, we followed the instructions to preprocess raw EEG data, as suggested by Makoto Miyakoshi's recommendation [36]. The pipeline is as follows:

(1) Import EEG data;

(2) High-pass filter the data at 8 Hz and low-pass filter the data at 30 Hz;

(3) Import channel info and use Montreal Neurological Institute (MNI) coordinate file for boundary element model (BEM) dipfit model;

(4) Remove line noise using CleanLine;

(5) Apply clean_rawdata to reject bad channels and correct continuous data using artefact subspace reconstruction (ASR);

(6) Interpolate all the removed channels;

(7) Reference the data to average; and

(8) Epoch data from −1 to 4 sec to event onset.

Power spectrum density (PSD) and individual channel's event-related spectral perturbation (ERSP) were used to analyze the MI-related activities.

2.3. Classic Motor Imagery Training. The classic MI group was set as the control group. The participants in this group also received 30 minutes of motor imagery training (MIT) per day. MIT was given in a fixed quiet room, and the training implementation was divided into four steps. One qualified therapist conducted all the training. The patients closed their eyes and listened to the therapist's instructions to complete the corresponding imagination tasks. The MIT procedure was as follows: first, patients were instructed to relax their body for two to three minutes. Then, they were told to close their eyes and imagine lying in a warm, relaxing place (such as a sofa, beach, or lawn). Second, the patients were prompted to perform MI of each joint in the upper limb for 10 minutes, including flexion and extension of the shoulder, elbow, wrist and fingers, and pronation and supination of the affected forearm. Third, for the next 15 minutes, patients were asked to imagine familiar, daily hand movements with their paretic upper limb, for example, "extending the affected arm to touch the red apple in front and then withdrawing the arm back" or "reaching out and grasping a cup on the table, bringing it to the mouth and reaching out to put it back." The content of the imagery task could be combined with occupational therapy, and the therapist could adjust the content of each MI task. Finally, the therapist directed the patient to return their attention to their surroundings within two to three minutes. To inform the patients that they were back in the room, the therapist asked them to listen to the sounds around as the therapist slowly counted down from 10 to 1. Then, the patients slowly opened their eyes while the therapist counted to one [37, 38]. To monitor whether the patients were cooperating with the imagery, the therapist could ask the patients about the fidelity and clarity of the imagery movements during the process to better help them enter the imagery state.

2.4. MI-Based BCI Training. Before intervention, the patients were first fitted with an EEG cap and plugged into the electrode with a conductive paste. During the intervention, the patients received both sensory input (with a brush) in both hands and visual feedback (the movements of virtual hands with VR glasses). The procedure of MI-based BCI training is as given below.

The patients first received sensory feedback in the back of both hands. After the sensory input stopped, grasping or extending actions of right/left virtual hand appeared randomly. After seeing the action of the virtual hand in the screen, the patients needed to perform the MI task of the same side simultaneously, namely, by grasping or extending this certain hand. The real-time EEG signals were collected and analysed by a computer to extract the characteristics of EEG patterns. If this pattern was in accordance with the preset pattern, the virtual hand would display the movements (grasping or extending) according to the MI of the patients. So, the patient received both sensory and visual feedback during the process. The above process was repeated during the intervention. Each session lasted 30 minutes (four cycles of six minutes each with two-minute intervals). The whole procedure is listed in Figure 1.

2.5. Clinical Outcome Measures. The primary outcome measure was the motor part of the Fugl-Meyer assessment-upper extremity (FMA-UE) score, which is widely recommended for the evaluation of motor impairments in stroke rehabilitation research.

Secondary outcome measures included the following: (1) action research arm test (ARAT); (2) motor status scale (MSS); (3) increased range of motion (ROM) of the affected wrist or the amplitude and cocontraction of the extensor carpi radialis on the surface electromyography (sEMG); and (4) Barthel index (BI).

2.6. Statistical Analysis. For clinical outcome measures, SPSS (version 20.0, Chicago, IL, USA) was used for all analyses. The general $\chi 2$ test or Fisher's exact test was used in the enumeration data. Paired sample t-tests were used to compare the differences within the groups, and an independent sample t-test was used to determine the difference between groups. The parameters of the major efficacy evaluation indicators were estimated, and the 95% confidence intervals (CI) of the differences before and after the intervention were given. Significant differences were considered if $p < 0.05$.

For EEG data, EEGLAB was used to perform all preprocessing routines and statistical analyses. For each participant, we performed a simple two-tailed paired t-test at each trial. We used 0.05 for the bootstrap significance level. For PSD, p values were computed at every frequency; for ERSP, p values were computed at every time/frequency point. Only those results with $p < 0.05$ showing statistical significance were preserved.

3. Results

3.1. Participants. Twelve stroke patients were enrolled and randomly divided into two groups: seven in the MI-BCI group and five in the MI group. All patients completed the entire training and assessment sessions. The demographic characteristics are listed in Table 1.

4. Clinical Outcome Analysis

4.1. Primary Outcome Measure. Compared with baseline, the FMA-UE score of the experimental group improved significantly ($p = 0.006$), while the control group did not show a significant improvement ($p = 0.068$). However, there was no significant difference when comparing the two groups (Table 2).

4.2. Secondary Outcome Measures. After treatment, both groups showed significant differences in MSS scores. The score for MI-based BCI increased from 19.17 ± 10.33 to

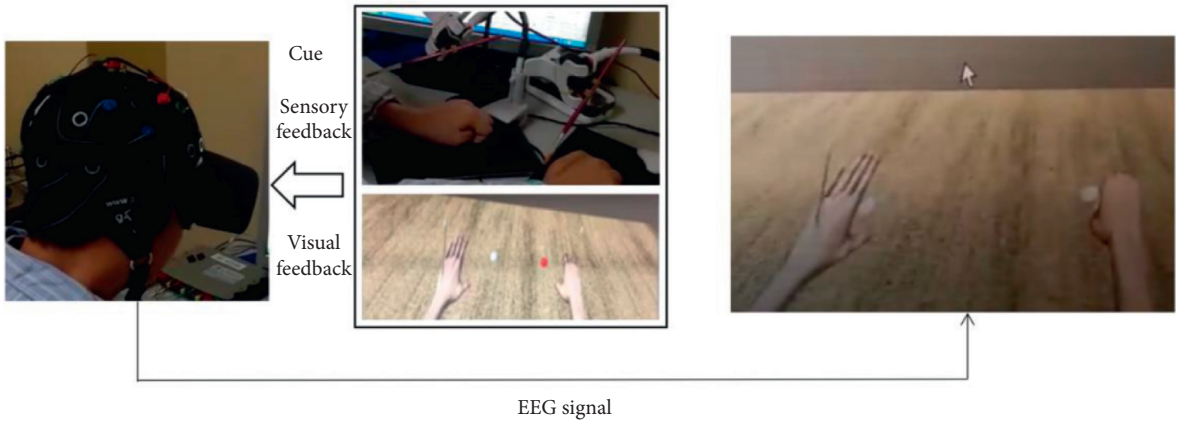

Figure 1: Illustration of the MI-BCI intervention procedures combined with multimodal feedback.

Table 1: Demographic characteristics of the participants ($N = 12$).

Characteristics	MI-based BCI group ($n = 7$)	Classic MI group ($n = 5$)	p value
Sex			0.408
Male	4	4	
Female	3	1	
Age (yr)	44.9 ± 7.5	60.4 ± 16.8	0.053
Stroke type			0.558
Ischemic	3	3	
Hemorrhagic	4	2	
Affected side			0.091
Right	3	0	
Left	4	5	
Poststroke duration (mo)	7.9 ± 6.5	7.3 ± 4.5	0.868

Mean ± standard deviation was used for the different baseline characteristics. MI-based BCI = motor imagery-based brain-computer interface; classic MI = classic motor imagery.

Table 2: Patients' performance and treatment effects in all outcome measures and comparison of the treatment effects between the experimental and control groups after the interventions.

Parameters	MI-based BCI group ($n = 7$)		Classic MI group ($n = 5$)		*Sig.*[a]	*Sig.*[b]	*Sig.*[c]
	Baseline	After intervention	Baseline	After intervention			
FMA-UE	12.7(8.88)	15.4(10.11)	13.8(6.65)	20.6(12.67)	**0.006**	0.068	0.214
ARAT	3.29(5.79)	5.57(7.66)	6.60(12.29)	8.60(9.10)	0.089	0.058	0.375
MSS	15.9(8.97)	19.17(10.33)	18.60(10.98)	23.90(11.11)	**0.010**	**0.002**	0.112
BI	66.43(22.31)	69.00(11.93)	75.71(11.34)	72.00(6.71)	0.174	0.374	0.376
sEMG	2.55(1.83)	4.86(5.02)	2.14(1.95)	3.99(2.90)	0.305	0.130	0.866
	44.00(18.28)	43.90(16.43)	49.41(8.09)	57.20(12.24)	0.989	0.110	0.389

[a,b]Main effect of assessment (pre-post), within-group comparisons in MI-BCI and MI group, respectively. [c]Interaction effect between treatment type (MI-BCI/MI) and assessment time (pre-post), between-groups comparisons, all significant p values are in bold. Mean (standard deviation) for all parameters. MI-based BCI = motor imagery-based brain-computer interface; classic MI = classic motor imagery; FMA-UE = Fugl-Meyer assessment-upper extremity; ARAT = action research arm test; MSS = motor status scale; BI = Barthel index; sEMG = the amplitude and cocontraction of the extensor carpi radialis on the surface electromyography. The bold values denote statistical significance.

15.94 ± 8.97 ($p = 0.010$), while the score for classic MI was from 23.90 ± 11.11 to 18.60 ± 10.98 ($p = 0.002$).

The ARAT scores and modified BI did not differ significantly between the two groups ($p = 0.375$ and $p = 0.376$, respectively). After MI-based BCI training, the scores of the ARAT and the BI were 5.57 ± 7.66 and 69.00 ± 11.93, respectively, while after classic MI training, the scores of the ARAT and the BI were 8.60 ± 9.10 and 72.00 ± 6.71, respectively.

All the participants were unable to actively extend their affected wrists at baseline. After completing all the training, two patients from each group were able to actively extend the paretic wrist. Further analysis of the surface electromyogram (sEMG) results showed a certain degree of improvement in each group, but no significant difference was observed within or between the two groups in the amplitude change of the extensor carpi radialis longus ($p = 0.305$ and $p = 0.130$, respectively) (Table 2).

5. Analysis of EEG Signals

5.1. Frequency Analysis. For the time-frequency analysis of EEG, we used ERSP as an indicator. According to prior knowledge, when a healthy person performs a left or right hand motor imagery task, oscillations in the alpha and beta bands can display either an event-related blocking response or an event-related amplitude enhancement. The former is named event-related desynchronisation (ERD) and the latter event-related synchronisation (ERS). In ERSP measurements, ERD indicated a power spectrum reduction, while ERS indicated a power spectrum increase [39]. For example, when the subjects perform the right hand motor imagery, it will correspondingly cause the left motion area to produce ERD, of which C3 is generally the most typical character. Same pheromone occurs with the left hand imagery. For one participant, we observed improvement after MI-BCI training by drawing ERSP graphs for the time-frequency analysis.

The all-channel ERSP diagram (Figure 2(a)) showed that in the early stage of rehabilitation training, in addition to FC3, C1, other channels presented two clusters of ERD: one centred at 5–10 Hz (ranging from about 2000 to 3000 ms), and the others centred at 20–30 Hz (ranging from about 500 to 3500 ms).

After 10 sessions of training (Figure 3), the ERSP of the left and right hemispheres differentiated. We could observe an alpha band of ERD appearing in the range of 10–15 Hz from 500 to 1500 ms in the left hemisphere. A beta band of ERS also appeared in the range of 20–30 Hz after 2500 ms. At the same time, only C4 in the right hemisphere showed a similar response.

At session 19 (Figure 4), the participant's ERSP concentrated on a single channel. We could observe that C3 had an obvious ERS centred at 15–25 Hz in the range of 2500–3000 ms when compared with other channels.

5.2. Power Spectral Analysis. The PSD shows the power distribution of the EEG series in the frequency domain (Figure 5). Each coloured trace represents the spectrum of the activity of one data channel. The leftmost scalp map shows the scalp distribution of power at 6 Hz. The black vertical line corresponding to the scalp map shows all channels' log PSD and relative amplitude under a specific frequency band. Taking the 10th session of the same participants as an example, the PSD of all channels is the highest at 6 Hz, and the PSD of C6 is the highest among all channels.

6. Discussion

Stroke patients could benefit from rehabilitation therapy [40, 41]. However, the recovery of the upper limb is still a great challenge, especially for patients in chronic stage. In the current study, stroke patients received MI-based BCI training to see whether they could benefit more from this multimodal feedback training than the classic MI training. BCI technology has developed rapidly during the past few years. It does not require the involvement of peripheral nerves and muscles but allows the central nervous system to directly interact with the surrounding environment. Concerning its potential to promote brain remodelling and structural restructuring, it has been widely applied in neurorehabilitation together with exoskeleton robots, functional electric stimulation, and other end-effectors [15, 31, 42, 43]. Although, there was some heterogeneity among various studies, the effectiveness of BCI in motor recovery was worthy of affirmation [19, 26–28].

Mental task exercise in MI can be linked to the brain regions that control motor execution. Repeated participation of these motor regions during training might effectively promote brain plasticity and the obtained functional outcomes [44, 45]. Some studies have indicated that the patterns of neurons activated during mental tasks were similar to those generated during actual movement [46]. Thus, the motor patterns involved in actual functional activities might be enhanced during MI, which contributes to functional recovery; this theory has been validated by subsequent studies [47]. In terms of poststroke rehabilitation, task-oriented training was considered one of the most effective interventions [48]. In fact, though, we found that patients with severe upper limb paralysis may not be able to adapt to these options in clinical practice. Under these circumstances, MI is presented as an alternative of easy application that is economical and that has the possibility of being carried out by these patients, which we should take into account as a complement to clinical care.

In our previous study [34], we combined wrist CPM with MI-based BCI, finding that chronic stroke patients with severe upper limb motor impairment might improve paretic wrist ROM after the intervention. This might indicate that they could benefit from this therapy. However, it was a before and after study. To further investigate the effect of MI-based BCI in upper limb motor recovery, we compared MI-based BCI intervention with the classic MI to see their effect on the recovery of upper limb motor function in stroke patients. The following results were obtained from this study: MI-based BCI combined with multimodal feedback had beneficial effects on the recovery of severe upper limb impairments after stroke and had the potential to restore control of the paralysed wrist.

In the current study, the motor section of the FMA-UE score was used as the primary outcome. Before the intervention, there was no difference between the MI-BCI group and MI group. After the intervention, upper limb motor function improved more significantly in the MI-BCI group than in the MI group. However, when comparing the control of the paretic wrist, MI-BCI did not show a better efficacy. The following reasons might explain this: first, we found that five of the seven patients in the MI-BCI group were in the chronic stroke stage, while only one in the control group was in the chronic stage after stroke. Hence, disease duration might be a nonnegligible factor. In addition, MSS scores as secondary endpoints performed well in both groups. Further analysis revealed that the MSS scale could be subdivided into the shoulder elbow part and wrist hand part, and both groups showed excellent improvement in the shoulder elbow part, which produced effective functional movements (such

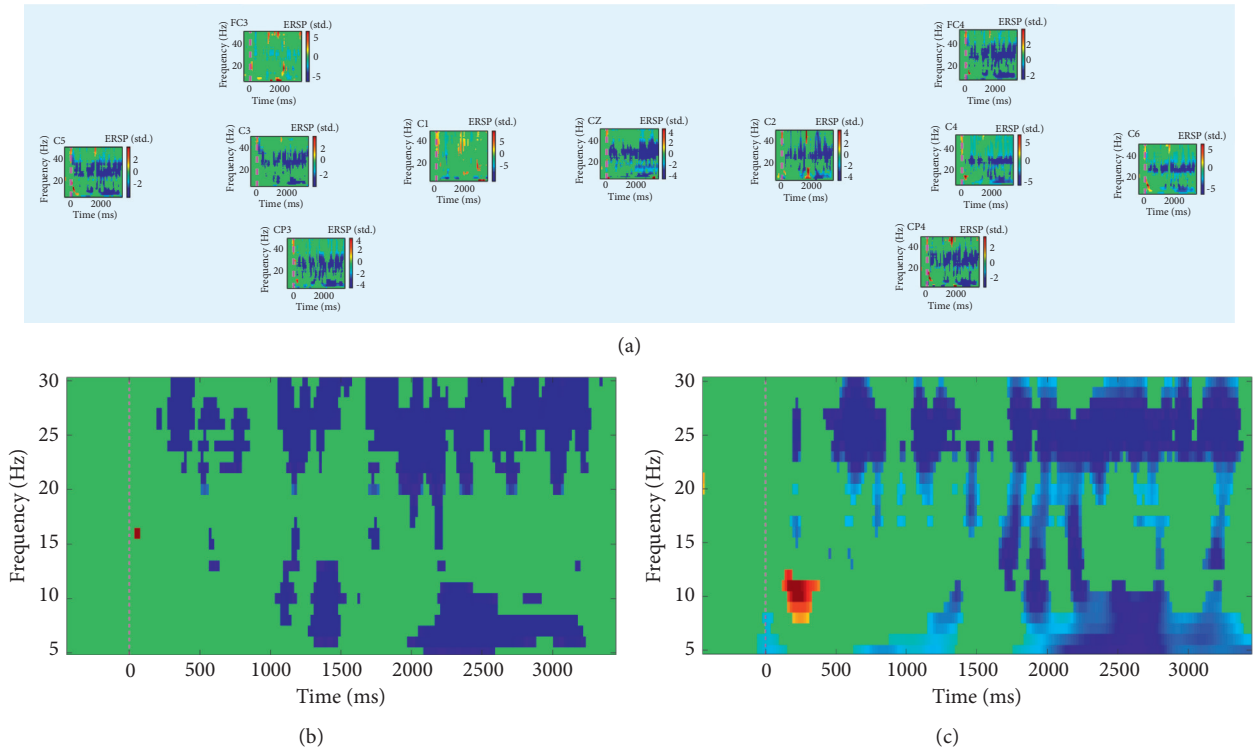

Figure 2: ERSP time-frequency measurements for session 1. (a) All channels, (b) C3, and (c) C4.

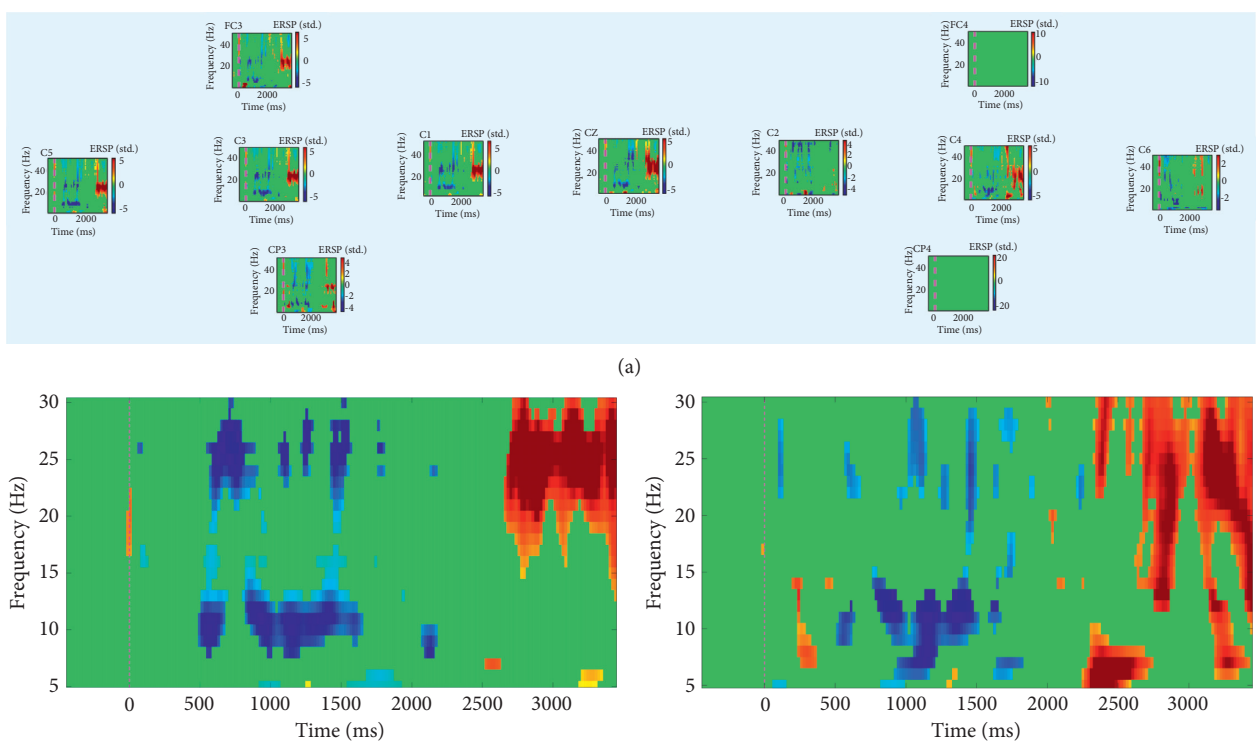

Figure 3: ERSP time-frequency measurements for session 11. (a) All channels, (b) C3, and (c) C4.

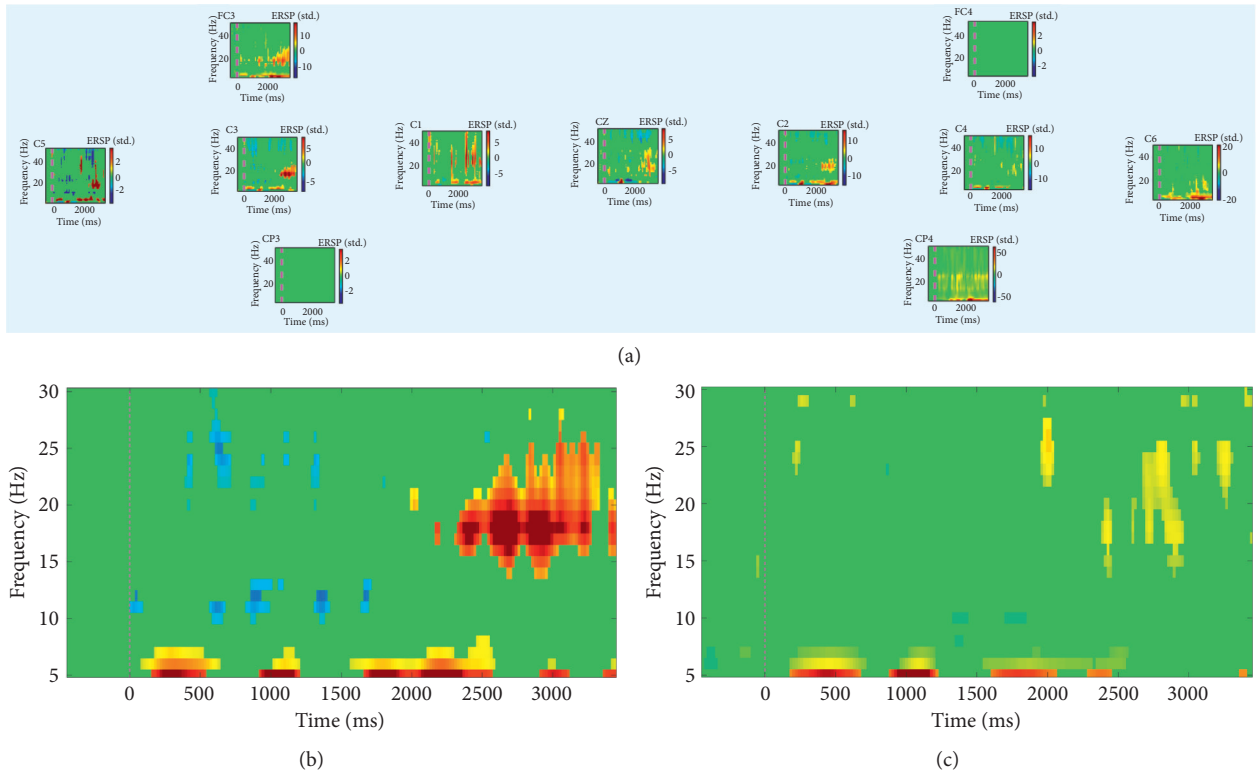

Figure 4: ERSP time-frequency measurements for session 19. (a) All channels, (b) C3, and (c) C4.

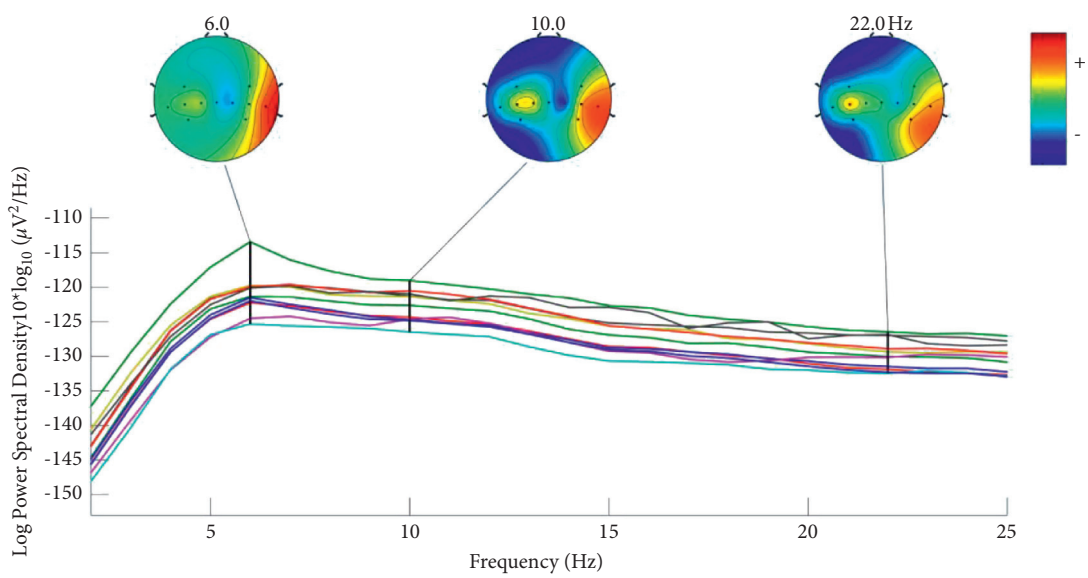

Figure 5: Power spectra analysis.

as lifting the arm and touching the mouth in supine position). Previous study indicated that if stroke patients show no measurable grasp strength by four weeks and a prolonged flaccidity period, they may have poor prognosis of the hand [49]. Therefore, although the reemergence of wrist extension is relatively minor and cannot be immediately translated into functional activities, it has some meaning for patients with tiny residual hand function. Simultaneously, the reappearance of new movement increased the patient's confidence and mobilised their enthusiasm, which may help with long-term recovery.

There was no difference in the ARAT scores between the two groups. Both groups improved in the MSS score. However, further analysis indicated that the MSS scale could be subdivided into the shoulder elbow part and wrist hand part. Both groups showed excellent improvement in the

shoulder and elbow, leading to the improvement for certain functional movements (such as lifting the arm and touching the mouth in supine position), whereas the score on the wrist hand part differed only in the control group.

The improvement of modified BI was not obvious between the two groups. There might be some possible explanations for this. First, the ultimate goal of rehabilitation is to help patients return to their families and society. During rehabilitation, patients have undergone standardised rehabilitation to increase their self-independence, regardless of their severity of motor impairment. Second, improvement in motor function did not directly equal improvement in ADL.

Our results also indicated that even in patients with central nervous system disease, MI ability could also be enhanced by multimodal feedback. MI could not be controlled well in the initial stage because of factors such as stroke and ERD appeared in almost all channels. This situation then improved after MI-based BCI training. The control level of the left hemisphere is relatively stronger than that of the right hemisphere, with ERD at the alpha band (5–10 Hz) and ERS at the beta band (20–30 Hz). In the later stage, the C3 channel had a clear ERS response at 20–30 Hz, indicating that this intervention could help improve the control of MI.

In the current study, we also investigated the security of MI-BCI. Conductive paste allergy, dizziness, and blurred vision might be common side effects. A questionnaire was surveyed, and none of the seven participants had the above adverse reactions.

The potential mechanism of BCI promoting motor function recovery is still being explored. However, it has been shown that BCI can change the neural network involved in motor recovery [4]. Studies have shown that the neural structures activated by MI are similar to those activated when certain movements are actually performed [50]. In addition, BCI is combined with an auditory, visual, or tactile system. All of these might reactivate and reorganize the brain structures and, through their feedback-based learning, lead to Hebbian-like plasticity-based cortical mechanisms. Generally, we believe that the ipsilateral limb is dominated by the contralateral brain. In fact, the ipsilateral motor cortex also contains important information about the state of the ipsilateral limb [51]. Therefore, even if the ipsilateral brain is severely damaged, the contralateral brain may also support the recovery of motor function through functional compensation. However, it is not unclear whether it is the recanalisation of the motor pathways on the affected side or the functional compensation on the healthy side that truly plays a role in the BCI system. According to the analysis of our EEG data, the brain remodelling of these patients may not be revealed by a single hypothesis, and the dual-mode equilibrium recovery may reflect the changes in brain remodelling after BCI training. In further studies, fMRI and diffusion tensor imaging (DTI) will be used to verify this hypothesis.

Therefore, we could conclude that MI-BCI could be used in stroke patients which might have some beneficial effect. There are still several limitations in the current study. First, it was only a preliminary study, and the sample size was not adequate enough to draw a conclusion. Second, improvement in upper limb motor function was still insufficient for functional use in daily life. This treatment may not substitute for the whole conventional rehabilitation therapy. Third, only the EEG signal of the participants in BCI group were collected and analysed, so the EEG patterns of the participants in the control group were not revealed and compared with those in BCI group. Forth, in the inclusion criteria, we did not standardize the motor function of the shoulder and elbow, which might affect the results of this study. Moreover, studies including motor-evoked potential (MEP) and DTI may further our understanding of the brain reorganisation mechanisms underlying this treatment.

7. Conclusion

Despite the current sample size being limited, the results suggest that stroke patients with severe restriction of residual upper limbs could gain a beneficial impact on motor function from MI-based BCI combined with multimodal feedback training. A potential in wrist extension movement was also observed. With further studies to provide stronger evidence, MI-based BCI combined with multimodal training might be a promising intervention for chronic stroke patients with severe upper limb impairment to further improve their motor function.

Data Availability

The original data could be processed by writing an email to Dr. Rongrong Lu (0356213@fudan.edu.cn).

Conflicts of Interest

The authors declare that they have no conflicts of interest.

Authors' Contributions

Yi-Qian Hu, Tian-Hao Gao, and Jie Li contributed equally to this work.

Acknowledgments

This work was supported by the Natural Science Foundation of China (NSFC) (grant no. 81902280), Medical Research Project in Jing'an District (grant no. 2015QN06), Shanghai Municipal Science and Technology Major Project (grant no. 2021SHZDZX0100), and the Fundamental Research Funds for the Central Universities.

References

[1] C. Warlo, J. van Gijn, and M. Dennis, *Stroke: Practical management*, Blackwell Publishing, Oxford, UK, 2008.

[2] E. Taub, G. Uswatte, D. K. King, D. Morris, J. E. Crago, and A. Chatterjee, "A placebo-controlled trial of constraint-induced movement therapy for upper extremity after stroke," *Stroke*, vol. 37, no. 4, pp. 1045–1049, 2006.

[3] A. E. Q. Van Delden, C. E. Peper, K. N. Nienhuys, N. I. Zijp, P. J. Beek, and G. Kwakkel, "Unilateral versus bilateral upper

limb training after stroke," *Stroke*, vol. 44, no. 9, pp. 2613–2616, 2013.

[4] A. Ramos-Murguialday, D. Broetz, M. Rea et al., "Brain-machine interface in chronic stroke rehabilitation: a controlled study," *Annals of Neurology*, vol. 74, no. 1, pp. 100–108, 2013.

[5] C. Schuster-Amft, K. Eng, Z. Suica et al., "Effect of a four-week virtual reality-based training versus conventional therapy on upper limb motor function after stroke: a multicenter parallel group randomized trial," *PLoS One*, vol. 13, no. 10, Article ID e0204455, 2018.

[6] S. Doyle, S. Bennett, and S. E. Fasoli, "Interventions for sensory impairment in the upper limb after stroke[J]," *Cochrane Database of Systematic Reviews*, vol. 16, no. 6, Article ID CD006331, 2010.

[7] S. F. Tyson, M. Hanley, J. Chillala, A. B. Selley, and R. C. Tallis, "Sensory loss in hospital-admitted people with stroke: characteristics, associated factors, and relationship with function," *Neurorehabilitation and Neural Repair*, vol. 22, no. 2, pp. 166–172, 2008.

[8] G. Abbruzzese and A. Berardelli, "Sensorimotor integration in movement disorders," *Movement Disorders*, vol. 18, no. 3, pp. 231–240, 2003.

[9] S. Schabrun and S. Hillier, "Evidence for the retraining of sensation after stroke: a systematic review," *Clinical Rehabilitation*, vol. 23, no. 1, pp. 27–39, 2009.

[10] M. C. Ridding, B. Brouwer, T. S. Miles, J. B. Pitcher, and P. D. Thompson, "Changes in muscle responses to stimulation of the motor cortex induced by peripheral nerve stimulation in human subjects," *Experimental Brain Research*, vol. 131, no. 1, pp. 135–143, 2000.

[11] D. J. Edwards, L. Dipietro, and A. Demirtas-Tatlidede, "Movement-generated afference paired with transcranial magnetic stimulation: an associative stimulation paradigm," *Journal of NeuroEngineering and Rehabilitation*, vol. 5, no. 11, p. 31, 2014.

[12] P. R. Kennedy and K. D. Adams, "A decision tree for brain-computer interface devices," *IEEE Transactions on Neural Systems and Rehabilitation Engineering*, vol. 11, no. 2, pp. 148–150, 2003.

[13] A. McConnell, R. Moioli, F. Brasil et al., "Robotic devices and brain-machine interfaces for hand rehabilitation post-stroke," *Journal of Rehabilitation Medicine*, vol. 49, no. 6, pp. 449–460, 2017.

[14] M. R. Curado, E. G. Cossio, D. Broetz et al., "Residual upper arm motor function primes innervation of paretic forearm muscles in chronic stroke after brain-machine interface (BMI) training," *PLoS One*, vol. 10, no. 10, Article ID e0140161, 2015.

[15] D. T. Bundy, L. Souders, K. Baranyai et al., "Contralesional brain-computer interface control of a powered exoskeleton for motor recovery in chronic stroke survivors," *Stroke*, vol. 48, no. 7, pp. 1908–1915, 2017.

[16] G. Prasad, P. Herman, D. Coyle, S. McDonough, and J. Crosbie, "Applying a brain-computer interface to support motor imagery practice in people with stroke for upper limb recovery: a feasibility study," *Journal of NeuroEngineering and Rehabilitation*, vol. 14, no. 1, p. 60, 2010.

[17] K.-S. Hong and M. J. Khan, "Hybrid brain-computer interface techniques for improved classification accuracy and increased number of commands: a review," *Frontiers in Neurorobotics*, vol. 24, p. 35, 2017.

[18] G. Pfurtscheller and C. Neuper, "Future prospects of ERD/ERS in the context of brain-computer interface (BCI) developments," *Progress in Brain Research*, vol. 159, pp. 433–437, 2006.

[19] E. Buch, C. Weber, L. G. Cohen et al., "Think to move: a neuromagnetic brain-computer interface (BCI) system for chronic stroke," *Stroke*, vol. 39, no. 3, pp. 910–917, 2008.

[20] M. Ietswaart, M. Johnston, H. C. Dijkerman et al., "Mental practice with motor imagery in stroke recovery: randomized controlled trial of efficacy," *Brain*, vol. 134, no. 5, pp. 1373–1386, 2011.

[21] S. J. Page, P. Levine, and A. C. Leonard, "Effects of mental practice on affected limb use and function in chronic stroke," *Archives of Physical Medicine and Rehabilitation*, vol. 86, no. 3, pp. 399–402, 2005.

[22] A. Sirigu, L. Cohen, J. R. Duhamel et al., "Congruent unilateral impairments for real and imagined hand movements," *NeuroReport*, vol. 6, no. 7, pp. 997–1001, 1995.

[23] H. C. Dijkerman, M. Ietswaart, M. Johnston, and R. S. MacWalter, "Does motor imagery training improve hand function in chronic stroke patients? A pilot study," *Clinical Rehabilitation*, vol. 18, no. 5, pp. 538–549, 2004.

[24] A. Guttman, A. Burstin, R. Brown, S. Bril, and R. Dickstein, "Motor imagery practice for improving sit to stand and reaching to grasp in individuals with poststroke hemiparesis," *Topics in Stroke Rehabilitation*, vol. 19, no. 4, pp. 306–319, 2012.

[25] S.-S. Kim and B.-H. Lee, "Motor imagery training improves upper extremity performance in stroke patients," *Journal of Physical Therapy Science*, vol. 27, no. 7, pp. 2289–2291, 2015.

[26] K. K. Ang, C. Guan, and K. S. Phua, "Transcranial direct current stimulation and EEG-based motor imagery BCI for upper limb stroke rehabilitation," *Annual International Conference of the IEEE*, vol. 2012, pp. 4128–4131, 2012.

[27] F. Pichiorri, G. Morone, M. Petti et al., "Brain-computer interface boosts motor imagery practice during stroke recovery," *Annals of Neurology*, vol. 77, no. 5, pp. 851–865, 2015.

[28] D. Mattia, F. Pichiorri, E. Colamarino et al., "The Promotoer, a brain-computer interface-assisted intervention to promote upper limb functional motor recovery after stroke: a study protocol for a randomized controlled trial to test early and long-term efficacy and to identify determinants of response," *BMC Neurology*, vol. 20, no. 1, p. 254, 2020.

[29] K. E. Laver, B. Lange, and S. George, "Virtual reality for stroke rehabilitation[J]," *Cochrane Database of Systematic Reviews*, vol. 11, Article ID CD008349, 2017.

[30] A. Vourvopoulos and S. Bermúdez i Badia, "Motor priming in virtual reality can augment motor-imagery training efficacy in restorative brain-computer interaction: a within-subject analysis," *Journal of NeuroEngineering and Rehabilitation*, vol. 13, no. 1, p. 69, 2016.

[31] A. A. Frolov, O. Mokienko, R. Lyukmanov et al., "Post-stroke rehabilitation training with a motor-imagery-based brain-computer interface (BCI)-Controlled hand exoskeleton: a randomized controlled multicenter trial," *Frontiers in Neuroscience*, vol. 11, no. 11, p. 400, 2017.

[32] T. Kim, S. Kim, and B. Lee, "Effects of action observational training plus brain-computer interface-based functional electrical stimulation on paretic arm motor recovery in patient with stroke: a randomized controlled trial," *Occupational Therapy International*, vol. 23, no. 1, pp. 39–47, 2016.

[33] A. Ramos-Murguialday, M. R. Curado, D. Broetz et al., "Brain-Machine interface in chronic stroke: randomized trial long-term follow-up," *Neurorehabilitation and Neural Repair*, vol. 33, no. 3, pp. 188–198, 2019.

[34] R.-R. Lu, M.-X. Zheng, J. Li et al., "Motor imagery based brain-computer interface control of continuous passive motion for wrist extension recovery in chronic stroke patients," *Neuroscience Letters*, vol. 718, Article ID 134727, 2020.
[35] F. Malouin, C. L. Richards, P. L. Jackson, M. F. Lafleur, A. Durand, and J. Doyon, "The kinesthetic and visual imagery questionnaire (KVIQ) for assessing motor imagery in persons with physical disabilities: a reliability and construct validity study," *Journal of Neurologic Physical Therapy*, vol. 31, no. 1, pp. 20–29, 2007.
[36] Makoto's Preprocessing Pipeline. (n.d.). Retrieved April 23, 2020, from https://sccn.ucsd.edu/wiki/Makoto's_preprocessing_pipeline.
[37] S. J. Page, P. Levine, S. A. Sisto, and M. V. Johnston, "Mental practice combined with physical practice for upper-limb motor deficit in subacute stroke," *Physical Therapy*, vol. 81, no. 8, pp. 1455–1462, 2001.
[38] S. J. Page, P. Levine, S. Sisto, and M. V. Johnston, "A randomized efficacy and feasibility study of imagery in acute stroke," *Clinical Rehabilitation*, vol. 15, no. 3, pp. 233–240, 2001.
[39] A. M. Cebolla, M. Petieau, C. Cevallos, A. Leroy, B. Dan, and G. Cheron, "Long-lasting cortical reorganization as the result of motor imagery of throwing a ball in a virtual tennis court," *Frontiers in Psychology*, vol. 6, p. 1869, 2015.
[40] D. Hebert, M. P. Lindsay, A. McIntyre et al., "Canadian stroke best practice recommendations: stroke rehabilitation practice guidelines, update 2015," *International Journal of Stroke*, vol. 11, no. 4, pp. 459–484, 2016.
[41] K.-C. Lin, H.-Y. Chung, C.-Y. Wu et al., "Constraint-Induced therapy versus control intervention in patients with stroke," *American Journal of Physical Medicine & Rehabilitation*, vol. 89, no. 3, pp. 177–185, 2010.
[42] L. I. Jovanovic, N. Kapadia, L. Lo, V. Zivanovic, M. R. Popovic, and C. Marquez-Chin, "Restoration of upper limb function after chronic severe hemiplegia," *American Journal of Physical Medicine & Rehabilitation*, vol. 99, no. 3, pp. e35–e40, 2020.
[43] M. Mukaino, T. Ono, K. Shindo et al., "Efficacy of brain-computer interface-driven neuromuscular electrical stimulation for chronic paresis after stroke," *Journal of Rehabilitation Medicine*, vol. 46, no. 4, pp. 378–382, 2014.
[44] P. Cicinelli, B. Marconi, M. Zaccagnini, P. Pasqualetti, M. M. Filippi, and P. M. Rossini, "Imagery-induced cortical excitability changes in stroke: a transcranial magnetic stimulation study," *Cerebral Cortex*, vol. 16, no. 2, pp. 247–253, 2006.
[45] N. Sharma and J.-C. Baron, "Does motor imagery share neural networks with executed movement: a multivariate fMRI analysis," *Frontiers in Human Neuroscience*, vol. 12, p. 564, 2013.
[46] S. Hétu, M. Grégoire, A. Saimpont et al., "The neural network of motor imagery: an ALE meta-analysis," *Neuroscience & Biobehavioral Reviews*, vol. 37, no. 5, pp. 930–949, 2013.
[47] E. Fernandez-Gomez and A. Sanchez-Cabeza, "Motor imagery: a systematic review of its effectiveness in the rehabilitation of the upper limb following a stroke[J]," *Revue Neurologique*, vol. 66, no. 5, pp. 137–146, 2018.
[48] R. P. Van Peppen, G. Kwakkel, S. Wood-Dauphinee, H. J. Hendriks, P. J. Van der Wees, and J. Dekker, "The impact of physical therapy on functional outcomes after stroke: what's the evidence?" *Clinical Rehabilitation*, vol. 18, no. 8, pp. 833–862, 2004.
[49] T. E. Twitchell, "The restoration of motor function following hemiplegia in man," *Brain*, vol. 74, no. 4, pp. 443–480, 1951.
[50] M. Jeannerod and J. Decety, "Mental motor imagery: a window into the representational stages of action," *Current Opinion in Neurobiology*, vol. 5, no. 6, pp. 727–732, 1995.
[51] K. Ganguly, L. Secundo, G. Ranade et al., "Cortical representation of ipsilateral arm movements in monkey and man," *Journal of Neuroscience*, vol. 29, no. 41, pp. 12948–12956, 2009.

Hindawi
Evidence-Based Complementary and Alternative Medicine
Volume 2021, Article ID 3671800, 16 pages
https://doi.org/10.1155/2021/3671800

Review Article

Repetitive Transcranial Magnetic Stimulation for Neuropathic Pain on the Non-Motor Cortex: An Evidence Mapping of Systematic Reviews

Yaning Zang,[1] **Yongni Zhang**,[2] **Xigui Lai**,[1] **Yujie Yang**,[3] **Jiabao Guo**,[4] **Shanshan Gu**,[5] **and Yi Zhu**[6]

[1]*Department of Kinesiology, Shanghai University of Sport, Shanghai, China*
[2]*School of Health Sciences, Duquesne University, Pittsburgh, PA, USA*
[3]*Department of Biomedical Sciences, City University of Hong Kong, Kowloon, Hong Kong, China*
[4]*Department of Rehabilitation Medicine, The Second School of Clinical Medicine, Xuzhou Medical University, Xuzhou, Jiangsu, China*
[5]*Department of Physical Therapy, University of Toronto, Toronto, ON, Canada*
[6]*Department of Musculoskeletal Pain Rehabilitation, The Fifth Affiliated Hospital of Zhengzhou University, Zhengzhou, Henan, China*

Correspondence should be addressed to Yi Zhu; zhuyi1010@163.com

Received 28 July 2021; Revised 4 October 2021; Accepted 12 October 2021; Published 29 October 2021

Academic Editor: Feng Zhang

Objective. This study was aimed to summarize and analyze the quality of the available evidence in systematic reviews (SRs) of repetitive transcranial magnetic stimulation (rTMS) on the non-motor cortex (non-M1) for neuropathic pain (NP) through an evidence mapping approach. *Methods*. We follow the Global Evidence Mapping (GEM) methodology. Searches were conducted in PubMed, EMBASE, Epistemonikos, and the Cochrane Library. The study type was restricted to SRs with or without meta-analysis. All literature published before January 23, 2021, were included. The methodological quality of the included SRs was assessed using A Measurement Tool to Assess Systematic Reviews (AMSTAR-2). Data were extracted according to a defined population-intervention-comparison-outcome (PICO) framework from primary studies that included SRs. The same PICO was categorized into PICOs according to interventions (stimulation target, frequency, number of sessions (short: 1–5 sessions, medium: 5–10 sessions, and long: >10 sessions)) and comparison (sham rTMS or other targets). The evidence mapping was presented in tables and a bubble plot. *Results*. A total of 23 SRs were included. According to the AMSTAR-2, 20 SRs scored "very low" in terms of methodological quality, 2 SRs scored "low," and 1 SR scored "high." A total of 17 PICOs were extracted. The dorsolateral prefrontal cortex (DLPFC) is the most studied of the non-motor cortex targets. PICOs of DLPFC, premotor cortex (PMC), frontal cortex, and secondary somatosensory cortex (S2) were mainly categorized with a "potentially better" conclusion. High-frequency (5–20 Hz) rTMS of non-M1 usually lead to "potentially better" conclusions. *Conclusions*. DLPFC, PMC, frontal cortex, and S2 seem to be promising new targets for rTMS treatment of certain NP. Evidence mapping is a useful and reliable methodology to identify and present the existing evidence gap that more research efforts are necessary in order to highlight the optimal stimulation protocols for non-M1 targets and standardize parameters to fill the evidence gaps of rTMS. Further investigation is advised to improve the methodological quality and the reporting process of SRs.

1. Introduction

Neuropathic pain (NP) is a chronic pain caused by lesions or dysfunction of the peripheral or central nervous system; it is often characterized by persistent pain, hyperalgesia, or even spontaneous pain [1]. NP not only disturbs daily activities, work, and sleep but also increases the incidence of emotional disorders such as patient depression and anxiety [2]. The mechanisms of NP are still unclear, which lead to the challenge of NP prevention and management. Pathological

changes such as spontaneous activity in damaged non-nociceptive fibers, peripheral and central, hyperactivity in nociceptors, and changes in central neuroplastic may be the possible reasons for NP [3, 4]. Currently, pharmacological treatment is the primary treatment for NP, including tricyclic anti-depressants, anti-convulsants, anti-epileptics, non-steroidal anti-inflammatory drugs, opioids, and so on. [5, 6]. However, pharmacological treatments provide less satisfaction with pain relief in many patients. In addition, drugs cause many adverse effects and even lead to drug dependence and abuse [7], wherein recommendation levels are not high [2, 8]. Thus, the treatment of NP remains a major unmet need, and the exploration of alternative approaches, especially evidence-based non-pharmacological interventions, is particularly important.

Repetitive transcranial magnetic stimulation (rTMS), as a non-invasive, safe non-pharmacological treatment, has been widely applied for NP. The rTMS technique uses magnetic pulses from an external stimulator to target specific cortical areas to generate induced currents that can alter the action potential of cortical nerve cells, induce depolarization of neurons, and ultimately lead to functional and even structural plasticity changes in the nervous system [9]. rTMS for NP has been published extensively. Stimulation target, frequency, and session are considered to be critical variables for analgesic efficacy. In terms of target, primary motor cortex (M1) is a commonly used stimulation target for rTMS and has been used for pain relief related to poststroke central pain, postherpetic neuralgia, and trigeminal facial pain. Although M1 has shown some efficacy in the treatment of NP, some studies have found that patients do not respond to M1 stimulation or only have short-lived effects. One study found the overall effectiveness rate was only about 40% [10]. This leaves a large gap in the search to find better management options for non-responders. Given the complexity of the disease type and the unclear mechanism of NP, M1 is not the suitable stimulation target for all types of NP. Therefore, the lack of individualized targeted therapy based on the characteristics of plasticity [11] may explain why rTMS is effective only in some patients, with a non-persistent efficacy and pain recurrence.

However, evidence-based evidence on non-M1 stimulation targets, treatment parameters, and treatment efficacy for the treatment of NP is still to be provided. Traditionally, SRs are a common methodology for evidence synthesis. SRs tend to focus on specific types of pain, whereas compared with M1, studies in non-M1 targets are insufficient and unfocused on specific NP, deeming SRs unable to provide a comprehensive overview of non-M1 regions for the treatment of NP. To overcome this barrier, an emerging synthesis method, evidence mapping [12–14], has been developed to provide an overview of the research area. Evidence mapping can provide both the breadth of evidence by extracting and analyzing primary data in SRs and the credibility of evidence by AMSTAR-2. The knowledge gaps identified by using evidence mapping can also inform future studies. This study aims to summarize, identify, and analyze the currently available evidence in SRs regarding rTMS on non-M1 for NP. This information is provided in a user-friendly manner that helps identify research gaps and assist evidence users in decision-making.

2. Methods

2.1. Setting the Boundaries and Context of the Evidence Mapping. This evidence mapping is based on the methodology proposed by GEM [15] and previous key studies [16–18]. The study process was divided into five stages (Figure 1). Studies and guidelines related to NP were referred, and an expert with a research background in NP was consulted to frame the evidence mapping. With the help of experts in this area, the specific terminology of the search strategy was confirmed, and the possible evidence users (pain, neurology, psychiatry, anesthesiology, and rehabilitation) involved were discussed. On the basis of the above information, the eligibility criteria have been established for inclusion in the study. Studies containing rTMS for NP were considered eligible. Studies on patients with NP were included, whereas experimental subjects that were animals or healthy people were excluded. The intervention should be rTMS, and the comparison could be rTMS, sham rTMS, other treatments of relieving pain, or no treatment. The outcome should be pain measured with various clinically validated tools such as visual analog scale (VAS), numerical rating scale (NRS), short-form McGill Pain Questionnaire, and brief pain inventory. Studies that did not address intervention outcomes, such as those aimed to explore NP-related pathophysiology and focusing on cost-effectiveness, were excluded. Studies that reported other outcomes (e.g., fatigue, motor function, spasticity, sensory function, and cognition) with the exception of pain were also excluded. Only SRs (with or without meta-analysis) were included as they could provide more reliable evidence. Literature published in non-English languages were excluded. Posters and conference abstracts were excluded.

2.2. Search and Select Evidence. We conducted searches of systematic literature published before January 23, 2021, on PubMed, EMBASE, Epistemonikos, and the Cochrane Library. Medical subject headings were used in combination with free-text terms for the search, such as "neuralgia," "neurodynia," "atypical neuralgia," "nerve pain," and "stump neuralgia." Literature published in non-English languages were excluded. In addition, references of included studies were also searched to ensure the integrity of the search. The details of the search strategies are provided in Supplementary Material 1.

EndNote (version X9) was used to manage all retrieved results. After removing duplicated SRs, two reviewers (Zang and Lai) independently screened titles and abstracts to exclude irrelevant studies. Full-text studies were obtained and reviewed to make a terminal decision. Any disagreements in the decision-making process were resolved by negotiation or discussion with a third reviewer (Zhang).

2.3. Assessing the Methodological Quality of SRs. The methodological quality for each SRs was assessed with the AMSTAR-2 [19]. Almost half of published SRs have included both randomized controlled trials (RCT) and non-randomized studies. AMSTAR-2 is suitable for evaluating

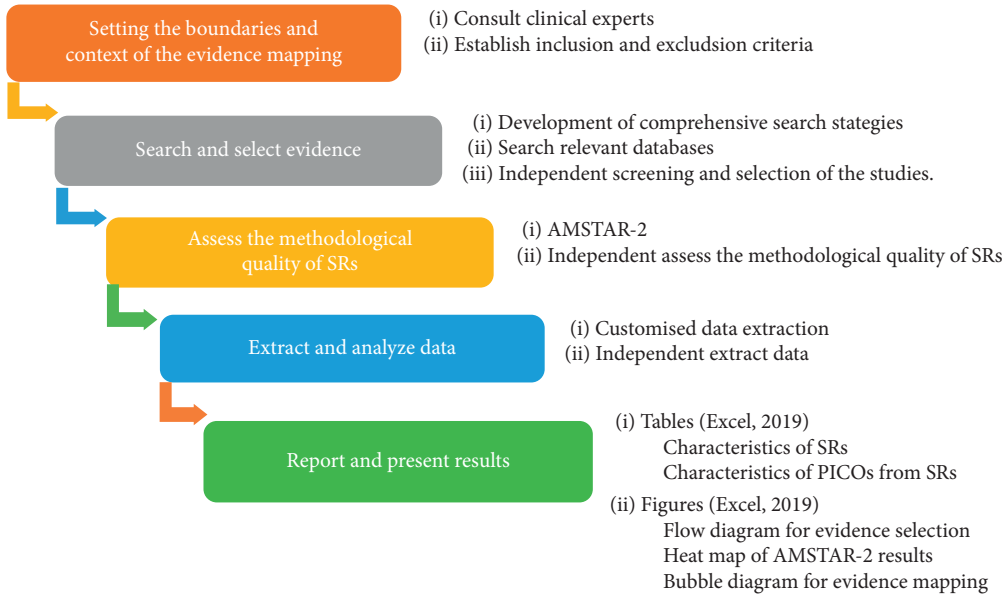

Figure 1: Core tasks for conducting evidence mapping.

the methodological quality of SRs that include RCT and non-RCT. A total of 16 items were included, covering the entire process of SRs and including topic selection, design, registration, data extraction, data statistical analysis, and discussion. AMSTAR-2 recommends 7 items (items: 2, 4, 7, 9, 11, 13, and 15) as key items for evaluating the quality of SRs (Figure 2). According to the absence of items, the evaluation results of the SRs are divided into the following four categories: "high," no key items missing and on more than one non-critical item missing; "moderate," no key items missing and more than one non-key item missing; "low," one key item missing and with or without non-key items missing; and "critically low," more than one key item missing and with or without non-critical items missing.

2.4. Extract and Analyze Data. Two data extraction tables were designed to record the main characteristics of the included SRs. Data were grouped into two categories:

(a) General characteristics of the SRs: authors, years of publication, types of SRs (with or without meta-analysis), objectives, dates of search, sample sizes, designs, and numbers of included primary studies.

(b) Characteristics of research questions: the PICO framework was used to extract data from primary studies that had been included in SRs. The four key components are study population, interventions, comparative measures, and assessment methods for outcomes. Due to the unavoidable heterogeneity of rTMS protocol among studies, it is difficult to classify and categorize all parameters. Targets, frequency, and sessions were most often reported for each primary study included in the SRs. They have been shown to influence analgesic effects and are identified as the most clinically significant factors [20–23]. High and low frequencies of rTMS could induce transient excitatory and inhibitory effects, respectively [24]. Sessions of rTMS are considered to be an important factor in maintaining the effects. Thus, the PICO characteristics are mainly focused on interventions (targets, frequency, and sessions) and comparison (sham rTMS or other targets).

According to the criteria reported previously, the conclusions of rTMS on NP reported by the systematic evaluation were classified into five categories: "potentially better," "mixed results," "unclear," "no difference," and "potentially worse." "Potentially better" is defined as statistically significant efficacy of rTMS, with the authors of the SR having no doubt about the current evidence and recommending the therapy. "Mixed results" means that the results of SRs with similar content are controversial (e.g., some SRs found no difference between transcranial magnetic stimulation with the control group in the same study, whereas others found potential benefits of transcranial magnetic stimulation over the control group. "Unclear" is defined as the SR authors concluding that the evidence is inconclusive or that the conclusions of a specific study were not reported by the authors of the SR. "No difference" is defined as comparable efficacy of rTMS as compared to the control group or no statistical difference. "Potentially worse" is defined as better efficacy in the control group as compared with rTMS. When SRs yielded consistent results for the same study, it was added to the appropriate group, and conflicting results were included in the "mixed results" group.

Two authors (Zang and Lai) assessed the methodological quality and extracted data independently. Any difference of

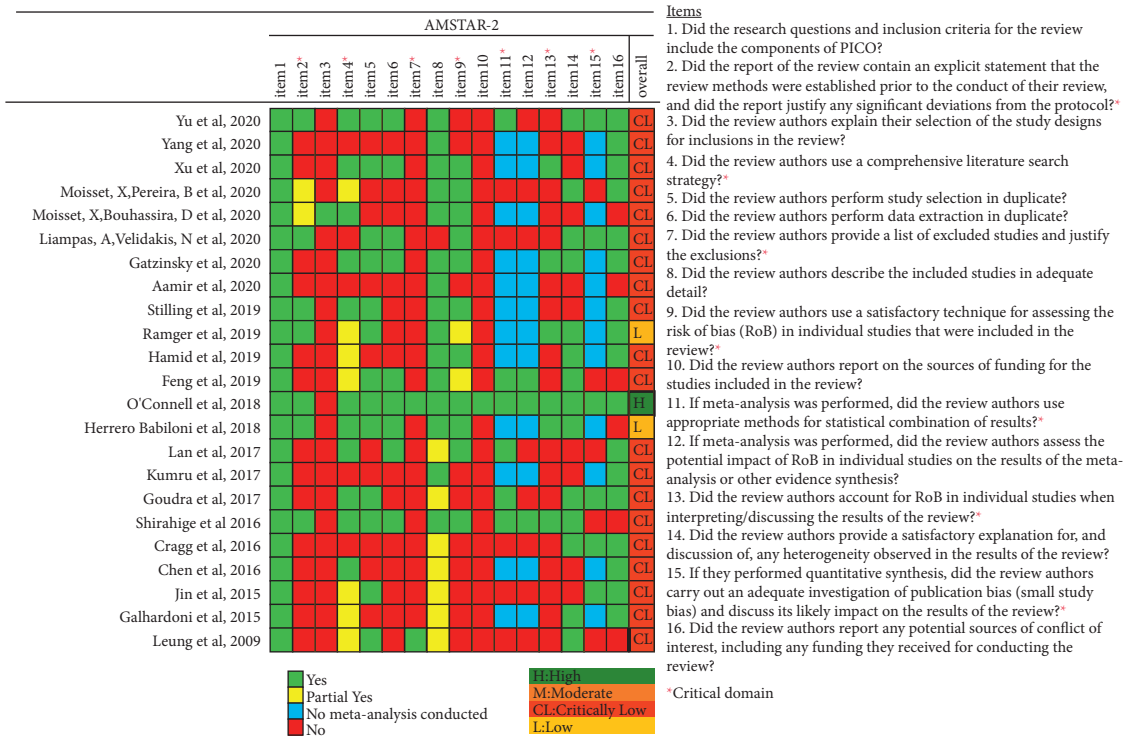

Figure 2: Methodological quality of the included systematic reviews.

opinions was discussed with the third author (Zhang). The original authors were contacted for missing information when necessary.

2.5. Report and Present Results. The evidence mapping was presented in three visualizations, and the findings were summarized in a narrative synthesis:

(a) Tables were used to describe the basic characteristics of the included SRs and characteristics of all identified PICOs.

(b) A heat map was displayed to present the quality of SRs.

(c) A bubble plot was used to present a comprehensive visualization of the conclusions of included SRs, methodological quality, sample size, and distribution of interventions. The bubble plot can display the following information: (1) authors' conclusions: ratings on the x-axis are: "potentially better," "mixed results," "unclear," "no difference," or "potentially worse"; (2) AMSTAR-2 evaluation results: presented in four different colors on the y-axis (red indicating critically very low, orange indicating low, yellow indicating medium, and green indicating high quality); (3) research characteristics: different colored bubbles indicate different PICOs; (4) the number of primary studies included in the SRs, shown in each bubble and indicated by the bubble size; and (5) interpretation of bubble plot: some primary studies may be included in multiple SRs. If SRs synthesized different conclusions for the same primary study, the same PICOs would appear in different classifications on the X-axis. If the same primary study was included by SRs of different quality, then the same PICOs classified by the primary study would appear in different classifications on the Y-axis. The included SRs covering similar topics may have overlapped considerably in terms of the primary studies they contained. Therefore, when interpreting the evidence mapping, it is critical that all figures in the bubble are not added up and that any overlapping studies are removed. Due to SRs serving as the unit of analysis rather than the primary study, the risk of bias is reduced when multiple reviews reach the same conclusion. When higher-quality SRs cover the same primary study, these findings may be interpreted with more confidence than the findings of lower quality reviews [25]. Conversely, the potential for bias appears when the primary study is concluded by only one low-quality SR, presented as "critically low" at the bottom of the bubble plot. Multiple bubbles with different results may indicate that this type of evidence highlights the preliminary stage or unclear nature of the evidence.

3. Results

3.1. Studies Selected. The study selection process is shown in Figure 3. The list of excluded studies and the reasons for exclusion are provided in Supplementary Material 2.

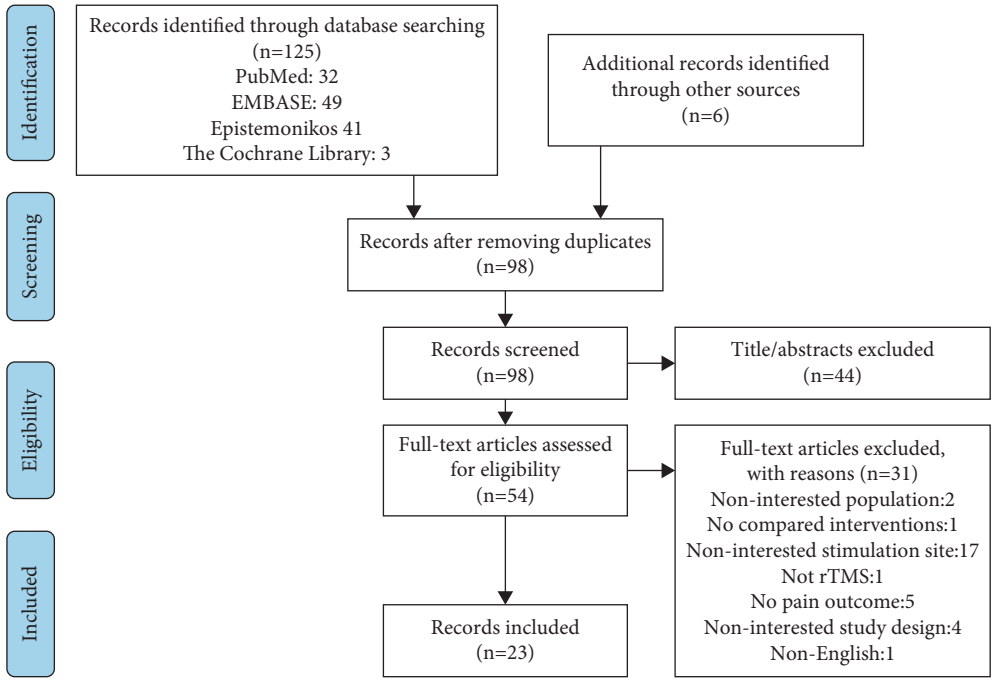

Figure 3: Flow diagram for evidence selection.

3.2. The Methodological Quality of SRs. As shown in Figure 2, according to AMSTAR-2 criteria, 1 Cochrane SR [23] was graded as "high." Two SRs [26, 27] were graded as "low," and 20 SRs [18, 27–45] were graded as "critically low" [22, 28–46]. The SRs were downgraded mainly due to the following reasons: absence of a predesigned and registered protocol [22, 29, 30, 34, 36, 40, 42–46]; no explanation for the selection of study design included in the SRs [22, 23, 26, 31, 33–46]; no list of the excluded studies or reasons for the exclusion [22, 26–45]; no statement of the funding or support for each included primary study in the SRs [22, 26–46]; and no investigation of the impact of the risk of bias in the included studies on the overall effect [28, 29, 31, 40, 42–46]. The detailed evaluation process is provided in Supplementary Material 3.

3.3. Characteristics of SRs. Table 1 shows the characteristics of the included SRs. All SRs [22, 23, 26–46] were published between 2009 and 2020. Among the 23 included SRs, 11 [23, 28, 31, 33, 37, 38, 40, 42, 44, 46] conducted a meta-analysis. The number of included primary studies ranged from 5 to 131, and they were conducted between 2004 and 2020. Each SR included patients ranging from 109 to 15,776. A total of 3 SRs [33, 39, 43] did not report or incompletely reported the designs of the included studies. Among the available data, a total of 509 randomized controlled trials (RCTs) accounted for 80.3% of the included studies in all SRs. Of all SRs, 13 [23, 27, 28, 30, 32, 36, 38, 41, 42, 45, 46] included only RCTs; 12 SRs [22, 23, 29, 31, 34, 36, 39, 40, 42, 44–46] included patients with NP with different causes; and 11 were specially conducted on NP with specific etiologies or due to a single disease. One SR [28] included pain after spinal cord injury (SCI); 4 SRs [26, 30, 33, 43] included central poststroke pain after stroke (CPSP); 4 SRs [31, 37, 38, 41] included migraine, 1 SR [35] included headache, and 1 SR [27] included orofacial pain (OFP). As for the intervention, 9 SRs [22, 29, 34, 36, 38, 40, 44–46] only assessed TMS; 8 SRs [23, 26, 28, 35, 37, 39, 41] also assessed other non-invasive stimulations; 1 SR [31] assessed neuromodulation techniques; 1 SR [30] assessed non-pharmacological interventions; 3 SRs [32, 33, 42] assessed pharmacological and non-pharmacological management of NP; and 1 SR [43] assessed non-invasive physical modalities.

3.4. Characteristics of PICOs from SRs. After merging the duplicated primary studies included in the 23 SRs, 24 primary studies that provide the mandatory parameter information were integrated into 17 PICOs groups according to the PICO characteristics.

The key characteristics of PICOs are listed in Table 2. The details of the characteristics are enumerated in Supplementary Material 4. In terms of the stimulation target, 6 PICOs stimulated the left DLPFC; 2 PICOs stimulated the S2; 2 PICOs stimulated the vertex; 1 PICO stimulated the PFC; 1 PICO stimulated the frontal cortex; 4 PICOs stimulated multiple different targets; and 1 PICO stimulated over the superior trapezius muscle. In terms of the stimulation frequency, 14 PICOs used high-frequency rTMS (>1 Hz); 2 PICOs used low-frequency rTMS (<1 Hz); and 1 PICO used both high and low frequencies. In terms of the number of sessions, 1–5 sessions were considered as short sessions, 6–10 as medium sessions, and more than 10 as long sessions. Three PICOs had long sessions; 6 PICOs had medium sessions; and 8 had short sessions. All PICOs used sham stimulation or placebo as a control to study the effectiveness of rTMS in patients with NP. In addition, 3 PICOs also

Table 1: Characteristics of included systematic reviews.

Author and year	Study design	Search date	Objective	Number of studies included	Design and number of included studies	Participants (*n*)
Yu et al., 2020 [28]	SRM	January 2019	To investigate the effect of non-invasive brain stimulation for SCI	11	RCT: 11	274
Yang et al., 2020 [29]	SR	June 2019	To explore the effect of rTMS on different types of pain	106	RCT: 69; OLT: 16; CR: 21	3,264
Xu et al., 2020 [30]	SR	August 2020	To assess the efficacy and safety of non-pharmacological therapies for CPSP	11	RCT: 11	210
Moisset et al., 2020 [31]	SRM	July 2020	To investigate the efficacy of neurostimulation techniques in migraine	38	RCT: 38	2,899
Moisset et al., 2020 [32]	SR	August 2019	To propose all the alternative treatment options for NP	131	RCT: 131	15,776
Liampas et al., 2020 [33]	SRM	November 2019	To describe the prevalence and characteristics of CPSP and investigate the relevant management methods	69	NR	NA
Gatzinsky et al., 2020 [22]	SR	June 2019	To review the efficacy and safety of rTMS on M1	32	RCT: 24; CS: 8	682 (RCT)
Aamir et al., 2020 [34]	SR	June 2019	To evaluate the effect of rTMSfor peripheral NP	12	RCT: 5; CS: 2; CR: 5	188
Stilling et al., 2020 [35]	SR	September 2018	To review the use of TMS and tDCS for specific headache disorders	34	Randomized trials: 20; NRC/prospective cohort/OLT: 14	1,787
Ramger et al., 2019 [26]	SR	2018	To evaluate the efficacy of rTMS and tDCS for CPSP	6	RCT: 1; prospective cohort: 1; CS: 2; cross-over: 2	109
Hamid et al., 2019 [36]	SR	2018	To explore the effect of rTMS on chronic refractory pain, especially in adults with central NP	12	RCT: 12	350
Feng et al., 2019 [37]	SRM	September 2018	To evaluate the efficacy of rTMS and tDCS for migraine	9	RCT: 9	276
O'Connell et al., 2018 [23]	SRM	October 2017	To assess the efficacy of non-invasive cortical stimulation techniques on chronic pain	94	RCT: 94	2,983
Herrero babiloni et al., 2018 [27]	SR	NR	To explore the effect of TMS and tDCS for chronic OFP	14	RCT: 14	228
Lan et al., 2017 [38]	SRM	April 2017	To explore the efficacy of TMS for migraine	5	RCT: 5	313
Kumru et al., 2017 [39]	SR	August 2015	To assess the role of rTMS or peripheral magnetic stimulation for NP	39	NR	892
Goudra et al., 2017 [40]	SRM	NR	To evaluate the effect of rTMS for chronic pain	9	RCT: 6; prospective observational: 3	183
Shirahige et al., 2016	SRM	November 11, 2015, to January 15, 2016	To assess the effect of NIBS on migraine patients	8	RCT: 8	296
Cragg et al., 2016 [42]	SRM	May 2015	To explore the predictors of placebo responses in central NP clinical trials	39	RCT: 39	1,153
Chen et al., 2016 [43]	SR	September 2015	To evaluate the antalgic effects of non-invasive physical modalities on CPSP	16	NA	184
Jin et al., 2015 [44]	SRM	December 2014	To evaluate the optimal parameters of rTMS for NP	25	RCT: 20; self-controlled: 5	589
Galhardoni et al., 2015 [45]	SR	2014	To review the studies on the analgesic effects of rTMS in chronic pain	33	RCT: 33	842

Table 1: Continued.

Author and year	Study design	Search date	Objective	Number of studies included	Design and number of included studies	Participants (*n*)
Leung et al., 2009 [46]	SRM	August 2007	To evaluate the overall effect of rTMS for NP and evaluate the effect of treatment parameters.	5	RCT: 5	149

SRs: systematic reviews (with or without meta-analysis); SR: systematic review; SRM: systematic review with meta-analysis; NP: neuropathic pain; SCI: spinal cord injury; rTMS: repetitive transcranial magnetic stimulation; CPSP: central poststroke pain; M1: motor cortex; TMS: transcranial magnetic stimulation; tDCS: transcranial direct current stimulation; OFP: orofacial pain; NIBS: non-invasive brain stimulation; RCT: randomized controlled trial; OLT: open-label trial; CR: case report; NR: not reported; CS: case series; and NA: not available.

compared the efficacy of different targets. The PICOs were concentrated in the following characteristics: 10 Hz, short-term sessions (4 PICOs from 7 primary studies); 10 Hz, medium-term sessions (3 PICOs from 6 primary studies); and 10 Hz, long-term sessions (2 PICOs from 5 primary studies).

3.5. Specific Findings from SRs in the Evidence Mapping. The evidence mapping of the rTMS for NP is presented in Figure 5. The bubble diagram is a visual display of data represented in Table 2. Evidence mapping showed that DLPFC is the most studied of the targets (5 PICOs from 9 primary studies) and showing a majority of "potentially better" treatment effects. In addition, the PICOs of PMC, frontal cortex, and S2 in trigeminal NP were mainly categorized with a "potentially better" conclusion and seem to be promising new targets for rTMS treatment of certain NP. PFC, S1, SMA, preM, and S2 in chronic visceral pain were categorized as "mixed" conclusions.

High-frequency (5–20 Hz) rTMS of non-M1 usually lead to "potentially better" conclusions as compared with sham stimulation, although some had transient effects. In contrast, the synthesis results for the lower frequencies (1 Hz) showed either no difference, unclear, or mixed.

Nine PICOs included 10 primary studies rated as "potentially better," and one of these PICOs involved one primary study that was also included in a high-quality meta-analysis [47]. In accordance with the AMSTAR-2 quality assessment, the interventions in these four PICOs were considered beneficial in most cases. Six PICOs included 7 primary studies with different findings within different SRs that were rated as "mixed," and this implies that the interventions in these eight PICOs had limited confidence in the effect estimates; true effects may be different from the study reports [48]. One PICO conclusion was rated as "unclear" due to its effect and was not reported in the SR [23]. Six PICOs included 7 primary studies that concluded that rTMS showed no difference when compared with the controls. Of these, 4 PICOs included 5 primary studies showing a potentially better effect of rTMS in the short term but no difference during long-term follow-up (Table 2; Supplementary Material 4). After the exclusion of studies that were ineffective during follow-up, no primary studies were included by a high-quality meta-analysis [47]. Two PICOs included 2 primary studies that showed a "potentially worse" conclusion. This finding indicated less effectiveness of these intervention protocols or inapplicability to particular NP, and the treatment effects could be uncertain [49].

4. Discussion

As far as we know, this evidence mapping may be the first synthesis of evidence on non-M1 targets for the treatment of NP. Following the classification criteria for interventions, this evidence mapping has described and organized existing evidence for non-M1 targets for NP. The majority of non-M1 targets reported as "potentially better" were DLPFC, probably due to DLPFC can coordinate the interaction between the cognitive pathway and the "pain matrix", or play a direct role in promoting or inhibiting pain through the nociceptive downstream inhibitory pathway [25, 47]. In addition, the PMC, the left frontal cortex, and the S2 also seem to be promising therapeutic targets. These targets are also importantly involved in nociceptive modulation; they share some common mechanisms, such as the involvement in altering human temperature pain thresholds [50], inducing striatal dopamine release that modulates pain [51], and causing cerebral hemodynamic changes in broader cortical regions (e.g., cingulate cortex, anterior frontal cortex, thalamus, and other subcortical areas involved in pain modulation) [52]. Another important finding was that most studies tend to suggest that high-frequencies produce better effects [49, 53–61]. This may be due to the factor that high-frequency rTMS can directly excite the injured hemisphere, thus directly improving pain. However, this evidence mapping does not significantly find the specific number of sessions that may possibly lead to a "potentially better" conclusion. This may be due to the small number of primary studies of different PICOs, making the differences insignificant.

We were able to identify some research gaps by this evidence mapping to orient further research. (1) The included SRs have covered most non-M1 targets of NP, including the DLPFC, ACC, PSI, S2, and S1, while there are still evidence gaps for other targets, such as the premotor cortex (PMC), the supplementary motor complex (SMC), and so on. (2) Low-frequency rTMS inhibited the non-injured side and the high-frequency rTMS excited the injured side. Evidence needs to be evaluated as to whether low and high frequency are used simultaneously to achieve a rebalancing of reciprocal inhibition in both hemispheres and whether the therapeutic effect can be enhanced. (3) Studies have only been conducted from a single cortical target to a

Table 2: PICOs included in systematic reviews.

PICOs number	PICOs in bubble chart	Stimulation site	Frequency (Hz)	Session schedule	Comparison	Population	Outcomes	Systematic reviews included	Individual studies included in the systematic review: Controlled trial (parallel)	Controlled trial (cross)	Number of studies	Number of SRs involving the Quality (high/moderate/low/critically low) of Individual studies:	Conclusion
1	DLPFC, 20 Hz, long sessions vs. sham rTMS	Left DLPFC	20 Hz	12 sessions	Sham	Migraine	Headache index	Yang [29], Stilling [35], Feng [37], Lan [38], Shirahige [41]	Brighina 2004		1	0/0/0/1	Mixed
2	DLPFC, 10 Hz, long sessions vs. sham rTMS	Left DLPFC	10 Hz	23 sessions	Sham	Migraine	MIDAS	Stilling [35]	Conforto 2014		1	0/0/0/1	Potentially worse: immediately
		Left DLPFC	10 Hz	23 sessions	Sham	Migraine	MIDAS	Yang [29], Stilling [35], Hamid [36], Feng [37], Lan [38], Shirahige [41]	Conforto 2014		1	0/0/0/1	No difference: follow-up at 8 weeks
		Left DLPFC	10 Hz	15 sessions	Sham	Chronic widespread pain	NRS	Hamid et al. [36], O'Connell [23]*	Avery 2015 *		1	1/0/0/1	Mixed
		Left DLPFC	10 Hz	12 sessions	Standard pharmacotherapy	Migraine	VAS	Yang [29], Stilling [35], Feng [37]	Rapinesi 2016		1	0/0/0/1	Potentially better
3	DLPFC, 10 Hz, medium sessions vs. sham rTMS	Left DLPFC	10 Hz	10 sessions	Sham	BMS	VAS	Yang [29], O'Connell [23] *, Herrero Babiloni [27] &	Umezaki 2016 * &		1	1/0/1/1	Mixed
4	DLPFC, 10 Hz, short sessions vs. sham rTMS	Left DLPFC	10 Hz	4 sessions	Sham	Mild traumatic brain injury related headache	NRS	Yang [29], Stilling [35]	Leung 2018		1	0/0/0/1	Potentially better: at 1 and 4 weeks

Table 2: Continued.

PICOs number	PICOs in bubble chart	Stimulation site	Frequency (Hz)	Session schedule	Comparison	Population	Outcomes	Systematic reviews included	Individual studies included in the systematic review			Number of SRs involving the Quality (high/ moderate/ low/ critically low) of Individual studies:	Conclusion
									Controlled trial (parallel)	Controlled trial (cross)	Number of studies		
		Left DLPFC	10 Hz	2 rTMS sessions, 1 rTMS + 1 sham	Sham	Postsurgical pain	VAS, morphine use	Yang [29]	Borckardt 2014		1	0/0/0/1	No difference
5	DLPFC, 5 Hz, medium sessions vs. sham rTMS	Left DLPFC	5 Hz	10 sessions		Migraine	MIDAS	Yang [29], Moisset [31]		Sahu 2019	1	0/0/0/1	Potentially better
6	DLPFC, 5 Hz, short sessions vs. sham rTMS	Left DLPFC	5 Hz	5 sessions	Sham	Episodic migraine	Attack frequency	Moisset [31]	Amin 2020		1	0/0/0/1	Potentially better
7	S2,1 Hz, medium sessions vs. sham rTMS	S2	1 Hz	10 sessions	Sham	Chronic visceral pain (visceral pain due to chronic pancreatitis)	VAS	Yang [29], Hamid [36], O'Connell [23]*, Galhardoni [45]	Fregni 2011 *		1	1/0/0/1	Mixed
8	S2,1 Hz or 20 Hz, short sessions vs. sham rTMS	S2	1 Hz or 20 Hz	1 session	Sham	Chronic pancreatitis pain	VAS	O'Connell [23]*		Fregni 2005*	1	1/0/0/0	Unclear
9	Vertex,10 Hz, medium sessions vs. sham rTMS	Vertex	10 Hz	10 sessions	Sham	SCI		Galhardoni et al. [45]	Yılmaz 2014		1	0/0/0/1	No difference
10	Vertex,1 Hz, short sessions vs. sham rTMS	Vertex	1 Hz	5 sessions	Sham	Migraine	NRS	Yang [29], Stilling [35], Moisset [31], Feng [37], Shirahige [41]	Teepker 2010		1	0/0/0/1	No difference

Table 2: Continued.

PICOs number	PICOs in bubble chart	Stimulation site	Frequency (Hz)	Session schedule	Comparison	Population	Outcomes	Individual studies included in the systematic review: Systematic reviews included	Controlled trial (parallel)	Controlled trial (cross)	Number of studies	Number of SRs involving the Quality (high/moderate/low/critically low) of Individual studies:	Conclusion
11	PFC, 10 Hz, short sessions vs. sham rTMS	Left PFC	10 Hz	3 sessions	Sham	Intractable neuropathic pain of various origins	NRS	Yang [29], Hamid [36], O'Connell [23]*, Herrero Babiloni&, Kumru [39]		Borckardt 2009*,&	2	1/0/1/2	Mixed
		Left PFC	10 Hz	1 session	Sham	Postsurgical pain	VAS	Yang [29], Goudra [40], Galhardoni [45]	Borckardt 2006				Mixed
		Left PFC	10 Hz	1 session	Sham	Postsurgical pain	VAS	Yang [29]	Borckardt 2008		1	0/0/0/1	Potentially better
12	S2 vs. S1/M1 vs. sham rTMS, 10 Hz, short sessions	Right S2	10 Hz	3 sessions	S1/M1 and sham	Non-specified orofacial pain, trigeminal neuropathic pain	NRS	Yang [29] Herrero Babiloni [27] &, Kumru [39]		Lindholm 2015&	1	0/0/1/1	Potentially better (S2)
13	PMC/DLPFC vs. sham rTMS, 10 Hz, medium sessions	Left PMC/DLPFC	10 Hz	10 sessions	Sham	SCI	Pain intensity: VAS	Yu [28], Yang [29], O'Connell [23]*	Nardone 2017 *		2	1/0/0/2	Potentially better (immediate effect)
		Left PMC/DLPFC	10 Hz	10 sessions	Sham	CPSP	VAS	Xu [30]	de Oliveira 2014				Potentially better (immediate effect)
		Left PMC/DLPFC	10 Hz	10 sessions	Sham	SCI	Pain intensity: VAS	Yu [28]	Nardone 2017		2	1/0/1/2	No difference (follow-up)

Table 2: Continued.

PICOs number	PICOs in bubble chart	Stimulation site	Frequency (Hz)	Session schedule	Comparison	Population	Outcomes	Individual studies included in the systematic review: Systematic reviews included	Controlled trial (parallel)	Controlled trial (cross)	Number of studies	Number of SRs involving the Quality (high/ moderate/ low/ critically low) of Individual studies:	Conclusion
		Left PMC/ DLPFC	10 Hz	10 sessions	Sham	CPSP	VAS	Yang [29], Xu [30], Moisset and Bouhassira [30], Liampas [33], Ramger [26]&, O'Connell [23]*, Kumru [39], Cragg [42], Chen [43]	de Oliveira 2014*, &				No difference (from D1 to W4)
14	Left frontal cortex vs. sham rTMS, 10 Hz, short sessions	Left frontal cortex	10 Hz	3 sessions	Sham	Migraine	VAS	Yang [29], Lan [38]	Misra 2013		1	0/0/0/1	Potentially better
15	Over the superior trapezius muscle vs. sham rTMS, 3 Hz/15 Hz, 10 sessions	Over the superior trapezius muscle	3 Hz/15 Hz	10 sessions	Sham	Brachial plexopathy	VAS	Aamir [34], Kumru [39]	Khedr 2012		1	0/0/0/1	Potentially better(1 month)
16	ACC vs. PSI vs. sham rTMS, 10 Hz, 16 sessions	ACC vs. PSI	10 Hz	16 sessions	Sham	CPSP or SCI	NRS	Yang [29], Moisset and Bouhassira [32]	Galhardoni 2019		1	0/0/0/1	No difference

Table 2: Continued.

PICOs number	PICOs in bubble chart	Stimulation site	Frequency (Hz)	Session schedule	Comparison	Population	Outcomes	Individual studies included in the systematic review: Systematic reviews included	Controlled trial (parallel)	Controlled trial (cross)	Number of studies	Number of SRs involving the Quality (high/moderate/low/critically low) of Individual studies:	Conclusion
17	S1, SMA, preM vs. M1 vs. sham rTMS, 5 Hz, short sessions	S1, SMA, preM	5 Hz	4 sessions	M1 and sham	NP	VAS	Yang [29], Gatzinsky [22], O'Connell [23]*, Kumru [39], Chen [43], Jin [44], Galhardoni [45], Leung [46]		Hirayama 2006*	1	1/0/0/1	Mixed
		S1, SMA, preM	5 Hz	2 sessions	M1 and sham	CPSP, SCI, TGNI, PNI, RA	VAS, SF-MPQ	Kumru [39]	Saitoh 2006		1	0/0/0/1	Potentially better (M1, maintained 3 hours)

PICO: population, intervention, control group, outcome; rTMS: repetitive transcranial magnetic stimulation; DLPFC: dorsolateral prefrontal cortex; S2: secondary somatosensory cortex; PFC: prefrontal cortex; PMC: premotor cortex; ACC: anterior cingulate cortex; PSI: posterior superior insula; S1: postcentral gyrus; SMA: supplementary motor area; preM: premotor area. BMS: burning mouth syndrome; SCI: spinal cord injury; CPSP: central poststroke pain; NP: neuropathic pain; TGNI: trigeminal neuropathic pain; PNI: peripheral nerve injury; RA: root avulsion. MIDAS: migraine disability assessment; NRS: numerical rating scale; VAS: visual analog scale; and SF-MPQ: short form of the McGill pain questionnaire. Note: (i) short: 1–5 sessions, medium: 5–10 sessions, and long: >10 sessions. (ii) In the included SRs: high-quality SRs are marked as *; &low-quality SRs; and the rest are critically low-quality SRs; (iii) in the primary studies included in SRs: *included by high- and critically low-quality SRs, and included by low- and critically low-quality SRs; (iv) in the number of SRs involving the quality (high/moderate/low/critically low) of primary studies): taking the 13th PICO (PMC/DLPFC vs. sham rTMS, 10 Hz, medium sessions), as an example, a total of 2 primary studies were involved. The meaning of 1/0/0/2 and 1/0/1/2 is shown below in Figure 4.

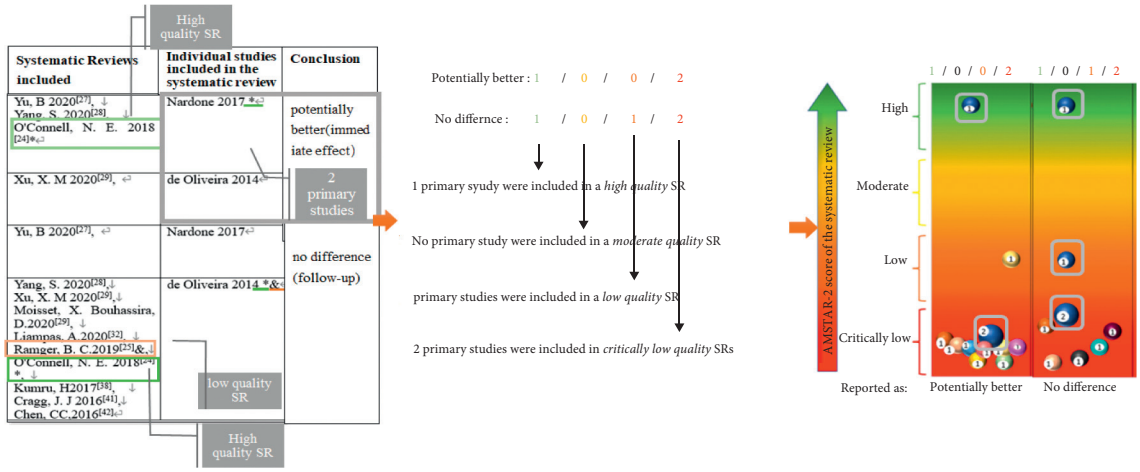

Figure 4: Interpretation of evidence mapping.

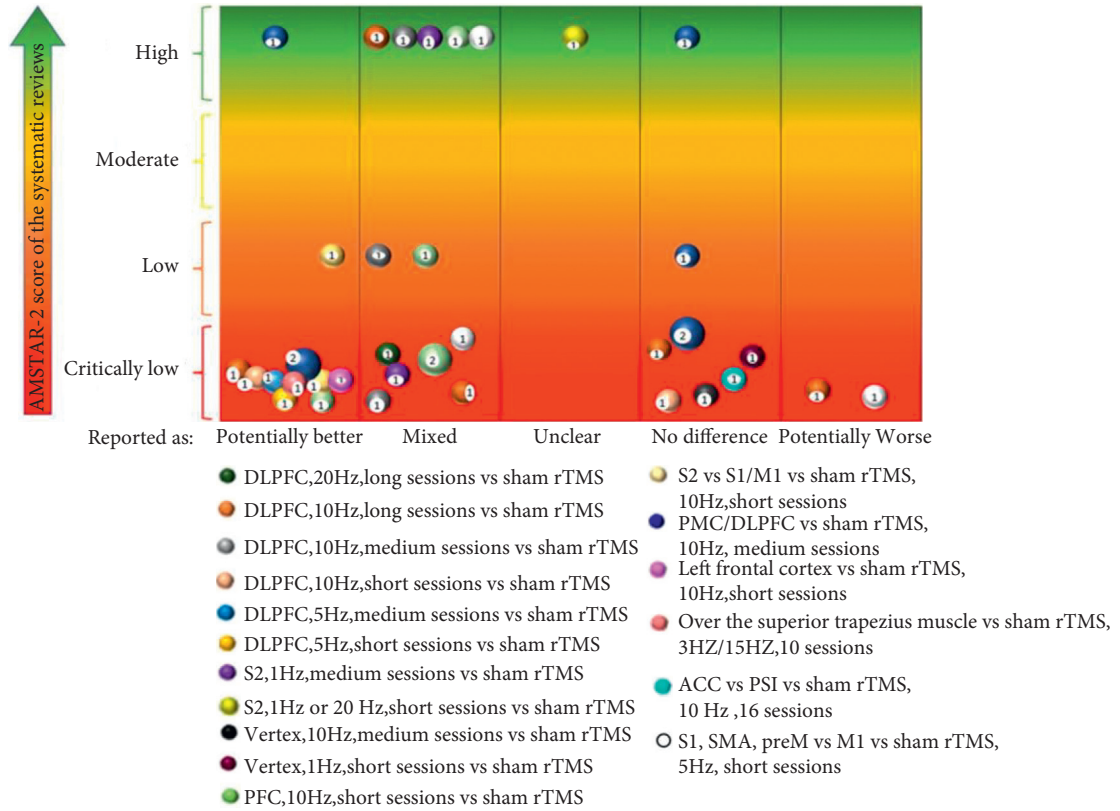

Figure 5: Evidence mapping of the rTMS on NP. Short: 1–5 sessions, medium: 5–10 sessions, and long: >10 sessions. rTMS = repetitive transcranial magnetic stimulation; DLPFC: dorsolateral prefrontal cortex; S2: secondary somatosensory cortex; PFC: prefrontal cortex; PMC: premotor cortex; ACC: anterior cingulate cortex; PSI: posterior superior insula; S1: postcentral gyrus; SMA: supplementary motor area; and preM: premotor area.

deep area of the brain; however, the fact is that any deep area is functionally connected to multiple superficial cortices. It would be interesting to examine whether combining different stimulation targets for treatment would enhance the analgesic effect. Similarly, combining transcranial direct current stimulation (tDCS) or prestimulation of a target to enhance the analgesic effect of rTMS could be experimented. (4) In addition to stimulating the target site, special stimulation coils can be designed for the deep brain structures involved in pain information processing, such as anterior cingulate cortex (ACC). (5) Clinical trials of non-M1 targets are mostly small samples with insufficient evidence reliability and an older publication year. Therefore, in future clinical studies, it is necessary to conduct large-scale, multicenter, randomized placebo-controlled trials while establishing safe and effective stimulation parameters,

selecting homogenous subjects, and reporting the treatment plan with detail and clarity. (6) When multiple SRs in an evidence mapping overlap in the inclusion of primary studies, it may be necessary to cross-check these SRs to determine whether the reported conclusions are the same as well as the extent of the overlap and the impact of the quality of SRs on the applicability of the conclusions. For example, 7 SRs categorized as second PICOs (DLPFC,10 Hz, long sessions) had different findings, with one in each of the categories of "potentially better," "mixed," "no difference," and "potentially worse." Future reviews could integrate the studies included in all 7 SRs and form new findings. (7) PICOs with multiple bubbles, and particularly those drawing mixed conclusions, may be an area where SRs need to be updated.

The quality of SRs is also an important consideration when conducting SRs. Assessment in this field suggested room for improving SR quality. Future SRs should place more emphasis on the following domains to improve the quality of studies and the validity of the results: reporting explicit statements about the description of the methodology should be designed prior to the conduction of the review; any significant deviations from the protocol should be justified to explain the selection of the study designs for inclusion in the review; a list of excluded studies should be provided and the exclusions should be justified; sources of funding or support for the individual studies included in the SRs should be indicated; and the effect of the risk of bias in individual studies on the total effect should be interpreted and discussed.

4.1. Limitations of the Study. Certain limitations in this evidence mapping should be taken into account. First, our SRs search was done in 2021. However, respective study searches were conducted in 2020 or earlier. Thus, studies that were newly published but may not be included in the SRs may have been overlooked. Nevertheless, we believe that these limitations do not substantially impact our results. Secondly, several different types of studies in SRs comparing therapeutic interventions for NP were included. Although most trials were RCTs, observational, open-label, and cohort studies as well as some case reports were also available. Furthermore, the methodologies of some SRs had limitations, and their conclusions can be subject to bias. Therefore, when multiple reviews reach the same conclusion, the conclusion should be explained carefully. Nevertheless, these are reported in detail in our results, and each conclusion can be assessed by the reader, including the limitations of the SRs. Another limitation was found in the selection of studies published solely in the English language, which limited the scope of the evidence mapping.

5. Conclusion

NP is a complex and refractory group of diseases. This evidence mapping could encourage clinical workers in the fields of pain, neurology, psychiatry, anesthesiology, and rehabilitation to pay more attention to individual patient characteristics and target the relevant brain regions. The small number of clinical trials in the area of non-M1 target therapy for NP is noteworthy, but the most important clinical issues have been covered as a result of evidence mapping. Evidence mapping is a useful and reliable method to identify currently available research as a suggestion for future research. In the future, more research effort is needed in order to highlight the optimal stimulation protocols and standardize all parameters to fill evidence gaps. More homogenous groups of participants should also be considered. Meanwhile, further efforts are needed to improve the methodological quality and reporting process of SRs.

Data Availability

The data generated in this study can be obtained in the supplementary materials provided.

Conflicts of Interest

The authors declare that the research was conducted in the absence of any commercial or financial relationships that could be construed as a potential conflict of interest.

Authors' Contributions

The study was designed by Yaning Zang, Yongni Zhang, and Yi Zhu. Screening studies and extraction data were collected by Yaning Zang and Xigui Lai under the guidance of Yongni Zhang. The data were analyzed by Yaning Zang and Yongni Zhang. Charting was done by Yaning Zang. The manuscript was drafted by Yaning Zang and Yongni Zhang. Yi Zhu reviewed the results. Shanshan Gu, Yujie Yang, Jiabao Guo, and Yi Zhu revised the manuscript for important intellectual content. All the authors approved the final version of the manuscript. Yaning Zang and Yongni Zhang contributed equally to this work.

Acknowledgments

This work was supported by the National Natural Science Foundation of China Project (No. 81860875).

Supplementary Materials

Supplementary Material 1: Database search strategies. Supplementary Material 2: SRs excluded. Supplementary Material 3: AMSTAR-2 assessment. Supplementary Material 4: PICOs' characteristics in the SRs. (*Supplementary Materials*)

References

[1] L. Colloca, T. Ludman, D. Bouhassira et al., "Neuropathic pain," *Nature Reviews Disease Primers*, vol. 3, no. 1, Article ID 17002, 2017.

[2] N. B. Finnerup, N. Attal, S. Haroutounian et al., "Pharmacotherapy for neuropathic pain in adults: a systematic review and meta-analysis," *The Lancet Neurology*, vol. 14, no. 2, pp. 162–173, 2015.

[3] R. Baron, "Neuropathic pain: a clinical perspective," *Handbook of Experimental Pharmacology*, vol. 194, pp. 3–30, 2009.
[4] N. B. Finnerup, R. Kuner, and T. S. Jensen, "Neuropathic pain: from mechanisms to treatment," *Physiological Reviews*, vol. 101, no. 1, pp. 259–301, 2021.
[5] E. Cavalli, S. Mammana, and F. Nicoletti, "The neuropathic pain: an overview of the current treatment and future therapeutic approaches," *International Journal of Immunopathology and Pharmacology*, vol. 33, Article ID 2058738419838383, 2019.
[6] D. P. Kuffler, "Mechanisms for reducing neuropathic pain," *Molecular Neurobiology*, vol. 57, no. 1, pp. 67–87, 2020.
[7] K.-H. Kim, H.-J. Seo, S. Abdi, and B. Huh, "All about pain pharmacology: what pain physicians should know," *The Korean Journal of Pain*, vol. 33, no. 2, pp. 108–120, 2020.
[8] R. H. Dworkin, A. B. O'Connor, J. Kent et al., "Interventional management of neuropathic pain: NeuPSIG recommendations," *Pain*, vol. 154, no. 11, pp. 2249–2261, 2013.
[9] A. H. Iglesias, "Transcranial magnetic stimulation as treatment in multiple neurologic conditions," *Current Neurology and Neuroscience Reports*, vol. 20, no. 1, p. 1, 2020.
[10] A. Hirayama, Y. Saitoh, and H. Kishima, "Reduction of intractable deafferentation pain by navigation-guided repetitive transcranial magnetic stimulation of the primary motor cortex," *Pain*, vol. 122, no. 1-2, pp. 22–27, 2006.
[11] K. Bannister, J. Sachau, R. Baron, and A. H. Dickenson, "Neuropathic pain: mechanism-based therapeutics," *Annual Review of Pharmacology and Toxicology*, vol. 60, no. 1, pp. 257–274, 2020.
[12] M. J. Grant and A. Booth, "A typology of reviews: an analysis of 14 review types and associated methodologies," *Health Information and Libraries Journal*, vol. 26, no. 2, pp. 91–108, 2009.
[13] N. R. Haddaway, C. Bernes, B.-G. Jonsson, and K. Hedlund, "The benefits of systematic mapping to evidence-based environmental management," *Ambio*, vol. 45, no. 5, pp. 613–620, 2016.
[14] I. M. Miake-Lye, S. Hempel, R. Shanman, and P. G. Shekelle, "What is an evidence map? a systematic review of published evidence maps and their definitions, methods, and products," *Systematic Reviews*, vol. 5, no. 1, p. 28, 2016.
[15] P. Bragge, O. Clavisi, T. Turner, E. Tavender, A. Collie, and R. L. Gruen, "The global evidence mapping initiative: scoping research in broad topic areas," *BMC Medical Research Methodology*, vol. 11, no. 1, p. 92, 2011.
[16] M. Ballesteros, N. Montero, A. López-Pousa et al., "Evidence mapping based on systematic reviews of therapeutic interventions for gastrointestinal stromal tumors (GIST)," *BMC Medical Research Methodology*, vol. 17, no. 1, p. 135, 2017.
[17] V. Welch, T. E. Howe, and S. Marcus, "Protocol: health, social care and technological interventions to improve functional ability of older adults: evidence and gap map," *Campbell Systematic Reviews*, vol. 15, no. 4, Article ID e1054, 2019.
[18] M. Madera Anaya, J. V. A. Franco, and M. Ballesteros, "Evidence mapping and quality assessment of systematic reviews on therapeutic interventions for oral cancer," *Cancer Management and Research*, vol. 11, pp. 117–130, 2019.
[19] B. J. Shea, B. C. Reeves, G. Wells et al., "AMSTAR 2: a critical appraisal tool for systematic reviews that include randomised or non-randomised studies of healthcare interventions, or both," *BMJ*, vol. 358, Article ID j4008, 2017.
[20] M. A. Ahmed, E. S. Darwish, E. M. Khedr, Y. M. El serogy, and A. M. Ali, "Effects of low versus high frequencies of repetitive transcranial magnetic stimulation on cognitive function and cortical excitability in Alzheimer's dementia," *Journal of Neurology*, vol. 259, no. 1, pp. 83–92, 2012.
[21] K. Pacheco-Barrios, X. Meng, and F. Fregni, "Neuromodulation techniques in phantom limb pain: a systematic review and meta-analysis," *Pain Medicine*, vol. 21, no. 10, pp. 2310–2322, 2020.
[22] K. Gatzinsky, C. Bergh, A. Liljegren et al., "Repetitive transcranial magnetic stimulation of the primary motor cortex in management of chronic neuropathic pain: a systematic review," *Scandinavian Journal of Pain*, vol. 21, 2020.
[23] N. E. O'Connell, L. Marston, B. M. Wand, S. Spencer, and L. H. Desouza, "Non-invasive brain stimulation techniques for chronic pain," *Cochrane Database of Systematic Reviews*, vol. 9, no. 4, 2018.
[24] M. M. Klein, R. Treister, T. Raij et al., "Transcranial magnetic stimulation of the brain: guidelines for pain treatment research," *Pain*, vol. 156, no. 9, pp. 1601–1614, 2015.
[25] K. B. Jensen, C. Berna, M. L. Loggia, A. D. Wasan, R. R. Edwards, and R. L. Gollub, "The use of functional neuroimaging to evaluate psychological and other non-pharmacological treatments for clinical pain," *Neuroscience Letters*, vol. 520, no. 2, pp. 156–164, 2012.
[26] B. C. Ramger, K. A. Bader, S. P. Davies et al., "Effects of non-invasive brain stimulation on clinical pain intensity and experimental pain sensitivity among individuals with central post-stroke pain: a systematic review," *Journal of Pain Research*, vol. 12, pp. 3319–3329, 2019.
[27] A. Herrero Babiloni, S. Guay, D. Nixdorf, L. De Beaumont, and G. Lavigne, "Non-invasive brain stimulation in chronic orofacial pain: a systematic review," *Journal of Pain Research*, vol. 11, pp. 1445–1457, 2018.
[28] B. Yu, H. Qiu, J. Li, C. Zhong, and J. Li, "Noninvasive brain stimulation does not improve neuropathic pain in individuals with spinal cord injury," *American Journal of Physical Medicine and Rehabilitation*, vol. 99, no. 9, pp. 811–820, 2020.
[29] S. Yang and M. C. Chang, "Effect of repetitive transcranial magnetic stimulation on pain management: a systematic narrative review," *Frontiers in Neurology*, vol. 11, p. 114, 2020.
[30] X.-M. Xu, H. Luo, B.-B. Rong et al., "Nonpharmacological therapies for central poststroke pain," *Medicine (Baltimore)*, vol. 99, no. 42, Article ID e22611, 2020.
[31] X. Moisset, B. Pereira, D. Ciampi de Andrade, D. Fontaine, M. Lantéri-Minet, and J. Mawet, "Neuromodulation techniques for acute and preventive migraine treatment: a systematic review and meta-analysis of randomized controlled trials," *The Journal of Headache and Pain*, vol. 21, no. 1, p. 142, 2020.
[32] X. Moisset, D. Bouhassira, J. Avez Couturier et al., "Pharmacological and non-pharmacological treatments for neuropathic pain: systematic review and French recommendations," *Revue Neurologique*, vol. 176, no. 5, pp. 325–352, 2020.
[33] A. Liampas, N. Velidakis, T. Georgiou et al., "Prevalence and management challenges in central post-stroke neuropathic pain: a systematic review and meta-analysis," *Advances in Therapy*, vol. 37, no. 7, pp. 3278–3291, 2020.
[34] A. Aamir, A. Girach, P. G. Sarrigiannis et al., "Repetitive magnetic stimulation for the management of peripheral neuropathic pain: a systematic review," *Advances in Therapy*, vol. 37, no. 3, pp. 998–1012, 2020.
[35] J. M. Stilling, O. Monchi, F. Amoozegar, and C. T. Debert, "Transcranial magnetic and direct current stimulation (TMS/tDCS) for the treatment of headache: a systematic review,"

Headache: The Journal of Head and Face Pain, vol. 59, no. 3, pp. 339–357, 2019.

[36] P. Hamid, B. H. Malik, and M. L. Hussain, "Noninvasive transcranial magnetic stimulation (TMS) in chronic refractory pain: a systematic review," *Cureus*, vol. 11, no. 10, Article ID e6019, 2019.

[37] Y. Feng, B. Zhang, J. Zhang, and Y. Yin, "Effects of non-invasive brain stimulation on headache intensity and frequency of headache attacks in patients with migraine: a systematic review and meta-analysis," *Headache: The Journal of Head and Face Pain*, vol. 59, no. 9, pp. 1436–1447, 2019.

[38] L. Lan, X. Zhang, X. Li, X. Rong, and Y. Peng, "The efficacy of transcranial magnetic stimulation on migraine: a meta-analysis of randomized controlled trails," *The Journal of Headache and Pain*, vol. 18, no. 1, p. 86, 2017.

[39] H. Kumru, S. Albu, J. Vidal, and J. M. Tormos, "Effectiveness of repetitive trancranial or peripheral magnetic stimulation in neuropathic pain," *Disability and Rehabilitation*, vol. 39, no. 9, pp. 856–866, 2017.

[40] B. Goudra, D. Shah, G. Balu et al., "Repetitive transcranial magnetic stimulation in chronic pain: a meta-analysis," *Anesthesia: Essays and Researches*, vol. 11, no. 3, pp. 751–757, 2017.

[41] L. Shirahige, L. Melo, F. Nogueira, S. Rocha, and K. Monte-Silva, "Efficacy of noninvasive brain stimulation on pain control in migraine patients: a systematic review and meta-analysis," *Headache: The Journal of Head and Face Pain*, vol. 56, no. 10, pp. 1565–1596, 2016.

[42] J. J. Cragg, F. M. Warner, N. B. Finnerup et al., "Meta-analysis of placebo responses in central neuropathic pain," *Pain*, vol. 157, no. 3, pp. 530–540, 2016.

[43] C.-C. Chen, Y.-F. Chuang, A. C.-W. Huang, C.-K. Chen, and Y.-J. Chang, "The antalgic effects of non-invasive physical modalities on central post-stroke pain: a systematic review," *Journal of Physical Therapy Science*, vol. 28, no. 4, pp. 1368–1373, 2016.

[44] Y. Jin, G. Xing, and G. Li, "High frequency repetitive transcranial magnetic stimulation therapy for chronic neuropathic pain: a meta-analysis," *Pain Physician*, vol. 18, no. 6, pp. E1029–E1046, 2015.

[45] R. Galhardoni, G. S. Correia, and H. Araujo, "Repetitive transcranial magnetic stimulation in chronic pain: a review of the literature," *Archives of Physical Medicine and Rehabilitation*, vol. 96, no. 4 Suppl, pp. S156–S172, 2015.

[46] A. Leung, M. Donohue, R. Xu et al., "rTMS for suppressing neuropathic pain: a meta-analysis," *The Journal of Pain*, vol. 10, no. 12, pp. 1205–1216, 2009.

[47] A. V. Apkarian, M. N. Baliki, and P. Y. Geha, "Towards a theory of chronic pain," *Progress in Neurobiology*, vol. 87, no. 2, pp. 81–97, 2009.

[48] I. M. Miake-Lye, S. Mak, J. Lee et al., "Massage for pain: an evidence map," *Journal of Alternative and Complementary Medicine*, vol. 25, no. 5, pp. 475–502, 2019.

[49] R. Nardone, Y. Höller, P. B. Langthaler et al., "rTMS of the prefrontal cortex has analgesic effects on neuropathic pain in subjects with spinal cord injury," *Spinal Cord*, vol. 55, no. 1, pp. 20–25, 2017.

[50] R. A. A. de Oliveira, D. C. de Andrade, A. G. G. Machado, and M. J. Teixeira, "Central poststroke pain: somatosensory abnormalities and the presence of associated myofascial pain syndrome," *BMC Neurology*, vol. 12, no. 1, p. 89, 2012.

[51] S. Huang, S. L. Borgland, and G. W. Zamponi, "Dopaminergic modulation of pain signals in the medial prefrontal cortex: challenges and perspectives," *Neuroscience Letters*, vol. 702, pp. 71–76, 2019.

[52] C. Nuti, R. Peyron, and L. Garcia-Larrea, "Motor cortex stimulation for refractory neuropathic pain: four year outcome and predictors of efficacy," *Pain*, vol. 118, no. 1-2, pp. 43–52, 2005.

[53] A. K. Sahu, V. K. Sinha, and N. Goyal, "Effect of adjunctive intermittent theta-burst repetitive transcranial magnetic stimulation as a prophylactic treatment in migraine patients: a double-blind sham-controlled study," *Indian Journal of Psychiatry*, vol. 61, no. 2, pp. 139–145, 2019.

[54] J. Korzhova, I. Bakulin, D. Sinitsyn et al., "High-frequency repetitive transcranial magnetic stimulation and intermittent theta-burst stimulation for spasticity management in secondary progressive multiple sclerosis," *European Journal of Neurology*, vol. 26, no. 4, pp. 680–e44, 2019.

[55] R. Amin, T. Emara, S. Ashour et al., "The role of left prefrontal transcranial magnetic stimulation in episodic migraine prophylaxis," *The Egyptian Journal of Neurology, Psychiatry and Neurosurgery*, vol. 56, no. 1, p. 19, 2020.

[56] A. Leung, V. Metzger-Smith, Y. He et al., "Left dorsolateral prefrontal cortex rTMS in alleviating MTBI related headaches and depressive symptoms," *Neuromodulation: Technology at the Neural Interface*, vol. 21, no. 4, pp. 390–401, 2018.

[57] P. Lindholm, S. Lamusuo, T. Taiminen et al., "Right secondary somatosensory cortex-a promising novel target for the treatment of drug-resistant neuropathic orofacial pain with repetitive transcranial magnetic stimulation," *Pain*, vol. 156, no. 7, pp. 1276–1283, 2015.

[58] R. A. A. de Oliveira, D. C. de Andrade, M. Mendonça et al., "Repetitive transcranial magnetic stimulation of the left premotor/dorsolateral prefrontal cortex does not have analgesic effect on central poststroke pain," *The Journal of Pain*, vol. 15, no. 12, pp. 1271–1281, 2014.

[59] J. J. Borckardt, S. T. Reeves, P. Kotlowski et al., "Fast left prefrontal rTMS reduces post-gastric bypass surgery pain: findings from a large-scale, double-blind, sham-controlled clinical trial," *Brain Stimulation*, vol. 7, no. 1, pp. 42–48, 2014.

[60] U. K. Misra, J. Kalita, and S. K. Bhoi, "High-rate repetitive transcranial magnetic stimulation in migraine prophylaxis: a randomized, placebo-controlled study," *Journal of Neurology*, vol. 260, no. 11, pp. 2793–2801, 2013.

[61] E. M. Khedr, M. A. Ahmed, E. A. M. Alkady, M. G. Mostafa, and H. G. Said, "Therapeutic effects of peripheral magnetic stimulation on traumatic brachial plexopathy: clinical and neurophysiological study," *Neurophysiologie Clinique/Clinical Neurophysiology*, vol. 42, no. 3, pp. 111–118, 2012.

Hindawi
Evidence-Based Complementary and Alternative Medicine
Volume 2021, Article ID 3051750, 7 pages
https://doi.org/10.1155/2021/3051750

Research Article

Effect of Executive Dysfunction on Posture Control and Gait after Stroke

Huixian Yu,[1,2] **Qianqian Zhang**,[1,2] **Sihao Liu**,[2] **Changbin Liu**,[2] **Pei Dai**,[1,2] **Yue Lan**,[3] **Guangqing Xu**,[4] **and Hao Zhang**[1]

[1]*School of Rehabilitation, Capital Medical University, China Rehabilitation Research Center, Beijing 100068, China*
[2]*Department of Rehabilitation Medicine, Beijing Tiantan Hospital, Capital Medical University, Beijing 100060, China*
[3]*Department of Rehabilitation Medicine, Guangzhou First People's Hospital, School of Medicine, South China University of Technology, Guangzhou 510050, China*
[4]*Department of Rehabilitation Medicine, Guangdong General Hospital, Guangdong Academy of Medical Sciences, Guangzhou 510080, China*

Correspondence should be addressed to Hao Zhang; crrczh2020@163.com

Received 19 August 2021; Accepted 20 September 2021; Published 12 October 2021

Academic Editor: Feng Zhang

Objective. The purpose of the study was to observe the effects of executive dysfunction (ED) on gait and postural control during walking after stroke. *Methods*. In this study, 34 subjects with stroke and ED (8 women and 26 men; age, 55.41 ± 7.89 years; time since stroke onset, 1.3 ± 0.12 months) were recruited. Stroop color-word test (SCWT), 10-meter walk test (10MWT), timed-up-and-go test (TUGT), and gait analysis were evaluated. The correlation among the correct number of Stroop tasks (SCWT-C), the number of time-consuming tasks (SCWT-T), the amount of interference (SIE-M and SIE-T) and posture control, and gait-related parameters was analyzed. *Results*. The results indicated that SCWT-C was negatively correlated with 10MWT, TUGT, and bilateral symmetry ($P < 0.05$). However, there was no significant correlation between SCWT-C and stride ($P > 0.05$). A significant negative correlation was seen between SCWT-C and bilateral symmetry ($P < 0.05$). There was no significant correlation between SCWT-T and stride ($P > 0.05$). SCWT-T was positively correlated with TUGT, 10MWT, and bilateral symmetry ($P < 0.05$). SIE-T was positively correlated with TUGT and bilateral symmetry ($P < 0.05$). There was no significant correlation between SIE-T and 10MWT or stride ($P > 0.05$). SIE-M was positively correlated with TUGT and bilateral symmetry ($P < 0.05$). There was no significant correlation between SIE-T and 10MWT or stride ($P > 0.05$). *Conclusions*. ED is closely related to the decline in postural control and the occurrence of falls. In the early phases of stroke rehabilitation, physiotherapists should focus on the patients' executive function to accelerate the recovery of postural control.

1. Introduction

Hemiplegic gait is the most common sequela of stroke [1]. The difficulty in walking or shifting restricts the range of the patients' activities, increases the burden of the caregivers, and also affects the patients' psychology [2]. Functional community walking needs attention to aspects such as flexibility and multitasking [3]. The ability to switch between tasks or simultaneously perform multiple tasks is damaged after stroke. Therefore, falls may result from the inability to effectively allocate attention to posture control rather than balance dysfunction [4]. Attention and anti-interference are important components of executive function (EF). The prevalence of EF impairment was 49% amongst all stroke patients and 34% amongst those with excellent clinical recovery [5]. According to the existing statistics for patients in the early stage (<3 months) of stroke, the incidence rate of executive dysfunction (ED) is quite high. ED is a common poststroke cognitive symptom and compromises the patients' independence in daily activities. Previous studies have often relied on brief cognitive tests without fully considering the wide spectrum of EF subdomains [6]. After stroke,

people with ED may show worse balance due to difficulty performing novel, targeted activities, such as standing up and moving from bed to chair [7]. In China, most cognitive rehabilitation and physical rehabilitation in rehabilitation facilities are separate. Physiotherapists seldom pay attention to the influence of patients' cognitive components on balance function during physical rehabilitation.

Hence, this study aimed to recruit poststroke patients with ED, conduct gait analysis, walk test, and timed-up-and-go test, and analyze the correlation of ED with gait parameters and stand up and walk test. Furthermore, this research intended to observe the effects of ED on gait and postural control during walking after stroke.

2. Methods

2.1. Participants. We collected the data of 34 patients (8 women and 26 men; age, 55.41 ± 7.89 years; time since stroke onset, 1.3 ± 0.12 months) with hemiplegic gait developed after stroke and who had visited the department of rehabilitation medicine, Beijing Tiantan Hospital, Capital Medical University, from November 2020 until June 2021. The patient inclusion criteria were as follows: (1) the definitive diagnosis of the first-ever stroke; (2) right or left basal ganglia region stroke; (3) age of 40–60 years, either male or female sex; (4) ≤3 months poststroke; (5) >12 years of education; (6) MoCA score of 20–30; (7) lower-limb Fugl–Meyer motor assessment score of 20–30; and (8) the ability to walk for 10 m without help. The exclusion criteria were as follows: (1) other cerebrovascular diseases; (2) sensory aphasia; (3) traumatic hemorrhage; (4) sensory impairment; (5) combination with other osteoarticular system diseases; and (6) failure to cooperate with the inspection process.

The Ethics Committee of Beijing Tiantan Hospital Affiliated to the Capital Medical University approved this study. All participants provided their written informed consent before data collection. The study was conducted in accordance with the Declaration of Helsinki.

2.2. Screening Measures

(1) Montreal Cognitive Assessment (MoCA): MoCA is a rapid screening assessment tool used for cognitive dysfunction. It included 11 items from across eight cognitive areas, including attention and concentration, executive function, memory, language, visual structure skills, abstract thinking, computation, and orientation. Patients with scores ranging from 20 to 30 points were recruited.

(2) 10 m walking test (10MWT): for this test, the patients were required to walk along a corridor of >10 m, with two invisible marking lines made at either end of the distance of the walking path. The time to test began with the first step of the marking line and ended when the second marking line was crossed.

(3) Timed-up-and-go test (TUGT): for the TUGT, during the evaluation, the patients were asked to remain seated in an armrest chair (seat height 45 cm, armrest height 20 cm), with the body leaning against the back of the chair and hands resting on the armrest. Next, a cone was placed on the floor 3 m away from the seat. When the experimenter gave the "go" command, the patient was required to stand up from the armchair. After standing firmly, the patient would walk for 3 m forward with the usual walking gait, turn around the cone, walk back to the chair, and then turn to sit down and lean back. No physical assistance was allowed during the test [8].

(4) Plantar pressure center of pressure (COP) of the gait analysis test: the patient was allowed to walk naturally on the plantar pressure plate and maintain the stride. The distance difference between the left-right swing of the center of gravity transfer trajectory (bilateral symmetry of COP) was recorded. The normal pressure trajectory of the center of gravity is a "butterfly" distribution, with the left-right symmetry, and the difference in the left-right swing amplitude was 0. The "butterfly" type of hemiplegic gait becomes atypical or even disappears (as shown in Figure 1).

(5) The Stroop color-word test (SCWT): it was divided into the following three steps: (i) in the first step, card A was presented, which consisted of four types of color words (i.e., yellow, red, blue, and green). A total of 50 words were read out as quickly and correctly as possible. (ii) Next, card B was presented, which consisted of dots in four different colors (i.e., yellow, red, blue, and green). (iii) Finally, card C was presented, and the above four-color words were printed in four different colors. The subjects were asked to try to read out the color of the words as quickly and correctly as possible, rather than thinking about the meaning of the words. The analysis indicators included the amount of time taken to complete reading each card, the number of correct readings, and the number of mistakes, among others. Stroop interference effects (SIE) indicators are as follows:

SIE time (SIE-T) = time of card C − time of card B;

SIE mistake count (SIE-M) = mistake number of card C − mistake number of card B.

The larger the SIE, the lower was the interference inhibition efficiency.

2.3. Data Analysis. Statistical analysis and graphing were performed using GraphPad Prism 8.0 (GraphPad Software, Inc., San Diego, California, USA). Continuous variables were expressed as mean ± standard deviation. Correlations between SCWT time (SCWT-T), SCWT correct count (SCWT-C), SIE-T, SIE-M, and the posture change, as well as the gait, were analyzed by Pearson bivariate correlation analysis. $P < 0.05$ was considered to be statistically significant.

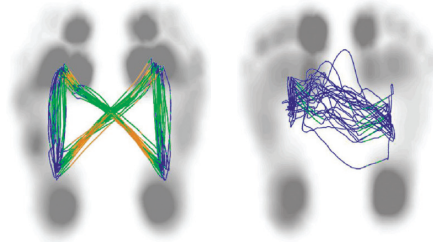

(a) (b)

Figure 1: (a) The normal central pressure trajectory is of butterfly distribution, with a left and right cross symmetry and each gait cycle almost overlapping straight lines. (b) The pressure lines of stroke patients were asymmetric, and the closer to the affected side, the more disordered they were, and the pressure lines of each gait cycle did not overlap.

3. Results

The participant characteristics are presented in Table 1. The mean time since stroke onset was 1.3 ± 0.12 months (range, 0–3 months). The mean score of MoCA was 25.78 ± 8.19 (range, 20–30). The mean lower-limb Fugl–Meyer motor assessment score was 24.56 ± 10.54(range, 20–28).

Correlation of SCWT-C with 10MWT, TUGT, stride, and bilateral symmetry of COP (Figure 2): the result showed significant negative correlation between SCWT-C and 10MWT ($R^2 = 0.666$, $P = 0.001$) and moderately negative correlation between SCWT-C and TUGT ($R^2 = 0.383$, $P \leq 0.001$). There was no significant correlation between SCWT-C and stride ($R^2 = 0.045$, $P = 0.230$). A moderately negative correlation was present between SCWT-C and bilateral symmetry ($R^2 = 0.353$, $P = 0.002$).

Correlation of SCWT-T with 10MWT, TUGT, stride, and bilateral symmetry of COP (Figure 3): there was no significant correlation between SCWT-T and 10MWT ($R^2 = 0.001$, $P = 0.900$). However, a moderately positive correlation was seen between SCWT-T and TUGT ($R^2 = 0.289$, $P = 0.001$). There was no significant correlation between SCWT-T and stride ($R^2 = 0.008$, $P = 0.613$). Furthermore, a moderately positive correlation was observed between SCWT-T and bilateral symmetry ($R^2 = 0.249$, $P = 0.003$).

Correlation of SIE-T with 10MWT, TUGT, stride, and bilateral symmetry of COP (Figure 4): there was no significant correlation between SIE-T and 10MWT ($R^2 = 0.001$, $P = 0.938$). The result suggested a moderately positive correlation between SIE-T and TUGT ($R^2 = 0.355$, $P = 0.002$). There was no significant correlation between SIE-T and stride ($R^2 = 0.038$, $P = 0.269$). A moderately positive correlation was noted between SIE-T and bilateral symmetry ($R^2 = 0.389$, $P \leq 0.001$).

Correlation of SIE-M with 10MWT, TUGT, stride, and bilateral symmetry of COP (Figure 5): there was no significant correlation between SIE-M and 10MWT ($R^2 = 0.011$, $P = 0.558$). The findings implied a moderately positive correlation between SIE-M and TUGT ($R^2 = 0.387$, $P \leq 0.001$). There was no significant correlation between SIE-M and stride ($R^2 = 0.042$, $P = 0.244$). Nonetheless, a significant positive correlation was seen between SIE-M and bilateral symmetry ($R^2 = 0.520$, $P \leq 0.001$).

4. Discussion

ED seriously affects the quality of life of the patients [9–11]. It is the core and first symptom of cognitive impairment [12], and its impact is comparable to that of limb dysfunction as it hinders the comprehensive rehabilitation of the patients [9]. ED also affects the activities of daily living (ADL), social participation, work performance, functional prognosis, and return to work [13]. Compared with normal patients, people with ED may show worse balance due to difficulty performing novel, targeted activities, such as standing up and moving from bed to chair. EF is a group of higher cognitive functions that control or monitor other low-level functions to achieve a selected goal. These functions include working memory, inhibitory control, attentional control, cognitive flexibility, reasoning, planning, concept formation, and problem-solving [14, 15]. It is generally agreed that there are three core EFs, namely, inhibitory control (including behavioral inhibition executive dysfunction) and interference control (selective attention and cognitive inhibition), working memory (WM), and cognitive flexibility.

ED is the reduced ability to do something, and the decline or loss of problem-solving ability is the main feature. ED can be divided into the following three aspects: initiation, termination, and self-regulation disorder [16]. The brain areas related to EF include the prefrontal-striatal circuit and the cerebellum, among which the prefrontal-striatal circuit also includes the dorsolateral prefrontal lobe, orbitofrontal lobe, anterior cingulate gyrus, and basal ganglia [17]. Patients with stroke who have infarction or hemorrhage in the above locations tend to exhibit significant ED.

Our present understanding of cognitive-motor networks and the influence of cognition on movement, gait characteristics, and postural control is limited. The existing research findings on the effect of cognition on gait speed and stride are controversial [18, 19]. The present study demonstrated a significant positive correlation between SCWT-T and 10MWT. Nevertheless, we did not see significant correlations between 10MWT and SCWT-C or SIE. The correlation analysis among SCWT, SIE, and stride length did not show any significance. In the process of walking in a straight line, muscle strength, endurance, and coordination may be more important than attention and posture control.

Falls after stroke are common [20]. Many studies have established a high correlation between TUGT and fall-risk

Table 1: Demographic characteristics of the participants.

Age (years)	Hemiplegic limb (number)		Onset time (M)	Sex (n)		Type of stroke		Fugl–Meyer	MoCA
	Left	Right		F	M	Inf.	Hem.		
55.41 ± 7.89	19	15	1.3 ± 0.12	8	26	24	10	24.56 ± 10.54	25.78 ± 8.19

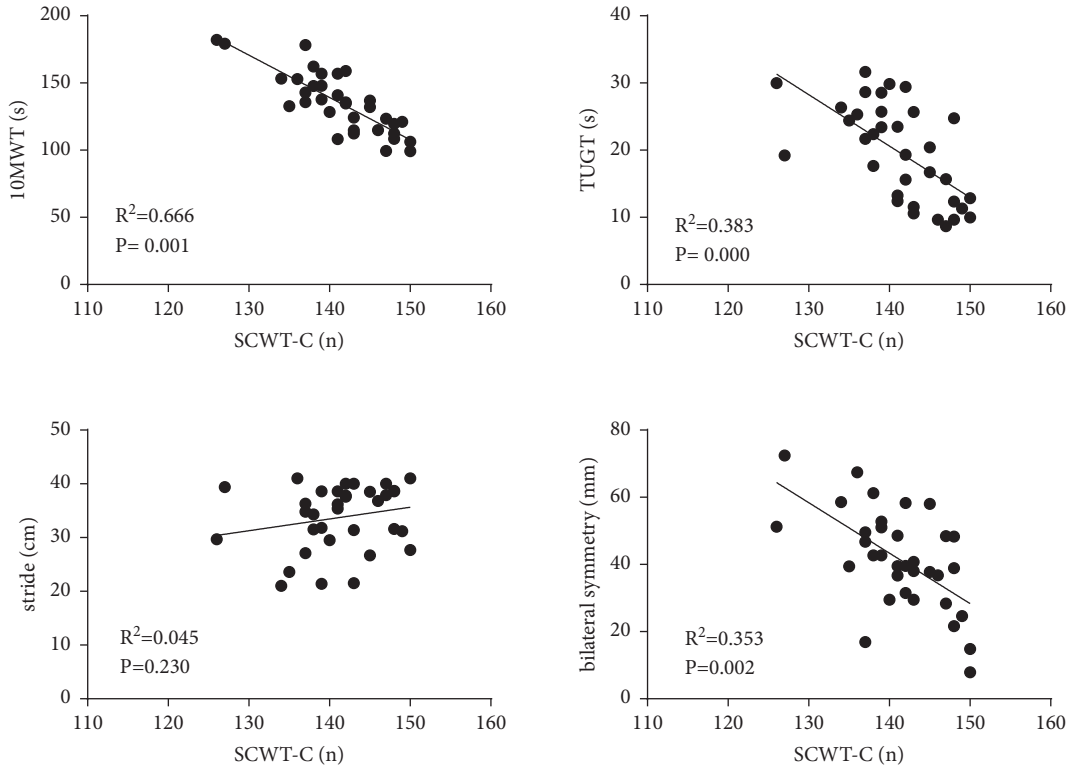

Figure 2: Correlation of SCWT-C with 10MWT, TUGT, stride, and bilateral symmetry of COP; SCWT-C and 10MWT, a significant negative correlation; SCWT-C and TUGT, a significant negative correlation; SCWT-C and stride, no significant correlation; SCWT-C and bilateral symmetry, a significant negative correlation.

prediction [21]. In this study, there were significant correlations between TUGT and SCWT (SCWT-T, SCWT-C, SIE-T, and SIE-M). Unlike walking along a straight line, in the TUGT, the complex control of the center of the body weight in getting up, walking, stopping, turning around, and sitting down requires more cognitive resources. In the analysis of central pressure, we found that the curve of people with cognitive dysfunction was more asymmetric and that the force line was more disordered. Instead of the normal straight-line distribution, the central pressure was curved, which meant that these patients had a poorer center of gravity control, higher energy consumption during walking, and a more unsteady gait. This study revealed the strong correlation between EF and the distribution of COP. Gait variability and symmetry are commonly used as quantifiable measures of mobility. COP trajectory during walking is commonly represented using the butterfly diagram. Previous research used the butterfly diagram to present essential gait characteristics, such as variability, stride width, and symmetry between legs [22]. Asymmetrical gait features are more significant. SCWT is a test developed by Stroop in 1935 to study the influence of interference. This test is often employed in the evaluation of EF in scientific research and clinical practice and is of great significance in the early detection of EF impairment. SCWT is a test of attention, and SIE reflects the dominant inhibitory component of EF. This research signified that decreased inhibition and attentional ability could reduce postural control and center of gravity control. Asymmetrical gait features are more significant.

In this study, there was no significant correlation between SCWT and step length or speed. Executive function is more affected by postural shift, while straight walking may require fewer cognitive resources.

In the past decade, conventional stroke rehabilitation has encompassed a spectrum of evidence-based exercise training interventions that involve improving strength, flexibility, endurance, balance, and gait [23]. Previously, studies have exploited repetitious and intense balance training to improve clinically relevant fall-risk predictors and balance confidence. However, systematic reviews (SRs) and meta-analyses have found that virtual reality-based training is

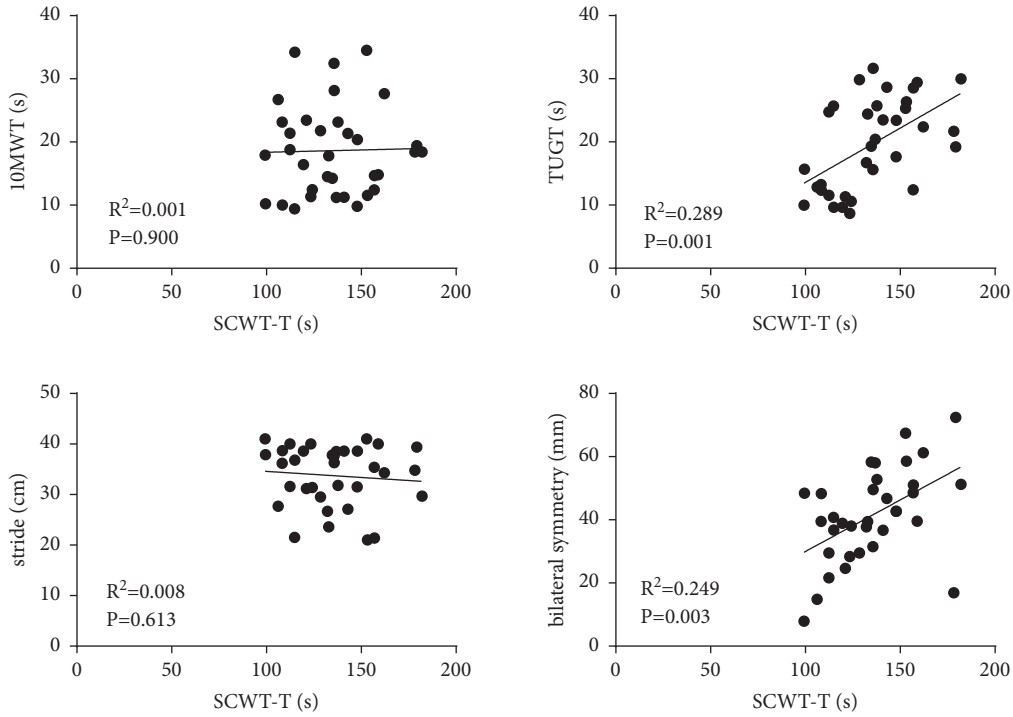

Figure 3: Correlation of SCWT-T with 10MWT, TUGT, stride, and bilateral symmetry of COP; SCWT-T and 10MWT, no significant correlation; SCWT-T and TUGT, a significant positive correlation; SCWT-T and stride, no significant correlation; SCWT-T and bilateral symmetry, a significant positive correlation.

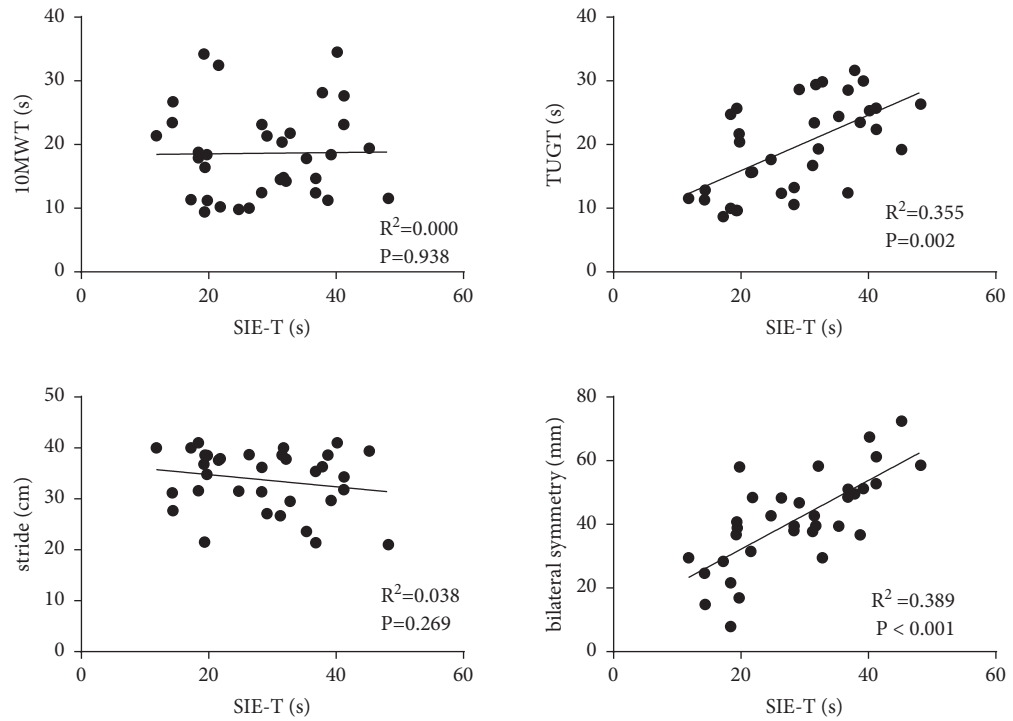

Figure 4: Correlation of SIE-T with 10MWT, TUGT, stride, and bilateral symmetry of COP; SIE-T and 10MWT, no significant correlation; SIE-T and TUGT, a significant positive correlation; SIE-T and stride, no significant correlation; SIE-T and bilateral symmetry, a significant positive correlation.

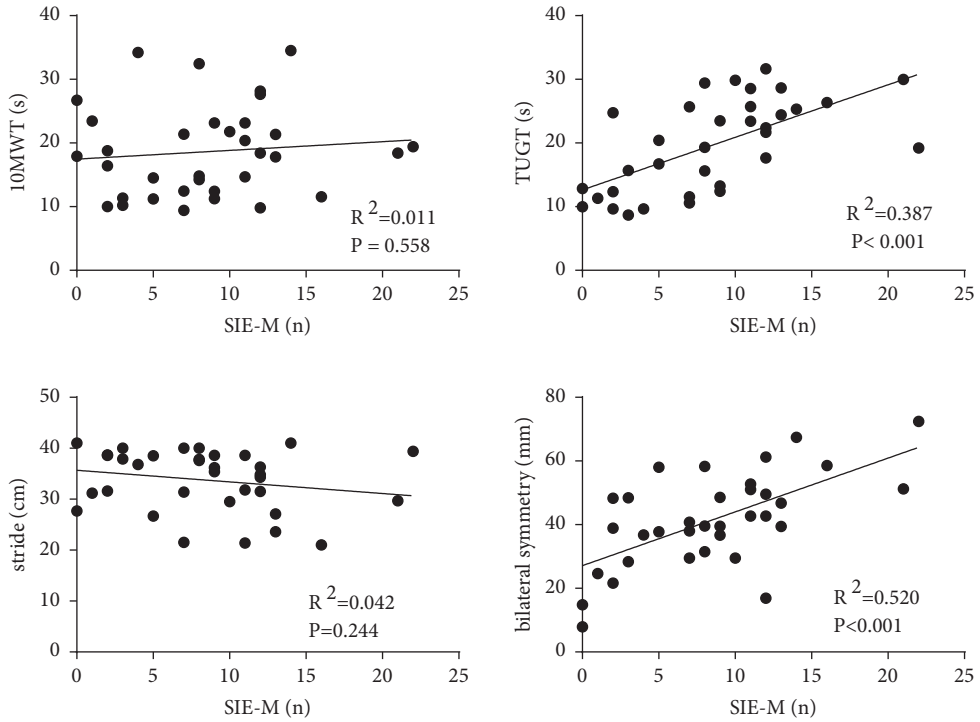

Figure 5: Correlation of SIE-M with 10MWT, TUGT, stride, and bilateral symmetry of COP; SIE-M and 10MWT, no significant correlation; SIE-M and TUGT, a significant positive correlation; SIE-M and stride, no significant correlation; SIE-M and bilateral symmetry, a significant positive correlation.

more effective in improving clinical balance measures [24]. After the stroke, the patients' ability to perform other tasks during walking is lowered or even lost completely, and the ability to notice obstacles and avoid them is decreased, which results in falls.

Many factors lead to falls in stroke patients, and the major ones are abnormal walking patterns, impaired balance function, and poor postural control. Postural control requires multiple sensory inputs, which are processed by the central nervous system and executed by the motor system. A framework for the study of postural control has been proposed, which includes biomechanical factors, spatial orientation, motor strategy, dynamic control ability, sensory strategy, and cognitive processing [25]. An SR on the effects of balance and motor function rehabilitation (248 primary studies and 10,638 participants) showed a defective result. A wide variety of balance and postural control outcomes were included. It was observed that 61% of the SRs focused on the effectiveness of physical therapy, 20% on virtual reality, 6% on electromechanical devices, 4% on Tai-Chi, whole-body vibration, and circuit training intervention, and 2% on cognitive rehabilitation [26]. The findings suggested that cognition is not sufficiently valued in balance function and motor rehabilitation. Recently, mounting evidence has indicated that cognitive function is involved in complex motor and posture control and that posture control during walking receives instructions from the cognitive regions of the brain [27]. The basal ganglia are a common stroke site and an important part of the execution-motor functional brain network [28]. This study identified that the incidence of early EF impairment after basal ganglia stroke is very high and that it tends to affect the patients' posture control ability, thereby increasing the occurrence of falls.

5. Conclusions

Our study demonstrated the strong correlation between EF and postural control in early of stroke. Furthermore, the findings suggested that impaired early ED is associated with a high fall rate in the early stage of stroke. In the early phases of stroke rehabilitation, physiotherapists should focus on the patients' ED to accelerate the recovery of postural control. In the next study, we aspire to perform early EF intervention for patients with stroke and observe the improvement in posture control ability. We hope to conduct more in-depth research on brain imaging and brain network analysis.

Data Availability

The data used in this study can be obtained by contacting the corresponding author.

Conflicts of Interest

The authors declare that they have no conflicts of interest.

Acknowledgments

This work was supported by grants from the National Natural Science Foundation of China (Grant nos. 82072548, 81974357, 81772438, and 82000723), the Science and Technology Planning Project of Guangdong Province, China (Grant no. 2016A020213003), the Science and Technology

Planning Project of Guangzhou, China (grant no. 201803010083), and the Fundamental Research Funds for the Central Universities (2018PY03).

References

[1] C. J. Winstein, J. Stein, and R. Arena, "Guidelines for adult stroke rehabilitation and recovery: a guideline for healthcare professionals from the American heart association/American stroke association," *Stroke*, vol. 47, pp. e98–e169, 2016.

[2] C. Beyaert, R. Vasa, and G. E. Frykberg, "Gait post-stroke: pathophysiology and rehabilitation strategies," *Neurophysiologie Clinique/Clinical Neurophysiology*, vol. 45, no. 4-5, pp. 335–355, 2015.

[3] Y Marco, Chung, Dual-task exercise reduces cognitive-motor interference in walking and falls after stroke," *Stroke*, vol. 49, no. 12, pp. 2990–2998, ., 2018.

[4] P. Plummer, G. Eskes, S. Wallace et al., "Cognitive-motor interference during functional mobility after stroke: state of the science and implications for future research," *Archives of Physical Medicine and Rehabilitation*, vol. 94, no. 12, pp. 2565–2574, 2013.

[5] H. Jokinen, S. Melkas, R. Ylikoski et al., "Post-stroke cognitive impairment is common even after successful clinical recovery," *European Journal of Neurology*, vol. 22, no. 9, pp. 1288–1294, 2015.

[6] H. M. Laakso, M. Hietanen, and S. Melkas, "Executive function subdomains are associated with poststroke functional outcome and permanent institutionalization," *European Journal of Neurology*, vol. 26, no. 3, 2018.

[7] U. PHlman, M. SVborg, and E. Tarkowski, "Cognitive dysfunction and physical activity after stroke: the gothenburg cognitive stroke study in the elderly," *Journal of Stroke and Cerebrovascular Diseases*, vol. 21, no. 8, pp. 652–658, 2012.

[8] C. Persson, P. Hansson, and K. Sunnerhagen, "Clinical tests performed in acute stroke identify the risk of falling during the first year: postural stroke study in Gothenburg (POSTGOT)," *Journal of Rehabilitation Medicine*, vol. 43, no. 4, pp. 348–353, 2011.

[9] S. Oveisgharan and V. Hachinski, "Executive dysfunction is a strong stroke predictor," *Journal of Neurological Science*, vol. 349, no. 1-2, pp. 161–167, 2015.

[10] L. E. Middleton, B. Lam, H. Fahmi et al., "Frequency of domain-specific cognitive impairment in sub-acute and chronic stroke," *NeuroRehabilitation*, vol. 34, no. 2, pp. 305–312, 2014.

[11] R. L. Brookes, V. Herbert, S. Paul, K. Hannesdottir, H. S. Markus, and R. G. Morris, "Executive dysfunction, awareness deficits and quality of life in patients with cerebral small vessel disease: a structural equation model," *Neuropsychology*, vol. 28, no. 2, pp. 247–253, 2014.

[12] E. H. Seo, H. Kim, K. H. Lee, and I. H. Choo, "Altered executive function in pre-mild cognitive impairment," *Journal of Alzheimer's Disease*, vol. 54, no. 3, pp. 933–940, 2016.

[13] S. H. Park, M. K. Sohn, S. Jee, and S. S. Yang, "The characteristics of cognitive impairment and their effects on functional outcome after inpatient rehabilitation in subacute stroke patients," *Annals of Rehabilitation Medicine*, vol. 41, no. 5, pp. 734–742, 2017.

[14] A. Diamond, "Executive functions," *Annual Review of Psychology*, vol. 64, no. 1, pp. 135–168, 2013.

[15] J. M. Povroznik, J. E. Ozga, C. V. Haar, and E. B. Engler-Chiurazzi, "Executive (dys)function after stroke: special considerations for behavioral pharmacology," *Behavioural Pharmacology*, vol. 29, no. 7, pp. 638–653, 2018.

[16] A. Jankowska, R. Klimkiewicz, A. Kubsik, P. Klimkiewicz, M. Woldańska - Okońska, and J. Śmigielski, "Location of the ischemic focus in rehabilitated stroke patients with impairment of executive functions," *Advances in Clinical and Experimental Medicine*, vol. 26, no. 5, pp. 767–776, 2017.

[17] J. S. Saczynski, S. Sigurdsson, M. K. Jonsdottir et al., "Cerebral infarcts and cognitive performance," *Stroke*, vol. 40, no. 3, pp. 677–682, 2009.

[18] C. San Martín Valenzuela, L. D. Moscardó, J. López-Pascual, P. Serra-Añó, and J. M. Tomás, "Effects of dual-task group training on gait, cognitive executive function, and quality of life in people with Parkinson disease: results of randomized controlled DUALGAIT trial," *Archives of Physical Medicine and Rehabilitation*, vol. 101, no. 11, pp. 1849–1856, 2020.

[19] Y. Y. Liao, I. H. Chen, and Y. J. Lin, "Effects of virtual reality-based physical and cognitive training on executive function and dual-task gait performance in older adults with mild cognitive impairment: a randomized control trial," *Frontiers in Aging Neuroence*, vol. 11, p. 62, 2019.

[20] N. Kerse, V. Parag, V. L. Feigin et al., "Falls after stroke," *Stroke*, vol. 39, no. 6, pp. 1890–1893, 2008.

[21] B. R. Greene, A. O'Donovan, R. Romero-Ortuno, L. Cogan, C. N. Scanaill, and R. A. Kenny, "Quantitative falls risk assessment using the timed up and go test," *IEEE Transactions on Biomedical Engineering*, vol. 57, no. 12, pp. 2918–2926, 2010.

[22] A. Kalron and L. Frid, "The "butterflfly diagram": a gait marker for neurological and cerebellar impairment in people with multiple sclerosis[J]," *Journal of Neurological Sciences*, vol. 358, no. 1-2, pp. 92–100, 2015.

[23] H. Gok, D. Geler-Kulcu, and N. Alptekin, "Effificacy of treatment with a kinaesthetic ability training device on balance and mobility after stroke: a randomized controlled study [J]," *Clinical Rehabilitation*, vol. 22, no. 10-11, pp. 922–930, 2008.

[24] I. J. M. de Rooij, I. G. L. van de Port, and J.-W. G. Meijer, "Effect of virtual reality training on balance and gait ability in patients with stroke: systematic review and meta-analysis," *Physical Therapy*, vol. 96, no. 12, pp. 1905–1918, 2016.

[25] G. Juras, K. Omka, and A. Fredyk, "Evaluation of the limits of stability (LOS) balance test," *Journal of Human Kinetics*, vol. 19, no. -1, pp. 39–52, 2008.

[26] C. Arienti, S. G. Lazzarini, A. Pollock, and S Negrini, "Rehabilitation interventions for improving balance following stroke: an overview of systematic reviews," *PloS one*, vol. 14, no. 7, p. e0219781, 2019.

[27] H.-x. Yu, Z.-x. Wang, C.-b. Liu, P. Dai, Y. Lan, and G.-q. Xu, "Effect of cognitive function on balance and posture control after stroke," *Neural Plasticity*, vol. 2021, no. 5, pp. 1–6, 2021.

[28] C. Blahak, H. Baezner, L. Pantoni et al., "Deep frontal and periventricular age related white matter changes but not basal ganglia and infratentorial hyperintensities are associated with falls: cross sectional results from the LADIS study," *Journal of Neurology, Neurosurgery & Psychiatry*, vol. 80, no. 6, pp. 608–613, 2009.

Hindawi
Evidence-Based Complementary and Alternative Medicine
Volume 2021, Article ID 7992688, 15 pages
https://doi.org/10.1155/2021/7992688

Research Article

Electroacupuncture Synergistically Inhibits Proinflammatory Cytokine Production and Improves Cognitive Function in Rats with Cognitive Impairment due to Hepatic Encephalopathy through p38MAPK/STAT3 and TLR4/NF-κB Signaling Pathways

Jiling Huang, Zhigang Gong, Yingnan Kong, Yanwen Huang, Hui Wang, Yingjie Kang, and Songhua Zhan

Department of Radiology, Shuguang Hospital Affiliated to Shanghai University of Traditional Chinese Medicine, Shanghai 201203, China

Correspondence should be addressed to Yingjie Kang; cry0109@foxmail.com and Songhua Zhan; zhansonghua@sina.com

Received 3 July 2021; Revised 31 August 2021; Accepted 13 September 2021; Published 1 October 2021

Academic Editor: Feng Zhang

Objective. To investigate the effect of electroacupuncture (EA) on cognitive dysfunction in rats with hepatic encephalopathy and its underlying mechanism. *Methods*. Fifty Wistar rats were randomly divided into a normal group ($n = 10$) and model group ($n = 40$). Rat models of hepatic encephalopathy were established by administration of carbon tetrachloride and thioacetamide for a total of 12 weeks. At the 9th week after modeling, rats with cognitive impairment in the model group were identified by conducting the Morris water maze test, which were then randomly divided into a control group (CCl_4) and treatment groups including EA group (CCl_4 + EA), lactulose group (CCl_4 + Lac), and EA plus lactulose group (CCl_4 + CM), with 9 rats in each group. At the end of the 9th week, rats in CCl_4 + Lac and CCl_4 + CM groups had lactulose gavage at a dose of 10 mL/kg body weight, while normal control and CCl_4 groups had gavage with the same volume of normal saline once a day for 21 days until the end of the experiment. Rats in CCl_4 + EA and CCl_4 + CM groups underwent acupuncture at Baihui (GV[DU]20), Shenting (GV[DU]24), and Zusanli (ST36) acupoints, among which EA at Baihui and Shenting acupoints were given once daily for 30 min lasting for 21 consecutive days. The effect of the treatment was measured by the Morris water maze test for learning and memory ability and magnetic resonance spectroscopy (MRS) for neuronal metabolism in the hippocampus of rats with hepatic encephalopathy. Pathological change in the rat hippocampus was observed by HE staining, while serum ammonia and liver function markers were detected. Western blot and real-time fluorescent quantitative PCR were used to detect the expressions of specific genes and proteins in the brain tissue. *Results*. Compared with those in the control group, rats undergoing EA had significantly shortened escape latency and increased number of platform crossing. H&E staining confirmed that EA improved brain tissue necrosis and ameliorated nuclear pyknosis in rats with hepatic encephalopathy. Significantly decreased levels of serum ammonia, alanine aminotransferase (ALT), aspartate transaminase (AST), total bilirubin (TBil), and total bile acid (TBA) were observed in rats undergoing EA, as well as improved levels of total protein (TP) and albumin (ALB). In addition, EA inhibited the brain expressions of TNF-α, IL-1β, IL-6, iNOS, TLR4, MyD88, NF-κB, p38MAPK, phosphorylated (p)-p38MAPK, STAT3, and p-STAT3 genes, as well as protein expressions of TNF-α, IL-6, TLR4, MyD88, NF-κB, p38MAPK, p-p38MAPK, STAT3, and p-STAT3. MRS showed increased Glx/Cr and decreased NAA/Cr, Cho/Cr and mI/Cr in the control group, and EA significantly reversed such changes in Glx/Cr and mI/Cr values. *Conclusion*. EA ameliorated the production of excessive proinflammatory cytokines in the hippocampus of rats with cognitive dysfunction secondary to hepatic encephalopathy, which also gave rise to subsequent changes such as reduced blood ammonia level, brain-protective activated astrocytes, and lower degree of brain tissue injury. The p38MAPK/STAT3 and TLR4/MyD88/NF-κB signaling pathways may be involved. EA can also improve the metabolism of NAA and Cho in the rat hippocampus and thereby improve learning and memory abilities.

1. Introduction

Hepatic encephalopathy (HE), a central nervous system dysfunction due to metabolic disorders, is caused by acute and chronic liver dysfunction or portal-systemic shunt [1]. It is characterized by extensive neuropsychiatric changes, consciousness disorders, behavioral abnormalities, and a series of dysfunction ranging from subclinical changes to coma, which is a continuous process of neurocognitive dysfunction [2]. Among others, C-type HE (CHE) is the most common type that is associated with cirrhosis, portal hypertension, and/or portal shunt. Studies have shown that CHE is independently associated with death in patients with cirrhosis, and the onset of HE in such patients may lead to persistent and cumulative cognitive impairments [3], including brain dysfunction affecting learning, memory, attention, executive function, and reasoning. These impairments would directly compromise patients' activities of daily living and quality of life and thereby bring huge economic burden and serious social issues [4]. However, therapeutic strategy to effectively improve cognitive dysfunction in patients with hepatic encephalopathy after cirrhosis remains to be discovered.

The exact pathogenesis of HE remains unclear. Studies have investigated on the synergistic effect of ammonia and inflammation on astrocyte swelling and brain edema by inducing oxidative stress and mitochondrial damage with the involvement of other factors [5, 6]. Hyperammonemia can induce neutrophil dysfunction, release reactive oxygen species, and trigger oxidative stress and inflammation. In rat models with hyperammonemia, ammonia induced the activation of astrocytes and microglia in the hippocampus and release of brain-derived inflammatory factors such as iNOS, IL-1β, and TNF-α, thereby damaging cerebral endothelial cells and disrupting the blood-brain barrier. This will result in increased permeability, which would act synergistically with intestinal ammonia to aggravate neuroinflammation and brain edema, trigger neuroinflammation, and affect brain function [7, 8]. Furthermore, abnormalities in neurotransmitters such as glutamate can be initiated by altered expressions of corresponding receptors, which leads to cognitive impairment [9]. Relevant studies have shown that anti-inflammatory treatment can reduce portal vein pressure and improve cognitive function in mice by mitigating inflammatory cytokines [10]. As one of the important members of MAPK, p38MAPK plays a regulatory role in neuronal growth, brain tissue development, and cardiac cell growth [11]. Toll-1ike receptor 4 (TLR4) also plays an important role in inflammation as a transmembrane protein receptor that mediates innate immunity, which is associated with host cell recognition of various microbial pathogenic agents [12]. TLR4 specifically identifies pathogen-associated molecular patterns (PAMPs) and transmembrane signal transduction to deliver pathogen-associated molecular stimulus signals intracellularly and triggers a cascade of signals through myeloid differentiation factor 88 (MyD88). The inhibiting unit of nuclear factor kappa-B (NF-κB), IκBα, is subsequently phosphorylated and degraded, allowing NF-κB and IκBα to dissociate into the nucleus and bind specifically to κB transcriptional regulation sequence located within the promoter or enhancer of downstream genes. As a result, the expression of inflammation-related genes would eventually lead to the release of various inflammatory cytokines and subsequent inflammatory responses [13].

The mainstay treatment for CHE is prompt removal of the precipitating factors and reversing the acute mental abnormality to a relatively stable state [14]. Lactulose is the first-line agent recommended in the current treatment guidelines for HE. Studies by Karakan et al. [15, 16] showed that lactulose can improve patients' cognitive function and reduce the incidence of symptomatic HE. However, the gastrointestinal adverse effects of lactulose have limited its usage, and it is not recommended for long-term clinical application due to its potential toxicity and the development of drug-resistant strains. Therefore, a safer and more effective treatment for HE is warranted. Acupuncture has been reported to play a regulatory role in the neuro-endocrine-immune network under stress. Mechanistically, acupuncture clears the meridians, regulates qi and the mind by stimulating the acupoints, and modulates the release of neurotransmitters and hormones in the neuro-endocrine-immune system. Thereby, it improves the ability of the body to cope with stress-related injury. Moreover, as a noninvasive alternative therapy, acupuncture can directly affect the nerve damage in the brain and improve cognitive dysfunction [17, 18]. However, the value and mechanism of acupuncture in the treatment of HE remain to be elucidated.

Magnetic resonance spectroscopy (MRS), a noninvasive approach to investigate the biochemical metabolic changes in the brain, reflects the concentration of compounds and metabolites in tissues and cells by utilizing the difference of hydrogen proton magnetic resonance frequency in different compounds and the height and area of the resonance peak [19]. MRS provides a new approach for early diagnosis and monitoring of HE by direct measurement of the concentration of osmotic substances such as mIns, Cho, and NAA. The hippocampus is an important functional region of the nervous system that is closely related to learning and memory. In this study, by observing the effect of electroacupuncture (EA) on the production of inflammatory factors such as IL-1β, TNF-α, and IL-6 in rats with cognitive impairment in CHE, we explored the role of TLR4/MyD88/NF-κB and p38MAPK/STAT3 signaling pathways in improving CHE-related cognitive impairment in rats undergoing EA, as well as the underlying mechanism and therapeutic targets.

2. Materials and Methods

2.1. Main Instruments and Reagents. The aspartate aminotransferase (AST) test kit (batch number: 01ast180109), alanine aminotransferase (ALT) test kit (batch number: 01ast180108), and total bile acid (TBA) test kit (batch number: 2401698) were purchased from Shanghai Huachen

Bearing Technology Co., Ltd. (Shanghai, China). The total bilirubin (TBil) test kit (Lot: 180824101), total protein (TP) test kit (Lot: 2401106), and serum albumin (ALB) test kit (Lot: 2400122) were purchased from Medical System Biotechnology Co., Ltd. (Ningbo, China). Carbon tetrachloride (CCl_4) (batch number: 89106125), thioacetamide (TAA) (batch number: 20160930), and olive oil (batch number: c10728873) were purchased from Shanghai Chemical Industry Park (Shanghai, China); lactulose (batch number: h20103621) made by Sichuan Jianneng Pharmaceutical Co., Ltd. The hematoxylin and eosin (H&E) staining test kit (batch number: 20180720) and blood ammonia assay kit (batch number: 2400505) were purchased from Nanjing Jiancheng Bioengineering Institute (Nanjing, China). TNF-α (60291-1-Ig), IL-1β (12703), IL-6 (12153), TLR4 (14358), MYD88 (4283), NF-κB (8242), p38MAPK (6417), (p)-p38MAPK (8690), STAT3 (9139), p-STAT3 (9145), and INOS (SBJ_M0506) were purchased from Cell Signaling Technology. Special fixation frames for rat acupuncture experiment (purchased from Beijing Global Biotechnology Co., Ltd.), 0.18 mm $*$ 13 mm acupuncture needles (batch number: 20071723; Beijing Zhongyan Taihe Medical Instrument Co., Ltd.), the Huatuo SDZ-V pulse acupuncture therapy instrument (Shanghai Huayi Medical Instrument Co., Ltd.), and the Siemens Skyra 3.0T scanner were used for magnetic resonance spectroscopy. Digbehv animal behavior analysis system includes Morris water maze, computer camera system, and software analysis system, purchased by Shanghai Jilu Software Technology Co., Ltd.

2.2. Experimental Animals and Modeling Methods. 50 Wistar male rats (200 ± 20 g, SPF grade)—provided by the Experimental Animal Center of Shanghai University of Traditional Chinese Medicine under animal license number SYXK (Shanghai, 2020-0009) and ethics committee document No.: PZSHUCM200703001—were maintained at an animal facility under pathogen-free conditions. The handling of rats and experimental procedures were conducted in accordance with experimental animal guidelines. Rat models with cirrhosis were established according to a previously reported protocol by Matei et al. [20, 21]. Fifty Wistar rats were randomly divided into a normal control group ($n = 10$) and model group ($n = 40$) according to the weight stratification method after adaptive feeding for one week. The HE model was established with carbon tetrachloride combined and thioacetamide (TAA) for 9 weeks. The model group was intraperitoneally injected with 1 mL/kg 35% carbon tetrachloride (diluted with olive oil) twice a week. At the end of the 9th week, TAA (3.5%, 250 mg/kg) was injected daily for 2 days in each group. After TAA injection in rats, the presence of any one of the symptoms such as drowsiness, slow reaction, reduced voluntary activity, ataxia, and coma can be diagnosed as HE. Before modeling, all rats were subjected to the Morris water maze test. At the 9th week after modeling, rats with cognitive impairment were screened through the Morris water maze test and randomly divided into a no-intervention group (CCl_4) and treatment groups including EA group (CCl4 + EA), lactulose group (CCl4 + Lac), and EA combined with lactulose group (CCl_4 + CM), with 9 rats in each group. Among them, therapeutic interventions were given in CCl4 + EA, CCl_4 + Lac, and CCl_4 + CM groups, which were regarded as interventional groups. At the end of the 9th week, the CCl_4 + Lac group and the CCl_4 + CM group were gavaged with lactulose at a dose of 10 mL/kg body weight, while normal control and CCl_4 groups were gavaged with the same volume of normal saline once a day for 21 days until the end of the experiment. All rats were fed with common fodder and had free intake of food and water during the study period. Finally, at the end of the 12th week of intervention, the rats' learning and memory function was measured by using the Morris water maze.

2.3. EA Treatment. At the end of week 9, EA was given to rats in the CCl_4 + EA and CCl_4 + CM groups. Rats were placed in a dedicated fixative for rat acupuncture and moxibustion, and acupoint selection was done by referring to the textbook of *experimental acupuncture* [22]. The skin areas of "Housanli" on both sides (equivalent to "Zusanli" point), "Baihui", and "Shenting" acupoints were disinfected with 75% ethanol. The acupoints were then treated with disposable sterile acupuncture needles (0.18 × 13 mm), and each point was twisted and supplemented for 1 min. The needle penetration depth is about 4 mm, which indicates the Deqi of acupuncture. Electric stimulation at "Baihui" and "Shenting" was conducted by using a Hwato EA therapeutic instrument with a frequency of 10 Hz and an intensity of 1 to 2 mA (continuous wave). The positive pole is connected to the Baihui point, and the negative pole is connected to the Shenting point, forming a loop. The appearance of slight tremor of rat limbs along with the frequency of EA apparatus was regarded as a sign of appropriate intensity. Each EA stimulus lasted for 30 min and was given once daily for consecutive 21 days.

2.4. Morris Water Maze Experiment. The Morris water maze test was used to measure the learning and memory ability of rats in each group before and after modeling and after treatment with EA. A black round pool with a diameter of about 150 cm and a height of about 60 cm was used, and the cross was divided into four quadrants, namely upper left, upper right, lower left, and lower right. A circular transparent platform with a diameter of about 12 cm was placed in the center of the upper right quadrant, and the position and size of the platform were recorded as the target area. Water was put into the pool at a height of about 2 cm higher than the platform, and the water temperature was adjusted to 25 ± 1 °C. The water in the pool was stained with carbon ink so that the rats could not see the location of the platform. All water maze experiments were carried out in the morning for 4 consecutive days. Directional sailing test: Rats were put into the water from any quadrant facing the markers each time and allowed to swim freely to find the platform under the water surface for 60 s. If the rats climbed to the platform within 60 s, this period was recorded as latency. The incubation period was 60 s, and the rats were artificially guided to the platform to rest for 20 s. The same procedure was done in

all four quadrants. Space exploration experiment: After the directional navigation test for 3 days, the cylindrical platform was removed and the rats were put into water. The computer automatic monitoring system tracked and recorded the number of times that the rats passed through the original platform position within 90 s, and the mean value of each group was taken for observation and comparative analysis. The escape latency and times of crossing the platform on the fourth day were used to assess the learning ability and memory of the rats.

2.5. MRI Examination. MRI was performed at the end of the third Morris water maze test. The Siemens 3.0T Skyra MRI scanner with special coil for rats (Shanghai Guangcheng Company; model CG-MUC40-H300-AS) was utilized for MRI imaging of rats. After anesthesia with intraperitoneal 3% pentobarbital at a dose of 2 mL/kg, the rats were placed in the coil with the prone position so that the brain was located in the middle part of the coil. After conventional transverse and coronal T2WI and T1WI MRI scanning, 1H-MRS scanning was performed [23]. Using single voxel spectroscopy (SVS)-stimulated echo acquisition mode spectroscopy (STEAM), the brain was scanned by 1H-MRS with TR/TE = 2000/9.53 ms and a turn angle of 90°. The mean acquisition time was 128, the scanning time was 4 minutes and 25 seconds, and the voxel size was $1 * 1 * 1$ cm. Scan was localized in the hippocampus of the rat brain, and the skull was avoided. Shimming was carried out in the VOI with the full width at half maximum of the water peak less than 8 Hz. Meanwhile, the resonance frequency of water was determined and input into the chemical shift selection sequence. The optimal water suppression effect was obtained by adjusting pulse excitation angle in the sequence.

After scanning, the baseline calibration, signal averaging, metabolite identification, and calculation of the area under the peak curve of metabolites were completed with the software attached to the device. The positions of the chemical shift of the metabolites were as follows: N-acetylaspartic acid (NAA): 2.01 ppm; alkali complex (Cho): 3.22 ppm; inositol (mI): 3.22 ppm; peak of creatinine (Cr): 3.03 ppm; glutamic acid-glutamine complex (Glx): 3.75 ppm. The ratios of the areas under the curve of each metabolite—i.e., NAA/Cr, CHO/Cr, MI/Cr, and GLX/Cr—were calculated with creatine (Cr) as the reference.

2.6. Sample Collection and Processing. After the MRS scan, craniotomy was performed under general anesthesia. The left brain was implanted with 10% formalin for fixation, and the right brain was separated from the hippocampus on a cryopreservation table. The hippocampus was placed in liquid nitrogen in a cryopreservation tube and stored at −80°C. Sampled brain tissues were dehydrated, embedded, and sliced before stained with H&E staining. Pathological changes of brain tissues were observed under a microscope. Blood sample was collected from the abdominal aorta, and part of the blood was treated with heparin sodium as an anticoagulant. The blood ammonia level was detected within 0.5 h. The remaining blood sample was placed at 4°C for 3 h before centrifugation at 3000 r/min for 15 min, and serum was obtained and stored at −70°C for later use.

2.7. Observation Index and Inspection Method

2.7.1. Serum Biochemistry Assays. Rats were anesthetized with pentobarbital, and blood was collected from the abdominal aorta. The levels of serum ammonia, serum TBil, ALT, AST, TBA, TP, and ALB were measured in accordance with the kit instructions of Nanjing Jiancheng Bioengineering Institute.

2.7.2. Evaluation of Brain Injury and Pathology. Brain tissues were fixed in 10% neutral-buffered formalin and embedded in paraffin. Sections of 5 μm thickness were affixed to slides, deparaffinized, and stained with hematoxylin/eosin to observe the histological changes of the hippocampal CA1 region, whether there is cell necrosis or neuronal degeneration.

2.7.3. Real-Time PCR. Real-time reverse transcription polymerase chain reaction (RT-PCR) primers were designed and synthesized by Shanghai Sangon Biological Engineering (Shanghai, China). Primers of TNF-α, IL-1β, IL-6, iNOS, TLR4, MyD88, NF-κB, P38MAPK, and STAT3 mRNAs were designed and synthesized by BioTNT (Shanghai, China). Information of the aforementioned genes and their primer sequences are shown in Table 1. Total RNA was extracted from tissues using an RNA extraction kit (MagExtractor) according to the manufacturer's instructions; and the RNA concentration detector was corrected before 5 μL of each sample was taken, and NanoDrop 2000 was used to detect the concentration and purity of RNAs. Extracted total RNAs were reverse-transcribed using reverse transcriptase kits according to the manufacturer's instructions. Using cDNA as a template, amplification was conducted using 10 μL of SYBR Green qPCR mix system according to the instructions of the TOYOBO amplification kit.

2.7.4. Western Blot Assay. Brain tissue (25 μg) was added to an appropriate volume of RIPA (including protease inhibitor and phosphatase inhibitor) and let stand for 10 min before centrifuged at 12000 rpm, 4°C for 20 min, and the supernatant was collected. Protein concentrations were measured, and samples were prepared using the loading buffer. SDS-PAGE electrophoresis was done at 300 mA with constant flow, and a blocking solution was applied for 30 min. Primary antibodies were added and incubated overnight at 4°C. Primary antibodies were IL-6 (1:1000), iNOS (1 : 1000), p-p38 (1 : 1000), p38 (1 : 1000), TLR4 (1 : 1000), MyD88 (1 : 1000), NF-κB (1:1000), TNF-α (1 : 1000), IL-1β (1 : 1000), STAT3 (1 : 1000), and p-STAT3 (1 : 1000). The product was washed with PBST for 3 times, each lasting for 5 min. The secondary antibody (1 : 3000) was then added and incubated at room temperature for 1 h before being washed with PBST. The PVDF membrane was placed on the image scanner, covered with chromographic solution, and

Table 1: Sequences of primers used in real-time polymerase chain reactions.

Genes	Sequences of primers	GenBank accession number	Annealing Tm (°C)	Product size (bp)
iNOS	5′CTTGGAGCGAGTTGTGGATTGT3′ 5′GGTAGTGATGTCCAGGAAGTAGGTG 3′	NM_012611.3	60	148
TNF-α	5′CCACCACGCTCTTCTGTCTACTG3′ 5′ TGGGCTACGGGCTTGTCACT 3′	NM_012675.3	60	151
IL-1β	5′CTGTGACTCGTGGGATGATGA3′ 5′ CCACTTGTTGGCTTATGTTCTGTC 3′	NM_031512.2	60	161
IL-6	5′CAGCGATGATGCACTGTCAGA3′ 5′ GGAGAGCATTGGAAGTTGGGG 3′	NM_012589.2	60	287
TLR4	5′AGCCTTGAATCCAGATGAAAC3′ 5′ ACAGCAGAAACCCAGATGAA 3′	NM_019078	60	135
MyD88	5′TCCAACAGAAGCGACTGAT3′ 5′ GCAGATAGTGATGAACCGTAG 3′	NM_198130	60	83
NF-κB	5′GCTCCTTTTCTCAAGCCGATGT3′ 5′ CGTAGGTCCTTTTGCGTTTTTC 3′	NM_199267.2	60	145
P38MAPK	5′TGTGATTGGTCTGTTGGATGTGT3′ 5′ TGTGGATTATGTCAGCCGAGTG3′	NM_031020.2	60	200
STAT3	5′GCCATCCTAAGCACAAAGCC3′ 5′GGGAATGTCAGGGTAGAGGTAGA3′	NM_012747.2	60	249
β-Actin	5′CCTCTATGCCAACACAGT3′ 5′ AGCCACCAATCCACACAG 3′	NM_031144	60	155

reacted for 1–2 min. Discoloration was done with Photoshop software, and densitometric values of target bands were analyzed with the alpha software processing system. β-Actin was used as an internal reference, and the relative expression of the protein of interest was calculated as the ratio of the gray value of the protein of interest to the gray value of the internal reference.

2.8. Statistical Analysis. Statistical analysis was performed using IBM SPSS software, version 22.0 (Armonk, NY). Measurement data were expressed as mean ± standard deviation ($x \pm s$). One-way ANOVA was used for comparison among multiple groups, and the LSD-t test was used for post hoc analysis. $P \leq 0.05$ was considered statistically significant.

3. Results

3.1. EA Significantly Shortened the Escape Latency and Increased the Number of Platform Crossing. Morris water maze is a classic method to observe the spatial learning and memory abilities in experimental rodent models, in which animals are trained to navigate to a platform located below the water's surface for the spatial cognition test. In this study, no significant difference was found in the latency of water maze escape and the number of platform crossing ($P > 0.05$) in rats before HE modeling. After modeling, the escape latency in rats in the CCl_4 group and treatment groups was significantly prolonged ($P < 0.05$), while the number of platform crossing was decreased ($P < 0.05$). No significant difference was found among the four groups ($P > 0.05$). After intervention, the escape latency in the CCl_4 group was significantly prolonged ($P < 0.05$) compared with the normal group; contrarily, compared with the CCl_4 group, the escape latency in CCl_4 + EA, CCl_4 + LAC, and CCl_4 + CM groups was significantly shortened ($P < 0.05$) and the number of platform crossing was increased ($P < 0.05$), and the CCl_4 + CM group was the most significant, as shown in Figure 1. The above results showed that EA improved the learning and memory disorders caused by HE.

3.2. EA Can Reduce Serum Ammonia Value and Significantly Improve Liver Function in Rats with HE. The disorder of blood ammonia metabolism is an important pathogenetic factor of HE. Alanine aminotransferase (ALT), aspartate transaminase (AST), albumin (ALB), total protein (TP), albumin (ALB), and total bilirubin (TBil) are commonly used indicators for liver function. These indicators can effectively reflect the inflammatory state of the liver and the degree of hepatocyte injury. Compared with normal control, serum levels of TBil, ALT, AST, and TBA in the CCl_4 group were significantly increased ($P < 0.001$), and the levels of TP and ALB were significantly decreased ($P < 0.05$). Meanwhile, compared with the CCl_4 group, the levels of TBil, ALT, AST, and TBA in CCl_4+EA, CCl_4+Lac, and CCl_4+CM groups were significantly decreased ($P < 0.05$) and the TP level was significantly increased ($P < 0.05$), whereas the ALB level in the CCl_4 + CM group was significantly increased ($P < 0.05$). Compared with the CCl_4 group, AST levels in both CCl_4 + EA and CCl_4 + CM groups were significantly decreased ($P < 0.05$), while TBil and ALT levels in the CCl_4 + CM group were significantly decreased ($P < 0.05$) (Figures 2(a)–2(f)). Compared with the normal group, the blood ammonia level in the CCl_4 group was significantly increased ($P < 0.01$). Compared with the CCl_4 group, blood ammonia content in CCl_4 + EA, CCl_4 + Lac, and CCl_4 + CM groups was significantly decreased on average ($P < 0.01$), and the CCl_4 + CM group was the most significant

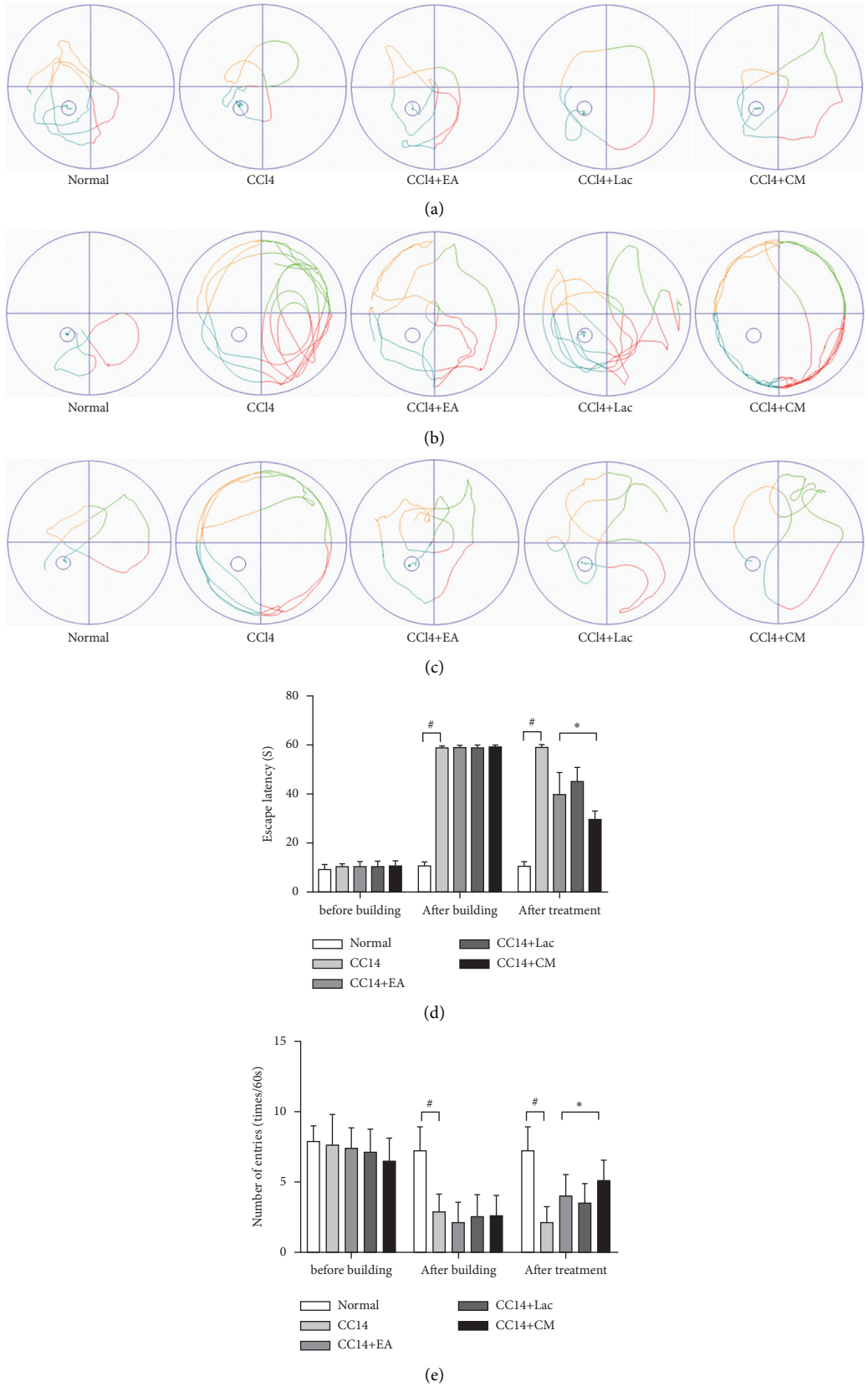

Figure 1: Wistar rats were treated with intraperitoneal injections of 1 mL/kg of 35% CCl_4 twice a week for 9 weeks. When liver cirrhosis models were established, rats with cognitive impairment were screened through the Morris water maze test and randomly divided into a no-intervention group (CCl_4) and treatment groups including EA group (CCl_4 + EA), lactulose group (CCl_4 + Lac), and EA combined with lactulose group (CCl_4 + CM), with 9 rats in each group. Ten rats in the normal group. (a–c) Behavior trajectory of rats before modeling, after modeling, and after treatment; (d) escape latency; and (e) times of crossing the platform. $^{\#}P < 0.05$ versus normal group. $^{*}P < 0.05$ versus CCl_4 model group.

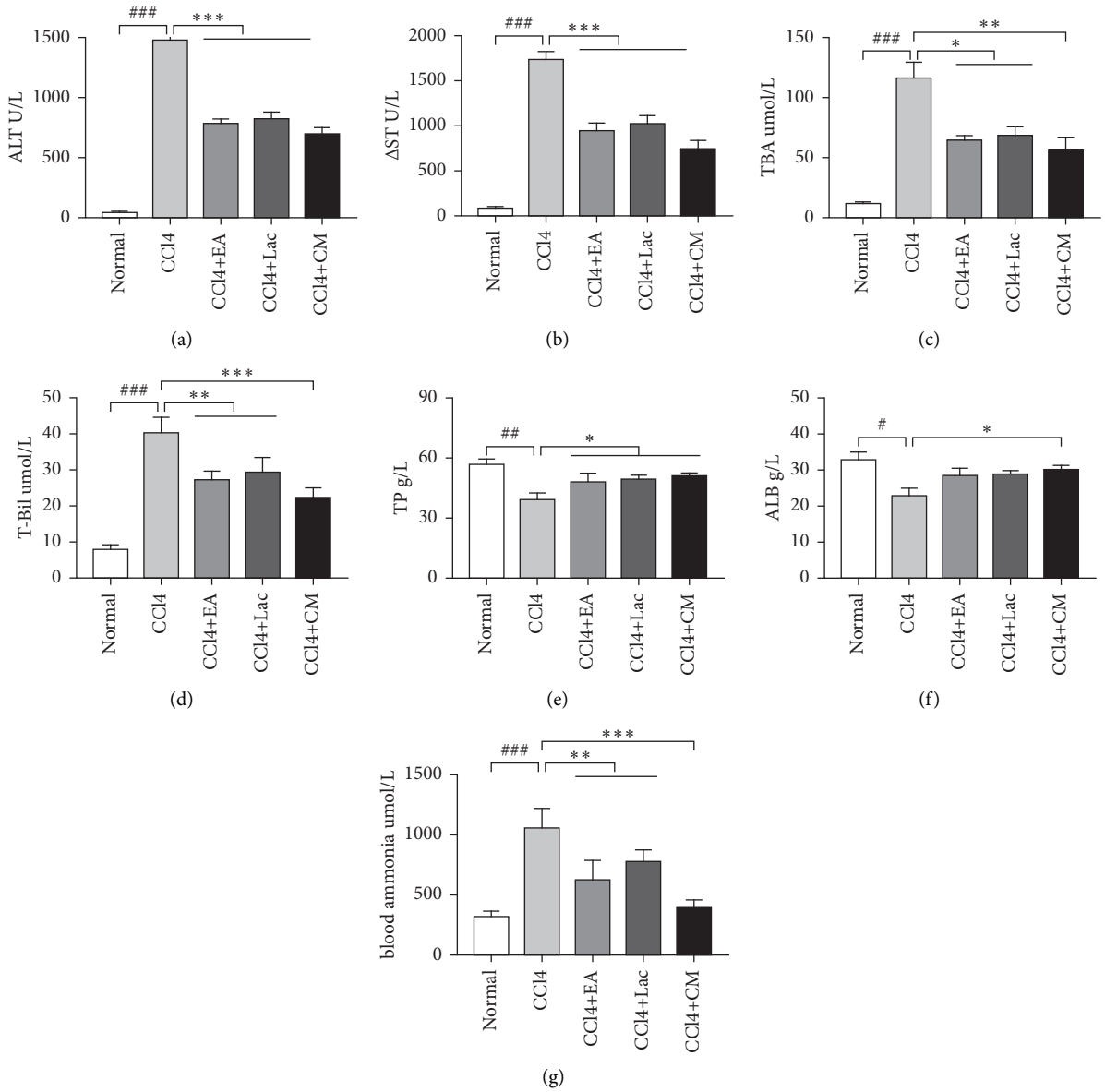

Figure 2: Wistar rats were treated with intraperitoneal injections of 1 mL/kg of 35% CCl_4 twice a week for 9 weeks. When liver cirrhosis models were established, rats with cognitive impairment were screened through the Morris water maze test and randomly divided into a no-intervention group (CCl_4) and treatment groups including EA group (CCl_4 + EA), lactulose group (CCl_4 + Lac), and EA combined with lactulose group (CCl_4 + CM), with 9 rats in each group. There are 10 rats in the normal group. (a–g) Serum levels of ALT, AST, TBA, TBil, TP, ALB, and blood ammonia. The results are expressed as mean ± SD. $^{###}P < 0.001$ and $^{##}P < 0.01$ versus normal group. $^{*}P < 0.05$, $^{**}P < 0.01$, and $^{***}P < 0.001$ versus CCl_4 model group. ALT: alanine aminotransferase; AST: aspartate aminotransferase; TBA: total bile acid; TBil: total bilirubin; TP: total protein; ALB: albumin.

(Figure 2(g)). These results indicate that EA can significantly improve the liver function of rats with hepatic encephalopathy and improve brain edema by reducing blood ammonia.

3.3. EA Improved Rat Brain Injury Induced by CCl_4 and TAA. HE staining of the brain tissues in the CA1 region of the hippocampus in rats of the normal group showed intact structure and normal size of neuron cells with absence of abnormal cells; while brain tissues in rats in the CCl_4 group presented with prominent necrosis with irregular nuclear morphology, disrupted cell membrane, decreased cytoplasm volume, condensed chromatin with cytoplasmic dispersion, pyknosis, and neuronal axonal disorganization. Compared with those in the CCl_4 group, rats in CCl_4 + EA, CCl_4 + Lac, and CCl_4 + CM groups had significantly improved brain structure, especially in the CCl_4 + CM group (Figure 3).

There are 10 rats in the normal group and 9 rats in each of no-intervention group (CCl_4) and treatment groups including EA group (CCl4 + EA), lactulose group (CCl4 + Lac), and EA combined with lactulose (CCl_4 + CM) group. H&E staining was used to evaluate the degree of brain inflammation. H&E (×200) staining.

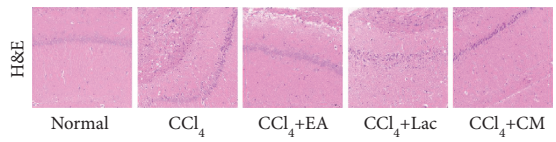

Figure 3: EA improved the brain injury induced by CCl_4 combined with TAA in HE rats.

3.4. EA Improved Nerve Cell Metabolism in the Hippocampus in Rats with Hepatic Encephalopathy. MRS was utilized for quantitative measurement of the changes in brain metabolites. Compared with the normal group, increased Glx/Cr values and decreased NAA/Cr, Cho/Cr, and mI/Cr values (all $P < 0.05$) were observed in the CCl_4 group. After intervention, we found decreased Glx/Cr values and increased Cho/Cr and mI/Cr values in all treatment groups (all $P < 0.05$), especially in the CCl_4 + EA group and CCl_4 + CM group ($P < 0.05$) (Figure 4). The results suggest that EA combined with other treatments may be able to modulate the metabolism of NAA, Glx, and Cho in the hippocampus in rats with HE and thereby improve the learning and memory performance in Morris water maze.

3.5. EA Effectively Ameliorated Inflammation in HE Rats by Inhibiting Inflammatory Factors Such as TNF-α, IL-6, and IL-1β. Inflammation can aggravate cognitive impairment in conjunction with ammonia. In this study, mRNA and protein expressions of TNF-α, IL-1β, and IL-6 in brain tissues of rats in the CCl_4 group were significantly upregulated compared with the normal control group ($P < 0.01$); Meanwhile, compared with the CCl_4 group, the mRNA and protein expressions of TNF-α, IL-1β, and IL-6 in brain tissues of rats in each treatment group were significantly downregulated ($P < 0.05$), especially those in CCl_4 + EA and CCl_4 + CM groups ($P < 0.05$) (Figures 5(a)–5(c), 6(a), 6(b), 7(a)). Therefore, it is suggested that EA inhibits the inflammatory reaction in the brain by reversing the imbalance between anti-inflammatory and inflammatory factors.

Liver failure can lead to toxin accumulation, elevated blood ammonia level, and secondary brain dysfunction [24]. Elevated blood ammonia can stimulate iNOS expression, promote NO production, increase cerebral blood flow, and result in astrocyte edema. Rats in the CCl_4 group had significantly increased expression of iNOS mRNA (vs normal group, $P < 0.01$). Meanwhile, rats in each treatment group had downregulated expression of iNOS mRNA in brain tissues (vs CCl_4 group, $P < 0.05$); among which, rats in CCl_4 + EA and CCl_4 + CM groups had significantly decreased iNOS mRNA compared with the CCl_4 + Lac group ($P < 0.05$) (Figure 5(d)).

3.6. EA Activated TLR4/MyD88/NF-κB Signaling Pathway. The TLR4/MyD88/NF-κB signaling pathway was widely distributed in various tissues and cells of the body, which can mediate the expression of inflammatory factors in cells [25]. Intervention of various targets in the TLR4/MyD88/NF-κB signaling transduction pathway has been found to reduce the inflammatory response of tissue to brain injury [26]. Our results showed that compared with normal control, the mRNA and protein expressions of TLR4, MyD88, and NF-κB in rat brains in the CCl_4 group were significantly increased (all $P < 0.001$), while expressions of those in the brain of HE rats were significantly decreased (all $P < 0.05$). Moreover, mRNA and protein expressions of TLR4, MyD88, and NF-κB in the CCl_4 + CM group were significantly decreased compared with the CCl_4+Lac group ($P < 0.05$) (Figures 5(e)–5(g), 6(c)–6(e), Figure 7(b)). Our results suggest that EA may alleviate brain injury in rats with HE by regulating the TLR4/MyD88/NF-κB signaling pathway.

3.7. EA Inhibited the p38MAPK/STAT3 Signaling Pathway and Thereby Reduced the Inflammatory Response. As an important member of the mitogen-activated protein kinase family, the p38MAPK signaling pathway plays an essential role in inflammatory response and cell apoptosis. STAT3 is considered one of the possible substrates of MAPK, which is the common pathway of intracellular signal transmission among different inflammatory cells and various inflammatory mediators and is involved in various biological reactions such as immune response and cell proliferation, differentiation, migration, and apoptosis [27]. In this study, after 3 weeks of acupuncture treatment, the mRNA and protein expressions of p38MAPK, p-p38MAPK, STAT3, and p-STAT3 in brain tissues of rats in the CCl_4 group were significantly increased compared with those in the normal control group ($P < 0.001$), indicating that MAPK and STAT3 signaling pathways could have simultaneously been activated under the inflammatory response in HE. Compared with the CCl_4 group, the mRNA and protein expressions of p38MAPK, p-p38MAPK, STAT3, and p-STAT3 in brain tissues of HE rats in all treatment groups were significantly decreased ($P < 0.05$). Compared with the CCl_4 + Lac group, expressions of p38MAPK, p-p38MAPK, STAT3, and p-STAT3 in the CCl_4 + CM group were significantly downregulated ($P < 0.05$). No significant difference in mRNA and protein expression levels between CCl4 + EA and CCl_4 + Lac groups ($P > 0.05$) was found (Figures 5(h), 5(i), 6(f)–6(i), 7(c)). In summary, EA downregulated the expressions of p38MAPK-STAT3 mRNA and related proteins by activating the p38MAPK-STAT3 signaling pathway and thereby modulated the inflammatory response in rats with HE.

4. Discussion

Currently, the pathogenesis of HE remains unclear, possible theories include toxication derived from excessive ammonia, γ-aminobutyric acid, manganese ions, and pseudo neurotransmitters, as well as oxidative stress and imbalance of serum amino acid [1]. Ammonia poisoning is the mainstay theory, and reducing the blood ammonia level serves as an important therapeutic strategy in the treatment of HE. A prospective clinical study has revealed a dose-dependent relationship between serum ammonia and cognitive

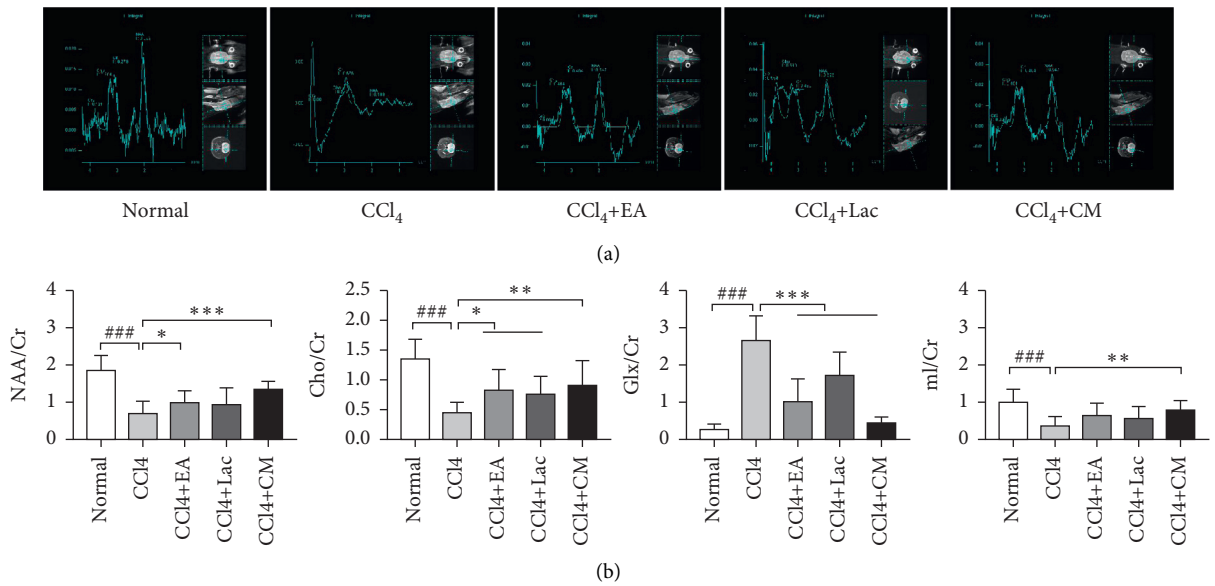

FIGURE 4: There are 10 rats in the normal group and 9 rats in each of no-intervention group (CCl_4) and treatment groups including EA group (CCl_4 + EA), lactulose group (CCl_4 + Lac), and EA combined with lactulose (CCl_4 + CM) group. (a) MRS map. (b) Comparison of the subpeak area ratio of metabolites in the brain tissue of five groups. The results are expressed as mean ± SD. $^{###}P < 0.001$ versus normal group. $^{*}P < 0.05$, $^{**}P < 0.01$, and $^{***}P < 0.001$ versus CCl_4 model group.

dysfunction [28]. Studies on the effects of ammonia toxication on the pathogenesis of HE and neurological damage have made some progress. A study [29] investigating chronic HE in rats found that reduced blood ammonia could affect the expressions of liver function biomarkers, inflammatory factors, apoptotic genes, and neurotransmitters. Recently, the synergistic effect of blood ammonia and inflammatory mediators on the initiation and development of HE has drawn more attention [30]. Acupuncture, as one of the classic therapeutic modalities in traditional Chinese medicine, has its unique advantages such as multitarget, multilevel, and omnidirectional treatment approaches. Acupuncture can deliver therapeutic effects by stimulating the internal potential of the body through activation of various regulatory mechanisms. Modern studies have shown that acupuncture at specific acupoints can play a therapeutic role in HE via inhibition of inflammatory response, improvement in liver function, and reduction of the blood ammonia level [31]. In addition, through observation of hippocampal neuron morphology and brain-derived neurotrophic factors in rats under chronic stress state, a study reported that acupuncture improved the damage of central neurons under stress state and had a benign regulatory effect on brain-derived neurotrophic factors [32]. However, few studies have investigated the specific mechanism of acupuncture therapy in mitigating HE-related cognitive dysfunction. The "Zusanli" acupoint chosen in this study is one of the most commonly adopted acupoints in current studies on the treatment of liver diseases [33]. Additionally, Baihui and Shenting acupoints belong to Du meridian, which is thought to bear the mind-awakening effect. Preliminary clinical and preclinical studies have demonstrated the efficacy of acupuncture at Baihui and Shenting acupoints in the treatment of cognitive dysfunction [34]. Therefore, these three acupoints were selected for rat experiments in this study.

We used Morris water maze to investigate the spatial learning and memory of rats with HE-related cognitive impairment. It is a well-established approach used to test cognitive impairment, especially learning dysfunction in rats. The escape latency period and the number of platform crossing were selected to reflect the cognitive changes. We found shortened escape latency and increased number of platform crossing after EA treatment for 3 weeks in rats in CCl_4 + Lac, CCl_4 + EA, and CCl_4 + CM groups, which indicates that EA can refresh the brain and resuscitate, regulate qi activity, relax tendons and activate collaterals, and promote the recovery of damaged brain tissue in rats, thus mitigating the learning and memory disturbances in rats with HE-related cognitive impairment.

The MRS technology uses the difference of hydrogen proton magnetic resonance frequency in different compounds and the peak height and area of the resonance peak to reflect the compound concentration, as well as the metabolism within tissues and cells, which can be used as an indicator for the early diagnosis of HE [35]. The metabolites commonly studied include N-acetylaspartate (NAA), creatine (Cr) and choline complex (Cho), glutamine and glutamate complex (Glx), myo-inositol (mIns), etc. Each metabolite is sensitive to different pathological processes. NAA peak mainly exists in neurons, which can reflect the density and functional state of neurons. Cho peak is a marker of cell membrane damage and glial cell proliferation and is a precursor of acetylcholine, an important neurotransmitter [36]. The peak of mIns is a marker of glial cells, and the abnormal changes of Cho and mI peaks indirectly

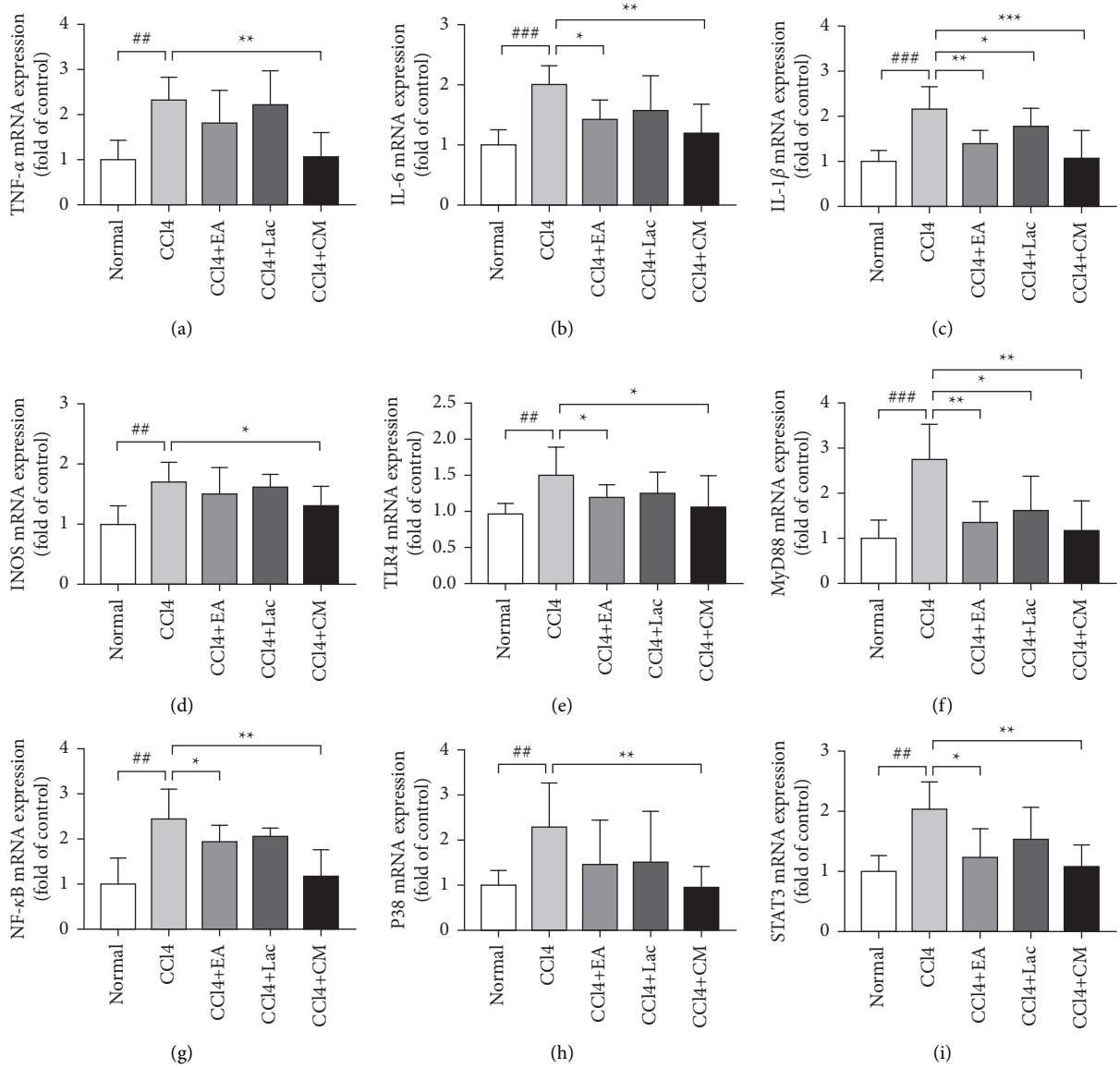

Figure 5: Wistar rats were treated with intraperitoneal injections of 1 mL/kg of 35% CCl_4 twice a week for 9 weeks. When HE models were established, the lactulose group (CCl_4 + Lac) and acupuncture combined with medicine group (CCl_4 + CM) were gavaged with 10 mL/kg body weight. EA was given to the EA (CCl_4 + EA) and the combination (CCl_4 + CM) groups 30 min per day with consecutive 21 days. There are 10 rats in the normal group, and 9 rats in each of no-intervention group (CCl_4) and treatment groups including EA group (CCl_4 + EA), lactulose group (CCl_4 + Lac), and EA combined with lactulose (CCl_4 + CM) group. Expressions of TNF-α, IL-6, IL-1β, iNOS, TLR4, MyD88, NF-κB, p38MAPK, and STAT3 genes were used to evaluate hepatic inflammation in the mRNA level detected by RT-qPCR.

reflect the changes in osmotic pressure inside and outside astrocytes. Glu is the most abundant amino acid in the brain and a major neurotransmitter. Glx composite peaks are mainly derived from the overlapping formants of glutamine (Gln) and glutamic acid (Glu) [37]. Since the level of Cr in the brain remains relatively stable, Cr is used as an internal parameter to quantify the levels of Glx, mIns, Cho, and NAA. Typical changes in patients with HE are decreased mI/Cr and Cho/Cr, increased Glx/Cr, and insignificant changes in NAA and NAA/Cr [38]. In this study, we found that compared with the normal group, mI/Cr, NAA/Cr, and Cho/Cr decreased and Glx/Cr increased in the HE model group, which was consistent with previous research results and also echoed the ammonia poisoning theory in HE. The underlying mechanism may be that liver dysfunction in HE patients may lead to hyperammonemia, which increases the blood ammonia concentration and damages the blood-brain barrier, thereby increasing glutamine synthesis in astrocytes and consequently increasing Glx peak. Elevated osmotic pressure in the brain leads to swelling of neurons, causing brain edema and further cognitive dysfunction [39]. Therefore, the elevation of Glx/Cr is closely related to the severity of HE. Meanwhile, the production of glutamine increases the osmotic pressure in astrocytes, and cells compensate for the high osmotic pressure by expulsing osmotic agents such as Mi and Cho, resulting in decreases in

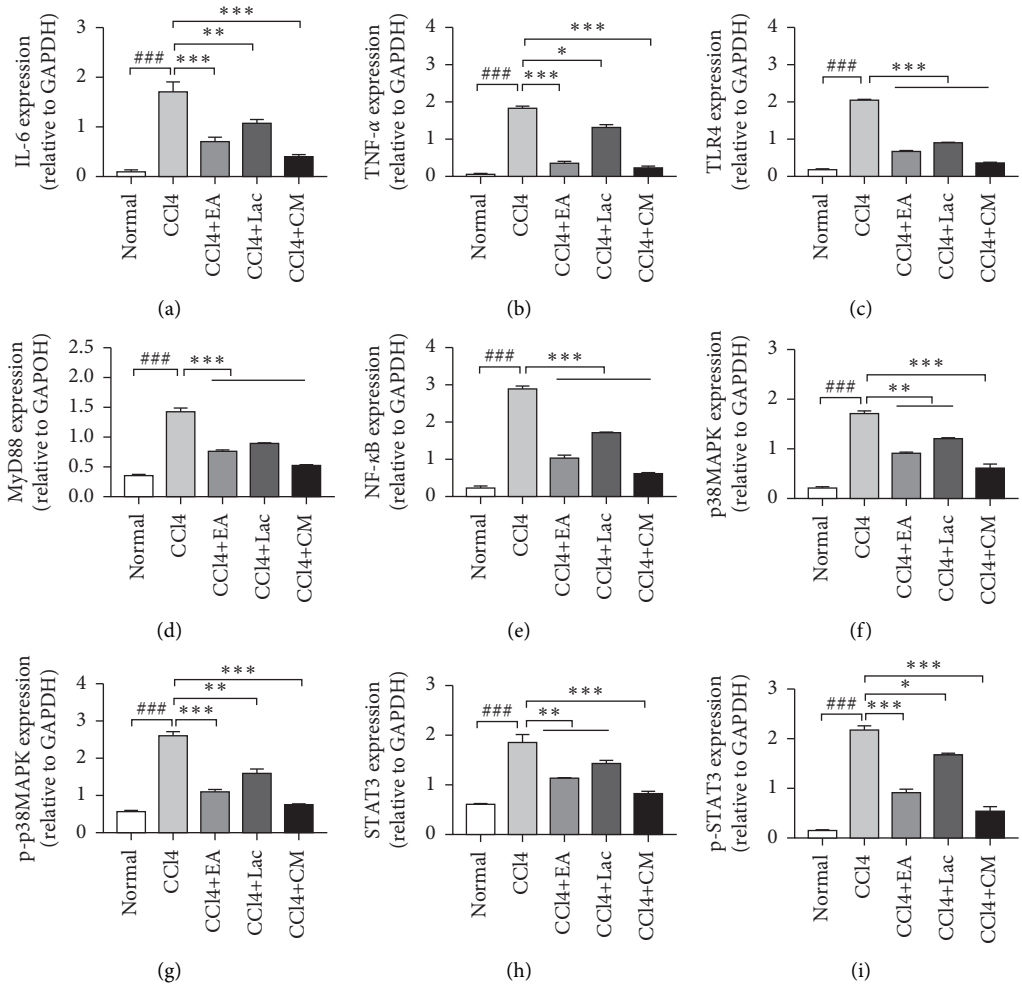

Figure 6: EA regulates the expression level of hepatic inflammation pathway-related proteins. There are 10 rats in the normal group and 9 rats in each of no-intervention group (CCl_4) and treatment groups including EA group (CCl_4 + EA), lactulose group (CCl_4 + Lac), and EA combined with lactulose (CCl_4 + CM) group. (a–i) TNF-α, IL-6, TLR4, MyD88, NF-κB, p38MAPK, p-p38MAPK, STAT3, and p-STST3 were used to evaluate the degree of inflammation in protein levels detected by Western blot. $^{###}P < 0.001$ versus normal group. $^{*}P < 0.05$, $^{**}P < 0.01$, and $^{***}P < 0.001$ versus CCl_4 model group.

mI/Cr and Cho/Cr ratios. However, the NAA/Cr value in rats in the CCl_4 group was found to be decreased in this study, indicating an advanced-stage HE and impaired neuronal function. These results further validated the success of the HE rat model and reflected that the changes in brain metabolites had certain diagnostic value in HE. After 3 weeks of EA treatment, Glx/Cr, NAA/Cr, Cho/Cr, and mI/Cr were significantly decreased in the CCl_4 + EA group, while the levels of NAA/Cr, Cho/Cr, and mI/Cr were significantly increased compared with the CCl_4 group. Compared with the CCl_4 + Lac group, the CCl_4 + EA group has no significant difference, while the CCl_4 + CM group has the most significant effect. These results indicate that abnormal brain metabolism shown by MRS is reversible, and EA may protect neurons and improve cognitive function by regulating the metabolism of NAA, Glx, and Cho in rats with HE.

Inflammatory response contributes to the pathological changes of HE to a large extent. A recent study [40] has confirmed that immune inflammatory response is involved in the occurrence and development of cognitive dysfunction. Inflammatory cytokines such as TNF-α, IL-1β, and IL-6 are main contributors for pathophysiological processes via maintaining chronic inflammatory state and inducing inflammatory cascade amplification. TNF-α induces the production of "secondary" cytokines such as IL-1β and IL-6 in the inflammatory response and thereby stimulates cytokine cascade reaction and inflammatory chain reaction. Studies have revealed a strong correlation between TNF-α level and HE, thus indicating that TNF-α can be used as a predictor of HE severity [41]. IL-6, also known as a proinflammatory factor, can activate microglia and astrocytes and cause neuronal damage and cognitive impairment by inducing the production of neurotoxic transmitters. Although inflammatory cytokines such as TNF-α, IL-1β, and IL-6 cannot directly penetrate the blood-brain barrier, they can damage the permeability of the blood-brain barrier to a certain extent. Meanwhile, active transport of substances to the brain could lead to swelling of astrocytes and

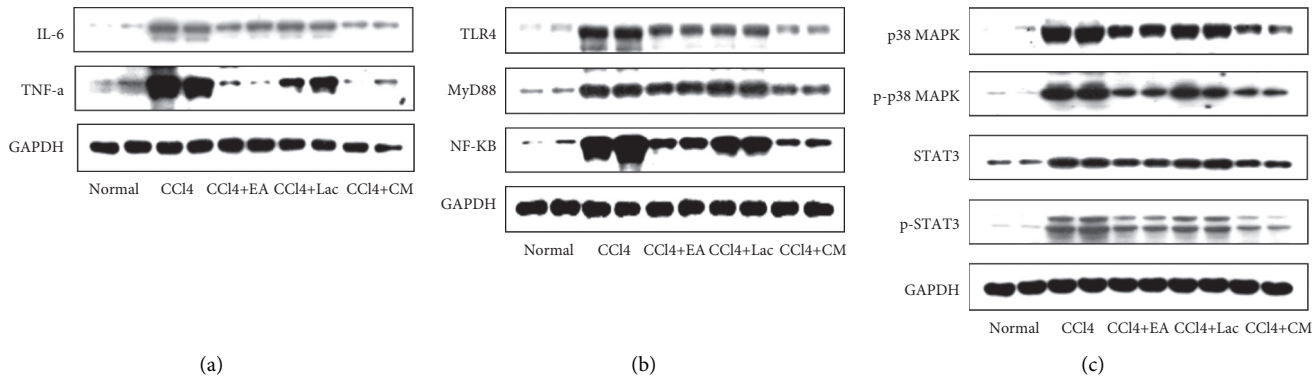

Figure 7: EA regulates the expression level of hepatic inflammation pathway-related proteins detected by Western blot. There are 10 rats in the normal group and 9 rats in each of no-intervention group (CCl_4) and treatment groups including EA group (CCl_4 + EA), lactulose group (CCl_4 + Lac), and EA combined with lactulose (CCl_4 + CM) group. (a) The protein expression of TNF-α and IL-6. (b) TLR4 pathway-associated signal proteins TLR4, MyD88, and NF-κB. (c) Proteins expressions of phosphorylated and total p38MAPK and STAT3.

inflammatory reactions in the brain. Impairment of liver function causes hyperammonemia, in which blood ammonia concentration increases and hampers the blood-brain barrier before entering the brain tissue. Increased osmotic pressure in the brain leads to swelling of neuronal cells, causing brain edema, which synergistically promotes the development of HE. Therefore, effective antagonization of TNF-α, IL-1β, and IL-6 could be a therapeutic strategy to mitigate hepatic encephalopathy.

Inflammatory response can be mediated by a variety of signaling pathways, among which TLR4/MyD88/NF-κB is one of the mainstay pathways mediating inflammatory reactions all over the body. In the central nervous system, TLR4 is mainly expressed in glial cells. Studies have demonstrated the relationship between TLR4 expression and blood ammonia level and found that the inhibition of TLR4 expression in rats can alleviate blood ammonia release, thereby preventing HE [42]. NF-κB is a protein complex widely involved in biological processes such as inflammation, apoptosis, immune response, and cell growth and development. During macrophage activation, upstream TLR4 triggers intracellular signal transduction, which ultimately activates NF-κB through stimulating MyD88 [43]. NF-κB activation can further trigger the release of inflammatory cytokines such as TNF-α, IL-1β, and IL-6 [44]. Consistently, TAA-induced NF-κB expression was found to be significantly upregulated in the liver of rats with HE [21]. After NF-κB activation, inflammatory factors released can in turn further activate NF-κB and amplify the inflammatory response cascade, thus generating a vicious cycle that would eventually lead to massive hepatocyte necrosis. Consequently, the synthesis, metabolism, and detoxification functions of the liver would be hampered and excessive ammonia and endotoxin that cannot be neutralized by the liver would enter blood circulation. Hyperammonemia can stimulate the expression of nitric oxide synthase (iNOS), upregulate the production of nitric oxide (NO), and increase cerebral blood flow, thus leading to edema of astrocytes and damage to the central nervous system [45], which ultimately causes cognitive dysfunction. On the other hand, inflammatory cytokines released after NF-κB activation can enter the peripheral blood circulation to aggravate infection and induce systemic inflammatory response, thereby playing an important role during pathogenesis and progression of HE synergistically with hyperammonemia [46]. In short, the NF-κB signaling pathway triggers the release of inflammatory factors, amplifies liver inflammatory response, accelerates liver function damage, and thereby contributes to the pathogenesis of HE. Mitigating inflammation, both systematically and locally in the liver, can potentially alleviate the severity of HE. In this study, we evaluated the role of EA treatment in an established rat HE model and found that EA therapy reduced IL-1β, IL-6, and TNF-α levels in the hippocampus, and combination of EA and drugs significantly downregulated mRNA and protein expressions of iNOS, TLR4, MyD88, and NF-κB. Compared with the CCl_4 + Lac group, the CCl_4 + EA and CCl_4 + CM groups had significant effects. Because EA and lactulose are both effective treatment methods, the combination of EA and lactulose has the best effect. Based on findings that the TLR4/MyD88/NF-κB signaling pathway plays an important role in mediating inflammatory response and that EA can inhibit inflammatory response through the NF-κB signaling pathway, we speculate that EA may inhibit intracerebral inflammatory response through the TLR4/MyD88/NF-κB signaling pathway, thereby improving the cognitive dysfunction in HE.

The P38MAPK signaling pathway is an important member of the mitogen-activated protein kinase family, which can be activated by a variety of stress stimuli including reactive oxygen species and plays an important role in processes such as inflammatory response, cellular stress response, and cell apoptosis. Studies have reported that signaling pathways including p38MAPK play an important role in the pathogenesis and treatment of HE [47] and that inhibition of MAPKs can improve the cognitive function in animal models of HE. Activation of p38 and JNKMAPKs in astrocytes may lead to astrocyte swelling that affects glutamate uptake [48]. P38MAPK also plays anti-inflammatory and antioxidative roles via mediating the STAT3 pathway

[49] through direct phosphorylation of the serine residues at the STAT3-C terminal, and STAT3 is therefore considered one of the possible substrates of MAPK. Under certain stimulating factors (such as inflammation and oxidative stress), MAPK and STAT3 signaling pathways may be concomitantly activated [50]. In this study, compared with the CCl_4 group, the mRNA and protein expressions of p38MAPK, p-p38MAPK, STAT3, and p-STAT3 in brain tissues of HE rats in all treatment groups were significantly decreased ($P < 0.05$). Compared with the CCl_4 + Lac group, expressions of p38MAPK, p-p38MAPK, STAT3, and p-STAT3 in the CCl_4 +CM group were significantly downregulated. Thus, the p38MAPK-STAT3 signaling pathway was found to be activated. EA treatment mitigated the phosphorylation of p38MAPK and STAT3 induced by combined treatment with CCl_4 and thioacetamide and downregulated the expressions of p38MAPK and STAT3 mRNAs, as well as their phosphorylated proteins. Additionally, pathologic injury to the liver in rats with HE was alleviated by EA therapy. These results suggest that the p38MAPK-STAT3 signaling pathway is involved in the regulation of HE and EA may play anti-inflammatory and antioxidative roles through regulating the p38MAPK-STAT3 signaling pathway, thus improving the cognitive impairment in HE.

In addition, as for the relationship among MRS, serum ammonia, liver function markers, and the expressions of certain genes and proteins in the brain tissue, the expressions of TNF-α, IL-1β, IL-6, and TLR4 were positively correlated with serum ammonia concentration in hepatic encephalopathy model rats. Serum ammonia and inflammatory mediators synergistically affect the occurrence and development of HE through Pearson's correlation analysis and literature review. Ammonia is a neurotoxin that leads to a variety of neurological complications, and it causes oxidative stress and brain edema and triggers neuroinflammation [51]. Inflammation is central to the pathogenesis of many human neurological disorders including HE. Systemic inflammation is a key player in precipitating and exacerbating HE, possibly by rendering the brain more susceptible to concurrent hyperammonemia [52]. Activated microglia also release proinflammatory mediators (e.g., cytokines TNF-α, IL-6, and IL-1β) that have also been directly linked to brain dysfunction [45]. It has been previously reported that activation of TLR4 initiates the NF-κB pathway as it stimulates the expression of proinflammatory cytokines TNF-α, IL-6, and IL-1β, which finally contributes to astrocyte swelling in HE [53]. MRS reflects the changes of brain metabolites such as mIns and Glx in the diagnosis of hepatic encephalopathy. Studies by Kooka et al. have shown that serum ammonia levels are negatively correlated with Cho and mIns levels in MRS and positively correlated with Glx levels [39]. Brain Glx levels are significantly positively correlated with serum TNF-α and IL-6 levels. The increase of TNF-α and IL-6 levels may increase the accumulation of Glx in astrocytes and promote the occurrence of cerebral edema. HE staining reflects the changes of astrocytes and neurons in the brain tissue. This experiment also shows that EA has a neuroprotective effect and can improve brain injury. AST, TBil, ALT, etc., are all typical biochemical test indicators, which can effectively reflect the inflammatory state of the liver and the degree of tissue cell damage. The correlation analysis shows that serum TNF-α, IL-6, and IL-1β levels are not significantly correlated with liver function indexes such as AST, ALT, TBil, and ALB. The reason may be due to the small sample size, a lot of experimental research is still needed in the future.

5. Conclusions

In conclusion, the synergistic role of inflammation and hyperammonemia can further aggravate the impaired cognitive function in HE. Treatment with EA may reduce the blood ammonia level, modulate inflammatory factors, ameliorate brain necrosis and apoptosis, and improve cognitive impairment through regulation of TLR4/MyD88/NF-κB and p38MAPK/STAT3 signaling pathways. MRS may be valuable in HE diagnosis of and evaluation of acupuncture efficacy. There are some limitations in the scope of this study, which are relatively simple compared with the complicated pathogenesis of HE involving multiple inflammatory reaction pathways. Future studies should adopt multimodal function imaging techniques, expand the sample size, and design rigorous experimental approaches to further explore the mechanism of acupuncture in improving cognitive dysfunction in HE.

Data Availability

The data used to support the findings of this study are available from the corresponding author upon request.

Conflicts of Interest

All authors declare no conflicts of interest.

Authors' Contributions

Huang JL performed most of the experiments, analyzed the data, and participated in the manuscript draft. Kong YN provided statistical advice. Gong ZG, Huang YW, and Wang H helped complete many experiments. Kang YJ and Zhan SH designed the study and drafted and finalized the manuscript. All authors read and approved the final manuscript.

Acknowledgments

The authors thank all participants and their families for participating and contributing to this research and the Key Laboratory of Department of Radiology (Shanghai University of Traditional Chinese Medicine) for providing the experimental support. This study was supported by the National Natural Science Foundation of China (No. 81573782) and Shanghai Science and Technology Commission 2018 "Science and Technology Innovation Action Plan" Clinical Medicine Field Project (No. 18401970300).

References

[1] Z. Marcel and A. S. Reichert, "Rapid metabolic and bioenergetic adaptations of astrocytes under hyperammonemia—a novel perspective on hepatic encephalopathy," *Biological Chemistry*, vol. 402, no. 9, pp. 1103–1113, 2021.

[2] V. Liere, G. Sandhu, and S. DeMorrow, "Recent advances in hepatic encephalopathy," *F1000Research*, vol. 6, p. 1637, 2017.

[3] K. Weissenborn, "Hepatic encephalopathy: definition, clinical grading and diagnostic principles," *Drugs*, vol. 79, pp. 5–9, 2019.

[4] M. Savva George and C. M. Stephan Blossom, "Alzheimer's society vascular dementia systematic review group, epidemiological studies of the effect of stroke on incident dementia: a systematic review," *Stroke*, vol. 41, pp. e41–46, 2010.

[5] D. R. Aldridge, E. J. Tranah, and D. L. Shawcross, "Pathogensis of hepatic encephalopathy:role of ammonia and systemic inflammation," *Journal of Clinical and Experimental Hepatology*, vol. 5, pp. S7–S20, 2015.

[6] M. Michele, B. Tiziano, C. C. Mari, L. Marta, and F. Vicente, "The dual role of the GABA receptor in peripheral inflammation and neuroinflammation: a study in hyperammonemic rats," *International Journal of Molecular Science*, vol. 22, no. 13, p. 6772, 2021.

[7] X. Y. Lyu and L. Li, "Clinical effect of rifaximin in treatment of complications associated with liver cirrhosis," *Journal of Clinical Hepatology*, vol. 34, no. 7, pp. 1551–1554, 2018, in Chinese.

[8] X. Zhu, Y. Han, J. Du, R. Liu, K. Jin, and W. Yi, "Microbiota-gut-brain axis and the central nervous system," *Oncotarget*, vol. 8, no. 32, pp. 53829–53838, 2017.

[9] V. Hernández-Rabaza, A. Cabrera-Pastor, L. Taoro-Gonzalez et al., "Hyperammonemia induces glial activation, neuroinflammation and alters neurotransmitter receptors in hippocampus, impairing spatial learning: reversal by sulforaphane," *Journal of Neuroinflammation*, vol. 13, no. 1, p. 41, 2016.

[10] A. S. Seyan, D. Hughes Robin, and L. Shawcross Debbie, "Changing face of hepatic encephalopathy: role of inflammation and oxidative stress," *World Journal of Gastroenterology*, vol. 16, no. 27, pp. 3347–3357, 2010.

[11] M. M. Guo, S. B. Qu, H. L. Lu et al., "In vivobiochanin a alleviates cerebral ischemia/reperfusion injury by suppressing endoplasmic reticulum stress-induced apoptosis and p38MAPK signaling pathway and," *Frontiers in Endocrinology*, vol. 12, Article ID 646720, 2021.

[12] K. Zhu, X. Zhu, S. Sun et al., "Inhibition of TLR4 prevents hippocampal hypoxic-ischemic injury by regulating ferroptosis in neonatal rats," *Experimental Neurology*, vol. 345, Article ID 113828, 2021.

[13] Q. Y. Yang, L. L. Ma, C. Zhang et al., "Exploring the mechanism of indigo naturalis in the treatment of ulcerative colitis based on TLR4/MyD88/NF-κB signaling pathway and gut microbiota," *Frontiers in Pharmacology*, vol. 12, Article ID 674416, 2021.

[14] Chinese Society of Hepatology and Chinese Medical Association, "Guidelines on the management of hepatic encephalopathy in cirrhosis," *Journal of Clinical Hepatology*, vol. 34, no. 10, pp. 2076–2089, 2018, in Chinese.

[15] K. Tarkan, T. Kieran Michael, and J. S. Gwendolyn, "Low-dose lactulose as a prebiotic for improved gut health and enhanced mineral absorption," *Frontiers Nutrition*, vol. 8, Article ID 672925, 2021.

[16] A. Moratalla, J. Ampuero, P. Bellot et al., "Lactulose reduces bacterial DNA translocation, which worsens neurocognitive shape in cirrhotic patients with minimal hepatic encephalopathy," *Liver International: Official Journal of the International Association for the Study of the Liver*, vol. 37, pp. 212–223, 2017.

[17] Y. Shan, J. J. Wang, Z. Q. Wang et al., "Neuronal specificity of acupuncture in alzheimer's disease and mildcognitive impairment patients:a functional MRI study," *Evidence-Based Complementary and Alternative Medicine: eCAM*, vol. 2018, Article ID 7619197, 10 pages, 2018.

[18] T. Li, H. Wu, F. Soto-Aguliar et al., "Efficacy of e;ectrical acupuncture on vascular cognitive impairment with no dementia: study protocol for a randomized controlled trial," *Trials*, vol. 19, no. 1, p. 52, 2018.

[19] R. A. Towner, R. Gulej, M. Zalles et al., "Rapamycin restores brain vasculature, metabolism, and blood-brain barrier in an inflammaging model," *GeroScience*, vol. 43, no. 2, pp. 563–578, 2021.

[20] V. Matei, A. Rodríguez-Vilarrupla, R. Deulofeu et al., "The eNOS cofactor tetrahydrobiopterin improves endothelial dysfunction in livers of rats with CCl4 cirrhosis," *Hepatology (Baltimore, Md.)*, vol. 44, pp. 44–52, 2006.

[21] S. A. El-Marasy, S. A. El Awdan, and R. M. Abd-Elsalam, "Protective role of chrysin on thioacetamide-induced hepatic encephalopathy in rats," *Chemico-Biological Interactions*, vol. 299, pp. 111–119, 2019.

[22] S. Yu and Y. Guo, *Experimental Acupuncture and Moxibustion*, Shanghai Science and Technology Press Society, Shanghai, China, 2nd edition, 2014.

[23] G. Xi, J. Hui, Z. Zhang et al., "Learning and memory alterations are associated with hippocampal N-acetylaspartate in a rat model of depression as measured by 1H-MRS," *PLoS One*, vol. 6, no. 12, pp. 286–295, 2011.

[24] I. Suárez, G. Bodega, M. Rubio, and B. Fernández, "Induction of NOS and nitrotyrosine expression in the rat striatum following experimental hepatic encephalopathy," *Metabolic Brain Disease*, vol. 24, pp. 395–408, 2009.

[25] G. J. Wu, Y. W. Lin, C. Y. Chuang, H. C. Tsai, and R. M. Chen, "Liver nitrosation and inflammation in septic rats were suppressed by propofol via downregulating TLR4/NF-κB-mediated iNOS and IL-6 gene expressions," *Life Sciences*, vol. 195, pp. 25–32, 2018.

[26] Z. Yan, Y. Chen, X. Zhang, L. Hua, and L. Huang, "Neuroprotective function of TNFAIP3 interacting protein 2 against oxygen and glucose deprivation/reoxygenation-induced injury in hippocampal neuronal HT22 cells through regulation of the TLR4/MyD88/NF-κB pathway," *Neuropsychiatric Disease and Treatment*, vol. 17, pp. 2219–2227, 2021.

[27] O. M. S. Khedr, S. M. El-Sonbaty, F. S. M. Moawed, E. L. Kandil, and B. E. Abdel-Maksoud, "Lactobacillus acidophilus ATCC 4356 exopolysaccharides suppresses mediators of inflammation through the inhibition of TLR2/STAT-3/P38-MAPK pathway in DEN-induced hepatocarcinogenesis in rats," *Nutrition and Cancer*, pp. 1–11, 2021.

[28] B. Duman, K. Can, E. Agtas-Ertan et al., "Risk factors for valproic acid induced hyperammonemia and its association with cognitive functions," *General Hospital Psychiatry*, vol. 59, pp. 67–72, 2019.

[29] L. Lu, C. Wu, B. J. Lu et al., "BabaoDan cures hepatic encephalopathy by decreasing ammonia levels and alleviating inflammation in rats," *Journal of Ethnopharmacology*, vol. 249, Article ID 112301, 2020.

[30] K. Wijarnpreecha, S. Chesdachai, C. Thongprayoon, V. Jaruvongvanich, P. Ungprasert, and W. Cheungpasitporn, "Association of helicobacter pylori with the risk of hepatic encephalopathy," *Digestive Diseases and Science*, vol. 62, no. 12, pp. 3614–3621, 2017.

[31] S. Hong-Hui, C. Hou-Song, and H. L. Su, "[Effect of acupuncture at thirteen evil acupoints on liver function, and the contents of blood ammonia and β-endorphin in patients with hepatic encephalopathy]," *Zhen Ci Yan Jiu*, vol. 42, pp. 342–345, 2017.

[32] S. Quiroz-Gonzalez, S. Torres-Castillo, R. E. López-Gómez, and I. Jimenez Estrada, "Acupuncture points and their relationship with multireceptive fields of neurons," *Journal of Acupuncture Meridian Studies*, vol. 10, pp. 81–89, 2017.

[33] R. S. Draz, Z. M. H. Serry, A. F. Rahmy, M. S. Ei Bardesi, and M. M. Taha, "Electroacupuncture versus aerobic interval training on liver functions in patients with nonalcoholic fatty liver," *Journal of Alternative and Complementary Medicine*, vol. 26, pp. 51–57, 2020.

[34] R. Lin, Y. Lin, J. Tao et al., "Electroacupuncture ameliorates learning and memory in rats with cerebral ischemia-reperfusion injury by inhibiting oxidative stress and promoting p-CREB expression in the hippocampus," *Molecular Medicine Reports*, vol. 12, no. 5, pp. 6807–6814, 2015.

[35] G. Zeng, R. Penninkilampi, J. Chaganti, S. Montagnese, B. J. Brew, and M. Danta, "Meta-analysis of magnetic resonance spectroscopy in the diagnosis of hepatic encephalopathy," *Neurology*, vol. 94, no. 11, pp. e1147–e1156, 2020.

[36] L. P. Meng, Y. C. Chen, Y. H. Li, J. S. Zhu, and J. L. Ye, "Viability assessment of magnetic resonance spectroscopy for the detection of minimal hepatic encephalopathy severity," *European Journal of Radiology*, vol. 84, no. 10, pp. 2019–2023, 2015.

[37] L. H. Chen, J. Y. Shi, T. X. Zou et al., "Disturbance of thalamic metabolism and its association with regional neural dysfunction and cognitive impairment in minimal hepatic encephalopathy," *European Journal of Radiology*, vol. 131, Article ID 109252, 2020.

[38] H. Bertrand, R. Marika, G. Damien, D. Thabut, and N. Weiss, "Magnetic resonance spectroscopy: a surrogate marker of hepatic encephalopathy?" *Journal of Hepatology*, vol. 71, pp. 1055–1057, 2019.

[39] Y. Kooka, K. Sawara, R. Endo, A. Kato, K. Suzuki, and Y. Takikawa, "Brain metabolism in minimal hepatic encephalopathy assessed by 3.0-tesla magnetic resonance spectroscopy," *Hepatology Research: the Official Journal of the Japan Society of Hepatology*, vol. 46, pp. 269–276, 2016.

[40] C. Trisha, I. J. Torres, D. J. Bond, and L. N. Yatham, "Inflammatory cytokines and cognitive functioning in early-stage bipolar I disorder," *Journal of Affective Disorder*, vol. 245, pp. 679–685, 2019.

[41] W. Zhuge, Q. Zhuge, W. Wang et al., "Hydrogen sulphide ameliorates dopamine-induced astrocytic inflammation and neurodegeneration in minimal hepatic encephalopathy," *Journal of Cellular and Molecular Medicine*, vol. 24, no. 23, pp. 13634–13647, 2020.

[42] B. Lu, C. Wu, N. L. B. Azami et al., "Babao dan improves neurocognitive function by inhibiting inflammation in clinical minimal hepatic encephalopathy," *Biomedicine & Pharmacotherapy*, vol. 135, Article ID 111084, 2021.

[43] M. Shafahi, G. Vaezi, H. Sharafi, S. Sharafi, and M. Khaksari, "Crocin inhibits apoptosis and astrogliosis of hippocampus neurons against methamphetamine neurotoxicity via antioxidant and anti-inflammatory mechanisms," *Neurochemical Research*, vol. 43, pp. 2252–2259, 2018.

[44] W. Liu, Y. Sun, Z. Cheng, Y. Guo, P. Liu, and Y. Wen, "Crocin exerts anti-inflammatory and anti-arthritic effects on type II collagen-induced arthritis in rats," *Pharmaceutical Biology*, vol. 56, no. 1, pp. 209–216, 2018.

[45] M. Elina, V. Oleksandr, F. Tetyana et al., "Hepatic encephalopathy aggravated by systemic inflammation," *Digestive Diseases*, vol. 37, pp. 509–517, 2019.

[46] L. D. Bobermin, R. H. A. Roppa, C. A. Gonçalves, and A. Quincozes-Santos, "Ammonia-induced glial-inflammaging," *Molecular Neurobiology*, vol. 57, pp. 3552–3567, 2020.

[47] X. X. Guo, S. An, Y. Yang et al., "Emerging role of the jun N-terminal kinase interactome in human health," *Cell Biology International*, vol. 42, pp. 756–768, 2018.

[48] V. Felipo, B. Piedrafita, J. A. Barios et al., "Rats with minimal hepatic encephalopathy show reduced cGMP-dependent proteikinase activity in hypothalamus correlating with circadian rhythms alterations," *Chronobiology International*, vol. 32, pp. 966–979, 2015.

[49] T. Li, Y. N. Wu, H. Wang, J. Y. Ma, S. S. Zhai, and J. Duan, "Dapk1 improves inflammation, oxidative stress and autophagy in LPS-induced acute lung injury via p38MAPK/NF-κB signaling pathway," *Molecular Immunology*, vol. 120, pp. 13–22, 2020.

[50] M. Wang, J. Li, Y. Ding, S. Cai, Z. Li, and P. Liu, "PEX5 prevents cardiomyocyte hypertrophy via suppressing the redox-sensitive signaling pathways MAPKs and STAT3," *European Journal of Pharmacology*, vol. 906, Article ID 174283, 2021.

[51] S. A. El-Marasy, R. F. Abdel-Rahman, and R. M. Abd-Elsalam, "Neuroprotective effect of vildagliptin against cerebral ischemia in rats," *Naunyn-Schmiedeberg's Archives of Pharmacology*, vol. 391, no. 10, pp. 1133–1145, 2018.

[52] M. Luo, H. Liu, S. J. Hu, and F. H. Bai, "Potential targeted therapies for the inflammatory pathogenesis of hepatic encephalopathy," *Clinics and Research in Hepatology and Gastroenterology*, vol. 39, no. 6, pp. 665–673, 2015.

[53] A. R. Jayakumar, K. V. Rama Rao, and M. D. Norenberg, "Neuroinflammation in hepatic encephalopathy: mechanistic aspects," *Journal of Clinical and Experimental Hepatology*, vol. 5, pp. S21–S28, 2015.

Hindawi
Evidence-Based Complementary and Alternative Medicine
Volume 2021, Article ID 6497568, 13 pages
https://doi.org/10.1155/2021/6497568

Research Article

GDF-15 Suppresses Atherosclerosis by Inhibiting oxLDL-Induced Lipid Accumulation and Inflammation in Macrophages

Hong Huang,[1,2] Zhongli Chen,[3] Yan Li,[2] Kunmei Gong,[4] Le Xiao,[4] Hao Fu,[5] Jingjing Yang,[2] Xianying Wang,[2] and Qiang Meng[5]

[1]*Faculty of Life Science and Technology, Kunming University of Science and Technology, Kunming 650500, China*
[2]*Department of Geriatric Medicine, The Affiliated Hospital of Kunming University of Science and Technology, The First People's Hospital of Yunnan Province, Kunming 650032, China*
[3]*Department of Cardiology, Ruijin Hospital, Shanghai Jiaotong University, Shanghai 200025, China*
[4]*Department of General Surgery, The First People's Hospital of Yunnan Province, Kunming 650032, China*
[5]*Department of Neurology, The First People's Hospital of Yunnan Province, No. 157 Jinbi Road, Xishan District, Kunming 650032, Yunnan Province, China*

Correspondence should be addressed to Qiang Meng; mengqiang1199@163.com

Received 16 June 2021; Accepted 8 August 2021; Published 8 September 2021

Academic Editor: Feng Zhang

The growth differentiation factor-15 (GDF-15) may be involved in atherosclerosis. However, the role of GDF-15 in atherosclerosis remains unclear. The main goal of this study was to verify the role and mechanism of GDF-15 in atherogenesis. We first compared the serum GDF-15 level between patients with coronary atherosclerosis and healthy people. And then one ApoE$^{-/-}$ mouse model of atherosclerosis was used to explore the effects of GDF-15 on oxidized low-density lipoprotein (oxLDL) accumulation, atherosclerosis-related gene expression, and lipid accumulation-related protein expression in mouse macrophages. As a result, the level of serum GDF-15 in patients with coronary atherosclerosis was significantly higher than that in healthy people. In the mouse model, GDF-15 expression was elevated in the core of plaque, and it was secreted mainly by the macrophages. In addition, GDF-15 decreased oxLDL-induced lipid accumulation and inflammation activation in macrophages. GDF-15 decreased the mRNA expressions of CD36, LOX1, and TLR4 that are associated with lipoprotein accumulation in macrophages. Further study showed that GDF-15 might suppress oxLDL-induced lipoprotein accumulation via inhibiting CD36 and LOX1 and decrease inflammation in macrophages by inhibiting TLR4. Thus, GDF-15 may suppress atherosclerosis and plaque formation by inhibiting lipoprotein accumulation and inflammation activation.

1. Introduction

Atherosclerosis is the leading cause of vascular diseases, including ischemic heart disease, ischemic stroke, and peripheral arterial disease [1]. As a chronic inflammatory disorder, atherosclerosis usually happens at the inner curvatures and branch points of arterial vessels, where endothelium was activated by the laminar flows [2]. Once activated, endothelium increases its permeability to lipoproteins, leading to the accumulation of lipoprotein in the arterial vessel wall. The sequestered lipoproteins induce an inflammatory response, and then circulating monocytes are recruited to this site and differentiate into macrophages that can ingest sequestered lipoproteins, thus fighting against inflammation. However, this process cannot clear lipoproteins but transforms macrophages to lipoprotein-laden foam cells, which can secrete various substances to initiate and promote atherosclerotic plaque formation. During the formation of plaque, proinflammatory cytokines and chemokines released by macrophages and other cells play a crucial role [3].

GDF-15 belongs to the transforming growth factor-β (TGF-β)/bone morphogenetic proteins (BMPs) superfamily [4], which are potent regulators of vascular development and vascular remodeling and play a key role in atherosclerosis and restenosis. TGF-β and BMPs regulate the proliferation, differentiation, and survival of endothelial cells, smooth muscle cells, macrophages, and T cells through activating

Smad-dependent and Smad-independent signaling via heteromeric type I and II receptor complexes and also participate in the response of vascular calcification cells [5]. Previous studies showed that GDF-15 expression was associated with the initiation and progression of multiple diseases [6]. For example, GDF-15 could induce the apoptosis of tumor cells to suppress the progression, invasiveness, and metastasis of tumors [7]. In addition, GDF-15 was reported to be correlated with cardiovascular and noncardiovascular mortality, and it played important roles in multiple cardiovascular diseases, such as heart failure, cardiac hypertrophy, and coronary heart disease [8–11]. A study of the atherosclerotic mouse model showed that GDF-15 increased the progress of the disease, and the expression defect of GDF-15 reduced the formation of early plaque and improved the stability of plaque [12]. Because the stability of plaque plays a blocking effect on the development of atherosclerosis and the deficiency of GDF-15 expression can improve the stability of plaque, some studies believe that the lack of GDF-15 is conducive to the body's resistance to vascular injury and inflammation [12, 13]. However, some other studies suggested that GDF-15 is a protective factor of the heart, which has the effect of antiatherosclerosis [14, 15]. It was reported that GDF-15 could inhibit apoptosis of endothelial cells induced by high glucose and improve the function of endothelial cells by activating PI3K/Akt/eNOS pathway [16]. Previous studies suggested GDF-15 might play an important role in inhibiting the occurrence of atherosclerosis, but the concrete role and mechanism of GDF-15 in atherosclerosis remain unclear.

In this study, we aimed to explore the role of GDF-15 in lipoprotein accumulation and inflammatory response in atherosclerosis. The serum GDF-15 level in atherosclerosis patients and healthy people and the expression and location of GDF-15 in the aorta atheromatous plaque in mice were detected first. Then the effect of GDF-15 on lipoprotein accumulation and proinflammatory cytokines releasing in oxidized low-density lipoprotein (oxLDL) treated macrophages was revealed. Further, we investigated the might mechanism of GDF-15 in oxLDL-induced lipoprotein accumulation and inflammation in macrophages in order to provide new clues for further understanding the role and mechanism of GDF-15 in atherosclerosis.

2. Materials and Methods

2.1. Human Sample Collection and Ethics Statement. This study involved the use of serum samples from healthy people and patients with atherosclerosis. Sixty-five health people and 101 patients were recruited in the First People's Hospital of Yunnan Province. After drawing blood, serum was isolated from collected blood and stored at −80°C until subsequent analysis. All samples were analyzed anonymously, and all researchers in this study have no access to any subject identification information. In addition, all recruited participants agree to the blood draw and signed written informed consents.

Ethical approval for the study and the informed consent process were approved by the Ethics Committee of the First People's Hospital of Yunnan Province (No. YYLH048). The research was conducted in accordance with the basic principles of the Helsinki declaration and the relevant international rules.

2.2. Enzyme-Linked Immunosorbent Assay (ELISA). GDF-15 in human serum and interleukin-6 (IL-6), interleukin-8 (IL-8), monocyte chemoattractant protein-1 (MCP-1), and matrix metalloproteinase-9 (MMP-9) in the cell culture supernatant and mice serum were measured using ELISA kits according to manufacturers' protocol (ELISA Genie, Ireland).

2.3. Mouse Model of Atherosclerosis. Wild-type (WT) C57BL/6 mice and ApoE$^{-/-}$ mice with a C57BL/6 background were purchased from the Model Animal Research Center of Nanjing University (Nanjing, China). The six-week-old C57BL/6 mice and ApoE$^{-/-}$ mice were fed a high-fat diet (KlibaNafag 3200 supplemented with 1.25% w/w cholesterol and 15% w/w cacao butter) for 20 weeks and subsequently sacrificed. For further study, recombinant GDF-15 (50 mg/kg/d) was intravenously injected into ApoE$^{-/-}$ mice after 10 weeks of high-fat feed once every three days. Aorta with plaques was collected at the end of 20 weeks of high-fat feed for subsequent H&E staining and immunohistochemical analysis. All animal experiments were approved by the Animal Ethics Committee of the First People's Hospital of Yunnan Province (Approval No. YYLH048).

2.4. Cell Culture and Treatment. Primary culture and identification of macrophages were derived from mouse bone marrow: the 6–8 week old mice were sacrificed and the femurs and tibias were taken. The bone marrow was placed in a 10 ml centrifuge tube. After lysis with RBC lysate, the supernatant was removed after centrifuged at 1,000 r/min for 5 min. The bone marrow cells were resuspended in the culture medium and inoculated evenly in a 10 cm culture dish. The cells were cultured overnight to remove other heterogeneous cells, such as fiber cells. The cells not attached to the wall were inoculated into a new culture plate and cultured with 50 ng/mL recombinant mouse M-CSF. On the third and seventh days, the activity and morphology of the cells were observed under an inverted microscope, including the adherent state, volume, morphology, and pseudopodia changes (photo recording). The macrophages from bone marrow were produced (the composition of the culture medium was α-MEM + 10% FBS + 1% double antibody). F4/80 and CD11 antibodies were used as a double standard to identify the purity of macrophages.

To study the effect of GDF-15 on macrophage functions, the macrophage was treated with oxLDL (50 μg/mL) or oxLDL (50 μg/mL) + GDF-15 (2 ng/mL) for a continuous 48 hours without changing the culture medium or other interruption. Cells and culture supernatant were collected at 48 hours post-treatment for the subsequent study. Then to

verify the potential mechanism of the inhibitory effect of lipoprotein accumulation and inflammation in oxLDL-induced macrophage by GDF-15, overexpression vectors of CD36 and LOX1 (pcDNA-CD36 and pcDNA-LOX1, respectively) were constructed by Guangzhou RiboBio Biotechnology Co. Ltd. (Guangzhou, China) and transfected into macrophage cells with Lipofectamine® 2000 transfection reagent (Thermo Fisher Scientific, Inc., USA) following the instructions. And agonist of TLR4, Neoseptin-3 (20 μM), was used to activate TLR4 in macrophage cells.

2.5. Oil Red O Staining. To evaluate the level of lipid accumulation in macrophages, the oil red O staining of macrophages was performed. Briefly, cells were fixed by 4% paraformaldehyde (PFA) for 15 min after being washed with PBS 3 times (5 min/time), then incubated with oil red O working solution (oil red:distilled water = 3:2) at room temperature for 10–15 min, subsequently differentiated by 60% isopropanol for 30 s, and washed with distilled water for 1 min. Finally, the filter paper was used to absorb the surrounding water, and glycerin gelatin was used to seal the cells. As a result, the lipid droplets are orange red to bright red stained.

2.6. Hematoxylin and Eosin and Nissl Staining. To verify whether atherosclerosis occurs in WT and ApoE$^{-/-}$ mice, the aorta tissues were harvested, fixed with 4% PFA for 24 h, and dehydrated by washing with a series of ethanol solutions (75% ethanol for 2 h; 80% ethanol for 2 h; 95% ethanol I for 2 h; 95% ethanol II for 1.5 h; 100% ethanol I for 1 h; and 100% ethanol II for 30 min) at room temperature and then paraffin-embedded and sectioned (transverse section, 7 μm thick). Then the sections were stained using the modified hematoxylin and eosin (H&E) staining kit (Solaria, China) in order to observe the morphological changes and plaques formation of aorta tissues. Images were captured under a light microscope (Nikon, Tokyo, Japan).

2.7. Immunohistochemistry Analysis. For immunohistochemistry analysis, the aorta tissue samples were fixed in 4% PFA for 24 h. Then the tissue block was put into the paraffin and sectioned into 7 μm thick sections in a microtome. The section frame was put into the antigen repair solution and heated for 10 min under low fire. The slicing frame was taken out and put into PBS for 5 min; it was repeated 3 times. After washing, the samples were prepared for blocking and incubating with the primary antibodies of GDF-15 or IL-6 at 4°C overnight. Isotype-matched IgG was used instead of the primary antibody as a negative control of the staining. Sections were then incubated with diluted streptavidin-peroxidase HRP at room temperature with DAB color- and hematoxylin-rendering staining kit, following the manufacturer's instructions. Finally, it was sealed with neutral gum after dehydrating and drying by gradient alcohol. The sections were then stained with hematoxylin for 5 min and mounted and observed with a phase-contrast microscope.

2.8. Immunofluorescence Analysis. Fresh tissue samples were taken and immediately immersed in 4% PFA fixative solution, changed into 30% sucrose solution for 24 h, transferred into OCT glue after 4°C for 48 h, froze at −80°C for 30 min, and then sliced. Next, wash with PBST for 3 times, 5 min each time, at room temperature. Add 200 μL sealing solution (10% goat serum) to the slice, and drop one prepared antibody (diluted with 10% goat serum, diluted according to the antibody manual, usually 1:200), and leave overnight to stay at 4°C. Wash three times with PBST, 5 min each time, add fluorescent second antibody, (1:2000) and incubate in dark for 1h; wash three times with 0.1% PBT, 5 min each time, at room temperature. DAPI was not exposed to light. Observe under the fluorescence microscope, and record the experimental results.

2.9. RNA Extraction and RT-qPCR Analysis. Total RNA was extracted from the macrophage using TRIzol (Ambion, USA) according to the manufacturer's protocol. Gene expression was quantified using iTaq Universal SYBR Green Supermix (Bio-Rad) and the CFX Connect real-time PCR detection system (Bio-Rad) after reverse transcription from RNA into cDNA using iScript reverse transcription supermix for RT-qPCR (Bio-Rad). Primers were designed to amplify the target genes. Primer sequences for gene expression analysis were shown in Table 1. The relative quantity of gene expression was calculated using the $2^{-\Delta\Delta Ct}$ method.

2.10. Western Blot Analysis. The macrophages were collected and lysed with RIPA buffer (Solarbio, China). Protein concentration was quantified using a Bio-Rad protein assay kit (Bio-Rad). Protein samples were separated by 12% SDS-PAGE. Then electrophoretically transferred onto polyvinylidene difluoride (PVDF) membranes (Bio-Rad). The membranes were incubated in primary antibodies (β-actin (Proteintech, China); IL-6 antibody; MCP-1 antibody; MMP-9 antibody, dilution 1:1,000 (CST, Germany); and IL-8 antibody, dilution 1:1,000 (Abcam, USA)) at 4°C overnight. Then membranes were incubated with horseradish peroxidase-coupled secondary antibody (antirabbit or antimouse antibodies, dilution 1:2,000 (Proteintech, China)) for 1 h at room temperature (Santa Cruz Biotechnology). The signals were detected by the chemiluminescence detection kit (Thermo Fisher Scientific). The protein bands were visualized by autoradiography and quantified by ImageJ software (National Institutes of Health, Bethesda, MD, USA).

2.11. Statistical Analyses. All results were confirmed in at least three independent experiments, and the data from one representative experiment was shown. All quantitative data are presented as mean ± SEM. The analysis was performed using GraphPad Prism version 7 (GraphPad Software, La Jolla, CA, USA). Statistical comparisons between each group were conducted with unpaired Student's *t*-test or one-way analysis of variance (ANOVA) followed by Bonferroni's

Table 1: The sequences of primers used in real-time PCR.

Gene name	Product size (bp)	Number gene primer (5′–3′)
β-actin	224	F: TGCTGTCCCTGTATGCCTCT R: TTTGATGTCACGCACGATTT
CD36	96	F: GGTGATGAGAAGGCAAAC R: CACCACACCAACACTGAG
LOX1	173	F: GGATGCCAAGTTGCTGA R: CGCCTCGGACTCTAAATA
LXRA	151	F: GTTTGCCTTGCTCATTGC R: TGGGAACATCAGTCGGTC
MSR1	143	F: CACTGATTGCCCTTTACC R: TCCCGTGAGACTTTGAG
SCARB1	187	F: CAGGGAGTTCAGGCACAAA R: CTTCAGGGTCATGGGCTTA
FABP4	102	F: TGGGATGGAAAATCAACC R: TCTCTCATAAACTCTCGTGG
TLR2	222	F: GATGCCTACTGGGTGGA R: AAGACGGAAATGGGAGA
TLR3	70	F: CAACGACTGATGCTCCGAAG R: GAAGAGGCTGGAATGGTGAA
TLR4	287	F: GGTATTTGACACCCTCCAT R: TTCTGTTCCTTGACCCACT
IL-6	256	F: GTGTCTTTCCCGTGGACCTTC R: TCATCTCGGAGCCTGTAGTGC
IL-8	140	F: CCTGGAAATCAACAGTTATGCT R: AGGTTCAGCAG GTAGACATCG
MCP-1	125	F: TCCTGTCATTTAT GCCTTTGTTG R: CACTCGATCTG CTGTCTCCCTAT
MMP-9	260	F: CCCACTTACTATGGAAACTCAA R: CTCAAAGATGAACGGGAACA

multiple comparisons test. For all comparisons, $P < 0.05$ was considered to indicate a statistically significant difference.

3. Results

3.1. Elevated Expression of GDF-15 in Atherosclerosis Patients. One previous atherosclerosis mouse model study demonstrated that GDF-15 deficiency attenuates early atherogenesis and improves plaque stability [12]. The clinical study suggested that a high level of GDF-15 is associated with coronary artery disease, a disease involving chronic inflammatory atherosclerosis [17]. To explore the relationship of GDF-15 with atherosclerosis, we recruited 65 healthy people and 101 patients with coronary atherosclerosis. After the blood draw, serum was isolated to measure GDF-15. As a result, GDF-15 levels were significantly higher in patients than that in healthy controls (960.1 ± 26.35 pg/mL vs. 769.6 ± 26.75 pg/mL; $P < 0.0001$, as can be seen in Figure 1) detected by ELISA assay. This finding indicates that the serum GDF-15 level may be associated with atherosclerosis.

3.2. High Expression of GDF-15 in Mice Macrophages with Atherosclerosis. To further determine the correlation of GDF-15 with atherosclerosis, we compared GDF-15

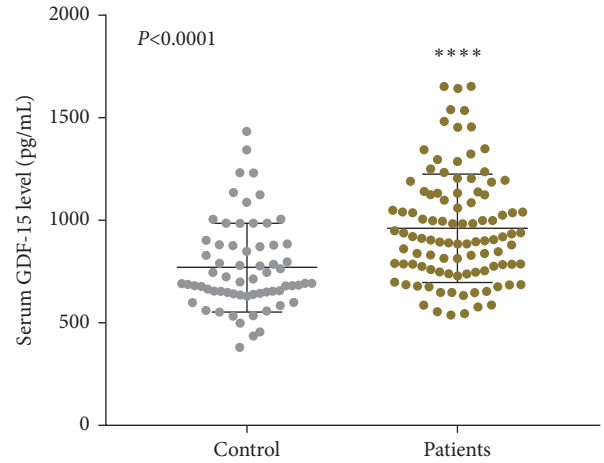

Figure 1: Level of serum GDF-15 in patients with atherosclerosis. Serum GDF-15 levels in patients with atherosclerosis were detected and compared with that of healthy people. Results showed the level of GDF-15 in patients was significantly higher than that in healthy controls. $^{****}P < 0.0001$ vs. control group.

expression in macrophages residing in blood vessels. Herein, the ApoE$^{-/-}$ mice model of atherosclerosis was used, and blood vessels with an atherosclerotic plaque were studied. As shown in Figure 2(a), compared with wild-type mice, ApoE$^{-/-}$ mice fed by a high-fat diet showed significant aortic arch stenosis, accompanied by obvious endothelial cell damage and atherosclerotic plaque formation. Meanwhile, immunohistochemical staining showed that the expression of GDF-15 in the aorta of ApoE$^{-/-}$ mice with atherosclerotic plaque was significantly higher than that of WT mice (Figure 2(b)), which is consistent with the expression of serum GDF-15 (Figure 1). Furthermore, immunofluorescence staining results showed that the level of CD68 positive macrophages and expression of GDF-15 in arterial tissue of WT mice were lower, while the positive rates of CD68 and GDF-15 in ApoE$^{-/-}$ mice were significantly higher than those in WT mice, and most GDF-15 producing cells were CD68 positive macrophages (Figure 2(c)), which suggested that macrophages may be the main cells producing GDF-15. Thus, our data suggested that the expression of GDF-15 was upregulated in atherosclerosis produced mainly by macrophages.

3.3. GDF-15 Suppressed Lipid Accumulation in Macrophages. Macrophages under endothelial cells play a decisive role in atherosclerosis initiation and progression [2, 18]. Macrophages in atherosclerotic lesions actively participate in lipoprotein ingestion and accumulation, which contributes to lipoprotein storage under endothelial cells and atherosclerosis initiation and progression [19]. To explore the role of GDF-15 in atherogenesis, we first induced primary culture macrophages, monocyte-derived macrophages (MDMs; Figure 3(a)), and studied the effect of GDF-15 on lipoprotein storage in macrophages by oil red O staining. As a result, oxLDL treatment alone induced lipoprotein accumulation in macrophages, while GDF-15 treatment significantly suppressed oxLDL-induced lipoprotein accumulation

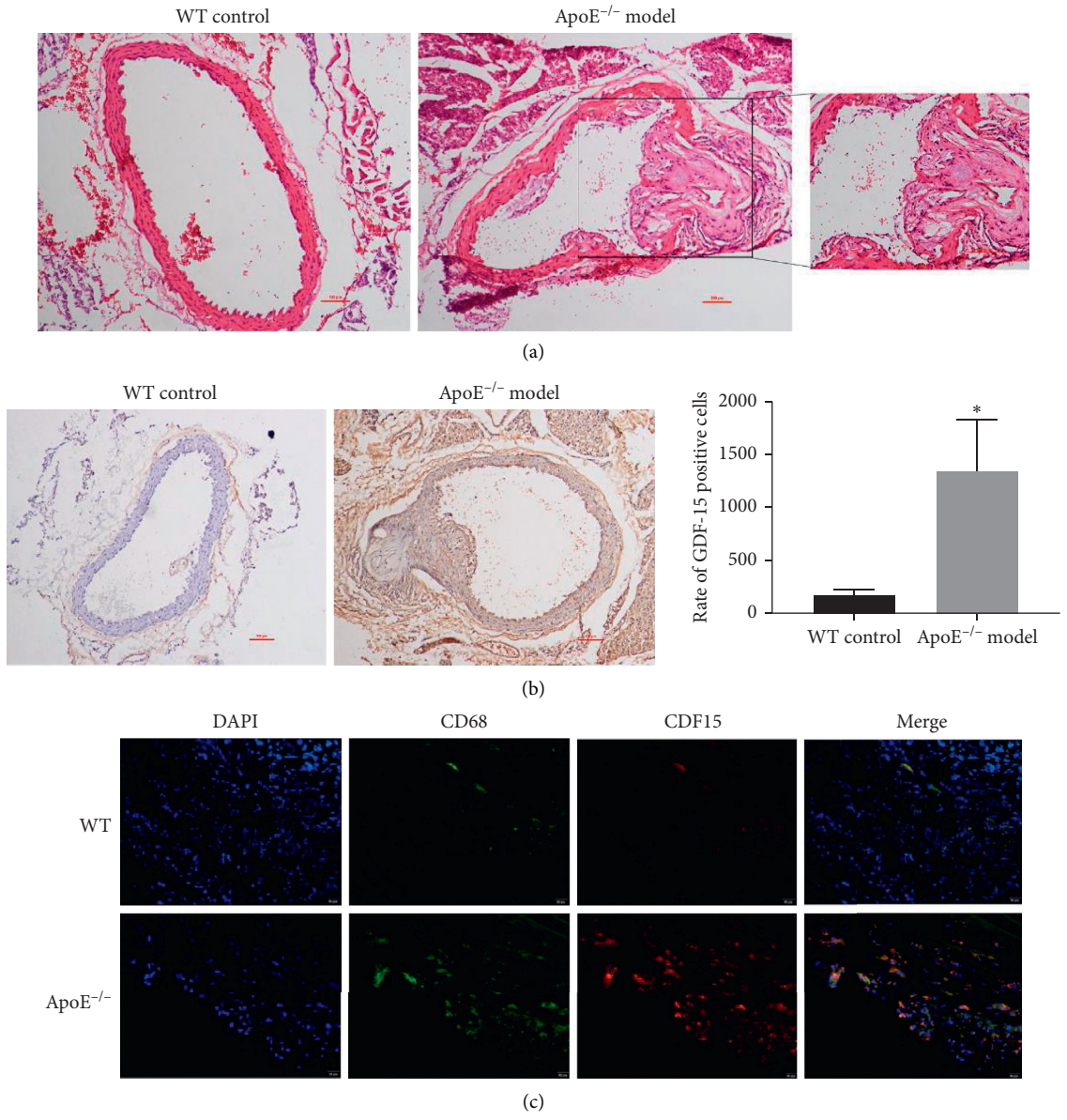

Figure 2: Macrophages are the major GDF-15 secreting cells in atherosclerotic plaque. (a) H&E staining. After fed by high-fat diet, the endothelium of the artery in ApoE$^{-/-}$ mice was damaged obviously, accompanied with the formation of atherosclerotic plaque, while there was no obvious change in wild-type mice artery. (b) GDF-15 was highly expressed in blood vessels of ApoE$^{-/-}$ mice compared with that in wild-type mice detected by immunohistochemical analyses. (c) Immunofluorescence staining showed most of GDF-15 were produced by CD68 positive macrophages, which suggested that macrophages may be the major cells, which producing GDF-15.

(Figure 3(b)). These results suggested that GDF-15 reduced lipoprotein accumulation in macrophages.

3.4. GDF-15 Suppressed Inflammation Response in Macrophages. The inflammation response is a remarkable feature of atherosclerosis, and oxLDL has been demonstrated to trigger inflammation response and proinflammatory cytokine production [3]. To determine the effect of GDF-15 on atherogenesis, we studied the effect of GDF-15 on proinflammatory cytokines, chemokines, and matrix protein, which all are correlated with atherosclerosis initiation and development in the presence of oxLDL. Consistent with a previous study [3], our results showed that oxLDL treatment upregulated the secretions of IL-6, IL-8, MCP-1, MMP-9, and GDF-15 treatment obviously suppressed the oxLDL-induced release of the above-studied proteins (Figure 4(a)). Next, to explore the mechanism that GDF-15 inhibits protein secretion, we performed RT-qPCR assay and western blot assay to study the effect of GDF-15 on transcription and protein expression of intracellular proteins. As a result, oxLDL treatment upregulated the intracellular expression of IL-6, IL-8, MCP-1, and MMP-9 in both mRNA and protein levels, while GDF-15 treatment suppressed the intracellular mRNAs and protein expressions of these proinflammatory

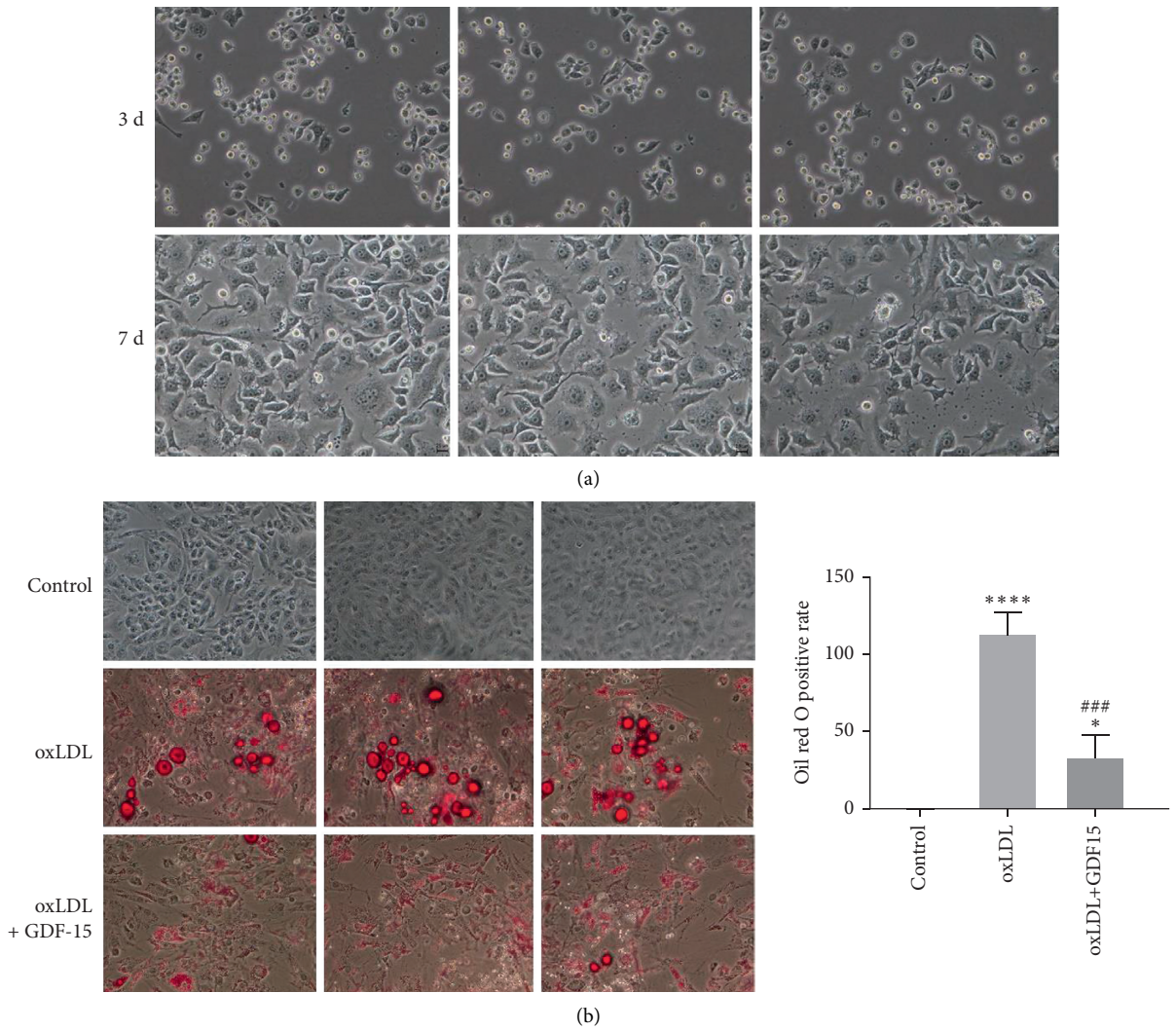

Figure 3: GDF-15 suppressed lipoprotein accumulation in oxLDL-treated monocyte-derived macrophages (MDMs): (a) representative images of primary cultured MDMs cells and (b) oil red O staining showed oxLDL treatment significantly induced lipoprotein accumulation in MDMs, while GDF-15 treatment inhibited oxLDL-induced lipoprotein accumulation. All images were obtained using a ZEISS LSM confocal microscope. Values are expressed as the mean ± standard deviation of three independent experiments as determined by Student's *t*-test. $^{*}P < 0.05$, $^{****}P < 0.0001$ vs. control group; $^{\#\#\#}P < 0.001$ vs. oxLDL-induced group.

cytokines (Figures 4(b) and 4(c)). Thus, the above data suggested that GDF-15 could inhibit the oxLDL-induced inflammatory response, which promotes atherosclerosis initiation and development.

3.5. GDF-15 Decreased Gene Expressions That Are Associated with Lipoprotein Accumulation. Subsequently, we explored the potential mechanism that GDF-15 blocks atherogenesis. Lipoprotein accumulation in macrophages is central to the pathogenesis of atherosclerosis and one of the earliest events in plaque formation [20]. Herein, we measured the impact of GDF-15 on gene expressions that are related to lipoprotein accumulation. The macrophages were treated with oxLDL (50 μg/mL) or oxLDL (50 μg/mL) + GDF-15 (2 ng/mL) for 48 hours. After treatment, the CD36, LOX1, LXRA, MSR1, SCARB1, FABP4, TLR2, TLR3, and TLR4 mRNA levels were measured by RT-qPCR assay. The results showed that GDF-15 significantly decreased levels of three genes, CD36, LOX1, and TLR4 (Figure 5), in oxLDL-induced macrophages. This result indicates that CD36, LOX1, and TLR4 might be involved in GDF-15-mediated lipoprotein accumulation suppression.

3.6. GDF-15 Suppressed oxLDL-Induced Lipoprotein Accumulation via Inhibiting DC36 and LOX1. To determine whether GDF-15 inhibits oxLDL-induced lipid accumulation in macrophages, Transfect pcDNA-CD36 and pcDNA-LOX1 into MDMs cells to overexpress CD36 and LOX1, then induce untransfected and transfected MDMs cells with oxLDL, and treat them with GDF15 for 48 hours. Oil red O staining showed GDF-15-inhibited lipid accumulation in oxLDL-induced MDMs, but overexpression of both CD36 and LOX1

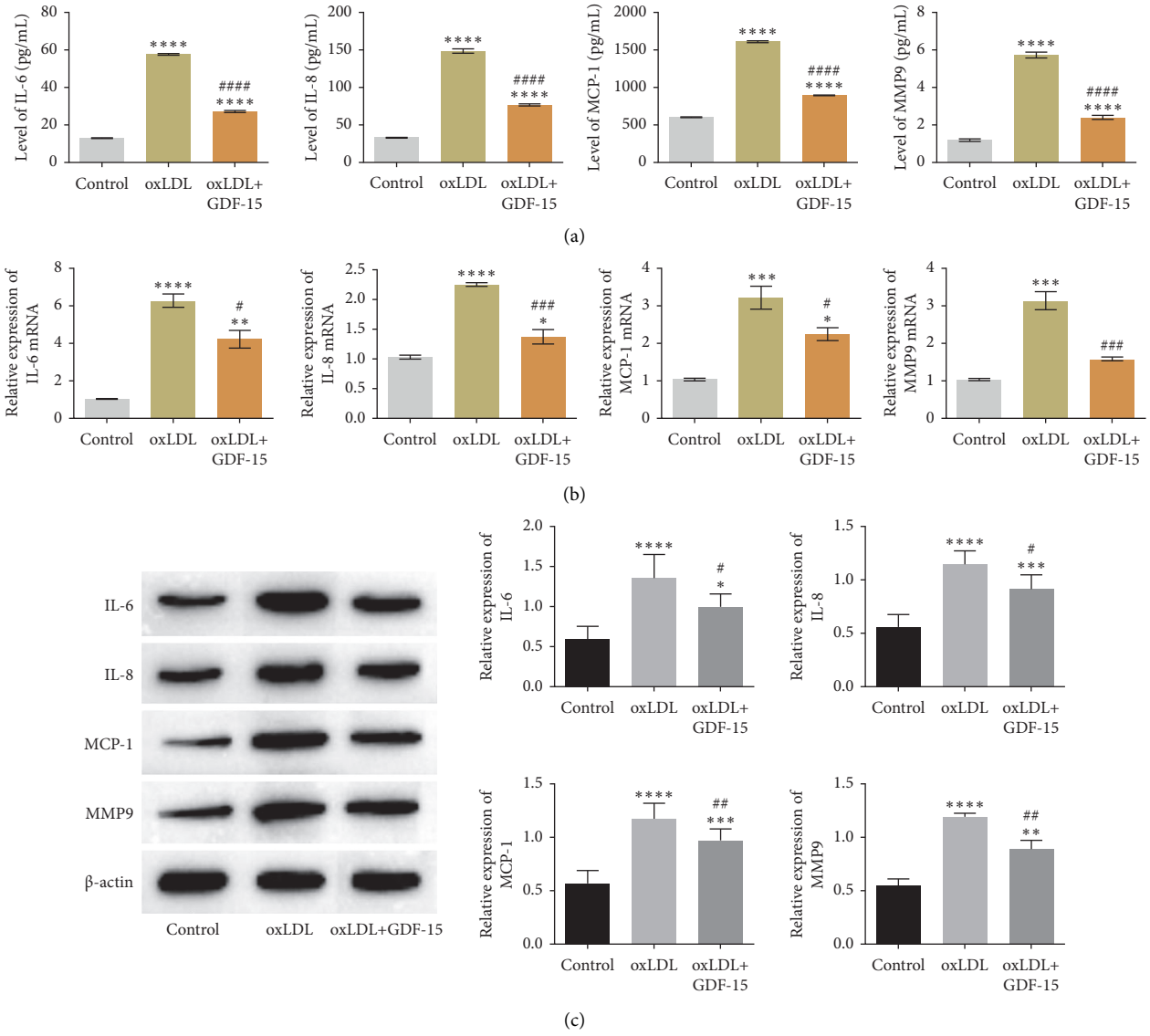

Figure 4: GDF-15 suppressed oxLDL-induced proinflammatory cytokine productions in MDMs. (a) The results of ELISA assay showed that oxLDL treatment promoted MDMs secret IL-6, IL-8, MCP-1, and MMP9, while GDF-15 inhibited oxLDL-induced proinflammatory cytokines releasing in MDMs. (b) After treated by oxLDL, the mRNA levels of IL-6, IL-8, MCP-1, and MMP-9 were significantly upregulated but then suppressed by GDF-15 treatment. (c) The protein levels of IL-6, IL-8, MCP-1, and MMP-9 were confirmed by western blotting assay, and the results showed that the protein levels of these proinflammatory cytokines in oxLDL-induced MDMs were obviously downregulated by GDF-15 treatment. Values are expressed as the mean ± standard deviation of three independent experiments as determined by one-way ANOVA test. $^{**}P < 0.01$, $^{***}P < 0.001$ vs. control group; $^{\#}P < 0.05$, $^{\#\#}P < 0.01$, $^{\#\#\#}P < 0.001$ vs. oxLDL-induced group.

reversed the effect of GDF-15 treatment (Figure 6(a)), which indicated that GDF-15 suppressed oxLDL-induced lipid accumulation partly by inhibiting CD36 and LOX1. Then, to verify whether GDF-15 inhibits oxLDL-induced macrophages inflammation via inhibiting TLR4, Neoseptin-3, an agonist of TLR4, was used to activate TLR4 when the oxLDL-induced cells were treated by GDF-15. The results showed that GDF-15 downregulated the expression of TLR4 induced by MDMs, while Neoseptin-3 reversed the inhibitory effect of GDF-15 (Figure 6(b)). Furthermore, the levels of IL-6, IL-8, MCP-1, and MMP9 in oxLDL-induced MDMs were significantly suppressed by GDF-15, while Neoseptin-3 treatment reversed the levels of these proinflammatory cytokines (Figures 6(c)–6(f)), which indicated that GDF-15 decreases proinflammatory cytokines releasing in oxLDL-induced macrophages by inhibiting the activation of TLR4 signaling.

3.7. Effect of Recombinant GDF-15 on High-Fat Fed ApoE$^{-/-}$ Mice. To determine the effect of recombinant GDF-15 on the inflammatory response and atherosclerotic plaque formation of ApoE$^{-/-}$ mice, recombinant GDF-15 was an intravenous injection to upregulate the level of circulating GDF-15. As the results showed, recombinant GDF-15 obviously alleviated the endothelial cell injury and atherosclerotic plaque formation in the aorta of ApoE$^{-/-}$ mice

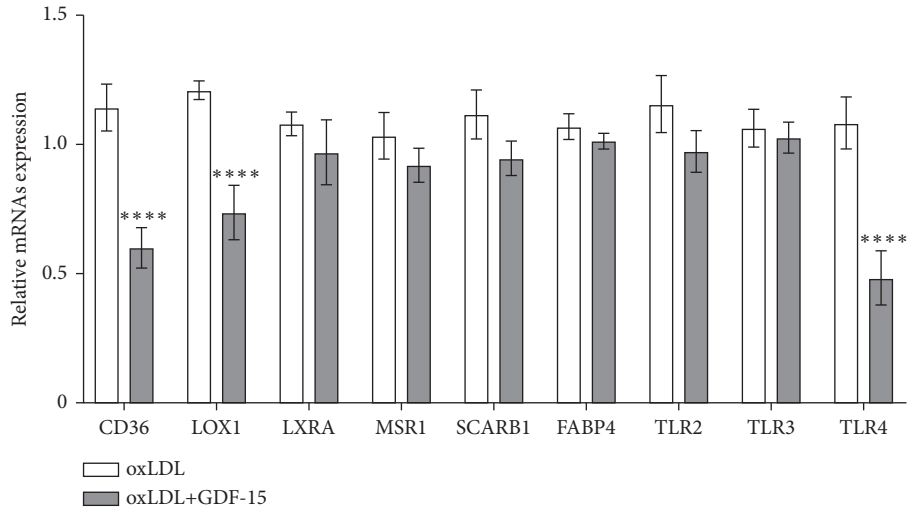

Figure 5: The effect of GDF-15 on gene expression associated with lipoprotein accumulation. oxLDL-induced MDMs were treated with GDF-15 (2 ng/mL) or untreated for 48 hours. After treatment, the mRNA expressions of CD36, LOX1, LXRA, MSR1, SCARB1, FABP4, TLR2, TLR3, and TLR4 were confirmed by real-time PCR assay. The results showed that the mRNA expressions of CD36, LOX1, and TLR4 were obviously downregulated by GDF-15 in oxLDL-induced MDMs. $^{****}P < 0.0001$ vs. oxLDL-induced group.

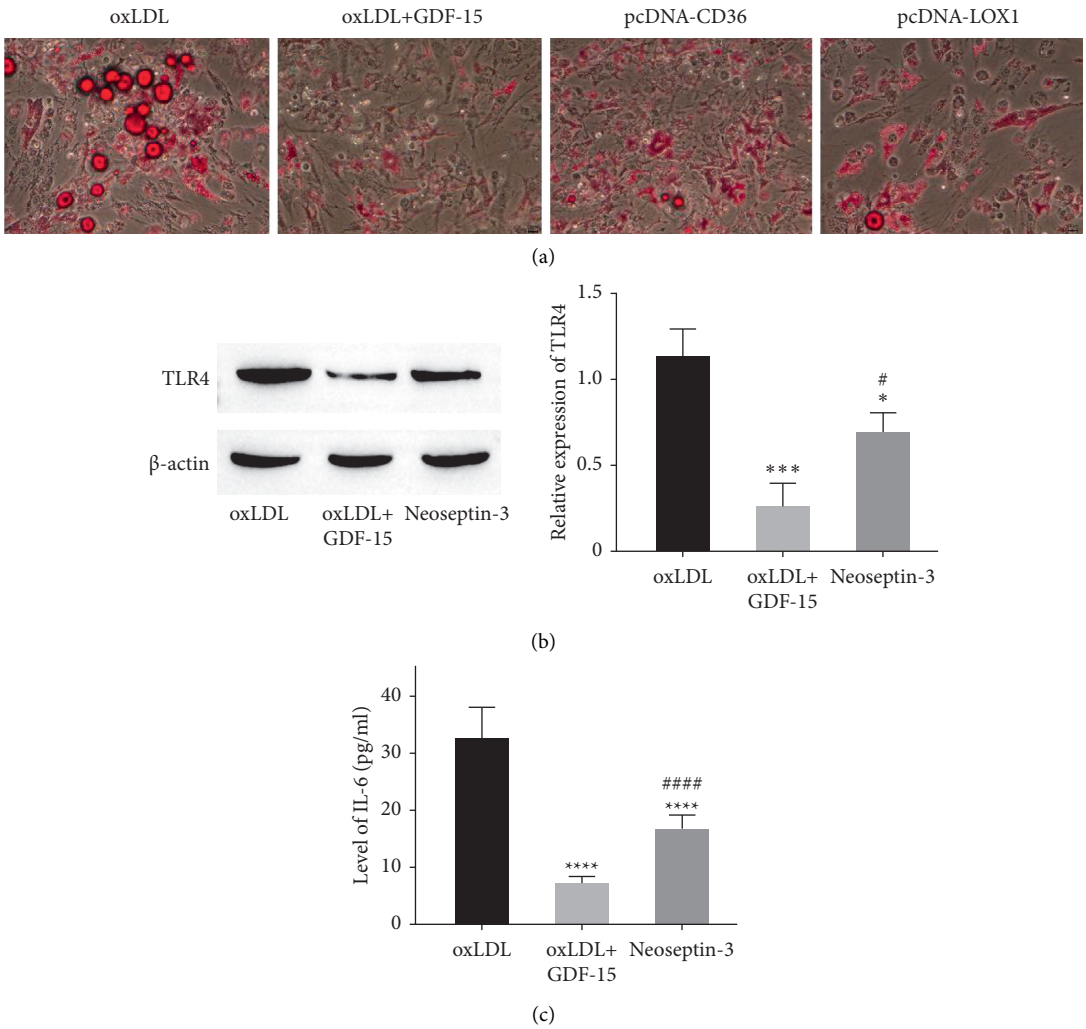

Figure 6: Continued.

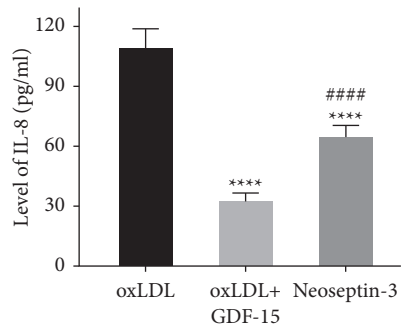

(d)

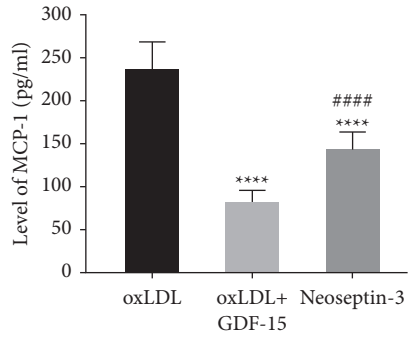

(e)

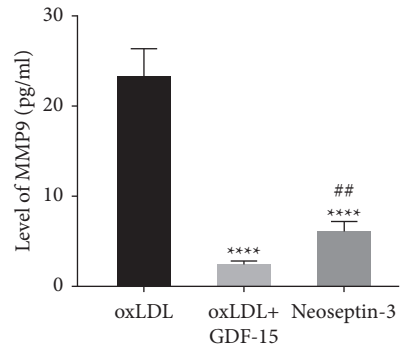

(f)

Figure 6: GDF-15 suppressed oxLDL-induced lipoprotein accumulation via inhibiting DC36 and LOX1. (a) Oil red O staining showed that GDF-15 inhibited lipoprotein accumulation in oxLDL-induced MDMs, but overexpression of both CD36 and LOX1 reversed the effect of GDF-15 treatment. (b) GDF-15 downregulated the expression of TLR4 induced by MDMs, while Neoseptin-3 reversed the inhibitory effect of GDF-15. (c–f) The levels of IL-6, IL-8, MCP-1, and MMP9 in oxLDL-induced MDMs were significantly suppressed by GDF-15, while Neoseptin-3 treatment reversed the levels of these proinflammatory cytokines. Values are expressed as the mean ± standard deviation of three independent experiments as determined by one-way ANOVA test. $^{*}P < 0.05$, $^{***}P < 0.001$, $^{****}P < 0.0001$ vs. oxLDL-induced group; $^{\#}P < 0.05$, $^{\#\#}P < 0.01$, $^{\#\#\#\#}P < 0.0001$ vs. oxLDL + GDF-15-treated group.

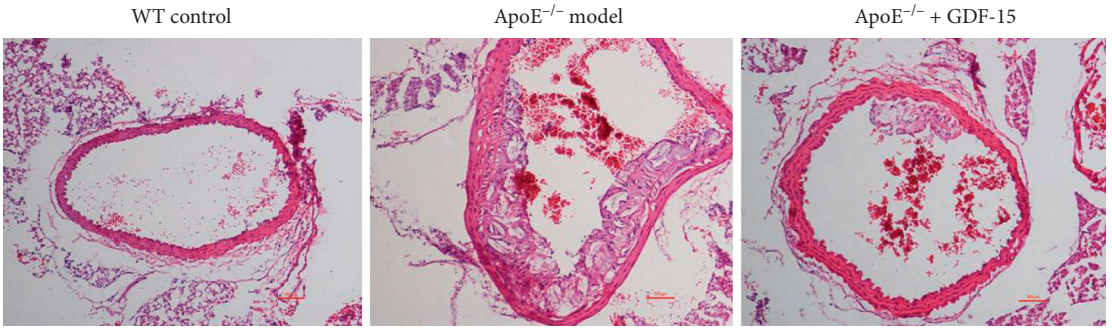

(a)

Figure 7: Continued.

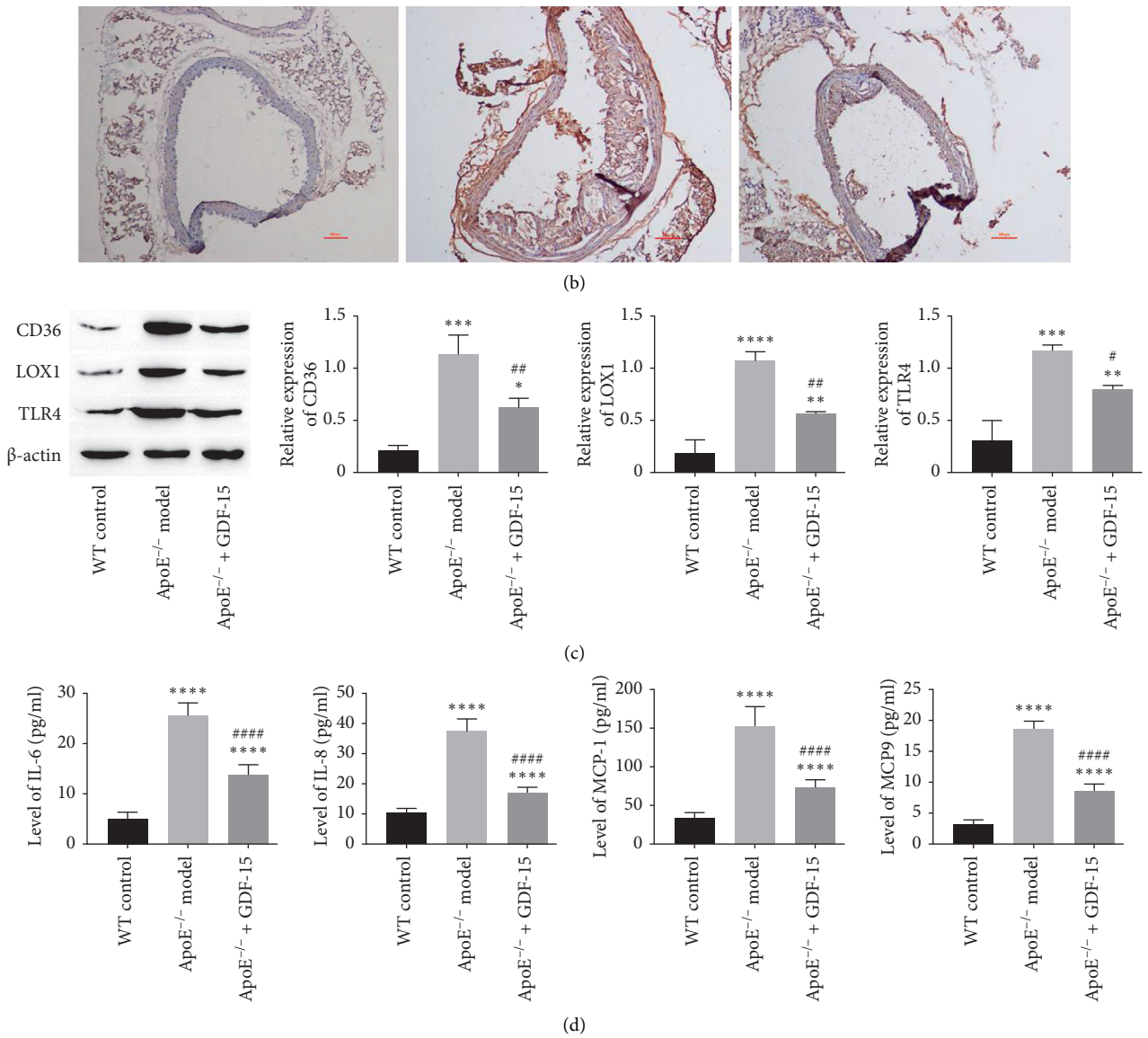

Figure 7: Effect of recombinant GDF-15 on high-fat fed ApoE$^{-/-}$ mice: (a) representative H&E staining images of artery vessels in WT mice, ApoE$^{-/-}$ mice, and recombinant GDF-15-treated ApoE$^{-/-}$ mice; (b) representative IL-6 immunohistochemical staining images of artery vessels in WT mice, ApoE$^{-/-}$ mice, and recombinant GDF-15-treated ApoE$^{-/-}$ mice; (c) expressions of CD36, LOX1, and TLR4 in artery vessels of WT mice, ApoE$^{-/-}$ mice, and recombinant GDF-15-treated ApoE$^{-/-}$ mice; and (d) levels of IL-6, IL-8, MCP-1, and MMP9 in artery vessels of each group. Values are expressed as the mean ± standard deviation of three independent experiments of five independent animal samples as determined by one-way ANOVA test. $^{**}P < 0.01$, $^{***}P < 0.001$, $^{****}P < 0.0001$ vs. WT control group; $^{\#}P < 0.05$, $^{\#\#}P < 0.01$, $^{\#\#\#\#}P < 0.0001$ vs. ApoE$^{-/-}$ model group.

(Figure 7(a)). Immunohistochemistry staining of IL-6 showed that IL-6 was highly expressed in the plaque of ApoE$^{-/-}$ mice aortic arch, while recombinant GDF-15 decreased the positive rate of IL-6 in the plaque of ApoE$^{-/-}$ mice aorta (Figure 7(b)). Further study showed that GDF-15 could inhibit the expression of CD36, LOX1, and TLR4 in the aorta of ApoE$^{-/-}$ mice (Figure 7(c)) and decrease the levels of IL-6, IL-8, MCP-1, and MMP9 in peripheral blood of ApoE$^{-/-}$ mice (Figure 7(d)). These results indicated that intravenous injection of recombinant GDF-15 could ameliorate atherosclerosis.

4. Discussion

GDF-15 is a new member of the transforming growth factor beta (TGF-β) superfamily, which has most recently been found in activated macrophages. GDF-15 is inducible in human macrophages by oxLDL and its mediators in vitro and is supposed to contribute to oxidative stress-dependent consequences in arteriosclerotic plaques modulating apoptosis and inflammatory processes in activated macrophages [21]. To determine the relationship of GDF-15 with atherosclerosis, we compared the serum GDF-15 levels in

patients with atherosclerosis and healthy people. As a result, GDF-15 was highly expressed in patients compared with healthy people (Figure 1). We also measured GDF-15 in atherosclerosis plaques from the ApoE$^{-/-}$ mice model of atherosclerosis. In mice with atherosclerosis, GDF-15 was highly expressed in the core of plaque and macrophages (Figure 2(b)). This study suggested that GDF-15 is possibly associated with atherosclerosis and can play a protective role.

Atherosclerosis is initiated by lipoprotein accumulation in the intimal layer of the arterial vessel wall, which results in the recruitment of circulating monocytes [22]. Once entered the arterial intima, the monocytes differentiate into macrophages; then the latter ingests lipoproteins, in particular oxidized lipoproteins, and finally converts into foam cells, which promotes atherosclerosis progression [23–26]. To determine the real role of GDF-15 in atherosclerosis, we detected the effect of GDF-15 on lipoprotein accumulation and inflammatory response in oxLDL-induced macrophages. Lipoprotein accumulation analysis showed that GDF-15 suppressed lipid accumulation in oxLDL-treated macrophages (Figure 3). Meanwhile, GDF-15 contributed to a decreased inflammatory response in oxLDL-treated macrophages (Figure 4). These data suggested that GDF-15 could suppress atherosclerosis initiation and progression. In this study, a GDF-15 inhibitor was not used to confirm the effect of GDF-15 on lipid accumulation and inflammatory factors, which can become future research directions.

Inflammation response plays an important role in the development and progression of atherosclerosis. Proinflammatory cytokine IL-6 is a proatherogenic cytokine, and sustained IL-6 production promotes the development of atherosclerosis [27–29]. Recombinant IL-6 treatment exacerbates atherosclerosis in wild-type and atherosclerosis-prone ApoE$^{-/-}$ mice fed with a high-fat diet, which shows a dramatically increased lesion size [26]. Another proinflammation cytokine, IL-8, and chemokine, MCP-1, are involved in monocyte adhesion and migration into the arterial vessel wall in atherosclerosis [29]. MMP belongs to a very large family of peptidases that can degrade the extracellular matrix [30]. MMP-9 is a member of the MMP family, and it has been determined to contribute to the destabilization of the plaque [3]. This study showed that GDF-15 could decrease the levels of IL-6, IL-8, MCP-1, and MMP-9 in oxLDL-treated macrophages (Figure 4). This result suggested that GDF-15 has pluripotential atheroprotective effects, that is, blocking the entry of monocytes into the arterial wall and suppressing plaque formation and expansion.

To study the atheroprotective mechanism of GDF-15, we studied the effect of GDF-15 on gene expressions that are associated with lipoprotein accumulation in macrophages. As a result, we found GDF-15 could decrease the expressions of CD36, LOX1, and TLR4 (Figure 5). Both CD36 and LOX1 are scavenged receptors, which recognize and process modified LDL (such as oxLDL) [31]. Previous studies indicate that CD36 locating in the surface of macrophages can bind oxLDL and then promotes oxLDL internalization [32]. On the other hand, the interaction of CD36 with oxLDL can also activate the immune response and then result in the secretion of cytokines, which lead to immune cell infiltrates and finally promote the progress of atherosclerosis [33]. Like CD36, LOX1 can also bind oxLDL, and ApoE$^{-/-}$ mouse model research indicated that LOX1 overexpression dramatically enhanced atherosclerosis [34]. This study showed that GDF-15 suppressed the expression of CD36 and LOX1, and GDF-15 might suppress oxLDL-induced lipoprotein accumulation by inhibiting the expression of CD36 and LOX1 (Figure 6(a)), but the concrete molecular mechanism needs further study. On the other hand, GDF-15 treatment also decreased TLR4 expression. Previous studies suggested that TLR4 plays a role in atherosclerosis. As a pattern recognition receptor, TLR4 activation can induce a proinflammatory response and then enhance atherogenesis. Moreover, minimally, oxLDL can be recognized by TLR4 and promotes TNF-α and IL-6 production [35]. Thus, our results showed that GDF-15 suppressed proinflammatory response induced by oxLDL and attenuated atherosclerosis initiation as well as progression by downregulating TLR4 (Figures 6(b) and 6(c)).

In conclusion, this study showed that GDF-15 suppressed atherosclerosis by inhibiting lipid accumulation and decreasing the expressions of IL-6, IL-8, MCP-1, and MMP-9 in macrophages. Furthermore, the expression of CD36, LOX1, and TLR4 may play an important role in the atheroprotective mechanism of GDF-15. However, the concrete molecular mechanism needs further exploration. This study indicated that GDF-15 may suppress atherosclerosis and plaque formation by inhibiting lipoprotein accumulation and inflammation activation. Although the results of this study are inconsistent with some existing studies, and the role of GDF-15 in atherosclerosis is still controversial, which needs further research and elucidation, GDF-15 still has the potential to become a target for the diagnosis and treatment of atherosclerosis.

Data Availability

The data sets used and/or analyzed during the current study are available from the corresponding author upon reasonable request.

Conflicts of Interest

The authors declare that there are no conflicts of interest.

Authors' Contributions

All the authors contributed substantially to this manuscript. All the authors read and approved the final manuscript. H H contributed majorly to this manuscript by participating in all the experiments and writing the manuscript. ZL C and Y L participated primarily in establishing the animal model and histopathological staining assay; KM G and L X contributed mainly to the cells culture and all in vitro tests; H F and JJ Y contributed to the collection of patients' serum and partly ELISA assays; XY W contributed the primary cell culture, data collation, and analysis; and Q M contributed to the

conception and design of this study and guided the writing of the manuscript.

Acknowledgments

This work was supported by the National Natural Science Foundation of China (nos. 81460188 and 81960228), Yunnan Provincial Department of Science and Technology—Kunming Medical University Joint Special Project on Applied Basic Research (no. 202001AY070001-118), Geriatric Prevention and Treatment Research Center of Yunnan Provincial Health and Family Planning Commission (no. 2016NS201), Yunnan Health Training Project of High Level Talents (no. L-2017013); and the Ten Thousand Talents Program-Famous Doctor Project of Yunnan Province (no. YNWR-MY-2018-018).

References

[1] W. Herrington, B. Lacey, P. Sherliker, J. Armitage, and S. Lewington, "Epidemiology of atherosclerosis and the potential to reduce the global burden of atherothrombotic disease," *Circulation Research*, vol. 118, no. 4, pp. 535–546, 2016.

[2] K. J. Moore, F. J. Sheedy, and E. A. Fisher, "Macrophages in atherosclerosis: a dynamic balance," *Nature Reviews Immunology*, vol. 13, no. 10, pp. 709–721, 2013.

[3] S. Bekkering, J. Quintin, L. A. B. Joosten, J. W. M. van der Meer, M. G. Netea, and N. P. Riksen, "Oxidized low-density lipoprotein induces long-term proinflammatory cytokine production and foam cell formation via epigenetic reprogramming of monocytes," *Arteriosclerosis, Thrombosis, and Vascular Biology*, vol. 34, no. 8, pp. 1731–1738, 2014.

[4] R. Adela and S. K. Banerjee, "GDF-15 as a target and biomarker for diabetes and cardiovascular diseases: a translational prospective," *Journal of Diabetes Research*, vol. 2015, Article ID 490842, 14 pages, 2015.

[5] A. Bobik, "Transforming growth factor-βs and vascular disorders," *Arteriosclerosis, Thrombosis, and Vascular Biology*, vol. 26, no. 8, pp. 1712–1720, 2006.

[6] T. Ago and J. Sadoshima, "GDF15, a cardioprotective TGF-β superfamily protein," *Circulation Research*, vol. 98, no. 3, pp. 294–297, 2006.

[7] M. Mimeault and S. K. Batra, "Divergent molecular mechanisms underlying the pleiotropic functions of macrophage inhibitory cytokine-1 in cancer," *Journal of Cellular Physiology*, vol. 224, no. 3, pp. 626–635, 2010.

[8] B. Lindahl, "The story of growth differentiation factor 15: another piece of the puzzle," *Clinical Chemistry*, vol. 59, no. 11, pp. 1550–1552, 2013.

[9] I. S. Anand, T. Kempf, T. S. Rector et al., "Serial measurement of growth-differentiation factor-15 in heart failure: relation to disease severity and prognosis in the Valsartan heart failure trial," *Circulation*, vol. 122, no. 14, pp. 1387–1395, 2010.

[10] A. Dominguez-Rodriguez, P. Abreu-Gonzalez, and P. Avanzas, "Relation of growth-differentiation factor 15 to left ventricular remodeling in ST-segment elevation myocardial infarction," *The American Journal of Cardiology*, vol. 108, no. 7, pp. 955–958, 2011.

[11] T. Kempf, J.-M. Sinning, A. Quint et al., "Growth-differentiation factor-15 for risk stratification in patients with stable and unstable coronary heart disease: results from the AtheroGene study," *Circulation: Cardiovascular Genetics*, vol. 2, no. 3, pp. 286–292, 2009.

[12] S. C. A. de Jager, B. Bermúdez, I. Bot et al., "Growth differentiation factor 15 deficiency protects against atherosclerosis by attenuating CCR2-mediated macrophage chemotaxis," *Journal of Experimental Medicine*, vol. 208, no. 2, pp. 217–225, 2011.

[13] K. Larissi, M. Politou, A. Margeli et al., "The growth differentiation factor-15 (GDF-15) levels are increased in patients with compound heterozygous sickle cell and beta-thalassemia (HbS/βthal), correlate with markers of hemolysis, iron burden, coagulation, endothelial dysfunction and pulmonary hypertension," *Blood Cells, Molecules, and Diseases*, vol. 77, pp. 137–141, 2019.

[14] J. Wang, L. Wei, X. Yang, and J. Zhong, "Roles of growth differentiation factor 15 in atherosclerosis and coronary artery disease," *Journal of the American Heart Association*, vol. 8, no. 17, Article ID e012826, 2019.

[15] J. Chen, F. Luo, Z. Fang, and W. Zhang, "GDF-15 levels and atherosclerosis," *International Journal of Cardiology*, vol. 257, p. 36, 2018.

[16] J. Li, L. Yang, W. Qin, G. Zhang, J. Yuan, and F. Wang, "Adaptive induction of growth differentiation factor 15 attenuates endothelial cell apoptosis in response to high glucose stimulus," *PLoS One*, vol. 8, no. 6, Article ID e65549, 2013.

[17] X. Wang, L.-L. Chen, and Q. Zhang, "Increased serum level of growth differentiation factor 15 (GDF-15) is associated with coronary artery disease," *Cardiovascular Therapeutics*, vol. 34, no. 3, pp. 138–143, 2016.

[18] K. J. Moore and I. Tabas, "Macrophages in the pathogenesis of atherosclerosis," *Cell*, vol. 145, no. 3, pp. 341–355, 2011.

[19] Y. V. Bobryshev, E. A. Ivanova, D. A. Chistiakov, N. G. Nikiforov, and A. N. Orekhov, "Macrophages and their role in atherosclerosis: pathophysiology and transcriptome analysis," *BioMed Research International*, vol. 2016, Article ID 9582430, 13 pages, 2016.

[20] I. Tabas and A. H. Lichtman, "Monocyte-macrophages and T cells in atherosclerosis," *Immunity*, vol. 47, no. 4, pp. 621–634, 2017.

[21] D. Schlittenhardt, A. Schober, J. Strelau et al., "Involvement of growth differentiation factor-15/macrophage inhibitory cytokine-1 (GDF-15/MIC-1) in oxLDL-induced apoptosis of human macrophages in vitro and in arteriosclerotic lesions," *Cell and Tissue Research*, vol. 318, no. 2, pp. 325–333, 2014.

[22] G. K. Hansson and A. Hermansson, "The immune system in atherosclerosis," *Nature Immunology*, vol. 12, no. 3, pp. 204–212, 2011.

[23] V. Braunersreuther, A. Zernecke, C. Arnaud et al., "Ccr5 but not Ccr1 deficiency reduces development of diet-induced atherosclerosis in mice," *Arteriosclerosis, Thrombosis, and Vascular Biology*, vol. 27, no. 2, pp. 373–379, 2007.

[24] L. Boring, J. Gosling, M. Cleary, and I. F. Charo, "Decreased lesion formation in CCR2$^{-/-}$ mice reveals a role for chemokines in the initiation of atherosclerosis," *Nature*, vol. 394, no. 6696, pp. 894–897, 1998.

[25] L. Gu, Y. Okada, S. K. Clinton et al., "Absence of monocyte chemoattractant protein-1 reduces atherosclerosis in low density lipoprotein receptor-deficient mice," *Molecular Cell*, vol. 2, no. 2, pp. 275–281, 1998.

[26] V. V. Kunjathoor, M. Febbraio, E. A. Podrez et al., "Scavenger receptors class A-I/II and CD36 are the principal receptors responsible for the uptake of modified low density lipoprotein leading to lipid loading in macrophages," *Journal of Biological Chemistry*, vol. 277, no. 51, pp. 49982–49988, 2002.

[27] S. A. Huber, P. Sakkinen, D. Conze, N. Hardin, and R. Tracy, "Interleukin-6 exacerbates early atherosclerosis in mice," *Arteriosclerosis, Thrombosis, and Vascular Biology*, vol. 19, no. 10, pp. 2364–2367, 1999.

[28] R. Elhage, S. Clamens, S. Besnard et al., "Involvement of interleukin-6 in atherosclerosis but not in the prevention of fatty streak formation by 17β-estradiol in apolipoprotein E-deficient mice," *Atherosclerosis*, vol. 156, no. 2, pp. 315–320, 2001.

[29] A. Tedgui and Z. Mallat, "Cytokines in atherosclerosis: pathogenic and regulatory pathways," *Physiological Reviews*, vol. 86, no. 2, pp. 515–581, 2006.

[30] A. Kousios, P. Kouis, and A. G. Panayiotou, "Matrix metalloproteinases and subclinical atherosclerosis in chronic kidney disease: a systematic review," *International Journal of Nephrology*, vol. 2016, Article ID 9498013, 11 pages, 2016.

[31] K. J. Moore and M. W. Freeman, "Scavenger receptors in atherosclerosis: beyond lipid uptake," *Arteriosclerosis, Thrombosis, and Vascular Biology*, vol. 26, no. 8, pp. 1702–1711, 2006.

[32] Y. Jiang, M. Wang, K. Huang et al., "Oxidized low-density lipoprotein induces secretion of interleukin-1β by macrophages via reactive oxygen species-dependent NLRP3 inflammasome activation," *Biochemical and Biophysical Research Communications*, vol. 425, no. 2, pp. 121–126, 2012.

[33] Y. M. Park, "CD36, a scavenger receptor implicated in atherosclerosis," *Experimental & Molecular Medicine*, vol. 46, no. 6, p. e99, 2014.

[34] A. Pirillo, G. D. Norata, and A. L. Catapano, "LOX-1, OxLDL, and atherosclerosis," *Mediators of Inflammation*, vol. 2013, Article ID 152786, 12 pages, 2013.

[35] Y. S. Bae, J. H. Lee, S. H. Choi et al., "Macrophages generate reactive oxygen species in response to minimally oxidized low-density lipoprotein: toll-like receptor 4- and spleen tyrosine kinase-dependent activation of NADPH oxidase 2," *Circulation Research*, vol. 104, no. 2, pp. 210–218, 2009.

Hindawi
Evidence-Based Complementary and Alternative Medicine
Volume 2021, Article ID 9567056, 10 pages
https://doi.org/10.1155/2021/9567056

Research Article

Aconitine Induces TRPV2-Mediated Ca^{2+} Influx through the p38 MAPK Signal and Promotes Cardiomyocyte Apoptosis

Chunai Yang,[1] **Xiaoyan Zeng**,[2] **Zhongfeng Cheng**,[1] **Junbo Zhu**,[1] **and Yangshan Fu**[1]

[1]*Department of Emergency, The Affiliated Hospital of Yunnan University, Kunming 650021, China*
[2]*Department of the Teaching Office, School of Continuing Education, Kunming Medical University, Kunming 650500, China*

Correspondence should be addressed to Chunai Yang; yangchunai2020@163.com and Xiaoyan Zeng; mzh2004@ynu.edu.cn

Received 7 May 2021; Revised 30 June 2021; Accepted 17 July 2021; Published 1 September 2021

Academic Editor: Feng Zhang

Aconitine is the main effective component of traditional Chinese medicine *Aconitum*, which has been proved to have severe cardiovascular toxicity. The toxic effect of aconitine on cardiomyocytes is related to intracellular calcium overload, but the mechanism remains unclear. The aim of this study was to explore the mechanism of aconitine inducing intracellular Ca^{2+} overload and promoting H9c2 cardiomyocyte apoptosis through transient receptor potential cation channel subfamily V member 2 (TRPV2). After treated with different concentrations of aconitine, the level of cell apoptosis, intracellular Ca^{2+}, and expression of p-p38 MAPK and TRPV2 of H9c2 cardiomyocytes were detected. The results showed that aconitine induced Ca^{2+} influx and H9c2 cardiomyocyte apoptosis in a dose-dependent manner and promoted p38 MAPK activation as well as TRPV2 expression and plasma membrane (PM) metastasis. siTRPV2, tranilast, and SB202190 reversed intracellular Ca^{2+} overload and H9c2 cardiomyocyte apoptosis induced by aconitine. These results suggested that aconitine promoted TRPV2 expression and PM metastasis through p38 MAPK signaling, thus inducing intracellular Ca^{2+} overload and cardiomyocyte apoptosis. Furthermore, TRPV2 is a potential molecular target for the treatment of aconitine poisoning.

1. Introduction

Aconitum species, containing aconitine, are widely used in the clinical treatment of rheumatism, arthritis, bruise, fracture, pain, and other diseases in China and other Asian countries because of their medicinal properties. However, due to their potential proarrhythmic effect, *Aconitum* and its related preparations are now restrictively used in the treatment of rheumatoid arthritis and some cardiovascular diseases [1]. As the main toxic ingredient and effective agent of *Aconitum*, aconitine is a natural diterpene alkaloid [2], which was reported to be an inducer of lethal ventricular arrhythmias through rapidly inhibiting or activating different ion channels on cardiac myocytes or conductive cells [3]. Although aconitine showed important biological activities in analgesia, diuresis, antitumor, antiasthmatic, anti-inflammatory, and other aspects [4, 5], its improper use can still lead to a high risk of serious toxic reactions, such as palpitation, vomiting, nausea, arrhythmia, shock, dizziness, hypotension, and coma [6]. Growing evidence showed that cardiotoxicity and neurotoxicity are the main toxic effects of aconitine [7]. According to previous studies, the mechanism of cardiotoxic effects may involve ion channel changes [8, 9], energy metabolism [10], oxidative damage [10], inflammation and apoptosis [11], and so on [12]. However, the cytotoxic signaling pathway of aconitine-induced cardiomyocyte injury remains to be further studied.

Transient receptor potential cation channel subfamily V member 2 (TRPV2) is a stretch-sensitive Ca^{2+} permeability channel. In myocardial tissue, TRPV2 was expressed in intercalated discs of the sarcomere and participated in the maintenance of appropriate electromechanical coupling and structure of the cardiomyocyte and myocardium [13]. It is also expressed in the cell pools of cardiomyocytes, mainly endoplasmic reticulum, and transferred to the sarcolemma under pathological conditions or stimulations, where it mediates a persistent Ca^{2+} influx and induces intracellular calcium overload [14]. Studies have shown that the p38

MAPK signaling pathway plays an important role in TRPV2 expression and transport to the plasma membrane (PM) because its activation can promote TRPV2 accumulation and transport to the PM [15, 16]. Meanwhile, it was reported that the arrhythmia induced by aconitine is related to the intracellular Ca^{2+} signal [17], and aconitine induces Ca^{2+} overload by activating the p38 MAPK signal, leading to arrhythmia and cardiomyocyte apoptosis [9]. p38 MAPK signaling plays an important role in cardiomyocyte differentiation, proliferation, apoptosis, inflammation, metabolism, and survival [18]. Studies have shown that p38 MAPK is related to cell cycle arrest of cardiomyocytes [19–21], which indicated that inhibition of p38 MAPK may be an effective strategy to enhance the proliferation of cardiomyocytes. The chronic activation of p38 MAPK was considered to be pathological and proapoptotic, and the inhibition of p38 MAPK activity was considered to be a potential therapy to alleviate acute injury of ischemic heart failure [22]. However, it is not clear whether aconitine-mediated cardiomyocyte Ca^{2+} overload and apoptosis are related to TRPV2 expression, PM metastasis, and p38 MAPK signal activation.

According to the above, here we hypothesized that aconitine could induce TRPV2-mediated Ca^{2+} influx through the p38 MAPK signal and thus promote cardiomyocyte apoptosis. The present study was designed to investigate this possibility *in vivo* which used the rat cardiomyocyte H9c2 cell line.

2. Materials and Methods

2.1. Cell Culture and Treatment. The rat cardiomyocyte H9c2 cells (#CRL-1446, ATCC) were cultured in the DMEM (Gibco, USA) with 10% FBS (Gibco, USA) and 0.1% penicillin-streptomycin solution (Sigma, USA) at 37°C in a 5% CO_2 humidified incubator. Aconitine (content ≥ 98%) was purchased from the National Institute for the Control of Pharmaceutical and Biological Products (China). H9c2 cells were treated with different dosages of aconitine (0, 0.25, 0.5, and 1.0 μM) for 24 h.

TRPV2 siRNA and negative siRNA were obtained from Shanghai GenePharma Co., Ltd., and transfected into H9c2 cells with a final concentration of 10 nM for 6 h by Lipofectamine® 2000 (Invitrogen, USA) according to the manufacturer's protocols. Tranilast (Sigma, USA) was used to inhibit the activation of TRPV2 at a dosage of 75 μM. SB202190 (Sigma, USA) was used to inhibit the activation of p38 at a dosage of 10 μM.

2.2. Flow Cytometry. Flow cytometry assay was used to measure the cell apoptosis rate according to the previous report [23]. The apoptotic cells were double-labeled with annexin V-FITC and PI using an annexin V-FITC/PI apoptosis detection kit (Beyotime Biotechnology, China). H9c2 cells in each group were harvested and resuspended. The H9c2 cells were washed in cold sterile PBS, pelleted, counted (to determine the cell number), and resuspended in 1X annexin binding buffer at a concentration of 1×10^5/100 μL. Subsequently, the cells were incubated for 30 minutes at room temperature in the dark with FITC annexin V and propidium iodide (PI, 100 μg/mL) and then further diluted with 400 μL 1X annexin binding buffer. Then, the fluorescence intensity of the cells was quantified by using a flow cytometer (Accuri C6, BD Biosciences, San Jose, CA) using fluorescence emission at 530 nm (FL1) and >575 nm (FL3). Single color stains for FITC annexin and PI and unstained cells were included in all experiments as positive and negative controls.

2.3. Measurements of Intracellular Ca^{2+} Variation. Intracellular Ca^{2+} concentration variations were detected using the fluorimetric assay with Fura-2AM (a ratiometric probe for intracellular Ca^{2+}) as essentially described [24]. The changes of intracellular Ca^{2+} were evaluated by fluorescence (510 nm) emission ratio at excitations at 340 and 380 nm, which can directly reflect the intracellular calcium content. In brief, the H9c2 cells were suspended in the buffer without Ca^{2+}, and the basic fluorescence level was recorded; then, Ca^{2+} was applied at 2 mM leading to calcium influx through opened membrane calcium channels (control calcium level) after 20 s. In order to detect the influence of aconitine and p38 MPAK/TRPV2 inhibitors on the intracellular calcium content, they were added into the resuspended cells just before the beginning of the measurement, then each group of H9c2 cells was resuspended in buffer solution containing 2 mM Ca^{2+}, and their fluorescence levels were recorded. To calculate the effect of inhibitors to aconitine, the normalized Ca^{2+} influx in the absence of aconitine and the channel activity at 2 mM Ca^{2+} are used as reference points.

2.4. Quantitative Reverse Transcription Polymerase Chain Reaction (qRT-PCR). The performance of the qRT-PCR assay followed the methods of Peng et al. with some modification [25]. Total RNA was extracted from H9c2 cells using TRIzol reagent (Invitrogen, USA) and then reverse transcribed using a PrimeScript RT reagent kit (Takara Biotechnology Co., Ltd.), following the manufacturer's instructions (with the temperature protocol of 37°C for 15 min and 85°C for 5 sec). qRT-PCR was carried out using SYBR Real-Time PCR Master Mix (Takara Biotechnology Co., Ltd.) on an ABI 7500 Real-Time PCR System (Applied Biosystems, USA). The thermocycling conditions were as follows: initial denaturation at 95°C for 10 sec, followed by 40 cycles of 95°C for 10 sec and 60°C for 30 sec. The mRNA level was normalized to GAPDH, and the relative levels were calculated by the $2^{-\Delta\Delta Cq}$ method [26]. The primer sequences used were as follows: rat TRPV2, forward: 5′-GCTGGCTGAACCTGCTTTAC-3′, reverse: 5′-CTACAGCAAAGCCGAAAAGG-3′; GAPDH, forward: 5′-GACATGCCGCCTGGAGAAAC-3′, reverse: 5′-AGCCCAGGATGCCCTTTAGT-3'.

2.5. Western Blotting. Western blotting was used to examine the expression levels of proteins in this study; the method

followed the methods of Peng et al. with some modifications [25]. Each group of H9c2 cells was harvested and lysed in RIPA buffer with protease inhibitors (Invitrogen, USA), and the protein concentrations were determined by the Pierce BCA assay (Invitrogen, USA), according to the manufacturer's protocols. Then, the proteins in lysates (40 ng of each sample) were separated by an SDS-PAGE and subsequently transferred onto PVDF membranes. The membranes were blocked with 5% nonfat milk for 1 h at room temperature and incubated with primary antibodies at 4°C overnight. Expression levels of the proteins of interest were analyzed using primary antibodies against the inhibitor of Bcl-2 (1 : 1000, CST, USA), Bax (1 : 1000, CST, USA), cleaved caspase-3 (1 : 1000, CST, USA), p38 (1 : 1000, CST, USA), p-p38 (1 : 1000, CST, USA), and TRPV2 (1 : 1000, Abcam, UK). Membranes were rinsed three times with 1X Tris-buffered saline with 0.5% Tween 20 (TBST) and then incubated with the anti-rabbit IgG (1 : 2000, Abcam, UK) horseradish peroxidase-conjugated secondary antibody for 1 h at room temperature. Membranes were rinsed three times with TBST and visualized using an ECL kit (Bio-Rad Laboratories Inc.). The protein bands were quantified using ImageJ software (version 1.52a, National Institutes of Health), and β-actin (1 : 1000, CST, USA) was used as a loading control. Each experiment was performed in triplicate.

2.6. Statistical Analysis. All the data are presented as the mean ± SEM. Differences between two or multiple groups were evaluated using a one-way ANOVA or two-way ANOVA followed by Bonferroni post hoc test. Statistical analyses were performed by GraphPad Prism 7.0 software (GraphPad Software Inc.). $P < 0.05$ was considered to indicate a statistically significant difference.

3. Results

3.1. Aconitine Promotes H9c2 Cardiomyocyte Apoptosis and Increases Ca^{2+} Influx. To detect the influence of aconitine on H9c2 cardiomyocyte, H9c2 cells were treated by aconitine at different dosages of 0, 0.25, 0.5, and 1.0 μM for 24 h, and then the cell apoptosis and intracellular Ca^{2+} were measured. As the results show, aconitine induced obvious H9c2 cell apoptosis at a lower dose of 0.25 μM, and the effect of aconitine on H9c2 cardiomyocyte apoptosis was dose dependent (Figures 1(a) and 1(b)). The levels of apoptosis-related proteins were carried out by western blotting (Figure 1(c)); the results showed that the expression of antiapoptotic protein Bcl-2 in H9c2 cells was reduced by aconitine at a dose-dependent manner, while the expressions of proapoptotic proteins Bax and cleaved caspase-3 were upregulated by aconitine at a dose-dependent manner (Figure 1(d)). In addition, aconitine obviously induced a Ca^{2+} influx which led to a significant intracellular Ca^{2+} overload of H9c2 cardiomyocytes in a dose-dependent manner (Figure 1(e)). These results indicated that aconitine could promote apoptosis by inducing intracellular Ca^{2+} overload.

3.2. Aconitine Activates the p38 MAPK Signal and Promotes TRPV2 PM Translocation. In order to further study the mechanism of aconitine on H9c2 cardiomyocyte apoptosis, the expressions of p38 MAPK and TRPV2 were determined. As shown in Figure 2(a), with the increase of the dosage of aconitine, there was a significant upregulation of the expression of p-p38, which was the activated form of p38 MAPK. For TRPV2, the results showed that both expression of TRPV2 mRNA and total TRPV2 protein level in H9c2 cardiomyocytes were all stimulated by aconitine in a dose-dependent manner (Figures 2(b) and 2(c)). Furthermore, aconitine not only induced the accumulation of TRPV2 in H9c2 cardiomyocytes but also promoted TRPV2 transfer to the PM which was established by increasing the cellular membrane expression of TRPV2 and the ratio between membrane TRPV2 and total TRPV2 (Figure 2(c)). These results implied that aconitine could activate the p38 MAPK signaling pathway and promote the expression and PM translocation of TRPV2.

3.3. Aconitine Promotes Ca^{2+} Influx by Upregulating TRPV2 Expression. To verify whether aconitine induced Ca^{2+} influx by promoting TRPV2 expression and PM transfer, siTRPV2 and specific TRPV2 inhibitor tranilast (TL) were used to inhibit TRPV2 expression and function. The results showed that TL had no obvious influence on the expression level of TRPV2, both mRNA and protein, which indicated TL could not inhibit the expression of TRPV2 but can inhibit the activation of TRPV2, while siTRPV2 significantly decreased the expression of TRPV2 mRNA and protein stimulated by aconitine (1.0 μM) (Figures 3(a)–3(c)). Importantly, from the results of the Fura-2AM fluorimetric assay, there was a significant decrease of intracellular Ca^{2+} both in TL- and siTRPV2-treated groups compared with aconitine treated only (Figure 3(d), $P < 0.001$ compared with the 1.0 μM aconitine treatment group), which indicated that TL has no obvious influence on TRPV2 expression but inhibits the activation of TRPV2, and TRPV2 inhibition by TL and siTRPV2 could reverse the Ca^{2+} influx induced by aconitine. These results suggested that the Ca^{2+} influx induced by aconitine was partly depended on the expression and activation of TRPV2.

3.4. Aconitine Promotes TRPV2 Transfer to the PM by Activating p38 MAPK Signaling. To detect whether aconitine promoted TRPV2 expression and PM translocation through p38 MAPK signaling, the p38 MAPK inhibitor SB202190 (SB) was used to inhibit the activation of p38 MAPK. As the results show, SB could effectively downregulate both mRNA and protein expression of TRPV2 stimulated by aconitine (1.0 μM) (Figures 4(a)–4(c)). Meanwhile, SB obviously inhibited the activation of p38 MAPK induced by aconitine (Figures 4(b) and 4(c)). In addition, the PM translocation of TRPV2 induced by aconitine was obviously reduced by SB (Figures 4(b) and 4(c)), and upregulated intracellular Ca^{2+} stimulated by aconitine was reversed by SB as well (Figure 4(e)). These results indicated that aconitine could promote TRPV2 expression and PM transfer through activating p38 MAPK signaling.

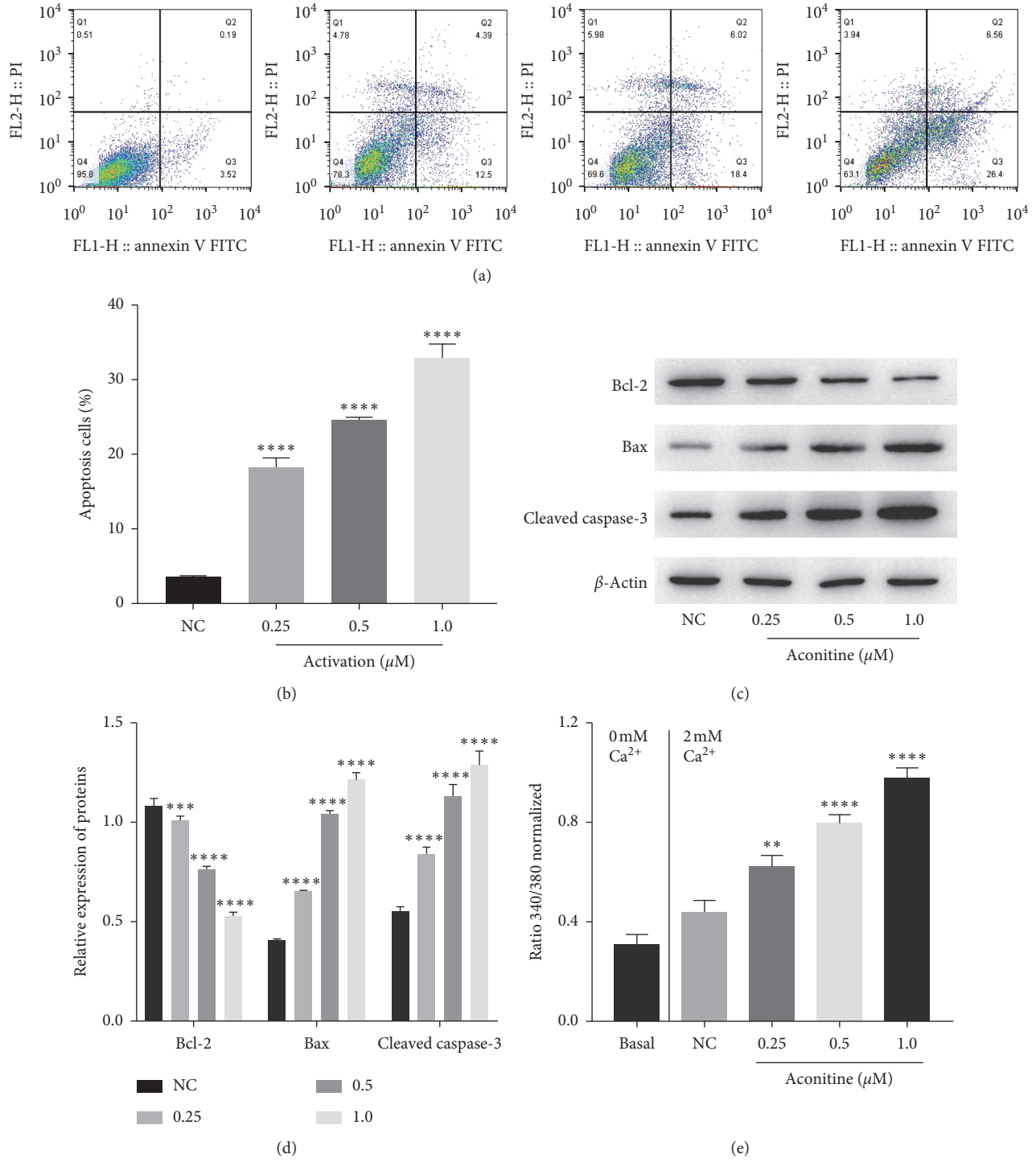

Figure 1: Influence of aconitine on apoptosis and Ca^{2+} influx of cardiomyocytes. (a, b) The rate of cell apoptosis was measured by flow cytometry. (c, d) The expressions of apoptosis-related proteins, Bcl-2, Bax, and cleaved caspase-3, were detected by western blotting. (e) The level of Ca^{2+} influx in each group was shown by the normalized ratio of 340/380. NC: negative control. $^{**}P < 0.01$, $^{***}P < 0.001$, and $^{****}P < 0.0001$ vs. the NC group.

3.5. p38 MAPK Inhibitor and TRPV2 Inhibitor Inhibit Aconitine-Induced Intracellular Ca^{2+} Overload and Cardiomyocyte Apoptosis. To further verify whether aconitine promoted TRPV2 expression and PM translocation through the p38 MAPK signal, thus mediating intracellular Ca^{2+} overload and inducing H9c2 cardiomyocyte apoptosis, SB and TL were used to inhibit the activation of p38 MAPK and TRPV2, respectively. As shown in Figures 5(a) and 5(b), both SB and TL alleviated the cell apoptosis induced by aconitine (1.0 μM). SB downregulated the expression of

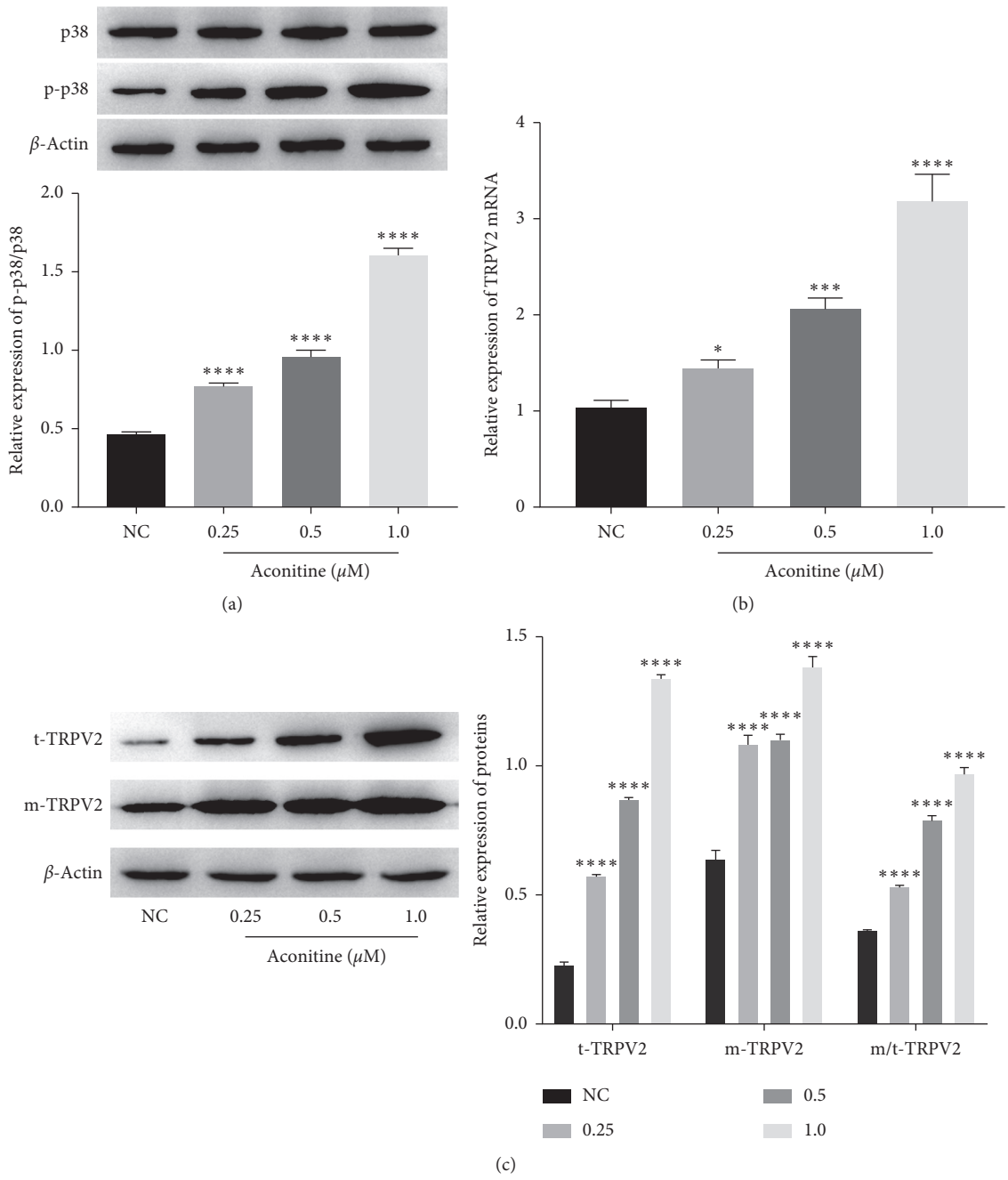

Figure 2: The effect of aconitine on p38 MAPK signaling and TRPV2 expression. (a) The expressions of p38 and p-p38 in each group. (b) The level of TRPV2 mRNA was measured by qRT-PCR. (c) The expressions of total TRPV2 and membrane TRPV2. NC: negative control; t-TRPV2: total TRPV2; m-TRPV2: membrane TRPV2. $^{*}P < 0.05$, $^{***}P < 0.001$, and $^{****}P < 0.0001$ vs. the NC group.

cleaved caspase-3, p-p38, and membrane TRPV2 induced by aconitine, while TL just reduced the expression of cleaved caspase-3 and membrane TRPV2 significantly but had no obvious influence on the expression of TRPV2 (Figures 5(c) and 5(d)). In addition, both SB and TL reversed the Ca^{2+} influx promoted by aconitine (Figure 5(e)). These results suggested that p38 MAPK activation-induced TRPV2 expression and PM transfer played an important role in aconitine-induced H9c2 cardiomyocyte Ca^{2+} overload and apoptosis.

4. Discussion

Aconitum, as a world-famous medicinal plant, has been used for more than 2000 years. However, aconitine, as the main effective component of *Aconitum*, is a diterpenoid alkaloid with severe cardiovascular toxicity, which often induced tachyarrhythmia and hypotension and led to high mortality [27, 28]. Previous studies have shown that aconitine has obvious cytotoxicity on cardiomyocytes, which can induce cardiomyocyte injury through various ways, such as BNIP3-

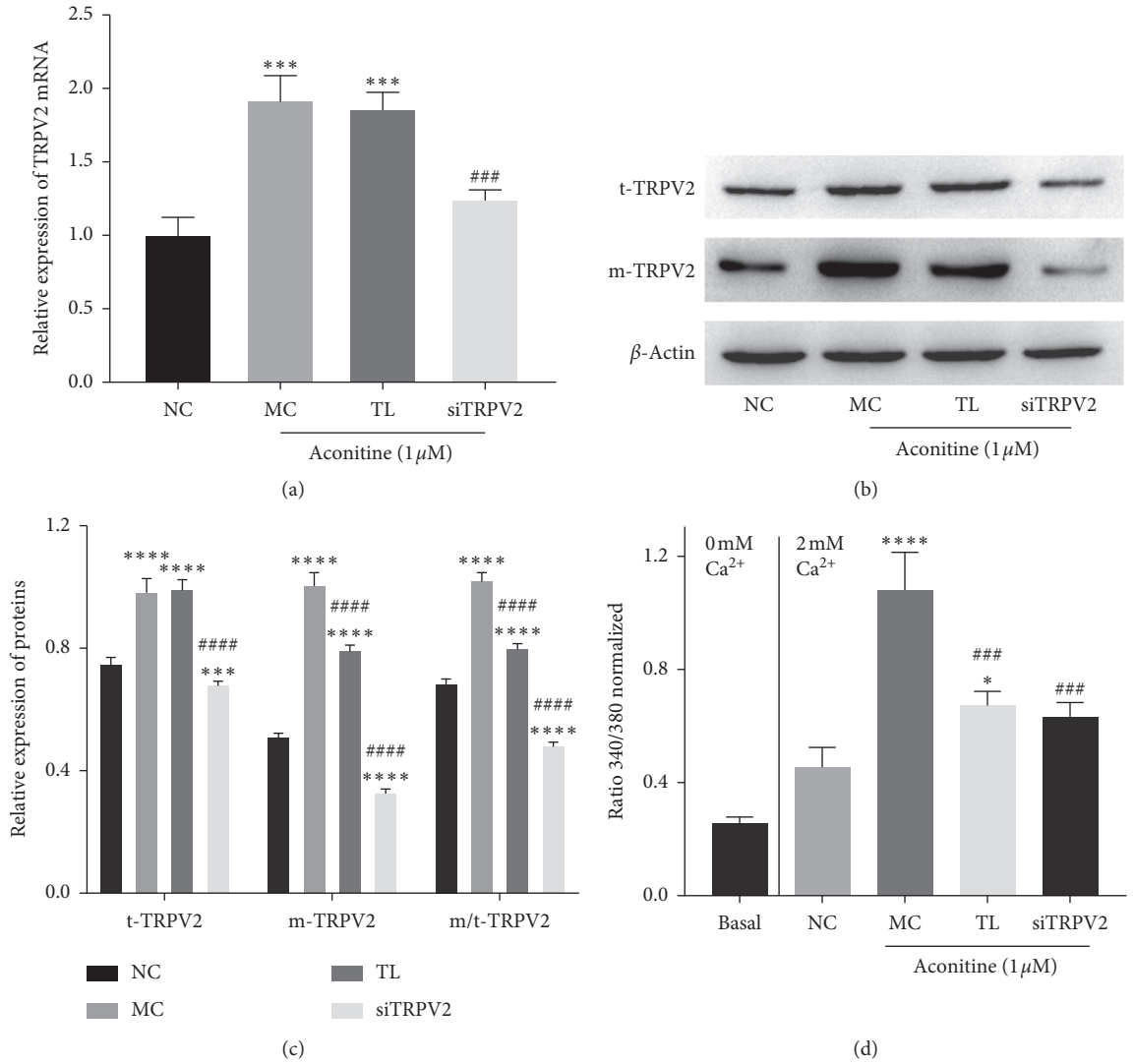

Figure 3: Aconitine induces intracellular Ca^{2+} overload by activating TRPV2. (a) The expression level of TRPV2 mRNA. (b, c) The protein expressions of TRPV2 and m/t-TRPV2. (d) The intracellular Ca^{2+} level in each group. NC: negative control; MC: model control; TL: tranilast; siTRPV2: siRNA of TRPV2; t-TRPV2: total TRPV2; m-TRPV2: membrane TRPV2. $^{*}P < 0.05$, $^{***}P < 0.001$, and $^{****}P < 0.0001$ vs. the NC group; $^{###}P < 0.001$ and $^{####}P < 0.0001$ vs. the MC group.

dependent mitophagy and TNF-α/NLRP3 signal transduction [11], Notch1-mediated histone demethylation of HCN4 [29], mitochondrial pathway [30], p38 MAPK signal, and Ca^{2+} overload [9]. In the present study, we demonstrated that aconitine could induce H9c2 cardiomyocyte apoptosis and Ca^{2+} influx in a dose-dependent manner (Figure 1), and the mechanism might be related to the activation of TRPV2 and p38 MAPK (Figure 2).

Growing evidence showed that the arrhythmia induced by aconitine is related to the activity of various ion channels, such as Na^{+} channel, Ca^{2+} channel, and K^{+} channel [31, 32]; among them, intracellular Ca^{2+} arrhythmia is most often reported to be related to the cardiotoxicity of aconitine [8, 9, 17, 33]. TRPV2 is a member of the TRPV channel family in the cardiovascular system and peripheral system and acts as a stretch-sensitive calcium permeability channel, and its plasma membrane translocation and activation lead to the sustained increase of intracellular Ca^{2+} [13]. TRPV2 is highly selective for Ca^{2+} and can be activated by lipids [34]. Under pathological conditions, the activation of TRPV2 mediates abnormal Ca^{2+} influx, thus accelerating disease progression [35], which is considered as a therapeutic target for cardiovascular diseases [13, 36]. Previous report has shown that inhibition of TRPV2 expression and intracellular Ca^{2+} overload plays an important role in maintaining cardiomyocyte activity and cardiac function [37]. The results of this study showed that both TRPV2 inhibitor tranilast and TRPV2 knockdown by siTRPV2 could reverse the Ca^{2+} influx stimulated by aconitine (Figure 3). Previous studies have revealed that the activation of the p38 MAPK signal could promote the expression and PM translocation of TRPV2 [15, 16], and the p38 MAPK signal could be activated by aconitine [9]. The present results showed that p38 MAPK inhibitor SB202190 reduced the expression and PM transfer

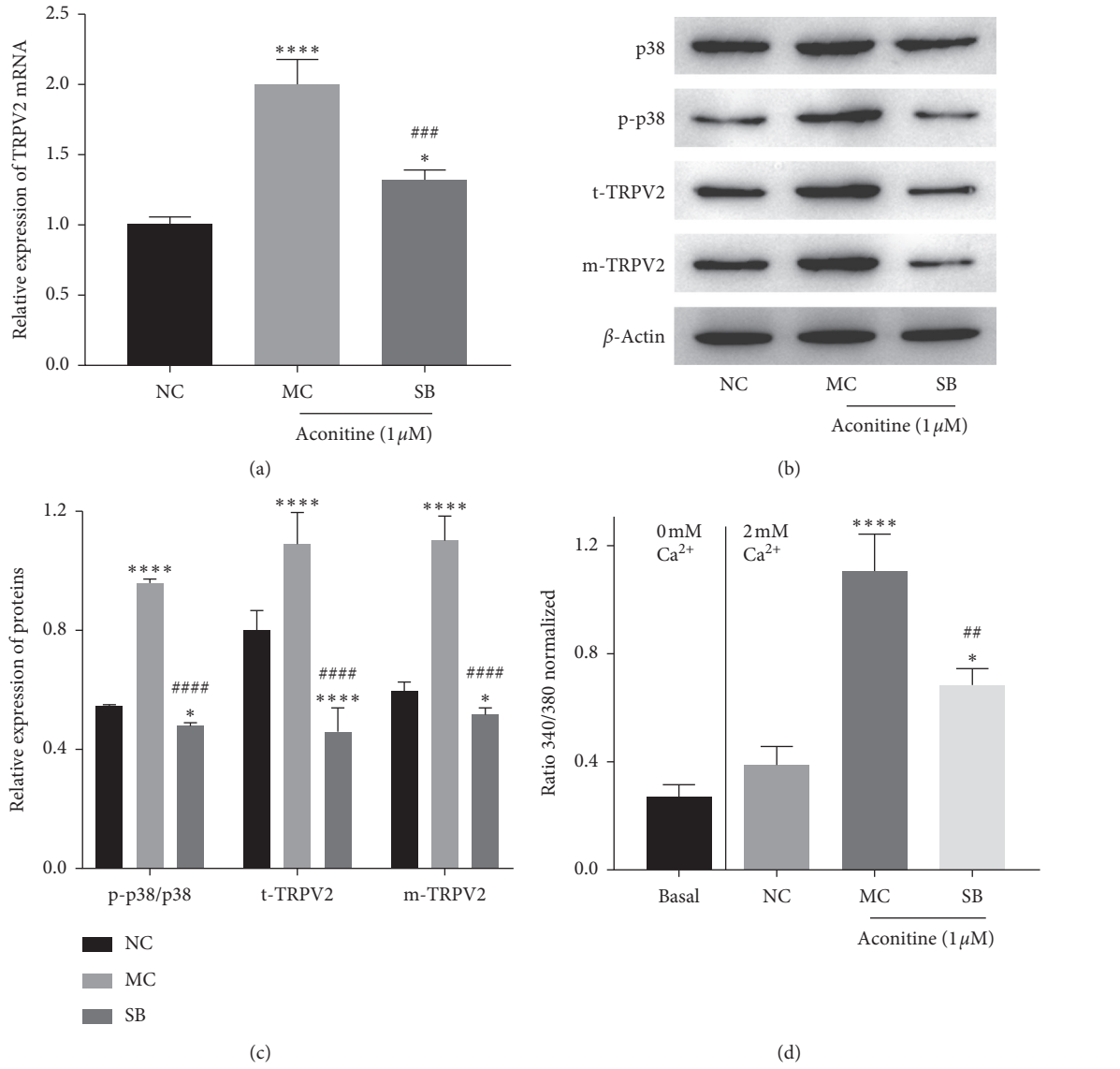

Figure 4: Aconitine promotes TRPV2 expression and PM translocation by activating p38 MAPK signaling. (a) The expression level of TRPV2 mRNA. (b, c) The protein expressions of p38, p-p38, and TRPV2. (d) The intracellular Ca^{2+} level in each group. NC: negative control; MC: model control; SB: SB202190; t-TRPV2: total TRPV2; m-TRPV2: membrane TRPV2. $^{*}P < 0.05$ and $^{****}P < 0.0001$ vs. the NC group; $^{\#\#}P < 0.01$, $^{\#\#\#}P < 0.001$, and $^{\#\#\#\#}P < 0.0001$ vs. the MC group.

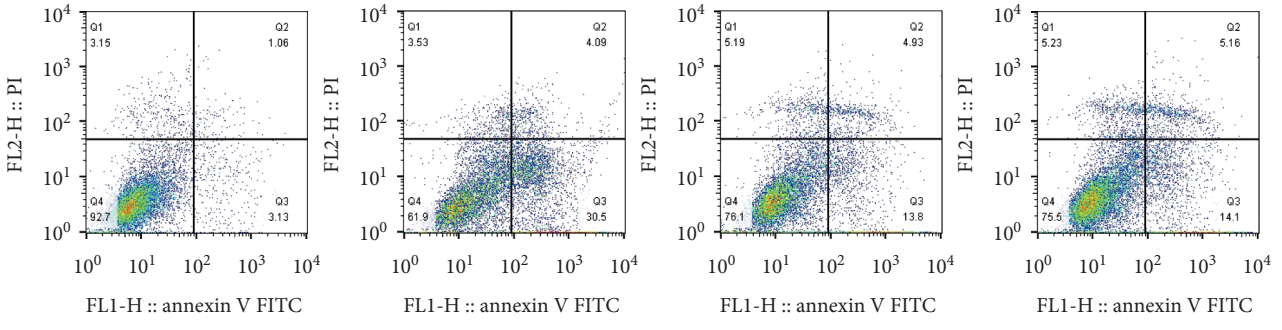

(a)

Figure 5: Continued.

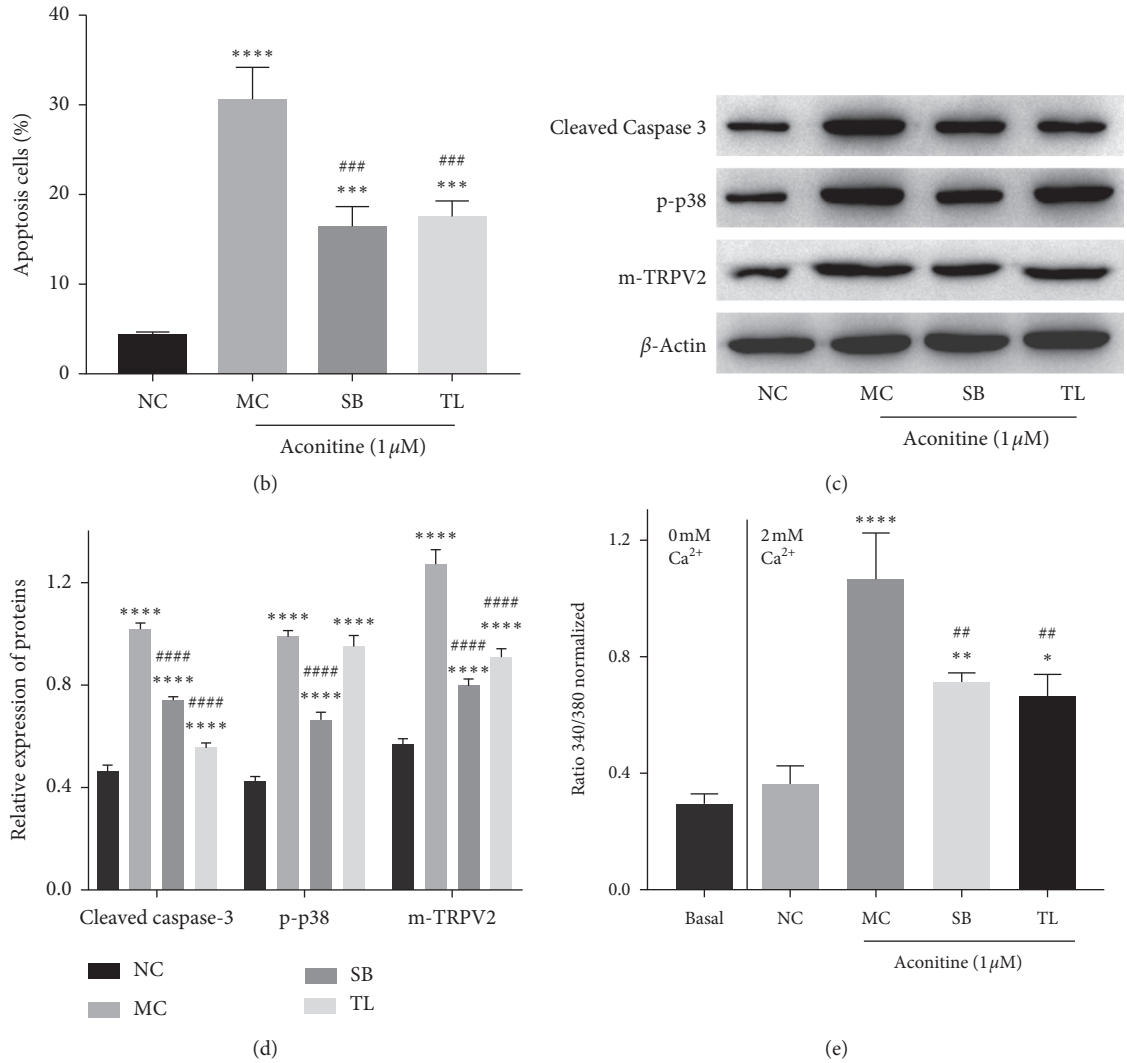

Figure 5: p38 MAPK inhibitor and TRPV2 inhibitor inhibit aconitine-induced intracellular Ca^{2+} overload and apoptosis. (a, b) The cell apoptosis rate of cardiomyocytes. (c, d) The protein expressions of cleaved caspase-3, p-p38, and m-TRPV2. (e) The intracellular Ca^{2+} content level in each group. NC: negative control; MC: model control; SB: SB202190; TL: tranilast; t-TRPV2: total TRPV2; m-TRPV2: membrane TRPV2. $^{*}P < 0.05$, $^{**}P < 0.01$, $^{***}P < 0.001$, and $^{****}P < 0.0001$ vs. the NC group; $^{\#\#}P < 0.01$, $^{\#\#\#}P < 0.001$, and $^{\#\#\#\#}P < 0.0001$ vs. the MC group.

of TRPV2 induced by aconitine, as well as Ca^{2+} influx (Figure 4), which indicated that aconitine could induce TRPV2-mediated Ca^{2+} influx by activating the p38 MAPK signal. Furthermore, tranilast and SB202190 reduced the H9c2 cardiomyocyte apoptosis stimulated by aconitine (Figure 5). These results suggested that aconitine-induced H9c2 cell apoptosis was partly depended on TRPV2-mediated intracellular Ca^{2+} overload promoted by p38 MAPK activation.

In summary, the effect of aconitine on cardiomyocytes was detected by *in vivo* assays in the present study, and results showed that aconitine promoted intracellular Ca^{2+} overload and cell apoptosis of H9c2 cardiomyocytes in a dose-dependent manner. Furthermore, aconitine promoted TRPV2 expression and PM metastasis through p38 MAPK signaling, thus inducing apoptosis mediated by intracellular calcium overload. These results indicated that TRPV2 may be a potential molecular target to treat aconitine poisoning and protect cardiac function.

Data Availability

The datasets used and/or analyzed during the current study are available from the corresponding author upon reasonable request.

Conflicts of Interest

The authors declare that they have no conflicts of interest.

Authors' Contributions

Chunai Yang and Xiaoyan Zeng contributed equally to this work. All authors contributed substantially to this

manuscript. XY Zeng contributed majorly for this manuscript, participated in all the experiments, and wrote the manuscript. ZF Cheng participated primarily in all the experiments and data analysis. JB Zhu contributed mainly to the assays of western blotting and qRT-PCR. YS Fu contributed majorly to the assays of flow cytometry. And CA Yang contributed to the conception and design of this study and guided the writing of the manuscript. All authors read and approved the final manuscript.

References

[1] L.-Q. Ma, Y. Yu, H. Chen et al., "Sweroside alleviated aconitine-induced cardiac toxicity in H9c2 cardiomyoblast cell line," *Frontiers in Pharmacology*, vol. 9, p. 1138, 2018.

[2] T. Y. K. Chan, "Aconitum alkaloid content and the high toxicity of aconite tincture," *Forensic Science International*, vol. 222, no. 1-3, pp. 1–3, 2012.

[3] F. Zhang, L. Cai, J. Zhang, X. Qi, and C. Lu, "Aconitine-induced cardiac arrhythmia in human induced pluripotent stem cell-derived cardiomyocytes," *Experimental and Therapeutic Medicine*, vol. 16, no. 4, pp. 3497–3503, 2018.

[4] B. Borcsa, U. Widowitz, D. Csupor, P. Forgo, R. Bauer, and J. Hohmann, "Semisynthesis and pharmacological investigation of lipo-alkaloids prepared from aconitine," *Fitoterapia*, vol. 82, no. 3, pp. 365–368, 2011.

[5] L. Tang, Y. Gong, C. Lv, L. Ye, L. Liu, and Z. Liu, "Pharmacokinetics of aconitine as the targeted marker of Fuzi (Aconitum carmichaeli) following single and multiple oral administrations of Fuzi extracts in rat by UPLC/MS/MS," *Journal of Ethnopharmacology*, vol. 141, no. 2, pp. 736–741, 2012.

[6] C.-C. Lin, T. Y. K. Chan, and J.-F. Deng, "Clinical features and management of herb-induced aconitine poisoning," *Annals of Emergency Medicine*, vol. 43, no. 5, pp. 574–579, 2004.

[7] N. G. Bisset, "Arrow poisons in China. part ii. aconitum -botany, chemistry, and pharmacology," *Journal of Ethnopharmacology*, vol. 4, no. 3, pp. 247–336, 1981.

[8] M. Fu, M. Wu, J.-F. Wang, Y.-J. Qiao, and Z. Wang, "Disruption of the intracellular Ca^{2+} homeostasis in the cardiac excitation-contraction coupling is a crucial mechanism of arrhythmic toxicity in aconitine-induced cardiomyocytes," *Biochemical and Biophysical Research Communications*, vol. 354, no. 4, pp. 929–936, 2007.

[9] G.-b. Sun, H. Sun, X.-b. Meng et al., "Aconitine-induced Ca^{2+} overload causes arrhythmia and triggers apoptosis through p38 MAPK signaling pathway in rats," *Toxicology and Applied Pharmacology*, vol. 279, no. 1, pp. 8–22, 2014.

[10] Y. Zhao, Q. Bu, Y. Zhou et al., "Mechanism study of Aconitum-induced neurotoxicity in PC12 cells: involvement of dopamine release and oxidative damage," *Neurotoxicology*, vol. 31, no. 6, pp. 752–757, 2010.

[11] F. Peng, N. Zhang, C. Wang et al., "Aconitine induces cardiomyocyte damage by mitigating BNIP3-dependent mitophagy and the TNFα-NLRP3 signalling axis," *Cell Proliferation*, vol. 53, no. 1, Article ID e12701, 2020.

[12] G. Sangiorgi, A. Mauriello, E. Bonanno et al., "Pregnancy-associated plasma protein-A is markedly expressed by monocyte-macrophage cells in vulnerable and ruptured carotid atherosclerotic plaques," *Journal of the American College of Cardiology*, vol. 47, no. 11, pp. 2201–2211, 2006.

[13] Y. Iwata and T. Matsumura, "Blockade of TRPV2 is a novel therapy for cardiomyopathy in muscular dystrophy," *International Journal of Molecular Sciences*, vol. 20, no. 16, 2019.

[14] M. Entin-Meer and G. Keren, "Potential roles in cardiac physiology and pathology of the cation channel TRPV2 expressed in cardiac cells and cardiac macrophages: a mini-review," *American Journal of Physiology-Heart and Circulatory Physiology*, vol. 318, no. 1, pp. H181–H188, 2020.

[15] J. Liu, Z. Zhao, J. Wen et al., "TNF-α differently regulates TRPV2 and TRPV4 channels in human dental pulp cells," *International Endodontic Journal*, vol. 52, no. 11, pp. 1617–1628, 2019.

[16] W. Ma, C. Li, S. Yin et al., "Novel role of TRPV2 in promoting the cytotoxicity of H2O2-mediated oxidative stress in human hepatoma cells," *Free Radical Biology and Medicine*, vol. 89, pp. 1003–1013, 2015.

[17] Y.-h. Zhou, X.-m. Piao, X. Liu et al., "Arrhythmogenesis toxicity of aconitine is related to intracellular Ca^{2+} signals," *International Journal of Medical Sciences*, vol. 10, no. 9, pp. 1242–1249, 2013.

[18] M. Ruiz, L. Coderre, B. G. Allen, and C. Des Rosiers, "Protecting the heart through MK2 modulation, toward a role in diabetic cardiomyopathy and lipid metabolism," *Biochimica et Biophysica Acta (BBA)-Molecular Basis of Disease*, vol. 1864, no. 5, pp. 1914–1922, 2018.

[19] F. B. Engel, P. C. H. Hsieh, R. T. Lee, and M. T. Keating, "FGF1/p38 MAP kinase inhibitor therapy induces cardiomyocyte mitosis, reduces scarring, and rescues function after myocardial infarction," *Proceedings of the National Academy of Sciences*, vol. 103, no. 42, pp. 15546–15551, 2006.

[20] F. B. Engel, M. Schebesta, M. T. Duong et al., "p38 MAP kinase inhibition enables proliferation of adult mammalian cardiomyocytes," *Genes & Development*, vol. 19, no. 10, pp. 1175–1187, 2005.

[21] F. B. Engel, M. Schebesta, and M. T. Keating, "Anillin localization defect in cardiomyocyte binucleation," *Journal of Molecular and Cellular Cardiology*, vol. 41, no. 4, pp. 601–612, 2006.

[22] M. S. Marber, B. Rose, and Y. Wang, "The p38 mitogen-activated protein kinase pathway-A potential target for intervention in infarction, hypertrophy, and heart failure," *Journal of Molecular and Cellular Cardiology*, vol. 51, no. 4, pp. 485–490, 2011.

[23] H. Ji, F. Xiao, S. Li, R. Wei, F. Yu, and J. Xu, "GRP78 effectively protect hypoxia/reperfusion-induced myocardial apoptosis via promotion of the Nrf2/HO-1 signaling pathway," *Journal of Cellular Physiology*, vol. 236, 2020.

[24] C. Habes, G. Weber, and C. Goupille, "Sulfated glycoaminoglycans and proteoglycan syndecan-4 are involved in membrane fixation of LL-37 and its pro-migratory effect in breast cancer cells," *Biomolecules*, vol. 9, no. 9, 2019.

[25] J. Peng, J. Jiang, H. Wang, X. Feng, and X. Dong, "miR-199a-3p Suppresses cervical epithelial cell inflammation by inhibiting the HMGB1/TLR4/NF-κB pathway in preterm birth," *Molecular Medicine Report*, vol. 22, no. 2, pp. 926–938, 2020.

[26] K. J. Livak and T. D. Schmittgen, "Analysis of relative gene expression data using real-time quantitative PCR and the $2^{-\Delta\Delta CT}$ method," *Methods*, vol. 25, no. 4, pp. 402–408, 2001.

[27] Y.-T. Tai, C.-P. Lau, K. Young, and P. P.-H. But, "Cardiotoxicity after accidental herb-induced aconite poisoning," *The Lancet*, vol. 340, no. 8830, pp. 1254–1256, 1992.

[28] T. Y. K. Chan, "Aconite poisoning," *Clinical Toxicology*, vol. 47, no. 4, pp. 279–285, 2009.

[29] W. Zhou, L.-z. Qiu, H. Liu, H.-F. Deng, L.-X. Yue, and Y. Gao, "Notch1-mediated histone demethylation of HCN4

contributes to aconitine-induced ventricular myocardial dysrhythmia," *Toxicology Letters*, vol. 327, pp. 19–31, 2020.

[30] X. Gao, X. Zhang, J. Hu et al., "Aconitine induces apoptosis in H9c2 cardiac cells via mitochondria-mediated pathway," *Molecular Medicine Reports*, vol. 17, no. 1, pp. 284–292, 2018.

[31] J. Wu, X. Wang, Y. Y. Chung et al., "L-type calcium channel inhibition contributes to the proarrhythmic effects of aconitine in human cardiomyocytes," *PloS One*, vol. 12, no. 1, Article ID e0168435, 2017.

[32] Z. Zhao, Y. Yin, H. Wu et al., "Arctigenin, a potential anti-arrhythmic agent, inhibits aconitine-induced arrhythmia by regulating multi-ion channels," *Cellular Physiology and Biochemistry*, vol. 32, no. 5, pp. 1342–1353, 2013.

[33] S.-W. Zhang, Y. Liu, G.-Z. Huang, and L. Liu, "Aconitine alters connexin43 phosphorylation status and [Ca^{2+}] oscillation patterns in cultured ventricular myocytes of neonatal rats," *Toxicology in Vitro*, vol. 21, no. 8, pp. 1476–1485, 2007.

[34] M. Guéguinou, R. Felix, S. Marionneau-Lambot et al., "Synthetic alkyl-ether-lipid promotes TRPV2 channel trafficking trough PI3K/Akt-girdin axis in cancer cells and increases mammary tumour volume," *Cell Calcium*, vol. 97, p. 102435, 2021.

[35] Z. Rozenbaum, L. Cohen, E. Bigelman, Y. Shacham, G. Keren, and M. Entin-Meer, "Downregulated expression of TRPV2 in peripheral blood cells following acute myocardial infarction is inversely correlated with serum levels of CRP and troponin I," *Cardiology*, vol. 139, no. 3, pp. 169–174, 2018.

[36] E. Aguettaz, P. Bois, C. Cognard, and S. Sebille, "Stretch-activated TRPV2 channels: role in mediating cardiopathies," *Progress in Biophysics and Molecular Biology*, vol. 130, pp. 273–280, 2017.

[37] Y. Li, Q. Li, O. Zhang et al., "miR-202-5p protects rat against myocardial ischemia reperfusion injury by downregulating the expression of Trpv2 to attenuate the Ca^{2+} overload in cardiomyocytes," *Journal of Cellular Biochemistry*, vol. 120, no. 8, pp. 13680–13693, 2019.